

**VIBRATIONS AND
BUCKLING
OF
BEAMS
AND
PLATES**

By

**Dr. Chellapilla
Kameswara Rao et.al**

Dr. CHELLAPILLA KAMESWARA RAO_REFEREED JOURNAL PUBLICATIONS

1. Lokavarapu Bhaskara Rao and Chellapilla Kameswara Rao, "Frequencies of circular plate with concentric ring and elastic edge support" *Front. Mech. Eng.* 2014, 9(2): 168–176
2. Lokavarapu Bhaskara Rao and Chellapilla Kameswara Rao, "Buckling of circular plate with foundation and elastic edge", *Int J Mech Mater Des*, 2014.
3. Lokavarapu Bhaskara Rao and Chellapilla Kameswara Rao, "Frequency analysis of annular plates with inner and outer edges elastically restrained and resting on Winkler foundation", *International Journal of Mechanical Sciences* 81(2014)184–1944
4. Lokavarapu Bhaskara Rao and Chellapilla Kameswara Rao, "Buckling of Annular Plates with Elastically Restrained External and Internal Edges", *Mechanics Based Design of Structures and Machines*, 41: 222–235, 2013
5. Lokavarapu Bhaskara Rao and Chellapilla Kameswara Rao, "Fundamental Buckling of Circular Plates with Elastically Restrained Edges and Resting on Concentric Rigid RingSupport", *Frontiers of Mechanical Engineering*, May 2013 issue.
6. Lokavarapu Bhaskara Rao and Chellapilla Kameswara Rao, "Frequencies of Circular Plates Weakened Along an Internal Concentric Circle and Elastically Restrained Edge Against Translation", *Journal of Applied. Mechanics*, Volume 80, Number 1, Paper No. 011005-1 to 011005-7, January 2013.
7. Lokavarapu Bhaskara Rao and Chellapilla Kameswara Rao, "Free Vibration of Circular Plates with Elastic Edge Support and Resting on an Elastic Foundation", *International Journal of Accoustics and Vibration*, Volume 17, Number 4, December 2012, pp.204-207.
8. Lokavarapu Bhaskara Rao and Chellapilla Kameswara Rao, " Buckling of Circular Plates with an Internal Elastic Ring Support and Outer Edge Restrained Against Translation", *Journal of Engineering Science and Technology*, Vol. 7, No.3, June 2012, pp. 393 – 401.
9. Lokavarapu Bhaskara Rao and Chellapilla Kameswara Rao "Vibrations of elastically restrained circular plates resting on Winkler Foundation", *The Arabian Journal for Science and Engineering*, March 2012.
10. Lokavarapu Bhaskara Rao and Chellapilla Kameswara Rao, "Vibrations of Circular Plates with Guided edge and Resting on Elastic Foundation", *Journal of Solid Mechanics*, Vol.4, No.3, 2012.
11. Lokavarapu Bhaskara Rao and Chellapilla Kameswara Rao "Buckling Analysis of Circular Plates with Elastically Restrained Edges and Resting on Internal Elastic Ring Support",

Mechanics Based Design of Structures and Machines: An International Journal, Vol. 38, 2010, pp. 440–452.

12. L. Bhaskara Rao and C. Kameswara Rao, “Vibrations of Elastically Restrained Circular Plates Resting on Partial Winkler Foundation”, The Open Acoustics Journal, 2009, 2, pp. 68-74.

13. L. Bhaskara Rao and C. Kameswara Rao, “Buckling of Circular Plates with an Internal Elastic Ring Support and Elastically Restrained Guided Edge Against Translation”, Mechanics Based Design of Structures and Machines: An International Journal, Vol. 37, 2009, pp. 60–72.

14. Kameswara Rao, C. and Simha, H. S. “Vibrations of Fluid-Conveying Pipes Resting on Two-parameter Foundation”, The Open Acoustics Journal, Banthem Publications, 2008, 1, 24-33.

15. Simha, H. S. and Kameswara Rao, C. “Critical Velocity of Fluid Conveying Pipes Resting on Two-parameter Foundation”, Journal of Sound and Vibration 302 (2007) 387–397.

16. Radhakrishna, M., and Kameswara Rao, C., “ Vibrations of Double Bellows Type Expansion Joint in Lateral and Rocking Modes”, International Journal of Structural Stability and Dynamics, WCM-2006-127, Published by World Scientific Publishing Co. Pte Ltd, London, U.K.,

17. Radhakrishna, M and Kameswara Rao, C. “Axial Vibrations of U Shaped Bellows with Elastically Restrained End Conditions”, Thin-walled Structures, Vol. 42, 2004, pp.415 – 426.

18. Kameswara Rao, C., "Frequency Analysis of Two-Span Uniform Euler-Bernoulli Beams," Journal of Sound and Vibration, Vol. 137, pp. 144-150, 1990.

19. Kameswara Rao, C., "Frequency Analysis of Clamped-Clamped Uniform Beams with Immediate Elastic Support," Journal of Sound and Vibration, Vol. 133, pp. 502-509, 1989.

20. Kameswara Rao, C., and Mirza, S., "Torsional Post-Buckling of Thin-Walled Beams Resting on Continuous Elastic Foundation," Thin-Walled Structures, Vol. 8, pp. 55-62, 1989.

21. Kameswara Rao, C., and Mirza, S., "Torsional Vibrations and Buckling of Thin-Walled Beams on Elastic Foundation," Thin-Walled Structures, Vol. 7, pp. 73-82, 1989.

22. Kameswara Rao, C., and Mirza, S., "Seismic Analysis of High Speed Rotating Machinery," Nuclear Engineering and Design, Vol. III, pp. 395-402, 1989.

23. Kameswara Rao, C., and Mirza, S., "A Note on Vibrations of Generally Restrained Beams," Journal of Sound and Vibration, Vol. 130, pp. 453-465, 1989.

24. Kameswara Rao, C., "Fundamental Frequencies of Cantilever Blades with Resilient Roots," Journal of Sound and Vibration, Vol. 126, pp. 363-366, 1988.

25. Kameswara Rao, C., "Torsional Frequencies and Mode Shapes of Generally Constrained Shafts and Piping," Journal of Sound and Vibration, Vol. 125, pp. 115-121, 1988.

26. Kameswara Rao, C., and Mirza, S., "Free Torsional Vibrations of Tapered Cantilever I-Beams," *Journal of Sound and Vibration*, Vol. 124, pp. 489-496, 1988.
27. Kameswara Rao, C., and Satyanarayana, B., "Effect of Thermal Gradient on Frequencies of Tapered Rectangular Plates," *AIAA Journal*, Vol. 13, No. 8, pp. 1123-1126, August 1975.
28. Kameswara Rao, C., "Nonlinear Torsional Vibrations of Thin-Walled Beams of Open Section," *J. of Appl. Mech., Trans. ASME*, pp. 241-243, March 1975.
29. Kameswara Rao, C., and Appala Satyam, A., "Torsional Vibrations and Stability of Thin-Walled Beams on Continuous Elastic Foundation," *AIAA Journal*, pp. 232-234, February 1975.

NATIONAL JOURNALS (7)

1. Rao, N. L. N., and Kameswara Rao, C., "Vibration Frequencies for Uniform Timoshenko Beams with Central Masses," *Machine Building Industry*, pp. 5-8, September 1978.
2. Kameswara Rao, C., "Free Torsional Vibrations of Viscoelastic Thin-Walled Beams of Open Section," *Journal of the Aeronautical Society of India*, Vol. 29, Nos. 1,2, pp. 43-48, February-May 1977.
3. Kameswara Rao, C., "Forced Torsional Vibrations of Thin-Walled Beams of Open Section with Longitudinal Inertia, Shear Deformation and Viscous Damping," *Journal of the Aeronautical Society of India*, Vol. 28, No. 4, pp. 405-412, November 1976.
4. Kameswara Rao, C., "On the Torsional Wave Propagation in Orthotropic Thin-Walled Beams of Open Section Including Longitudinal Inertia and Shear Deformation," *Journal of the Aeronautical Society of India*, Vol. 28, No. 3, pp. 283-288, September 1976.
5. Kameswara Rao, C., and Prasada Rao, K. S. R., "Frequency Analysis of Rectangular Isotropic Plates by Galerkin Method," *Journal of the Aeronautical Society of India*, Vol. 28, No. 1, pp. 113-120, February 1976.
6. Kameswara Rao, C., and Sarma, P. K., "The Fundamental Frequency of Simply Supported Beams with Uniform Taper," *Journal of the Aeronautical Society of India*, Vol. 27, No. 4, pp. 169-171, November 1975.
7. Kameswara Rao, C., Appa Rao, K. V., and Sarma, P. K., "Effect of Longitudinal Inertia and of Shear Deformation on the Torsional Frequency and Normal Modes of Thin-Walled Open Section Beams," *Journal of the Aeronautical Society of India*, Vol. 26, Nos. 1,2, pp. 32-41, May 1974.

CONFERENCE PAPERS

INTERNATIONAL CONFERENCES (16)

1. Chellapilla, Kameswara Rao., and Hari Simha, “Critical Flow Velocities of Elastically Restrained Multi-span Fluid Conveying Pipes Resting on Continuous Elastic Foundation”, Proceedings of the 13th International Conference on Nuclear Engineering, Beijing, China, May 2005 Paper No.50473
2. Kameswara Rao, C. “ Frequency Analysis of Boiler Support Structure Subjected to Earthquake Excitation”, (Keynote Speech), Proceedings of International Conference on Advances in Structural Dynamics and its Applications (ICASDA-2005), Conference held at GITAM, Visakhapatnam – 539 045, during 7-9 Dec. 2005, pp. 415 – 424.
3. Kameswara Rao, C., and Ramesh, M., “Free Torsional Vibrations of Generally Restrained Thin-walled Beams of Open Section”, Proceedings of ICASDA 2005, pp. 210 – 217.
4. Kameswara Rao, C., and Simha, H., “ Critical Velocity of Fluid Conveying Pipes Resting on Two-Parameter Foundation”, Proceedings of ICASDA 2005, pp. 609 – 617.
5. Kameswara Rao, C and Radhakrishna, M. “Seismic Response of Elastically Restrained Single Bellows Expansion Joint in Lateral Mode”, Proceedings of the Eleventh International Conference on Nuclear Engineering, April 20-24, 2003, Tokyo, Japan, Paper No. ICONE 11-36400, pp 1-6.
6. Kameswara Rao, C and Radhakrishna, M. “Transverse Vibrations of Single Bellows Expansion Joint Restrained Against Rotation”, Proceedings of the Tenth International Conference on Nuclear Engineering, April 14-18,2002, Arlington, Virginia, USA, Paper No. ICONE 10-22090, pp. 1-5.
7. Kameswara Rao, C and Radhakrishna, M. “Transverse Vibrations of Double Expansion Joint Restrained Against Rotation”, Proceedings of the Tenth International Conference on Nuclear Engineering, April 14-18, 2002, Arlington, Virginia, USA, Paper No. ICONE 10-22092.
8. Radhakrishna, M and Kameswara Rao, C. “Finite Element Analysis of Axial Vibrations of Single Bellows Elastically Restrained Against Rotation”, Proceedings of Second International Conference on Vibration Engineering and Technology of Machinery, VETOMAC-2, December 16-18, 2002, Mumbai, India.
9. Kameswara Rao, C., and Mirza, S., "Accurate Estimates of Natural Frequencies and Mode Shapes of Flexible Piping Carrying an Arbitrarily Located Heavy Valve," Chapter 3 - Pipeline Dynamics, Proc. of PVP Conference, Pittsburg, Pennsylvania, Seismic Engineering, PVP-Vol. 144, pp. 221-226, June 1988.

10. Kameswara Rao, C., and Mirza, S., "Seismic Analysis of High-Speed Rotating Machinery," Proc. of 9th International Conference on Structural Mechanics in Reactor Technology, Lausanne, Invited Paper No. K-18-1, August 1987.
11. Kameswara Rao, C., and Mirza, S., "Influence of Flexible Connections on the Seismic Response of a Nuclear Condenser," Proc. Canadian Conference on Earthquake Engineering, pp. 553-558, July 1987.
12. Kameswara Rao, C., and Mirza, S., "Seismic Response of Flexibly Connected Piping Systems, Proc. of ASME Pressure Vessels and Piping Conference, San Diego, Seismic Engineering, PVP Vol. 127, pp. 308-313, June 1987.
13. Kumar, G. V., Kameswara Rao, C., and Chary, S. R., "Pipe Support Design for Dynamic Loads," Proc. of ASME Pressure Vessels and Piping Conference, San Diego, Seismic Engineering, PVP Vol. 127, pp. 303-308, June 1987.
14. Kameswara Rao, C., and Mirza, S., "Vibration Frequencies and Mode Shapes for Generally Restrained Bernoulli-Euler Beams," Proc. of ASME Pressure Vessels and Piping Conference, San Diego, Recent Advances in Structural Dynamics, PVP-Vol. 124, pp. 117-121, June 1987.
15. Kameswara Rao, C., "Effects of Bellow and Pipe Support Stiffness on Dynamic Response of Piping Systems," Proc. of ASME Pressure Vessels and Piping Conference, New Orleans, Recent Advances in Seismic Design of Piping and Components, PVP-Vol. 98-3, pp. 267-271, June 1985.
16. Kameswara Rao, C., Ramadasa, K., Singh, A. K., and Bhatia, K. G., "Three Dimensional Analysis of 110 MW Boiler Supporting Structure Subjected to Seismic Excitation," Proc. of Seventh World Conference on Earthquake Engineering, Istanbul, Turkey, Vol. 5, pp. 601-608, September 1980.

NATIONAL CONFERENCES (27)

1. Simha, H. S. and Kameswara Rao, C. "Thermal Buckling of Fluid Conveying Single-Walled Carbon Nanotubes Embedded in an Elastic Medium", International Conference on Nanotechnology & Functional Materials, SNIST, Hyderabad, 2012.
2. Simha, H. S. and Kameswara Rao, C. "Free Vibrations of Fluid Conveying Single-Walled Carbon Nanotubes", International Conference on Nanotechnology & Functional Materials, SNIST, Hyderabad, 2012.
3. Lokavarapu Bhaskara Rao and Chellapilla Kameswara Rao, "Buckling of Circular Plates with an Internal Ring Support and Elastically Restrained edge", Proceedings of Vibration Engineering & Technology of Machinery (VETOMAC-IV), 17 – 19, December 2007, Osmania University, Hyderabad.

4. Kameswara Rao, C., Sravana Kumar, G., Vijaya Kumar, K., and Sameer, T., “ Fundamental Frequencies of Restrained Cantilever Blades including the Effects of Thermal Gradient”, Proceedings of RACE 2006, March 3-5, 2006, Osmania University, India.
5. Kameswara Rao, C., and Ratna Kiran V., “ Finite Element Analysis of Torsional Vibrations of Thin-Walled Beams on Two Parameter Foundation”, Proceedings of RACE 2006, March 3-5, 2006, Osmania University, India.
6. Kameswara Rao, C., and Bhaskara Rao, L., “ Vibrations of Elastically Restrained Circular Plates on Winkler’s Foundation”, Proceedings of RACE 2006, March 3-5, 2006, Osmania University, India.
7. Kameswara Rao, C., and Ratna Kiran, V., “Torsional Vibrations of Thin-walled Beams Resting on Continuous Two Parameter Foundation”, Proceedings of National Conference on Advances in CAD/ CAM, February 27-28, 2006, JNTU College of Engineering, Kakinada, A.P., India.
8. Radhakrishna, M and Kameswara Rao, C.”Finite Element Analysis of Transverse Vibrations of Single Bellows Expansion Joint Restrained Against Rotation”, Paper communicated to Journal of Thin-Walled Structures, Elsevier Applied Science Publishers, Great Britain, 2002.
9. Radhakrishna, M and Kameswara Rao, C.”Vibrations of Fluid Filled Bellows- A State-of-the-Art”, Proceedings of the National Symposium on Advances in Structural Dynamics and Design, Jan 9-11, 2001.
10. Simha, H. & Kameswara Rao, C., "Finite Element Analysis of Vibrations of Rotationally Restrained Fluid Conveying Pipes Resting on Soil Medium" Proceedings of the National Symposium on Advances in Structural Analysis and Design, pp 569-578, Allied Publishers, Chennai, January 2001.
11. Simha, H, and Kameswara Rao, C., “Finite Element Analysis of Vibrations of Rotationally Restrained Fluid Conveying Pipes Resting on Soil Medium”, Proceedings of the Conference on Advances in Structural Dynamics and Design held at SERC, Chennai, Jan 2001, pp.569-577.
12. Srinivasulu, N. V. & Kameswara Rao, C., "Galerkin Finite Element Analysis of Free Torsional Vibrations of Tapered Cantilever I-Beams" Paper no. CP071, Proceedings of Vibration Engineering and Technology of Machinery, IISc, Bangalore, October 2000.
13. Simha, H. & Kameswara Rao, C.,”Finite Element Analysis of Vibrations Fluid Conveying Pipes Resting on Soil Medium”, Proceedings of the Technical Conference on Pressure Vessels and Piping, pp 173-182, Hyderabad, October 1997.
14. Raghava Chary, S., Kameswara Rao, C., and Iyengar, R. N., "Vibration of Fluid Conveying Pipe on Winkler Foundation," Proc of 8th National Convention of Aerospace Engineers on Aeroelasticity, Hydroelasticity and other Fluid-Structure Interaction Problems, IIT Kharagpur, India, pp. 266-287, March 5-6, 1993.

15. Prasad, P. M. L., and Kameswara Rao, C., "Seismic Analysis of SF6 Circuit Breaker," Proc. Of National Symposium on Vibration of Power Plant Equipment, Bombay, pp. III-6.1 to III-6.9, March 1986.
16. Kameswara Rao, C., and Prasad, P. M. L., "Seismic Analysis of 70 MW Turbo-Generator Rotor Bearing System," Proc. of National Symposium on Vibration of Power Plant Equipment, Bombay, pp. II-9.1 to II-9.9, March 1986.
17. Rao, J. S., Prasad, P. M. L., and Kameswara Rao, C., "Seismic Analysis of Gasifier Support Structure," Proc. of Mid-Trem Symp. on Earthquake Effects on Plant and Equipment, Hyderabad, Vol. I, pp. 177-181, December 1984.
18. Kameswara Rao, C., Pillai, K. S., and Prasad, P. M. L., "Seismic / Wind Analysis of Common Condenser for a Chemical Plant," Proc. of Mid-Trem Symp. on Earthquake Effects on Plant and Equipment, Hyderabad, Vol. I, pp. 257-260, December 1984.
19. Kameswara Rao, C., and Prasad, P. M. L., "Seismic Analysis of 70 MW Turbo-Generator Foundation," Proc. of Mid-Trem Symp. on Earthquake Effects on Plant and Equipment, Hyderabad, Vol. I, pp. 143-149, December 1984.
20. Kameswara Rao, C., and Vijaya Kumar, G. V., "Effects of Support and Bellow Stiffnesses on Piping Seismic Response," Proc. of Mid-Trem Symp. on Earthquake Effects on Plant and Equipment, Hyderabad, Vol. I, pp. 107-111, December 1984.
21. Kameswara Rao, C., "Seismic Analysis of Rotating Mechanical Systems - State of the Art," 28th Congress of Indian Society of Theoretical and Applied Mechanics, December 1983.
22. Kameswara Rao, C., and Bhatia, K. G., "Evaluation of Seismic Analysis Techniques for Static Electrical Equipment," Proc. of Seventh Symp. on Earthquake Engineering, Roorkee, Vol. I, pp. 583-588, November 1982.
23. Singh, A. K., Ramadasa, K., Kameswara Rao, C., and Bhatia, K. G., "Seismic Analysis of General Piping System for Narora Atomic Power Plant," Proc. of Seventh Symp. on Earthquake Engineering, Roorkee, Vol. I, pp. 571-575, November 1982.
24. Kameswara Rao, C., and Bhatia, K. G., "Seismic Analysis of 220 kV Current and Voltage Transformers," Proc. of Seventh Symp. on Earthquake Engineering, Roorkee, Vol. I, pp. 565-569, November 1982.
25. Kameswara Rao, C., Ramadasa, K., Singh, A. K., and Bhatia, K. G., "An Approximate Analysis of 110 MW Boiler Supporting Structure Subjected to Seismic Excitation," Proc. of Seventh Symp. on Earthquake Engineering, Roorkee, Vol. I, pp. 561-564, November 1982.
26. Kameswara Rao, C., "Seismic Analysis of Instrument Transformers," Proc. of Symp. On Earthquake Disaster Mitigation, Roorkee, India, Vol. I, pp. 165-170, March 1981.

27. Kameswara Rao, C., "Non-linear Torsional Vibrations and Stability of Thin-Walled Beams on Elastic Foundation," Symposium on Large Deformations, IIT, New Delhi, December 1979.

28. Kameswara Rao, C., "Galerkin Finite Element Analysis of Torsional Vibrations of Tapered Cantilever I-Beams on Elastic Foundation," Proc. of AGM of Aeronautical Society of India, August 1978.

Effect of Longitudinal Inertia and of Shear Deformation on the Torsional Frequency and Normal Modes Thin-Walled Open Section Beams

C. Kameswara Rao, K. V. Appa Rao and P. K. Sharma

Effect of Longitudinal Inertia and of Shear Deformation on the Torsional Frequency and Normal Modes of Thin-Walled Open Section Beams

C. Kameswara Rao*, K. V. Appa Rao** and P. K. Sarma†

SUMMARY

The free torsional vibration of bars of thin-walled open section for which the shear centre and centroid coincide was dealt with, developing new frequency and normal mode equations, which include the effects of longitudinal inertia and shear deformation, for six common types of simple and finite beams. Solutions of the frequency equations for various end conditions are obtained on a digital computer and the results for the first two modes of vibration of ten Indian Standard wide-flanged I-beams for various end conditions are presented in graphical form, suitable for design use. Comparison is made with the results of a higher order theory and an excellent agreement is observed.

INTRODUCTION

It has been the usual practice to approximate the torsional vibrations of thin-walled open section beams by classical Saint-Venant torsion theory. Timoshenko¹ pointed out the inadequacy of the Saint-Venant torsion theory and introduced the effect of warping of the cross section for the case of an I-beam. Much work has been done²⁻¹⁰, based on Timoshenko torsion theory. Recently Aggarwal and Cranch¹¹ modified the Timoshenko torsion theory by including the effects of shear deformation and longitudinal inertia. Aggarwal¹², analysed the free and forced vibrations of an I-beam and presented curves for selected values of shear and longitudinal inertia parameters for the first three modes of vibration of simply supported beam. Results for other boundary conditions are not given. The natural frequency results for the simply supported beam have not been made available beyond his thesis.

Krishna Murty and Joga Rao¹³ presented a general theory of vibrations of cylindrical tubes which includes the secondary effects such as transverse shear, longitudinal inertia and shear lag.

In part IV of their theory¹⁴, results for simply-supported open tube of doubly symmetric I-section are presented. The other boundary conditions are not analysed. The first order approximation equations of Ref. 13, neglecting shear lag, for torsional vibrations of doubly symmetric open tubes, are observed to be the same as those obtained in Ref. 11, but for the only difference that the shear coefficient in the equations of Ref. 11 assumes a value of unity in those of Ref. 13, irrespective of the shape of the cross section.

In the present investigation, a somewhat different and simple method of solution used by Huang¹⁵, is applied to the coupled equations of Ref. 11, to derive a clear and neat set of frequency and normal mode equations for six common types of simple and finite beams. The advantage of this method is that the boundary conditions prescribed are homogeneous and the analysis is quite simple. Solutions are obtained on a digital computer, for the frequency equations of various end conditions. It is noted that the torsional natural frequency results for various end conditions for Indian Standard I-section have not been presented prior to this study. In the present paper, the results for the first two modes of vibration for the various types of end conditions are presented in graphical form, suitable for design use. (The results upto the tenth mode of vibration are available with the authors). The results for simply supported beams are compared with those of Ref. 13, and an excellent agreement is observed.

* Associate Lecturer, Dept. of Mech. Engg., A.U., Waltair, A.P., India.

** Late Professor, Dept. of Mech. Engg., A.U., Waltair, A.P., India.

† Professor, Dept. of Mech. Engg., Andhra University, Waltair, A.P., India.

Date of receipt of the Manuscript : March 3, 1972.

Date of receipt of the final revised version : June 26, 1973.

DIFFERENTIAL EQUATIONS AND BOUNDARY CONDITIONS

The coupled equations for the angle of twist $\Phi(z, t)$ and the warping angle $\Psi(z, t)$, for a wide flanged symmetric I-beam are given by Aggarwal and Cranch¹¹ as,

$$GC_s \frac{\partial^2 \Phi}{\partial z^2} + k' A_f G \left[\frac{h}{2} \frac{\partial^2 \Phi}{\partial z^2} - \frac{\partial \Psi}{\partial z} \right] - \rho I_p \frac{\partial^2 \Phi}{\partial t^2} = 0 \quad (1)$$

$$k' A_f G \left[\frac{h}{2} \frac{\partial \Phi}{\partial z} - \Psi \right] + \frac{2C_w}{h^2} \left[E \frac{\partial^2 \Phi}{\partial z^2} - \rho \frac{\partial^2 \Psi}{\partial t^2} \right] = 0 \quad (2)$$

in which,

E = modulus of elasticity

G = modulus of rigidity

C_s = Torsional constant for the section

k' = numerical shape factor for cross section

A_f = area of each flange

h = height between the centre lines of the flanges of the beam

ρ = mass density of the material of the beam

I_p = polar moment of inertia of the cross section about centroid

C_w = warping constant

= $I_f h^2/2$, for a wide-flanged symmetric I-beam.

I_f = moment of inertia of each flange area about Y-axis

t = time

z = distance along the axis of the beam.

Eliminating Ψ or Φ from equations (1) and (2), the following two complete differential equations in Φ and Ψ are obtained.

$$\left[\frac{EI_f C_s}{k' A_f} + EC_w \right] \frac{\partial^4 \Phi}{\partial z^4} - \left[\frac{E \rho I_p I_f}{k' A_f G} + \frac{C_s \rho I_f}{k' A_f} + \frac{\rho I_f h^2}{2} \right] \frac{\partial^4 \Phi}{\partial z^2 \partial t^2} - GC_s \frac{\partial^2 \Phi}{\partial z^2} + \rho I_p \frac{\partial^2 \Phi}{\partial t^2} + \frac{\rho I_p \rho I_f}{k' A_f G} \frac{\partial^4 \Phi}{\partial t^4} = 0 \quad (3)$$

$$\left[\frac{EI_f C_s}{k' A_f} + EC_w \right] \frac{\partial^4 \Psi}{\partial z^4} - \left[\frac{E \rho I_p I_f}{k' A_f G} + \frac{C_s \rho I_f}{k' A_f} + \frac{\rho I_f h^2}{2} \right] \frac{\partial^4 \Psi}{\partial z^2 \partial t^2} - GC_s \frac{\partial^2 \Psi}{\partial z^2} + \rho I_p \frac{\partial^2 \Psi}{\partial t^2} + \frac{\rho I_p \rho I_f}{k' A_f G} \frac{\partial^4 \Psi}{\partial t^4} = 0 \quad (4)$$

Let

$$\Phi = \phi e^{ipt} \quad (5)$$

$$\Psi = \psi e^{ipt} \quad (6)$$

$$\xi = z/L \quad (7)$$

where

ϕ = normal function of Φ

ψ = normal function of Ψ

ξ = non-dimensional length of beam

$i = \sqrt{-1}$

p = natural frequency of vibration

L = length of the beam

Omitting the factor e^{ipt} , equations (1) to (4) are reduced to

$$(c^2 + 1) \phi'' + r^2 b^2 s^2 d^2 \phi - \frac{2L}{h} \psi' = 0 \quad (8)$$

$$s^2 \Psi'' - (1 - r^2 b^2 s^2) \psi + \frac{h}{2L} \phi' = 0 \quad (9)$$

$$\frac{c^2 + 1}{r^2 b^2} \phi''' + (a^2 + s^2 d^2) \phi' - d^2 (1 - r^2 b^2 s^2) \phi = 0 \quad (10)$$

$$\frac{c^2 + 1}{r^2 b^2} \psi''' + (a^2 + s^2 d^2) \psi' - d^2 (1 - r^2 b^2 s^2) \psi = 0 \quad (11)$$

where

$$a^2 = 1 + c^2 - \frac{c^2}{r^2 b^2 s^2} \quad (12)$$

$$b^2 = \frac{1}{E I_f} \rho A_f L^4 p^2 \quad (13)$$

$$c^2 = \frac{2C_s}{k' A_f h^2} \quad (14)$$

$$d^2 = \frac{2 I_p L^2}{h^2 I_f} \quad (17)$$

$$r^2 = \frac{I_f}{A_f L^2} \quad (16)$$

$$s^2 = \frac{E I_f}{k' A_f G L^2} \quad (17)$$

and the primes for ϕ and ψ represent differentiation with respect to ξ .

The necessary and sufficient boundary conditions for the beam are found as follows :

Simply supported end

$$\phi = 0 \quad (18)$$

$$\psi' = 0 \quad (19)$$

Fixed end

$$\phi = 0 \quad (20)$$

$$\psi = 0 \quad (21)$$

Free end

$$\psi' = 0 \quad (22)$$

$$(c^2 + 1) \phi' - \frac{2L}{h} \psi = 0 \quad (23)$$

SOLUTIONS :

The solutions of (10) and (11) can be found as

$$\phi = A_1 \cosh r b \alpha \xi + A_2 \sinh r b \alpha \xi + A_3 \cos r b \beta \xi + A_4 \sin r b \beta \xi \quad (24)$$

$$\psi = A_1' \sinh r b \alpha \xi + A_2' \cosh r b \alpha \xi + A_3' \sin r b \beta \xi + A_4' \cos r b \beta \xi \quad (25)$$

where

$$\alpha = \frac{1}{\sqrt{2} (c^2 + 1)^{1/2}} \left\{ \mp (a^2 + s^2 d^2) + \left[(a^2 - s^2 d^2)^2 + \frac{4d^2}{r^2 b^2} \right]^{1/2} \right\} \quad (26)$$

and

$$\left[(a^2 - s^2 d^2)^2 + \frac{4d^2}{r^2 b^2} \right]^{1/2} > (a^2 + s^2 d^2)$$

is assumed.

In case

$$\left[(a^2 - s^2 d^2)^2 + \frac{4d^2}{r^2 b^2} \right]^{1/2} < (a^2 + s^2 d^2)$$

we write

$$\alpha = \frac{1}{\sqrt{2} (c^2 + 1)^{1/2}} \left\{ (a^2 + s^2 d^2) - \left[(a^2 - s^2 d^2)^2 + \frac{4d^2}{r^2 b^2} \right]^{1/2} \right\} \\ = i \alpha'$$

then (24) and (25) are replaced by

$$\phi = A_1 \cosh r b \alpha' \xi + i A_2 \sinh r b \alpha' \xi + A_3 \cos r b \beta \xi + A_4 \sin r b \beta \xi \quad (28)$$

$$\psi = i A_1' \sinh r b \alpha' \xi + A_2' \cosh r b \alpha' \xi + A_3' \sin r b \beta \xi + A_4' \cos r b \beta \xi \quad (29)$$

Solutions of (24) to (25) or (28) to (29) are naturally the solutions of the original coupled equations (8) and (9).

Only one half of the constants in equations (24) and (25) are independent. They are related by the equations (8) or (9) as follows :

$$A_1 = \frac{2L}{r b h \alpha} \left[1 - r^2 b^2 s^2 (\alpha^2 + 1) \right] A_1' \quad (30)$$

$$A_2 = \frac{2L}{r b h \alpha} \left[1 - r^2 b^2 s^2 (\alpha^2 + 1) \right] A_2' \quad (31)$$

$$A_3 = \frac{-2L}{r b h \beta} \left[1 + r^2 b^2 s^2 (\beta^2 - 1) \right] A_3' \quad (32)$$

$$A_4 = \frac{2L}{r b h \beta} \left[1 + r^2 b^2 s^2 (\beta^2 - 1) \right] A_4' \quad (33)$$

or

$$A_1' = \frac{r b h}{2L} \left[\frac{\alpha^2 (c^2 + 1) + s^2 d^2}{\alpha} \right] A_1 \quad (34)$$

$$A_2' = \frac{r b h}{2L} \left[\frac{\alpha^2 (c^2 + 1) + s^2 d^2}{\alpha} \right] A_2 \quad (35)$$

$$A_3' = \frac{-r b h}{2L} \left[\frac{\beta^2 (c^2 + 1) - s^2 d^2}{\beta} \right] A_3 \quad (36)$$

$$A_4' = \frac{r b h}{2L} \left[\frac{\beta^2 (c^2 + 1) - s^2 d^2}{\beta} \right] A_4 \quad (37)$$

FREQUENCY EQUATIONS

The application of appropriate boundary conditions (18 to 23) and relations of integration constants (30 to 37) to equations (24) and (25) yields for each type of beam a set of four homogeneous linear algebraic equations in four constants A_1 to A_4 with or without primes. In order that the solutions other than zero may exist the determinant of the coefficients of A 's must be equal to zero. This leads to the frequency equations in each case from which the natural frequencies can be determined.

In the following, six common types of beams will be identified by a compound adjective which describes the end conditions at $\xi=0$ and $\xi=1$ or $z=0$ and $z=L$. They are (a) simply-supported beam (b) Beam simply supported at one end, free at the other (c) Fixed-end beam (d) Beam fixed at one end, simply supported at the other. (e) Beam fixed at one end, free at the other. (f) Beam free at both ends.

The frequency equations thus obtained are as follows :

(a) Simply-supported beam

$$\sin r b \beta = 0 \quad (38)$$

(b) Beam simply supported at one end, free at the other

$$\delta \tanh r b \alpha - \theta \tan r b \beta = 0$$

in which

$$\delta = \alpha/\beta$$

$$\theta = \frac{\beta^2(c^2+1)-s^2d^2}{\beta^2(c^2+1)+s^2d^2} = \frac{\alpha^2(c^2+1)+a^2}{\beta^2(c^2+1)-a^2}$$

$$= \frac{\beta^2(c^2+1)-s^2d^2}{\beta^2(c^2+1)+s^2d^2} = \frac{\alpha^2(c^2+1)+a^2}{\alpha^2(c^2+1)+s^2d^2} \quad (41)$$

(c) Fixed-end beam

$$2-2 \cosh r b \alpha \cos r b \beta + \frac{r b / d}{(1-r^2 b^2 s^2)^{\frac{1}{2}} (c^2+1)^{\frac{1}{2}}}$$

$$[r^2 b^2 s^2 (s^2 d^2 - a^2)^2 + (3 s^2 d^2 - a^2)]$$

$$\sinh r b \alpha \sin r b \beta = 0 \quad (42)$$

(d) Beam fixed at one end, simply supported at the other

$$\theta \delta \tanh r b \alpha - \tan r b \beta = 0 \quad (43)$$

(e) Beam fixed at one end, free at the other

$$2 + \left[\frac{r^2 b^2}{d^2} (a^2 - s^2 d^2)^2 + 2 \right] \cosh r b \alpha \cos r b \beta$$

$$- \frac{(r b / d) (a^2 + s^2 d^2)}{(1-r^2 b^2 s^2)^{\frac{1}{2}} (c^2+1)^{\frac{1}{2}}} \sinh r b \alpha \sin r b \beta = 0 \quad (44)$$

(f) Beam free at both ends

$$2-2 \cosh r b \alpha \cos r b \beta + \frac{r b / d}{(1-r^2 b^2 s^2)^{\frac{1}{2}} (c^2+1)^{\frac{1}{2}}}$$

$$\left[\frac{r^2 b^2 a^2}{d^2} (a^2 - s^2 d^2)^2 + (3 a^2 - s^2 d^2) \right]$$

$$\sinh r b \alpha \sin r b \beta = 0 \quad (45)$$

When

$$\left[(a^2 - s^2 d^2)^2 + \frac{4 d^2}{r^2 b^2} \right]^{\frac{1}{2}} < (a^2 + s^2 d^2), \quad b^2 r^2 s^2 > 1$$

correspondingly. It is convenient to use $\alpha = i \alpha'$ and

$$(1-r^2 b^2 s^2)^{\frac{1}{2}} = i (r^2 b^2 s^2 - 1)^{\frac{1}{2}} \quad (46)$$

$$\delta = i \delta' \quad (47)$$

Where $\delta' = \alpha'/\beta$ and transform the frequency equations (38 to 45) for the case

$$\left[(a^2 - s^2 d^2)^2 + \frac{4 d^2}{r^2 b^2} \right]^{\frac{1}{2}} > (a^2 + s^2 d^2)$$

to those for the case

$$\left[(a^2 - s^2 d^2)^2 + \frac{4 d^2}{r^2 b^2} \right]^{\frac{1}{2}} < (a^2 + s^2 d^2)$$

(39) Thus we obtain the frequency equations as follows :

(a) Simply supported beam

$$\sin r b \beta \sin r b \alpha' = 0 \quad (48)$$

(b) Beam simply supported at one end, free at the other

$$\delta' \tan r b \alpha' + \theta \tan r b \beta = 0 \quad (49)$$

(c) Fixed-end beam

$$2-2 \cos r b \alpha' \cos r b \beta + \frac{r b / d}{(r^2 b^2 s^2 - 1)^{\frac{1}{2}} (c^2+1)^{\frac{1}{2}}}$$

$$[r^2 b^2 s^2 (s^2 d^2 - a^2)^2 + (3 s^2 d^2 - a^2)] \sin r b \alpha' \sin r b \beta = 0 \quad (50)$$

(d) Beam fixed at one end, simply supported at the other

$$\delta' \theta \tan r b \alpha' + \tan r b \beta = 0 \quad (51)$$

(e) Beam fixed at one end, free at the other

$$2 + \left[\frac{r^2 b^2}{d^2} (a^2 - s^2 d^2)^2 + 2 \right] \cos r b \alpha' \cos r b \beta$$

$$- \frac{(r b / d) (a^2 + s^2 d^2)}{r^2 b^2 s^2 - 1)^{\frac{1}{2}} (c^2+1)^{\frac{1}{2}}} \sin r b \alpha' \sin r b \beta = 0 \quad (52)$$

(f) Beam free at both ends

$$2-2 \cos r b \alpha' \cos r b \beta + \frac{r b / d}{(r^2 b^2 s^2 - 1)^{\frac{1}{2}} (c^2+1)^{\frac{1}{2}}}$$

$$\left[\frac{r^2 b^2 a^2}{d^2} (a^2 - s^2 d^2)^2 + (3 a^2 - s^2 d^2) \right]$$

$$\sin r b \alpha' \sin r b \beta = 0 \quad (53)$$

NORMAL MODES

For each type of beam the roots of the frequency equations b_i , ($i=1, 2, 3, \dots$) give the eigen values of the problem. The corresponding eigen functions, normal modes ϕ_i and ψ_i , can be obtained accordingly. In the following list of normal modes the subscript i is omitted for $\phi, \psi, b, \alpha, \beta$ and the constants B and C . Since the coefficients in ϕ and ψ are related, the constants B and C are connected through any one of the equations of (30-33) or (34-37).

The normal modes ϕ and ψ for various simple beams are as follows : In case there are two pairs of ϕ and ψ the first pair is for the case when

$$\left[(a^2 - s^2 d^2)^2 + \frac{4 d^2}{r^2 b^2} \right]^{\frac{1}{2}} > (a^2 + s^2 d^2)$$

and the second pair

$$\left[(a^2 - s^2 d^2)^2 + \frac{4d^2}{r^2 b^2} \right]^{\frac{1}{2}} < (a^2 + s^2 d^2)$$

(a) Simply-supported beam

$$\phi = B \sin rb\beta\xi \quad (54)$$

$$\psi = C \cos rb\beta\xi \quad (55)$$

(b) Beam simply supported at one end, free at the other

$$\phi = \delta \frac{\cos rb\beta}{\cosh rb\alpha} \sinh rb\alpha\xi + \sin rb\beta\xi \quad (56)$$

$$\psi = \frac{1}{\delta} \frac{\sin rb\beta}{\sinh rb\alpha} \cosh rb\alpha\xi + \cos rb\beta\xi \quad (57)$$

and

$$\phi = -\delta' \frac{\cos rb\beta}{\cos rb\alpha'} \sin rb\alpha'\xi + \sin rb\beta\xi \quad (58)$$

$$\psi = -\frac{1}{\delta'} \frac{\sin rb\beta}{\sin rb\alpha'} \cos rb\alpha'\xi + \cos rb\beta\xi \quad (59)$$

(c) Fixed-end beam

$$\phi = B (\cosh rb\alpha\xi + \delta\eta\theta \sinh rb\alpha\xi - \cos rb\beta\xi + \eta \sin rb\beta\xi) \quad (60)$$

$$\psi = C (\cosh rb\alpha\xi + \frac{\mu}{\delta\theta} \sinh rb\alpha\xi - \cos rb\beta\xi + \mu \sin rb\beta\xi) \quad (61)$$

Where

$$\eta = \frac{-\cosh rb\alpha + \cos rb\beta}{\delta\theta \sinh rb\alpha - \sin rb\beta} \quad (62)$$

$$\mu = \frac{-\cosh rb\alpha + \cos rb\beta}{\frac{1}{\delta\theta} \sinh rb\alpha + \sin rb\beta} \quad (63)$$

and

$$\phi = B (\cos rb\alpha'\xi - \delta'\lambda\theta \sin rb\alpha'\xi - \cos rb\beta\xi + \lambda \sin rb\beta\xi) \quad (64)$$

$$\psi = C (\cos rb\alpha'\xi + \frac{\nu}{\delta'\theta} \sin rb\alpha'\xi + \cos rb\beta\xi + \nu \sin rb\beta\xi) \quad (65)$$

Where

$$\lambda = \frac{\cos rb\alpha' - \cos rb\beta}{\delta'\theta \sin rb\alpha' - \sin rb\beta} \quad (66)$$

$$\nu = \frac{-\cos rb\alpha' + \cos rb\beta}{\frac{1}{\delta'\theta} \sin rb\alpha' + \sin rb\beta} \quad (67)$$

(d) Beam fixed at one end, simply supported at the other

$$\phi = B (\cosh rb\alpha\xi - \coth rb\alpha \sinh rb\alpha\xi - \cos rb\beta\xi + \cot rb\beta \sin rb\beta\xi) \quad (68)$$

$$\psi = C (\cosh rb\alpha\xi + \frac{\mu}{\delta\theta} \sinh rb\alpha\xi - \cos rb\beta\xi + \mu \sin rb\beta\xi) \quad (69)$$

Where

$$\mu = \frac{-(\delta \sinh rb\alpha + \sin rb\beta)}{\frac{1}{\theta} \cosh rb\alpha + \cos rb\beta} \quad (70)$$

and

$$\phi = B (\cos rb\alpha'\xi - \cot rb\alpha' \sin rb\alpha'\xi - \cos rb\beta\xi + \cot rb\beta \sin rb\beta\xi) \quad (71)$$

$$\psi = C (\cos rb\alpha'\xi - \frac{\nu}{\delta'\theta} \sin rb\alpha'\xi - \cos rb\beta\xi + \nu \sin rb\beta\xi) \quad (72)$$

$$\nu = \frac{\delta' \sin rb\alpha' - \sin rb\beta}{\frac{1}{\theta} \cos rb\alpha' + \cos rb\beta} \quad (73)$$

(e) Beam fixed at one end, free at the other

$$\phi = B (\cosh rb\alpha\xi - \delta\theta\eta \sinh rb\alpha\xi - \cos rb\beta\xi + \eta \sin rb\beta\xi) \quad (74)$$

$$\psi = C (\cosh rb\alpha\xi + \frac{\mu}{\delta\theta} \sinh rb\alpha\xi - \cos rb\beta\xi + \mu \sin rb\beta\xi) \quad (75)$$

Where

$$\eta = \frac{\frac{1}{\delta} \sinh rb\alpha - \sin rb\beta}{\theta \cosh rb\alpha + \cos rb\beta} \quad (76)$$

$$\mu = -\frac{\delta \sinh rb\alpha + \sin rb\beta}{\frac{1}{\theta} \cosh rb\alpha + \cos rb\beta} \quad (77)$$

and

$$\phi = B (\cos rb\alpha'\xi + \delta'\lambda\theta \sin rb\alpha'\xi - \cos rb\beta\xi + \lambda \sin rb\beta\xi) \quad (78)$$

$$\psi = C (\cos rb\alpha'\xi - \frac{\nu}{\delta'\theta} \sin rb\alpha'\xi - \cos rb\beta\xi + \nu \sin rb\beta\xi) \quad (79)$$

Where

$$\lambda = \frac{\frac{1}{\delta'} \sin rb\alpha' - \sin rb\beta}{\theta \cos rb\alpha' + \cos rb\beta} \quad (80)$$

$$\nu = \frac{\delta' \sin rb\alpha' - \sin rb\beta}{\frac{1}{\theta} \cos rb\alpha' + \cos rb\beta} \quad (81)$$

(f) Beam free at both ends

$$\phi = B (\cosh r\beta\alpha\xi + \eta\delta \sinh r\beta\xi + \frac{1}{\theta} \cos r\beta\xi + \eta \sin r\beta\xi) \quad (82)$$

$$\psi = C (\cosh r\beta\alpha\xi - \frac{\eta}{\delta} \sinh r\beta\xi + \theta \cos r\beta\xi + \frac{1}{\eta} \sin r\beta\xi) \quad (83)$$

Where

$$\eta = \frac{\cosh r\beta\alpha - \cos r\beta}{\delta \sinh r\beta\alpha - \theta \sin r\beta} \quad (84)$$

and

$$\phi = B (\cos r\beta\alpha'\xi - \delta\lambda \sin r\beta\xi + \frac{1}{\theta} \cos r\beta\xi + \lambda \sin r\beta\xi) \quad (85)$$

$$\psi = C (\cos r\beta\alpha'\xi - \frac{\lambda}{\delta} \sin r\beta\xi + \theta \cos r\beta\xi - \frac{1}{\lambda} \sin r\beta\xi) \quad (86)$$

Where

$$\lambda = - \frac{\cos r\beta\alpha' - \cos r\beta}{\delta \sin r\beta\alpha' - \theta \sin r\beta} \quad (87)$$

For a given beam with c, d, r , and s known, the b_i ($i=1,2,3, \dots$) can be found from the appropriate frequency equations and the corresponding p_i can be calculated by the equation (13). These frequency equations are highly transcendental and the solutions are obtained on a digital computer.

COMPARISON WITH HIGHER-ORDER THEORIES

The first order approximation equations (Eqs. 1.60) of Ref. 13, for torsional vibrations of uniform doubly symmetric open tubes are observed to be the same as Eqs. (1) and (2) of the present paper, but for the only difference that the shear coefficient k' in Eqs. (1) and (2) of the present paper, assumes a value of unity in those of Ref. 13.

SOLUTIONS OF THE FREQUENCY EQUATIONS:

(a) Simply supported beam :

Substituting the value of β from equations (26) in the frequency equation of the first set (38) and simplifying the expression we get

$$b^2 = \frac{[n^2 \pi^2 (s^2 d^2 + c^2 + 1) + d^2]}{2r^2 s^2 d^2} \rightarrow \frac{-[n^2 \pi^2 (s^2 d^2 - c^2 - 1) + d^2]^2 + 4n^2 \pi^2 d^2}{2r^2 s^2 d^2} \quad (88)$$

This frequency equation (88) in b^2 , has an infinite number of roots which in general represent two coupled frequency spectra.

The second spectrum appears at higher frequencies greater than the critical frequency b_c given by

$$b_c^2 r^2 s^2 = 1 \quad \dots \dots (89)$$

and is due to interaction between shear deformation and longitudinal inertia. It may be easily seen that this critical frequency represents the first thickness shear mode in this case. Eqn. (89) shows the thickness shear nature of the critical frequency while Eqn. (88) shows the two frequency spectra, uncoupled in the present case.

The classical Timoshenko torsion theory provides only one set of frequency spectrum, but Aggarwal and Cranch¹¹ theory provides two frequency spectra. The eigen values b of the first set of frequency spectrum cover the whole range from zero to infinity, but those of the second set range from the critical frequency b_c given by equation (89) to infinity. Two torsional frequency spectra are illustrated for simply supported beams in Ref. 13 also. It is to be mentioned here that for the range of c, d, r and s parameters covered in this paper, b is less than b_c . In case there is any extension from there on for b beyond b_c , care should be taken to account for the second spectrum.

Now let b_0 be the classical eigen values and p_0 , the natural torsional frequencies corresponding to b_0 .

The classical (Timoshenko) frequency equation derived by Gere⁴ can be written in terms of b_0 as

$$b_0^2 = \frac{n^2 \pi^2 A_f}{E I_f I_p} (n^2 \pi^2 E C_w + L^2 G C_s) \quad (90)$$

$$\text{and } b/b_0 = p/p_0 \quad (91)$$

Comparing the mechanism of vibration of Timoshenko and Aggarwal and Cranch beams, we note that the classical (Timoshenko) beam is equivalent to Aggarwal and Cranch beam with longitudinal and shear constraints.

Therefore,

$$p \leq p_0 \quad (92)$$

and

$$b/b_0 = p/p_0 = q, \quad q \leq 1 \quad (93)$$

The ratio of b/b_0 or p/p_0 , denoted by q , will be referred to as the 'modifying quotient.'

Table 1, contains values of c, d, r and s for one meter length of ten Indian Standard wide flanged I-beams considered in this paper. A value of 0.3 is chosen for poisson's ratio and $\pi^2/12$ for the shear coefficient k' , which is assumed to be constant for all the beams, in obtaining the results presented in this paper.

TABLE 1. Values of c, d, r and s for the ISW Beams.

poisson's ratio = 0.3, $E/G = 2.6$, $k' = \pi^2/12$, $L = 1$ meter.

Beam	C	dL	r/L	s/L
ISWB 150	0.0713888	43.9416	0.0259972	0.0462225
ISWB 175	0.0641706	35.8305	0.0319069	0.0567298
ISWB 200	0.0658632	31.3969	0.0361028	0.06419
ISWB 225	0.637969	29.0311	0.0388452	0.069066
ISWB 250	0.0528314	23.3791	0.0487886	0.086745
ISWB 300	0.049721	18.0905	0.0497493	0.0884533
ISWB 350	0.0485133	22.2714	0.0507509	0.090254
ISWB 400	0.0481979	21.8672	0.0516273	0.0917923
ISWB 500	0.0437731	17.7378	0.063717	0.113287
ISWB 600	0.0556116	16.5884	0.0669601	0.119053

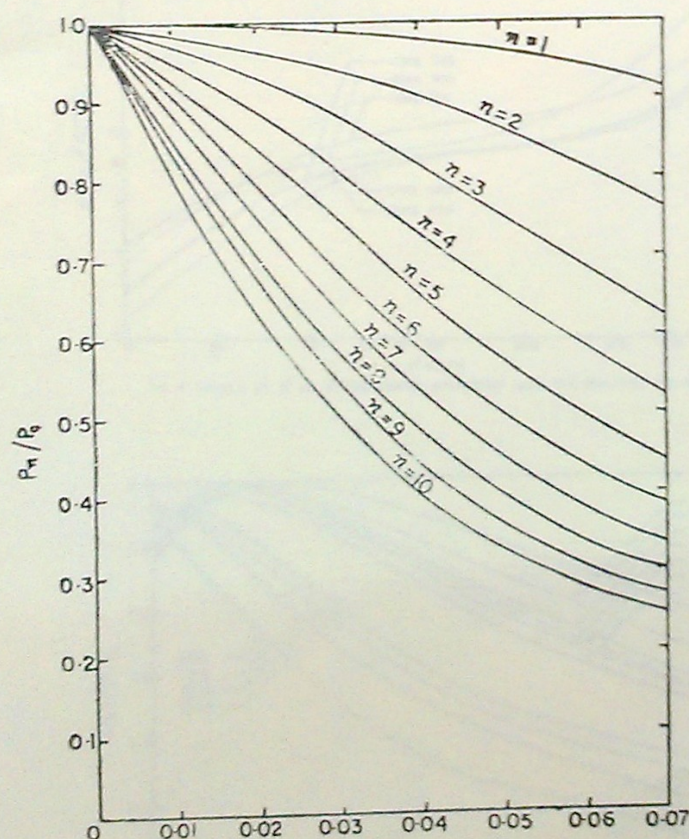


Fig. 1 Corrections in the torsional frequencies of a simply supported beam due to longitudinal inertia and shear deformation.

The values of c, d, r and s can be obtained for any length of the beam in meters, by properly multiplying and dividing the values by the length, as shown in the table, 1.

The graphical representation of p/p_0 versus r for the first ten modes of simply supported wide-flanged I-beams considered are presented in Fig. 1 with the range of r from 0 to 0.07. It is seen that the reduction of the ratio of the torsional natural frequencies is increased by increasing the values of r and s and reducing the values of c and d .

Fig. 2. Compares the values of B^* versus L^* obtained from Gere's analysis⁴ based on classical Timoshenko torsion theory, AVK and CVJ analysis¹³, and present analysis, considering the example of simply-supported ISWB 150, where

$$L^* = L/n \quad (94)$$

$$B^* = P_n L^{*2} \sqrt{\rho A_I / E I_r} \quad (95)$$

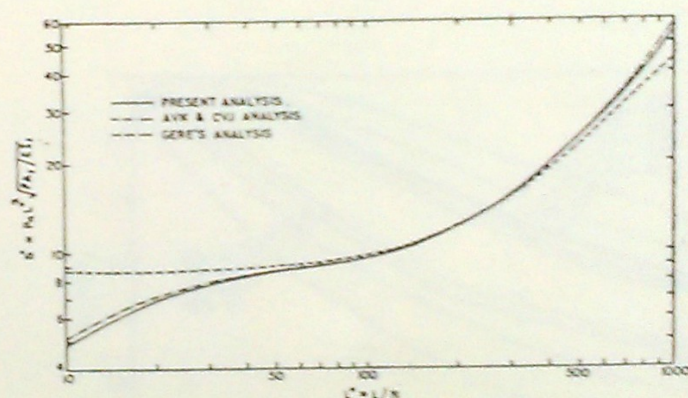


Fig. 2 Comparison of values of B^* VS. L^* for simply supported ISWB 150.

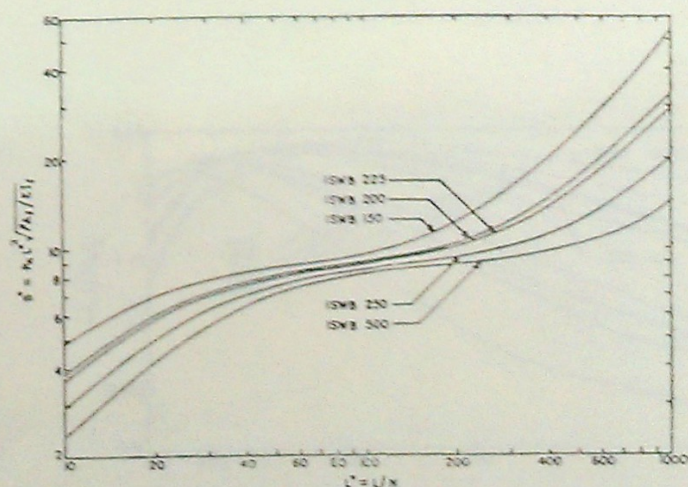


FIG. 3 VALUES OF B^* VS. L^* FOR SIMPLY SUPPORTED ISWB 150, 200, 225, 250, 300

It can be of interest to note from fig. 2., that the values obtained from the present analysis, agree well with those obtained from AVK and CVJ analysis¹³ and, that for lengthy beams and lower modes of vibration, the present analysis gives almost the same values as Gere's analysis. So, for short beams and higher modes of vibration, the effects of longitudinal inertia and shear deformation are quite significant and must be taken care of, in designing such beams

For a simply supported beam, its higher harmonic corresponds to the fundamental of another simply supported beam of shorter span. The n th frequency of simply-supported beam of span L is equal to the fundamental of another such beam with span L/n i.e. L^* . So, for the sake of simplicity and ease of presentation, the values of B^* are plotted versus L^* for simply-supported beams ISWB 150, 200, 225, 250 and 500 in fig. 3. and for beams ISWB 175, 300, 350, 400 and 600 in fig. 4.

(b) Other boundary conditions

Solutions of Eqns. (39) to (45) for ten Indian Standard wide flanged I-beams, are obtained on IBM 1130 Computer at the Computer center, Andhra University, Waltair.

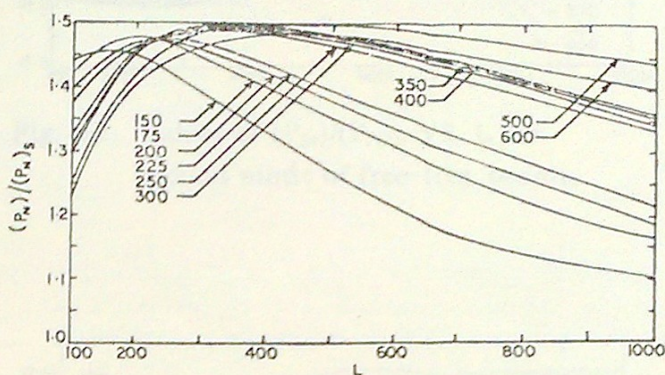


Fig. 6 Values of $(P_N)/(P_N)_S$ VS. L for the fixed end beams ($n=2$) second mode.

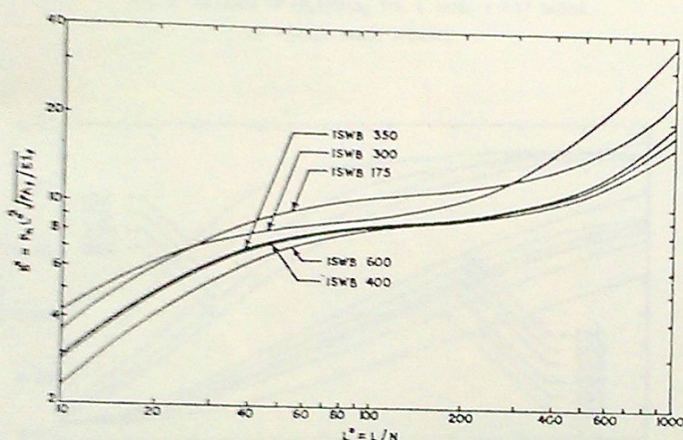


FIG. 4 VALUES OF B^* VS. L^* FOR SIMPLY SUPPORTED ISWB 175, 300, 350, 400, 600

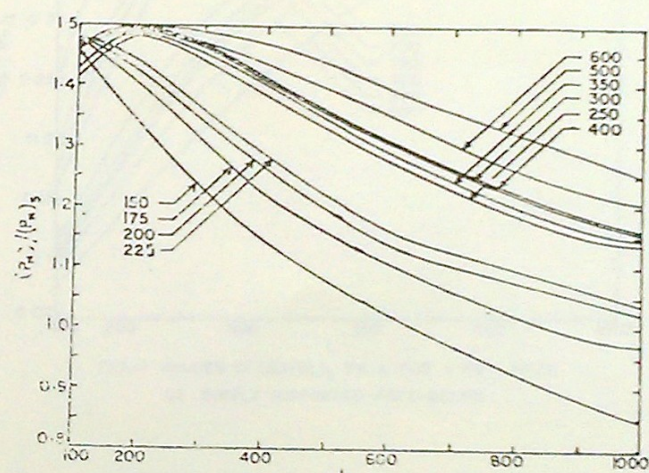


FIG. 7 VALUES OF $(P_N)/(P_N)_S$ VS. L FOR FIRST MODE OF FIXED-SIMPLY SUPPORTED BEAMS

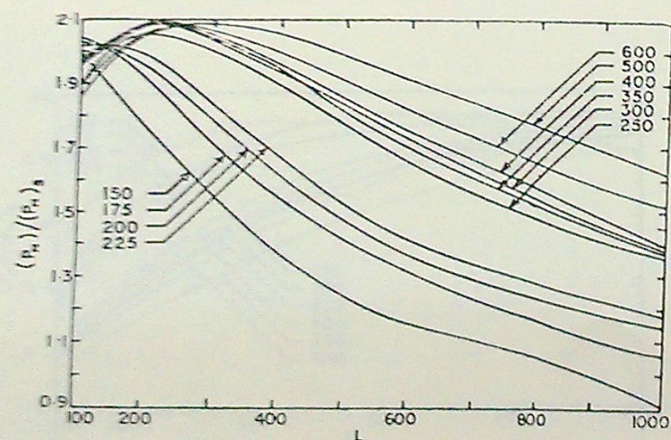


FIG. 5 VALUES OF $(P_N)/(P_N)_S$ VS. L FOR THE FIXED END BEAMS ($n=1$), FIRST

MODE

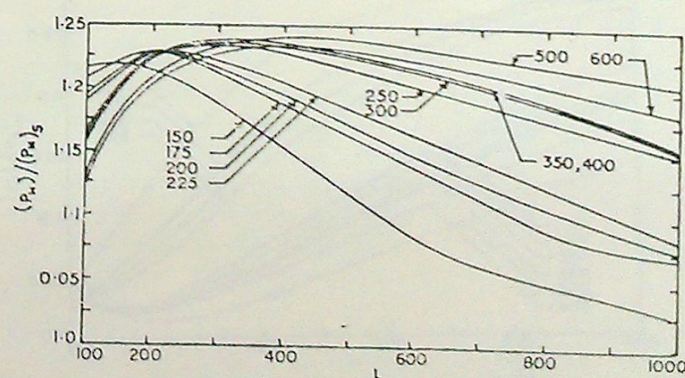


FIG. 8 VALUES OF $(P_N)/(P_N)_S$ VS. L FOR SECOND MODE OF FIXED-SIMPLY SUPPORTED BEAMS

The values of $(P_n)/(P_n)_s$ are plotted against the length of the beam L , in first, 5 to 14 for various boundary conditions for the first two modes of vibration where $(P_n)_s$ is the frequency for the simply supported beam that can be obtained from figs. 3, 4 and Eqn. (95). Knowing $(P_n)_s$ for a particular beam length and mode, the values of the frequency P_n can be obtained for various boundary conditions from these graphs. Other results upto the tenth mode are available with the authors.

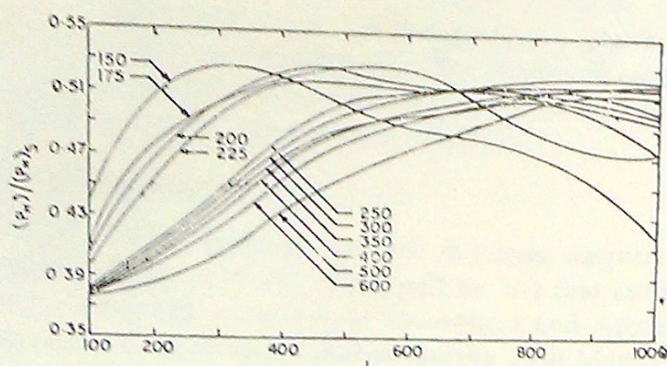


FIG. 9 VALUES OF $(P_n)/(P_n)_s$ VS. L FOR FIRST MODE OF FIXED-FREE BEAMS

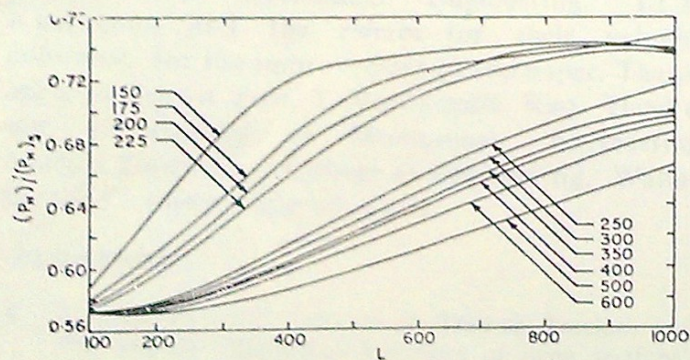


FIG. 10 VALUES OF $(P_n)/(P_n)_s$ VS. L FOR SECOND MODE OF FIXED-FREE BEAMS

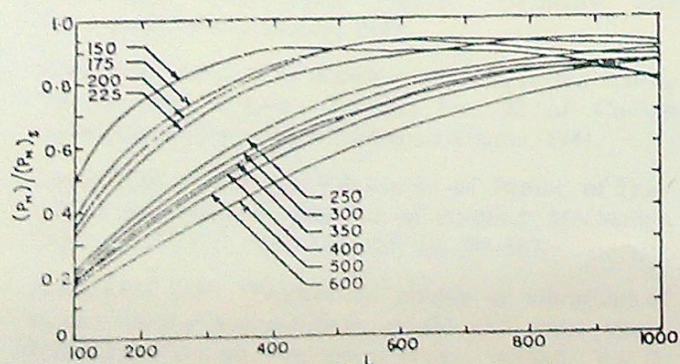


Fig. 11 Values of $(P_n)/(P_n)_s$ VS. L for first mode of free-free beams.

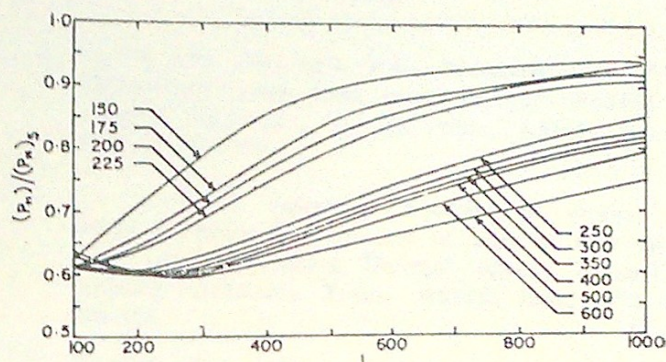


Fig. 12. Values of $(P_n)/(P_n)_s$ VS. L for second mode of free-free beams.

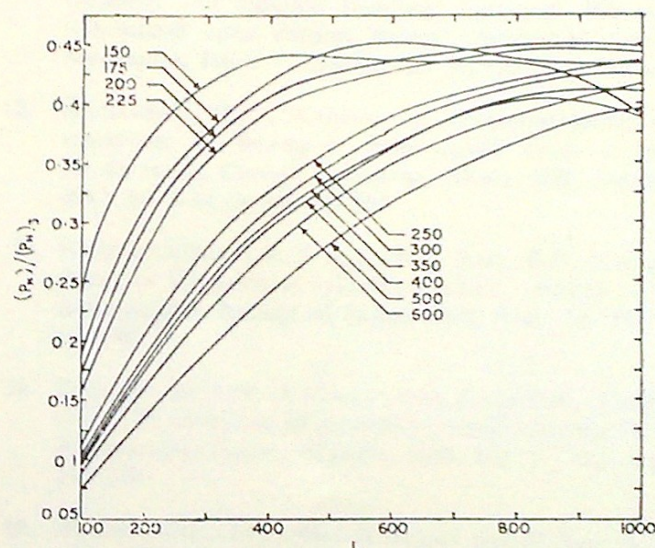


FIG. 13 VALUES OF $(P_n)/(P_n)_s$ VS. L FOR FIRST MODE OF SIMPLY SUPPORTED-FREE BEAMS

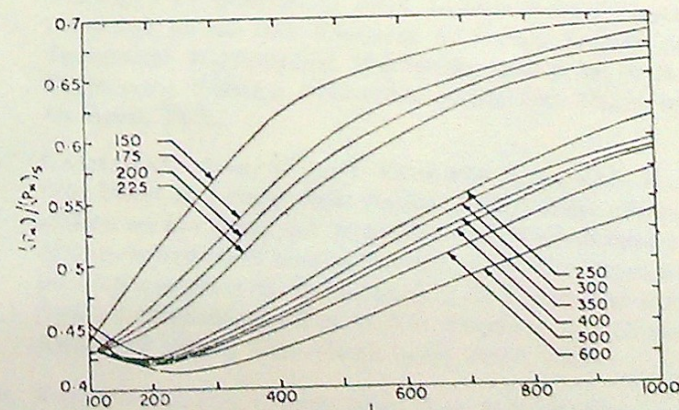


FIG. 14 VALUES OF $(P_n)/(P_n)_s$ VS. L FOR SECOND MODE OF SIMPLY SUPPORTED-FREE BEAMS

CONCLUSIONS

In this paper a comparison is drawn between the theories of torsional vibrations of thin-walled beams of open cross section. A clear and neat set of new frequency and normal mode equations for free torsional vibrations of six common types of simple and finite beams, including the second order effects, are presented. The solutions of the frequency equations are obtained on a digital computer and the results for the first two modes of vibration for ten Indian Standard wide-flanged I-beams for various end conditions are presented in graphical form, suitable for design use. The results of simply supported beams are compared with those of Ref.13 and an excellent agreement is observed.

ACKNOWLEDGEMENTS

The work reported here in, is partly abstracted from the papers 16-18, presented by the first author at the sixteenth congress on theoretical and Applied Mechanics, held at Allahabad during 29th March to 1st April 1972.

The authors wish to thank Dr. J. S. Rao, Professor in Mechanical Engineering, I.I.T., Kharagpur, and the referee for their valuable comments for the improvement of the paper. Thanks are also due to Prof. T. Venugopala Rao Head of the Department of Mechanical Engineering, Andhra University, College of Engineering, Waltair for the facilities made available.

REFERENCES

1. TIMOSHENKO, S.P., 'Theory of Bending, Torsion, and Buckling of Thin-walled members of open sections', Journal of Franklin Institute, Vol. 239, 1945, pp. 215-219, 249-254.
2. WAGNER, H., 'Torsion and Buckling of open sections', Technische Hochschule, Denzig, Germany 25th Anniversary Publications, 1929
3. GOODIER, J.N., 'The Buckling of compressed bar by Torsion and flexure', Bulletin No. 27 of Cornell University Engineering Experiment Station, 1941.
4. GERE, J.M. 'Torsional Vibrations of Beams of Thin-walled open section', Journal of Applied Mechanics, Trans., A.S.M.E., Vol. 21, 1954, pp. 381-387.
5. GARLAND, C.F., 'The normal modes of vibrations of Beams having non-collinear elastic and mass axes', Journal of Applied Mechanics, Trans. ASME, Vol. 7, A-97, June, 1940.
6. TIMOSHENKO, S.P., YOUNG, D.H., 'Vibration problems in Engineering', Third edition, D. Van Nostrand Company Inc., Princeton, N.J., 1955, pp. 407-409.
7. GERE, J.M., and LIN, Y.K., 'Coupled vibrations of thin-walled beams open cross section' Journal of Applied Mechanics, Vol. 25, Trans. ASME, Vol. 80, 1958, pp. 373-374.
8. YU, YI-YUAN, 'Variational equation of motion for coupled flexure and Torsion of Bars of thin-walled open section including Thermal effect', Journal of Applied Mechanics, Trans. ASME, June, 1971, pp. 502-506.
9. VLASOV, V.Z., 'Thin-walled elastic beams', Moscow, 1959, (English translation, Israel Program for Scientific Translation, Jerusalem, 1961).
10. CHILVER, A.H., 'Thin-walled Structures', Chatto and Windus Ltd., London, 1967.
11. AGGARWAL, H.R. and CRANCH, E.T., 'A theory of torsional and coupled Bending Torsional Waves in thin-walled open section Beams', Journal of Applied Mechanics, Trans. ASME, Vol. 34, 1967, pp. 337-343.
12. AGGARWAL, H.R., 'A theory of Torsional waves and vibrations in Beams of Thin-walled open section', Ph. D. thesis, Cornell University, Ithaca, N.Y. January, 1962, pp. 8-34, 96-99, 104-105.
13. KRISHNAMURTY, A.V. and JOGA RAO, C.V. 'General theory of Vibration of cylindrical tubes', Journal of the Aeronautical Society of India, 1968, Vol. 20, No. 1, pp.1-38.
14. KRISHNA MURTY, A.V. and JOGA RAO, C.V. 'General theory of vibrations of cylindrical tubes', Journal of the Aeronautical Society of India, 1968, Vol. 20, No. 4, pp. 235-258.
15. HUANG, T.C., 'The Effect of Rotary end of shear deformation on the frequency and normal mode equations of uniform beams with simple end conditions', Journal of Applied Mechanics, Trans. ASME, Vol.28, Series E., No. 4, Dec., 1961, pp. 579-584.
16. KAMESWARA RAO, C. and VENKATA APPA RAO, K., 'Influence of Longitudinal inertia on the Torsional frequency of thin-walled open section Beams' paper presented at the 16th Congress of Indian Society of Theoretical and Applied Mechanics, held at M. N. R. Engineering College, Allahabad, during 29th March to 1st April, 1972.
17. KAMESWARA RAO, C., and VENKATA APPA RAO, K., 'The Effect of Longitudinal Inertia and of shear deformation on the Torsional frequency and Normal modes of thin-walled open section Beams', paper presented at the 16th Congress of Indian Society of Theoretical and Applied Mechanics held at M.N.R. Engineering College Allahabad, during 29th March to 1st April, 1972.
18. KAMESWARA Rao, C., and APPA Rao, K.V., 'Orthogonality and Normalizing conditions of Normal modes of Aggarwal and Cranch Beams' Paper presented at the 16th Congress of Theoretical and Applied Mechanics held at M.N.R. Engineering College, Allahabad, during 29th March to 1st April, 1972.

can be improved. First, the code is written in such a way that eight N -vectors must be stored in addition to the two N -vectors which define the table being interpolated. By a simple rewriting of the code, the eight N -vectors can be reduced to one. Second, the algorithm of Ref. 4 sets up the linear system in terms of the second derivatives at the nodal points. Then, both the second and third derivatives are used in the interpolation computations. If the first derivatives at the nodal points are needed, additional computations would have to be made. An algorithm can be formulated such that the solution of the linear system yields the first derivatives at the nodal points and that this is the only N -vector which needs to be stored along with the two defining the table. The remainder of this Note presents the equations for such an algorithm.

Consider the cubic polynomial for the k th interval where the k subscripted quantities are evaluated at the beginning of the interval and the $k+1$ subscripted quantities are evaluated at the end of the interval. Let t denote the value of the independent variable within the k th interval for which the interpolated value of the dependent variable y is desired. Let A , B , C , and D represent the constant coefficients of the cubic polynomial in this interval, and write the following expressions:

$$\begin{aligned} y &= A + B(t - t_k) + (C/2)(t - t_k)^2 + (D/6)(t - t_k)^3 \\ y' &= B + C(t - t_k) + (D/2)(t - t_k)^2 \\ y'' &= C + D(t - t_k) \end{aligned} \quad (1)$$

In terms of the notation $h = t - t_k$, $H_k = t_{k+1} - t_k$, and $R = h/H_k$, the expressions which relate the constant coefficients of the cubic to the values of the dependent variable and its first derivative at the ends of the interval are given by

$$\begin{aligned} A &= y_k \\ B &= y'_k \\ C &= (6/H_k^2)(y_{k+1} - y_k) - (2/H_k)(y'_{k+1} + 2y'_k) \\ D &= (-12/H_k^3)(y_{k+1} - y_k) + (6/H_k^2)(y'_{k+1} + y'_k) \end{aligned} \quad (2)$$

These values may now be substituted into the expressions for the dependent variable and its derivatives to produce the following relations:

$$\begin{aligned} y &= y_k + (3R^2 - 2R^3)(y_{k+1} - y_k) + \\ &\quad H_k(R - 2R^2 + R^3)y'_k + H_k(-R^2 + R^3)y'_{k+1} \\ y' &= (6/H_k)(R - R^2)(y_{k+1} - y_k) + \\ &\quad (1 - 4R + 3R^2)y'_k + (-2R + 3R^2)y'_{k+1} \\ y'' &= (6/H_k^2)(1 - 2R)(y_{k+1} - y_k) + \\ &\quad (1/H_k)(-4 + 6R)y'_k + (1/H_k)(-2 + 6R)y'_{k+1} \end{aligned} \quad (3)$$

The equations written in this form assure continuity of the dependent variable and its first derivative at the ends of the interval as may be demonstrated by using $R = 0$ and $R = 1$ in the above equations to obtain values at the beginning of the k th interval and at the end of k th interval. In order to assure continuity of the second derivative between intervals, the value of y'' at the end of the k th interval is equated to the value of y'' at the beginning of the $k+1$ st interval. This yields the following recursive relationship for y'_k :

$$H_k y'_{k-1} + 2(H_{k-1} + H_k)y'_k + H_{k-1}y'_{k+1} = 3(H_{k-1}/H_k)(y_{k+1} - y_k) + 3(H_k/H_{k-1})(y_k - y_{k-1}) \quad (4)$$

The output of the Runge-Kutta-Fehlberg numerical integration process is the table of values of y_k and t_k . For N stepping points (including the first) used by the numerical integrator, N values of y'_k must be determined to construct the cubic spline. The recursive relations of Eq. (4) provide $N-2$ equations in y'_k . The input of y'_1 and y'_N , the values at the beginning and end of the integration interval, provides a solvable set of equations in y'_k . If conditions are imposed on y'_1 and y'_N , the corresponding conditions on the first derivatives can be obtained from the third of Eqs. (3).

The successive over-relaxation iterative method for solving the linear system is defined by the relation

$$y'_k = y'_k + 1.0717968\Delta_k \quad (5)$$

where

$$\Delta_k = \frac{1}{2(H_{k-1} + H_k)} \left[3 \frac{H_{k-1}}{H_k} (y_{k+1} - y_k) + 3 \frac{H_k}{H_{k-1}} (y_k - y_{k-1}) - H_k y'_{k-1} - H_{k-1} y'_{k+1} \right] - y'_k \quad (6)$$

To start the iterative process, the values of y'_k corresponding to a quadratic spline are used; that is,

$$y'_k = \frac{H_{k-1}}{H_k + H_{k-1}} \frac{1}{H_k} (y_{k+1} - y_k) + \frac{H_k}{H_k + H_{k-1}} \frac{1}{H_{k-1}} (y_k - y_{k-1}) \quad (7)$$

The iterative process is continued until the change in the values of y'_k at each nodal point between iterations satisfies a prescribed tolerance which should be correlated with the tolerance prescribed for the integrator. Convergence of the iterative method is assured since the coefficient matrix of the linear system is tridiagonal and irreducibly diagonally dominant. Finally, once the values of y'_k are known, interpolated values of y can be computed from the first of Eqs. (3).

From the previous relations, it is apparent that the only quantities which need to be stored during the computation process are t_k , y_k , and y'_k . The values of H_k , H_{k-1} , and Δ_k can be computed at each nodal point and do not need to be stored as vectors.

The use of variable-step integration with numerical optimization methods which iterate on variable histories requires interpolation. Furthermore, the interpolation method must be generated accurately and must use minimal storage. The procedure suggested here has a guaranteed accuracy and requires the minimum amount of storage.

References

- Gottlieb, R. G., Hull, D. G., and Fowler, W. T., "Generalized Perturbation Method for Solving Two-Point Boundary-Value Problems," *AIAA Journal*, Vol. 12, No. 5, May 1974, pp. 648-650.
- Hall, K. R., "Numerical Solutions to Interplanetary Trajectory Problems Involving Close Planetary Approaches," Applied Mechanics Research Laboratory Rept. 1060, 1974, University of Texas, Austin, Texas.
- Fehlberg, E., "Low-Order Classical Runge-Kutta Formulas with Step-size Control and Their Application to Some Heat Transfer Problems," Technical Rept. R-315, 1969, NASA.
- Ralston, A. and H. S. Wilf, *Mathematical Methods for Digital Computers*, Wiley, New York, 1967, pp. 156-168.

Torsional Vibrations and Stability of Thin-Walled Beams on Continuous Elastic Foundation

C. KAMESWARA RAO* AND A. APPALA SATYAM†
Andhra University, Waltair, A.P., India

Nomenclature

- A = area of cross section of the beam
 A_i = constants ($i = 1 \dots 4$)
 a_i, B_n = constants ($i = 0 \dots 4; n = 1, 2, \dots, \infty$)
 C_s = torsion constant

Received May 2, 1974; revision received July 16, 1974. The authors wish to thank Prof. P. K. Sarma and Prof. T. Venugopala Rao, Head of the Department of Mechanical Engineering, Andhra University, for their encouragement in the preparation of this paper.

Index categories: Structural Dynamic Analysis; Structural Stability Analysis.

* Associate Lecturer, Department of Mechanical Engineering.

† Post-Graduate Student, Department of Mechanical Engineering.

C_w = warping constant
 E = modulus of elasticity
 G = shear modulus
 I_p = polar moment of inertia of beam
 K_s = torsional foundation modulus
 K = warping parameter
 L = length of the beam
 N = mode number
 P = axial compressive load
 σ = P/A , axial compressive stress
 p_n = natural frequency of vibration
 t = time
 T = kinetic energy
 z = distance along the length of the beam
 Z = z/L , nondimensional distance along the length of the beam
 V = potential energy
 λ^2 = $\rho I_p L^4 p_n^2 / EC_w$, frequency parameter
 Δ^2 = $\sigma I_p L^2 / EC_w$, load parameter
 Δ_{cr}^2 = critical buckling load parameter
 γ^2 = $K_s L^4 / 4EC_w$, foundation parameter
 ϕ = angle of twist of the beam
 $X(Z)$ = normal function of angle of twist
 α, β = positive real quantities
 δ = variation operator
 ρ = mass density of the material of the beam

Introduction

STATIC and dynamic analysis of beams on elastic foundation occupies a prominent place in contemporary structural mechanics. The vibrations and buckling of continuously supported finite and infinite beams resting on elastic foundation have applications in the design of highway pavements and aircraft runways, and in the use of metal rails for rail road tracks. Very large numbers of studies have been devoted to this subject^{1,2} and valuable practical methods for the analysis of such beams have been worked out. Free torsional vibrations and stability of doubly-symmetric thin-walled beams of open section are investigated by Gere,³ Aggarwal and Cranch,⁴ Krishna Murty and Joga Rao,⁵ Kameswara Rao, Apparao and Sarma,⁶ and Timoshenko and Gere.⁷ Recently free torsional vibrations of restrained elastic thin-walled beams is also investigated by Christieno and Salmela.⁸ In all the preceding investigations which deal with free vibrations, the effects of elastic foundation and in-plane axial compressive force are not included. The purpose of the present investigation is to include these effects and to study their influence on the natural frequencies and buckling loads of simply supported, fixed and simply supported-fixed thin-walled beams of open section.

Formulation and Analysis

Neglecting the effects of longitudinal inertia and shear deformation, the total potential energy of the beam V , consisting of the strain energy of deformation of the beam, the work done by the external compressive load and the reaction offered by the elastic foundation, is given by⁹

$$V = \frac{1}{2} \int_0^L [EC_w(\phi'')^2 + (GC_s - \sigma I_p)(\phi')^2 + K_s(\phi)^2] dz \quad (1)$$

where primes denote differentiation with respect to z . The kinetic energy is

$$T = \frac{1}{2} \int_0^L \rho I_p (\dot{\phi})^2 dz \quad (2)$$

where dot denotes differentiation with respect to t . Applying Hamilton's principle which states

$$\delta \int_{t_1}^{t_2} (T - V) dt = 0 \quad (3)$$

and carrying out necessary variations and integrations we get

$$(GC_s - \sigma I_p)\phi'' - EC_w\phi'''' - K_s\phi = \rho I_p \ddot{\phi} \quad (4)$$

which is the governing differential equation of motion. The natural boundary conditions obtained are

$$\phi''\delta\phi' \Big|_0^L = 0 \quad (5)$$

and

$$[EC_w\phi''' - (GC_s - \sigma I_p)\phi'] \delta\phi \Big|_0^L = 0 \quad (6)$$

From Eqs. (5) and (6), for the beam simply supported at both ends, the boundary conditions to be satisfied are

$$\phi = \phi'' = 0 \quad \text{at } Z = 0 \quad \text{and } Z = 1 \quad (7)$$

where

$$Z = z/L \quad (8)$$

For the beam fixed at both ends, the boundary conditions are

$$\phi = \phi' = 0 \quad \text{at } Z = 0 \quad \text{and } Z = 1 \quad (9)$$

For the beam simply supported at one end and fixed at the other, the boundary conditions are

$$\phi = \phi'' = 0 \quad \text{at } Z = 0 \quad \text{and } \phi = \phi' = 0 \quad \text{at } Z = 1 \quad (10)$$

For sinusoidal vibration, we take

$$\phi(Z, t) = X(Z)e^{i\omega t} \quad (11)$$

Using Eqs. (8) and (11), Eq. (4) can be written as

$$X'''' - (K^2 - \Delta^2)X'' - (\lambda^2 - 4\gamma^2)X = 0 \quad (12)$$

where

$$K^2 = L^2 GC_s / EC_w, \quad \Delta^2 = \sigma I_p L^2 / EC_w \quad (13)$$

and

$$\gamma^2 = K_s L^4 / 4EC_w, \quad \lambda^2 = \rho I_p L^4 p_n^2 / EC_w \quad (14)$$

The general solution of Eq. (12) is

$$X(Z) = A_1 \cosh \alpha Z + A_2 \sinh \alpha Z + A_3 \cos \beta Z + A_4 \sin \beta Z \quad (15)$$

where

$$\alpha^2 = (1/2) \{ (K^2 - \Delta^2) + [(K^2 - \Delta^2)^2 + 4(\lambda^2 - 4\gamma^2)]^{1/2} \} \quad (16)$$

and

$$\beta^2 = (1/2) \{ -(K^2 - \Delta^2) + [(K^2 - \Delta^2)^2 + 4(\lambda^2 - 4\gamma^2)]^{1/2} \} \quad (17)$$

From Eqs. (16) and (17), the relation between α and β is

$$\alpha^2 = \beta^2 + (K^2 - \Delta^2) \quad (18)$$

The four arbitrary constants, A_i ($i = 1 \dots 4$) in Eq. (15) can be determined so as to satisfy the particular boundary conditions of the problem. For any beam there will be two boundary conditions at each end and these four conditions determine the frequency equation. Solving the frequency equation then determines the principal frequencies of vibration and hence the mode shapes.

Applying the boundary conditions given by Eqs. (7, 9, and 10), the following frequency equations are obtained:

$$\sin \beta = 0 \quad (19)$$

$$2\alpha\beta(1 - \cosh \alpha \cos \beta) + (\alpha^2 - \beta^2) \sinh \alpha \sin \beta = 0 \quad (20)$$

and

$$\tanh \alpha = (\alpha/\beta) \tan \beta \quad (21)$$

for the simply supported, fixed, and simply supported-fixed beams, respectively.

From Eq. (19), we have $\beta = N\pi$, and using Eq. (17), the expression for the natural frequency parameter λ , for the simply supported beam is obtained as

$$\lambda = \{ N^2 \pi^2 (N^2 \pi^2 + K^2 - \Delta^2) + 4\gamma^2 \}^{1/2} \quad (22)$$

By putting $\lambda = 0$, and $N = 1$, in Eq. (22), the expression for the buckling load parameter Δ_{cr} , in this case can be obtained as

$$\Delta_{cr}^2 = [\pi^2 + K^2 + (4/\pi^2)\gamma^2] \quad (23)$$

The frequency equations for the fixed and simply supported-fixed beams given by Eqs. (20) and (21) can be observed to be highly transcendental and can be solved in conjunction with Eqs. (16-18) by lengthy trial-and-error procedure.

In an attempt to derive approximate but satisfactory expressions for the frequency parameter λ and buckling load parameter Δ for the fixed beam, the normal function $X(Z)$ is assumed in the form

$$X(Z) = \sum_{n=1}^{\infty} B_n (1 - \cos 2n\pi Z) \quad (24)$$

which satisfies the boundary conditions given by Eq. (9).

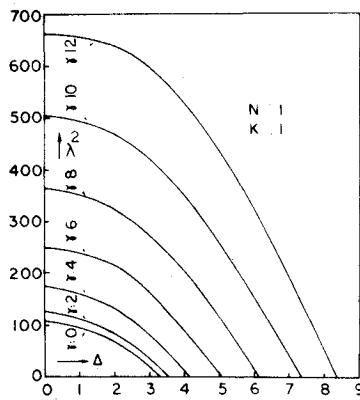


Fig. 1 Values of frequency and buckling parameters for a simply supported beam.

Substituting Eq. (24) in Eq. (12) and performing the Galerkin method of integrating the resulting expression over the whole length of the beam, the expression for the frequency parameter λ is obtained as

$$\lambda = 2\{(N^2\pi^2/3)(4N^2\pi^2 + K^2 - \Delta^2) + \gamma^2\}^{1/2} \quad (25)$$

In arriving at Eq. (25), only one term of the infinite series of Eq. (24) is utilized. Eq. (25) gives an upper bound for the natural frequency parameter λ for the fixed-end beam as it is obtained by the approximate method due to Galerkin. But it is quite handy and can give values within engineering accuracy.

By putting $\lambda = 0$, and $N = 1$, in Eq. (25), the expression for the buckling load parameter Δ_{cr} , for the clamped beam can be obtained as

$$\Delta_{cr}^2 = [4\pi^2 + K^2 + (3/\pi^2)\gamma^2] \quad (26)$$

For the simply supported-fixed beam, the approximate expressions obtained, for the fundamental frequency parameter λ ($N = 1$), and buckling load parameter Δ_{cr} , by the Galerkin method assuming a power series of the type

$$X(Z) = \sum_{i=0}^4 a_i Z^i \quad (27)$$

are

$$\lambda = [238.739 + 11.3686(K^2 - \Delta^2) + 4\gamma^2]^{1/2} \quad (28)$$

and

$$\Delta_{cr}^2 = [21 + K^2 + 0.352\gamma^2] \quad (29)$$

Out of the five constants a_i ($i = 0, 1, 2, 3, 4$) in Eq. (27), four constants as ratios of the fifth constant can be obtained by utilizing the boundary conditions of Eq. (10) for this case, and the fifth arbitrary constant cancels out in the Galerkin integral.

In the limiting case of the absence of elastic foundation, i.e., $\gamma = 0$, and the compressive load, $\Delta = 0$, all the approximate expressions are observed⁹ to be in complete agreement with those derived previously by Gere³ and Timoshenko and Gere.⁷

Conclusions

Results for the torsional frequency parameter λ , for the first mode ($N = 1$), for the simply supported and fixed beams, obtained from Eqs. (22) and (25) are plotted in Figs. 1 and 2 respectively, for various values of foundation parameter γ and load parameter Δ . The warping parameter is kept at $K = 1$. The values of the critical buckling loads for various values of γ can also be obtained from the graphs for $\lambda = 0$ (i.e., on the axis on which Δ is taken). When the axial load is not present the values of the frequency parameter λ for various values of γ can be obtained for values of $\Delta = 0$ (i.e., on the vertical axis on which λ is plotted). The combined influence of the foundation parameter γ and the load parameter Δ can be observed from the graphs, to be opposing each other. Independently, as the load parameter Δ increases, the frequency parameter λ drops to zero. In the absence of the axial load, the frequency parameter λ increases for increasing values of the foundation parameter γ . Hence the combined influence is the superimposition of the individual effects on the frequency of vibration.

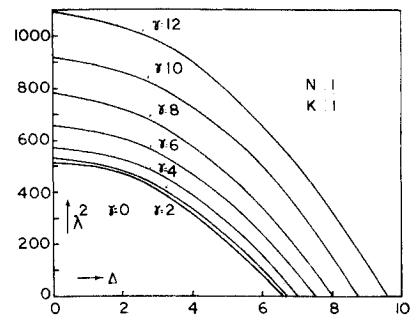


Fig. 2 Values of frequency and buckling parameters for a fixed-fixed beam.

It can be observed from Eqs. (22) and (25) that the influence of foundation parameter γ decreases for increasing values of N (i.e., for higher modes). It is interesting to see from Eq. (22) that for the simply supported beam, for the limiting condition $\gamma = 0.5N\pi\Delta$, the combined influence of elastic foundation and axial compressive load becomes zero. In the case of clamped beam this limiting condition, from Eq. (25), is $\gamma = 0.574N\pi\Delta$.

References

- Hatvani, M., *Beams on Elastic Foundation*, University of Michigan Press, Ann Arbor, Mich., March 1946.
- Vlasov, V. Z. and Leont'ev, U. N., "Beams, Plates and Shells on Elastic Foundations," translated from the Russian, Israel Program for Scientific Translations, Jerusalem.
- Gere, J. M., "Torsional Vibrations of Beams of Thin-Walled Open Section," *Journal of Applied Mechanics*, Transactions of the ASME, Dec. 1954, pp. 381-387.
- Aggarwal, H. R. and Cranch, E. T., "A Theory of Torsional and Coupled Bending Torsional Waves in Thin-Walled Open Section Beams," *Journal of Applied Mechanics*, Transactions of the ASME, Vol. 34, 1967, pp. 337-343.
- Krishna Murty, A. V. and Joga Rao, C. V., "General Theory of Vibrations of Cylindrical Tubes," *Journal of the Aeronautical Society of India*, Vol. 20, No. 1, 1968, pp. 1-38; No. 4, pp. 235-258.
- Kameswara Rao, C., Apparao, K. V., and Sarma, P. K., "Effect of Longitudinal Inertia and Shear Deformation on the Torsional Frequency and Normal Modes of Thin-Walled Open Section Beams," *Journal of the Aeronautical Society of India*, to be published.
- Timoshenko, S. P. and Gere, J. M., *Theory of Elastic Stability*, McGraw-Hill, New York, 1961.
- Christiano, P. and Salmela, L., "Frequencies of Beams with Elastic Warping Restraint," *Journal of the Structural Division, Proceedings of the ASCE*, Vol. 97, No. ST6, June 1971, pp. 1835-1840.
- Appala Satyam, A., "Torsional Vibrations and Stability of Thin-Walled Beams of Open Section Resting on an Elastic Foundation," M.E. thesis, 1974, Department of Mechanical Engineering, Andhra University, Waltair, India.

Vibration—Stability Relationships for Conservative Elastic Systems

C. SUNDARARAJAN*

University of Toronto, Toronto, Canada

Introduction

LURIE¹ observed that, for linearly elastic systems, the square of the lateral frequency is "practically" linearly related to the end thrust. According to Southwell's theorem² this straight

Received May 6, 1974; revision received August 12, 1974.

Index categories: Structural Dynamic Analysis; Structural Stability Analysis.

* Postdoctoral Fellow, Department of Mechanical Engineering.

LETTERS TO THE EDITOR

FUNDAMENTAL FREQUENCIES OF CANTILEVER BLADES WITH RESILIENT ROOTS

1. INTRODUCTION

A considerable amount of work has been done in the field of vibration dealing with the computation of natural frequencies and mode shapes of cantilever blades including the effects of root flexibility [1-7]. These investigations have revealed that the natural frequencies are considerably lowered when the roots are flexible. Justine and Krishnan [4] used a finite element method based on Bernoulli-Euler theory and presented results for the fundamental frequency of vibration for various values of rotational and linear spring stiffness parameters. A total of about 16 elements were found to be necessary to yield satisfactory results. Fossman and Sorensen [5] have studied in detail the dynamic response of elastically restrained cantilever beams and presented exact frequencies and mode shapes for a wide range of restraint parameters. Abbas [6] studied the Timoshenko beam problem using a higher order element and presented results for the degenerated cases also. Recently, Afolabi [7] has investigated the problem in much greater detail and tabulated the first three frequencies for a wide range of values of spring parameters.

In the early stages of design, a quick estimate of the fundamental frequency becomes necessary and simple but reliable expressions become quite handy in such circumstances. In the present note, a simple expression for approximately predicting the fundamental frequency is derived by using Galerkin's technique. A comparison of results obtained by using the expression show excellent agreement with the finite element and exact results [4, 7]. During the course of comparison serious inaccuracies are noticed in the fundamental as well as higher mode frequencies reported by Abbas [6], which were obtained by using a higher order finite element. These observations are also included in the note.

2. ANALYSIS

For a Bernoulli-Euler beam of length L , area of cross-section A , mass density ρ , Young's modulus E , moment of inertia I , the differential equation describing its sinusoidal vibratory motion can be expressed as

$$EIY'''' - \lambda^4 Y = 0, \quad (1)$$

where primes denote differentiation with respect to the non-dimensional distance $X = x/L$, along the length of the beam and, the frequency parameter is given by $\lambda^4 = \rho A \omega^2 L^4 / EI$, in which ω is the circular natural frequency of the beam.

The boundary conditions for a cantilever blade with linear and rotational springs of stiffnesses S_1 and S_2 respectively at the resilient root (see Figure 1) can be expressed as follows:

$$\text{at } X = 0, \quad Y'''(0) = -TY(0), \quad Y''(0) = RY'(0); \quad (2a)$$

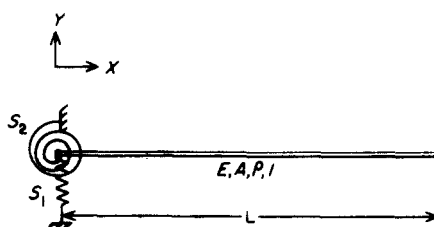


Figure 1.

$$\text{at } X = 1, \quad Y'''(1) = 0, \quad Y''(1) = 0. \quad (2b)$$

Here

$$T = S_1 L^3 / EI, \quad R = S_2 L / EI. \quad (3)$$

The fundamental mode-shape satisfying the boundary conditions (2) can be assumed as

$$Y(X) = A(X^4 - 4X^3 + 6X^2 + 12R^*X + 24T^*). \quad (4)$$

where $R^* = 1/R$, and $T^* = 1/T$. Substituting equation (4) in equation (1) and performing the minimization of the resulting error by utilizing the Galerkin integral, yields the expression determining the fundamental frequency as

$$\lambda^4 = 36288Z_4 / (60480Z_1 + 2912Z_2 + 72576Z_3), \quad (5)$$

where

$$Z_1 = 12T^{*2} + R^{*2}, \quad Z_2 = 1 + 9R^*, \quad Z_3 = T^*(1 + 5R^*), \quad Z_4 = 1 + 20T^* + 5R^*. \quad (6(a)-(d))$$

When the linear spring at the root is infinitely stiff ($T \rightarrow \infty$), i.e., $T^* \rightarrow 0$, then equation (5) reduces to

$$\lambda^4 = 36288(1 + 5R^*) / (2912 + 26208R^* + 60480R^{*2}). \quad (7)$$

TABLE 1

Values of λ_1 for cantilever blades with resilient roots for various values of R and T

R		Value of T				
		0.01	0.1	1	10	1000
0.01	F	0.2979	0.3941	0.4134	0.4154	0.4157
	E	0.297992	0.394250	0.413616	0.415701	0.415932
	G	0.298047	0.395127	0.413850	0.415729	0.415935
0.1	F	0.3141	0.5292	0.6980	0.7313	0.7354
	E	0.314227	0.529359	0.698245	0.731779	0.735742
	G	0.314227	0.529463	0.699847	0.732229	0.735789
1.0	F	0.3160	0.5582	0.9312	1.1951	1.2467
	E	0.315991	0.558157	0.931611	1.195670	1.247368
	G	0.315991	0.558157	0.931935	1.199138	1.248060
10	F	0.3161	0.5611	0.9814	1.5066	1.7189
	E	0.316168	0.561288	0.981460	1.507835	1.720254
	G	0.316119	0.561288	0.981482	1.512302	1.723775
100	F	—	—	—	—	—
	E	0.316186	0.561603	0.986917	1.569480	1.853372
	G	0.316186	0.561603	0.986928	1.573429	1.858149
1000	F	0.3161	0.5615	0.9870	1.5750	1.8466
	E	0.316188	0.561635	0.987467	1.576304	1.869694
	G	0.316188	0.561635	0.987477	1.580178	1.874608
10 000	F	0.3161	0.5615	0.9875	1.5765	1.8696
	E	0.316188	0.561638	0.987522	1.576994	1.871365
	G	0.316188	0.561638	0.987532	1.580860	1.876292
∞	F	0.3161	0.5615	0.9875	1.5766	1.8697
	E	0.316188	0.561638	0.987528	1.577071	1.871551
	G	0.316188	0.561638	0.987538	1.580935	1.876480

F, finite element results [4]; E, Exact results [7]; G, Galerkin results from equation (5).

TABLE 2

Comparison of values of λ_1 for cantilever blades with resilient roots obtained by Galerkin and higher order finite element methods for various values of R and T

R		Value of T				
		0.01	0.1	1	10	∞
0.01	A	0.0	0.0	0.0	0.0	0.0
	G	0.298047	0.395127	0.413850	0.415729	0.415937
0.1	A	0.232379	0.374166	0.435890	0.460435	0.531037
	G	0.314227	0.529463	0.699847	0.732229	0.735789
1.0	A	0.738918	1.158879	1.190798	1.192476	1.192896
	G	0.315991	0.558157	0.931935	1.199138	1.248538
10	A	0.802496	1.714351	1.8	1.802498	1.802498
	G	0.316119	0.561288	0.981460	1.507835	1.725696
∞	A	0.810555	1.791926	1.874033	1.875100	1.875100
	G	0.316188	0.561638	0.987538	1.580935	1.878854

A, finite element results by Abbas [6]; G, Galerkin results from equation (5).

TABLE 3

Comparison of λ_2 for cantilever blades with resilient roots obtained by higher order finite element and exact methods for various values of R and T

R		Value of T				
		0.01	0.1	1	10	1000
0.01	A	1.217785	3.305904	3.916504	3.924538	3.924666
	E	0.623990	0.838528	1.418276	2.455427	3.927805
0.1	A	1.222702	3.301060	3.916121	3.925685	3.926067
	E	1.043705	1.101487	1.481858	2.461235	3.938466
1.0	A	1.785777	3.271085	3.986853	4.009738	4.011484
	E	1.720136	1.731420	1.841351	2.505060	4.031139
10	A	2.328304	3.255457	4.490768	4.528797	4.530894
	E	2.235315	2.238866	2.274598	2.606356	4.399523
∞	A	2.376552	3.261135	4.660150	4.688603	4.689243
	E	2.365300	2.367816	2.393234	2.648238	4.694091

A, finite element results by Abbas [6]; E, exact results [7].

The case represented by equation (7) was studied by Chun [1] using an exact method of analysis. For a cantilever blade with complete fixity at the root, equation (5) gives the value of λ as 1.878853 against the exact value of 1.875104 which amounts to an error of only 0.2 percent.

3. NUMERICAL RESULTS AND DISCUSSION

By using equation (5), numerical values of fundamental frequency parameter λ were generated for various values of linear and rotational spring stiffness parameters T and R respectively in the range of 0.01 to ∞ . In Table 1, the results obtained by using

Galerkin's method are compared with those obtained by finite element [4] and exact methods [7]. It can be seen that equation (5) gives very accurate estimates of the fundamental frequency over the entire range of spring stiffness values and hence can be recommended for use in design.

In Table 2 is given the comparison of Galerkin results obtained from equation (5) with those reported by Abbas [6] for this case. In Table 3 the second mode frequency results reported by Abbas are compared with the exact ones reported by Afolabi [7]. From these comparisons, it can be observed that the results reported by Abbas are in serious error. It is therefore suggested that care should be taken in utilizing the higher order element developed by Abbas, especially for beams with elastically restrained ends.

*Seismic and Foundation Analysis Group,
Corporate R and D Division,
Bharat Heavy Electricals Limited,
Vikasnagar, Hyderabad 500 593, India*

C. KAMESWARA RAO

(Received 23 November 1987)

REFERENCES

1. K. R. CHUN 1972 *Journal of Applied Mechanics* **39**, 1154-1155. Free vibration of a beam with one end spring-hinged and other free.
2. J. C. MCBAIN and J. GENIN 1973 *Journal of Sound and Vibration* **27**, 197-206. Natural frequencies of a beam considering support characteristics.
3. J. C. MCBAIN and J. GENIN 1973 *Journal of the Franklin Institute* **296**, 259-273. Effect of support flexibility on the fundamental frequency of vibrating beams.
4. T. JUSTINE and A. KRISHNAN 1980 *Journal of Sound and Vibration* **68**, 310-312. Effect of support flexibility on fundamental frequency of beams.
5. R. FOSSMAN and A. SORENSEN 1980 *Journal of Mechanical Design* **102**, 829-834. Influence of flexible connections on response characteristics of a beam.
6. B. A. H. ABBAS 1984 *Journal of Sound and Vibration* **97**, 541-548. Vibration of Timoshenko beams with elastically restrained ends.
7. D. AFOLABI 1986 *Journal of Sound and Vibration* **110**, 429-441. Natural frequencies of cantilever blades with resilient roots.

FREE TORSIONAL VIBRATIONS OF TAPERED CANTILEVER I-BEAMS

C. KAMESWARA RAO† AND S. MIRZA

Department of Mechanical Engineering, University of Ottawa, Ottawa, Canada K1N 6N5

(Received 9 July 1987, and in revised form 17 November 1987)

Torsional vibration characteristics of linearly tapered cantilever I-beams have been studied by using the Galerkin finite element method. A third degree polynomial is assumed for the angle of twist. The analysis presented is valid for long beams and includes the effect of warping. The individual as well as combined effects of linear tapers in the width of the flanges and the depth of the web on the torsional vibration of cantilever I-beams are investigated. Numerical results generated for various values of taper ratios are presented in graphical form.

1. INTRODUCTION

It is commonly believed that material saving can be accomplished by using non-uniform beams. Non-uniform thin-walled beams are quite commonly used in aircraft, bridges and several other industrial structures. In view of the current emphasis on structural optimization, there is an urgent need to obtain a proper understanding of the vibration characteristics of non-prismatic structural members. Several investigations [1–4] have been reported on torsional vibrations and stability of long uniform thin-walled open section beams, such as I-beams.

Static torsional response and lateral-torsional stability of tapered I-beams has been investigated by many researchers [5–13]. Among these, Hamaychi [5], Lee [6], Wilde [7] and Lee and Szabo [8], presented basic derivations for a comprehensive theory of non-uniform torsion of tapered I-beams. Massey and McGuire [9] studied the lateral stability of stepped cantilever beams of rectangular and I-cross-section using a Runge-Kutta integration procedure. The problem of lateral-torsional buckling of tapered I-beams has been studied by Kitipornchai and Trahair [10], Brown [11], Culver and Preg [12] and Shiomi and Kurata [13]. In these studies, solutions were obtained for simply supported and cantilever beams using finite-difference or finite-integral methods.

A review of the literature clearly shows that very few studies [14–16, 18] have been conducted on the free vibration characteristics of non-uniform thin-walled beams. It can be also seen that especially little progress has been made in the area of torsional vibrations of I-beams with taper along their depth.

In the present paper, the governing differential equation for torsional vibrations of tapered doubly symmetric I-beams is derived and solved for the case of a cantilever I-beam fixed at its smaller end by utilizing the Galerkin finite element method [17]. An analysis is presented for the case of long beams including the effect of warping. The individual as well as combined effects of linear variations in the width of the flanges and the depth of the web on torsional natural frequencies are investigated.

† On leave from Corporate R&D Division, Bharat Heavy Electricals Ltd., Vikas Nagar, Hyderabad-500 593, India.

2. GOVERNING EQUATION OF TORSIONAL MOTION

Consider free torsional vibrations of a doubly symmetric thin-walled I-beam of variable cross-section and of length L . The variations in the width of the flanges and the depth of the web are respectively assumed to be of the form

$$b(z) = b_0(1 + \alpha z/L), \quad d(z) = d_0(1 + \beta z/L), \quad (1, 2)$$

where z is the distance along the length of the beam, and α and β are the taper ratios in the width of the flanges and depth of the web, respectively. The values with subscript zero are those at the smaller end of the beam (a list of nomenclature is given in the Appendix).

When the beam is executing torsional vibration, the bending moment, M , induced in the flanges is given by [4]

$$M(z) = EI_f(z) \partial^2 u / \partial z^2. \quad (3)$$

In equation (3), the warping displacement, u , in the flanges is given by

$$u(z) = [h(z)/2] \phi, \quad (4)$$

where $h(z)$ is the height between centerlines of the flanges. Hence, one has

$$h(z) = d(z) + t_f. \quad (5)$$

Substituting equation (4) in equation (3) gives

$$M(z) = EI_f(z) \frac{\partial^2}{\partial z^2} \left[\frac{h(z)}{2} \frac{\partial^2 u}{\partial z^2} \right]. \quad (6)$$

The torque, T , induced in the beam is given by [6]

$$T(z) = Gc_s(z) \partial \phi / \partial z - h(z) \partial M(z) / \partial z + M(z) dh(z) / dz. \quad (7)$$

For free torsional vibrations, the static torque is replaced by the inertia torque which has an intensity of $\rho I_p(z) \partial^2 \phi / \partial t^2$, in which I_p is the polar moment of inertia and ρ is the mass density of the material of the beam. Thus,

$$\partial T(z) / \partial z = \rho I_p(z) \partial^2 \phi / \partial t^2. \quad (8)$$

Substituting equation (7) in equation (8) gives

$$\begin{aligned} \frac{\partial}{\partial z} \left[Gc_s(z) \frac{\partial \phi}{\partial z} \right] - \frac{\partial^2}{\partial z^2} \left[EI_f(z) h(z) \frac{\partial^2}{\partial z^2} \left(\frac{h(z)}{2} \phi \right) \right] \\ + 2 \frac{\partial}{\partial z} \left[EI_f(z) \frac{dh(z)}{dz} \frac{\partial^2}{\partial z^2} \left(\frac{h(z)}{2} \phi \right) \right] = \rho I_p(z) \frac{\partial^2 \phi}{\partial t^2}. \end{aligned} \quad (9)$$

For harmonic vibration the angle of twist ϕ can be written in the form

$$\phi(z, t) = \theta(z) \sin \omega t. \quad (10)$$

Substituting equation (10) in equation (9) gives

$$\begin{aligned} \frac{d^2}{dz^2} \left[EI_f(z) h(z) \frac{d^2}{dz^2} \left(\frac{h(z)}{2} \theta \right) \right] - \frac{d}{dz} \left[Gc_s(z) \frac{d\theta}{dz} \right] \\ - 2 \frac{d}{dz} \left[EI_f(z) \frac{dh(z)}{dz} \frac{d^2}{dz^2} \left(\frac{h(z)}{2} \theta \right) \right] - \rho I_p(z) \omega^2 \theta = 0. \end{aligned} \quad (11)$$

When expanding the differential equation (11), terms containing $d^2 h(z) / dz^2$ are neglected as the depth taper considered in this study is linear.

Equation (11) is a fourth order differential equation with variable coefficients and a Galerkin-finite element method has been utilized in this study in obtaining the solutions for cantilever beams.

3. FINITE ELEMENT FORMULATION

In the Galerkin - finite element formulation [17], the domain of the beam is subdivided into a number of elements. A third degree polynomial for angle of twist in z is assumed over the element. The variation of torsional amplitude θ_e over each element, in terms of nodal degrees of freedom θ and θ' , is given by

$$\{\theta_e\} = [\chi]\{\delta_e\}, \quad (12)$$

where $[\chi]$ is the row matrix of shape functions

$$\{\delta\}_e = [\theta_1, \theta'_1, \theta_2, \theta'_2]^T. \quad (13)$$

Here primes denote differentiation with respect to z and subscripts 1 and 2 denote the two ends of the element.

Substituting equation (12) in equation (11) gives the residual R_e for the element as

$$R_e = \left[EI_f h \left(\frac{h}{2} \chi \right)'''' \right] \{\delta\}_e - [Gc_s \chi'] \{\delta\}_e - 2 \left[EI_f h' \left(\frac{h}{2} \chi \right)''' \right] \{\delta\}_e - \rho I_p \omega^2 \chi \{\delta\}_e. \quad (14)$$

In the Galerkin - finite element method, the weighted residual is minimized by setting

$$\frac{\partial}{\partial \{\delta\}_e} \int_0^L R_e \theta_e dz = 0. \quad (15)$$

This procedure is repeated for all elements and after the usual assembly procedure, the final matrix equation governing free vibration is obtained as

$$[A]\{\delta\} - \lambda_n^2 [B]\{\delta\} = 0, \quad (16)$$

where

$$\lambda_n^2 = A_{f0} \omega^2 L^4 / EI_{f0} \quad (17)$$

The quantities A_{f0} and I_{f0} are the flange area and moment of inertia respectively at the fixed end. Also, $[A]$ is the stiffness matrix, $[B]$ the mass matrix and $\{\delta\}$ the eigenvector. Equation (16) can be solved by using any standard eigenvalue algorithm to obtain the eigenvalues and eigenvectors $\{\delta\}$.

4. NUMERICAL RESULTS

Numerical values of the frequency parameter λ have been obtained, by dividing the beam into a sufficient number of elements, for the case of a tapered cantilever I-beam shown in the inset of Figure 1. It is found that 12-16 elements are sufficient to yield convergence. The cantilever beam chosen is of 76 cm in length and has the following dimensions at the fixed smaller end: width of the flanges, $b_0 = 31.55$ cm; depth of the web, $d_0 = 66.54$ cm. The boundary conditions considered at the fixed end ($z = 0$), are $\theta = \theta' = 0$.

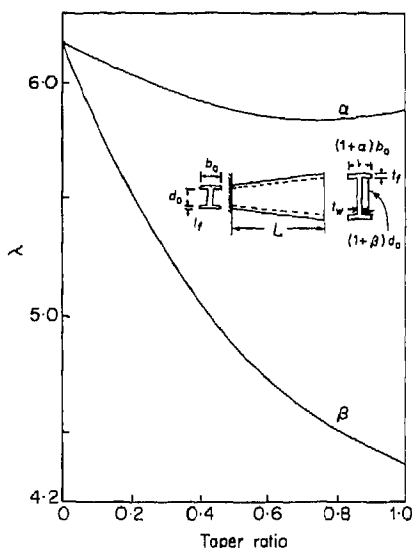


Figure 1. Effect of individual taper ratios (first mode). $b_0 = 31.55$; $d_0 = 66.54$; $t_{f0} = 3.11$; $t_w = 2.13$; $L = 760$ (all dimensions in mm).

The thickness of the flanges and the web are kept constant and are chosen as $t_f = 3.11$ cm and $t_w = 2.13$ cm respectively. The values of λ for various combinations of taper ratios α and β for the first three modes of vibration are presented in Figures 1-6. Figures 1-3 show the individual influences of taper ratios and Figures 4-6 show the combined effects.

4.1. INFLUENCE OF FLANGE WIDTH TAPER α

From Figure 1, it can be seen that, for $\beta = 0$, the first frequency decreases marginally up to a value of $\alpha = 0.7$ and thereafter increases slightly. It can be observed from Figures 2 and 3 that the torsional frequencies for the second and third modes increase significantly for increasing values of the taper ratio α . However, for higher modes it can be also noted

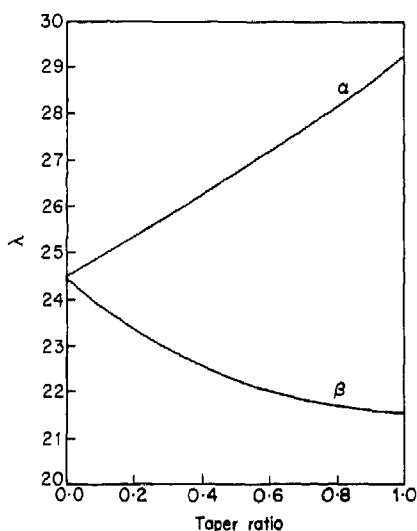


Figure 2. Effect of individual taper ratios (second mode).

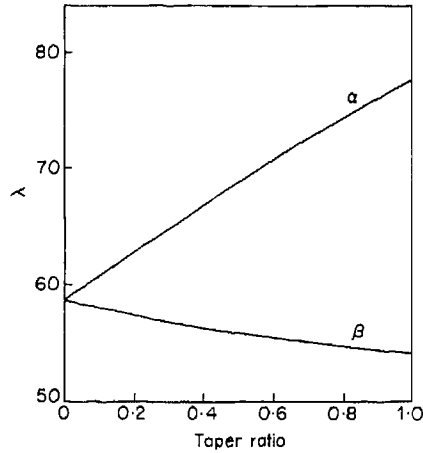


Figure 3. Effect of individual taper ratios (third mode).

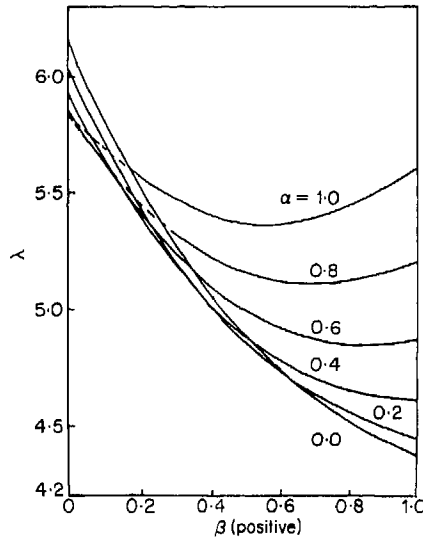


Figure 4. Combined influence of taper ratios (first mode).

that the flange taper α has a much larger influence on frequencies of vibration than the web taper β .

4.2. INFLUENCE OF WEB DEPTH TAPER β

Figures 1-3 clearly show that, for $\alpha = 0$, the first three torsional frequencies of vibration decreases significantly for increasing values of depth taper β . This decrease is comparatively significant in the first mode than that in other higher modes of vibration.

4.3. COMBINED INFLUENCE OF TAPER RATIOS α AND β

Figures 4-6 show the combined influence of the taper ratios α and β on the first three frequencies of vibration. In Figure 4, the intersection of various curves can be easily understood by recalling the opposite effects of the individual tapers α and β discussed in sections 4.1 and 4.2. It can be also observed that, for values of β in the range $0 < \beta \leq 0.4$,

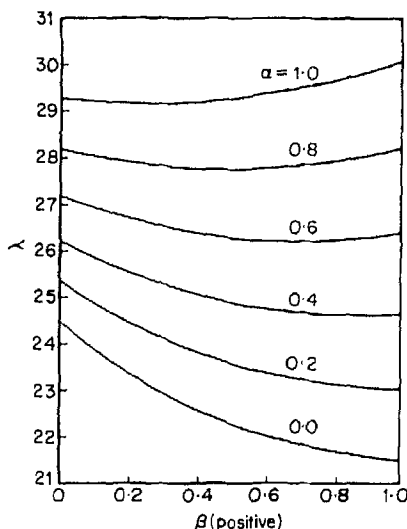


Figure 5. Combined influence of taper ratios (second mode).

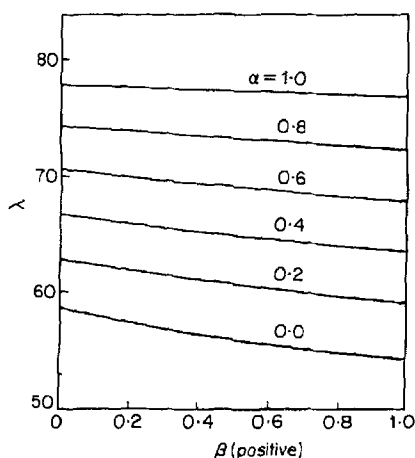


Figure 6. Combined influence of taper ratios (third mode).

the fundamental frequency decreases for increasing values of flange width taper α . In the range, $0.4 < \beta \leq 1.0$, the fundamental frequency increases for increasing values of α . Hence, the combined behaviour can be understood as a superposition of the individual influences of the taper ratios α and β on the frequencies.

Figures 5 and 6 reveal interesting trends. The various curves for the different values of the taper ratio α do not intersect. This is due to the opposing nature of the individual influences of α and β on the second and third mode frequencies. It can be observed from Figure 5 that for any constant value of α in the range $0 < \alpha \leq 0.6$ the influence of increasing values of β is to decrease the frequency of vibration. This is due to the fact that the percentage increase in the frequency due to increase in the taper ratio β is much higher than that due to α in this range. In the zone $0.6 < \alpha \leq 1.0$ the frequency of vibration marginally decreases up to a value of $\beta = 0.5$ and then increases for increasing values of β . From Figure 6, it can be seen that, for any constant value of α , the third mode frequency

decreases for increasing values of β . Further, for a constant value of β , the third mode frequency increases for increasing values of taper ratio α .

5. CONCLUDING REMARKS

The governing differential equation for the free torsional vibrations of tapered I-beams has been derived in this paper and solved for the case of a cantilever I-beam fixed at the smaller end by utilizing a Galerkin – finite element method. The effects of individual as well as combined linear tapers α and β in the flange width and web depth respectively on the first three torsional frequencies of vibration have been investigated. Except for a smaller range in the first mode of vibration, the effect of increase in flange width taper α in general is to increase significantly the frequencies of vibration. Interestingly, the effect of increase in web depth taper β is to decrease drastically the torsional frequency.

REFERENCES

1. V. Z. VLASOV 1961 *Thin-walled Elastic Beams*. Jerusalem: Israel Program of Scientific Translations.
2. J. M. GERE 1954 *Journal of Applied Mechanics* **21**, 381–387. Torsional vibrations of beams of thin-walled open section.
3. C. KAMESWARA RAO 1975 *Ph.D. thesis, Andhra University, Waltair*. Torsional vibrations and stability of thin-walled beams of open section resting on continuous elastic foundation.
4. C. SZYMCAK 1978 *Rozprawy Inzynierskie* **26**, 267–274. Torsional vibrations of thin-walled bars with bisymmetric cross-section (in Polish).
5. F. HAMAYCHI 1961 *Memorirs of the Faculty of Engineering, Hokkaido University*, **11**, 209. On torsion of I-beams with web of variable height.
6. G. C. LEE and B. A. SZABE 1967 *Proceedings of the American Society of Civil Engineers* **93**, *Journal of the Structural Division* **ST5**, 233–252. Torsional response of tapered I-girders.
7. P. WILDE 1968 *Archiwum Mechaniki Stosowanej* **20**, 431–443. On torsion of thin-walled bars with variable cross-section.
8. L. H. N. LEE 1956 *Journal of the Franklin Institute* **262**, 37–44. Non-uniform torsion of tapered I-beams.
9. C. MASSEY and P. J. MCGUIRE 1971 *Proceedings of the American Society of Civil Engineers* **97**, *Journal of the Engineering Mechanics Division* **EM3**, 673–686. Lateral stability of non-uniform cantilevers.
10. S. KITIPORNCHAI and N. S. TRAHAIR 1972 *Proceedings of the American Society of Civil Engineers* **98**, *Journal of the Structural Division* **ST3**, 713–728. Elastic stability of tapered I-beams.
11. T. G. BROWN 1981 *Proceedings of the American Society of Civil Engineers* **107**, *Journal of the Structural Division* **ST4**, 689–697. Lateral-torsional buckling of tapered I-beams.
12. G. C. CULVER and S. M. PREG 1968 *Proceedings of the American Society of Civil Engineers* **94**, *Journal of the Structural Division* **ST2**, 455–470. Elastic stability of tapered beam-columns.
13. H. SHIOMI and M. KURATA 1984 *Proceedings of the American Society of Civil Engineers* **110**, *Journal of Structural Engineering* **ST7**, 1630–1643. Strength formula for tapered beam-columns.
14. Z. CYWINSKI 1969 *Rozprawy Inzynierskie* **17**, 185–217. Statistics and dynamics in torsion of I-beams with variable bisymmetric cross-section (in Polish).
15. C. KAMESWARA RAO and P. K. SARMA 1975 *Journal of the Aeronautical Society of India* **27**, 169–171. The fundamental flexural frequency of simply-supported I-beams with uniform taper.
16. C. SZYMCAK 1983 *Journal of Sound and Vibration* **86**, 235–241. Optimal design of thin-walled I-beams for extreme natural frequency of torsional vibrations.
17. S. G. HUTTON and D. L. ANDERSON 1971 *Proceedings of the American Society of Civil Engineers* **97**, *Journal of the Engineering Mechanics Division* **EM5**, 1503–1520. Finite element method: a Galerkin approach.
18. R. H. GUTIERREZ and P. A. A. LAURA 1987 *Journal of Sound and Vibration* **114**, 393–397. Approximate analysis of coupled flexural-torsional vibrations of a beam of non-uniform cross-section using the optimized Rayleigh method.

APPENDIX: NOMENCLATURE

$[A]$	stiffness matrix
A_{f0}	area of the flanges at the smaller end of the beam
$[B]$	mass matrix
b	width of the flanges
b_0	width of flanges at smaller end
c_s	torsion constant
d	depth of the web
d_0	depth of web at smaller end
E	Young's modulus
G	shear modulus
h	distance between centerlines of the flanges
I_f	flange moment of inertia
I_p	polar moment of inertia
L	length of the beam
M	flange bending moment
R_e	residual, see equation (14)
T	twisting moment
t	time
t_f	thickness of the flange
z	distance along the length of the beam
α	taper parameter in width of the flanges
β	taper parameter in depth of the web
ϕ	angle of twist
θ	normal function of angle of twist
λ	torsional frequency parameter
ρ	mass density of the beam material
ω	natural frequency of vibration
$[\chi]$	row matrix of shape functions
$\{\delta\}$	eigenvector

See discussions, stats, and author profiles for this publication at: <https://www.researchgate.net/publication/256801045>

Free torsional vibrations of tapered cantilever I-beams

Article in *Journal of Sound and Vibration* · August 1988

DOI: 10.1016/S0022-460X(88)81390-7

CITATIONS

9

READS

217

2 authors:



Kameswara Rao Chellapilla

NNRG

105 PUBLICATIONS 461 CITATIONS

SEE PROFILE

Sashi Mirza

5 PUBLICATIONS 101 CITATIONS

SEE PROFILE

Some of the authors of this publication are also working on these related projects:



Vibrations of Fluid Conveying Carbon Nanotubes on Partial Elastic Foundation [View project](#)



Vibrations and Stability of Plates [View project](#)

FREE TORSIONAL VIBRATIONS OF TAPERED CANTILEVER I-BEAMS

C. KAMESWARA RAO† AND S. MIRZA

Department of Mechanical Engineering, University of Ottawa, Ottawa, Canada K1N 6N5

(Received 9 July 1987, and in revised form 17 November 1987)

Torsional vibration characteristics of linearly tapered cantilever I-beams have been studied by using the Galerkin finite element method. A third degree polynomial is assumed for the angle of twist. The analysis presented is valid for long beams and includes the effect of warping. The individual as well as combined effects of linear tapers in the width of the flanges and the depth of the web on the torsional vibration of cantilever I-beams are investigated. Numerical results generated for various values of taper ratios are presented in graphical form.

1. INTRODUCTION

It is commonly believed that material saving can be accomplished by using non-uniform beams. Non-uniform thin-walled beams are quite commonly used in aircraft, bridges and several other industrial structures. In view of the current emphasis on structural optimization, there is an urgent need to obtain a proper understanding of the vibration characteristics of non-prismatic structural members. Several investigations [1–4] have been reported on torsional vibrations and stability of long uniform thin-walled open section beams, such as I-beams.

Static torsional response and lateral-torsional stability of tapered I-beams has been investigated by many researchers [5–13]. Among these, Hamaychi [5], Lee [6], Wilde [7] and Lee and Szabo [8], presented basic derivations for a comprehensive theory of non-uniform torsion of tapered I-beams. Massey and McGuire [9] studied the lateral stability of stepped cantilever beams of rectangular and I-cross-section using a Runge-Kutta integration procedure. The problem of lateral-torsional buckling of tapered I-beams has been studied by Kitipornchai and Trahair [10], Brown [11], Culver and Preg [12] and Shiomi and Kurata [13]. In these studies, solutions were obtained for simply supported and cantilever beams using finite-difference or finite-integral methods.

A review of the literature clearly shows that very few studies [14–16, 18] have been conducted on the free vibration characteristics of non-uniform thin-walled beams. It can be also seen that especially little progress has been made in the area of torsional vibrations of I-beams with taper along their depth.

In the present paper, the governing differential equation for torsional vibrations of tapered doubly symmetric I-beams is derived and solved for the case of a cantilever I-beam fixed at its smaller end by utilizing the Galerkin finite element method [17]. An analysis is presented for the case of long beams including the effect of warping. The individual as well as combined effects of linear variations in the width of the flanges and the depth of the web on torsional natural frequencies are investigated.

† On leave from Corporate R&D Division, Bharat Heavy Electricals Ltd., Vikas Nagar, Hyderabad-500 593, India.

2. GOVERNING EQUATION OF TORSIONAL MOTION

Consider free torsional vibrations of a doubly symmetric thin-walled I-beam of variable cross-section and of length L . The variations in the width of the flanges and the depth of the web are respectively assumed to be of the form

$$b(z) = b_0(1 + \alpha z/L), \quad d(z) = d_0(1 + \beta z/L), \quad (1, 2)$$

where z is the distance along the length of the beam, and α and β are the taper ratios in the width of the flanges and depth of the web, respectively. The values with subscript zero are those at the smaller end of the beam (a list of nomenclature is given in the Appendix).

When the beam is executing torsional vibration, the bending moment, M , induced in the flanges is given by [4]

$$M(z) = EI_f(z) \partial^2 u / \partial z^2. \quad (3)$$

In equation (3), the warping displacement, u , in the flanges is given by

$$u(z) = [h(z)/2] \phi, \quad (4)$$

where $h(z)$ is the height between centerlines of the flanges. Hence, one has

$$h(z) = d(z) + t_f. \quad (5)$$

Substituting equation (4) in equation (3) gives

$$M(z) = EI_f(z) \frac{\partial^2}{\partial z^2} \left[\frac{h(z)}{2} \frac{\partial^2 u}{\partial z^2} \right]. \quad (6)$$

The torque, T , induced in the beam is given by [6]

$$T(z) = Gc_s(z) \partial \phi / \partial z - h(z) \partial M(z) / \partial z + M(z) dh(z) / dz. \quad (7)$$

For free torsional vibrations, the static torque is replaced by the inertia torque which has an intensity of $\rho I_p(z) \partial^2 \phi / \partial t^2$, in which I_p is the polar moment of inertia and ρ is the mass density of the material of the beam. Thus,

$$\partial T(z) / \partial z = \rho I_p(z) \partial^2 \phi / \partial t^2. \quad (8)$$

Substituting equation (7) in equation (8) gives

$$\begin{aligned} \frac{\partial}{\partial z} \left[Gc_s(z) \frac{\partial \phi}{\partial z} \right] - \frac{\partial^2}{\partial z^2} \left[EI_f(z) h(z) \frac{\partial^2}{\partial z^2} \left(\frac{h(z)}{2} \phi \right) \right] \\ + 2 \frac{\partial}{\partial z} \left[EI_f(z) \frac{dh(z)}{dz} \frac{\partial^2}{\partial z^2} \left(\frac{h(z)}{2} \phi \right) \right] = \rho I_p(z) \frac{\partial^2 \phi}{\partial t^2}. \end{aligned} \quad (9)$$

For harmonic vibration the angle of twist ϕ can be written in the form

$$\phi(z, t) = \theta(z) \sin \omega t. \quad (10)$$

Substituting equation (10) in equation (9) gives

$$\begin{aligned} \frac{d^2}{dz^2} \left[EI_f(z) h(z) \frac{d^2}{dz^2} \left(\frac{h(z)}{2} \theta \right) \right] - \frac{d}{dz} \left[Gc_s(z) \frac{d\theta}{dz} \right] \\ - 2 \frac{d}{dz} \left[EI_f(z) \frac{dh(z)}{dz} \frac{d^2}{dz^2} \left(\frac{h(z)}{2} \theta \right) \right] - \rho I_p(z) \omega^2 \theta = 0. \end{aligned} \quad (11)$$

When expanding the differential equation (11), terms containing $d^2 h(z) / dz^2$ are neglected as the depth taper considered in this study is linear.

Equation (11) is a fourth order differential equation with variable coefficients and a Galerkin-finite element method has been utilized in this study in obtaining the solutions for cantilever beams.

3. FINITE ELEMENT FORMULATION

In the Galerkin - finite element formulation [17], the domain of the beam is subdivided into a number of elements. A third degree polynomial for angle of twist in z is assumed over the element. The variation of torsional amplitude θ_e over each element, in terms of nodal degrees of freedom θ and θ' , is given by

$$\{\theta_e\} = [\chi]\{\delta_e\}, \quad (12)$$

where $[\chi]$ is the row matrix of shape functions

$$\{\delta\}_e = [\theta_1, \theta'_1, \theta_2, \theta'_2]^T. \quad (13)$$

Here primes denote differentiation with respect to z and subscripts 1 and 2 denote the two ends of the element.

Substituting equation (12) in equation (11) gives the residual R_e for the element as

$$R_e = \left[EI_f h \left(\frac{h}{2} \chi \right)'''' \right] \{\delta\}_e - [Gc_s \chi'] \{\delta\}_e - 2 \left[EI_f h' \left(\frac{h}{2} \chi \right)''' \right] \{\delta\}_e - \rho I_p \omega^2 \chi \{\delta\}_e. \quad (14)$$

In the Galerkin - finite element method, the weighted residual is minimized by setting

$$\frac{\partial}{\partial \{\delta\}_e} \int_0^L R_e \theta_e dz = 0. \quad (15)$$

This procedure is repeated for all elements and after the usual assembly procedure, the final matrix equation governing free vibration is obtained as

$$[A]\{\delta\} - \lambda_n^2 [B]\{\delta\} = 0, \quad (16)$$

where

$$\lambda_n^2 = A_{f0} \omega^2 L^4 / EI_{f0} \quad (17)$$

The quantities A_{f0} and I_{f0} are the flange area and moment of inertia respectively at the fixed end. Also, $[A]$ is the stiffness matrix, $[B]$ the mass matrix and $\{\delta\}$ the eigenvector. Equation (16) can be solved by using any standard eigenvalue algorithm to obtain the eigenvalues and eigenvectors $\{\delta\}$.

4. NUMERICAL RESULTS

Numerical values of the frequency parameter λ have been obtained, by dividing the beam into a sufficient number of elements, for the case of a tapered cantilever I-beam shown in the inset of Figure 1. It is found that 12-16 elements are sufficient to yield convergence. The cantilever beam chosen is of 76 cm in length and has the following dimensions at the fixed smaller end: width of the flanges, $b_0 = 31.55$ cm; depth of the web, $d_0 = 66.54$ cm. The boundary conditions considered at the fixed end ($z = 0$), are $\theta = \theta' = 0$.

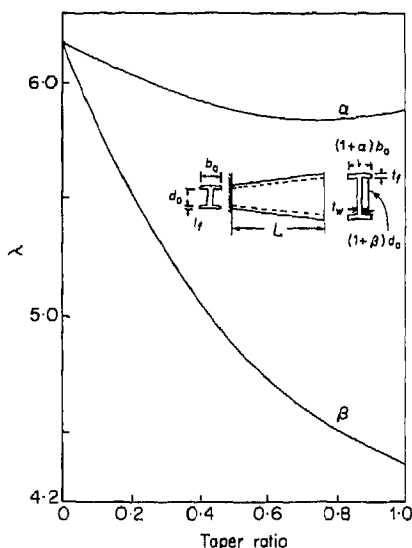


Figure 1. Effect of individual taper ratios (first mode). $b_0 = 31.55$; $d_0 = 66.54$; $t_{f0} = 3.11$; $t_w = 2.13$; $L = 760$ (all dimensions in mm).

The thickness of the flanges and the web are kept constant and are chosen as $t_f = 3.11$ cm and $t_w = 2.13$ cm respectively. The values of λ for various combinations of taper ratios α and β for the first three modes of vibration are presented in Figures 1-6. Figures 1-3 show the individual influences of taper ratios and Figures 4-6 show the combined effects.

4.1. INFLUENCE OF FLANGE WIDTH TAPER α

From Figure 1, it can be seen that, for $\beta = 0$, the first frequency decreases marginally up to a value of $\alpha = 0.7$ and thereafter increases slightly. It can be observed from Figures 2 and 3 that the torsional frequencies for the second and third modes increase significantly for increasing values of the taper ratio α . However, for higher modes it can be also noted

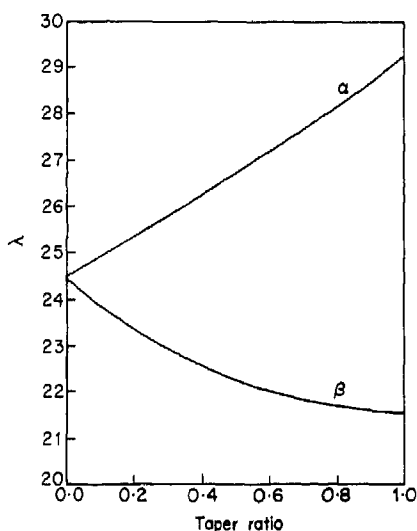


Figure 2. Effect of individual taper ratios (second mode).

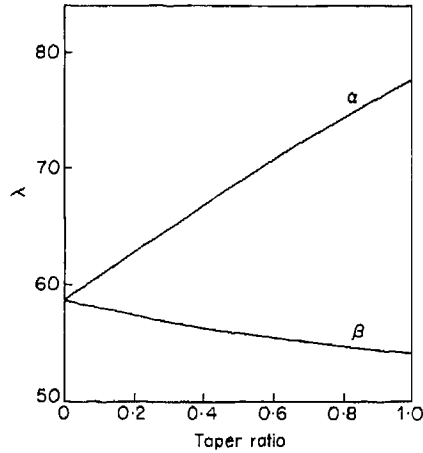


Figure 3. Effect of individual taper ratios (third mode).

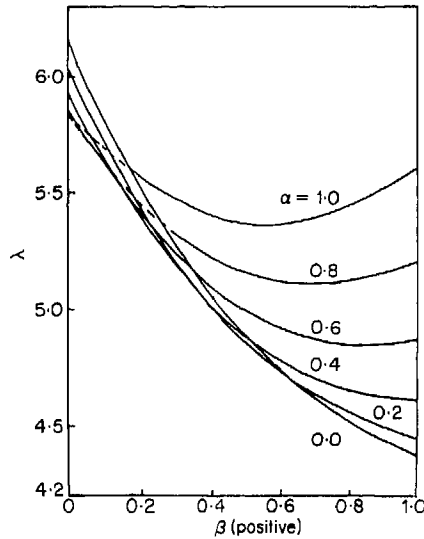


Figure 4. Combined influence of taper ratios (first mode).

that the flange taper α has a much larger influence on frequencies of vibration than the web taper β .

4.2. INFLUENCE OF WEB DEPTH TAPER β

Figures 1-3 clearly show that, for $\alpha = 0$, the first three torsional frequencies of vibration decreases significantly for increasing values of depth taper β . This decrease is comparatively significant in the first mode than that in other higher modes of vibration.

4.3. COMBINED INFLUENCE OF TAPER RATIOS α AND β

Figures 4-6 show the combined influence of the taper ratios α and β on the first three frequencies of vibration. In Figure 4, the intersection of various curves can be easily understood by recalling the opposite effects of the individual tapers α and β discussed in sections 4.1 and 4.2. It can be also observed that, for values of β in the range $0 < \beta \leq 0.4$,

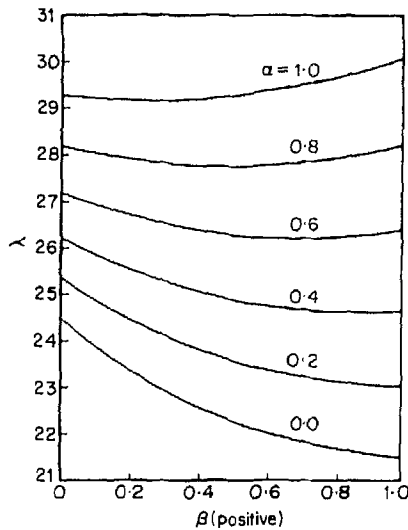


Figure 5. Combined influence of taper ratios (second mode).

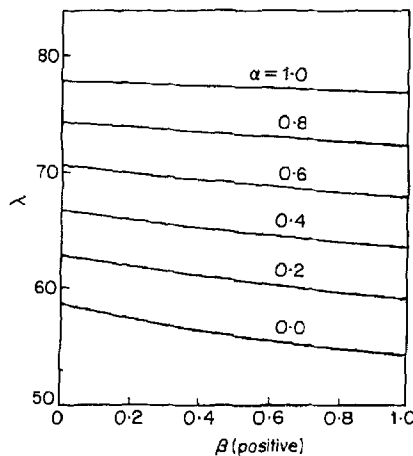


Figure 6. Combined influence of taper ratios (third mode).

the fundamental frequency decreases for increasing values of flange width taper α . In the range, $0.4 < \beta \leq 1.0$, the fundamental frequency increases for increasing values of α . Hence, the combined behaviour can be understood as a superposition of the individual influences of the taper ratios α and β on the frequencies.

Figures 5 and 6 reveal interesting trends. The various curves for the different values of the taper ratio α do not intersect. This is due to the opposing nature of the individual influences of α and β on the second and third mode frequencies. It can be observed from Figure 5 that for any constant value of α in the range $0 < \alpha \leq 0.6$ the influence of increasing values of β is to decrease the frequency of vibration. This is due to the fact that the percentage increase in the frequency due to increase in the taper ratio β is much higher than that due to α in this range. In the zone $0.6 < \alpha \leq 1.0$ the frequency of vibration marginally decreases up to a value of $\beta = 0.5$ and then increases for increasing values of β . From Figure 6, it can be seen that, for any constant value of α , the third mode frequency

decreases for increasing values of β . Further, for a constant value of β , the third mode frequency increases for increasing values of taper ratio α .

5. CONCLUDING REMARKS

The governing differential equation for the free torsional vibrations of tapered I-beams has been derived in this paper and solved for the case of a cantilever I-beam fixed at the smaller end by utilizing a Galerkin – finite element method. The effects of individual as well as combined linear tapers α and β in the flange width and web depth respectively on the first three torsional frequencies of vibration have been investigated. Except for a smaller range in the first mode of vibration, the effect of increase in flange width taper α in general is to increase significantly the frequencies of vibration. Interestingly, the effect of increase in web depth taper β is to decrease drastically the torsional frequency.

REFERENCES

1. V. Z. VLASOV 1961 *Thin-walled Elastic Beams*. Jerusalem: Israel Program of Scientific Translations.
2. J. M. GERE 1954 *Journal of Applied Mechanics* **21**, 381–387. Torsional vibrations of beams of thin-walled open section.
3. C. KAMESWARA RAO 1975 *Ph.D. thesis, Andhra University, Waltair*. Torsional vibrations and stability of thin-walled beams of open section resting on continuous elastic foundation.
4. C. SZYMCAK 1978 *Rozprawy Inzynierskie* **26**, 267–274. Torsional vibrations of thin-walled bars with bisymmetric cross-section (in Polish).
5. F. HAMAYCHI 1961 *Memorirs of the Faculty of Engineering, Hokkaido University*, **11**, 209. On torsion of I-beams with web of variable height.
6. G. C. LEE and B. A. SZABE 1967 *Proceedings of the American Society of Civil Engineers* **93**, *Journal of the Structural Division* **ST5**, 233–252. Torsional response of tapered I-girders.
7. P. WILDE 1968 *Archiwum Mechaniki Stosowanej* **20**, 431–443. On torsion of thin-walled bars with variable cross-section.
8. L. H. N. LEE 1956 *Journal of the Franklin Institute* **262**, 37–44. Non-uniform torsion of tapered I-beams.
9. C. MASSEY and P. J. MCGUIRE 1971 *Proceedings of the American Society of Civil Engineers* **97**, *Journal of the Engineering Mechanics Division* **EM3**, 673–686. Lateral stability of non-uniform cantilevers.
10. S. KITIPORNCHAI and N. S. TRAHAIR 1972 *Proceedings of the American Society of Civil Engineers* **98**, *Journal of the Structural Division* **ST3**, 713–728. Elastic stability of tapered I-beams.
11. T. G. BROWN 1981 *Proceedings of the American Society of Civil Engineers* **107**, *Journal of the Structural Division* **ST4**, 689–697. Lateral-torsional buckling of tapered I-beams.
12. G. C. CULVER and S. M. PREG 1968 *Proceedings of the American Society of Civil Engineers* **94**, *Journal of the Structural Division* **ST2**, 455–470. Elastic stability of tapered beam-columns.
13. H. SHIOMI and M. KURATA 1984 *Proceedings of the American Society of Civil Engineers* **110**, *Journal of Structural Engineering* **ST7**, 1630–1643. Strength formula for tapered beam-columns.
14. Z. CYWINSKI 1969 *Rozprawy Inzynierskie* **17**, 185–217. Statistics and dynamics in torsion of I-beams with variable bisymmetric cross-section (in Polish).
15. C. KAMESWARA RAO and P. K. SARMA 1975 *Journal of the Aeronautical Society of India* **27**, 169–171. The fundamental flexural frequency of simply-supported I-beams with uniform taper.
16. C. SZYMCAK 1983 *Journal of Sound and Vibration* **86**, 235–241. Optimal design of thin-walled I-beams for extreme natural frequency of torsional vibrations.
17. S. G. HUTTON and D. L. ANDERSON 1971 *Proceedings of the American Society of Civil Engineers* **97**, *Journal of the Engineering Mechanics Division* **EM5**, 1503–1520. Finite element method: a Galerkin approach.
18. R. H. GUTIERREZ and P. A. A. LAURA 1987 *Journal of Sound and Vibration* **114**, 393–397. Approximate analysis of coupled flexural-torsional vibrations of a beam of non-uniform cross-section using the optimized Rayleigh method.

APPENDIX: NOMENCLATURE

$[A]$	stiffness matrix
A_{f0}	area of the flanges at the smaller end of the beam
$[B]$	mass matrix
b	width of the flanges
b_0	width of flanges at smaller end
c_s	torsion constant
d	depth of the web
d_0	depth of web at smaller end
E	Young's modulus
G	shear modulus
h	distance between centerlines of the flanges
I_f	flange moment of inertia
I_p	polar moment of inertia
L	length of the beam
M	flange bending moment
R_e	residual, see equation (14)
T	twisting moment
t	time
t_f	thickness of the flange
z	distance along the length of the beam
α	taper parameter in width of the flanges
β	taper parameter in depth of the web
ϕ	angle of twist
θ	normal function of angle of twist
λ	torsional frequency parameter
ρ	mass density of the beam material
ω	natural frequency of vibration
$[\chi]$	row matrix of shape functions
$\{\delta\}$	eigenvector

A NOTE ON VIBRATIONS OF GENERALLY RESTRAINED BEAMS

C. KAMESWARA RAO AND S. MIRZA

*Department of Mechanical Engineering, University of Ottawa, 770 King Edward Avenue, Ottawa,
Ontario, Canada K1N 6N5*

(Received 15 August 1987, and in revised form 28 September 1988)

Exact frequency and normal mode shape expressions are derived in this note for generally restrained Bernoulli–Euler beams with unsymmetrical translations and rotations at either end. The eigenfrequencies and mode shape parameters are presented for a wide range of restraint parameters. Several degenerate cases have been studied, and some of these have been compared with those available in the published literature. It is believed that the results presented in this paper will be of use in design of beams, shafts and piping under dynamic considerations.

1. INTRODUCTION

Several investigators have studied the influence of flexible connections on the response characteristics of Bernoulli–Euler beams. These essential characteristics for classical [1–4] and some non-classical [5, 6] boundary conditions have already been documented in the literature. These dynamic characteristics are more useful in quickly estimating the response of beams for a specified dynamic loading. Exact expressions for frequency and mode shapes of a beam with one end on a spring and the other end free were derived by Chun [7]. The problem of free vibration of a beam supported by a rotational spring on one end and having a translational spring at the other end has been studied by Maurizi, Rossi and Reyes [8].

In an attempt to estimate the fundamental frequency of vibrating fuel rods, Passig [9] derived an exact frequency equation for a beam supported by symmetrical springs at either end of the beam. The problem of free vibration of a beam supported by non-symmetric springs was attempted by Hibbeler [10], but his frequency expression and results are found to be incorrect in view of improper boundary conditions [16]. Sundararajan [12] derived a simple algebraic expression for an upper bound to the fundamental frequency of beams with unsymmetric springs.

Fossman and Sorensen [13] have studied the response of elastically restrained cantilever Bernoulli–Euler beams and presented exact frequencies and mode shapes for the first four modes of vibration for a number of restraint parameters. Recently, Abbas [14, 15] has studied the problem of elastically restrained Timoshenko beams and presented some results for the degenerate case of Bernoulli–Euler beams also. However, with the exception of Chun [1] and Fossman and Sorensen [13], investigators did not pay much attention to the study of influence of flexible connections on the normal mode shapes of Bernoulli–Euler beams.

The present paper is concerned with the general problem of free vibration of partially restrained Bernoulli–Euler beams. Exact expressions for frequencies and normal mode shapes for the restrained beams with unsymmetric translations and rotations at either

end have been obtained. The eigenvalues are presented for a wide range of restraint parameters. Several degenerate cases have been discussed. It is believed that the expressions derived and the results presented will be of value in the design of beams, shafts and piping subjected to dynamic loads.

2. ANALYSIS

We consider a uniform Bernoulli-Euler beam of length L , shown in Figure 1, which is partially restrained against translation and rotation at its ends. The translational restraint is characterized by the spring constant S_1 at one end and S_3 at the other end and the rotational restraint by the spring constants S_2 and S_4 .

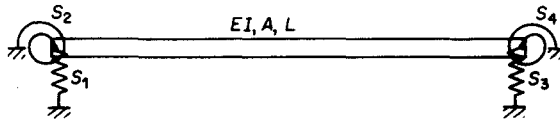


Figure 1. Geometry of generally restrained Bernoulli-Euler beam, showing the support system.

The differential equation for small-amplitude free flexural vibrations of a uniform beam can be stated as

$$EI \partial^4 y / \partial x^4 + \rho A \partial^2 y / \partial t^2 = 0, \quad (1)$$

where y is the lateral deflection, EI is the flexural rigidity of the beam, ρ the mass density, A the cross-sectional area, x the distance along the length of the beam and t is time.

The boundary conditions for this beam can be written, at $x=0$, as

$$EI \partial^3 y(0, t) / \partial x^3 = -S_1 y(0, t), \quad EI \partial^2 y(0, t) / \partial x^2 = S_2 \partial y(0, t) / \partial x, \quad (2a, b)$$

and, at $x=L$, as

$$EI \partial^3 y(L, t) / \partial x^3 = S_3 y(L, t), \quad EI \partial^2 y(L, t) / \partial x^2 = -S_4 \partial y(L, t) / \partial x. \quad (3a, b)$$

Using the method of separation of variables one assumes a solution of the form,

$$y(x, t) = \sum_{n=1}^{\infty} y_n(x) T(t), \quad (4)$$

where $y_n(x)$ is the n th mode of natural vibration and is given by

$$y_n(x) = c_1 \cosh \beta x + c_2 \sinh \beta x + c_3 \cos \beta x + c_4 \sin \beta x. \quad (5)$$

In equation (5), the parameter β is given by

$$\beta^4 = (\lambda / L)^4 = \omega_n^2 \rho A / (EI). \quad (6)$$

3. GENERAL FREQUENCY EQUATION

Substitution of equation (5) in equation (4), and then in equations (2) and (3), results in a set of four homogeneous equations in four constants, c_1 , c_2 , c_3 and c_4 . For a non-trivial solution the determinant of the coefficient matrix is set equal to zero, yielding the frequency

equation

$$\begin{aligned}
 & (\lambda^4 + R_1 T_1)(\lambda^4 + R_2 T_2) - 2\lambda^2(\lambda^4 R_1 R_2 - T_1 T_2) \sinh \lambda \sin \lambda \\
 & + [2\lambda^4(R_1 T_2 + R_2 T_1) - (\lambda^4 - R_1 T_1)(\lambda^4 - R_2 T_2)] \cosh \lambda \cos \lambda \\
 & - \lambda[(\lambda^4 - R_1 T_1)(\lambda^2 R_2 + T_2) + (\lambda^4 - R_2 T_2)(\lambda^2 R_1 + T_1)] \sin \lambda \cosh \lambda \\
 & - \lambda[(\lambda^4 - R_1 T_1)(\lambda^2 R_2 - T_2) + (\lambda^4 - R_2 T_2)(\lambda^2 R_1 - T_1)] \cos \lambda \sinh \lambda = 0, \quad (7)
 \end{aligned}$$

where

$$T_1 = S_1 L^3 / (EI), \quad R_1 = S_2 L / (EI), \quad T_2 = S_3 L^3 / (EI), \quad R_2 = S_4 L / (EI). \quad (8a, b)$$

Equation (7) can be conveniently used to obtain expressions for several degenerate cases by substituting extreme values of restraint parameters T_1 , R_1 , T_2 and R_2 . Some of these special cases are given below.

4. DEGENERATE CASES

Eight degenerate cases are to be considered, as follows.

(a) One end rotationally restrained ($T_1 \rightarrow \infty$, $R_1 = R$), the other free ($T_2 \rightarrow 0$ and $R_2 \rightarrow 0$):

$$R(1 + \cosh \lambda \cos \lambda) - \lambda(\sin \lambda \cosh \lambda - \cos \lambda \sinh \lambda) = 0. \quad (10)$$

Equation (10) agrees well with the one derived by Chun [7].

(b) One end rotationally restrained ($T \rightarrow \infty$, $R_1 = R$), the other with translational restraint ($T_2 = T$, $R_2 \rightarrow 0$):

$$\begin{aligned}
 & \lambda^3 R(1 + \cosh \lambda \cos \lambda) + 2\lambda T \sinh \lambda \sin \lambda \\
 & - (\lambda^4 - RT)(\sin \lambda \cosh \lambda - \cos \lambda \sinh \lambda) = 0. \quad (11)
 \end{aligned}$$

Equation (11) is similar to the one obtained in reference [8].

(c) Unsymmetric rotational restraints at the two ends ($T_1 \rightarrow \infty$, $T_2 \rightarrow \infty$):

$$\begin{aligned}
 & R_1 R_2 (1 - \cosh \lambda \cos \lambda) + 2\lambda^2 \sinh \lambda \sin \lambda \\
 & + \lambda(R_1 + R_2)(\sin \lambda \cosh \lambda - \cos \lambda \sinh \lambda) = 0. \quad (12)
 \end{aligned}$$

Equation (12) can be seen to be exactly the same as the one derived by Goel [16] for the case of zero concentrated mass. For $R_1 = R_2 = R$, equation (12) agrees well with the one derived by Passig [9].

(d) One end free ($T_1 \rightarrow 0$, $R_1 \rightarrow 0$) and the other with translational and rotational restraints ($T_2 \rightarrow T$, $R_2 \rightarrow R$):

$$\begin{aligned}
 & [(\lambda^4 - RT) - (\lambda^4 - RT) \cosh \lambda \cos \lambda] \\
 & - \lambda[(\lambda^2 R + T) \sin \lambda \cosh \lambda + (\lambda^2 R - T) \cos \lambda \sinh \lambda] = 0, \quad (13)
 \end{aligned}$$

which agrees exactly with the equations presented in reference [13].

(e) One end clamped ($T_1 \rightarrow \infty$, $R_1 \rightarrow \infty$) and the other with translational and rotational springs ($R_2 = R$, $T_2 = T$):

$$\begin{aligned}
 & [(\lambda^4 + RT) + (\lambda^4 - RT) \cosh \lambda \cos \lambda] \\
 & + \lambda[(\lambda^2 R + T) \sin \lambda \cosh \lambda + (\lambda^2 R - T) \cos \lambda \sinh \lambda] = 0. \quad (14)
 \end{aligned}$$

(f) One end simply supported ($T_1 \rightarrow \infty$, $R_1 \rightarrow 0$) and the other with translational and

rotational springs ($T_2 = T$, $R_2 = R$):

$$2\lambda^3 R \cosh \lambda \cos \lambda + 2\lambda T \sinh \lambda \sin \lambda - (\lambda^4 - RT)(\sin \lambda \cosh \lambda - \cos \lambda \sinh \lambda) = 0. \quad (15)$$

(g) One end guided vertically ($T_1 \rightarrow 0$, $R_1 \rightarrow \infty$) and the other with translational and rotational springs ($T_2 = T$, $R_2 = R$):

$$2\lambda T \cosh \lambda \cos \lambda - 2\lambda^3 R \sinh \lambda \sin \lambda - (\lambda^4 - RT)(\sin \lambda \cosh \lambda + \cos \lambda \sinh \lambda) = 0. \quad (16)$$

(h) Beam supported by unsymmetrical translational springs ($R_1 \rightarrow 0$, $R_2 \rightarrow 0$) (this case is for rotor bearing systems):

$$\lambda^6(1 - \cosh \lambda \cos \lambda) + 2T_1 T_2 \sinh \lambda \sin \lambda - \lambda^3(T_1 + T_2)(\sin \lambda \cosh \lambda - \cos \lambda \sinh \lambda) = 0. \quad (17)$$

Several other special cases can be derived and in each case computational techniques can be used to generate the frequencies.

5. MODAL SHAPE

For each frequency there exists a corresponding mode shape of vibration which can be obtained from the expression

$$Y_n(\xi) = c_1(\cosh \lambda \xi - \delta \sinh \lambda \xi + \gamma_1 \cos \lambda \xi + \gamma_2 \sin \lambda \xi), \quad (18)$$

where

$$\xi = x/L, \quad \delta = \frac{f_1 + g_1 f_2 - g_2 f_3}{f_4 - g_1 f_3 - g_3 f_2} = \frac{f'_4 - g_1 f'_3 - g_2 f'_2}{f'_1 - g_1 f'_2 + g_3 f'_3}, \quad (19a)$$

$$\gamma_1 = g_1 + g_3 \delta, \quad \gamma_2 = g_2 - g_1 \delta, \quad (19b)$$

$$g_1 = (\lambda^4 - R_1 T_1)/(\lambda^4 + R_1 T_1), \quad g_2 = 2\lambda T_1/(\lambda^4 + R_1 T_1), \quad (19c)$$

$$g_3 = 2\lambda^3 R_1/(\lambda^4 + R_1 T_1),$$

$$\begin{aligned} f_1 &= \lambda^3 \sinh \lambda - T_2 \cosh \lambda, & f'_1 &= \lambda \sinh \lambda + R_2 \cosh \lambda, \\ f_2 &= \lambda^3 \sin \lambda - T_2 \cos \lambda, & f'_2 &= \lambda \sin \lambda - R_2 \cos \lambda, \\ f_3 &= \lambda^3 \cos \lambda + T_2 \sin \lambda, & f'_3 &= \lambda \cos \lambda + R_2 \sin \lambda, \\ f_4 &= \lambda^3 \cosh \lambda - T_2 \sinh \lambda, & f'_4 &= \lambda \cosh \lambda + R_2 \sinh \lambda. \end{aligned} \quad (19d)$$

Equation (18) was found to agree very well with all the various degenerate cases available in the published literature.

6. NUMERICAL RESULTS

For a given uniform Bernoulli-Euler beam with partial translational and rotational restraints, T_1 , R_1 , T_2 and R_2 are defined and the frequencies and corresponding mode shapes can be obtained from equations (7) and (18) respectively. Although a wide range of numerical results have been generated, due to space limitations, only a few typical cases showing the influence of partial restraints on the first five frequencies and mode shape factors are presented in this paper. The other results will be reported elsewhere.

The following three cases are chosen for discussion in this paper: Case 1: symmetrical translational and rotational springs at either end, $R_2 = R_1 = R$ and $T_2 = T_1 = T$; Case 2: symmetrical rotational springs, but unsymmetrical translational springs at either end, $R_2 = R_1 = R$ and $T = T_1 = T_2/100$; Case 3: unsymmetrical translational and rotational springs at either end, $R = R_1 = R_2/100$ and $T = T_1 = T_2/100$.

Tables 1, 2 and 3 contain the frequency parameter $\lambda(\beta L)$ for the above three cases. It may be pointed out that the mode shape equation (18) is defined in terms of non-dimensional parameters δ , γ_1 and γ_2 . The values of the parameter δ for the three cases are presented in Tables 4, 5 and 6, respectively. For Case 3, the values of γ_1 and γ_2 are presented in Tables 7 and 8 corresponding to the first five values of the frequency parameter λ which are given in Table 3.

TABLE 1

First five values of λ for generally restrained Bernoulli-Euler beams for various values of R and T ($R_2 = R_1 = R$, $T_2 = T_1 = T$)

R	Mode				
	1	2	3	4	5
<i>T = 0.10</i>					
0.01	0.668464	0.956995	4.735993	7.856163	10.997575
0.10	0.668473	1.309211	4.771548	7.878716	11.013751
1.00	0.668539	2.110991	5.050215	8.073408	11.159847
10.00	0.668655	2.891977	5.839931	8.830518	11.853961
100.00	0.668689	3.114298	6.223295	9.335775	12.449364
1000.00	0.668694	3.141694	6.277334	9.415527	12.553946
<i>T = 1.00</i>					
0.01	1.184305	1.579241	4.752892	7.859877	10.998928
0.10	1.184479	1.696265	4.787949	7.882388	11.015097
1.00	1.185645	2.233310	5.063136	8.076710	11.161117
10.00	1.187696	2.933358	5.846051	8.832472	11.854824
100.00	1.188301	3.144179	6.227220	9.336969	12.449880
1000.00	1.188374	3.170358	6.280993	9.416615	12.554406
<i>T = 10</i>					
0.01	2.032659	2.768866	4.916849	7.897181	11.012509
0.10	2.035385	2.788458	4.947253	7.919256	11.028597
1.00	2.054026	2.933271	5.189702	8.109836	11.173850
10.00	2.088258	3.270873	5.906928	8.852036	11.863475
100.00	2.098730	3.403000	6.266457	9.348932	12.455050
1000.00	2.099997	3.420269	6.317602	9.427513	12.559013
<i>T = 100</i>					
0.01	2.878769	4.663787	6.077217	8.277362	11.152463
0.10	2.896360	4.663806	6.086466	8.294714	11.167635
1.00	3.029676	4.663961	6.165789	8.445450	11.304408
10.00	3.361188	4.664462	6.462484	9.049539	11.951128
100.00	3.497751	4.664729	6.648886	9.470611	12.507389
1000.00	3.515830	4.664770	6.677590	9.538559	12.605675

TABLE 2

First five values of λ for generally restrained Bernoulli-Euler beams for various values of R and T ($R = R_1 = R_2$, $T = T_1 = T_2/100$)

R	Mode				
	1	2	3	4	5
$T = 0.10$					
0.01	0.773035	2.459819	4.831716	7.876835	11.005057
0.10	0.960041	2.484818	4.864344	7.899144	11.021189
1.00	1.391053	2.675441	5.122811	8.091744	11.166862
10.00	1.644356	3.115533	5.873967	8.841314	11.858723
100.00	1.686817	3.279332	6.245097	9.342368	12.452209
1000.00	1.691388	3.300382	6.297662	9.421532	12.556481
$T = 1.00$					
0.01	1.315227	3.624708	5.633820	8.086649	11.077385
0.10	1.366623	3.646422	5.647211	8.106033	11.093029
1.00	1.654075	3.802732	5.763474	8.274346	11.234190
10.00	2.112540	4.122149	6.199292	8.944860	11.903536
100.00	2.269050	4.224131	6.460114	9.405242	12.478831
1000.00	2.289285	4.236410	6.499061	9.478813	12.580200
$T = 10$					
0.01	2.231039	4.066281	6.907516	9.562281	11.956471
0.10	2.242055	4.092155	6.922573	9.569687	11.964209
1.00	2.328941	4.297243	7.051167	9.635639	12.035706
10.00	2.578979	4.923981	7.526142	9.921744	12.414734
100.00	2.701713	5.287801	7.829838	10.129361	12.788030
1000.00	2.719110	5.345134	7.878408	10.162703	12.857943
$T = 100$					
0.01	2.989992	5.144780	7.371291	10.256407	13.266117
0.10	3.011413	5.150857	7.385468	10.268246	13.274934
1.00	3.177594	5.206735	7.509945	10.375725	13.356758
10.00	3.623440	5.491684	8.058015	10.915833	13.814301
100.00	3.817067	5.752920	8.548016	11.489735	14.373666
1000.00	3.842622	5.800003	8.642199	11.613812	14.506334

TABLE 3

First five values of λ for generally restrained Bernoulli-Euler beams for various values of R and T ($R = R_1 = R_2/100$, $T = T_1 = T_2/100$)

R	Mode				
	1	2	3	4	5
$T = 0.10$					
0.01	1.238122	2.510150	4.977661	7.985393	11.086464
0.10	1.536584	2.636521	5.358913	8.377352	11.446125
1.00	1.634071	2.847163	5.650639	8.708708	11.806661
10.00	1.681749	3.183474	6.074594	9.123442	12.200960
100.00	1.690798	3.288558	6.273368	9.385670	12.509540
1000.00	1.691790	3.301338	6.300611	9.426106	12.562619
$T = 1.00$					
0.01	1.531633	3.655384	5.667830	8.177654	11.155761
0.10	1.870949	3.756650	5.780093	8.500828	11.496614
1.00	2.075799	3.903110	5.939151	8.786629	11.838017
10.00	2.243645	4.142369	6.295445	9.185769	12.226591
100.00	2.286114	4.226178	6.475621	9.443001	12.533211
1000.00	2.291046	4.236614	6.500707	9.482816	12.586029
$T = 10$					
0.01	2.324034	4.145887	6.944055	9.563429	11.975898
0.10	2.535983	4.456845	7.121630	9.575803	12.067017
1.00	2.644496	4.794548	7.366170	9.643060	12.205476
10.00	2.702192	5.178009	7.687266	9.921949	12.529087
100.00	2.718858	5.329757	7.856992	10.129463	12.811061
1000.00	2.720894	5.349618	7.881330	10.162720	12.860489
$T = 100$					
0.01	3.107827	5.193899	7.422552	10.294993	13.291462
0.10	3.444654	5.404187	7.691510	10.525668	13.456763
1.00	3.652671	5.604957	8.059137	10.918002	13.798358
10.00	3.783499	5.737043	8.422038	11.314610	14.169702
100.00	3.837305	5.796210	8.620374	11.580250	14.463721
1000.00	3.844697	5.804663	8.650176	11.624110	14.516931

TABLE 4

First five values of δ for generally restrained Bernoulli-Euler beams for various values of R and T ($R_2 = R_1 = R$, $T_2 = T_1 = T$)

R	Mode				
	1	2	3	4	5
$T = 0.10$					
0.01	0.318874	2.246995	0.982605	1.000774	0.999967
0.10	0.322096	1.739849	0.983208	1.000757	0.999967
1.00	0.322333	1.275618	0.987266	1.000623	0.999972
10.00	0.322397	1.117448	0.994199	1.000292	0.999986
100.00	0.322416	1.092949	0.996042	1.000176	0.999992
1000.00	0.322417	1.090331	0.996250	1.000162	0.999993
$T = 1.00$					
0.01	0.531409	1.519308	0.982894	1.000772	0.999967
0.10	0.531517	1.449080	0.983478	1.000754	0.999967
1.00	0.531931	1.240076	0.987428	1.000621	0.999971
10.00	0.532665	1.112419	0.994234	1.000291	0.999986
100.00	0.532874	1.090087	0.996058	1.000175	0.999992
1000.00	0.532906	1.087658	0.996264	1.000162	0.999993
$T = 10$					
0.01	0.768367	1.133863	0.985462	1.000744	0.999967
0.10	0.768927	1.131097	0.985895	1.000728	0.999967
1.00	0.772711	1.112429	0.988914	1.000601	0.999972
10.00	0.779512	1.078943	0.994573	1.000285	0.999986
100.00	0.781560	1.068837	0.996210	1.000174	0.999992
1000.00	0.781807	1.067618	0.996399	1.000160	0.999993
$T = 100$					
0.01	0.893574	1.019048	0.995421	1.000508	0.999971
0.10	0.895334	1.019068	0.995463	1.000499	0.999972
1.00	0.907795	1.019043	0.995809	1.000430	0.999975
10.00	0.932939	1.019031	0.996881	1.000235	0.999987
100.00	0.941247	1.019026	0.997413	1.000154	0.999993
1000.00	0.942270	1.019018	0.997486	1.000143	0.999993

TABLE 5

First five values of δ for generally restrained Bernoulli-Euler beams for various values of R and T ($R = R_1 = R_2$, $T = T_1 = T_2/100$)

R	Mode				
	1	2	3	4	5
$T = 0.10$					
0.01	1.512054	1.286930	0.982753	1.000774	0.999967
0.10	1.204728	1.280595	0.983332	1.000757	0.999967
1.00	0.672163	1.240899	0.987233	1.000624	0.999972
10.00	0.161736	1.253462	0.993766	1.000296	0.999986
100.00	0.049742	4.101789	0.993515	1.000199	0.999992
1000.00	0.037821	-0.344027	0.974675	1.000364	0.999990
$T = 1.00$					
0.01	1.148581	1.024701	0.990094	1.000737	0.999967
0.10	1.102421	1.025949	0.990201	1.000722	0.999967
1.00	0.876442	1.037868	0.991010	1.000605	0.999972
10.00	0.483730	1.160060	0.991872	1.000325	0.999986
100.00	0.275605	12.660498	0.976757	1.000392	0.999989
1000.00	0.241855	-0.507629	0.884113	1.001933	0.999966
$T = 10$					
0.01	1.021346	1.002141	0.999468	1.000120	0.999982
0.10	1.014576	1.002579	0.999449	1.000121	0.999983
1.00	0.966170	1.006483	0.999260	1.000130	0.999983
10.00	0.850149	1.032566	0.997648	1.000216	0.999986
100.00	0.792461	1.148323	0.984912	1.001032	0.999968
1000.00	0.783619	1.273911	0.949931	1.005309	0.999821
$T = 100$					
0.01	1.003100	1.000169	0.999971	1.000005	0.999999
0.10	0.994563	1.000279	0.999962	1.000006	0.999999
1.00	0.966674	1.001292	0.999882	1.000009	0.999999
10.00	0.965152	1.006556	0.999357	1.000035	0.999998
100.00	0.969645	1.012197	0.997900	1.000170	0.999989
1000.00	0.970274	1.013453	0.997009	1.000381	0.999962

TABLE 6

First five values of δ for generally restrained Bernoulli-Euler beams for various values of R and T ($R = R_1 = R_2/100$, $T = T_1 = T_2/100$)

R	Mode				
	1	2	3	4	5
$T = 0.10$					
0.01	0.817908	1.199075	0.987760	1.000614	0.999972
0.10	0.568518	1.084713	0.996724	1.000192	0.999989
1.00	0.401251	1.055576	0.999315	1.000026	0.999999
10.00	0.138024	1.115679	0.999466	1.000008	1.000000
100.00	0.048855	3.091267	0.997414	1.000024	1.000000
1000.00	0.037754	-0.349476	0.978041	1.000205	0.999997
$T = 1.00$					
0.01	0.931357	1.031631	0.991648	1.000593	0.999972
0.10	0.779198	1.051801	0.995445	1.000216	0.999990
1.00	0.698799	1.069913	0.997140	1.000057	0.999998
10.00	0.447912	1.191409	0.996137	1.000050	0.999999
100.00	0.270415	16.179428	0.979925	1.000220	0.999997
1000.00	0.241298	-0.506074	0.885783	1.001789	0.999973
$T = 10$					
0.01	0.970867	1.006060	0.999309	1.000124	0.999984
0.10	0.905423	1.015680	0.998694	1.000137	0.999989
1.00	0.875590	1.019865	0.998186	1.000154	0.999994
10.00	0.817220	1.039381	0.996756	1.000221	0.999993
100.00	0.787361	1.152610	0.984201	1.001025	0.999974
1000.00	0.783076	1.275180	0.949660	1.005304	0.999825
$T = 100$					
0.01	0.931296	1.001193	0.999888	1.000008	0.999999
0.10	0.872169	1.004176	0.999586	1.000026	0.999998
1.00	0.913119	1.005816	0.999422	1.000037	0.999998
10.00	0.958877	1.008950	0.999124	1.000051	0.999997
100.00	0.969081	1.012675	0.997838	1.000175	0.999989
1000.00	0.970219	1.013507	0.996999	1.000381	0.999961

TABLE 7

First five values of γ_1 for generally restrained Bernoulli-Euler beams for various values of R and T ($R = R_1 = R_2/100$, $T = T_1 = T_2/100$)

R	Mode				
	1	2	3	4	5
$T = 0.10$					
0.01	1.01235	1.00950	1.00397	1.00251	1.00180
0.10	1.07028	1.08185	1.03717	1.02387	1.01747
1.00	1.45665	1.73733	1.35347	1.22962	1.16938
10.00	2.23679	7.92231	4.28676	3.19157	2.63905
100.00	2.49838	174.03435	32.58151	22.27957	16.98044
1000.00	2.53085	-114.86171	292.81445	210.54071	159.55721
$T = 1.00$					
0.01	1.00851	1.00553	1.00348	1.00244	1.00179
0.10	1.06643	1.05496	1.03426	1.02349	1.01738
1.00	1.53666	1.53730	1.33391	1.22726	1.16884
10.00	3.29701	6.49767	4.13195	3.17153	2.63415
100.00	4.50456	583.45728	29.52887	21.89638	16.88506
1000.00	4.70145	-58.72514	174.97775	188.81155	153.73555
$T = 10$					
0.01	1.00149	1.00417	1.00279	1.00207	1.00166
0.10	1.02251	1.04041	1.02726	1.02065	1.01648
1.00	1.21027	1.38038	1.26333	1.20489	1.16288
10.00	1.79894	4.28010	3.46539	2.97520	2.58173
100.00	2.10457	19.20818	20.42958	18.87639	15.98067
1000.00	2.14848	35.24100	66.65125	102.14421	114.32745
$T = 100$					
0.01	0.98472	1.00111	1.00203	1.00176	1.00144
0.10	0.91465	1.01356	1.02022	1.01736	1.01425
1.00	0.60073	1.14188	1.19597	1.16793	1.13904
10.00	0.20215	1.86897	2.64764	2.55105	2.32888
100.00	0.11434	2.74680	7.94754	11.38623	11.88367
1000.00	0.10473	2.94244	11.32798	25.88213	41.98274

TABLE 8

First five values of γ_2 for generally restrained Bernoulli-Euler beams for various values of R and T ($R = R_1 = R_2/100$, $T = T_1 = T_2/100$)

R	Mode				
	1	2	3	4	5
$T = 0.10$					
0.01	-0.711882	-1.186370	-0.986135	-1.000220	-0.999824
0.10	-0.511455	-1.073352	-0.995400	-0.999846	-0.999855
1.00	-0.344949	-1.043715	-0.998009	-0.999687	-0.999867
10.00	-0.069973	-1.088021	-0.997107	-0.999456	-0.999799
100.00	0.023520	-2.599088	-0.983812	-0.997208	-0.999081
1000.00	0.035165	0.033023	-0.860571	-0.974947	-0.991898
$T = 1.00$					
0.01	-0.372360	-0.990571	-0.980644	-0.996931	-0.998530
0.10	-0.463671	-1.013038	-0.984910	-0.996920	-0.998661
1.00	-0.415199	-1.027241	-0.985999	-0.996774	-0.998690
10.00	-0.067456	-1.085926	-0.975567	-0.994667	-0.998010
100.00	0.190297	-8.436342	-0.867498	-0.973027	-0.990912
1000.00	0.232817	-0.253042	-0.245197	-0.779195	-0.922362
$T = 10$					
0.01	0.623642	-0.724815	-0.939496	-0.977237	-0.988329
0.10	0.334660	-0.785200	-0.942568	-0.977129	-0.988513
1.00	0.319542	-0.803890	-0.941559	-0.975570	-0.988098
10.00	0.601331	-0.659058	-0.898458	-0.959544	-0.981780
100.00	0.757330	0.182158	-0.542381	-0.809772	-0.919212
1000.00	0.779951	1.092004	0.432242	-0.022607	-0.457623
$T = 100$					
0.01	5.680637	0.427009	-0.510322	-0.816551	-0.914764
0.10	3.812221	0.271593	-0.555605	-0.827031	-0.917340
1.00	2.371514	0.210588	-0.579895	-0.833460	-0.918578
10.00	1.260743	0.510416	-0.388520	-0.754899	-0.882989
100.00	1.003066	0.911428	0.398934	-0.202575	-0.574195
1000.00	0.973661	1.002233	0.907661	0.711150	0.405018

7. CONCLUSIONS

Exact frequency and normal mode expressions for generally restrained Bernoulli-Euler beams have been derived and results for the first five eigenfrequencies and mode shape parameters for typical cases have been presented. The expressions derived and results presented check with the degenerate cases available in the published literature.

It can be seen from the various results presented in this paper that both the translational and rotational spring constants have a significant effect on the first three frequencies and mode shapes of vibration. It is seen that the higher mode frequencies, comparatively, do not show much variation with the range of spring constants considered in this investigation. This study also shows that, in general, the translational spring constant has relatively greater influence on frequencies and mode shapes than the rotational spring constant.

REFERENCES

1. R. E. D. BISHOP and D. C. JOHNSON 1956 *Vibration Analysis Tables*. Cambridge University Press.

2. T. C. CHANG and R. R. CRAIG 1969 *Journal of the Engineering Mechanics Division*, American Society of Civil Engineers **11**, 1027-1031. Normal modes of uniform beams.
3. S. TIMOSHENKO, D. H. YOUNG and W. WEAVER JR. 1974 *Vibration Problems in Engineering*. New York: Wiley.
4. D. YOUNG and R. P. FELGAR JR. 1949 *Tables of Characteristic Functions Representing Normal Modes of Vibration of a Beam*. University of Texas publication, No. 4913.
5. D. J. GORMAN 1975 *Free Vibration Analysis of Beams and Shafts*. New York: Wiley.
6. R. D. BLEVINS 1979 *Formulas for Natural Frequency and Mode Shape*. New York: Van Nostrand.
7. K. R. CHUN 1972 *Journal of Applied Mechanics* **39**, 1154-1155. Free vibration of a beam with one end spring-hinged and the other free.
8. M. J. MAURIZI, R. E. ROSSI and J. A. REYES 1976 *Journal of Sound and Vibration* **48**, 565-568. Vibration frequencies for a beam with one end spring-hinged and subjected to a translational restraint at the other end.
9. E. G. PASSIG 1970 *Nuclear Engineering and Design* **14**, 198-200. End slope and fundamental frequency of vibrating fuel rods.
10. R. C. HIBBELER 1975 *Journal of Applied Mechanics* **42**, 501-502. Free vibration of a beam supported by unsymmetrical spring-hinges.
11. E. M. NASSAR and W. H. HORTON 1976. *American Institute of Aeronautics and Astronautics Journal* **14**, 122-123. Static deflection of beams subjected to elastic rotational restraints.
12. C. SUNDARARAJAN 1979 *Journal of Mechanical Design* **101**, 711-712. Fundamental frequency of beams with elastic rotational restraints.
13. R. FOSSMAN and A. SORENSEN JR. 1980 *Journal of Mechanical Design* **102**, 829-834. Influence of flexible connections on response characteristics of a beam.
14. B. A. H. ABBAS 1984 *Journal of Sound and Vibration* **97**, 541-548. Vibrations of Timoshenko beams with elastically restrained ends.
15. B. A. H. ABBAS 1985 *The Aeronautical Journal* **89**, 10-16. Dynamic analysis of thick rotating blades with flexible roots.
16. R. P. GOEL 1976 *Journal of Sound and Vibration* **47**, 9-14. Free vibrations of a beam-mass system with elastically restrained ends.

FREQUENCY ANALYSIS OF CLAMPED-CLAMPED UNIFORM BEAMS WITH INTERMEDIATE ELASTIC SUPPORT

1. INTRODUCTION

Several researchers studied the problem of free lateral vibration of single-span and multi-span uniform Bernoulli-Euler beams [1-9]. Many handbooks have also appeared in the literature [10-12] giving frequency tables and mode-shape expressions for various cases. However, a thorough literature search carried out by the author revealed the lack of explicit and exact frequency and mode-shape expressions, even for double-span beams with classical end conditions and with an arbitrarily located intermediate elastic support.

The problem of free lateral vibrations of clamped-clamped uniform Bernoulli-Euler beams with arbitrarily located intermediate elastic support was first treated by Gorman [11] in his book (case 3.16, ch. 3, p. 85). He presented a set of simultaneous equations for mode shapes which can be used in conjunction with frequency tables given in his book. Very recently, Maurizi and Bambill De Rossit [14] treated this problem again in a slightly more complicated way and presented an 8×8 matrix frequency equation. In addition, they have given a frequency chart showing only the variation of the fundamental frequency. Results for higher mode frequencies were not reported. Further, none of the above studies attempted to provide explicit and exact frequency and mode-shape expressions for this important case. With the increasing availability of personal computers and high-precision programmable calculators, the utility of explicit and exact frequency and mode-shape expressions need not be over-emphasized. In the present paper, explicit and exact frequency and mode-shape expressions for the title problem are given, and extensive design data is provided for the first five frequencies of vibration for various values of non-dimensional position and stiffness parameters of the intermediate elastic support.

2. ANALYSIS

A two-span clamped-clamped uniform Bernoulli-Euler beam with an intermediate elastic support of stiffness S is considered here (see Figure 1). When the beam is assumed to undergo harmonic free oscillations, the governing differential equation can be written as

$$Y''''(\xi) - \beta^4 Y(\xi) = 0, \quad (1)$$

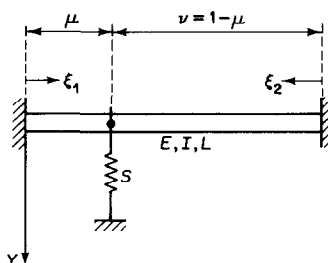


Figure 1. Clamped-clamped beam with intermediate elastic support.

where $\beta^4 = \rho A \omega^2 L^4 / (EI)$, ρ is the mass density of the beam material, A is the area of cross-section, E is the Young's modulus, I is the area moment of inertia, ω is the circular frequency, L is the overall length of the beam, and $\xi = x/l$ is the non-dimensional beam length.

The spatial co-ordinates measured along the spans as well as the transverse displacements are normalized with respect to the overall beam length L . The first span length is designated as μ , with limits $0 < \mu < 1$. The second span length then becomes $\nu = 1 - \mu$.

The governing differential equation (1) is satisfied by expressing the first and second span deflections, respectively, as

$$Y_1(\xi_1) = A_1 \cosh \beta \xi_1 + B_1 \sinh \beta \xi_1 + C_1 \cos \beta \xi_1 + D_1 \sin \beta \xi_1, \quad (2)$$

$$Y_2(\xi_2) = A_2 \cosh \beta \xi_2 + B_2 \sinh \beta \xi_2 + C_2 \cos \beta \xi_2 + D_2 \sin \beta \xi_2, \quad (3)$$

where subscripts 1 and 2 refer to the left-hand and right-hand spans respectively.

3. BOUNDARY CONDITIONS

The problem of enforcing the boundary conditions is simplified by measuring ξ 's in each span from the beam outer end. Evidently, a total of eight boundary conditions are required in order to determine the arbitrary constants A_1, B_1, C_1, D_1 and A_2, B_2, C_2, D_2 of equations (2) and (3) given above. Four of these equations can be written on the basis of the boundary conditions existing at the beam outer ends. Three more equations can be written by enforcing the conditions of continuity of beam displacement, slope and bending moment across the intermediate elastic support. The last equation can be written for the continuity of the shear force across the support, taking into account the contribution from the elastic support.

The first four boundary conditions at the two outer ends of the clamped-clamped beam can be written as follows:

At $\xi_1 = 0$,

$$Y_1(0) = 0, \quad Y_1'(0) = 0 \quad (4)$$

and at $\xi_2 = 0$,

$$Y_2(0) = 0, \quad Y_2'(0) = 0. \quad (5)$$

At this stage, using the above boundary conditions, one can express the span deflections Y_1 and Y_2 as follows:

$$Y_1(\xi_1) = C_1(\cos \beta \xi_1 - \cosh \beta \xi_1) + D_1(\sin \beta \xi_1 - \sinh \beta \xi_1), \quad (6)$$

$$Y_2(\xi_2) = C_2(\cos \beta \xi_2 - \cosh \beta \xi_2) + D_2(\sin \beta \xi_2 - \sinh \beta \xi_2). \quad (7)$$

The remaining four boundary conditions at the intermediate elastic support at $\xi_1 = \mu$ and $\xi_2 = \nu$ are

$$Y_1(\mu) - Y_2(\nu) = 0, \quad Y_1'(\mu) + Y_2'(\nu) = 0, \quad (8)$$

$$Y_1''(\mu) - Y_2''(\nu) = 0, \quad Y_1'''(\mu) + Y_2'''(\nu) - TY_1(\mu) = 0, \quad (9)$$

where

$$T = SL^3 / (EI). \quad (10)$$

4. FREQUENCY EQUATIONS

Substituting equations (6) and (7) in the boundary conditions (8) and (9), a set of four homogeneous linear algebraic equations in four constants C_1, C_2, D_1 and D_2 are obtained.

In order that the solutions other than zero may exist, the determinant of the coefficients of these arbitrary constants must be equal to zero. This leads to the frequency equation for the clamped-clamped beam with intermediate elastic support, from which the natural frequencies can be determined by utilising numerical methods in conjunction with efficient algorithms [13].

Without much difficulty, we obtain the explicit frequency equation for this important case as follows:

$$2\beta^3(1 - \cos \beta \cosh \beta) + T[(1 - \cos \beta \mu \cosh \beta \mu)(\sin \beta \nu \cosh \beta \nu - \cos \beta \nu \sinh \beta \nu) + (1 - \cos \beta \nu \cosh \beta \nu)(\sin \beta \mu \cosh \beta \mu - \cos \beta \mu \sinh \beta \mu)] = 0. \quad (11)$$

When the intermediate support is pinned, i.e., $T \rightarrow \infty$, equation (11) reduces to

$$(1 - \cos \beta \mu \cosh \beta \mu)(\sin \beta \nu \cosh \beta \nu - \cos \beta \nu \sinh \beta \nu) + (1 - \cos \beta \nu \cosh \beta \nu)(\sin \beta \mu \cosh \beta \mu - \cos \beta \mu \sinh \beta \mu) = 0. \quad (12)$$

which tallies exactly with the one derived earlier by this author [9].

5. MODE-SHAPE EXPRESSIONS

For various values of μ and $\nu = 1 - \mu$, the roots of equation (11), β_n , $n = 1, 2, 3, \dots$, give the eigenvalues of the problem. The corresponding eigenfunctions, normal modes Y_1 and Y_2 can be explicitly expressed as

$$Y_1(\xi_1) = (\sin \beta \xi_1 - \sinh \beta \xi_1) + \alpha_1(\cos \beta \xi_1 - \cosh \beta \xi_1), \quad (13)$$

$$Y_2(\xi_2) = \alpha_2[(\sin \beta \xi_2 - \sinh \beta \xi_2) + \alpha_3(\cos \beta \xi_2 - \cosh \beta \xi_2)], \quad (14)$$

in which

$$\alpha_1 = F_1/F_2, \quad \alpha_2 = F_3/F_4, \quad \alpha_3 = F_5/F_6, \quad (15)$$

where

$$F_1 = \Phi_4 f_6 + \Phi_1 f_5 - \Phi_2 f_4, \quad F_2 = \Phi_5 f_5 - \Phi_3 f_6 + \Phi_1 f_4, \quad (16, 17)$$

$$F_3 = \Psi_1 f_2 - \Psi_2 f_1 + \Psi_4 f_3, \quad (18)$$

$$F_4 = \Phi_1 f_5 - \Phi_2 f_4 + \Phi_4 f_6, \quad F_5 = \Psi_1 f_1 + \Psi_4 f_2 - \Psi_3 f_3, \quad (19, 20)$$

$$F_6 = \Psi_1 f_2 - \Psi_2 f_1 + \Psi_4 f_3. \quad (21)$$

Here

$$f_1 = 1 - \cos \beta \mu \cosh \beta \mu, \quad f_2 = \cos \beta \mu \sinh \beta \mu - \sin \beta \mu \cosh \beta \mu, \quad (22)$$

$$f_3 = \sin \beta \mu \sinh \beta \mu, \quad f_4 = 1 - \cos \beta \nu \cosh \beta \nu, \quad (23)$$

$$f_5 = \cos \beta \nu \sinh \beta \nu - \sin \beta \nu \cosh \beta \nu, \quad f_6 = \sin \beta \nu \sinh \beta \nu, \quad (24)$$

$$\Phi_1 = \sin \beta \mu + \sinh \beta \mu, \quad \Phi_2 = \cos \beta \mu + \cosh \beta \mu, \quad (25)$$

$$\Phi_3 = \sin \beta \mu - \sinh \beta \mu, \quad \Phi_4 = \cos \beta \mu - \cosh \beta \mu, \quad (26)$$

$$\Psi_1 = \sin \beta \nu + \sinh \beta \nu, \quad \Psi_2 = \cos \beta \nu + \cosh \beta \nu, \quad (27)$$

$$\Psi_3 = \sin \beta \nu - \sinh \beta \nu, \quad \Psi_4 = \cos \beta \nu - \cosh \beta \nu. \quad (28)$$

6. RESULTS AND DISCUSSION

For a given two-span beam with μ and $\nu = 1 - \mu$ known, the values of β_n ($n = 1, 2, 3, \dots$) can be found by solving numerically the frequency equation (11), and the corresponding ω_n are then calculated by using the relation $\omega_n^2 = EI\beta_n^4/(\rho AL^4)$.

An efficient algorithm proposed by Wittrick and Williams [13] is utilized in extracting the eigenvalues. In order that the designer can immediately use these results, values of β_n for the first five modes of vibration are given for various values of intermediate elastic support stiffness parameter T such as $T = 10, 100, 1000, 5000$ and ∞ , respectively, in Figures 2–6, for various values of position parameter μ . By taking advantage of symmetry, results are given for values of μ in the range 0.0 – 0.5 in steps of 0.02 . The corresponding values for $\mu > 0.5$ can be read from these tables by suitably choosing the axis such that $\mu \leq 0.5$. It can be easily seen that the fundamental frequencies obtained here exactly coincide with those reported in reference [14]. It is believed that the exact frequency data presented in Table 1 will enable the designer to immediately determine the fundamental frequencies of clamped–clamped beams with an arbitrarily placed intermediate elastic support. Further, the table can be also utilized in assessing the accuracy of various approximate methods, such as energy methods.

7. CONCLUSIONS

Exact frequency and mode-shape expressions for clamped–clamped uniform Bernoulli–Euler beams with an arbitrarily placed intermediate elastic support are explicitly presented in this paper. Extensive frequency tables giving the first five natural frequencies of vibration are provided for immediate use in design.

The various results presented in this paper clearly demonstrate that the natural frequencies and mode shapes are sensitive to the position and stiffness of the intermediate elastic

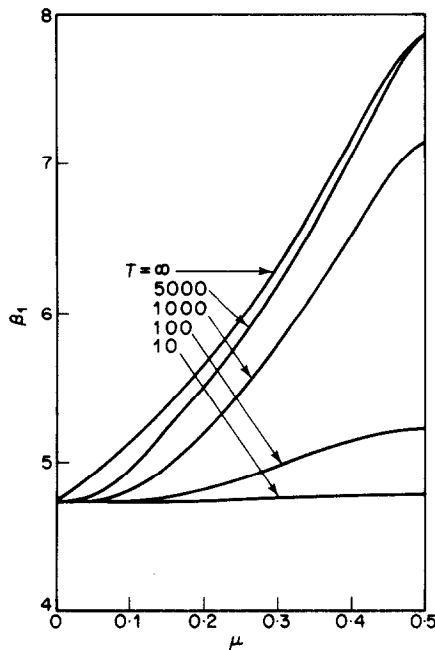


Figure 2. First mode values of β_n for clamped–clamped beams for various values of T and μ .

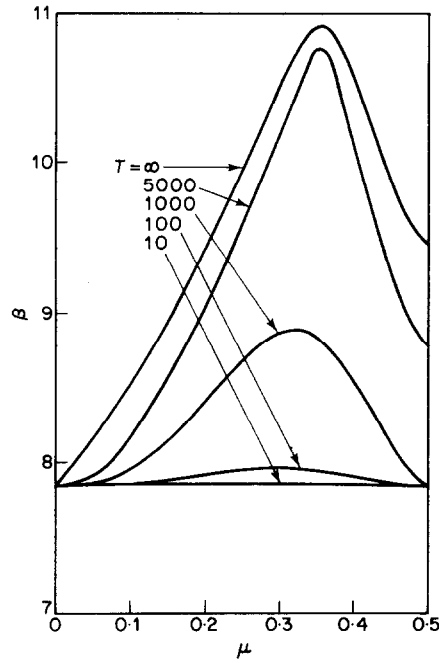


Figure 3. Second mode values of β_n for clamped-clamped beams for various values of T and μ .

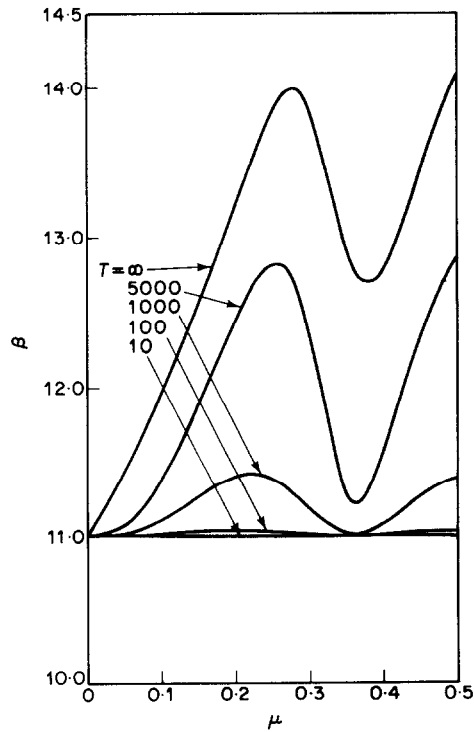


Figure 4. Third mode values of β_n for clamped-clamped beams for various values of T and μ .

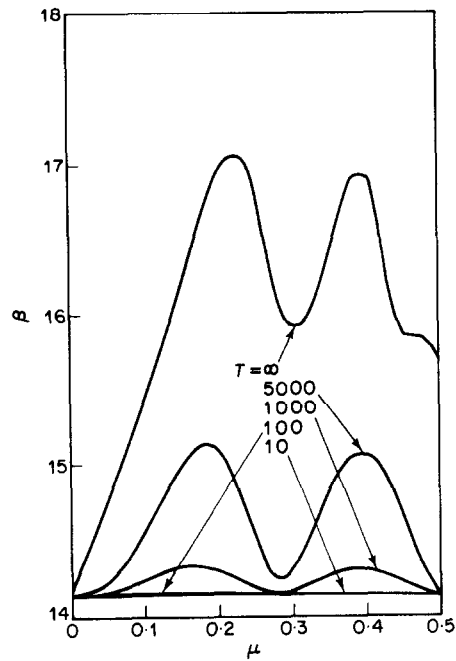


Figure 5. Fourth mode values of β_n for clamped-clamped beams for various values of T and μ .

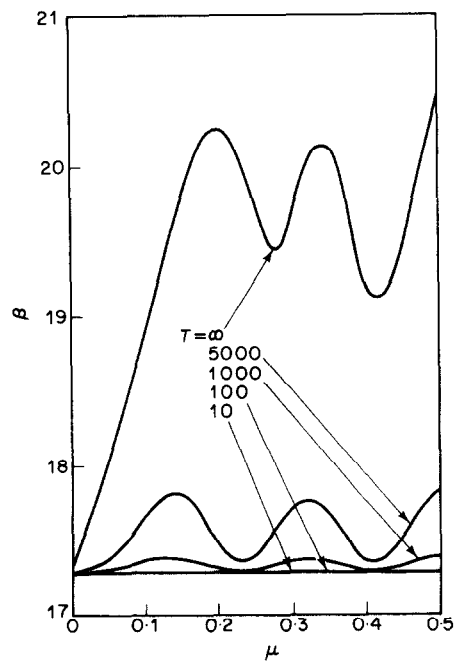


Figure 6. Fifth mode values of β_n for clamped-clamped beams for various values of T and μ .

TABLE 1

Fundamental mode values of β_n for clamped-clamped beams with intermediate spring support for various values of T and μ

μ	Values of T				
	10	100	1000	5000	∞
0.00	4.73004	4.73004	4.73004	4.73004	4.73004
0.02	4.73004	4.73006	4.73022	4.73091	4.80251
0.04	4.73007	4.73031	4.73266	4.74227	4.87863
0.06	4.73017	4.73129	4.74199	4.77949	4.95832
0.08	4.73041	4.73372	4.76329	4.84676	5.04186
0.1	4.73088	4.73832	4.79992	4.93616	5.12954
0.12	4.73166	4.74579	4.85271	5.03811	5.22162
0.14	4.73282	4.75670	4.92047	5.14677	5.31837
0.16	4.73441	4.77142	5.00100	5.25962	5.42012
0.18	4.73647	4.79013	5.09202	5.37605	5.52718
0.20	4.73902	4.81280	5.19163	5.49623	5.63991
0.22	4.74205	4.83922	5.29844	5.62066	5.75866
0.24	4.74552	4.86902	5.41155	5.74998	5.88382
0.26	4.74938	4.90172	5.53041	5.88482	6.01577
0.28	4.75356	4.93671	5.65475	6.02581	6.15488
0.30	4.75795	4.97328	5.78445	6.17356	6.30150
0.32	4.76245	5.01065	5.91949	6.32865	6.45593
0.34	4.76694	5.04795	6.05984	6.49160	6.61830
0.36	4.77130	5.08426	6.20540	6.66284	6.78853
0.38	4.77540	5.11860	6.35590	6.84259	6.96605
0.40	4.77910	5.14997	6.51063	7.03066	7.14942
0.42	4.78231	5.17736	6.66806	7.22594	7.33546
0.44	4.78492	5.19984	6.82479	7.42514	7.51761
0.46	4.78685	5.21657	6.97286	7.61911	7.68260
0.48	4.78803	5.22689	7.09256	7.8212	7.80584
0.50	4.78843	5.23038	7.14282	7.85320	7.85320

support. It can be also seen that the effect of finite stiffness of the elastic support is considerable on the first few modes and becomes negligible on higher mode frequencies. The explicit and exact frequency and mode-shape expressions provided in this paper can be effectively utilized in determining the dynamic behaviour of such beams.

*Department of Mechanical Engineering,
University of Ottawa, 770 King Edward Avenue,
Ottawa, Ontario, Canada K1N 6N5*

C. KAMESWARA RAO†

(Received 9 February 1989)

REFERENCES

1. H. WAGNER and V. RAMAMURTI 1977 *Shock and Vibration Digest* 9(9), 17-24. Beam vibrations—a review.

† On leave from Corporate R and D division, Bharat Heavy Electricals Limited, Vikasnagar, Hyderabad-500 593, India.

2. C. KAMESWARA RAO and S. MIRZA 1987 *American Society of Mechanical Engineers Proceedings of Pressure Vessels and Piping Conference*, PVP—Vol. 124, 117–121. Vibration frequencies and mode-shapes for generally restrained Bernoulli–Euler beams.
3. C. M. HARRIS and C. E. CREDE 1961 *Shock and Vibration Handbook*. New York: McGraw-Hill.
4. T. M. WANG 1970 *Journal of Sound and Vibration* **13**, 409–414. Natural frequencies of continuous Timoshenko beams.
5. D. J. GORMAN 1974 *International Journal of Mechanical Sciences* **16**, 345–351. Free lateral vibration analysis of double-span uniform beams.
6. P. A. A. LAURA, P. V. D. IRASSAR and G. M. FICCADENTI 1983 *Journal of Sound and Vibration* **86**, 279–284. A note on transverse vibrations of continuous beams subject to an axial force and carrying concentrated masses.
7. C. PIERRE, D. M. TANG and E. H. DOWELL 1988 *American Institute of Aeronautics and Astronautics Journal* **25**, 1249–1257. Localized vibrations of disordered multi-span beams: theory and experiment.
8. P. A. A. LAURA, G. SANCHEZ SARMIENTO and A. N. BERGMANN 1983 *Applied Acoustics* **16**, 95–104. Vibrations on double-span uniform beams subject to an axial force.
9. C. KAMESWARA RAO 1988 *Journal of Sound and Vibration* (Submitted). Frequency analysis of two-span uniform Bernoulli–Euler beams.
10. R. E. D. BISHOP and D. C. JOHNSON 1956 *Vibration Analysis Tables*. Cambridge University Press.
11. D. J. GORMAN 1975 *Free Vibration Analysis of Beams and Shafts*. New York: John Wiley.
12. R. D. BLEVINS 1979 *Formulas for Natural Frequency and Mode Shape*. New York: Van Nostrand Reinhold.
13. W. H. WITTRICK and F. W. WILLIAMS 1971 *Quarterly Journal of Mechanics and Applied Mathematics* **24**, 263–284. A general algorithm for computing natural frequencies of elastic structures.
14. M. J. MAURIZI and D. V. BAMBILL DE ROSSIT 1987 *Journal of Sound and Vibration* **119**, 173–176. Free vibration of a clamped-clamped beam with an intermediate elastic support.

SEISMIC ANALYSIS OF HIGH-SPEED ROTATING MACHINERY

C. KAMESWARA RAO ¹ and S. MIRZA ²

Department of Mechanical Engineering, University of Ottawa, Ottawa, Canada K1N 6N5

Received 16 October 1987

Seismic analysis of high-speed rotating machinery such as turbo-generators and fan-motor systems are of main concern in this paper. A comprehensive review of some important studies made in this area, as well as new results of seismic response of a fan-motor system are presented here. The effects of several design parameters, namely, bearing oil-film stiffnesses and pedestal flexibilities on seismic response of high-speed rotating machinery are discussed. Important qualitative and quantitative conclusions are presented

1. Introduction

High-speed rotating machinery like vertical or horizontal pumps, turbine-generator systems and fan-motor systems located in a nuclear power plant are required to remain operational even during a seismic event as the supply of power is essential to carry out necessary relief operations. In many cases, testing of such equipment on shaker tables for seismic qualification is not feasible because of their excessive weight and large size. Consequently, one may have to necessarily resort to an analytical investigation.

The main objective of such an analytical investigation is to determine the seismic response of structures and equipment and to check the seismic deflections of the critical portions in view of the design limitations. In rotor-bearing systems, it is necessary to check the seismic deflections of the rotor at various bearing locations so that the lubricating fluid-film maintains a minimum thickness at all times in order to keep the rotor and bearing surfaces away from rubbing against each other. The additional seismic forces coming on to the bearings and the seismic deflections and forces experienced by the foundation are also to be computed and should be checked against their corresponding allowable limits. In order to create a realistic mathematical model, this analysis should account for the stiffness and damping coefficients of bearings, pedestal mass and stiffnesses

and flexibility of the foundation. In situations where reliable data is not available, appropriate assumptions may have to be made in order to obtain conservative estimates of seismic response.

The purpose of the present paper is to briefly review some important studies made in the area of seismic response of high-speed rotating machinery and to present new results from a seismic response analysis of a typical fan-motor rotor-bearing system. The fan-motor rotor-bearing system is analyzed utilizing an in-house finite element computer programme and the natural frequencies and mode shapes are obtained using determinant search method. Later, the seismic response is computed based on response spectrum approach.

2. Brief review of earlier studies

2.1. Dynamic response of machine foundations

Pile supported frame foundations and nuclear turbine-generator foundations are large three-dimensional structures whose critical feature is that the economic consequences of their failure far exceed their cost. The dynamic response of such foundations were studied by many investigators both theoretically and experimentally [1–4]. Recently, Kameswara Rao et al. [5] studied the seismic response of a 70 MW turbine-generator foundation shown in fig. 1. The finite-element model adopted in this study is shown in fig. 2. Fig. 3 shows the response spectrum curve for the prescribed site (site 1). The structural damping for concrete was

¹ Post Doctoral Fellow

² Professor.

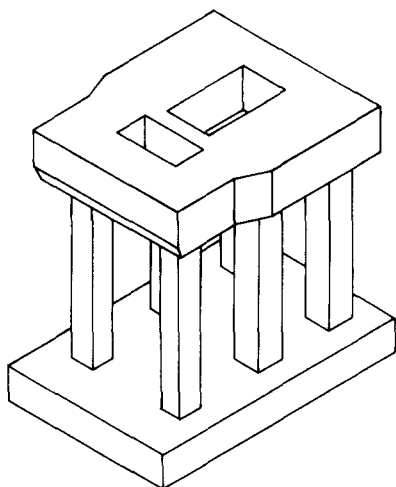


Fig. 1. Isometric view of 70 MW TG foundation.

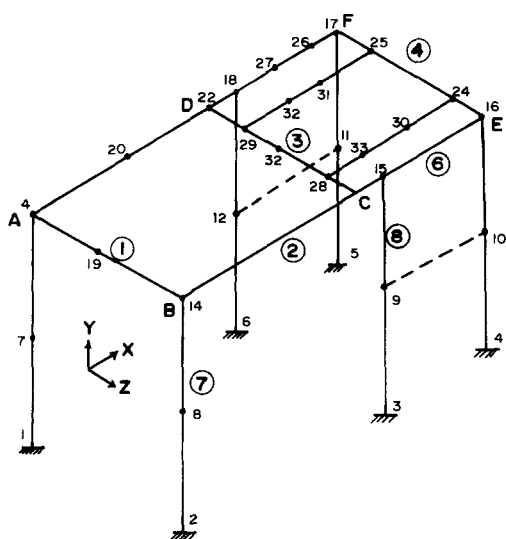


Fig. 2. Mathematical model of 70 MW TG foundation frame.

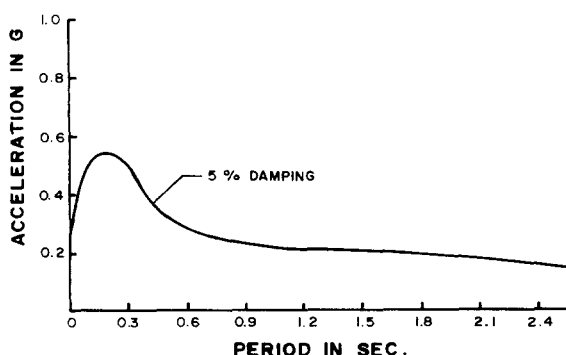


Fig. 3. Response spectrum for Site 1.

assumed to be 5%. The free-vibration mode shapes of the foundation for the first and second modes were presented in ref. [5]. As this study was carried out during the preliminary stages of design, the rotor was assumed to be rigid and the weights of the turbine-generator system were lumped at appropriate nodal points of the foundation. Some structural modifications were proposed in order to reduce unacceptable horizontal displacements especially on the generator side.

Some studies [2,4] in this area suggest the use of rigorous three-dimensional finite element models in order to obtain meaningful results for seismic response, especially at some critical portions of the foundation.

2.2. Dynamic stability of rotor-bearing systems

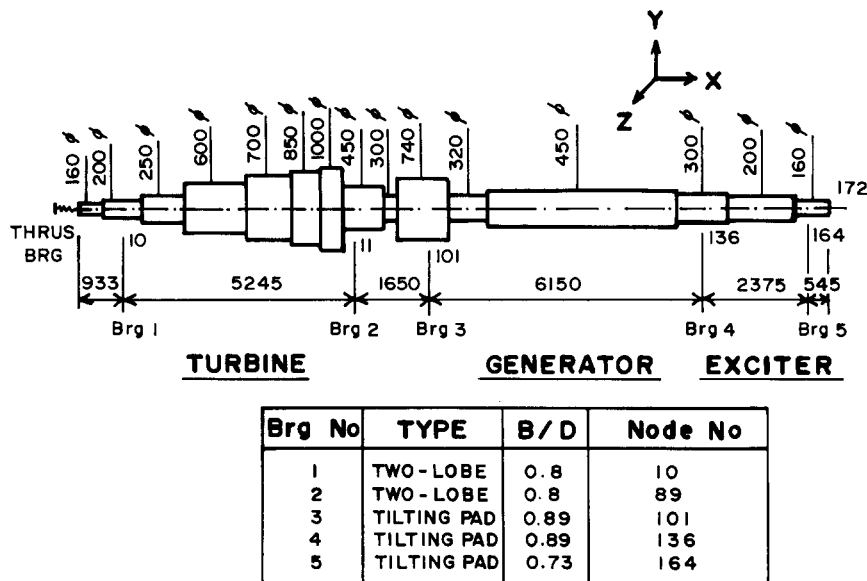
The oil-film stiffness and damping properties of various types of bearings, in general, lead to non-symmetric matrices and thus show a greater influence on dynamic stability of rotating machinery. Consequently, the unbalanced response and dynamic stability analysis become very important. Some of the investigators [6–11] addressed to this problem and developed improved methods of response calculations. In view of the rigid couplings being increasingly used these days in high-speed machinery, it is necessary to include all critical portions of the rotor-bearing system to obtain reliable and meaningful response information.

2.3. Seismic response of rotating machinery

Currently, there is wide interest in this topic. This may be due to some stringent requirements imposed by various design codes. Several authors [12,15] have presented comprehensive summaries in this area.

Villasor [13], Soni et al. [14], Srinivasan et al. [15], Ly [16], utilized response spectrum technique or time-history method in order to estimate the seismic response in a deterministic way. Recently, Kameswara Rao et al. [17] studied the companion problem of seismic response of 70 MW turbine-generator of rotor-bearing system. Fig. 4 shows the details of this system. The entire rotor in [17] was supported by two two-lobe fluid-film bearings on the turbine side and by three tilted-pad bearings on the generator and exciter side. To support the rotor horizontally, a thrust bearing was provided on the turbine front end. This study revealed that the influence of bearing pedestal mass and stiffness on the rotor response is of the order of about 20%.

Due to the nature and approximations involved in the analytical approach, the response spectrum technique [23] yields conservative response results and, con-



ALL DIMENSIONS ARE IN MM

Fig. 4. 70 MW TG rotor-bearing system.

sequently, is widely used in industry. Besides this, the time-history type of analysis becomes more costly and is generally adopted only when more exact estimates are required to be obtained for critically reviewing the equipment performance under transient and stochastic loading conditions.

Reliability and random seismic response studies were carried out by Iwatsubo et al. [19], Shimogo [20], Subbiah et al. [21] and more recently by Somali et al. [22]. In these studies the seismic excitation and response are analyzed as random vibrations using spectral density functions.

After a thorough search of the available literature, it is the opinion of the authors that there is a critical need

to develop simple but efficient techniques of modeling as well as seismic analysis methodologies in order to ensure structural safety and integrity of rotating machinery at optimum analysis costs.

3. Response spectrum analysis

In the present investigation, the response spectrum method of analysis [23] is chosen since the input motion is provided as plots of the maximum average response of a single-degree-of-freedom oscillator with different natural frequencies to a given support motion and structural damping. Fig. 7 shows the response spectrum

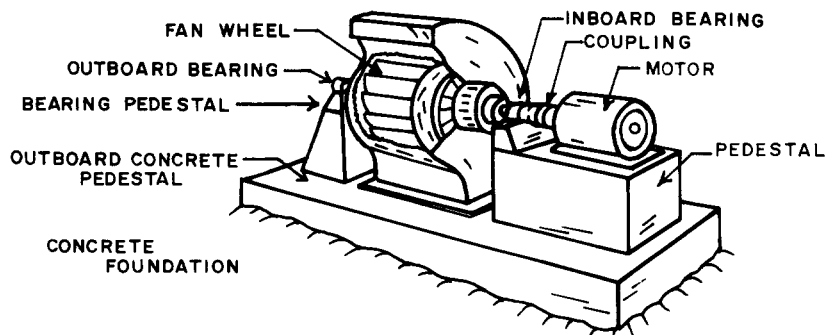


Fig. 5. Typical fan-motor system.

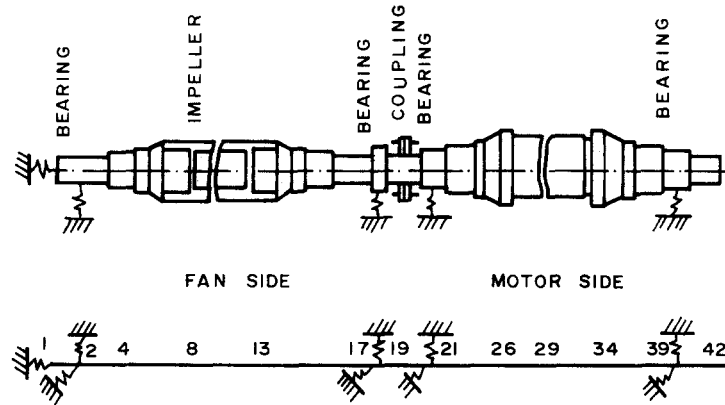


Fig. 6. Mathematical model of the fan-motor rotor-bearing system.

for site 2 which is utilized in carrying out the response calculations for the system chosen in the present study (fig. 5).

For a linear multi-degree of freedom system, subjected to earthquake excitation, the equation of motion is:

$$[M]\{\ddot{\bar{X}}\} + [C]\{\dot{\bar{X}}\} + [K]\{\bar{X}\} = -[M]\{\bar{P}\}\{\ddot{Y}_g\}, \quad (1)$$

where $\{\ddot{Y}_g\}$ is the time dependent prescribed ground acceleration, $\{\bar{P}\}$ is the vector with components of unity in all directions parallel to support movement and zero otherwise, $[M]$ is the mass matrix, $[K]$ is the stiffness matrix, $[C]$ is the damping matrix and $\{\bar{X}\}$, $\{\dot{\bar{X}}\}$ and $\{\ddot{\bar{X}}\}$ represent time dependent relative displacement, velocity and acceleration vectors respectively.

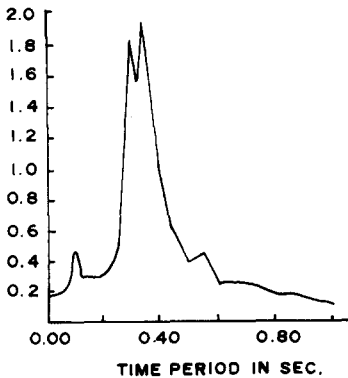


Fig. 7. Response spectrum for Site 2.

The displacement $\bar{X}(t)$ in eq. (1) can be expressed in terms of the normalized modes, ϕ_i , and the generalized coordinates, q_i , as

$$X(t) = \sum_{i=1}^N \phi_i q_i. \quad (2)$$

Substituting eq. (2) into eq. (1) and premultiplying by $\{\phi\}^T$ and the resulting equation by M^*-1 , we obtain a set of single degree of freedom equations:

$$\ddot{q}_i + 2\omega_i \xi_i \dot{q}_i + \omega_i^2 q_i = -\nu_i \ddot{Y}_g, \quad (3)$$

where $[M^*] = \{\phi\}^T [M] \{\phi\}$, ω_i is the natural frequency of the i th mode, ν_i is the mode participation factor $= \phi_i^T M \bar{P}$ in mode i and ξ_i is the modal damping. Maximum values of q_i are then obtained utilizing the given response spectra. Once q_i has been determined, the maximum displacement X_i for mode i , is given by

$$(X_i)_{\max} = \phi_i q_i. \quad (4)$$

Based on the maximum modal displacement vector given by eq. (4), member forces, nodal displacements and reactions are computed for each mode. Since these maximum responses are not expected to occur at the same instant of time, empirical rules have to be used for combining modal responses to obtain the total response. In the present study, the square root sum of squares (SRSS) method is used in combining the modal responses. The SRSS combination is the most commonly used rule for maximum modal responses.

In SRSS method, the probable response is evaluated as

$$R_a = \left[\sum_{k=1}^N R_k^2 \right]^{1/2}, \quad (5)$$

Table 1
Bearing stiffnesses (N/m) at various rotor speeds

Bearing location	Stiffness type	Stiffness ($\times 10^8$) vs. speed			
		375 rpm	750 rpm	1000 rpm	750 rpm with pedestals
1	K_x	82.21	81.12	80.02	81.12
2	K_y	1.65	1.08	0.77	1.01
	K_z	19.82	14.81	13.83	5.92
17	K_y	1.82	1.18	0.84	1.09
	K_z	21.88	16.97	16.28	6.29
21	K_y	1.73	1.77	2.03	1.60
	K_z	16.78	15.89	18.15	6.81
39	K_y	1.68	1.73	2.00	1.57
	K_z	16.28	15.60	17.95	6.76

where R_k denotes the maximum modal response in the k th mode and R_a the total response.

4. Fan-motor rotor-bearing system

4.1. System configuration and modeling

Induced draft fans are generally located between the boiler and the stack of power generator units to pull combustion gases from the boiler and exhaust them up the stack. At the center of the shaft and between the bearings, is located the fan wheel of the double-inlet type centrifugal fan. A thrust bearing is included at the left end of the rotor-bearing system to provide axial restraint.

Fig. 5 shows a typical induced draft fan-motor rotor-bearing system studied in this paper. The fan-motor system is driven at a speed of 750 rpm with an over-speeding capacity up to 1000 rpm. The combined fanmotor rotor-bearing system is 5.515 m long and weighs about 61 kN. The rotor is supported totally on four fluid-film bearings and their horizontal (K_z) and

vertical (K_y) stiffness coefficients at various rotor speeds are listed in table 1. Table 2 gives the typical weights of bearing pedestals and their horizontal and vertical stiffnesses utilized in the present analysis.

The flexible rotor is modeled using three-dimensional beam elements [24] which account for the effects of rotary inertia and shear deformation. The bearing and pedestal stiffnesses are modeled utilizing spring elements. The neglect of the effects of bearing damping coefficients in the present analysis, eventually leads to conservative estimates of rotor seismic response under different rotor speed conditions. The masses of various parts such as impeller, rotor shaft, etc., are lumped at appropriate nodal points.

4.2. Discussion of results

The individual rigid critical speeds of the fan-rotor and the motor-rotor at a speed of 750 rpm are obtained by determinant search method and these results for the first five modes of vibration are presented in table 3. The values of first ten natural frequencies and modal

Table 2
Steel bearing pedestal weights and stiffnesses

Node	Weight (kN)	$K_y \times 10^8$ (N/m)	$K_z \times 10^8$ (N/m)
2	50.22	15.0	10.0
17	15.03	15.0	10.0
21	21.58	17.0	12.0
39	21.58	17.0	12.0

Table 3
Individual rotor rigid critical speeds (Hz) at 750 rpm

Mode	Fan rotor (Hz)	Mode	Motor rotor (Hz)
1	35.9	1	42.6
2	55.0	2	53.5
3	95.6	3	83.9
4	175.4	4	207.2
5	177.8	5	224.2

Table 4

First ten natural frequencies (Hz) and mode participation factors (mpf) at various rotor speeds

Mode	375 rpm		750 rpm		1000 rpm	
	Freq.	mpf	Freq.	mpf	Freq.	mpf
1	26.6	2.4(y)	26.7	2.3(y)	27.6	2.2(y)
2	35.6	-2.3(z)	35.5	2.3(z)	32.6	1.9(y)
3	41.1	-1.8(y)	36.3	1.8(y)	35.7	-2.3(z)
4	58.0	-0.5(y)	58.2	1.6(z)	58.0	1.5(z)
5	59.2	1.5(z)	58.7	0.5(y)	62.1	-0.6(y)
6	94.6	-2.9(x)	94.6	2.9(x)	92.2	0.3(y)
7	114.4	0.4(y)	102.2	0.3(y)	94.6	2.9(x)
8	120.7	-0.6(y)	117.4	-0.3(y)	118.6	0.4(y)
9	126.1	0.2(z)	125.4	0.3(z)	127.2	-0.2(z)
10	167.8	-1.1(z)	165.2	-1.1(z)	173.7	1.1(z)

participation factors for the rigidly coupled fan-motor rotor-bearing system at various rotor speeds are given in table 4. A comparison of tables 3 and 4 clearly shows that the natural frequencies of the combined system at a rotor speed of 750 rpm are considerably lower than those obtained for individual rigid rotors of the fan and the motor. From table 4, it can be also observed that the change in rotor speed influences the resulting natural frequencies of the combined rotor-bearing system to an extent of about $\pm 5\%$.

The vertical bearing reactions under static self-weight loading with bearing stiffnesses computed at a rotor speed of 750 rpm are presented in table 5. A maximum

Table 5

Bearing forces (kN) under self-weight at 750 rpm

Force (kN)	Bearing points			
	2	17	21	39
F_y	7.412	4.836	24.407	22.661

Table 6

Bearing forces (kN) at various rotor speeds under seismic loading.

Speed (rpm)	Forces (kN)	Bearing points			
		2	17	21	39
375	F_y	1.985	1.629	3.562	3.819
	F_z	2.469	2.713	6.229	4.585
750	F_y	2.074	1.564	3.513	3.755
	F_z	2.492	2.717	6.203	4.573
1000	F_y	2.276	1.568	3.377	3.496
	F_z	2.490	2.722	6.210	4.593

force of 24.41 kN can be seen to occur at the left end bearing of the generator-rotor. The bearing seismic forces in the vertical and horizontal directions are presented in table 6. It can be observed that the overall maximum forces of magnitude 3.82 kN and 6.23 kN in vertical and horizontal directions respectively occur at the generator bearings. This, therefore, indicates that a maximum increase of 16% results in bearing reactions due to seismic loading.

The seismic displacements of the rotor are obtained by combining the responses of the first ten modes of vibration using the square root sum of the squares (SRSS) method outlined in section 3. These values, in microns (10^{-6} mm), at salient nodal points for various cases considered here, are given in table 7. From these results, we can see that the maximum displacements in all the x , y , z -directions occur at the center node of the motor-rotor span (node No. 29) and their values are 5.8, 51.3 and 42.9 microns, respectively, which are well within the limit. We can, therefore, see that the motor-rotor should withstand higher seismic displacements in comparison with the fan-rotor.

In order to study the influence of pedestal mass and stiffness on the overall seismic response of the system, combined oil-film and pedestal stiffnesses are worked out [25] at a selected rotor speed of 750 rpm. The first ten natural frequencies corresponding to this case are presented in table 8. A close look at tables 4 and 8 reveals that the pedestal mass and stiffnesses have a decreasing effect of the order of 6% on the natural frequencies of the system. The values of seismic displacements and bearing reactions, for this case, are presented in tables 9 and 10, respectively.

From table 9, we observe that while the axial and vertical seismic displacements remain unchanged (see

Table 7

Seismic displacements (microns) at salient nodal points of the rotor-bearing system (SRSS method with 10 modes included)

Node	Displ. (microns)	Displacements (microns) vs. speed (Hz)		
		375 rpm	750 rpm	1000 rpm
2B	x	1.3	1.3	1.3
	y	12.0	19.2	29.4
	z	1.2	1.7	1.8
4	x	2.0	2.0	2.0
	y	20.5	27.5	37.7
	z	12.4	12.9	13.0
8	x	2.4	2.4	2.4
	y	21.0	27.6	37.0
	z	13.5	14.0	14.1
13	x	3.1	3.1	3.1
	y	17.5	23.2	30.8
	z	9.9	10.3	10.4
17B	x	3.7	3.7	3.7
	y	8.9	13.3	18.8
	z	1.2	1.6	1.7
19	x	4.5	4.5	4.5
	y	7.8	8.1	8.0
	z	5.3	5.2	5.5
21B	x	5.1	5.1	5.1
	y	20.6	19.9	16.6
	z	3.7	3.9	3.4
26	x	5.6	5.6	5.7
	y	44.3	43.2	38.2
	z	33.0	33.2	32.6
29	x	5.8	5.8	5.8
	y	51.3	50.0	44.5
	z	42.7	42.9	42.3
34	x	5.6	5.6	5.7
	y	41.8	40.5	35.3
	z	29.7	29.8	29.3
398	x	5.4	5.4	5.4
	y	22.8	21.8	17.5
	z	2.8	2.9	2.6

table 7 for comparison), the horizontal (z) displacements became more than twice the displacements occurring when pedestal mass and stiffnesses are not included in the analysis. However, from table 10 and 6,

Table 8

First ten natural frequencies (Hz) with pedestal masses at 750 rpm rotor speed

Mode	Freq.	mpf	Mode	Freq.	mpf
1	26.13	2.4(y)	6	94.57	-2.9(x)
2	33.38	2.3(z)	7	99.54	0.3(y)
3	35.51	-1.8(y)	8	102.0	-0.7(z)
4	52.98	-1.6(z)	9	116.5	0.3(y)
5	56.48	-0.5(y)	10	134.9	-0.7(z)

Table 9

Seismic displacements (microns) at bearing points at 750 rpm rotor speed considering pedestal stiffnesses

Displ. (microns)	Bearing point			
	2	17	21	39
x	1.3	3.7	5.1	5.4
y	20.5	14.1	21.8	24.4
z	4.5	4.3	8.9	6.9

Table 10

Seismic forces (kN) at bearing points at 750 rpm rotor speed considering pedestal stiffnesses.

Force (kN)	Bearing point			
	2	17	21	39
F_y	2.074	1.537	3.479	3.829
F_z	2.662	2.699	6.004	4.657

we observe that the resulting seismic forces did not differ significantly.

5. Conclusions

From the results presented in this paper, the following can be concluded:

- (1) The variation in bearing oil-film stiffnesses due to change in rotor speed has resulted in only a marginal deviation in the natural frequencies of fan-motor rotor-bearing system considered in this study.
- (2) Inclusion of pedestal masses and stiffnesses has shown a significant influence on horizontal seismic displacements but only marginally affected the bearing seismic reactions.
- (3) Though not explicitly shown here, the authors found during the course of this investigation that the effects to rotary inertia and shear deformation are significant especially on higher modes of vibration and hence should be necessarily included in seismic response calculations of rotating machinery.

References

- [1] F. Aboul-Ella and M. Novak, Dynamic response of pile-supported frame foundations, *J. Engrg. Mech.*, ASCE 106 (1980) 1215–1232.
- [2] I.K. Aneja and B.W. Dimmick, Nuclear turbine-generator foundation modal tests, *J. Engrg. Mech.*, ASCE 103 (1977) 243–255.
- [3] L. Gaul, Dynamics of frame foundations interacting with soil, *J. Mech. Des.*, ASME 102 (1980) 303–310.
- [4] B. Chandra and S.R. Reddy, Seismic behaviour of framed foundation for turbo-generators, *Proceedings of 6th World Conf. on Earthquake Engrg.*, New Delhi, Vol. 4 (1977), paper No. 4–157.
- [5] C. Kameswara Rao and P.M.L. Prasad, Seismic analysis of 70 MW turbo-generator foundation, *Proceedings of Symp. Earthquake Effects on Plant and Equipment*, Hyderabad, I (1984) 143–149.
- [6] R. Gasch, Vibration of large turbo-rotors in fluid-film bearings on an elastic foundation, *J. Sound Vib.* 47 (1976) 53–73.
- [7] N. Hagiwara et al., Analysis of coupled vibration response in a rotating flexible shaft-impeller system, *J. Mech. Des.*, ASME 102 (1980) 163–167.
- [8] M. Jacker, Vibration analysis of large rotor-bearing-foundation systems using a model condensation for the reduction of unknowns, *I. Mech. E.*, C280/80, 195–202.
- [9] R. Gasch, J. Maurer and W. Sarfeld, The influence of the elastic half-space on stability and unbalance-response of a simple rotor-bearing-foundation system, *I. Mech. E.*, C 300/84, 1–12.
- [10] S.C. Ulm, Application of modal analysis to the design of a large-foundation system, *Proceedings 2nd Int. Modal Analysis Conf.*, Florida (1984).
- [11] Z. Wang and J.W. Lund, Calculations of long rotors with many bearings on a flexible foundation, *I. Mech. E.*, C 291/84, 13–16.
- [12] C. Kameswara Rao, Seismic analysis of rotating mechanical systems – State of the art, 28th Congress of Ind. Soc. of Theor. and Appl. Mech., Waltair, 1983.
- [13] A.P. Villasor, Seismic analysis of a reactor coolant pump by the response spectrum method, *Nucl. Engrg. Des.* 38 (1976) 527–542.
- [14] A.H. Soni and V. Srinivasan, Seismic analysis of a gyroscopic mechanical system, *J. Vib. Acc. Str. and Reliab. in Des.*, ASME 105 (1983) 449–455.
- [15] V. Srinivasan and A.H. Soni, Seismic analysis of a rotor-bearing system, *J. Earthg. Engrg. and Str. Dyn.* 12 (1984) 287–311.
- [16] B.L. Ly, Seismic response of gyroscopic system by the response spectrum method, 8th SMiRT Conf., K 11/5 (1985) 547–552.
- [17] C. Kameswara Rao and P.M.L. Prasad, Seismic analysis of 70 MW turbogenerator rotor-bearing system, *Proceedings Nat. Symp. on Vibration of Power Plant Equipment*, Bombay, DAE: 86:02, II 9.1–9.9.
- [18] C. Kameswara Rao and S. Mirza, Seismic analysis of high-speed rotating machinery, *Proceedings of the 9th SMiRT Conf.*, Vol. K 2 (1987) 1017–1026.
- [19] T. Iwatsubo et al., Reliability design of rotating machinery against earthquake excitation, *Bull. JSME* 22 (1979) 1632–1639.
- [20] T. Shimogo et al., Seismic response of a flexible rotor, *I. Mech. E.*, C 298/80, 321–326.
- [21] R. Subbiah et al., Response of rotors subjected to random support excitations, *J. Vib. Acc. Str. and Reliab. in Des.*, ASME 107 (1985) 453–459.
- [22] B. Samali et al., Random vibration of rotating machines under earthquake excitations, *J. Engrg. Mech.*, ASCE 112 (1986) 550–565.
- [23] J.M. Biggs, *Introduction to Structural Dynamics* (McGraw-Hill, New York, 1964).
- [24] J.S. Przemieniecki, *Theory of Matrix Structural Analysis* (McGraw-Hill, New York, 1968).
- [25] W.D. Pilkey and P.Y. Chang, *Modern formulas for statics and dynamics – A stress-and-strain approach* (McGraw-Hill, New York, 1978).

TORSIONAL FREQUENCIES AND MODE SHAPES OF GENERALLY CONSTRAINED SHAFTS AND PIPING

C. KAMESWARA RAO†

Department of Mechanical Engineering, University of Ottawa, 770 King Edward Avenue, Ottawa
Ontario, Canada K1N 6N5

(Received 3 September 1987, and in revised form 21 December 1987)

In this note, exact frequency and normal mode expressions are derived for the free torsional vibrations of circular shafts or piping systems constrained by unsymmetrical torsional springs and carrying unequal rotational masses at either end. For use in design, extensive tables of natural torsional frequency and mode shape parameters are provided for a wide range of values of torsional spring and rotational mass parameters.

1. INTRODUCTION

A considerable number of studies have been made in determining the lateral frequencies and mode shapes of straight beams and shafts subjected to partial edge restrains. However, corresponding torsional behaviour of such beams and shafts have received considerably less attention. In 1975 Gorman [1] and in 1979 Blevins [2] presented exact expressions for torsional frequencies and mode shapes of shafts with various non-classical boundary conditions. Gorman [1] had also presented a vast number of tables of frequencies for various cases considered. However, the problem in its generality was not discussed in the published literature.

In the present note, a circular shaft or pipe constrained by unsymmetrical torsional springs and with unequal rotational masses such as heavy discs or valves or bellows at either ends is considered. Exact expressions for torsional frequencies and mode shapes are derived and numerical results for the first five frequency and mode shape parameters are presented in tabular form for a wide range of values of the torsional spring stiffness and rotational mass parameters. The reliability of the present results have been verified by checking various degenerate cases published earlier [1, 2].

2. ANALYSIS

The differential equation for small-amplitude, free torsional vibrations of a generally restrained shaft or pipe of length L (see Figure 1) executing harmonic oscillations is given by [1]

$$GI_p \theta''(\xi) + \rho I_p \omega^2 L^2 \theta(\xi) = 0 \quad (1)$$

where G is the shear modulus, I_p the polar moment of inertia, ρ the mass density, ω the torsional radian frequency of the constrained shaft and primes denote differentiation with respect to the non-dimensional length $\xi = x/L$.

The general solution of equation (1) is

$$\theta(\xi) = A \sin \lambda \xi + B \cos \lambda \xi. \quad (2)$$

† On leave from Corporate R & D Division, Bharat Heavy Electricals Limited, Vikasnagar, Hyderabad-500 593, India

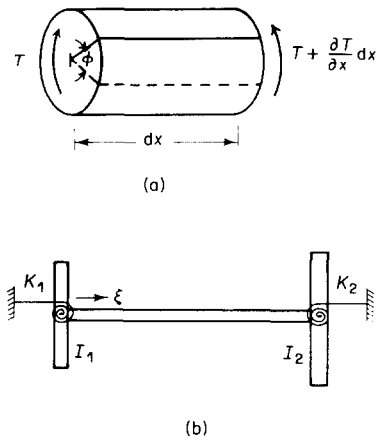


Figure 1. Generally constrained shaft.

TABLE 1

First five values of λ for generally restrained circular shafts for various values of R and T
($R_2 = R_1 = R, T_2 = T_1 = T$)

T	Mode				
	1	2	3	4	5
R = 0.10					
0.00	0.443521	3.203994	6.314854	9.445950	12.58227
0.01	0.439291	3.142390	6.191715	9.261506	12.33686
0.10	0.405895	2.686702	5.332782	8.080572	10.91640
1.00	0.257959	1.338660	3.676510	6.585277	9.631902
10.00	0.097588	0.454473	3.204054	6.314861	9.445952
100.00	0.031544	0.144793	3.147946	6.286366	9.426899
R = 1.00					
0.00	1.306542	3.673194	6.584620	9.631684	12.72324
0.01	1.297144	3.613781	6.462900	9.447522	12.47718
0.10	1.219178	3.147512	5.562953	8.205151	10.98783
1.00	0.808675	1.598398	3.707706	6.591303	9.633881
10.00	0.308548	0.543193	3.204596	6.314933	9.445973
100.00	0.099751	0.173061	3.147952	6.286367	9.426899
R = 10.00					
0.00	2.627675	5.307324	8.067135	10.90871	13.81919
0.01	2.624806	5.286901	8.009071	10.79635	13.64220
0.10	2.598133	5.081849	7.386277	9.591338	11.89511
1.00	2.267871	3.158143	4.169544	6.665645	9.655761
10.00	0.973877	1.086248	3.210552	6.315663	9.446189
100.00	0.315434	0.346121	3.148010	6.286374	9.426902
R = 100.00					
0.00	3.080011	6.160137	9.240491	12.32118	15.40232
0.01	3.079954	6.159679	9.238944	12.31752	15.39516
0.10	3.079433	6.155403	9.223825	12.27917	15.31310
1.00	3.073730	6.090171	8.724368	9.883852	10.69867
10.00	2.845124	3.161773	3.474177	6.325334	9.448613
100.00	0.997283	1.009117	3.148657	6.286448	9.426923

where $\lambda = \omega L \sqrt{\rho/G}$ and the constants A and B are to be determined based on the boundary conditions.

The boundary conditions for the shaft or pipe restrained by unsymmetrical torsional springs of stiffnesses K_1 and K_2 and carrying unequal rotational masses with inertias I_1 and I_2 at either ends are, at $\xi = 0$,

$$\theta'(\xi) = (R_1 - \lambda^2 T_1) \theta(\xi). \quad (3)$$

and at $\xi = 1$,

$$\theta'(\xi) = (\lambda^2 T_2 - R_2) \theta(\xi). \quad (4)$$

where the torsional spring parameters R_1 and R_2 and rotational mass parameters T_1 and T_2 are given by

$$R_1 = K_1 L / GI_p, \quad R_2 = K_2 L / GI_p \quad \text{and} \quad T_1 = I_1 / \rho I_p L, \quad T_2 = I_2 / \rho I_p L. \quad (5a, b)$$

Substitution of equation (2) in equations (3) and (4) leads to the frequency equation

$$[\lambda^4 T_1 T_2 - \lambda^2 (1 + R_1 T_2 + R_2 T_1) + R_1 R_2] \sin \lambda + \lambda [R_1 + R_2 - \lambda^2 (T_1 + T_2)] \cos \lambda = 0. \quad (6)$$

TABLE 2

First five values of λ for generally restrained circular shafts for various values of R and T
($R_2 = R_1 = R$, $T = T_1 = T_2/100$)

T	Mode				
	1	2	3	4	5
$R = 0.10$					
0.01	0.312971	2.060081	4.886670	7.913480	10.98601
0.10	0.131735	1.545986	4.345040	7.249596	10.21419
1.00	0.043318	0.908226	3.430455	6.439173	9.530485
10.00	0.013754	0.327674	3.173440	6.299221	9.435483
100.00	0.004351	0.105142	3.144804	6.284792	9.425849
$R = 1.00$					
0.01	0.938651	2.408577	5.061105	8.024250	11.06614
0.10	0.375716	1.936127	4.509382	7.329772	10.25714
1.00	0.121964	1.211160	3.450877	6.442469	9.531514
10.00	0.038670	0.440458	3.173721	6.299257	9.435493
100.00	0.012232	0.141365	3.144807	6.284792	9.425849
$R = 10.00$					
0.01	2.394114	3.635269	5.959204	8.793309	11.72174
0.10	1.024043	2.877144	5.614770	8.238192	10.84404
1.00	0.329666	2.531569	3.830734	6.484374	9.543002
10.00	0.104423	1.030509	3.176833	6.299626	9.435601
100.00	0.033027	0.331121	3.144836	6.284796	9.425850
$R = 100.00$					
0.01	3.076832	6.124109	8.922553	10.32393	12.64651
0.10	2.918098	3.361135	6.239909	9.334971	12.42902
1.00	1.003122	3.110751	6.185009	8.988283	10.36914
10.00	0.317735	2.934078	3.377451	6.304535	9.436820
100.00	0.100492	1.003194	3.145161	6.284833	9.425861

Corresponding to each frequency, the mode shape can be expressed as

$$\theta(\xi) = B (\cos \lambda \xi + \delta \sin \lambda \xi). \quad (7)$$

where

$$\delta = \lambda / (R_1 - \lambda^2 T_1). \quad (8a)$$

Also

$$\delta = [\lambda \sin \lambda - (R_2 - \lambda^2 T_2) \cos \lambda] / [\lambda \cos \lambda + (R_2 - \lambda^2 T_2) \sin \lambda]. \quad (8b)$$

3. NUMERICAL RESULTS

The roots of the frequency equation (6) have been obtained carrying out a lengthy trial-and-error procedure with use of interpolation and bisection methods and allowance for an error of $\epsilon = 10^{-6}$. Numerical results for frequency parameter λ and the mode shape

TABLE 3

First five values of λ for generally restrained circular shafts for various values of R and T
($R = R_1 = R_2/100$, $T = T_1 = T_2/100$)

T	Mode				
	1	2	3	4	5
<i>R = 0.01</i>					
0.00	0.867662	3.428323	6.438815	9.530372	12.64607
0.01	0.678953	2.104851	4.876587	7.904231	10.97872
0.10	0.301235	1.498341	4.329012	7.241941	10.21007
1.00	0.099507	0.871900	3.428537	6.438851	9.530383
10.00	0.031607	0.314252	3.173412	6.299218	9.435481
100.00	0.010000	0.100830	3.144804	6.284792	9.425849
<i>R = 0.10</i>					
0.00	1.489910	4.327111	7.241068	10.209599	13.22148
0.01	1.444881	3.155434	5.003595	7.936007	10.99391
0.10	0.936119	1.581211	4.346203	7.249844	10.21428
1.00	0.314623	0.909110	3.430478	6.439177	9.530486
10.00	0.099950	0.327820	3.173440	6.299221	9.435483
100.00	0.031621	0.105185	3.144804	6.284792	9.425849
<i>R = 1.00</i>					
0.00	2.011949	4.866431	7.901031	10.97709	14.06836
0.01	1.997944	4.808464	7.717735	9.804620	11.34628
0.10	1.874888	3.161302	4.527617	7.332608	10.25810
1.00	0.992609	1.218030	3.451117	6.442505	9.531526
10.00	0.316066	0.441100	3.173724	6.299257	9.435493
100.00	0.099995	0.141543	3.144807	6.284792	9.425849
<i>R = 10.00</i>					
0.00	2.860154	5.755204	8.700082	11.69146	14.71920
0.01	2.858144	5.741461	8.662762	11.62193	14.61235
0.10	2.839005	5.592048	8.207350	9.970117	10.88596
1.00	2.525614	3.162175	3.834039	6.484829	9.543128
10.00	0.999248	1.031510	3.176867	6.299630	9.435603
100.00	0.316211	0.331269	3.144836	6.284796	9.425850

factor δ were generated for the following three cases: (1) $R_1 = R_2 = R$ and $T_1 = T_2 = T$; (2) $R_1 = R_2 = R$ and $T = T_1 = T_2/100$; (3) $R = R_1 = R_2/100$ and $T = T_1 = T_2/100$. For use in design, values of λ and δ for a wide range of values of parameters R and T are presented in Tables 1-6.

4. CONCLUSIONS

Exact frequency and normal mode expressions for torsional vibrations of circular shafts or pipes constrained by unsymmetrical torsional springs and carrying unequal rotational masses such as discs or heavy valves or bellows have been derived. Results for the first five modes of vibration for a wide range of non-dimensional parameters are presented.

From the various results presented in this note, the following can be concluded: (1) The torsional frequency increases significantly with an increase in the torsional spring stiffness. (2) An increase in the rotational mass results in a considerable decrease in the torsional frequency. (3) At the design stage itself, by a judicious choice of values of

TABLE 4

First five values of δ for generally restrained circular shafts for various values of R and T
($R_2 = R_1 = R$, $T_2 = T_1 = T$)

T	Mode				
	1	2	3	4	5
<i>R = 0.10</i>					
0.00	0.2255	0.0312	0.0158	0.0106	0.0079
0.01	0.2232	0.0004	-0.046	-0.082	-0.115
0.10	0.2058	-0.231	-0.515	-0.796	-1.083
1.00	0.1297	-1.264	-3.649	-6.570	-9.622
10.00	0.0488	-4.325	-32.01	-63.13	-94.47
100.00	0.0158	-13.79	-314.8	-628.6	-942.7
<i>R = 1.00</i>					
0.00	0.7654	0.2722	0.1519	0.1038	0.0786
0.01	0.7580	0.2406	0.0901	0.0114	-0.045
0.10	0.6983	0.0030	-0.377	-0.699	-1.008
1.00	0.4279	-0.973	-3.438	-6.440	-9.531
10.00	0.1555	-3.591	-31.73	-62.99	-94.35
100.00	0.0499	-11.528	-314.5	-628.5	-942.6
<i>R = 10.00</i>					
0.00	3.8056	1.8842	1.2396	0.9167	0.7236
0.01	3.7836	1.8386	1.1685	0.8183	0.5966
0.10	3.5891	1.4596	0.6152	0.0835	-0.349
1.00	2.1416	0.0083	-1.771	-5.165	-8.629
10.00	0.5295	-1.657	-28.99	-61.57	-93.40
100.00	0.1591	-5.721	-311.6	-627.0	-941.6
<i>R = 100.00</i>					
0.00	32.467	16.233	10.8219	8.1161	6.4925
0.01	32.437	16.173	10.7314	7.9953	6.3416
0.10	32.166	15.630	9.9191	6.9160	4.9990
1.00	29.460	10.330	2.7378	0.2337	-1.152
10.00	6.6966	0.0101	-5.958	-47.44	-83.91
100.00	0.5443	-1.814	-283.1	-612.7	-932.1

TABLE 5

*First five values of δ for generally restrained circular shafts for various values of R and T
($R_2 = R_1 = R$, $T = T_1 = T_2/100$)*

T	Mode				
	1	2	3	4	5
$R = 0.10$					
0.01	0.3164	0.0279	-0.028	-0.067	-0.101
0.10	0.7459	-0.090	-0.412	-0.711	-1.012
1.00	2.2652	-0.798	-3.401	-6.424	-9.520
10.00	7.1331	-2.973	-31.70	-62.98	-94.34
100.00	22.547	-9.563	-314.4	-628.5	-942.6
$R = 1.00$					
0.01	1.0560	0.3911	0.1470	0.0444	-0.020
0.10	2.6240	0.3229	-0.229	-0.597	-0.928
1.00	8.0772	-0.386	-3.161	-6.287	-9.427
10.00	25.473	-2.134	-31.42	-62.83	-94.25
100.00	80.531	-7.063	-314.2	-628.3	-942.5
$R = 10.00$					
0.01	4.1530	2.7145	1.6185	1.0493	0.7359
0.10	9.6628	3.1880	1.2195	0.3900	-0.162
1.00	30.004	1.4186	-1.220	-4.942	-8.495
10.00	94.721	-0.601	-28.62	-61.41	-93.30
100.00	299.48	-2.912	-311.3	-626.9	-941.5
$R = 100.00$					
0.01	32.470	16.268	11.118	9.5830	7.7809
0.10	33.977	29.416	15.402	9.7789	6.8028
1.00	98.686	29.036	9.9831	2.1373	-0.725
10.00	311.55	4.7415	-4.166	-47.18	-83.77
100.00	985.10	-0.638	-282.7	-612.6	-932.0

TABLE 6

First five values of δ for generally restrained circular shafts for various values of R and T
 ($R = R_1 = R_2/100$, $T = T_1 = T_2/100$)

T	Mode				
	1	2	3	4	5
$R = 0.01$					
0.00	0.0115	0.0029	0.0016	0.0010	0.0008
0.01	0.0079	-0.016	-0.047	-0.078	-0.109
0.10	0.0031	-0.143	-0.431	-0.723	-1.020
1.00	0.0010	-0.860	-3.426	-6.437	-9.529
10.00	0.0003	-3.111	-31.73	-62.99	-94.35
100.00	0.0001	-9.984	-314.5	-628.5	-942.6
$R = 0.10$					
0.00	0.0671	0.0231	0.0138	0.0098	0.0076
0.01	0.0548	0.0001	-0.030	-0.067	-0.101
0.10	0.0132	-0.095	-0.412	-0.711	-1.012
1.00	0.0032	-0.799	-3.401	-6.424	-9.529
10.00	0.0010	-2.973	-31.70	-62.98	-94.34
100.00	0.0003	-9.568	-314.4	-628.5	-942.6
$R = 1.00$					
0.00	0.4970	0.2055	0.1266	0.0911	0.0711
0.01	0.4805	0.1599	0.0524	0.0039	-0.025
0.10	0.3459	0.0002	-0.232	-0.597	-0.928
1.00	0.0148	-0.397	-3.161	-6.287	-9.427
10.00	0.0032	-2.144	-31.42	-62.83	-94.23
100.00	0.0010	-7.0893	-314.2	-628.3	-942.5
$R = 10.00$					
0.00	3.4963	1.7376	1.1494	0.8553	0.6794
0.01	3.4702	1.6843	1.0677	0.7442	0.5382
0.10	3.2385	1.2290	0.3977	0.0060	-0.170
1.00	1.4338	0.0002	-1.226	-4.943	-8.495
10.00	0.0151	-0.621	-28.62	-61.41	-93.30
100.00	0.0033	-2.940	-311.3	-626.9	-941.5

parameters R and T , the torsional frequencies of the shaft or piping system can be controlled in a practical situation.

REFERENCES

1. D. J. GORMAN 1975 *Free Vibration Analysis of Beams and Shafts*. New York: John Wiley.
2. R. D. BLEVINS 1979 *Formulas for Natural Frequency and Mode Shape*. New York: Van Nostrand.

Torsional Post-buckling of Thin-Walled Open Section Beams Resting on a Continuous Elastic Foundation

C. Kameswara Rao* & S. Mirza

Department of Mechanical Engineering, University of Ottawa, Ottawa, Ontario, Canada, K1N 6N5

(Received 10 August 1988; revised version received 22 August 1988; accepted 27 September 1988)

ABSTRACT

The post-buckling behaviour of thin-walled beams of open section subjected to an axial compressive load and resting on a Winkler-type continuous elastic foundation is discussed. We assume the strains to be small and elastic, shear deformations and the in-plane cross-sectional deformations to be negligible. The post-buckling paths are determined for simply supported and clamped beams with constant cross-section. The points of bifurcation in both cases are found to be symmetric and stable for various values of warping and foundation parameters.

NOTATION

A, L	Area of cross-section and length of the beam
C_s	Torsion constant
C_w	Warping constant
E, G	Modulus of elasticity and shear modulus
F	$I_R - (I_{pc}/A)^2$, cross-sectional property
I_p	Polar moment of inertia of beam, also $I_{pc} = 1/2 I_p$
I_R	Fourth moment of inertia of beam

*Present address: Corporate R & D Division, Bharat Heavy Electricals Ltd, Vikas Nagar, Hyderabad 500593, India.

K_t	Torsional foundation modulus
K	Warping parameter
P	Axial compressive load
P_{cr}, P_{cr}^*	Linear and nonlinear buckling loads
$x(z)$	Normal function of angle of twist
z	Distance along the length of beam
γ^2	$K_t L / 4EC_w$; foundation parameter
δ	F/C_w
Δ^2	$\sigma I_p L^2 / EC_w$; load parameter
$\Delta_{cr}, \Delta_{cr}^*$	Linear and nonlinear buckling load parameters
ϕ	Angle of twist
σ	P/A , axial compressive stress

INTRODUCTION

The study of the post-buckling behaviour of thin-walled prismatic beams of open section has wide-ranging applications in aircraft structures, runways and railroads. In addition, many of the base-frame structures of rotating machinery consist of thin-walled beams of open section which are either continuously or periodically supported by other structural members or concrete foundations. Under some critical loading conditions these beams undergo either pure torsional or coupled flexural-torsional buckling which poses severe design problems in the power industry.

The problem of linear torsional buckling has been extensively studied and the results for many cases are documented in standard books.^{1,2} However, the classical linear buckling theories for elastic beams necessarily predict buckling at loads that remain constant as the buckling amplitudes increase. The nonlinear behaviour of members in uniform torsion was first investigated by Young³ who considered circular cross-sections. The related problem of torsional stiffness of narrow rectangular sections under uniform axial tension, was examined by Buckley.⁴ Weber³ investigated the nonlinear behaviour of narrow rectangular strips in pure torsion. Cullimore⁵ studied the behaviour of thin-walled I and Z sections. A more accurate theory of nonlinear non-uniform torsion of thin-walled beams of open section was presented by Ghobarah and Tso^{6,7} using the principle of minimum potential energy and taking into account large torsional deformations under general loading and boundary conditions.

Bazant and El Nimeiri,⁸ Epstein and Murray,⁹ Szymzak,¹⁰ Roberts and Azizian¹¹ and Wekezer^{12,13} studied the nonlinear torsional behaviour of

thin-walled beams in a greater detail. However, in all these studies the effect of continuous elastic foundation was not considered. Kameswara Rao *et al.*^{14, 15} studied the effect of Winkler-type elastic foundation on the linear torsional stability of thin-walled beams of open section, but its effect on post-buckling behaviour was not studied. The present paper investigates the effect of continuous Winkler-type elastic foundation on the torsional post-buckling behaviour of uniform thin-walled I-beams.

THEORETICAL FORMULATION

Let us consider a doubly symmetric thin-walled beam of constant cross-section of length L undergoing pure torsion and subjected to an axial compressive load P . The beam is resting on Winkler-type elastic foundation. In the present formulation, we neglect the effects of (i) large and inelastic strains, (ii) shear deformations and (iii) in-plane cross-sectional deformations. The total potential energy V , consisting of the strain energy of deformation of the beam, the work done by the external axial compressive load and the reaction offered by the continuous elastic foundation, is given by^{10, 14, 16}

$$V = \frac{1}{2} \int_0^L [EC_w(\phi'')^2 + (GC_s - \sigma I_p)(\phi')^2 + EF(\phi')^4 + k_t(\phi)^2] dz \quad (1)$$

where primes denote differentiation with respect to z .

The fundamental differential equation resulting from the Euler condition of stationary potential energy given by eqn (1) can be written as

$$EC_w \phi^{iv} - 6EF(\phi')^2 \phi'' - (GC_s - \sigma I_p) \phi'' + k_t \phi = 0 \quad (2)$$

Two cases of simply supported and clamped end conditions are considered here. The boundary conditions associated with these cases are

$$(a) \text{ simply supported end } \phi = 0; \phi'' = 0 \quad (3)$$

$$(b) \text{ clamped end } \phi = 0; \phi' = 0 \quad (4)$$

The general solution of eqn (2) with the associated boundary conditions can be obtained by numerical methods using computer techniques. However, in this study approximate solutions are obtained by using Galerkin's technique.

Simply supported beam

For a simply supported beam, the boundary conditions are

$$\phi = 0 \quad \text{and} \quad \phi'' = 0 \quad \text{at} \quad Z = 0 \quad (5)$$

$$\phi = 0 \quad \text{and} \quad \phi'' = 0 \quad \text{at} \quad Z = 1 \quad (6)$$

where primes denote differentiation with respect to the dimensionless length $Z = z/L$.

Equation (2) can be written in non-dimensional form as

$$\phi^{iv} - 6\delta(\phi')^2\phi'' - (K^2 - \Delta^2)\phi'' + 4\gamma^2\phi = 0 \quad (7)$$

In the above equation the parameter $\delta = F/C_w$. In order to solve eqn (7) by Galerkin's method, the angle of twist $\phi(Z)$ is assumed to be of the form

$$\phi(Z) = \beta x(Z) \quad (8)$$

where β is the torsional amplitude. The approximate function $x(Z)$ is assumed to satisfy the boundary conditions. On substituting eqn (8) in (7), we can estimate the error ε as

$$\varepsilon = \beta[x^{iv} - 6\beta^2\delta(x')^2x'' - (K^2 - \Delta^2)x'' + 4\gamma^2x] \quad (9)$$

In order to minimize the error ε , the Galerkin's integral is given by the following equation:

$$\int_0^1 \varepsilon x \, dZ = 0 \quad (10)$$

Keeping in view the boundary conditions for this case, which are given by eqns (5) and (6), we assume

$$x(Z) = \sin \pi Z \quad (11)$$

Substituting eqns (9) and (11) into eqn (10), the expression for the torsional post-buckling load for a simply supported beam can be established:

$$\Delta_{cr}^{*2} = K^2 + \pi^2 + 4\gamma^2/\pi^2 + (3/2)\pi^2\delta\beta^2 \quad (12)$$

The corresponding linear torsional buckling load is given by

$$\Delta_{cr}^2 = K^2 + \pi^2 + 4\gamma^2/\pi^2 \quad (13)$$

Hence, the ratio of the nonlinear buckling load to linear buckling load is given by

$$P^*/P_{cr} = \Delta_{cr}^{*2}/\Delta_{cr}^2 = 1 + (3/2)\pi^4\delta\beta^2/[\pi^2(K^2 + \pi^2) + 4\gamma^2] \quad (14)$$

In the absence of an elastic foundation, i.e. $\gamma = 0$, eqn (14) reduces to

$$P^*/P_{cr} = \Delta_{cr}^{*2}/\Delta_{cr}^2 = 1 + 3\pi^2\delta\beta^2/[2(K^2 + \pi^2)] \quad (15)$$

Clamped beam

The boundary conditions for a beam clamped at both ends are given as

$$\phi = 0 \quad \text{and} \quad \phi' = 0 \quad \text{at} \quad Z = 0 \quad (16)$$

$$\phi = 0 \quad \text{and} \quad \phi' = 0 \quad \text{at} \quad Z = 1 \quad (17)$$

For this case, the function $x(Z)$ is assumed to be of the form

$$x(Z) = \beta(1 - \cos 2\pi Z) \quad (18)$$

The expression for the torsional post-buckling load for a clamped beam is obtained by inserting eqns (9) and (18) in eqn (10). This yields

$$\Delta_{cr}^{*2} = K^2 + 4\pi^2 + 3\gamma^2/\pi^2 + 6\pi^2\delta\beta^2 \quad (19)$$

The corresponding linear torsional buckling load for a clamped beam is

$$\Delta_{cr}^2 = K^2 + 4\pi^2 + 3\gamma^2/\pi^2 \quad (20)$$

Hence, the ratio of the nonlinear buckling load to linear buckling load is given by

$$P^*/P_{cr} = \Delta_{cr}^{*2}/\Delta_{cr}^2 = 1 + 6\pi^4\delta\beta^2/[\pi^2(K^2 + 4\pi^2) + 3\gamma^2] \quad (21)$$

In the absence of an elastic foundation, i.e. $\gamma = 0$, eqn (21) reduces to

$$P^*/P_{cr} = \Delta_{cr}^{*2}/\Delta_{cr}^2 = 1 + 6\pi^2\delta\beta^2/[(K^2 + 4\pi^2)] \quad (22)$$

RESULTS AND CONCLUSIONS

In order to demonstrate the torsional post-buckling behaviour of doubly symmetric thin-walled beams, an American steel I-beam of 760 mm length with the following cross-sectional dimensions is chosen:

Flange width = 31.55 mm,

Distance between centre lines of flanges = 69.65 mm,

Flange thickness = 3.11 mm

Web thickness = 2.13 mm.

Using the beam properties selected above, we obtain the values of the non-dimensional parameters K and δ as $K = 3.106$ and $\delta = 1.1095$. Numerical values of P^*/P_{cr} against values of torsional amplitude β for four typical values of foundation parameter $\gamma(0, 4, 8, 12)$ are generated for simply supported and clamped beams using eqns (14) and (21) and the resulting plots are shown in Figs 1 and 2 respectively. The selected γ

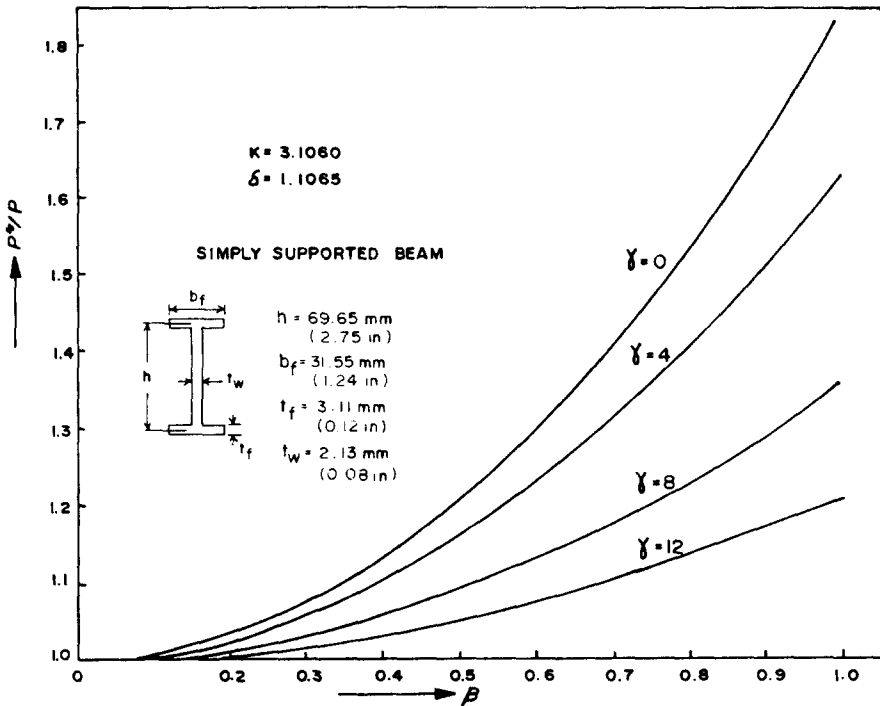


Fig. 1. Effect of elastic foundation on the torsional post-buckling behaviour of simply supported thin-walled beams of open section.

values, provide a wide range of foundation characteristics varying from no torsional stiffness to high torsional stiffness values. In both cases, we observe that the ratio of the nonlinear buckling load to linear torsional buckling load P^*/P_{cr} increases with increasing values of the torsional amplitude β for a given value of γ . The nonlinearity is of the hardening type as in the case of columns and plates and further, the equilibrium configurations in the torsional post-buckling region exist only for axial compressive loads in excess of the critical load of small deflection theory.

It is observed that for lower values of γ the nonlinear buckling load increases rapidly as β increases. As γ increases, the P^* - β curves become flatter indicating that the influence of β on P^* becomes gradually less significant. Equations (14) and (21) indicate that as δ increases the nonlinear buckling load P^* increases for constant values of K , γ and β . Also, the effect of increase in the values of warping parameter K and (or) foundation parameter γ is to decrease the nonlinear buckling load P^* considerably.

Comparing Figs 1 and 2 and also eqns (14) and (21), we notice that the rate of change in the nonlinear torsional buckling load P^* due to an

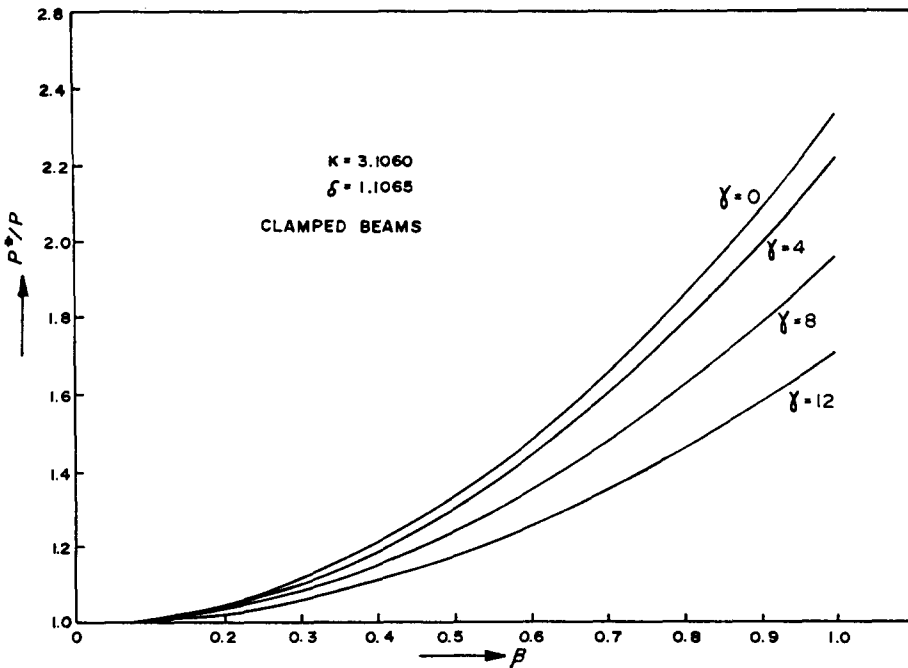


Fig. 2. Effect of elastic foundation on the torsional post-buckling behaviour of clamped thin-walled beams of open section.

increase in β , for any constant values of K and δ , is more significant in clamped beams than in simply supported beams. Hence, simply supported beams lose stability earlier than clamped beams.

REFERENCES

1. Timoshenko, S. P. & Gere, J. M., *Theory of Elastic Stability*, 2nd ed., McGraw-Hill, New York, 1961, pp. 212-29.
2. Vlasov, V. Z., *Thin-walled Elastic Beams*, 2nd ed., National Science Foundation, Washington, DC, 1961.
3. Timoshenko, S. P., *Strength of Materials—Part II*, 3rd ed, D. Van Nostrand Co. Inc., Princeton, NJ, 1956.
4. Buckley, J. C., The bifilar property of twisted strips. *Phil. Mag., London*, **28** (1914) 778.
5. Cullimore, M. S. G., The shortening effect—A non-linear feature of pure torsion, *Engineering Structures*. Butterworths, London, 1949, p. 153.
6. Tso, W. K. & Ghobarah, A. A., Non-linear non-uniform torsion of thin-walled beams. *Int. J. Mech. Sci.*, **13** (1971) 1039-47.
7. Ghobarah, A. A. & Tso, W. K., A non-linear thin-walled beam theory. *Int. J. Mech. Sci.*, **13** (1971) 1025-38.

8. Bazant, Z. P. & El Nimeiri, M., Large deflection spacial buckling of thin-walled beams and frames. *J. Engng Mech. Div., ASCE*, **99** (1973) 1259-81.
9. Epstein, M. & Murray, D. W., Three-dimensional large deformation analysis of thin-walled beams. *Int. J. Solids Struct.*, **12** (1976) 867-76.
10. Szymzak, C., Buckling and initial post-buckling behaviour of thin-walled I-columns. *Comput. Struct.*, **11** (1980) 481-7.
11. Roberts, T. M. & Azizian, Z. G., Instability of thin-walled bars. *J. Engng Mech., ASCE*, **109** (1983) 781-94.
12. Wekezer, J. W., Instability of thin-walled bars. *J. Engng Mech., ASCE*, **111** (1985) 923-35.
13. Wekezer, J. W., Non-linear torsion of thin-walled bars of variable cross-sections. *Int. J. Mech. Sci.*, **27** (1985) 631-41.
14. Kameswara Rao, C., Gupta, B. V. R. & Rao, D. L. N., Torsional vibrations of thin-walled beams on continuous elastic foundation using finite element method. In *Proceedings of the Int. Conf. on Finite Element Methods in Engineering*, Coimbatore Institute of Technology, Coimbatore, December 1974, pp. 231-48.
15. Kameswara Rao, C. & Appala Satyam, A., Torsional vibrations and stability of thin-walled beams on continuous elastic foundation. *AIAA Journal*, **13** (1975) 232-4.
16. Hatenyi, M., *Beams on Elastic Foundation*, University of Michigan Press, Ann Arbor, 1946, pp. 151-5.

Torsional Post-buckling of Thin-Walled Open Section Beams Resting on a Continuous Elastic Foundation

C. Kameswara Rao* & S. Mirza

Department of Mechanical Engineering, University of Ottawa, Ottawa, Ontario, Canada, K1N 6N5

(Received 10 August 1988; revised version received 22 August 1988; accepted 27 September 1988)

ABSTRACT

The post-buckling behaviour of thin-walled beams of open section subjected to an axial compressive load and resting on a Winkler-type continuous elastic foundation is discussed. We assume the strains to be small and elastic, shear deformations and the in-plane cross-sectional deformations to be negligible. The post-buckling paths are determined for simply supported and clamped beams with constant cross-section. The points of bifurcation in both cases are found to be symmetric and stable for various values of warping and foundation parameters.

NOTATION

A, L	Area of cross-section and length of the beam
C_s	Torsion constant
C_w	Warping constant
E, G	Modulus of elasticity and shear modulus
F	$I_R - (I_{pc}/A)^2$, cross-sectional property
I_p	Polar moment of inertia of beam, also $I_{pc} = 1/2 I_p$
I_R	Fourth moment of inertia of beam

*Present address: Corporate R & D Division, Bharat Heavy Electricals Ltd, Vikas Nagar, Hyderabad 500593, India.

K_t	Torsional foundation modulus
K	Warping parameter
P	Axial compressive load
P_{cr}, P_{cr}^*	Linear and nonlinear buckling loads
$x(z)$	Normal function of angle of twist
z	Distance along the length of beam
γ^2	$K_t L / 4EC_w$; foundation parameter
δ	F/C_w
Δ^2	$\sigma I_p L^2 / EC_w$; load parameter
$\Delta_{cr}, \Delta_{cr}^*$	Linear and nonlinear buckling load parameters
ϕ	Angle of twist
σ	P/A , axial compressive stress

INTRODUCTION

The study of the post-buckling behaviour of thin-walled prismatic beams of open section has wide-ranging applications in aircraft structures, runways and railroads. In addition, many of the base-frame structures of rotating machinery consist of thin-walled beams of open section which are either continuously or periodically supported by other structural members or concrete foundations. Under some critical loading conditions these beams undergo either pure torsional or coupled flexural-torsional buckling which poses severe design problems in the power industry.

The problem of linear torsional buckling has been extensively studied and the results for many cases are documented in standard books.^{1,2} However, the classical linear buckling theories for elastic beams necessarily predict buckling at loads that remain constant as the buckling amplitudes increase. The nonlinear behaviour of members in uniform torsion was first investigated by Young³ who considered circular cross-sections. The related problem of torsional stiffness of narrow rectangular sections under uniform axial tension, was examined by Buckley.⁴ Weber³ investigated the nonlinear behaviour of narrow rectangular strips in pure torsion. Cullimore⁵ studied the behaviour of thin-walled I and Z sections. A more accurate theory of nonlinear non-uniform torsion of thin-walled beams of open section was presented by Ghobarah and Tso^{6,7} using the principle of minimum potential energy and taking into account large torsional deformations under general loading and boundary conditions.

Bazant and El Nimeiri,⁸ Epstein and Murray,⁹ Szymzak,¹⁰ Roberts and Azizian¹¹ and Wekezer^{12,13} studied the nonlinear torsional behaviour of

thin-walled beams in a greater detail. However, in all these studies the effect of continuous elastic foundation was not considered. Kameswara Rao *et al.*^{14, 15} studied the effect of Winkler-type elastic foundation on the linear torsional stability of thin-walled beams of open section, but its effect on post-buckling behaviour was not studied. The present paper investigates the effect of continuous Winkler-type elastic foundation on the torsional post-buckling behaviour of uniform thin-walled I-beams.

THEORETICAL FORMULATION

Let us consider a doubly symmetric thin-walled beam of constant cross-section of length L undergoing pure torsion and subjected to an axial compressive load P . The beam is resting on Winkler-type elastic foundation. In the present formulation, we neglect the effects of (i) large and inelastic strains, (ii) shear deformations and (iii) in-plane cross-sectional deformations. The total potential energy V , consisting of the strain energy of deformation of the beam, the work done by the external axial compressive load and the reaction offered by the continuous elastic foundation, is given by^{10, 14, 16}

$$V = \frac{1}{2} \int_0^L [EC_w(\phi'')^2 + (GC_s - \sigma I_p)(\phi')^2 + EF(\phi')^4 + k_t(\phi)^2] dz \quad (1)$$

where primes denote differentiation with respect to z .

The fundamental differential equation resulting from the Euler condition of stationary potential energy given by eqn (1) can be written as

$$EC_w \phi^{iv} - 6EF(\phi')^2 \phi'' - (GC_s - \sigma I_p) \phi'' + k_t \phi = 0 \quad (2)$$

Two cases of simply supported and clamped end conditions are considered here. The boundary conditions associated with these cases are

$$(a) \text{ simply supported end } \phi = 0; \phi'' = 0 \quad (3)$$

$$(b) \text{ clamped end } \phi = 0; \phi' = 0 \quad (4)$$

The general solution of eqn (2) with the associated boundary conditions can be obtained by numerical methods using computer techniques. However, in this study approximate solutions are obtained by using Galerkin's technique.

Simply supported beam

For a simply supported beam, the boundary conditions are

$$\phi = 0 \quad \text{and} \quad \phi'' = 0 \quad \text{at} \quad Z = 0 \quad (5)$$

$$\phi = 0 \quad \text{and} \quad \phi'' = 0 \quad \text{at} \quad Z = 1 \quad (6)$$

where primes denote differentiation with respect to the dimensionless length $Z = z/L$.

Equation (2) can be written in non-dimensional form as

$$\phi^{iv} - 6\delta(\phi')^2\phi'' - (K^2 - \Delta^2)\phi'' + 4\gamma^2\phi = 0 \quad (7)$$

In the above equation the parameter $\delta = F/C_w$. In order to solve eqn (7) by Galerkin's method, the angle of twist $\phi(Z)$ is assumed to be of the form

$$\phi(Z) = \beta x(Z) \quad (8)$$

where β is the torsional amplitude. The approximate function $x(Z)$ is assumed to satisfy the boundary conditions. On substituting eqn (8) in (7), we can estimate the error ε as

$$\varepsilon = \beta[x^{iv} - 6\beta^2\delta(x')^2x'' - (K^2 - \Delta^2)x'' + 4\gamma^2x] \quad (9)$$

In order to minimize the error ε , the Galerkin's integral is given by the following equation:

$$\int_0^1 \varepsilon x \, dZ = 0 \quad (10)$$

Keeping in view the boundary conditions for this case, which are given by eqns (5) and (6), we assume

$$x(Z) = \sin \pi Z \quad (11)$$

Substituting eqns (9) and (11) into eqn (10), the expression for the torsional post-buckling load for a simply supported beam can be established:

$$\Delta_{cr}^{*2} = K^2 + \pi^2 + 4\gamma^2/\pi^2 + (3/2)\pi^2\delta\beta^2 \quad (12)$$

The corresponding linear torsional buckling load is given by

$$\Delta_{cr}^2 = K^2 + \pi^2 + 4\gamma^2/\pi^2 \quad (13)$$

Hence, the ratio of the nonlinear buckling load to linear buckling load is given by

$$P^*/P_{cr} = \Delta_{cr}^{*2}/\Delta_{cr}^2 = 1 + (3/2)\pi^4\delta\beta^2/[\pi^2(K^2 + \pi^2) + 4\gamma^2] \quad (14)$$

In the absence of an elastic foundation, i.e. $\gamma = 0$, eqn (14) reduces to

$$P^*/P_{cr} = \Delta_{cr}^{*2}/\Delta_{cr}^2 = 1 + 3\pi^2\delta\beta^2/[2(K^2 + \pi^2)] \quad (15)$$

Clamped beam

The boundary conditions for a beam clamped at both ends are given as

$$\phi = 0 \quad \text{and} \quad \phi' = 0 \quad \text{at} \quad Z = 0 \quad (16)$$

$$\phi = 0 \quad \text{and} \quad \phi' = 0 \quad \text{at} \quad Z = 1 \quad (17)$$

For this case, the function $x(Z)$ is assumed to be of the form

$$x(Z) = \beta(1 - \cos 2\pi Z) \quad (18)$$

The expression for the torsional post-buckling load for a clamped beam is obtained by inserting eqns (9) and (18) in eqn (10). This yields

$$\Delta_{cr}^{*2} = K^2 + 4\pi^2 + 3\gamma^2/\pi^2 + 6\pi^2\delta\beta^2 \quad (19)$$

The corresponding linear torsional buckling load for a clamped beam is

$$\Delta_{cr}^2 = K^2 + 4\pi^2 + 3\gamma^2/\pi^2 \quad (20)$$

Hence, the ratio of the nonlinear buckling load to linear buckling load is given by

$$P^*/P_{cr} = \Delta_{cr}^{*2}/\Delta_{cr}^2 = 1 + 6\pi^4\delta\beta^2/[\pi^2(K^2 + 4\pi^2) + 3\gamma^2] \quad (21)$$

In the absence of an elastic foundation, i.e. $\gamma = 0$, eqn (21) reduces to

$$P^*/P_{cr} = \Delta_{cr}^{*2}/\Delta_{cr}^2 = 1 + 6\pi^2\delta\beta^2/[(K^2 + 4\pi^2)] \quad (22)$$

RESULTS AND CONCLUSIONS

In order to demonstrate the torsional post-buckling behaviour of doubly symmetric thin-walled beams, an American steel I-beam of 760 mm length with the following cross-sectional dimensions is chosen:

Flange width = 31.55 mm,

Distance between centre lines of flanges = 69.65 mm,

Flange thickness = 3.11 mm

Web thickness = 2.13 mm.

Using the beam properties selected above, we obtain the values of the non-dimensional parameters K and δ as $K = 3.106$ and $\delta = 1.1095$. Numerical values of P^*/P_{cr} against values of torsional amplitude β for four typical values of foundation parameter $\gamma(0, 4, 8, 12)$ are generated for simply supported and clamped beams using eqns (14) and (21) and the resulting plots are shown in Figs 1 and 2 respectively. The selected γ

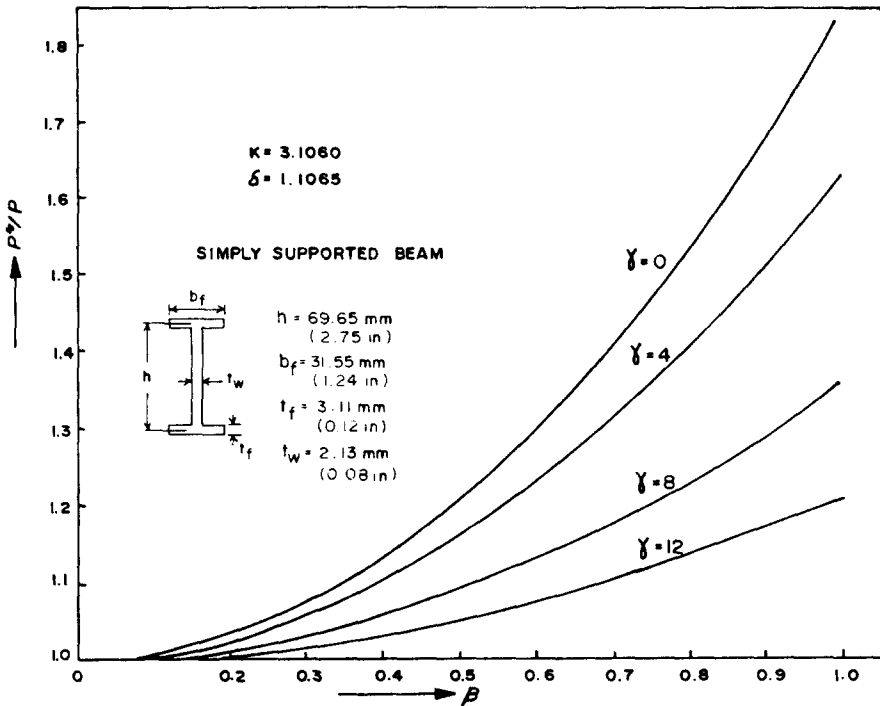


Fig. 1. Effect of elastic foundation on the torsional post-buckling behaviour of simply supported thin-walled beams of open section.

values, provide a wide range of foundation characteristics varying from no torsional stiffness to high torsional stiffness values. In both cases, we observe that the ratio of the nonlinear buckling load to linear torsional buckling load P^*/P_{cr} increases with increasing values of the torsional amplitude β for a given value of γ . The nonlinearity is of the hardening type as in the case of columns and plates and further, the equilibrium configurations in the torsional post-buckling region exist only for axial compressive loads in excess of the critical load of small deflection theory.

It is observed that for lower values of γ the nonlinear buckling load increases rapidly as β increases. As γ increases, the P^* - β curves become flatter indicating that the influence of β on P^* becomes gradually less significant. Equations (14) and (21) indicate that as δ increases the nonlinear buckling load P^* increases for constant values of K , γ and β . Also, the effect of increase in the values of warping parameter K and (or) foundation parameter γ is to decrease the nonlinear buckling load P^* considerably.

Comparing Figs 1 and 2 and also eqns (14) and (21), we notice that the rate of change in the nonlinear torsional buckling load P^* due to an

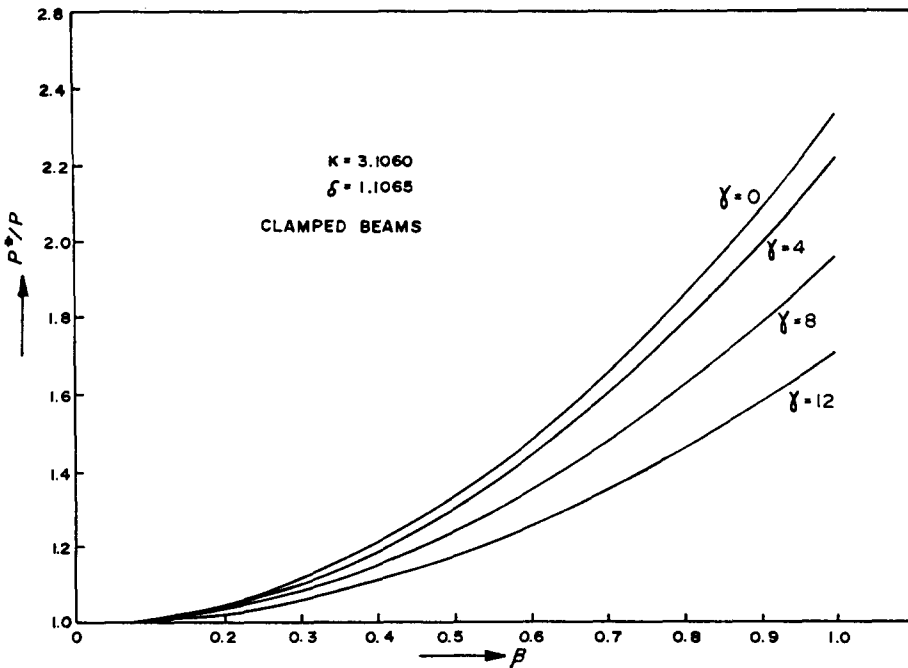


Fig. 2. Effect of elastic foundation on the torsional post-buckling behaviour of clamped thin-walled beams of open section.

increase in β , for any constant values of K and δ , is more significant in clamped beams than in simply supported beams. Hence, simply supported beams lose stability earlier than clamped beams.

REFERENCES

1. Timoshenko, S. P. & Gere, J. M., *Theory of Elastic Stability*, 2nd ed., McGraw-Hill, New York, 1961, pp. 212-29.
2. Vlasov, V. Z., *Thin-walled Elastic Beams*, 2nd ed., National Science Foundation, Washington, DC, 1961.
3. Timoshenko, S. P., *Strength of Materials—Part II*, 3rd ed, D. Van Nostrand Co. Inc., Princeton, NJ, 1956.
4. Buckley, J. C., The bifilar property of twisted strips. *Phil. Mag., London*, **28** (1914) 778.
5. Cullimore, M. S. G., The shortening effect—A non-linear feature of pure torsion, *Engineering Structures*. Butterworths, London, 1949, p. 153.
6. Tso, W. K. & Ghobarah, A. A., Non-linear non-uniform torsion of thin-walled beams. *Int. J. Mech. Sci.*, **13** (1971) 1039-47.
7. Ghobarah, A. A. & Tso, W. K., A non-linear thin-walled beam theory. *Int. J. Mech. Sci.*, **13** (1971) 1025-38.

8. Bazant, Z. P. & El Nimeiri, M., Large deflection spacial buckling of thin-walled beams and frames. *J. Engng Mech. Div., ASCE*, **99** (1973) 1259-81.
9. Epstein, M. & Murray, D. W., Three-dimensional large deformation analysis of thin-walled beams. *Int. J. Solids Struct.*, **12** (1976) 867-76.
10. Szymzak, C., Buckling and initial post-buckling behaviour of thin-walled I-columns. *Comput. Struct.*, **11** (1980) 481-7.
11. Roberts, T. M. & Azizian, Z. G., Instability of thin-walled bars. *J. Engng Mech., ASCE*, **109** (1983) 781-94.
12. Wekezer, J. W., Instability of thin-walled bars. *J. Engng Mech., ASCE*, **111** (1985) 923-35.
13. Wekezer, J. W., Non-linear torsion of thin-walled bars of variable cross-sections. *Int. J. Mech. Sci.*, **27** (1985) 631-41.
14. Kameswara Rao, C., Gupta, B. V. R. & Rao, D. L. N., Torsional vibrations of thin-walled beams on continuous elastic foundation using finite element method. In *Proceedings of the Int. Conf. on Finite Element Methods in Engineering*, Coimbatore Institute of Technology, Coimbatore, December 1974, pp. 231-48.
15. Kameswara Rao, C. & Appala Satyam, A., Torsional vibrations and stability of thin-walled beams on continuous elastic foundation. *AIAA Journal*, **13** (1975) 232-4.
16. Hatenyi, M., *Beams on Elastic Foundation*, University of Michigan Press, Ann Arbor, 1946, pp. 151-5.

Torsional Vibrations and Buckling of Thin-Walled Beams on Elastic Foundation

C. Kameswara Rao* & S. Mirza

Department of Mechanical Engineering, University of Ottawa, Ottawa, Canada K1N 6N5

(Received 23 November 1987; revised version received 15 March 1988; accepted 5 May 1988)

ABSTRACT

The problem of free torsional vibration and buckling of doubly symmetric thin-walled beams of open section, subjected to an axial compressive static load and resting on continuous elastic foundation, is discussed in this paper. An analytical method based on the dynamic stiffness matrix approach is developed, including the effects of warping. The resulting transcendental equation is solved for thin-walled beams clamped at one end and simply supported at the other. A computer program is developed, based on the dynamic stiffness matrix approach. The software consists of a master program to set up the dynamics stiffness matrix and to call specific sub-routines to perform various system calculations. Numerical results for natural frequencies and buckling load for various values of warping and elastic foundation parameter are obtained and presented.

1 INTRODUCTION

The vibrations and buckling of continuously-supported finite and infinite beams on elastic foundation have applications in the design of aircraft structures, base frames for rotating machinery, railroad tracks, etc. Several studies have been conducted on this topic, and valuable practical methods for the analysis of beams on elastic foundation have been suggested.¹⁻³ A discussion of various foundation models was presented by Kerr.⁴

While there are a number of publications on flexural vibrations of

Correspondence address: Group Co-ordinator (SFA), Bharat Heavy Electricals Ltd, Corporate R & D Division, Vikas Nagar, Hyderabad-500593, India.

rectangular beams and plates on elastic foundation, the literature on torsional vibrations and buckling of beams on elastic foundation is rather limited. Free torsional vibrations and stability of doubly-symmetric long thin-walled beams of open section were investigated by Gere,⁵ Krishna Murthy and Joga Rao⁶ and Christiano and Salmela.⁷ Kameswara Rao *et al.*⁸ used a finite element method to study the problem of torsional vibration of long, thin-walled beams of open sections resting on elastic foundations. In another publication⁹ Kameswara Rao and Appala Satyam developed approximate expressions for torsional frequency and buckling loads for thin-walled beams resting on Winkler-type elastic foundation and subjected to a time-invariant axial compressive force.

It is known that higher mode frequencies predicted by approximate methods are generally in considerable error. In order to improve this situation, a large number of elements or terms in the series have to be included in the computations to get values with acceptable accuracy. In view of the same, more and more effort is being put into developing frequency dependent 'exact' finite elements or dynamic stiffness and mass matrices. In the present paper, an improved analytical method based on the dynamic stiffness matrix approach is developed including the effects of Winkler-type elastic foundation and warping torsion. The resulting transcendental frequency equation is solved for a beam clamped at one end and simply supported at the other. Numerical results for torsional natural frequencies and buckling loads for some typical values of warping and foundation parameters are presented. The approach presented in this paper is quite general and can be utilized in analyzing continuous thin-walled beams also.

2 FORMULATION AND ANALYSIS

Consider a long doubly-symmetric thin-walled beam of open section of length L and resting on a Winkler-type elastic foundation of torsional stiffness K_s . The beam is subjected to a constant static axial compressive force P and is undergoing free torsional vibrations. The corresponding differential equation of motion can be written as:⁹

$$EC_w \partial^4 \phi / \partial z^4 - (GC_s - PI_p/A) \partial^2 \phi / \partial z^2 + K_s \phi + \rho I_p \partial^2 \phi / \partial t^2 = 0 \quad (1)$$

in which E is the modulus of elasticity; C_w , the warping constant; G , the shear modulus; C_s , the torsion constant; I_p , the polar moment of inertia; A , the area of cross-section; ρ , the mass density of the material of the beam; ϕ , the angle of twist; z , the distance along the length of the beam and t , the time.

For free torsional vibrations, the angle of twist $\phi(z, t)$ can be expressed in the form.

$$\phi(z, t) = x(z) e^{ipt} \quad (2)$$

in which $x(z)$ is the modal shape function corresponding to each beam torsional natural frequency p .

The expression for $x(z)$ which satisfies eqn (1) can be written as:

$$x(z) = A \cos \alpha z + B \sin \alpha z + C \cosh \beta z + D \sinh \beta z \quad (3)$$

in which,

$$\alpha L, \beta L = (1/\sqrt{2}) \{ \mp (K^2 - \Delta^2) + [(K^2 - \Delta^2)^2 + 4(\lambda^2 - 4\gamma^2)]^{1/2} \} \quad (4)$$

$$K^2 = L^2 GC_s / EC_w, \Delta^2 = PI_p L^2 / AEC_w \quad (5)$$

and

$$\lambda^2 = \rho I_p L^4 p_n^2 / EC_w, \gamma^2 = K_s L^4 / 4EC_w \quad (6)$$

From eqn (4), we have the following relation between αL and βL :

$$(\beta L)^2 = (\alpha L)^2 + K^2 - \Delta^2 \quad (7)$$

Knowing α and β , the frequency parameter λ can be evaluated using the following equation:

$$\lambda^2 = (\alpha L)(\beta L) + 4\gamma^2 \quad (8)$$

The four arbitrary constants A , B , C and D in eqn (3) can be determined from the boundary conditions of the beam. For any single-span beam, there will be two boundary conditions at each end and these four conditions then determine the corresponding frequency and mode shape expressions.

3 DYNAMIC STIFFNESS MATRIX

In order to proceed further, we must first introduce the following nomenclature: the variation of angle of twist ϕ with respect to z is denoted by $\theta(z)$; the flange bending moment and the total twisting moment are given by $M(z)$ and $T(z)$. Considering clockwise rotations and moments to be positive, we have,

$$\theta(z) = d\phi/dz, hM(z) = -EC_w(d^2\phi/dz^2) \quad (9)$$

and

$$T(z) = -EC_w(d^3\phi/dz^3) + (GC_s - PI_p/A)d\phi/dz \quad (10)$$

where $EC_w = I_f h^2/2$, I_f being the flange moment of inertia and h the distance between the center lines of the flanges of a thin-walled I-beam.

Consider a uniform thin-walled I-beam element of length l as shown in Fig. 1. By combining eqns (3) and (9), the end displacements, $\phi(0)$ and $\theta(0)$ and end forces, $hM(0)$ and $T(0)$, of the beam at $z = 0$, can be expressed as:

$$\begin{Bmatrix} \phi(0) \\ \theta(0) \\ hM(0) \\ T(0) \end{Bmatrix} = \begin{bmatrix} 1 & 0 & 1 & 0 \\ 0 & \alpha & 0 & \beta \\ EC_w \alpha^2 & 0 & -EC_w \beta^2 & 0 \\ 0 & EC_w \alpha \beta^2 & 0 & -EC_w \alpha^2 \beta \end{bmatrix} \begin{Bmatrix} A \\ B \\ C \\ D \end{Bmatrix} \quad (11a)$$

Equation (11a) can be written in an abbreviated form as follows:

$$\delta(0) = V(0)U \quad (11b)$$

In a similar manner, the end displacements, $\phi(L)$ and $\theta(L)$ and end forces $hM(L)$ and $T(L)$, of the beam where $z = l$ can be expressed as follows:

$$\delta(L) = V(L)U \quad (12a)$$

where

$$\{\delta(L)\}^T = \{\phi(L), \theta(L), hM(L), T(L)\} \quad (12b)$$

$$\{U\}^T = \{A, B, C, D\} \quad (12c)$$

and

$$[V(l)] = \begin{bmatrix} c & s & C & S \\ -\alpha s & \alpha c & \beta S & \beta C \\ EC_w \alpha^2 c & EC_w \alpha^2 s & -EC_w \beta^2 C & -EC_w \beta^2 S \\ -EC_w \alpha \beta^2 s & EC_w \alpha \beta^2 c & -EC_w \alpha^2 \beta S & -EC_w \alpha^2 \beta C \end{bmatrix} \quad (12d)$$

in which $c = \cos \alpha L$; $s = \sin \alpha L$; $C = \cos h \beta L$; $S = \sin h \beta L$.

By eliminating the integration constant vector U from eqns (11) and (12), and designating the left end of element as i and the right end as j , the equation relating the end forces and displacements can be written as:

$$\begin{Bmatrix} T \\ hM_i \\ T_j \\ hM_j \end{Bmatrix} = \begin{bmatrix} J_{11} & J_{12} & J_{13} & J_{14} \\ & J_{22} & J_{23} & J_{24} \\ & & J_{33} & J_{34} \\ \text{Sym} & & & J_{44} \end{bmatrix} \begin{Bmatrix} \phi_i \\ \theta_i \\ \phi_j \\ \theta_j \end{Bmatrix} \quad (13a)$$

Symbolically it is written

$$\{F\} = [J]\{U\} \quad (13b)$$

where

$$\{F\}^T = \{T_i, hM_i, T_j, hM_j\} \quad (13c)$$

$$\{U\}^T = \{\phi_i, \theta_i, \phi_j, \theta_j\} \quad (13d)$$

In eqns (13a) and (13b) the matrix $[J]$ is the 'exact' element dynamic stiffness matrix, which is also a square symmetric matrix. The elements of $[J]$ are given:

$$\begin{aligned} J_{11} &= H(\alpha^2 + \beta^2)(\alpha Cs + \beta Sc) \\ J_{12} &= -H[(\alpha^2 - \beta^2)(1 - Cc) + 2\alpha\beta Ss] \\ J_{13} &= -H(\alpha^2 + \beta^2)(\alpha s + \beta S) \\ J_{14} &= -H(\alpha^2 + \beta^2)(C - c) \\ J_{22} &= -(H/\alpha\beta)(\alpha^2 + \beta^2)(\alpha Sc - \beta Cs) \\ J_{24} &= (H/\alpha\beta)(\alpha^2 + \beta^2)(\alpha S - \beta s) \\ J_{23} &= -J_{14} \\ J_{33} &= J_{11} \\ J_{34} &= -J_{12} \\ J_{44} &= J_{22} \end{aligned} \quad (14)$$

and

$$H = EC_w \alpha\beta / [2\alpha\beta(1 - Cc) + (\beta^2 - \alpha^2)Ss]$$

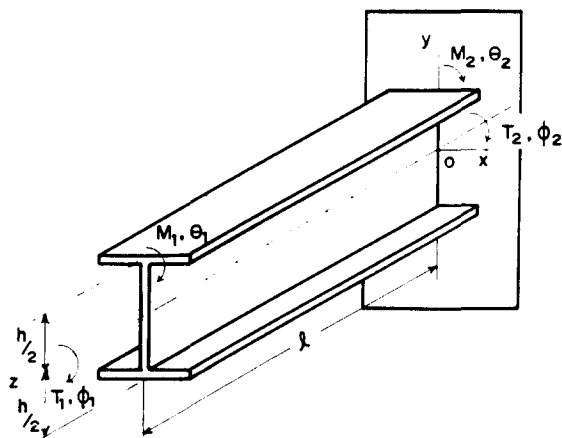


Fig. 1. Differential element of thin-walled I-beam.

Using the element dynamic stiffness matrix defined by eqns (13) and (14), one can easily set up the general equilibrium equations for multi-span thin-walled beams, adopting the usual finite element assembly methods. Introducing the boundary conditions, the final set of equations can be solved for eigenvalues by setting up the determinant of their matrix to zero. For convenience in programming, the signs of end forces and end displacements used in eqns (13) and (14) are all positive and are defined as shown in Fig. 1.

4 METHOD OF SOLUTION

Denoting the assembled and modified dynamic stiffness matrix as $[DS]$, we state that

$$\det |DS| = 0 \quad (15)$$

Equation (15) yields the frequency equation of continuous thin-walled beams in torsion resting on continuous elastic foundation and subjected to a constant axial compressive force. It can be noted that eqn (15) is highly transcendental in terms of the eigenvalues λ . The roots of eqn (15) can, therefore, be obtained by applying the Regula-Falsi method¹⁰ and the Wittrick-Williams algorithm¹¹ on a high-speed digital computer. Exact values of the frequency parameter λ for simply supported and built-in thin-walled beams are obtained in this paper using an error factor $\epsilon = 10^{-6}$.

A computer program was developed based on the above-discussed approach. The software includes a master program to evaluate and assemble

the various element stiffness matrices and to finally solve the frequency equations. Various checks are incorporated in order to identify and eliminate any false frequencies. Care is also taken to suitably adjust the required number of iterations to avoid missing any frequency in the specified range.

5 RESULTS AND DISCUSSION

The approach developed in this paper can be applied to the calculation of natural torsional frequencies and mode shapes of multi-span doubly symmetric thin-walled beams of open section such as beams of I-section. Beams with non-uniform cross-sections also can be handled very easily as the present approach is almost similar to the finite element method of analysis but with exact displacement shape functions. All classical and non-classical (elastic restraints) boundary conditions can be incorporated in the present model without any difficulty.

To demonstrate the effectiveness of the present approach, a single-span, thin-walled I-beam, clamped at one end ($z = 0$) and simply supported at the other end ($z = l$), is chosen. The boundary conditions for this problem can be written as:

$$\phi(0) = 0; \theta(0) = 0 \quad (16)$$

$$\phi(l) = 0 \text{ and } M(l) = 0 \quad (17)$$

Considering a one element solution and applying the boundary conditions defined by eqns (16) and (17) gives,

$$J_{22} = 0 \quad (18a)$$

This gives,

$$(H/\alpha\beta)(\alpha^2 + \beta^2)(\alpha Sc - \beta Cs) = 0 \quad (18b)$$

As H and $(\alpha^2 + \beta^2)$ are, in general, non-zero, the frequency equation for the clamped, simply supported beam can, therefore, be written as,

$$\alpha \tanh \beta L = \beta \tan \alpha L \quad (18c)$$

Equation (18c) is solved for values of warping parameter $K = 1$ and $K = 10$ and for various values of foundation parameter γ in the range 0–12. Figures 2 and 3 show the variation of fundamental frequency and buckling

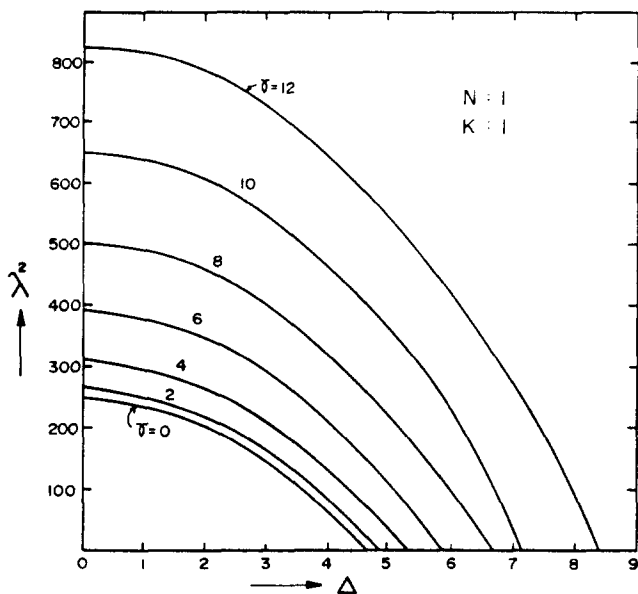


Fig. 2. Effect of elastic foundation on torsional frequencies and buckling loads of I-beams ($N = 1$, $K = 1$).

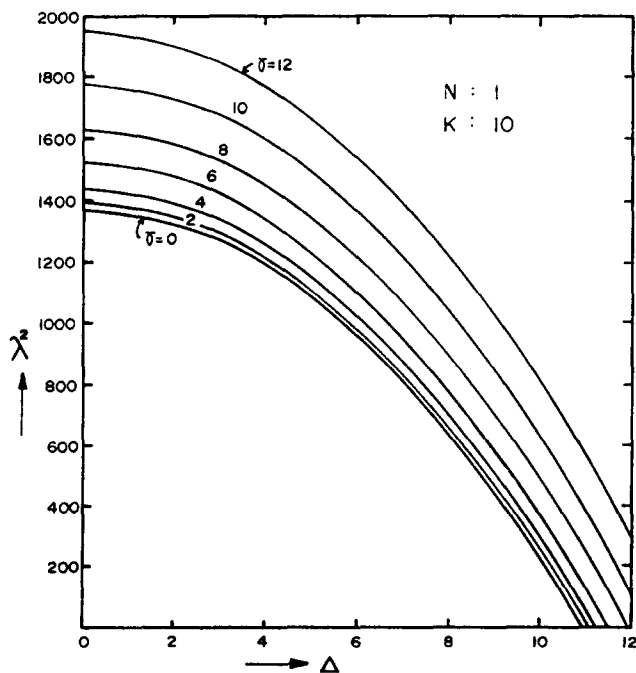


Fig. 3. Effect of elastic foundation on torsional frequencies and buckling loads of I-beams ($N = 1$, $K = 10$).

TABLE 1

Comparison between Exact and Approximate Values of λ^2 for the First Mode of Vibration of a Fixed, Simply Supported Beam Resting on Elastic Foundation

		Values of λ^2 from exact and approximate analyses ^a					
K	Δ	$\gamma = 4.0$		$\gamma = 8.0$		$\gamma = 12.0$	
		Exact	Approx.	Exact	Approx.	Exact	Approx.
1.0	0.0	314.265	325.950	506.302	517.894	826.253	837.892
	2.0	268.632	276.602	460.548	468.596	780.735	788.735
	4.0	132.226	128.557	324.676	320.624	644.378	640.655
10.0	0.0	1 439.762	1 547.319	1 631.753	1 739.526	1 951.865	2 059.296
	4.0	1 257.879	1 349.926	1 449.536	1 541.898	1 769.758	1 861.886
	8.0	712.010	757.747	904.893	949.692	1 224.926	1 269.686

^aResults from Galerkin's technique.⁹

load parameters with foundation parameter for values of K equal to 1 and 10 respectively. To give an idea about the accuracy of the results obtained, comparison is made with results obtained using approximate methods such as Galerkin's technique.⁹ Table 1 shows the comparison between the approximate values⁹ and those from the present analysis. It can be stated that even for beams with non-uniform sections, multiple spans and complicated boundary conditions, accurate estimates of natural frequencies can be obtained using the approach presented in this paper.

A close look at the results presented in Figs 2 and 3 clearly reveals that the effect of an increase in axial compressive load parameter Δ is to drastically decrease the fundamental frequency $\lambda(N = 1)$. Furthermore, the limiting load where λ becomes zero is the buckling load of the beam for a specified value of warping parameter K and foundation parameter γ . One can easily read the values of buckling load parameter Δ_{cr} from these figures for $\lambda = 0$. As can be expected, the effect of elastic foundation is found to increase the frequency of vibration especially for the first few modes. However, this influence is seen to be quite negligible on the modes higher than the third.

6 CONCLUDING REMARKS

A dynamic stiffness matrix approach has been developed for computing the natural torsion frequencies and buckling loads of long, thin-walled beams of open section resting on continuous Winkler-type elastic foundation and subjected to an axial time-invariant compressive load. The approach

presented in this paper is quite general and can be applied for treating beams with non-uniform cross-sections and also non-classical boundary conditions. Using Wittrick and Williams' algorithm¹¹, a computer program has been developed to accurately determine the torsional buckling loads, frequencies and corresponding modal shapes. Results for a beam clamped at one end and simply supported at the other have been presented, showing the influence of elastic foundation, axial compressive load and warping. While an increase in the values of elastic foundation parameter resulted in an increase in frequency, the effect of an increase in axial load parameter is found to be to drastically decrease the frequency to zero at the limit when the load equals the buckling load for the beam.

REFERENCES

1. Hetenyi, M., *Beams on elastic foundation*. University of Michigan Press, Ann Arbor, 1946.
2. Vlasov, V. Z. & Leont'ev, U. N., *Beams, plates and shells on elastic foundations*. Translation from Russian, Israel program for scientific translations, Jerusalem, 1961.
3. Timoshenko, S. P. & Gere, J. M., *Theory of elastic stability* (2nd Edition). McGraw-Hill, New York, 1961.
4. Kerr, A. D., Elastic and viscoelastic foundation models. *Journal of Applied Mechanics*, **31** (1964) 491-8.
5. Gere, J. M., Torsional vibrations of beams of thin walled open section. *Journal of Applied Mechanics*, **21** (1954) 381-7.
6. Krishna Murthy, A. V. & Joga Rao, C. V., General theory of vibrations of cylindrical tubes. *Journal of Aeronautical Society of India*, **20** (1968) 1-38, 235-58.
7. Christiano, P. & Salmela, L., Frequencies of beams with elastic warping restraint. *Journal of the Structures Division*, **97** (1971) 1835-40.
8. Kameswara Rao, C., Gupta, B. V. R. & Rao, D. L. N., Torsional vibrations of thin walled beams on continuous elastic foundation using finite element method. Proceedings of International Conference on Finite Element Methods in Engineering, Coimbatore, 1974, pp. 231-48.
9. Kameswara Rao, C. & Appala Satyam, A., Torsional vibration and stability of thin walled beams on continuous elastic foundation. *AIAA Journal*, **13** (1975) 232-4.
10. Wendroff, B., *Theoretical numerical analysis*. Academic Press, New York, 1966.
11. Wittrick, W. H. & Williams, F. W., A general algorithm for computing natural frequencies of elastic structures. *Quarterly Journal of Mechanics and Applied Mathematics*, **24** (1971) 263-84.

FREQUENCY ANALYSIS OF TWO-SPAN UNIFORM BERNOULLI-EULER BEAMS

1. INTRODUCTION

Free lateral vibration analysis of single-span uniform Bernoulli–Euler beams with various classical and non-classical boundary conditions has been studied extensively by various researchers [1, 2]. Over the years, several handbooks have appeared in the literature [3–5] giving exact frequency and mode-shape expressions and providing detailed frequency tables. However, a thorough literature search carried out by the author revealed that the problem of multi-span beams with unequal spans is still not fully investigated.

Harris and Crede [6], Wang [7], Gorman [4, 8], Laura *et al.* [9], and Pierre [10] studied various cases of multi-span beam problems and presented useful results. In all these studies, no attempt has been made to derive explicit and exact frequency expressions even for some simple cases. Furthermore, the problem of vibrations of two-span beams with guided end conditions has not been treated earlier. The present letter attempts to correct this situation, by providing explicit expressions for frequencies and mode shapes of two-span beams resting on a pinned intermediate support and with possible combinations of classical boundary conditions, including the guided ones. Frequency charts and tables are provided for some specific cases which permit immediate use in design.

2. ANALYSIS

A two-span uniform Bernoulli–Euler beam with an intermediate pinned support is considered here. With the beam undergoing harmonic free oscillations, the governing differential equation can be written as

$$Y''''(\xi) - \beta^4 Y(\xi) = 0, \quad (1)$$

where $\beta^4 = \rho A \omega^2 L^4 / (EI)$, ρ is the mass density of the beam material, A is the area of cross-section, E is the Young's modulus, I is the area moment of inertia, ω is the circular frequency, L is the overall length of the beam, and $\xi = x/L$ is the non-dimensional beam length.

The spatial co-ordinates measured along the spans as well as the transverse displacements are normalized with respect to the overall beam length L . The first span length is designated as μ with limits $0 < \mu < 1$. The second span length then becomes $\nu = 1 - \mu$.

The governing differential equation (1) is satisfied by expressing the first and second span deflections, respectively, as

$$Y_1(\xi_1) = A_1 \cosh \beta \xi_1 + B_1 \sinh \beta \xi_1 + C_1 \cos \beta \xi_1 + D_1 \sin \beta \xi_1, \quad (2)$$

$$Y_2(\xi_2) = A_2 \cosh \beta \xi_2 + B_2 \sinh \beta \xi_2 + C_2 \cos \beta \xi_2 + D_2 \sin \beta \xi_2. \quad (3)$$

where subscripts 1 and 2 refer to the left-hand and right-hand spans respectively.

The problem of enforcing the boundary conditions is simplified by measuring the ξ s in each span from the beam outer end (see inset of Figure 1). Evidently a total of eight boundary conditions are required in order to determine the arbitrary constants A_1, B_1, C_1, D_1 and A_2, B_2, C_2, D_2 of equations (2) and (3). Four of these equations can be written based on the boundary conditions existing at the beam outer ends. Two more equations can be obtained by requiring zero displacement at the intermediate pinned

support. Finally, the last two equations can be written by enforcing the conditions of continuity of beam slope and bending moment across the intermediate support.

The necessary and sufficient boundary conditions for any prescribed outer end of the beam can be written as follows:

$$(a) \text{ free end, } Y'' = 0, \quad Y''' = 0; \quad (4)$$

$$(b) \text{ guided end, } Y' = 0, \quad Y''' = 0; \quad (5)$$

$$(c) \text{ pinned end, } Y = 0, \quad Y'' = 0; \quad (6)$$

$$(d) \text{ clamped end, } Y = 0, \quad Y' = 0. \quad (7)$$

The four boundary conditions at the intermediate pinned support at $\xi_1 = \mu$ and $\xi_2 = \nu$ are

$$Y_1(\mu) = 0, \quad Y_2(\nu) = 0, \quad Y'_1(\mu) + Y'_2(\nu) = 0, \quad Y''_1(\mu) - Y''_2(\nu) = 0. \quad (8, 9)$$

3. FREQUENCY EQUATIONS

For each two-span beam, therefore, one obtains a set of eight homogeneous linear algebraic equations in eight constants A_1, A_2 etc. In order that the solutions other than zero may exist, the determinant of the coefficients of these arbitrary constants must be equal to zero. This leads to the frequency equation in each case from which the natural frequencies can be determined by utilizing numerical methods in conjunction with efficient algorithms [11]. In the following, a total of ten common types of two-span beams are identified by a compound adjective which describes the end conditions at $\xi_1 = 0$ and $\xi_2 = 0$: (a) pinned-pinned-pinned; (b) pinned-pinned-free; (c) clamped-pinned-pinned; (d) clamped-pinned-clamped; (e) clamped-pinned-free; (f) free-pinned-free; (g) guided-pinned-free; (h) guided-pinned-guided; (i) guided-pinned-pinned; (j) guided-pinned-clamped.

The frequency equations thus obtained are as follows:

$$(a), \sin \beta \nu \sinh \beta \nu (\cos \beta \mu \sinh \beta \mu - \sin \beta \mu \cosh \beta \mu) \\ + \sin \beta \mu \sinh \beta \mu (\cos \beta \nu \sinh \beta \nu - \sin \beta \nu \cosh \beta \nu) = 0; \quad (10)$$

$$(b), 2 \sin \beta \mu \sinh \beta \mu (1 + \cos \beta \nu \cosh \beta \nu) \\ - (\cos \beta \mu \sinh \beta \mu - \sin \beta \mu \cosh \beta \mu)(\cos \beta \nu \sinh \beta \nu - \sin \beta \nu \cosh \beta \nu) = 0; \quad (11)$$

$$(c), 2 \sin \beta \nu \sinh \beta \nu (1 - \cos \beta \mu \cosh \beta \mu) \\ + (\cos \beta \nu \sinh \beta \nu - \sin \beta \nu \cosh \beta \nu)(\cos \beta \mu \sinh \beta \mu - \sin \beta \mu \cosh \beta \mu) = 0; \quad (12)$$

$$(d), (1 - \cos \beta \mu \cosh \beta \mu)(\cos \beta \nu \sinh \beta \nu - \sin \beta \nu \cosh \beta \nu) \\ + (1 - \cos \beta \nu \cosh \beta \nu)(\cos \beta \mu \sinh \beta \mu - \sin \beta \mu \cosh \beta \mu) = 0; \quad (13)$$

$$(e), (1 - \cos \beta \mu \cosh \beta \mu)(\cos \beta \nu \sinh \beta \nu - \sin \beta \nu \cosh \beta \nu) \\ - (1 + \cos \beta \nu \cosh \beta \nu)(\cos \beta \mu \sinh \beta \mu - \sin \beta \mu \cosh \beta \mu) = 0; \quad (14)$$

$$(f), (1 + \cos \beta \mu \cosh \beta \mu)(\cos \beta \nu \sinh \beta \nu - \sin \beta \nu \cosh \beta \nu) \\ + (1 + \cos \beta \nu \cosh \beta \nu)(\cos \beta \mu \sinh \beta \mu - \sin \beta \mu \cosh \beta \mu) = 0; \quad (15)$$

$$(g), \quad 2 \cos \beta\mu \cosh \beta\mu (1 + \cos \beta\nu \cosh \beta\nu) \\ + (\cos \beta\mu \sinh \beta\mu + \sin \beta\mu \cosh \beta\mu)(\cos \beta\nu \sinh \beta\nu - \sin \beta\nu \cosh \beta\nu) = 0; \quad (16)$$

$$(h), \quad \cos \beta\mu \cosh \beta\mu (\cos \beta\nu \sinh \beta\nu + \sin \beta\nu \cosh \beta\nu) \\ + \cos \beta\nu \cosh \beta\nu (\cos \beta\mu \sinh \beta\mu + \sin \beta\mu \cosh \beta\mu) = 0; \quad (17)$$

$$(i), \quad \cos \beta\mu \cosh \beta\mu (\cos \beta\nu \sinh \beta\nu - \sin \beta\nu \cosh \beta\nu) \\ - \sin \beta\nu \sinh \beta\nu (\cos \beta\mu \sinh \beta\mu + \sin \beta\mu \cosh \beta\mu) = 0; \quad (18)$$

$$(j), \quad 2 \cos \beta\mu \cosh \beta\mu (1 - \cos \beta\nu \cosh \beta\nu) \\ - (\cos \beta\mu \sinh \beta\mu + \sin \beta\mu \cosh \beta\mu)(\cos \beta\nu \sinh \beta\nu - \sin \beta\nu \cosh \beta\nu) = 0. \quad (19)$$

5. MODE-SHAPE EXPRESSIONS

For each type of beam, for various values of μ and $\nu = 1 - \mu$, the roots of the frequency equations, β_n , $n = 1, 2, 3, \dots$, give the eigenvalues of the problem. The corresponding eigenfunctions, normal modes Y_1 and Y_2 , can be obtained accordingly. The mode-shape expressions obtained for cases (a)–(f) are the same as those presented by Gorman [4, 8] and hence will not be listed here. The mode-shape expressions for the rest of the cases (g)–(j) are as follows:

$$(g), \quad Y_1(\xi_1) = \cos \beta\xi_1 + \alpha_1 \cosh \beta\xi_1, \quad (20)$$

$$Y_2(\xi_2) = \alpha_2 [\sin \beta\xi_2 + \sinh \beta\xi_2 + \alpha_3 (\cos \beta\xi_2 + \cosh \beta\xi_2)], \quad (21)$$

where

$$\alpha_1 = -\cos \beta\mu / \cosh \beta\mu. \quad (22)$$

$$\alpha_2 = -\cos \beta\mu (\cos \beta\nu + \cosh \beta\nu) / (\cos \beta\nu \sinh \beta\nu - \sin \beta\nu \cosh \beta\nu), \quad (23)$$

$$\alpha_3 = -(\sin \beta\nu + \sinh \beta\nu) / (\cos \beta\nu + \cosh \beta\nu); \quad (24)$$

$$(h), \quad Y_1(\xi_1) = \cos \beta\xi_1 + \alpha_1 \cosh \beta\xi_1, \quad Y_2(\xi_2) = \alpha_2 (\cos \beta\xi_2 + \alpha_3 \cosh \beta\xi_2), \quad (25, 26)$$

where

$$\alpha_1 = -\cos \beta\mu / \cosh \beta\mu, \quad \alpha_2 = \cos \beta\mu / \cos \beta\nu, \quad \alpha_3 = -\cos \beta\nu / \cosh \beta\nu; \quad (27-29)$$

$$(i), \quad Y_1(\xi_1) = \cos \beta\xi_1 + \alpha_1 \cosh \beta\xi_1, \quad Y_2(\xi_2) = \alpha_2 (\sin \beta\xi_2 + \alpha_3 \sinh \beta\xi_2). \quad (30, 31)$$

where

$$\alpha_1 = -\cos \beta\mu / \cosh \beta\mu, \quad \alpha_2 = \cos \beta\mu / \sin \beta\nu, \quad \alpha_3 = -\sin \beta\nu / \sinh \beta\nu; \quad (32-34)$$

$$(j), \quad Y_1(\xi_1) = \cos \beta\xi_1 + \alpha_1 \cosh \beta\xi_1, \quad (35)$$

$$Y_2(\xi_2) = \alpha_2 [\sin \beta\xi_2 - \sinh \beta\xi_2 + \alpha_3 (\cos \beta\xi_2 - \cosh \beta\xi_2)], \quad (36)$$

where

$$\alpha_1 = -\cos \beta\mu / \cosh \beta\mu, \quad (37)$$

$$\alpha_2 = \cos \beta\mu (\cos \beta\nu - \cosh \beta\nu) / (\cos \beta\nu \sinh \beta\nu - \sin \beta\nu \cosh \beta\nu), \quad (38)$$

$$\alpha_3 = -(\sin \beta\nu - \sinh \beta\nu) / (\cos \beta\nu - \cosh \beta\nu). \quad (39)$$

6. RESULTS AND DISCUSSION

For a given two-span beam with μ and $\nu = 1 - \mu$ known, the values of β_n ($n = 1, 2, 3, \dots$) can be found by solving numerically the appropriate frequency equation, and the corresponding ω_n are then calculated by using the relation

$$\omega_n^2 = EI\beta_n^4/(\rho AL^4). \quad (40)$$

An efficient algorithm proposed by Wittrick and Williams [11] has been utilized in extracting the eigenvalues. In order that the designer can immediately use these results, frequency charts are drawn for beams with arbitrary values of intermediate support position parameter μ . Frequency charts obtained for cases (a)–(f) are exactly the same as those presented by Gorman [4, 8] and are therefore not included here. The frequency charts for the rest of the cases (g)–(j) are given in Figures 1–4 respectively. Frequency values for the first five modes of vibration for arbitrary values of μ can be easily read from these figures.

As small an interval as 0.01 in μ has been found necessary in generating reliable frequency data plotted in Figures 1–4. From these figures it can be clearly seen that the frequencies are sensitive to the changes in the position of the intermediate pinned support. With advantage taken of symmetry, results for case (h) are plotted in Figure 2 for values of μ in the range 0.0–0.5 only. The corresponding values for $\mu > 0.5$ can be read from this figure by suitably choosing the axis such that $\mu \leq 0.5$. Exact values of the frequency parameter β_n for the first mode of vibration are also presented in Table 1 for cases (g)–(j). This data will facilitate the designer's determination of accurate values of the frequencies when found necessary. This data can be also utilized in assessing the accuracy of various approximate methods utilized by various analysts [9, 10].

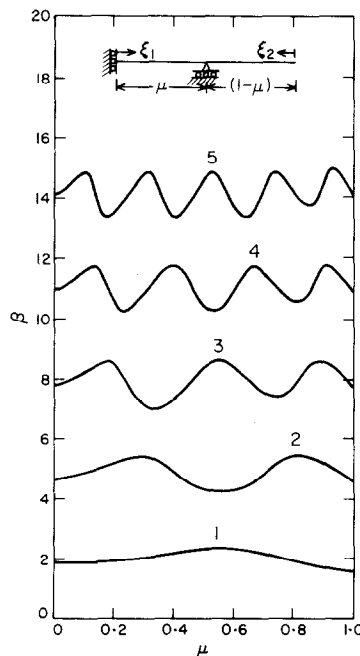


Figure 1. Frequency parameter values β for the first five modes of vibration as a function of μ for guided-pinned-free two-span beams.

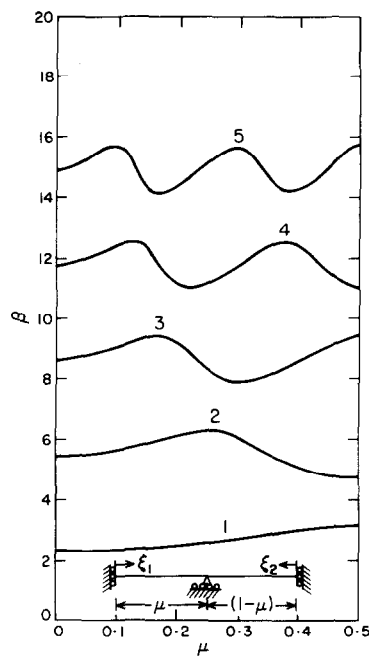


Figure 2. As Figure 1, but for guided-pinned-guided two-span beams.

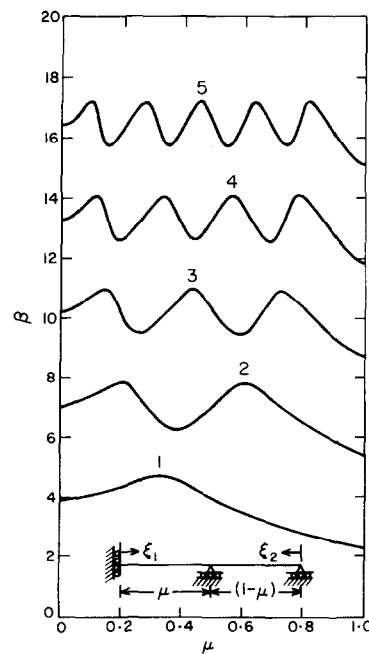


Figure 3. As Figure 1, but for guided-pinned-pinned two-span beams.

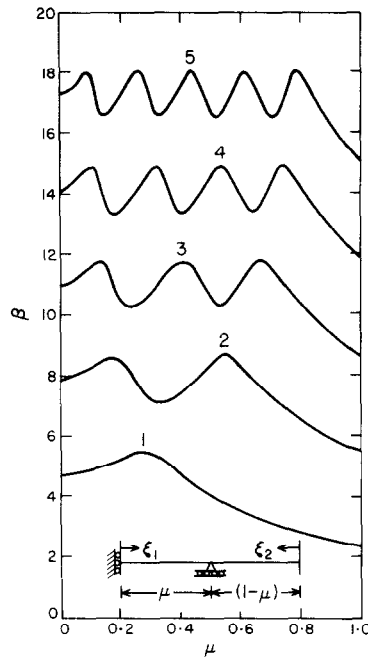


Figure 4. As Figure 1, but for guided-pinned-clamped two-span beams.

TABLE 1

Values of β_n (fundamental) for guided-pinned-XX beams for various values of μ and end condition XX

μ	End condition XX			
	Free	Guided	Pinned	Clamped
0.00	1.8751	2.3650	3.9266	4.7300
0.05	1.8813	2.3778	3.9608	4.7777
0.10	1.8990	2.4136	4.0504	4.8985
0.15	1.9276	2.4696	4.1817	5.0691
0.20	1.9664	2.5447	4.3441	5.2670
0.25	2.0153	2.6379	4.5107	5.4462
0.30	2.0739	2.7479	4.6716	5.4800
0.35	2.1408	2.8705	4.7000	5.2177
0.40	2.2132	2.9956	4.5197	4.8046
0.45	2.2842	3.0991	4.2254	4.4056
0.50	2.3409	3.1416	3.9266	4.0590
0.55	2.3650	3.0991	3.6582	3.7641
0.60	2.3416	2.9956	3.4247	3.5128
0.65	2.2725	2.8705	3.2229	3.2971
0.70	2.1741	2.7479	3.0482	3.1102
0.75	2.0631	2.6379	2.8960	2.9469
0.80	1.9510	2.5447	2.7627	2.8030
0.85	1.8438	2.4696	2.6453	2.6752
0.90	1.7444	2.4136	2.5411	2.5610
0.95	1.6534	2.3778	2.4482	2.4581
1.00	1.5708	2.3650	2.3650	2.3650

7. CONCLUSIONS

Exact frequency and mode-shape expressions for two-span beams resting on a pinned intermediate support with all possible combinations of classical boundary conditions have been presented. Frequency charts giving the first five natural frequencies of vibration for beams involving guided ends are provided for immediate use by designers. Exact frequency values for the first mode of vibration for various discrete values of intermediate support position parameter μ are presented in tabular form to facilitate accurate estimates where necessary.

The various results presented clearly demonstrate that the natural frequencies of two-span beams with various end conditions are sensitive to the position of the intermediate pinned support. The various frequency and mode-shape expressions provided can be used effectively in obtaining free vibration characteristics of two-span beams with an intermediate pinned support and with combinations of classical boundary conditions at the outer ends.

*Seismic & Foundation Analysis Group,
Corporate R&D Division,
Bharat Heavy Electricals Limited,
Vikas Nagar, Hyderabad-500 593, India*

C. KAMESWARA RAO

(Received 13 June 1989)

REFERENCES

1. H. WAGNER and V. RAMAMURTI 1977 *Shock and Vibration Digest* 9(9), 17–24. Beam vibrations—a review.
2. C. KAMESWARA RAO and S. MIRZA 1987 *American Society of Mechanical Engineers Proceedings of Pressure Vessels and Piping Conference, PVP-Vol. 124*, 117–121. Vibration frequencies and mode-shapes for generally restrained Bernoulli-Euler beams.
3. R. E. D. BISHOP and D. C. JOHNSON 1956 *Vibration Analysis Tables*. Cambridge University Press.
4. D. J. GORMAN 1975 *Free Vibration Analysis of Beams and Shafts*. New York: John Wiley.
5. R. D. BLEVINS 1979 *Formulas for Natural Frequency and Mode Shape*. New York: Van Nostrand Reinhold.
6. C. M. HARRIS and C. E. CREDE 1961 *Shock and Vibration Handbook*. New York: McGraw-Hill.
7. T. M. WANG 1970 *Journal of Sound and Vibration* 13, 409–414. Natural frequencies of continuous Timoshenko beams.
8. D. J. GORMAN 1974 *International Journal of Mechanical Sciences* 16, 345–351. Free lateral vibration analysis of double-span uniform beams.
9. P. A. A. LAURA, P. V. D. IRASSAR and G. M. FICCADENTI 1983 *Journal of Sound and Vibration* 86, 279–284. A note on transverse vibrations of continuous beams subject to an axial force and carrying concentrated masses.
10. C. PIERRE, D. M. TANG and E. H. DOWELL 1988 *American Institute of Aeronautics and Astronautics Journal* 25, 1249–1257. Localized vibrations of disordered multi-span beams: theory and experiment.
11. W. H. WITTRICK and F. W. WILLIAMS 1971 *Quarterly Journal of Mechanics and Applied Mathematics* 24, 263–284. A general algorithm for computing natural frequencies of elastic structures.



Natural Frequencies of U-Shaped Bellows

Li Ting-Xin

Chemical Machinery Department, South China University of Technology,
Guangzhou 510641, People's Republic of China

Guo Bing-Liang

Chemical Engineering Department, Inner Mongolia Institute of Technology,
Huhehaote 010062, People's Republic of China

&

Li Tian-Xiang

Chemical Machinery Department, South China University of Technology,
Guangzhou 510641, People's Republic of China

(Received 12 October 1989; accepted 6 December 1989)

ABSTRACT

It is assumed in this paper that the mass distribution of bellows is uniform. On this basis, the authors have deduced the equations for calculating the axial and the lateral natural frequencies of U-shaped bellows with different end conditions. This paper also discusses the influence of different amounts of axial extension and compression on the natural frequencies of bellows which either contain gas or are filled with liquids. Eleven U-shaped bellows specimens were chosen to perform experiments, applying the 'shock' method and the 'resonance' method respectively. The resulting experimental data have proven that the deduced equations are accurate enough to meet standard engineering requirements.

THE AXIAL NATURAL FREQUENCY OF BELLOWS

As shown in Fig. 1(a), it is assumed that a straight pipe with continuously and uniformly distributed mass is fixed at its bottom. A weight W_0 is

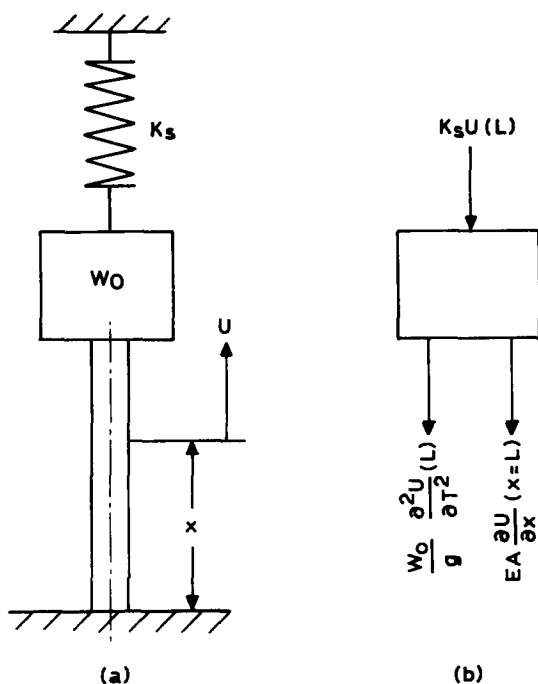


Fig. 1. Pipe with end condition.

attached to its top, and the weight is connected with a spring. The differential equation to express the axial vibration for the straight pipe can be given by:¹

$$\frac{\partial^2 u}{\partial T^2} = a^2 \frac{\partial^2 u}{\partial x^2}$$

where u is the axial displacement of the pipe (mm), T is the time (s), $a = \sqrt{Eg/v}$, E is the elastic modulus of the pipe material (MPa), g is the gravitational acceleration ($9806.65 \text{ mm s}^{-2}$) and v is the weight per unit volume of the pipe material (N mm^{-3}).

The solution of the above differential equation is:

$$u(x, t) = \left(C \sin \frac{\omega_i}{a} x + D \cos \frac{\omega_i}{a} x \right) \sin (\omega_i T + \phi) \quad (1)$$

where ω_i is the angular frequency (rad s^{-1}), ϕ is the phase angle (degrees), and C and D are integration constants. From the end condition: $x = 0$, $u(0, T) = 0$, we can obtain

$$D = 0 \quad (2)$$

When $x = L$ (L is the length of the pipe, mm) as shown in Fig. 1(b), the equilibrium equation of force along the x -axis is

$$AE \frac{\partial u}{\partial x} + \frac{W_0}{g} \frac{\partial^2 u}{\partial T^2} + K_s u = 0 \quad (3)$$

where A is the cross-sectional area of the pipe (mm^2) and K_s is the stiffness of the spring (N mm^{-1}).

Substituting eqn (2) into eqn (1) and then substituting eqn (1) into eqn (3) again yields:

$$AE \frac{\omega_i}{a} \cos \frac{\omega_i}{a} L - \frac{W_0}{g} \omega_i^2 \sin \frac{\omega_i}{a} L + K_s \sin \frac{\omega_i}{a} L = 0 \quad (4)$$

in which

$$\frac{L}{a} = \sqrt{\frac{LA\nu}{AEg/L}} = \sqrt{\frac{G/g}{Q/L(\partial u/\partial x)}} = \sqrt{\frac{G}{gK_n}} \quad (5)$$

where G is the weight of the pipe (N), Q is the applied axial force (N) and K_n is the axial spring rate of the pipe (N mm^{-1}). Therefore, $G = LA\nu$, $E = (Q/A)/(\partial u/\partial x)$, $K_n = Q/L(\partial u/\partial x)$. Substituting eqn (5) into eqn (4) yields the frequency equation of the system as follows:

$$AE \frac{\omega_i}{a} \cos \omega_i \sqrt{\frac{G}{gK_n}} - \frac{W_0}{g} \omega_i^2 \sin \omega_i \sqrt{\frac{G}{gK_n}} + K_s \sin \omega_i \sqrt{\frac{G}{gK_n}} = 0 \quad (6)$$

The axial natural frequencies of bellows with three different end conditions may be calculated by using the following three different methods.

(1) One end of the bellows is fixed and the other end is only attached by a weight W_0 (i.e. $W_0 \neq 0$, $K_s = 0$). Equation (6) becomes

$$AE \frac{\omega_i}{a} \cos \omega_i \sqrt{\frac{G}{gK_n}} = \frac{W_0}{g} \omega_i^2 \sin \omega_i \sqrt{\frac{G}{gK_n}}$$

Rearranging terms in the above equation yields

$$\omega_i \sqrt{\frac{G}{gK_n}} \tan \omega_i \sqrt{\frac{G}{gK_n}} = \frac{G}{W_0} \quad (7)$$

Assuming that

$$\beta_i = \omega_i \sqrt{\frac{G}{gK_n}} \quad \text{and} \quad \alpha = \frac{G}{W_0}$$

eqn (7) can be reduced to

$$\beta_i \tan \beta_i = \alpha \quad (8)$$

Here

$$\beta_i = (i - 1)\pi + \varepsilon_i \quad (9)$$

where i is the order number of the frequency, $i = 1, 2, 3, \dots$

$$0 < \varepsilon_i < \pi/2$$

Substituting eqn (9) into eqn (8), according to the value of α and by means of a trial and error method, the value of ε_i can be obtained. Therefore, the value of β_i in eqn (9) can also be obtained. The axial natural frequency of the bellows, f_i (Hz), is

$$f_i = \frac{\omega_i}{2\pi} = \frac{\beta_i}{2\pi} \sqrt{\frac{K_n g}{G}} = 15.76 \beta_i \sqrt{\frac{K_n}{G}} \quad (10)$$

(2) One end of the bellows is fixed, and the other end is free (i.e. $W_0 = 0$, $K_s = 0$). Equation (6) becomes

$$\cos \omega_i \sqrt{G/gK_n} = 0 \quad (11)$$

Therefore

$$f_i = \omega_i/2\pi = 49.5(i - 0.5)\sqrt{K_n/G} \quad (12)$$

(3) Both ends of the bellows are fixed (i.e. $W_0 = 0$, $K_s = \infty$). Equation (6) becomes

$$\sin \omega_i \sqrt{G/gK_n} = 0 \quad (13)$$

Therefore

$$f_i = \omega_i/2\pi = 49.5i\sqrt{K_n/G} \quad (14)$$

THE LATERAL NATURAL FREQUENCY OF BELLWS

When both ends of a straight pipe are fixed, the lateral natural frequency can be calculated for a pipe with continuously and uniformly distributed mass as follows:¹

$$f_i = \frac{k_i^2}{2\pi} \sqrt{\frac{EJg}{AvL^4}} \quad (15)$$

When $i = 1, 2, 3, 4, 5$, the corresponding k_i in eqn (15) equals 4.73, 7.85, 11, 14.14 and 17.28 respectively. EJ in eqn (15) is the bending stiffness of the pipe. For bellows EJ can be calculated by²

$$EJ = K_n n w d_p^2 / 8 \quad (16)$$

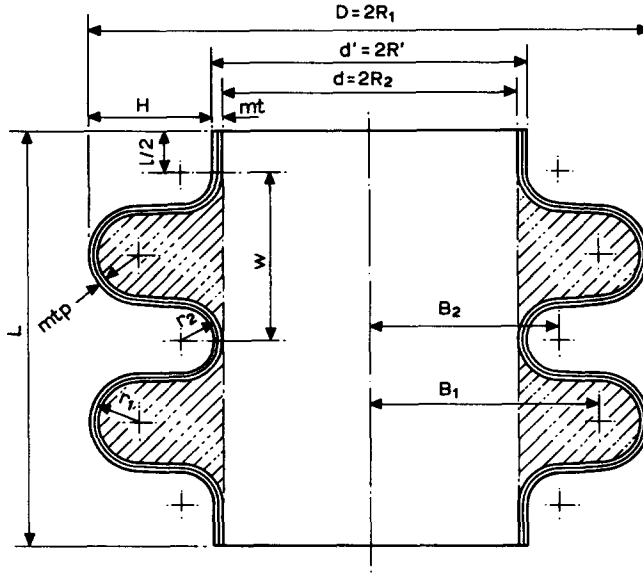


Fig. 2. U-shaped bellows.

where w is the bellows pitch (mm) (see Fig. 2), n is the total number of convolutions in one bellows, $d_p = d' + H$, d' is the outside diameter of the cylindrical tangent (mm, Fig. 2) and H is the convolution depth (mm).

Substituting eqn (16) into eqn (15), and noting that $G = \nu AL$ and $L = nw$, the lateral natural frequency of the bellows can be obtained as follows:

$$f_i = 5.57 k_i^2 \frac{d_p}{L} \sqrt{\frac{K_n}{G}}$$

or

$$f_i = C_i \frac{d_p}{L} \sqrt{\frac{K_n}{G}} \quad (17)$$

When $i = 1, 2, 3, 4, 5$, the corresponding C_i in eqn (17) equals 124.63, 343.53, 673.53, 1113.28 and 1663.13 respectively.

CALCULATION OF BELLOWS WEIGHT

The variable G in eqns (10), (12), (14) and (17) is the weight of the bellows. If the bellows contains only gas, the weight of the gas might be considered negligible, so that G is only the weight of the bellows material itself, G_1 (i.e. $G = G_1$). But if the bellows are filled with liquids, the weight of liquids, G_2 , in

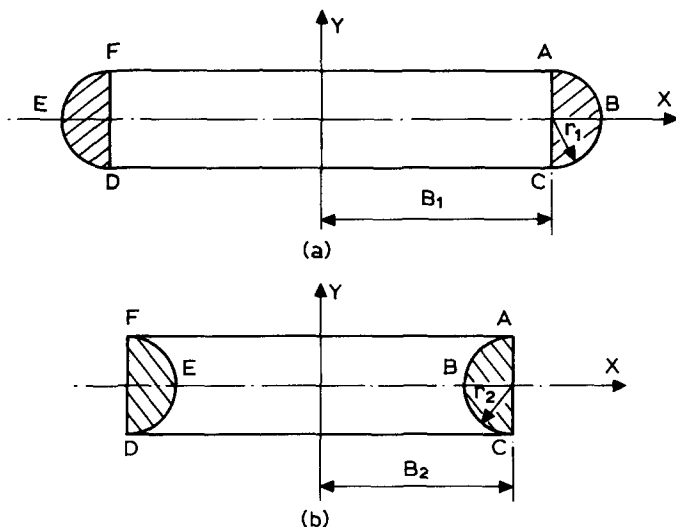


Fig. 3. Illustration of geometrical bodies.

the shaded area shown in Fig. 2 will have an effect on the axial natural frequency of bellows. Thus in eqns (10), (12) and (14), $G = G_1 + G_2$, and the weight of liquids in whole bellows, G_3 , will have an effect on the lateral natural frequency of bellows; so that, in eqn (17), $G = G_1 + G_3$. In order to derive the equations for calculating the values of G_1 , G_2 and G_3 , attention must first be given to those equations to determine the volumes of four kinds of geometric bodies (see Fig. 3). The volume V_1 , of the revolutionary body, which is formed by rotating cross-section ABCDEFA in Fig. 3(a) around the Y-axis, can be calculated by

$$V_1 = 2 \int_0^{r_1} (B_1 + \sqrt{r_1^2 - x^2})^2 \pi dx = 2\pi r_1 B_1^2 + \frac{4}{3}\pi r_1^3 + \pi^2 B_1 r_1^2 \quad (18)$$

The volume, V_2 , of the circular body shaded in Fig. 3(a) can be determined by

$$V_2 = V_1 - 2r_1 \pi B_1^2 = \pi^2 B_1 r_1^2 + \frac{4}{3}\pi r_1^3 \quad (19)$$

The volume, V_3 , of the revolutionary body, which is formed by rotating cross-section ABCDEFA in Fig. 3(b) around the Y-axis, can be calculated by

$$V_3 = 2 \int_0^{r_2} (B_2 - \sqrt{r_2^2 - x^2})^2 \pi dx = 2\pi r_2 B_2^2 + \frac{4}{3}\pi r_2^3 - \pi^2 B_2 r_2^2 \quad (20)$$

The volume, V_4 , of the circular body shaded in Fig. 3(b) can be determined by

$$V_4 = 2r_2 \pi B_2^2 - V_3 = \pi^2 B_2 r_2^2 - \frac{4}{3}\pi r_2^3 \quad (21)$$

Applying eqns (19) and (21), the value of G_1 can be obtained as follows:

$$G_1 = 2\pi n v t_0 [(B_1^2 - B_2^2) + \pi(B_1 r_1 + B_2 r_2) + 2(r_1^2 - r_2^2)] + v\pi(R_2 + R')lmt \quad (22)$$

If $r_1 = r_2 = r$, eqn (22) can be simplified to

$$G_1 = 2\pi n v t_0 (B_1 + B_2)(\pi r + B_1 - B_2) + v\pi(R_2 + R')lmt$$

where v is the weight per unit volume of the bellows material (N mm^{-3}), t_0 is the thickness of the bellows ($=mt_p$, mm), m is the number of plies of thickness t_p , t_p is the thickness of the bellows in one ply to correct for thinning during formation ($=t(d'/d_p)^{0.5}$, mm), t is the nominal material thickness of one ply (mm), r_1 is the middle radius of the crown torus (mm, Fig. 2), r_2 is the middle radius of the root torus (mm, Fig. 2), $B_1 = R_1 - r_1 - t_0/2$, R_1 is the outside radius of the convolution (mm, Fig. 2), $B_2 = R_2 + r_2 + t_0/2$, R_2 is the inside radius of the convolution (mm, Fig. 2), R' is the outside radius of the cylindrical tangent (mm), and l is the total length of cylindrical tangent at both ends (mm).

From eqns (18) and (20), the value of G_2 can be obtained as follows:

$$G_2 = n v' \pi \left[B_1^2(2r_1 - t_0) + \frac{\pi}{4} B_1(2r_1 - t_0)^2 + \frac{1}{6}(2r_1 - t_0)^3 + B_2^2(2r_2 + t_0) - \frac{\pi}{4} B_2(2r_2 + t_0)^2 + \frac{1}{6}(2r_2 + t_0)^3 - R_2^2 w \right] \quad (23)$$

and

$$G_3 = G_2 + L\pi R_2^2 v'$$

where v' is the weight per unit volume of the liquid (N mm^{-3}).

THE BELLOWS AXIAL SPRING RATE

The variable K_n in eqns (10), (12), (14) and (17) expresses the spring rate of bellows at the corresponding vibration conditions. Since bellows have different values of K_n when they have different amounts of axial tension and compression,^{3,4} the larger the amount of axial compression the smaller the value of K_n . The spring rate of bellows also changes with temperature;⁴ it decreases with an increase in temperature. The deflection hysteresis of bellows also leads to the kinetic spring rate being slightly lower than the static one.⁴ Hence the axial spring rate of bellows is not a constant under different vibration conditions, and it follows that the axial and the lateral natural frequencies are not constants. This conclusion has been proven by the experiments described later in this paper.

If the actual spring rate of bellows for the corresponding vibration conditions is unknown the initial elastic spring rate measured by experiments on bellows can be used. Alternatively K_n can be calculated by the formula in the *Standards of the Expansion Joint Manufacturers Association* (EJMA),⁵ as follows:

$$K_n = 1.7 \frac{E d_p t_p^3 m}{C_f H^3 n} \quad (25)$$

where E is the modulus of elasticity of the bellows material at working temperature (MPa) and C_f is a factor (see Ref. 5). However, some errors may be introduced when calculating the f_i in eqns (10), (12), (14) and (17) by using the K_n in eqn (25).

EXPERIMENTS

The U-shaped bellows specimens used in these experiments are shown in Fig. 2, and are made from austenitic stainless steel (1Cr18Ni9Ti). The dimensions of the specimens are listed in Table 1.

The experiments on the bellows spring rate were conducted on an electronic universal testing machine. The change of time rate of bellows deflection was 10 mm min^{-1} . The correlation between load and deflection was recorded continuously and automatically on a chart. The experimental spring rate data for all the specimens were listed in Table 1.

The 'shock' method was used to test the natural frequency of the bellows. Strain gauges were cemented onto the exterior of the bellows. When the bellows were shocked axially or laterally, they vibrated axially or laterally respectively, causing alternating variations of resistance in the strain gauges. A galvanometer-oscillograph chart was arranged to record the signals coming from the strain gauges as a result of vibration. The frequency of those signals illustrated the axial and the lateral natural frequencies of the bellows.

The 'resonance' method was an alternative way of measuring the axial natural frequency of bellows, and was also used to prove the results of the 'shock' method. The bellows, which was equipped with strain gauges, together with a vibration transducer, was mounted on the vibro-bench for testing. When the vertical vibration frequency of the vibro-bench equalled the axial natural frequency of the bellows, the ratio of resistance change caused by the deflection of the bellows to the vibration amplitude of the vibro-bench reached its maximum value. Similar recordings were taken subsequently at different frequencies on the galvanometer-oscillograph chart. A simple study of the chart enables us to determine the resonance

TABLE I
Bellows Dimensions and Elastic Spring Rate

Specimen number	Dimensions (mm)					Convolution number <i>n</i>	Elastic spring rate ($K_s/N\text{ mm}^{-1}$)			
	Bellows outside diameter <i>D</i>	Cylindrical tangent inside diameter <i>d</i>	Convolution depth <i>H</i>	Convolution pitch <i>W</i>	Nominal material thickness (<i>t</i>) of one ply \times number of plies, <i>m</i>		Middle radius of the crown torus <i>r</i> ₁	Middle radius of the root torus <i>r</i> ₂	Over length of two ends cylindrical tangent <i>l</i>	Experimental value
1	372.4	322.5	24.5	22.4	0.49 \times 1	6.3	4.9	30	67.35	65.51
2	372	320	25.5	22.4	0.49 \times 2	6.3	4.9	50	155.44	152.00
3	251	198	25.5	33	1 \times 1	8.25	8.25	60	398.84	336.37
4	249	198	24.5	33	0.5 \times 2	8.25	8.25	60	258.60	169.75
5	249.4	198	24.7	33	0.5 \times 2	8.25	8.25	60	226.53	165.83
6	245	192	26	22	0.5 \times 1	6.25	4.75	30	40.50	40.89
7	245	192	26	22	0.5 \times 1	6.25	4.75	30	40.80	40.89
8	245	192	26	22	0.5 \times 1	6.25	4.75	30	32.36	36.77
9	210	164	22.5	20	0.5 \times 1	5.5	4.5	30	49.82	52.25
10	210	164	22.5	20	0.5 \times 1	5.5	4.5	30	39.03	39.91
11	301	219	40	40	0.5 \times 2	10	10	30	112.77	89.53

TABLE 2
Axial Natural Frequencies of the Specimens (both ends fixed)

TABLE 3

Axial Primary Natural Frequencies of the Specimens (one end fixed, the other end free or attached by a weight)

Medium filling the specimen	Specimen number	Weights W_0 (N)	Experimental value f_1 (Hz)	Calculated value substituting the value (K_n) in Table 1 into eqn (10) or eqn (12) f_1 (Hz)	Error corresponding to the experimental value (%)
Air	1	0	37.5	40.4	7.7
	6	0	40	38.6	-3.5
Water	1	0	27.5	27.5	0
Air	6	62.76	11	12.17	10.6
		203.48	6.1	6.94	13.8
	7	62.76	11.5	12.22	6.3
		203.48	6.4	6.97	8.9
	11	71.6	18.8	18.4	-2.1
		212.3	11	11.14	1.3
Water	7	62.76	11.1	11.89	6.9
		203.48	6.36	6.28	6.9
	11	71.6	17.6	17	-3.4
		212.3	10.7	10.96	2.4

frequency of the bellows. The experimental data obtained by using the two methods were the same.

Experimental data and calculation values of the natural frequencies for all specimens with different end conditions are listed in Tables 2-5.

All experiments were carried out at room temperature.

CONCLUSIONS

On the basis of the above experimentation and application of the theory, several conclusions were reached which are summarized as follows:

- (1) When bellows contain gas or are filled with liquids, and have the three types of different end conditions described previously, it can be seen from Tables 2 and 3 that the calculated values of the axial natural frequencies, according to eqns (10), (12) and (14) respectively, are in good agreement with the experimental data. When bellows

TABLE 4

Axial Secondary Natural Frequencies of the Specimens (filled with air, having an axial pre movement)

Specimen number	Amount of axial pre-movement (mm)	Experimental spring rate with axial pre-movement ($N\text{ mm}^{-1}$)	Natural frequency (Hz)		Error of the calculated value corresponding to the experimental value (%)
			Calculated value substituting the experimental value (K_n) into eqn (14)	Experimental value	
6	-18	40.3	158.9	152	4.5
	-9	40.40	159	155	2.6
	0	40.50	160.6	160	0.4
7	-18	37.36	153	157	-2.6
	-9	40.21	158.7	160	-0.8
	0	40.70	160.6	165	-2.7
	4.5	41.19	160.6	171	-6.1
	9	41.68	161.5	175	-7.7
	13.5	43.64	165.3	183	-9.7
11	-9	63.25	135.8	130	4.4
	0	104.93	184.2	165	11.6
	9	145.33	205.8	200	2.9

TABLE 5

Lateral Primary Natural Frequencies of the Specimens (both ends fixed)

Medium filling the specimen	Specimen number	Experimental value (Hz)	Calculated value substituting the measured K_n into eqn (17) (Hz)	Error corresponding to the experimental value (%)	Calculated value substituting the K_n calculated using eqn (25) into eqn (17) (Hz)	Error corresponding to the experimental value (%)
Air	1	325	318	-2.2	313.5	-3.5
	2	260	266	2.3	244.3	-6
	3	383	428	11.7	423.6	10.6
	4	200	215	7.5	174.5	-12.7
Water	1	117	100	-14.8	98.5	-15.8
	2	137	121	-11.7	111.2	-18.8
	3	177	175	-1.1	173.1	-2.2
	4	109	98	-10.1	79.5	-27

contain gas or are filled with liquids and both ends are fixed, the values of the lateral natural frequencies of the bellows calculated by using eqn (17) approach the experimental data (see Table 5). Therefore, such equations can be considered accurate enough to meet standard engineering requirements.

- (2) It can be seen from Table 4 that the spring rate of the bellows changes with different amounts of axial pre-movement. In addition, the deflection hysteresis and the change of temperature can also cause a change in the spring rate of the bellows.⁴ For these reasons, the spring rate corresponding to the amount of axial pre-movement, temperature, and state of vibration should be used to calculate the natural frequencies. If there is no such spring rate value, both the initial elastic spring rate measured by experiments and the spring rate calculated by eqn (25) can be used. Note that the initial elastic spring rate should be considered first. It must be kept in mind that the spring rate will vary greatly in the case of large amounts of axial pre-movement or of high temperature. Such changes will have a great effect on the natural frequencies of the bellows.
- (3) The results of the theory and the experimentation listed in Tables 2–4 have shown that the axial natural frequency of the bellows is a maximum in the case of both ends fixed, and is a minimum in the case of one end fixed and the other end being attached by a weight. In addition, the axial natural frequency of bellows containing gas is larger than that of bellows filled with liquids. Therefore, the corresponding equations should be used to calculate the axial natural frequency of bellows for different cases.
- (4) During the design and use of bellows, the natural frequency of the bellows should be adjusted by changing the dimensions, material, temperature, end conditions and amount of pre-movement, to avoid the coincidence of the natural frequency of the bellows with the frequency of the pipe system. In order to avoid a resonant response in the bellows, the natural frequency of the bellows should be either lower than that of the system or at least 50% higher.

REFERENCES

1. Timoshenko, S., Young, D. H. & Weaver, W., Jr, *Vibration problems in engineering*. John Wiley, New York, 1974.
2. Li Ting-Xin, Cen Han-Zhao, Hu Jian, Hong Xi-Gang, Li Tian-Xiang & Cao Yong-Biao, Calculating and measuring of the natural frequency of expansion joint. *Chem. General Equip.*, No. 6 (1983) 44–51 (in Chinese).

3. Li Ting-Xin, Hu Jian, Cen Han-Zhao, Hong Xi-Gang & Li Tian-Xiang, Research in the field of axial natural frequency and spring rate behavior of bellows. In *Proc. 5th Int. Conf. Pres. Ves. Technol.*, San Francisco. American Society of Mechanical Engineers (ASME), New York, 1984, pp. 519–29.
4. Li Ting-Xin, Axial deflection stresses and spring rate of U-shaped expansion joint. *Design Petrol Proc. Equip.*, No. 3 (1981) 9–17 (in Chinese).
5. *Standards of the expansion joint manufacturers association*, 5th edn (EJMA), New York, 1980.

FIRST AUTHOR'S REPLY†

C. KAMESWARA RAO

Seismic and Foundation Analysis, Corporate R & D, BHEL, Vikasnagar, Hyderabad-500593, India

(Received 16 July 1990)

The authors wish to thank Professors M. J. Maurizi, R. E. Rossi and J. A. Reyes for bringing to their notice the existence of an earlier report of theirs [2] on the frequency equation for generally restrained Bernoulli-Euler beams. In this context they wish to inform that they were not aware of this work at the time of submission of the paper to the *Journal* in its final form. Further, the results reported in their paper [1] were obtained in 1986, and an earlier version of the same was presented at the ASME PVP Conference held at San Diego in June 1987 [3]. The authors sincerely hope that the frequency and mode shape expressions, along with the tabulated results for a wide range of restraint parameters, given in their paper will be of interest to structural design engineers.

REFERENCES

1. C. KAMESWARA RAO and S. MIRZA 1989 *Journal of Sound and Vibration* **130**, 453-465. A note on vibrations of generally restrained beams.
2. M. J. MAURIZI, R. E. ROSSI and J. A. REYES 1976 *Department of Engineering, Universidad Nacional del Sur, Bahia Blanca, Argentina*. General equation of frequencies for vibrating uniform one-span beams.
3. C. K. RAO and S. MIRZA 1987 *Proceedings of ASME PVP Conference, San Diego, California, PVP-Vol. 124*, 117-121. Vibration frequencies and mode shapes for generally restrained Bernoulli-Euler beams.

† *Editor's Note:* Because of their present geographical separation, the authors have sent in separate replies, and as they are complementary, I have decided to publish them separately.

FINITE ELEMENT ANALYSIS OF VIBRATIONS OF FLUID CONVEYING PIPES RESTING ON SOIL MEDIUM

SUMMARY

The effect of velocity of fluid on the natural frequencies of a straight pipe conveying the fluid is investigated. It is a well documented fact that the natural frequency decreases with increasing flow velocity. Likewise, it is generally found that the natural frequency increases with increasing foundation stiffness. This paper aims to analyze the dynamic behaviour of straight Bernoulli-Euler pipes inclusive of the effects of flow velocity and foundation stiffness by the finite element method. Mass and stiffness matrices are developed and numerical results obtained are presented for the first three frequencies for three boundary conditions : Hinged-hinged, fixed-hinged and fixed-fixed. The results are found to be in good agreement with previously published literature.

INTRODUCTION

Investigations on the effect of flow velocity on the natural frequencies of straight pipes conveying fluid are of considerable practical importance. In general, it is found that the natural frequency of vibration decreases with increasing values of flow velocity and this effect may be very important in industrial systems involving high fluid velocities through flexible thin-walled pipes. One such practical problem is the effect of flow velocity on the dynamics of feed water lines to water turbines and rocket motors. If the flow velocity reaches a critical value, the effective natural frequency becomes zero, which leads to pipe buckling. Under some critical circumstances, the pipe may become vulnerable to resonant vibrations leading to fatigue failure if its natural frequency falls below certain limits.

In 1947, Goldenblatt [1] considered a pipeline divided symmetrically into two sections with counter-current equal velocity flows in each section, neglecting the influence of elastic medium. Ashley and Haviland [2] attempted to describe vibrations of a simply supported pipe span using an approximate power series solution. Feodosyev [3] subsequently demonstrated that the equation of motion derived did not adequately describe the governing inertial forces. He developed a more complete equation and solved it using the Galerkin method. Using Hamilton's principle, Housner [4] derived an equation of motion identical with Feodosyev's equation and both the authors concluded that axial buckling occurs when the flow velocity exceeds a critical value. Both the above authors did not consider the effects of elastic medium.

The vibrations of finite beams subjected to various end conditions were investigated by Handelman [5], who analysed the structure of the differential equations of motion without resort to specific solutions. Naguleswaran and Williams [7] developed exact solutions for the natural frequencies, axial distribution of phase and modal envelopes of pinned-pinned, fixed-pinned and fixed-fixed pipes. Effects of internal pressure and axial applied tension were taken into account. They compared their results with those obtained from Galerkin, Raleigh-Ritz and Fourier series

solutions. Their experimental results are in agreement with theoretical results at low flow rates, but reveal difficulty in predicting the critical flow velocity.

Stein and Tobriner [8] developed equations of motion for a fluid conveying pipe resting on elastic foundation and solved the same for an infinitely long pipe. Their main study was focussed on the wave propagation characteristics of the system. Very recently, Dermendjian-Ivanova [9] studied the effects of Winkler foundation on the critical flow velocities of a simply supported pipeline. The main concern in his study was to determine the influence of pipe length, cross-sectional rigidity, and the foundation spring constant on the critical flow velocities of the pipe. In a recent paper, Raghava Chary, Kameswara Rao and Iyengar [10] presented approximate solutions for the lateral vibrations of a fluid conveying pipe resting on Winkler type elastic medium. Solutions were presented for the natural frequencies and critical flow velocities for a hinged-hinged pipe using Fourier series solutions and for fixed-hinged and fixed-fixed pipes using Galerkin method. They have presented the results of the fundamental natural frequency and critical flow velocity for various values of pipe-fluid mass ratio and foundation stiffness parameter.

As can be seen from the above discussion, many methods have been utilised by investigators in solving this problem, but the finite element method was utilised by only a few investigators such as Kohli and Nakra [11] and Pramila, Laukkanen and Liukkonen [12]. While Kohli and Nakra studied the problem of vibrations of Bernoulli-Euler pipes, Pramila, et. al. addressed the problem of vibrations of Timoshenko pipes, wherein the effects of shear deformation and rotary inertia are included in the element formulations. However, the effect of foundation modulus is not included in both these studies.

As a first step, it is therefore found necessary to develop a finite element computer program to analyze the dynamic behaviour of long straight pipes including the effects of flow velocity and soil medium, based on the Bernoulli-Euler pipe theory. The effects of soil inertia along with shear deformation and rotary inertia are not considered.

The present paper deals with development of a finite element program for long pipes with internal flow and resting on Winkler foundation. Different types of pipe end conditions are considered in generating results for the natural frequencies of the piping system with variations in the non-dimensional parameters defining the flow velocity and foundation stiffness. The generated numerical results are compared with closed form results given by Raghava Chary et. al. [10]. The comparison is found to be quite good, even for a crude mesh of finite elements utilizing six beam elements. The paper also presents explicitly the stiffness and mass matrices derived.

Equations of motion

The system under consideration consists of a pipe of length L with cross-sectional area A , flexural rigidity EI , mass of pipe per unit length m_p , constant axial flow velocity v_f , mass of fluid per unit

length m_f and foundation stiffness k_f . Here the extended Hamilton's principle [6] is used which takes into account the energies associated with inflow and outflow.

The extended Hamilton's principle states that

$$\delta \int_{t_1}^{t_2} (T - V) dt - \int_{t_1}^{t_2} m_f u (\dot{w} + u w') \delta w \Big|_{x=L} dt = 0, \quad (1)$$

where the possible free end is assumed to be the right end, $x = L$. In this expression, T and V denote the kinetic energy of the pipe with fluid and the potential energy respectively. The dot indicates differentiation with respect to time, t , and a prime indicates differentiation with respect to the spatial coordinate x . δ is the variation symbol.

The equation for kinetic energy is

$$T = \frac{1}{2} \int_0^L [m_p \dot{w}^2 + m_f u^2 (w')^2 + m_f (\dot{w} + u w')^2] dx, \quad (2)$$

The expression for potential energy is

$$V = \frac{1}{2} \int_0^L [EI w''^2 + k_f w^2] dx, \quad (3)$$

The displacements and rotations of the nodes are interpolated independently, i.e.

$$w = N_w a = [N_1 \ 0 \ N_2 \ 0 \ \dots] a, \quad (4)$$

and

$$w' = N_\theta a = [0 \ N_1 \ 0 \ N_2 \ \dots] a, \quad (5)$$

Here, the vector of nodal parameters is

$$a = [w_1 \ w_1' \ w_2 \ w_2' \ \dots]^T, \quad (6)$$

and N_1, N_2 , etc. are the linear shape functions.

The first time-integral of equation (1) yields a system of ordinary differential equations :

$$M \ddot{a} + G \dot{a} + K a = 0, \quad (7)$$

The mass matrix is

$$M = \int_0^L (m_p + m_f) N_w^T N_w dx, \quad (8)$$

The gyroscopic matrix is given by

$$G = \int_0^L m_f u \left(N_w^T N_w' - N_w'^T N_w \right) dx , \quad (9)$$

The stiffness matrix is composed of three parts :

$$K_b = \int_0^L E I N_\theta'^T N_\theta' dx , \quad (10)$$

due to bending,

$$K_g = - \int_0^L m_f u^2 N_w'^T N_w' dx , \quad (11)$$

due to the centripetal acceleration of fluid particles, and

$$K_f = \int_0^L k_f N_w^T N_w dx , \quad (12)$$

due to continuous elastic foundation.

Contributions from a typical element to the stiffness and mass matrices respectively are explicitly given below :

STIFFNESS MATRIX

$$\begin{aligned} k_{11} &= \left\{ 12 - 1.2v_f / n^2 + (39 / 105)\gamma / n^4 \right\} n^2 ; k_{21} = \left\{ 6 - v_f / 10n^2 + (11 / 210)\gamma / n^4 \right\} n \\ k_{22} &= \left\{ 4 - (2 / 15)v_f / n^2 + (1 / 105)\gamma / n^4 \right\} ; k_{31} = \left\{ -12 + 1.2v_f / n^2 + (9 / 70)\gamma / n^4 \right\} n^2 \\ k_{32} &= \left\{ -6 + v_f / 10n^2 + (13 / 420)\gamma / n^4 \right\} n ; k_{33} = \left\{ 12 - 1.2v_f / n^2 + (39 / 105)\gamma / n^4 \right\} n^2 \\ k_{41} &= -k_{32} ; k_{42} = \left\{ 2 + v_f / 30n^2 - (1 / 140)\gamma / n^4 \right\} \\ k_{43} &= -k_{21} ; k_{44} = k_{22} \end{aligned}$$

MASS MATRIX

$$\begin{aligned} m_{11} &= 156/(420n^2) & ; m_{21} &= 22/(420n^3) & ; m_{22} &= 4/(420n^4) \\ m_{31} &= 54/(420n^2) & ; m_{32} &= 13/(420n^3) & ; m_{33} &= m_{11} \\ m_{41} &= -m_{32} & ; m_{42} &= -3/(420n^4) & ; m_{43} &= -m_{21} & ; m_{44} &= m_{22} \end{aligned}$$

where n is the number of elements.

As the present investigation is limited to the study of free vibration characteristics only, the damping matrix [G], which effects the dynamic stability of the pipe is neglected in the computations carried out.

NUMERICAL RESULTS

Numerical results obtained from the computer program developed using the above matrices for the vibration of fluid conveying pipes resting on soil medium for the first three frequencies are listed in tables 2, 3 and 4. The results are obtained using 10 elements for beams with hinged-hinged, fixed-hinged and fixed-fixed boundary conditions. The tables show the frequencies for various values of fluid velocity/fluid mass and soil/foundation stiffness parameters. A comparison of the present results with those obtained from an earlier study [10], using an approximate method analogous to modal expansion has shown that the accuracy obtained is well within the allowable engineering norms. Table 1 shows the results in a typical convergence study of the finite element procedure used, for the case when the pipe is fixed at one end and hinged at the other.

The effect of flow velocity and foundation stiffness on the frequencies can be observed from figures 1 to 9. While an increase in flow velocity reduces the frequencies, the foundation stiffness tends to increase the same. For constant values of flow velocity and foundation stiffness, it can be seen that increase in fluid mass (due to an increase in fluid density) decreases the frequencies. It can be clearly seen that the foundation on which the pipe rests contributes significantly to the dynamics of fluid conveying pipes. However, the influence of fluid velocity and foundation stiffness decreases for higher mode frequencies as can be observed from the tables and figures.

ACKNOWLEDGEMENTS

The first author sincerely thanks Mr. R. N. Parlikar, Sr. Deputy Director and Head, Design & Engineering Division, IICT, for his constant support and encouragement during the course of this study. Both authors are grateful to the managements of their respective organisations for granting permission to carry out the study and publish the results.

REFERENCES

1. I. I. GOLDENBLATT 1947 Stroeizat. Modern Problems of Vibrations and Resistance in Engineering Construction.
2. H. ASHLEY and G. HAVILAND 1950 *Journal of Applied Mechanics* Vol. 17, Trans. ASME, Vol. 72, 229-232. Bending Vibrations of a Pipeline Containing Flowing Fluid.
3. V. P. FEODOSYEV 1951 *Inzhenernyisbornik* Vol. 10, 169-170. Vibrations and Stability of a Pipeline when a Liquid Flows Through it.
4. G. W. HOUSNER 1952 *Journal of Applied Mechanics* Vol. 19, 205-208. Bending Vibrations of a Pipe when a Liquid Flows Through it.
5. G. H. HANDELMANN 1955 *Quarterly of Applied Mathematics* Vol. 13, No. 3. A Note on the Transverse Vibration of a Tube Containing Flowing Fluid.
6. D. B. MCIVER 1973 *Journal of Engineering Mathematics* Vol. 7, 243-261. Hamilton's Principle for Systems of Changing Mass.

7. S. NAGULESWARAN AND C. J. H. WILLIAMS 1968 *Journal of Mechanical Engineering Science* Vol. 10, No. 3, 228-238. Lateral Vibration of a Pipe Conveying Fluid.
8. R. A. STEIN AND M. W. TOBRINER 1970 *Journal of Applied Mechanics* Vol. , 906-916. Vibration of Pipes Containing Flowing Fluids.
9. D. S. DERMENDJIAN-IVANOVA 1992 *Journal of Sound and Vibration* Vol. 157, No. 2, 370-374. Critical Flow Velocities of a Simply-Supported Pipeline on an Elastic Foundation.
10. S. RAGHAVA CHARY, C. KAMESWARA RAO AND R. N. IYENGAR 1993 *Proceedings of 8th National Convention of Aerospace Engineers*, 266-287, Institution of Engineers (India). Vibrations of Fluid Conveying Pipes on Winkler Foundation.
11. A. K. KOHLI AND B. C. NAKRA 1984 *Journal of Sound and Vibration* Vol. 93, No. 2, 307-311. Vibration Analysis of Straight and Curved Tubes Conveying Fluids by means of Straight Beam Finite Elements.
12. A. PRAMILA, J. LAUKKANEN AND S. LIUKKONEN 1991 *Journal of Sound and Vibration* Vol. 144, No. 3, 421-425. Dynamics and Stability of Short Fluid Conveying Timoshenko Element Pipes.

Table 1 : Fundamental frequencies for various values of v_f and γ for fixed-hinged pipe showing convergence for number of elements upto 10.

$v_f \downarrow$	$\gamma \downarrow$	Number of elements				
		1	2	3	4	5
0.00	0.00	.204939E+02	.155608E+02	.154485E+02	.154279E+02	.154222E+02
5.00	500.00	.291548E+02	.261554E+02	.260929E+02	.260807E+02	.260772E+02
9.00	1000.00	.359722E+02	.337269E+02	.336781E+02	.336681E+02	.336652E+02

Table 1 : Contd..

$v_f \downarrow$	$\gamma \downarrow$	Number of elements				
		6	7	8	9	10
0.00	0.00	.154202E+02	.154193E+02	.154188E+02	.154186E+02	.154185E+02
5.00	500.00	.260760E+02	.260754E+02	.260752E+02	.260750E+02	.260749E+02
9.00	1000.00	.336642E+02	.336637E+02	.336635E+02	.336634E+02	.336633E+02

Table 2 : First three frequencies for various values of flow velocity parameter v_f and foundation stiffness parameter γ for hinged-hinged pipe

$\gamma \rightarrow$	0.00			100.00		
$v_f \downarrow$	λ_1	λ_2	λ_3	λ_1	λ_2	λ_3
0.00	.986967E+01	.394826E+02	.888739E+02	.140503E+02	.407293E+02	.894347E+02
1.00	.935632E+01	.389795E+02	.883727E+02	.136946E+02	.402418E+02	.889367E+02
5.00	.693270E+01	.368983E+02	.863390E+02	.121681E+02	.382294E+02	.869162E+02
9.00	.292984E+01	.346925E+02	.842563E+02	.104204E+02	.361050E+02	.848476E+02

Table 2 : *Contd.*

$\gamma \rightarrow$	500.00			1000.00		
$v_f \downarrow$	λ_1	λ_2	λ_3	λ_1	λ_2	λ_3
0.00	.244420E+02	.453749E+02	.916437E+02	.331272E+02	.505854E+02	.943322E+02
1.00	.242392E+02	.449377E+02	.911578E+02	.329779E+02	.501936E+02	.938602E+02
5.00	.234107E+02	.431449E+02	.891876E+02	.323738E+02	.485951E+02	.919480E+02
9.00	.225518E+02	.412744E+02	.871729E+02	.317582E+02	.469422E+02	.899951E+02

Table 3 : First three frequencies for various values of flow velocity parameter v_f and foundation stiffness parameter γ for fixed-hinged pipe

$\gamma \rightarrow$	0.00			100.00		
$v_f \downarrow$	λ_1	λ_2	λ_3	λ_1	λ_2	λ_3
0.00	.154185E+02	.499734E+02	.104324E+03	.183774E+02	.509641E+02	.104802E+03
1.00	.150402E+02	.495423E+02	.103873E+03	.180612E+02	.505415E+02	.104353E+03
5.00	.134128E+02	.477787E+02	.102046E+03	.167303E+02	.488140E+02	.102535E+03
9.00	.115420E+02	.459469E+02	.100185E+03	.152715E+02	.470225E+02	.100683E+03

Table 3 : *Contd.*

$\gamma \rightarrow$	500.00			1000.00		
$v_f \downarrow$	λ_1	λ_2	λ_3	λ_1	λ_2	λ_3
0.00	.271612E+02	.547480E+02	.106694E+03	.351814E+02	.591383E+02	.109012E+03
1.00	.269482E+02	.543548E+02	.106252E+03	.350172E+02	.587745E+02	.108580E+03
5.00	.260749E+02	.527523E+02	.104467E+03	.343497E+02	.572958E+02	.106833E+03
9.00	.251638E+02	.510991E+02	.102650E+03	.336633E+02	.557774E+02	.105058E+03

Table 4 : First three frequencies for various values of flow velocity parameter v_f and foundation stiffness parameter γ for fixed-fixed pipe

$\gamma \rightarrow$	0.00			100.00		
$v_f \downarrow$	λ_1	λ_2	λ_3	λ_1	λ_2	λ_3
0.00	.223741E+02	.616889E+02	.121023E+03	.245071E+02	.624942E+02	.121435E+03
1.00	.220972E+02	.613144E+02	.120613E+03	.242547E+02	.621245E+02	.121027E+03
5.00	.209498E+02	.597914E+02	.118961E+03	.232141E+02	.606219E+02	.119381E+03
9.00	.197291E+02	.582258E+02	.117286E+03	.221187E+02	.590783E+02	.117711E+03

Table 4 : *Contd.*

$\gamma \rightarrow$	500.00			1000.00		
$v_i \downarrow$	λ_1	λ_2	λ_3	λ_1	λ_2	λ_3
0.00	.316322E+02	.656165E+02	.123071E+03	.387376E+02	.693219E+02	.125086E+03
1.00	.314371E+02	.652645E+02	.122669E+03	.385783E+02	.689888E+02	.124690E+03
5.00	.306414E+02	.638359E+02	.121045E+03	.379327E+02	.676389E+02	.123093E+03
9.00	.298201E+02	.623718E+02	.119398E+03	.372725E+02	.662589E+02	.121474E+03

Figure 1 Variation of λ_1 with v_f for various values of γ for hinged-hinged pipe

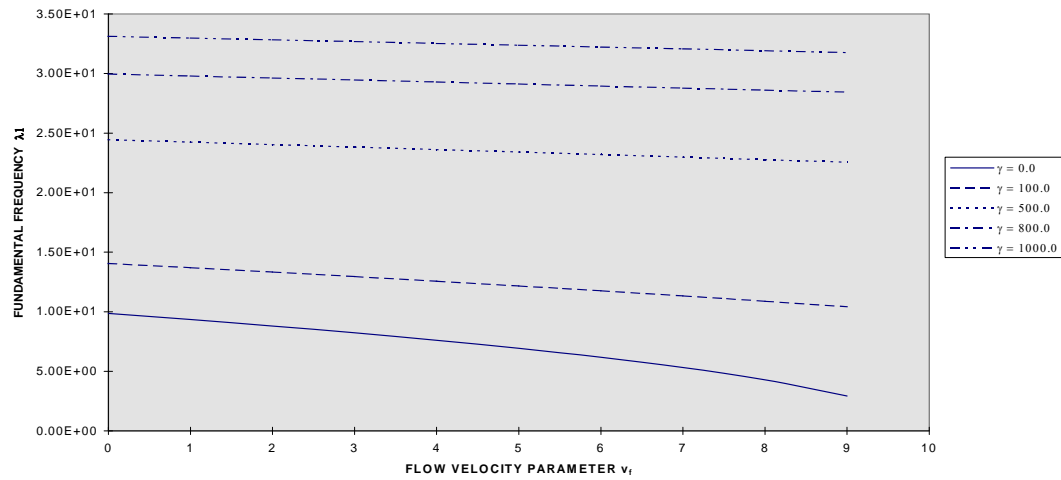


Figure 2 Variation of λ_2 with v_f for various values of γ for hinged-hinged pipe

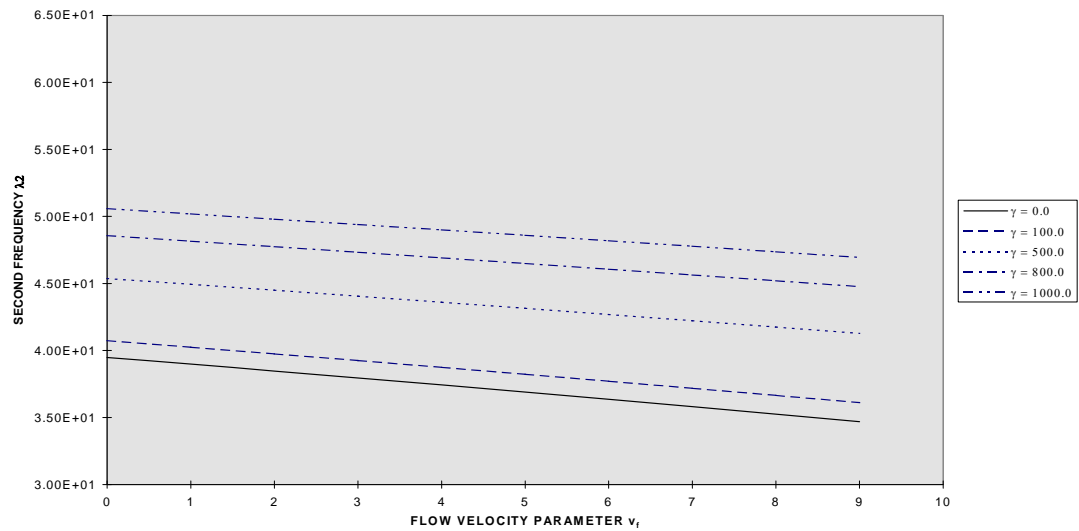


Figure 3 Variation of λ_3 with v_f for various values of γ for hinged-hinged pipe

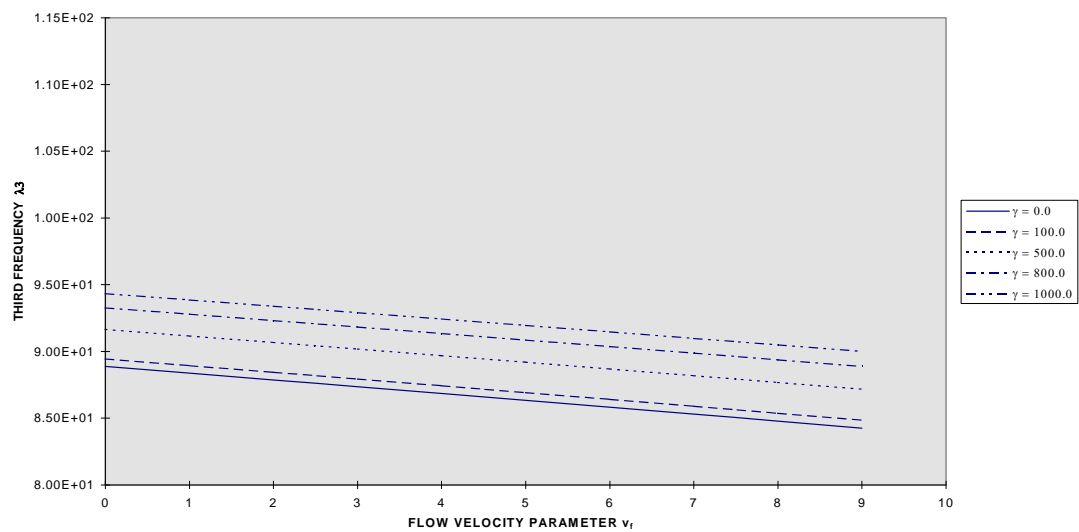


Figure 4 Variation of λ_1 with v_f for various values of γ for fixed-hinged pipe

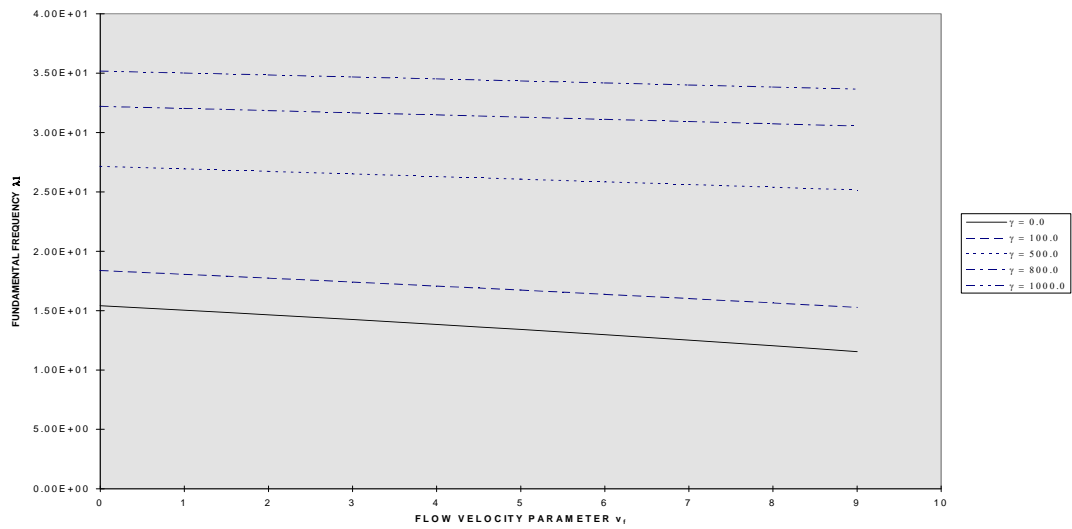


Figure 5 Variation of λ_2 with v_f for various values of γ for fixed-hinged pipe

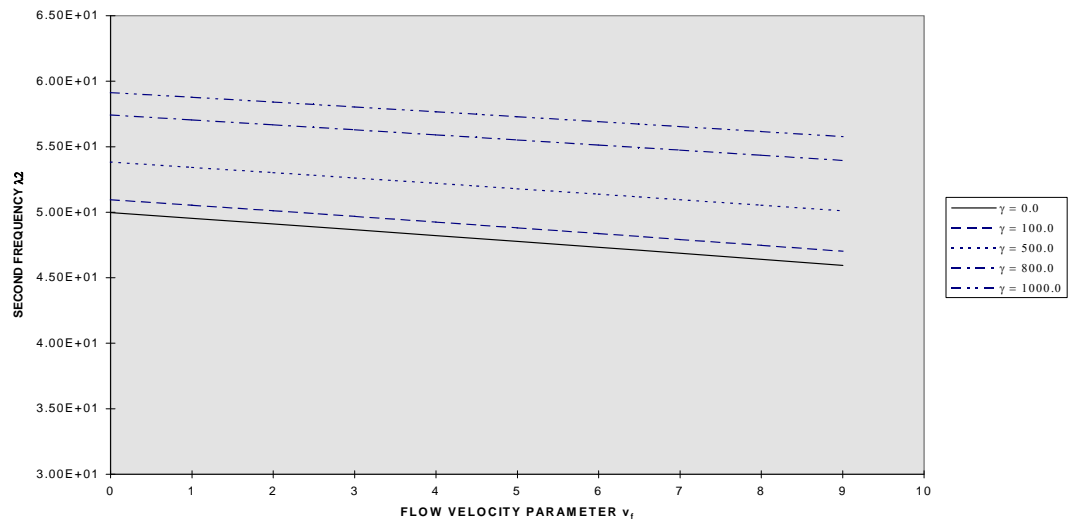


Figure 6 Variation of λ_3 with v_f for various values of γ for fixed-hinged pipe

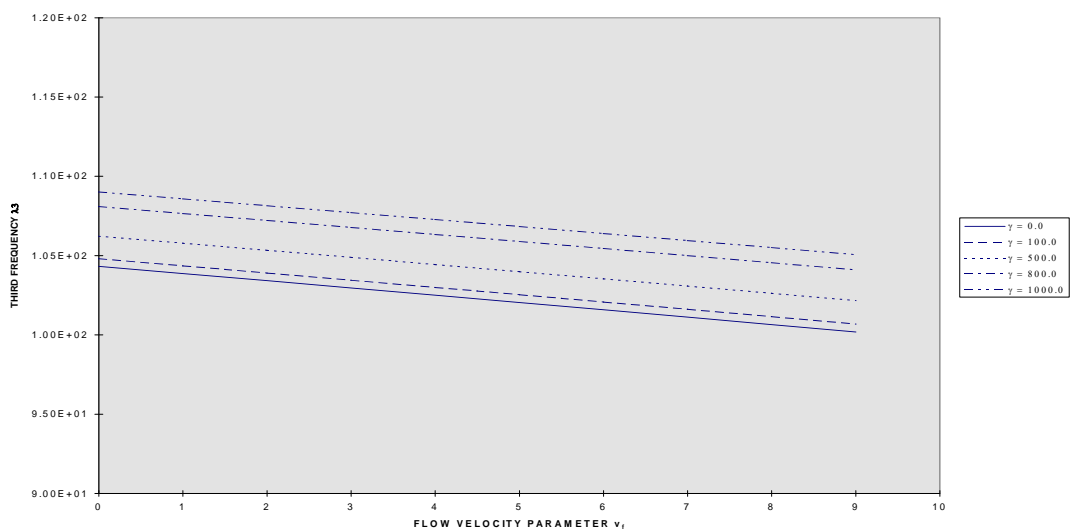


Figure 7 Variation of λ_1 with v_f for various values of γ for fixed- fixed pipe

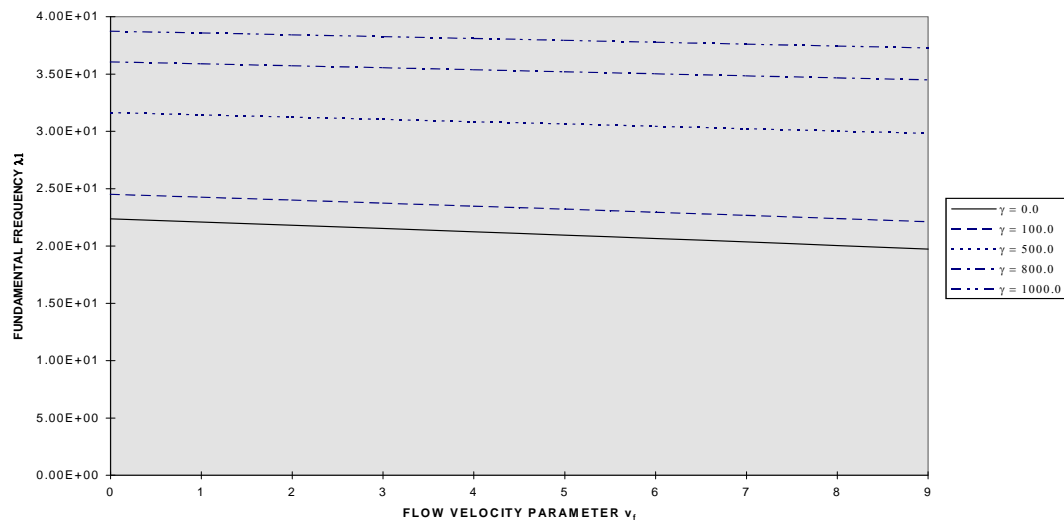


Figure 8 Variation of λ_2 with v_f for various values of γ for fixed- fixed pipe

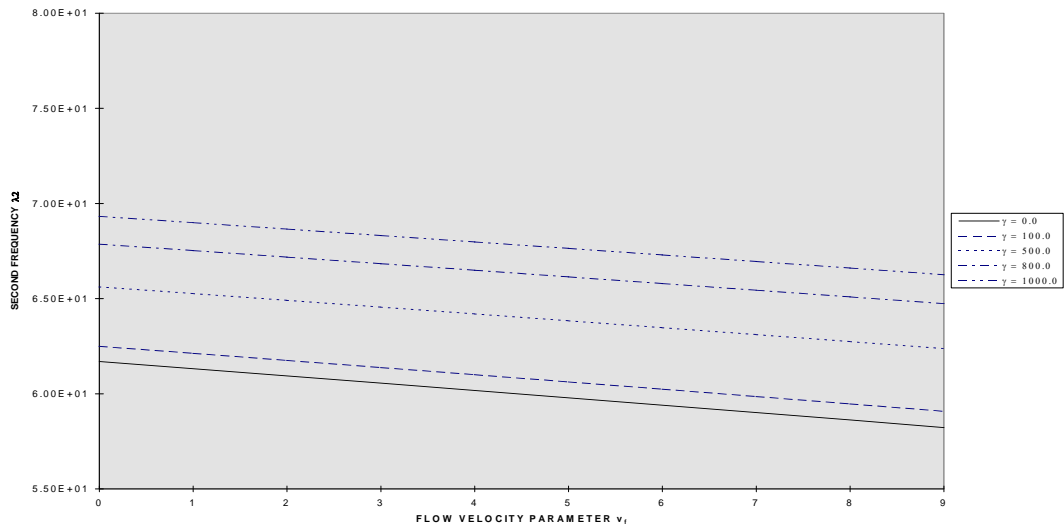
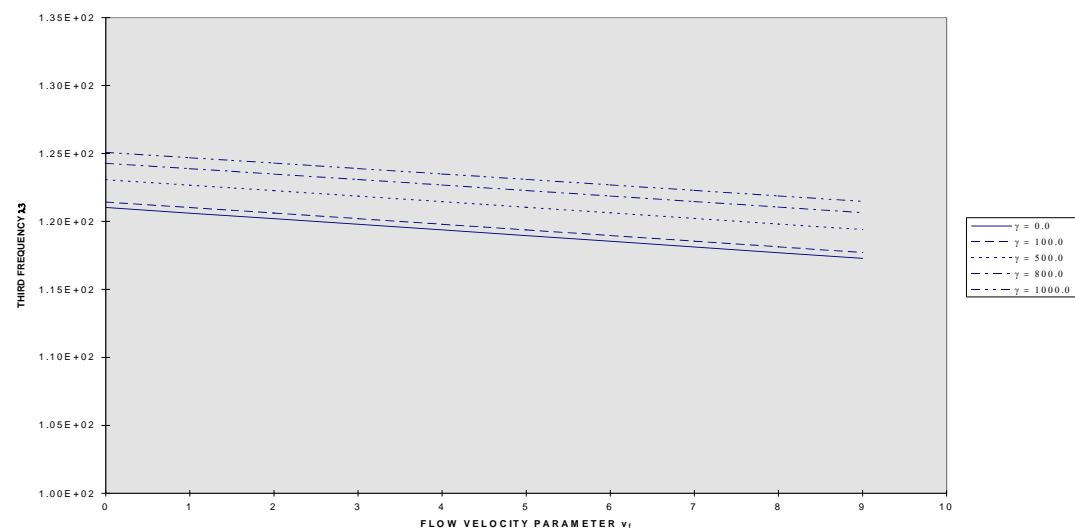


Figure 9 Variation of λ_3 with v_f for various values of γ for fixed- fixed pipe



Finite Element Analysis of Vibrations of Rotationally Restrained Fluid Conveying Pipes Resting on Soil Medium

Simha, H.⁺ and Kameswara Rao, C.⁺⁺

⁺Design & Engineering Division, Indian Institute of Chemical Technology,
Hyderabad 500 007, INDIA. simha@iict.ap.nic.in; ⁺⁺Patents & Standards
Translation Group, BHEL Corporate R&D Division, Hyderabad 500 093, INDIA

Abstract

This paper deals with the vibrations of rotationally restrained straight pipes conveying fluid and resting on soil medium. An attempt has been made to analyse the dynamic behaviour of straight Bernoulli-Euler pipes rotationally restrained at either ends including the effects of flow velocity and foundation stiffness using the finite element approach. For the first time, results are presented for the first two natural frequencies of rotationally restrained fluid conveying pipes for varying values of the rotational restraint parameter, fluid flow velocity parameter and foundation stiffness parameter. For extreme values of the rotational stiffness parameter (0 and infinity), which represent the ideal boundary conditions, the results are found to be in good agreement with those available in published literature.

INTRODUCTION

It is a well known fact that the velocity of the fluid has considerable effect on the natural frequencies of the straight pipe conveying the fluid. There have been many investigations on the effect of flow velocity on the natural frequencies of straight pipes conveying fluid with simple boundary conditions such as hinged-hinged, hinged-fixed and fixed-fixed. These boundary conditions are idealised cases and are difficult to realise practically. A more realistic boundary condition is the rotational restraint at both ends of the pipe. However, results are not available for rotationally

⁺ Scientist, ⁺⁺Sr. DGM

restrained straight Bernoulli-Euler fluid conveying pipes resting on soil medium in the published literature.

Since 1947, many investigations [1 - 7] have been carried out for studying the vibration behaviour of fluid conveying pipes utilising various methods such as Galerkin, Rayleigh-Ritz and Fourier series solutions. Stein and Tobriner [8], Dermendjian-Ivanova [9] and Raghava Chary, Kameswara Rao and Iyengar [10], have devoted their studies on fluid conveying pipes resting on elastic foundation.

As can be seen from the above discussion, many methods have been utilised by investigators in solving this problem, but the finite element method was utilised by only a few investigators such as Kohli and Nakra [11] and Pramila, Laukkanen and Liukkonen [12]. However, the effect of foundation modulus is not included in both these studies. In an earlier paper [13], the authors have presented numerical results for the first three natural frequencies obtained from the mass and stiffness matrices developed for straight Bernoulli-Euler fluid conveying pipes resting on soil medium. These results were however for the three classical boundary conditions of hinged-hinged, hinged-fixed and fixed-fixed.

The present paper deals with development of a finite element program for rotationally restrained long pipes with internal flow and resting on Winkler foundation. Different values of pipe rotational restraint parameter are considered in generating results for the natural frequency of the piping system with variations in the non-dimensional parameters defining the flow velocity and foundation stiffness. For extreme values of the rotational restraint parameter, the results are in good agreement with those available in published literature. The effects of soil inertia along with shear deformation are not considered in the analysis.

EQUATIONS OF MOTION

The system under consideration consists of a pipe of length L with cross-sectional area A , flexural rigidity EI , mass of pipe per unit length m_p , constant axial flow velocity v_f , mass of fluid per unit length m_f and foundation stiffness k_f . Here the extended Hamilton's principle [6] is used and states that

$$\delta \int_{t_1}^{t_2} (T - V) dt - \int_{t_1}^{t_2} m_f v_f (\dot{w} + v_f w') dw \Big|_{x=L} dt = 0, \quad (1)$$

where the possible free end is assumed to be the right end, $x = L$. Here, T and V denote the kinetic energy of the pipe with fluid and the potential energy respectively. δ is the variation symbol. The dot indicates differentiation with respect to time, t , and a prime indicates differentiation with respect to the spatial coordinate x . The equation for kinetic energy is

$$T = \frac{1}{2} \int_0^L \left[m_p \dot{w}^2 + m_f v_f^2 (w')^2 + m_f (\dot{w} + v_f w')^2 \right] dx, \quad (2)$$

Potential energy is given by

$$V = \frac{1}{2} \int_0^L \left[E I w''^2 + k_f w^2 \right] dx, \quad (3)$$

The displacements and rotations of the nodes are interpolated independently, i.e.

$$w = N_w \mathbf{a} = [N_1 \quad 0 \quad N_2 \quad 0 \cdots] \mathbf{a}, \quad (4)$$

and

$$w' = N_q \mathbf{a} = [0 \quad N_1 \quad 0 \quad N_2 \cdots] \mathbf{a}, \quad (5)$$

Here, the vector of nodal parameters is

$$\mathbf{a} = \left[w_1 \quad w_1' \quad w_2 \quad w_2' \cdots \right]^T, \quad (6)$$

and N_1, N_2 , etc. are cubic functions. The first time-integral of equation (1) yields a system of ordinary differential equations :

$$\mathbf{M} \ddot{\mathbf{a}} + \mathbf{G} \dot{\mathbf{a}} + \mathbf{K} \mathbf{a} = \mathbf{0}, \quad (7)$$

The mass matrix is

$$\mathbf{M} = \int_0^L (m_p + m_f) N_w^T N_w dx, \quad (8)$$

The gyroscopic matrix is given by

$$\mathbf{G} = \int_0^L m_f v_f \left(N_w^T N_w' - N_w'^T N_w \right) dx, \quad (9)$$

The stiffness matrix is composed of three parts :

$$\mathbf{K}_b = \int_0^L E I \mathbf{N}_q'^T \mathbf{N}_q' dx, \quad (10)$$

$$\mathbf{K}_g = - \int_0^L m_f v_f^2 \mathbf{N}_w'^T \mathbf{N}_w' dx, \quad (11)$$

$$\mathbf{K}_f = \int_0^L k_f \mathbf{N}_w^T \mathbf{N}_w dx, \quad (12)$$

Equation (10) is due to bending, equation (11) is due to the centripetal acceleration of fluid particles, and equation (12) is due to continuous elastic foundation. For free vibration analysis, we assume

$$\mathbf{a} = A e^{i \omega_n t}, \text{ where } A \text{ is a constant and } \omega_n \text{ is the circular natural frequency}$$

As the present investigation is limited to the study of free vibration characteristics only, the damping matrix [G], which effects the dynamic stability of the pipe is neglected in the computations carried out. The final non-dimensional eigenvalue problem solved here is

$$\mathbf{K} \mathbf{a} - I \mathbf{M} \mathbf{a} = \mathbf{0}, \text{ where } I = \frac{m_p L^3 \omega_n^2}{EI(m_p + m_f)} \text{ is the frequency parameter}$$

Contributions from a typical element to the stiffness and mass matrices respectively are explicitly given below :

Stiffness Matrix

$$\begin{aligned} k_{11} &= \{12 - 1.2v_f / n^2 + (39/105)g / n^4\} n^2; k_{21} = \{6 - v_f / 10n^2 + (11/210)g / n^4\} n \\ k_{22} &= \{4 - (2/15)v_f / n^2 + (1/105)g / n^4\}; \\ k_{31} &= \{-12 + 1.2v_f / n^2 + (9/70)g / n^4\} n^2 \\ k_{32} &= \{-6 + v_f / 10n^2 + (13/420)g / n^4\} n \\ k_{33} &= \{12 - 1.2v_f / n^2 + (39/105)g / n^4\} n^2; k_{41} = -k_{32}; \\ k_{42} &= \{2 + v_f / 30n^2 - (1/140)g / n^4\}; k_{43} = -k_{21}; k_{44} = k_{22} \end{aligned}$$

Mass Matrix

$$\begin{aligned} m_{11} &= 156/(420n^2) & ; m_{21} &= 22/(420n^3) & ; m_{22} &= 4/(420n^4) \\ m_{31} &= 54/(420n^2) & ; m_{32} &= 13/(420n^3) & ; m_{33} &= m_{11} \\ m_{41} &= -m_{32} & ; m_{42} &= -3/(420n^4) & ; m_{43} &= -m_{21} \\ m_{44} &= m_{22} \end{aligned}$$

where n is the number of elements and

$$g = \frac{k_f L^4}{EI}, \text{ the foundation stiffness parameter.}$$

NUMERICAL RESULTS

Figure 1 shows the Bernoulli-Euler pipe element conveying fluid and resting on soil medium. SR_1 and SR_2 are the rotational restraint stiffness parameters at either ends of the pipe. For the purpose of this study, both the ends are assumed to have linear restraint stiffness parameters ST_1 and ST_2 equal to infinity. Each node of the element has two degrees of freedom as shown.

Numerical results are obtained from the computer program developed using the above matrices with suitable modifications in the stiffness matrix to include the effects of the rotational restraint stiffness parameters. The values of the first two natural frequency parameter λ for various values of flow parameter v_f and foundation stiffness parameter γ for the case of equal rotational restraint at either end ($SR_1 = SR_2$) are presented in Table 1. Table 2 gives the values of the first two natural frequency parameter for various values of v_f and γ for the case of $SR_2 = SR_1 / 100$.

Figures 2 and 3 show the variation of the first two natural frequency parameters λ_1 and λ_2 respectively for various values of SR_2 , V_f and γ keeping the rotational restraint parameter $SR_1 = 0.1$. Similar results for $SR_1 = 10.0$ and $SR_1 = 1000.0$ are presented in Figures 4 and 5, Figures 6 and 7 respectively.

The tables and figures presented in this paper give a wide range of results for the vibrations of rotationally restrained Bernoulli-Euler pipes conveying fluid and resting on elastic foundation. The authors believe that these results will be of considerable use in the design of such piping systems.

CONCLUSIONS

The following conclusions can be drawn from the above study :

- The results for the cases when the rotational restraint $SR_1 = SR_2 = 0.0$ (hinged-hinged); $SR_1 = SR_2 = \text{infinity}$ (fixed-fixed) and $SR_1 = 0.0$, $SR_2 = \text{infinity}$ (hinged-fixed) are found to exactly tally with the results for classical boundary conditions reported in a previous paper by the authors [13].
- In all the cases studied here, the natural frequency of the piping system starts to increase appreciably for values of SR_2 in the range 0.01 to 10.0, for given values of V_f , γ and SR_1 . Values of the natural frequency parameter remain essentially constant for the values of $SR_2 < 0.01$ and $SR_2 > 10$. However, in all cases, the natural frequency parameter decreases with increasing flow velocity parameter and increase consistently with increasing foundation stiffness parameter.
- The effect of foundation stiffness parameter γ on the first natural frequency parameter λ_1 is most profound. The frequency parameter increases appreciably with increasing values of γ . This effect is not as appreciable for λ_2 .
- The results are presented in a non-dimensional form and hence a designer can obtain values of natural frequencies for any fluid conveying pipe by proper interpolation.

ACKNOWLEDGEMENTS

Both authors are grateful to the managements of their respective organisations for granting permission to carry out the study and publish the results.

REFERENCES

1. I. I. GOLDENBLATT 1947 Stroeizat. Modern Problems of Vibrations and Resistance in Engineering Construction.
2. H. ASHLEY and G. HAVILAND 1950 *Journal of Applied Mechanics* Vol. 17, Trans. ASME, Vol. 72, 229-232. Bending Vibrations of a Pipeline Containing Flowing Fluid.
3. V. P. FEODOSYEV 1951 *Inzheneryisbornik* Vol. 10, 169-170. Vibrations and Stability of a Pipeline when a Liquid Flows Through it.
4. G. W. HOUSNER 1952 *Journal of Applied Mechanics* Vol. 19, 205-208. Bending Vibrations of a Pipe when a Liquid Flows Through it.

National Symposium on Advances in Structural Dynamics and Design
Structural Engineering Research Centre, Madras
January, 9 to 11, 2001

5. G. H. HANDELMANN 1955 *Quarterly of Applied Mathematics* Vol. 13, No. 3. A Note on the Transverse Vibration of a Tube Containing Flowing Fluid.
6. D. B. MCIVER 1973 *Journal of Engineering Mathematics* Vol. 7, 243-261. Hamilton's Principle for Systems of Changing Mass.
7. S. NAGULESWARAN AND C. J. H. WILLIAMS 1968 *Journal of Mechanical Engineering Science* Vol. 10, No. 3, 228-238. Lateral Vibration of a Pipe Conveying Fluid.
8. R. A. STEIN AND M. W. TOBRINER 1970 *Journal of Applied Mechanics* Vol. , 906-916. Vibration of Pipes Containing Flowing Fluids.
9. D. S. DERMENDJIAN-IVANOVA 1992 *Journal of Sound and Vibration* Vol. 157, No. 2, 370-374. Critical Flow Velocities of a Simply-Supported Pipeline on an Elastic Foundation.
10. S. RAGHAVA CHARY, C. KAMESWARA RAO AND R. N. IYENGAR 1993 *Proceedings of 8th National Convention of Aerospace Engineers*, 266-287, Institution of Engineers (India). Vibrations of Fluid Conveying Pipes on Winkler Foundation.
11. A. K. KOHLI AND B. C. NAKRA 1984 *Journal of Sound and Vibration* Vol. 93, No. 2, 307-311. Vibration Analysis of Straight and Curved Tubes Conveying Fluids by means of Straight Beam Finite Elements.
12. A. PRAMILA, J. LAUKKANEN AND S. LIUKKONEN 1991 *Journal of Sound and Vibration* Vol. 144, No. 3, 421-425. Dynamics and Stability of Short Fluid Conveying Timoshenko Element Pipes.
13. H. SIMHA AND C KAMESWARA RAO 1998 *Paper communicated to the Journal of Sound and Vibration*. Finite Element Analysis of Vibrations of Fluid Conveying Pipes Resting on Soil Medium.

Table 1 Values of first two natural frequency parameters λ for various values of flow velocity parameter v_f and foundation stiffness parameter g with rotational stiffness parameters $SR_1 = SR_2$

$SR_1 = SR_2$	v_f	$\gamma = 0.0$		$\gamma = 500.0$		$\gamma = 1000.0$	
		λ_1	λ_2	λ_1	λ_2	λ_1	λ_2
1.00E-01	0	11.40749	41.14778	25.10241	46.83097	33.61742	51.89547
1.00E-01	1	10.96567	40.66497	24.90474	46.40733	33.47007	51.51349
1.00E-01	3	10.02374	39.68173	24.5046	45.54821	33.17341	50.74091
1.00E-01	6	8.4153	38.15938	23.89178	44.22825	32.72335	49.55944
1.00E-01	9	6.41534	36.57369	23.26277	42.86764	32.26696	48.34909
1.00E+01	0	21.45771	59.2499	30.99086	63.32891	38.21562	67.16064
1.00E+01	1	21.17999	58.87406	30.79922	62.97741	38.06037	66.8293
1.00E+01	3	20.61224	58.11459	30.41158	62.26802	37.74737	66.16121
1.00E+01	6	19.72708	56.95516	29.81875	61.18733	37.27141	65.14514
1.00E+01	9	18.79645	55.77005	29.21141	60.08576	36.78732	64.11161
1.00E+03	0	22.36453	61.66984	31.6255	65.59855	38.73206	69.3049
1.00E+03	1	22.08772	61.29542	31.43036	65.24667	38.57288	68.97194
1.00E+03	3	21.52237	60.53914	31.03566	64.53671	38.25196	68.30071
1.00E+03	6	20.64247	59.3854	30.43208	63.4557	37.76389	67.2802
1.00E+03	9	19.7196	58.20722	29.8138	62.35448	37.26745	66.24259

Table 2 Values of first two natural frequency parameters λ for various values of flow velocity parameter v_f and foundation stiffness parameter g with rotational stiffness parameters $SR_2 = SR_1 / 100.0$

SR ₁	SR ₂	v _f	$\gamma = 0.0$		$\gamma = 500.0$		$\gamma = 1000.0$	
			λ_1	λ_2	λ_1	λ_2	λ_1	λ_2
1.00E-01	1.00E-03	0	10.65084	40.32901	24.76773	46.11322	33.36825	51.2487
1.00E-01	1.00E-03	1	10.17603	39.83647	24.56729	45.68308	33.21975	50.86201
1.00E-01	1.00E-03	3	9.15272	38.83266	24.16138	44.81044	32.9207	50.07969
1.00E-01	1.00E-03	6	7.35513	37.27635	23.53928	43.46868	32.46687	48.88278
1.00E-01	1.00E-03	9	4.94124	35.65222	22.90013	42.08421	32.0065	47.65586
1.00E+01	1.00E-01	0	15.92336	49.79661	27.45093	54.58665	35.40556	58.98901
1.00E+01	1.00E-01	1	15.56861	49.37198	27.24668	54.19956	35.24744	58.63098
1.00E+01	1.00E-01	3	14.83202	48.51135	26.83261	53.41677	34.92834	57.90812
1.00E+01	1.00E-01	6	13.648	47.1905	26.19671	52.22014	34.44224	56.80619
1.00E+01	1.00E-01	9	12.34398	45.83105	25.54161	50.99496	33.94663	55.682
1.00E+03	1.00E+01	0	21.90432	60.44271	31.30174	64.44627	38.46816	68.21526
1.00E+03	1.00E+01	1	21.62704	60.06756	31.10834	64.09456	38.31095	67.88308
1.00E+03	1.00E+01	3	21.06048	59.30966	30.71716	63.38483	37.994	67.21336
1.00E+03	1.00E+01	6	20.17794	58.15305	30.11892	62.30391	37.51199	66.19499
1.00E+03	1.00E+01	9	19.25119	56.97138	29.50607	61.20243	37.02173	65.15933

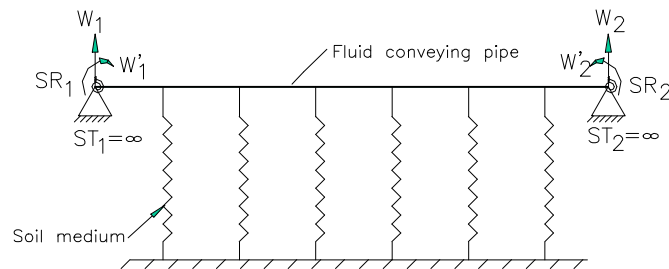


Fig. 1 Rotationally Restrained Fluid Conveying Pipe Element

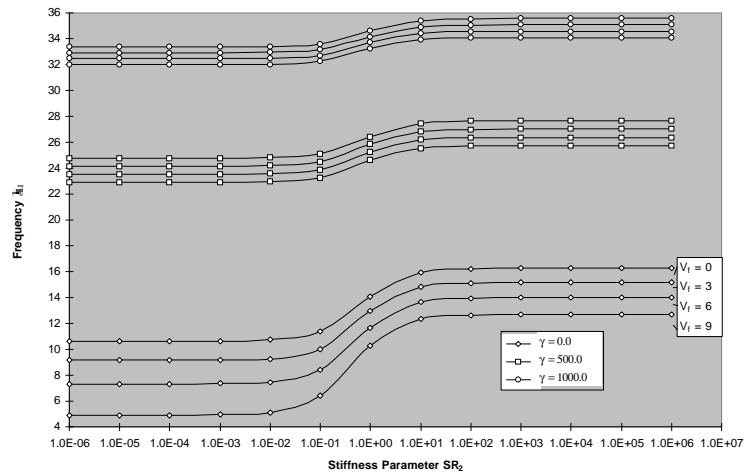


Fig. 2 Variation of l_1 with SR_2 for various values of v_f & g with $SR_1=0.1$

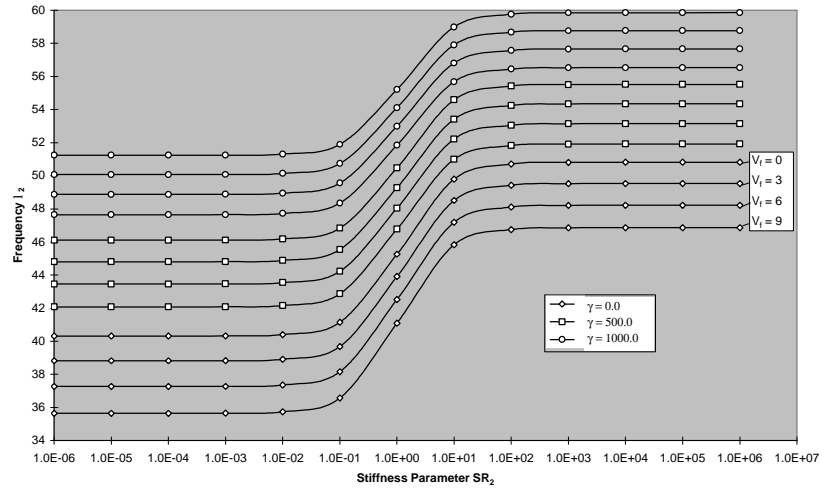


Fig. 3 Variation of l_2 with SR_2 for various values of v_f & g with $SR_1=0.1$

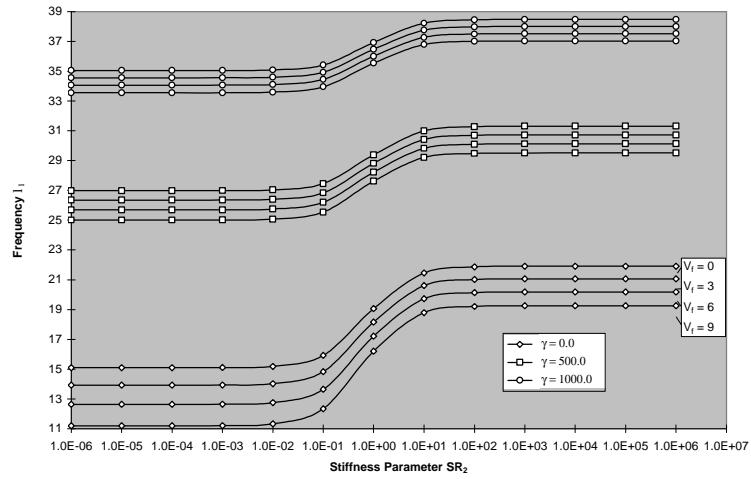


Fig. 4 Variation of l_1 with SR_2 for various values of v_f & g with $SR_1=10.0$

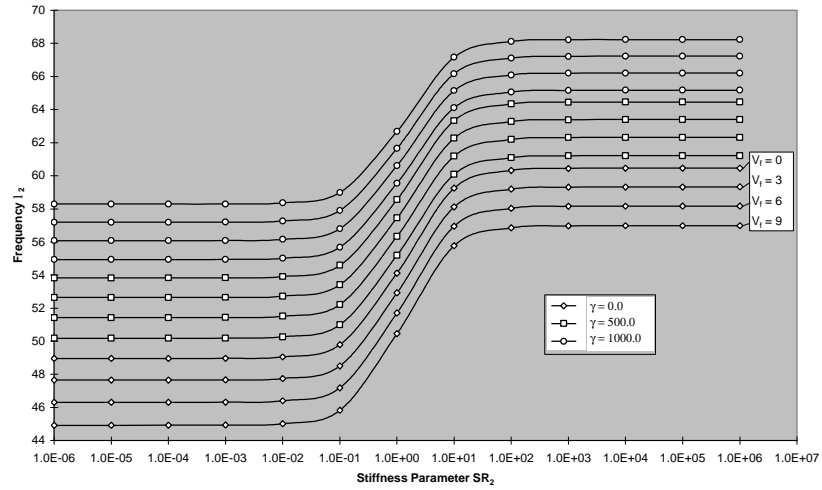


Fig. 5 Variation of l_2 with SR_2 for various values of v_f & g with $SR_1=10.0$

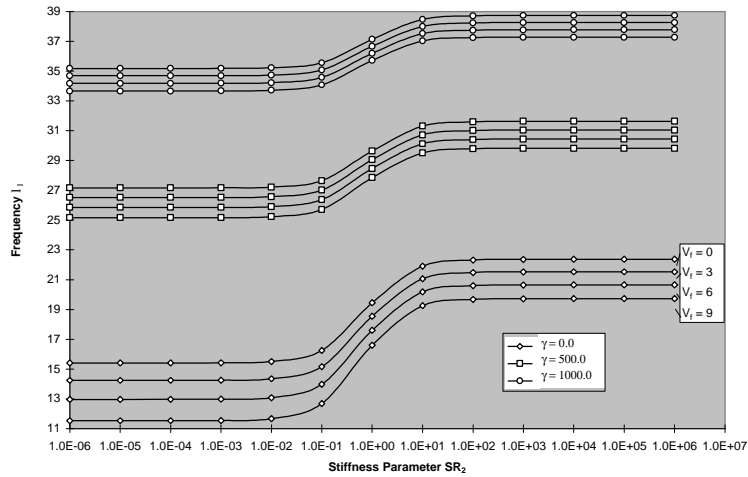


Fig. 6 Variation of l_1 with SR_2 for various values of v_f & g with $SR_1=1000.0$

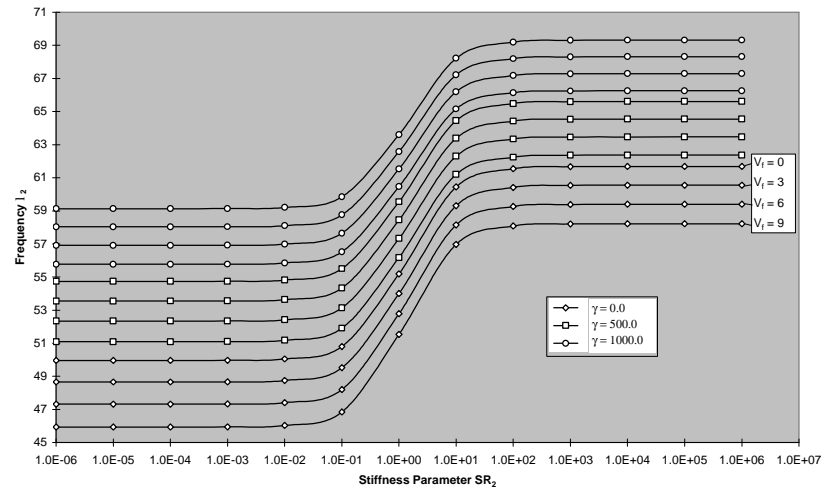


Fig. 7 Variation of l_2 with SR_2 for various values of v_f & g with $SR_1=1000.0$

FINITE ELEMENT ANALYSIS OF TRANSVERSE VIBRATIONS OF SINGLE BELLOWS RESTRAINED AGAINST ROTATION

RADHAKRISHNA.M

*Scientist, Design Engineering Division
Indian Institute of Chemical Technology, Hyderabad
India*

KAMESWARA RAO.C

*Senior Deputy General Manager
Intellectual Property Management Group
Corporate R&D,
Bharat Heavy Electricals Limited, Hyderabad
India*

Keywords

Bellows vibration, single bellows, transverse frequency, elastic restraint & finite element

Abstract

The paper presents the results of investigation of transverse vibrations of single bellows expansion joint restrained against rotation on either end using the finite element method. The aim of this work is to model flexible U shaped bellows using beam elements. The effect of rotatory inertia on the natural frequency is included in the beam element matrices. Results obtained from the numerical analysis are presented and compared with the exact frequencies for the first three modes of vibration. Experimental results are used for verification. The effect of variation of internal pressure and velocity on the natural frequencies are also studied and presented.

Introduction

Bellows expansion joints are commonly used in nuclear /power and chemical piping systems so as to absorb the axial and transverse displacements due to thermal loading. In order to design the bellows expansion joint along with the piping system for specified design response spectra, it is essential to obtain reliable solutions for the transverse vibrations frequencies of bellows expansion joints. Thus metal bellows have become an important component in a number of applications.

The formulae presented in the EJMA code and those derived by investigators, [1,4] cover classical boundary conditions only. It is observed that the flange-bellow-flange junction - as clamped end conditions or infinitely stiff compared to the bellows stiffness is not a practical situation compared to the bellows welded on either end in many of the piping systems. Hence, this assumption of clamped-clamped will lead to over estimation of natural frequencies. Rao.C.K and Radhakrishna.M [6] analyzed U-shaped bellows subjected to axial force and internal pressure, and obtained an exact solution for the transverse vibrations of single bellows that are elastically restrained against rotation on either end using the *Bernoulli-*

Euler beam theory. The paper presents a finite element representation of single bellows and to validate the frequencies obtained by exact analysis for first three modes of vibration.

Characteristics of Bellows

The various geometrical dimensional parameters of U-shaped bellows are given in Fig 1. R_1 is the meridional radius of the convolution root, R_2 is the meridional radius of the convolution crown and h is the convolution height. R_m is the mean radius of the bellows, that is, the distance from the bellows centerline to mid convolution height, and t is the bellow material thickness. It is assumed that $t \ll R_1$, R_2 and $h \ll R_m$. With 'N' as number of convolutions the total length of the bellows is $L = 2(R_1 + R_2) N$. Therefore, with these assumptions bellows are considered as equivalent pipe / bar of radius R_m and wall thickness t .

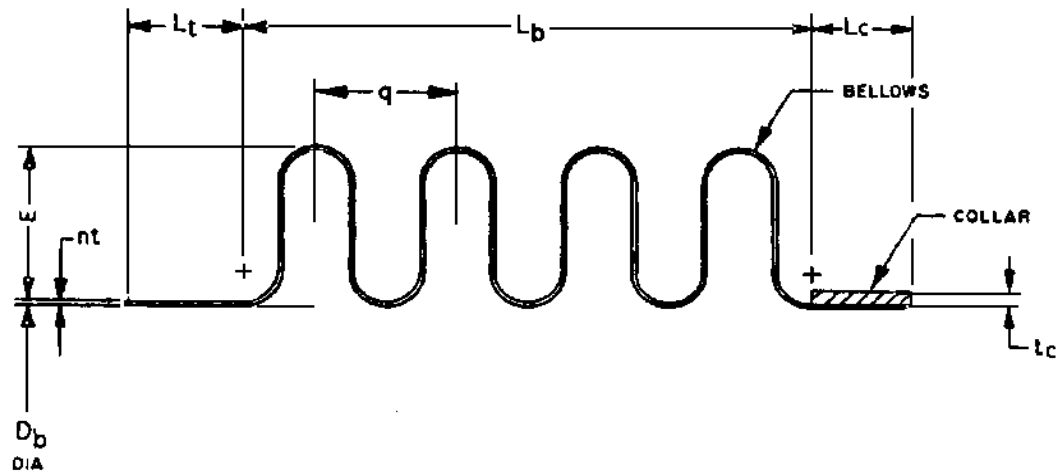


Fig.1: Geometrical Dimensions of bellow

Theory of Free Vibrations of Bellows

The matrix equation for the free vibration of bellows can be written as –

$$[M] \{q\} + [K] \{q\} = 0 \quad (1)$$

Where

$\{q\}$ - Generalized coordinates

$[M]$ - Mass matrix

$[K]$ - Elastic stiffness matrix

Formulations of Elastic Stiffness Matrix

The strain energy U of a bellow element of length 'l' including the effect of rotatory inertia is given by the relation-

$$U = \frac{1}{2} EI \int_0^l \left(\frac{d^2 y}{dx^2} \right)^2 dx - \frac{1}{2} P \pi R_m^2 \int_0^l \left(\frac{dy}{dx} \right)^2 dx \quad (2)$$

Where

y - deflection of the bellow

EI -bending stiffness of bellow
 P -internal pressure and
 R_m -mean radius of bellows

Now on non-dimensionalizing and substituting the following relations, $\eta = x / l$ and $\phi = y / l$ the above expression of strain energy becomes as follows –

$$U = \frac{1}{2} EI/l \int_0^l (d^2\phi/d\eta^2)^2 d\eta - \frac{1}{2} P\pi R_m^2/l \int_0^l (d\phi/d\eta)^2 d\eta \quad (3)$$

Assuming a cubic polynomial expression for ϕ to be of the form –

$$\phi = \sum a^r \eta^r \quad (4)$$

Now substituting in to equation (1) and replacing the coefficient of a_r ($r=0,1,2,3$), the strain energy expression becomes -

$$U = \frac{1}{2} EI/l \{\xi\}^T [K] \{\xi\} \quad (5)$$

ξ is the degree of freedom (DOF)

$$\therefore [K] = [K_e] - \Delta^2 [K_v] \quad (6)$$

Where

$$\Delta^2 = P\pi R_m^2 l^2 / EI$$

$[K]$ -Elastic stiffness matrix

$[K_e]$ -Velocity stiffness matrix and are defined as follows –

$$\begin{aligned}
 [K_e] &= \begin{bmatrix} 12 & -6 & -12 & -6 \\ & 4 & 6 & 2 \\ & \text{sym} & 12 & 6 \\ & & & 4 \end{bmatrix} \\
 [K_v] &= \begin{bmatrix} -36 & -3 & -36 & -3 \\ & 4 & -3 & -1 \\ & \text{sym} & -36 & 3 \\ & & & 4 \end{bmatrix}
 \end{aligned}$$

$$\text{Where } \xi^T = \{\phi_i, \phi_i', \phi_{i+1}, \phi_{i+1}'\} \quad (7)$$

Formulation of Mass and Rotatory Inertia Matrices

The kinetic energy 'T' of a bellow element of length including the effects of rotatory inertia is given by –

$$T = \frac{1}{2} \rho A I^3 \int_0^l (\ddot{\varphi})^2 d\eta + \frac{1}{2} \rho J I \int_0^l (\ddot{\varphi}')^2 d\eta \quad (8)$$

The mass of bellows per unit length is computed by using the formula given in equation (9)-

$$m = \rho_b 2\pi R_m [\pi (R_1 + R_2) + 2(h - R_1 - R_2)]t + 2\pi(R_1 + R_2) \quad (9)$$

Where

ρ_b - mass density of bellows material

ρ_f - mass density of fluid flowing through bellows

A - area of cross-section of the bellow

Now substituting for φ from equation (2) and replacing the coefficient a_r ($r=0,1,2,3$) by the nodal coordinates the expression becomes-

$$T = \frac{1}{2} \rho A I^3 \{\ddot{\xi}\}^T + [M] \{\ddot{\xi}\} \quad (10)$$

Where

$$[M] = [M_1] + R \lambda^4 [M_2]$$

$$R = J / m I^2$$

$$\lambda^4 = (m I^4 P_n^2) / EI$$

The mass moment of inertia of the bellow per unit length is given by-

$$J = J_{xx} = J_{yy} = \pi R_m^3 [(2h/q + 0.571)t \rho_b + h/q (2R_2 - t) \rho_f] \quad (11)$$

Now the mass matrices M_1 and M_2 are defined as follows-

$$M_1 = 1/420 \begin{bmatrix} 156 & 22 & 54 & -13 \\ & 4 & 13 & -3 \\ & & 156 & -22 \\ & & & 4 \end{bmatrix}$$

$$M_2 = 1/30 \begin{bmatrix} -36 & -3 & -36 & -3 \\ & 4 & -3 & -1 \\ & & \text{sym} & 3 \\ & & & 4 \end{bmatrix}$$

The matrix equation for free vibration of single bellows is given by-

$$\{[K] - \lambda^4 [M]\} \{\xi\} = 0 \quad (12)$$

Where

$$\lambda^4 = \{\rho A I^4 P_n^2\} / EI$$

The matrix eigenvalue equation is solved for the bellows restrained against rotation using the following boundary conditions

Boundary Conditions

At the end 'A' - bellows are connected to a pipe nipple, and are considered to have a rotational stiffness of R_1 and R_2 at either end as shown in figure 2.

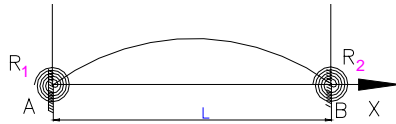


Fig. 2: Mathematical model of single expansion joint fixed at both ends (lateral mode)

At the end A ($x = 0$)

$$X(0) = 0 \text{ and} \quad (13)$$

$$\frac{\partial^2 X(0)}{\partial x^2} = T_1 \frac{\partial X(0)}{\partial x} \quad (14)$$

At the end B ($x = L$) the boundary conditions are given by -

$$X(L) = 0 \text{ and} \quad (15)$$

$$\frac{\partial^2 X(L)}{\partial x^2} = T_2 \frac{\partial X(L)}{\partial x} \quad (16)$$

$$T_1 = SR_1 L / EI \quad (17)$$

$$T_2 = SR_2 L / EI \quad (18)$$

Results and Discussion

A single bellows with the following geometrical and physical parameters is considered –bellows length $L = 0.0693\text{m}$, mass moment of inertia per unit length, $J = 0.001153\text{kgm}$, $EI = 5.078\text{Nm}$ and total mass $m_{\text{tot}} = 5.138\text{kg/m}$ respectively. The geometrical properties data specified above is taken from the thesis of Jakubauskas.V.F (5). The Jacobi method is used for solving the frequency equation.

The first three modes of lateral natural frequencies are obtained for internal pressure of $P=166.0\text{ MPa}$ and are given in Tables 1 & 2 and the same is graphically represented in figures 3 & 4 respectively. Firstly, it is seen that as internal pressure of the bellows increases, the lateral mode natural frequency decreases. For example at $P = 0.0\text{MPa}$ and mode number

N=1, natural frequency obtained is $\omega = 1690.20$ rad/s and at P=166.0 MPa and N=1, and $\omega = 1069.06$ rad/s a drastic drop by about 37%. The same is true for even higher order of mode numbers of N=2 & 3 respectively.

It is also seen that as the value of rotational restraint T ($T=T_1=T_2$) -increases from 0.01 to 10^{10} , the frequencies tend to increase for all the mode numbers. As the rotational stiffness value $T \rightarrow \alpha$, the frequency value increases by about 54.1% for N=1, P=0.0 MPa and by 68.56% for N=1 & P=166.0 MPa. However, it is observed that there is no change in frequency and it becomes constant from $T=10^4$ onwards.

Table1: Natural Frequencies for $T=T_1=T_2$ and N=1 to3 & PR=0.0 MPa

#	T	N=1	N=2	N=3
1	0.01	1690.2	4846.58	8112.22
2	0.1	1717.17	4866.0	8126.83
3	1.0	1927.65	5028.8	8252.68
4	10	2821.56	5938.55	9104.02
5	10^2	3544.04	6944.05	10343.6
6	10^3	3669.43	7138.60	10608.4
7	10^4	3682.84	7159.61	10637.1
8	10^5	3684.19	7161.73	10640.0
9	10^6	3684.33	7161.94	10640.3
10	10^7	3684.34	7161.94	10640.3
11	10^8	3684.34	7161.94	10640.3
12	10^9	3684.34	7161.94	10640.3
13	10^{10}	3684.34	7161.94	10640.3

Fig 3: Transverse Natural Frequencies of Rotationally Restrained Single Bellows
SR=0.01 to $1.E+10$, Pressure PR=0.0 MPa, RIX=0.04673 & V=0 m/s

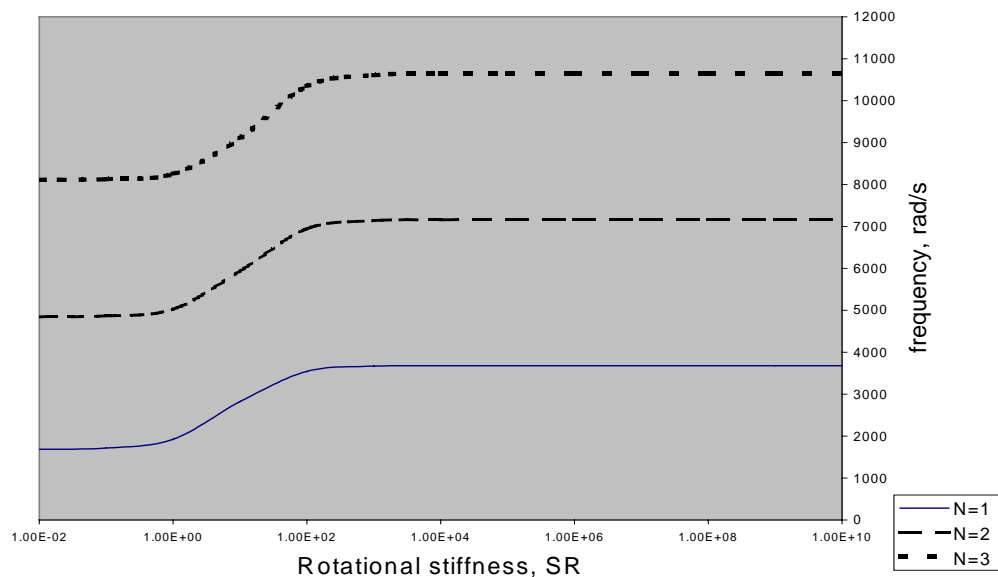


Table2: Natural Frequencies for $T=T_1=T_2$ and $N=1$ to 3 & $PR=166.0$ MPa

#	T	N=1	N=2	N=3
1	0.01	1069.06	4468.55	7837.89
2	0.1	1111.2	4489.69	7852.98
3	1.0	1414.32	4665.5	7983.22
4	10	2486.92	5631.27	8862.16
5	10^2	3256.51	6672.85	10131.0
6	10^3	3385.25	6871.85	10400.1
7	10^4	3398.95	6893.31	10429.2
8	10^5	3400.33	6895.47	10432.1
9	10^6	3400.47	6895.69	10432.4
10	10^7	3400.48	6895.71	10432.5
11	10^8	3400.48	6895.71	10432.5
12	10^9	3400.48	6895.71	10432.5
13	10^{10}	3400.48	6895.71	10432.5

Fig 4: Transverse frequencies of Rotationally Restrained Singles Bellows for $SR=0.01$ to $1.E+10$ and Pressure $PR = 166.0$ MPa & $V=0$ m/s, $RIX=0.04673$

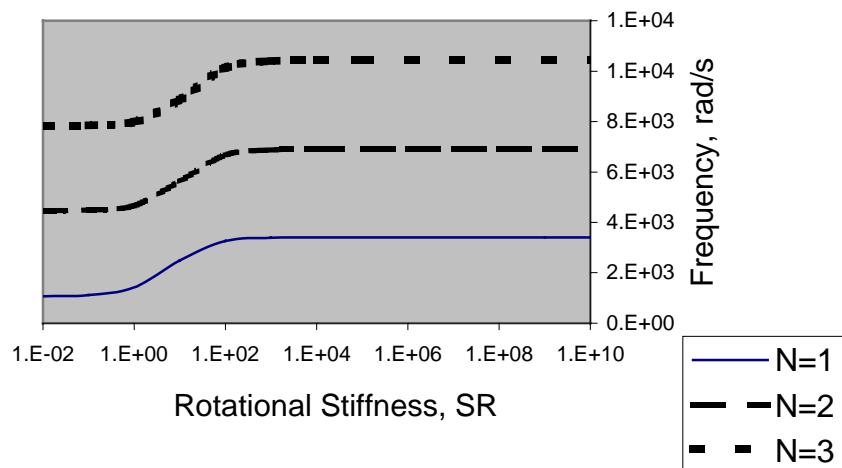


Table 5 gives a comparison of the exact frequency solutions obtained using the finite element method for a single bellows elastically restrained at both ends with rotational restraint vis-a-vis to the results presented in the thesis [5] and in paper [6] by the present authors for a rotationally restrained case.

Table 5 Comparison of Frequency Solutions for $T=\alpha$ and $P_{\max}=166\text{MPa}$

Mode #	Exact [6] ω , rad/s	Thesis [5] ω , rad/s	FEA, ω rad/s	Error, %
1	3400.159	3400.334	3400.48	0.004
2	6890.181	6890.356	6895.71	0.077

The first two natural frequencies are calculated for the bellows data as given above using the frequency formula derived in equation (12) using the FE analysis. It is seen that the results obtained by the FEA method is found to be in good agreement with the exact method. The percentage error in the frequency obtained from the present analysis and the exact bisection method is less and about 0.004%. Therefore, since the percent of error is found to be less it is precise enough to estimate the natural frequency of single bellows expansion joint using this formula.

The effect of variation of velocity of flow at $V= 1.0, 5.0$ and 10 m/s on the first three frequencies is studied. It is seen that for a constant value of rotational stiffness $SR = 10^{10}$ the frequency increases with increase in the velocity of flow and also with increase in mode numbers.

Table 6 Frequencies at different velocities and constant value $SR= 10^{10}$

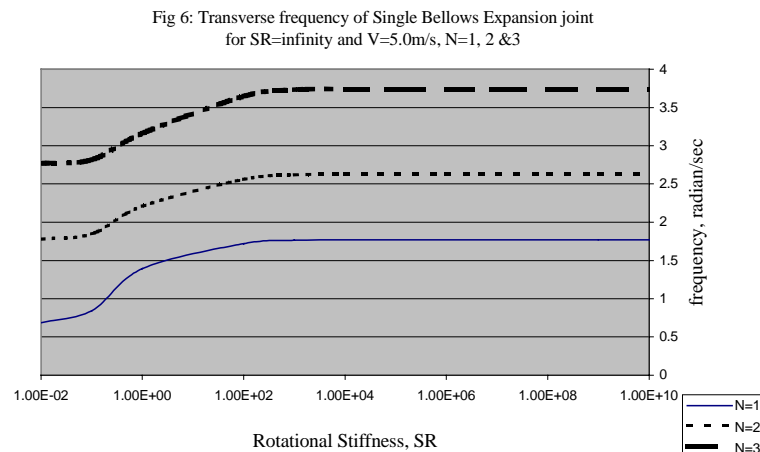
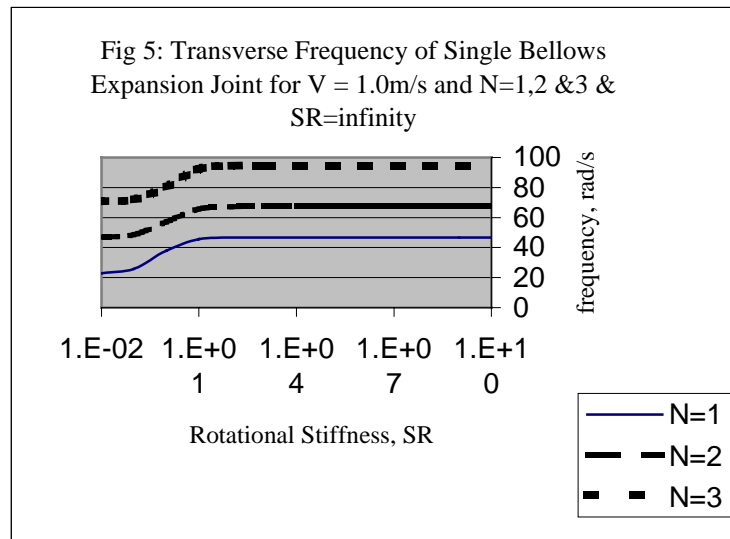
Mode Number	V=1.0	V=5.0	V=10.0
	Frequency, Hz	Frequency, Hz	Frequency, Hz
N=1	0.08	2.0	7.4
N=2	0.16	4.0	15.5
N=3	0.25	6.0	23.7

It is seen that the effect of variation of pressure and velocity of flow on the natural frequency is marginal because the dimensions of bellows given in thesis (5) are small. The effect of variation of pressure and flow velocity on the transverse natural frequencies for modes $N=1, 2$ & 3 is significant. In order to demonstrate this clearly a large dimensioned bellow is considered that has the following geometric properties - $D_b= 1.2\text{m}$, $R_m = 0.6395\text{m}$, $BL= 0.254\text{m}$, $EI=5449\text{Nm}^2$, $J=1485.36\text{kgm}$ and $m_{\text{tot}}= 912.13\text{kg/m}$ respectively.

Firstly, the effect of velocity of flow for $V=1.0$ m/s and 5.0 m/s is studied on the natural frequency. It is found that for a constant value of $SR \rightarrow \infty$ and velocity of flow increasing the natural frequency decreases. It is also observed that the frequency, ω_n increases with increase in the mode number $N=1, 2$ & 3 . Table 7 shows the frequencies in radians/s obtained for different velocities of flow of liquid inside the bellow and figures 5 & 6 depict the same.

Table 7 Frequencies at $SR=10^{10}=\infty$ & varying velocities

Velocity	V=1.0	V=2.0	V=3.0	V=4.0	V=5.0
N=1	46.71	11.53	5.054	2.8	1.76
N=2	67.38	16.75	7.39	4.13	2.62
N=3	94.77	23.61	10.46	5.867	3.742



Similarly, the effect of variation of internal pressure on natural frequency is investigated for the same geometrical dimensions of bellows. It is found that for $SR \rightarrow \infty$ and pressure increasing from 10.0 MPa to 150.0 MPa, the transverse natural frequencies for the first three modes of vibration decreases. Table 8 shows the frequencies obtained at different internal pressures of bellows.

Figures 7 to 10, shows the frequencies obtained by varying the pressures by an interval of 50.0 MPa. It is seen that for $P=10.0$ MPa & $N=1$, the percentage increase in frequency for $SR=0.01$ to $SR=10^6$ is 50% and then the frequency remains constant as SR approaches infinity. At same pressure of 10MPa and $N=2$, the percentage increase in frequency for $SR=0.01$ to 10^6 is 30% and for $N=3$ the percentage increase in frequency is 25%. Similarly for a maximum pressure of 160MPa and $N=1$, the percentage increase in frequency for $SR=0.01$ to 10^6 is 69%. At same pressure of 160MPa and $N=2$, the percentage increase in frequency for $SR=0.01$ to 10^6 is 33% and for $N=3$ the percentage increase in frequency is 26%.

Table 8 Frequencies at $SR=10^{10}=\infty$ & varying pressures

Pressure	PR=10MPa	PR=50MPa	PR=100MPa	PR=150MPa
N=1	105.35	20.58	9.97	6.43
N=2	151.41	29.94	14.75	9.69
N=3	212.60	42.28	20.98	13.81

Fig 7: Transverse Frequency of Single Bellows Expansion Joint for $SR=\infty$ and $PR=10.0$ MPa, $N=1,2,3$

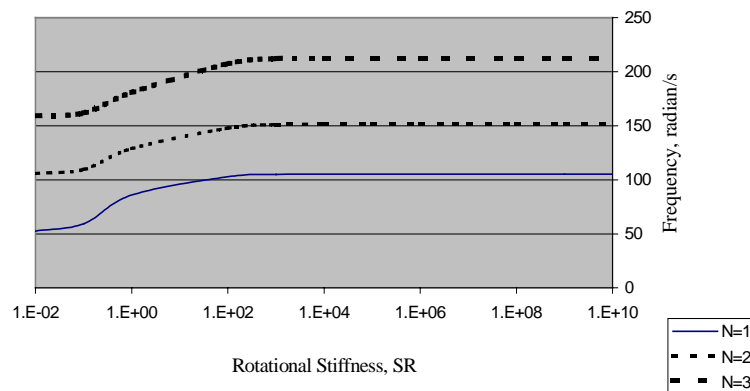


Fig 8: Transverse Frequency of Single Bellows Expansion Joint
for SR=infinity, PR=50MPa and N=1,2 &3

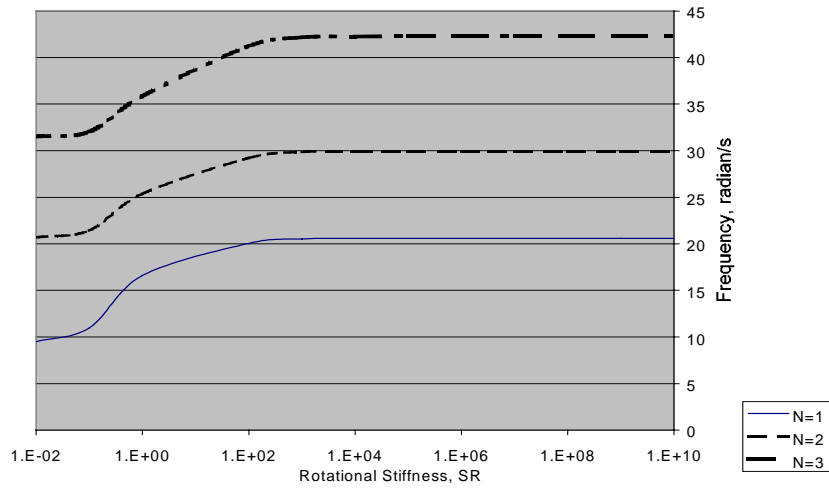


Fig9: Transverse Frequency of Single Bellows Expansion Joint
for SR=infinity, PR=100.0MPa and N=1,2&3

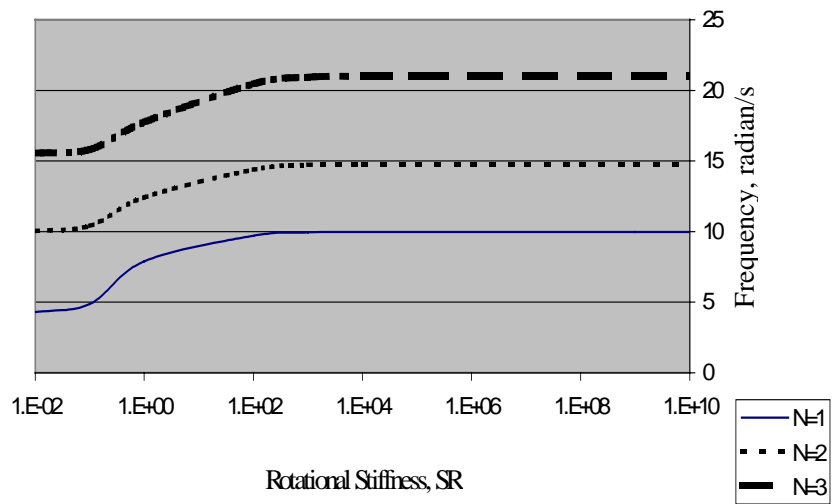
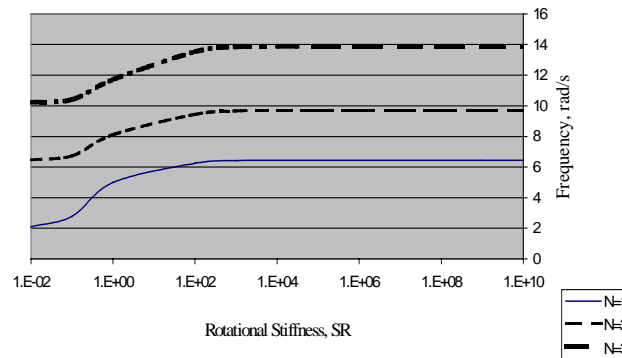


Fig 10: Transverse Frequency of Single Bellows Expansion Joint for SR=infinity and PR=150.0 MPa and N=1,2 &3



Conclusions

Theoretical and experimental comparisons confirm that the finite element method developed used in this study is well adapted to the dynamic response of bellows gives fairly exact results. From the various results presented in this paper the following can be concluded-

- i. As the internal pressure of the bellow is doubled the transverse frequency of vibrations for the first three mode numbers is reduced by nearly 50%.
- ii. Similar kind of analysis has been done to study the effect of velocity of flow on frequency. It is seen that as the flow velocity is doubled the frequency decreases by about 4 times for all the first three modes of vibration.

References

1. EJMA – “The Standards of the Expansion joint Manufacturers Association Inc”. New York, ASME, 1984, p221.
2. Li Ting-Xin, Li Tian-Xiang and Guo Bing-Liang, “Research on Axial and Lateral Natural Frequencies of Bellows with different end conditions”, International Symposium 86 PVP-14, ASME, p367-373.
3. Jakubauskas V.F and Weaver. D.S, “Transverse Vibrations of Bellows Expansion Joints Part-II: Beam Model Development & Experimental Verification”.
4. Jakubauskas V.F, “Practical Predictions of Natural Frequencies of Transverse Vibrations of Bellows Expansion Joints”, Mechanika-Kaunas, Technologija, 1998, No.3 (14), p47-52.
5. Jakubauskas.V.F, “Transverse Vibrations of bellows Expansion Joints”- PhD. Thesis – Hamilton, Ontario, Canada: McMaster University, 1995, PP145-150.
6. Rao.C.K and Radhakrishna.M, “Transverse Vibrations of Single Bellows Expansion Joints restrained against Rotation”, Presented at Tenth International Conference on Nuclear Engineering, April 14-18, 2002, USA.

“DRAFT”

ICON 10-22092

TRANSVERSE VIBRATIONS OF DOUBLE BELLOWS EXPANSION JOINT RESTRAINED AGAINST ROTATION

KAMESWARA RAO.C
Bharat Heavy Electricals Limited
Hyderabad, India

RADHAKRISHNA.M
Indian Institute of Chemical Technology
Hyderabad, India

Keywords:

Bellow vibration, double bellows, transverse frequency & elastic constraints

ABSTRACT

The paper presents the results of investigation of transverse vibrations of single bellows expansion joint restrained against rotation on either end. A theoretical model is developed based on the Bernoulli-Euler beam theory and includes added mass of the fluid flowing inside the pipe-bellow-pipe assembly. Neglecting effects of shear and rotary inertia an exact frequency equation is derived for the transverse vibrations of single bellows expansion joint including the effects of end elastic restraints against rotation. Numerical results are presented for an example bellow showing the effects of variation of elastic restraints and internal pressure on the first four modes of vibration.

Introduction

Bellows expansion joints are designed to absorb the axial or transverse displacements in pipeline systems. It is observed that any piping system is more or less flexible, and so has the natural flexibility to accept small elongation or contraction. However, in many of the applications such as the fossil/nuclear power plants or in aircraft and space

industry, the elongation/ contraction of the piping system is quite significant and frequent changes in temperature or relative mechanical motion of structures with respect to each other. Therefore, the bellows are very susceptible to vibrations that can be easily excited either structurally through the fixed ends of the expansion joints or by the fluid flowing inside the bellows. Most studies of transverse vibration of double bellows expansion joint consider the bellows directly welded to pipe flange and uses fixed-fixed beam approach for investigation of transverse mode shapes and natural frequency [1].

However, in real practice the bellow is welded to a short pipe nipple. The other end of the nipple has a flange and is connected to the pipe flange. Figure 1 depicts the bellow-nipple-flange assembly.

The paper presents an analysis of estimating the frequency and mode shapes of transverse vibrations of double bellows expansion joint restrained against rotation on either end. The analysis forms the basis of development of a theoretical model for the bellow considering as a *Bernoulli-Euler Beam*. The model considers fluid filled bellows and neglects the effect of shear and rotatory inertia.

More precise formulae are developed based on the solution of Bernoulli-Euler differential equation for calculating the natural frequency of bellows. Results obtained using the Bisection method are compared with results presented in thesis [1].

The Differential Equation

Figure 2 shows the various geometrical dimensions of U-shaped bellows –where R_1 and R_2 is the inner and outer radius of bellow, p is the pitch, h is the convolution height, t is the thickness of bellows wall and L is the length of bellow.



Fig. 1 : Flange-Pipe Nipple-Bellow assembly

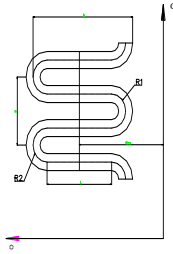


Fig. 2 : Geometry of Bellows

The general form of the differential equation of vibration of bellows for single or double bellows expansion joint is given by –

$$EI \frac{\partial^4 W}{\partial x^4} + P\pi R_m^2 \frac{\partial^2 W}{\partial x^2} - \frac{J}{\partial x^2} \frac{\partial^4 \omega}{\partial t^2} + m_{tot} \frac{\partial^2 W}{\partial t^2} = 0 \quad (1)$$

Where EI is the bending stiffness, P -internal pressure, J -mass moment of inertia per unit length, m_{tot} –total mass of bellows per unit length includes bellows material mass and fluid mass, x – axial coordinate, R_m –is the mean radius of bellow, W -deflection and t -time [2].

Using the technique of *Separation of variables*, the lateral deflection of the bellows axis ‘ w ’ can be expressed as-

$$W(x, t) = X(x) T(t) \quad (2)$$

Differentiating the above equation (2) and substituting into differential equation (1) –

$$X \frac{d^4 X}{dx^4} + \frac{[P\pi R_m^2 + J\omega^2]}{EI} \frac{d^2 X}{dx^2} - W^2 \frac{m_{tot}}{EI} = 0 \quad (4)$$

$$\text{If } c = \frac{\sqrt{(P\pi R_m^2 + J\omega^2)}}{\sqrt{2EI}} \quad (5)$$

$$\lambda = \frac{(m_{tot} W^2)^{1/4}}{(EI)^{1/4}} \quad (6)$$

$$\frac{d(X^4)}{dx^4} + 2c^2 \frac{dX^2}{dx^2} - \lambda^4 X = 0 \quad (7)$$

The general solution of the equation is given by-

$$X = A \sinh \alpha x + B \cosh \alpha x + C \sin \beta x + D \cos \beta x \quad (8)$$

The first three derivatives of equation (8) are given as follows–

$$\frac{d(X)}{dx} = A\alpha \cosh \alpha x + B\alpha \sinh \alpha x + C\beta \cos \beta x - D\beta \sin \beta x \quad (9)$$

$$\frac{d^2(X)}{dx^2} = A\alpha^2 \sinh \alpha x + B\alpha^2 \cosh \alpha x - C\beta^2 \sin \beta x - D\beta^2 \cos \beta x \quad (10)$$

$$\frac{d^3(X)}{dx^3} = A\alpha^3 \cosh \alpha x + B\alpha^3 \sinh \alpha x - C\beta^3 \cos \beta x + D\beta^3 \sin \beta x \quad (11)$$

Where the roots of the equation are α & β and their values are given by -

$$\alpha = \sqrt{-c^2 + \sqrt{c^4 + \lambda^4}} \quad (12)$$

$$\beta = \sqrt{c^2 + \sqrt{c^4 + \lambda^4}} \quad (13)$$

A, B, C, D are arbitrary constants

Exact Solution of Double Bellows Expansion Joint Lateral Mode Natural Frequency

A case of vibration of bellows in lateral mode is shown in figure 2. It is seen that the pipe has pure translational motion due to the geometry and physical symmetry of the system provided the coriolis component of force acting on the bellows from the fluid flowing inside is neglected.

As a mathematical approximation one half of the system is considered with its left end having a rotational stiffness 'R' and right end fixed to the vertical rollers and is shown in figure 2.

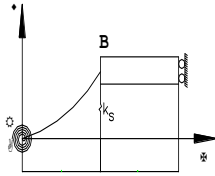


Fig. 3 : Mathematical model of universal expansion joint for lateral mode

Boundary Conditions

As shown in figure 3, end 'A' of the bellow is connected to a pipe nipple, and considered to have a rotational stiffness of 'R'. Now the first two boundary conditions are written as follows -

Deflection is zero at $W(0, t) = 0$ and (14)

$$\frac{EI}{L^2} \frac{\partial^2 X(0)}{\partial x^2} = \frac{R}{L} \frac{\partial X(0)}{\partial x} \quad (15)$$

$$\frac{\partial^2 X(0)}{\partial x^2} = T \frac{\partial X(0)}{\partial x}$$

As the end B does not rotate the third boundary condition, slope is zero and given by -

$$\frac{\partial W(L, t)}{\partial x} = 0 \quad (18)$$

The fourth boundary condition at end 'B' is the shear force $Q(L, t)$ of the bellows and is given by-

$$\frac{\partial^3 W(L, t)}{\partial x^3} = \frac{\{M_s + (m_p + m_{f3})a\}}{EI} \frac{\partial^2 W(L, t)}{\partial x^2} + \frac{k_s W(L, t)}{EI} \quad (19)$$

$$\frac{d^3 X(L)}{dx^3} = \frac{-W^2 \{M_s + (m_p + m_{f3})a\}}{EI} * X(L) + \frac{k_s}{EI} X(L) \quad (20)$$

$$\text{If } b = \frac{-W^2 \{M_s + (m_p + m_{f3})a\}}{EI} - \frac{k_s X(L)}{EI} \quad (21)$$

M_s is the equivalent lateral support mass, k_s is the equivalent spring stiffness of the lateral support, m_p is the mass per unit length of the connecting pipe of length 'a' and m_B is the mass of the fluid per unit length in the connecting pipe.

Substitution of the general solution (8) and its derivatives into boundary condition expressions (14), (15), (16) and (17) will give a set of linear equations with respect to the constants A, B, C and D.

$$B + D = 0 \quad (22)$$

$$\{B(\alpha L)^2 - D(\beta L)^2 - T(A\alpha L + C\beta L)\} = 0 \quad (23)$$

$$A\alpha \cosh \alpha L + B\alpha \sinh \alpha L + C\beta \cos \beta L - D\beta \sin \beta L = 0 \quad (24)$$

$$[\alpha^3 \cosh \alpha L + b \sinh \alpha L] A + [\alpha^3 \sinh \alpha L + b \cosh \alpha L] B - [\beta^3 \cos \beta L - b \sin \beta L] C + [\beta^3 \sin \beta L + b \cos \beta L] D = 0 \quad (25)$$

Substituting c_1, c_2, c_3, c_4 for the terms in the brackets in equation (25) we get -

$$c_1 = \alpha^3 \cosh \alpha L + b \sin \alpha L \quad (26)$$

$$c_2 = \alpha^3 \sinh \alpha L + b \cosh \alpha L \quad (27)$$

$$c_3 = \beta^3 \cos \beta L - b \sin \beta L \quad (28)$$

$$c_4 = \beta^3 \sin \beta L + b \cos \beta L \quad (29)$$

For a non-trivial solution the determinant formed by the coefficients of the system of algebraic equations above must be equal to zero -

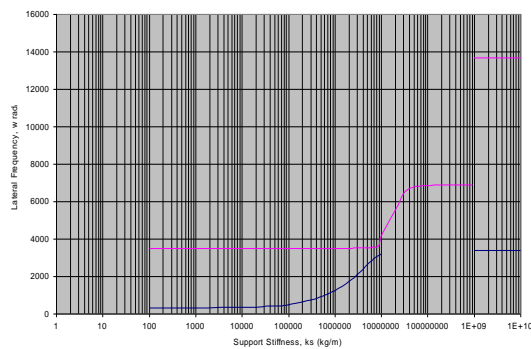
The expansion of the above determinant results in the frequency equation for the system shown in figure 2.

0	1	0	1		A
$+T(\alpha)$	$(\alpha)^2$	$+T(\beta)$	$+(\beta)^2$		B
$\alpha \cosh(\alpha L)$	$\alpha \sinh(\alpha L)$	$\beta \cos \beta L$	$-\beta \sin \beta L$		C
c_1	c_2	c_3	c_4		D

$$=0 \quad (30)$$

$$T \{ b [(\alpha^2 - \beta^2) \sin \beta L \sinh \alpha L + 2\alpha\beta (1 - \cos \beta L \cosh \alpha L) - \alpha\beta (\alpha^2 + \beta^2) (\alpha \sinh \alpha L \cos \beta L + \beta \cosh \beta L \sin \beta L) + b (\alpha^2 + \beta^2) (\alpha \sin \beta L \cosh \alpha L - \beta \cos \beta L \sinh \alpha L - \alpha\beta (\alpha^2 + \beta^2) \cos \beta L \cosh \beta L \} \quad (31)$$

Fig 4: Transverse Vibrations-Double Bellows
(Lateral Mode) & for N=1 and N=2 & $M_0=0$



Results and Discussion

Let us take a double bellows expansion joint having the following geometrical and physical parameters -bellow length $L=0.0693m$, mass moment of inertia per unit length $J=0.001153kgm$, $EI = 5.078Nm^2$, total bellows mass $m_{tot} = 5.138kg/m$, total connecting pipe mass, $m_b + mf_3 = 5.0kg/m$ and assuming $a = L$.

According to [1], the maximum allowable pressure in bellows is -

$$P_{max} = \frac{\pi k^* P}{6.666L^2} \quad (32)$$

Where k is the equivalent axial stiffness of bellows -

Substitution of the above numerical values into the expressions 4 & 5, we get -

$$c = \sqrt{616.49 + 0.0001135\omega^2} \quad (33)$$

$$\lambda = 1.0029\sqrt{\omega} \quad (34)$$

$$b = 0.10235\omega^2 \quad (35)$$

The study involves the effect of varying the equivalent support stiffness and mass on the frequency of vibration. Using expressions in (12), (13), (32), (33), (34) and (35) the frequency equation (31) is solved by applying bisection method. The results are presented in Tables 1,2 and 3 and the same are also graphically represented in figures 4 and 5 respectively.

Tables 1 and 2 presents the frequencies obtained by varying the support stiffness k_s for mode numbers $N=1$ and 2. It is seen that as stiffness increases from a value of 10^2 to 10^{15} , frequency increases from 331.40rad/s to 3400.1597rad/s, a steep rise by almost 90%. The frequency attains almost a constant value from 10^8 onwards.

The effect of varying the support mass on the frequency of vibration is also studied and the results presented in Table 3. It is seen that there is a steep drop of 87% in frequency as the support mass increases from 1.0 to 100 for $N=1$ and by a small drop of 1% for $N=2$.

“DRAFT”

ICONE 11-36400

**SEISMIC RESPONSE OF ELASTICALLY RESTRAINED SINGLE BELLOWS
EXPANSION JOINT IN LATERAL MODE**

KAMESWARA RAO.C
Bharat Heavy Electricals Limited
Hyderabad, India

RADHAKRISHNA . M
Indian Institute of Chemical Technology
Hyderabad, India

Keywords

Single bellows, elastic restraint, seismic, lateral mode

Introduction

Bellows expansion joints are used for absorbing thermal movements of piping that results in a substantial shortening of pipe length and thereby reducing the plant construction costs considerably.

It is seen that most of the nuclear and thermal power plants around the world are located in the seismic zones. The piping in these plants consists of expansion bellows and needs to be analyzed from seismic design point of view.

Hence, while designing an expansion bellow from structural point of view, the seismic design aspect is also to be given utmost importance.

The formulae presented in EJMA and those derived by Morishita et al, [1,3] cover classical boundary conditions only like the fixed-fixed

type of ends, which are infinitely stiff and have used the approximate method to determine the natural frequencies. Hence, it is observed that this assumption will lead to an over estimation of natural frequencies and incorrect determination of seismic response.

The paper attempts to derive an exact solution for the seismic response of U type of single bellows that are considered elastically restrained against rotation on either end. The fundamental equation of motion of the equivalent Timoshenko beam is used to calculate the spectral response of the bellows to a seismic excitation in the lateral direction. The shear terms are neglected. The first and second lateral mode frequencies are obtained keeping the rotational spring stiffness values equal.

The Differential Equation

The fundamental equation of motion of the equivalent Timoshenko beam [5] is given by-

$$EI \frac{\partial^4 w}{\partial x^4} + P\pi R_m^2 \frac{\partial^2 w}{\partial x^2} \rho A - J \frac{\partial^4 w}{\partial x^2 \partial t^2} + m_{tot} \frac{\partial^2 w}{\partial t^2} = 0 \quad (1)$$

Where EI is bending stiffness, P- internal pressure in bellows, J – rotatory inertia per unit length, w –lateral deflection x-axial coordinate, R_m –mean radius of bellows, m_{tot} is the total mass of bellows per unit length includes mass of bellows and fluid mass and t-time [5].

Using the technique of Separation of variables, the lateral deflection of the bellows axis ‘w’ is expressed as-

$$w(x, t) = X(x) \cdot T(t) \quad (2)$$

Where w (t) is a parameter of x only and T (t) is the time harmonic function such as -

$$T(t) = X(x) e^{i\omega t} \quad (3)$$

Where ‘ ω ’ is the natural frequency

The modal expansion technique is used to obtain the seismic response of the beam. Applying the modal expansion to equation (1) –we obtain the equation of motion in modal space-

$$[M] \ddot{y} + [c] \dot{y} + [k] y = \beta_b \ddot{y}_0(T) \quad (4)$$

$$[M] \ddot{y} + [k] x = \beta_b \ddot{y}_0(T) \quad (5)$$

β_b is the participation factor which for the present study becomes equal to 1.0.

Differentiating the above equation (5) we get-

$$y(x, T) = y(x) \cdot e^{(i\omega T)} \quad (6)$$

$$\dot{y}(x, T) = y(x) (i\omega) e^{(i\omega T)} \quad (7)$$

$$\ddot{y}(x, T) = y(x) (i\omega)^2 e^{(i\omega T)} \quad (8)$$

$$\therefore \ddot{y}(x, T) = -\omega^2 y(x, T) \quad (9)$$

Where ‘y’ is generalized coordinate in modal space. Assuming damping factor is equal to zero i.e. [c] = 0

Let the solution of equation (9) be given as-

$$Y = A \sinh \alpha x + B \cosh \alpha x + C \sin \beta x + D \cos \beta x \quad (10)$$

Where A, B, C&D are arbitrary constants

Boundary conditions are as follows-

i.) $y=0$ at $x=0$

$$\partial^2 y / \partial x^2 = + T_1 \partial y / \partial x \quad (11)$$

ii.) And $y = 0$ at $x = L$ or $x = 1$

$$\partial^2 y / \partial x^2 = - T_2 \partial y / \partial x \quad (12)$$

Now applying B.C (i) & (ii) we get-

$$B + D = 0 \text{ or } B = -D$$

$$A + C = 0 \text{ or } A = -C$$

Substituting in equation (10) and rewriting-

$$y = C (\sin \beta x - \sinh \alpha x) + D (\cos \beta x - \cosh \alpha x) \quad (13)$$

$$y = D \{ [T_2 (\sinh \alpha x + \sin \beta x) + \phi (\cosh \alpha x + \cos \beta x)] \}$$

$$\begin{aligned} & / T_2 (\cos \beta x - \cosh \alpha x) - \phi (\sinh \alpha x + \sin \beta x) \\ & (\sin \beta x - \sinh \alpha x) + (\cos \beta x - \cosh \alpha x) \end{aligned} \quad (14)$$

Applying the boundary condition (ii) we get –

$$y = D \{ (\cos \beta x - \cosh \alpha x) + \delta (\sin \beta x - \sinh \alpha x) \} \quad (15)$$

Where

$$\delta = \frac{T_2 (\sinh \alpha x + \sin \beta x) + \phi (\cosh \alpha x + \cos \beta x)}{T_2 (\cos \beta x - \cosh \alpha x) - \phi (\sinh \alpha x + \sin \beta x)} \quad (16)$$

At $x = l$

$$\delta = \frac{\sin \beta + \sinh \alpha}{\cos \beta - \cosh \alpha} \quad (17)$$

Also equation (17) can be written as -

$$\delta = - \left\{ \frac{\sin \beta - \sinh \alpha}{\cos \beta - \cosh \alpha} \right\} \quad (18)$$

We know

$$c = \frac{\sqrt{(P \pi R_m^2 + J \omega^2)}}{\sqrt{2 EI}} \quad (19)$$

Let the roots of the equation (10) be α & β are given as in reference [3]-

$$\alpha = \sqrt{-c^2 + \sqrt{(c^4 + \phi^4)}} \quad (20)$$

$$\beta = \sqrt{c^2 + \sqrt{(c^4 + \phi^4)}} \quad (21)$$

Exact Analysis –Seismic Response

The various dimensional parameters of U-shaped bellows are taken to be same as those that have been considered by Morishita et al. [5]-

Bellows inner diameter (D_i) –545.8mm, convolution height, $h=30$ mm; convolution pitch, $p=25$ mm; bellows thickness, $t_b=0.563$ mm; Bellows mean diameter, $D_m=550.8$ mm; number of convolutions, $N=20$; pitch diameter of bellows, $D_p=575.8$ mm and Bellows length $L = 0.5$ m respectively.

The theoretical stiffness of bellows is computed by using the expression given in EJMA, $k=387.02$ N/m.

According to [3] the maximum internal pressure in bellows and bending stiffness are given by the expressions -

$$P_{max} = \pi \cdot kp / (6.666L^2) \quad (22)$$

$$EI = \frac{1}{4} \cdot kp \cdot R_m^2 \quad (23)$$

Substituting the values for k , p , L and R_m , we get-

$$P_{max} = 18.23 \text{ Pa}$$

$$EI = 0.1834 \text{ Nm}^2.$$

Also the total mass (m_{tot}) and rotatory inertia (J) of bellows per unit length are found out as-

$$m_{tot} = 440.76 \text{ kg/m.}$$

$$J = 2.3894 \text{ kg m}$$

Substituting the above numerical values in equation (19), (20) and (21) we get –

$$c = \sqrt{(0.00001184 + 6.5141 \omega^2)} \quad (24)$$

$$\lambda = 7.0016\sqrt{\omega} \quad (25)$$

Using the frequency expression derived and given in reference [4] the first and second lateral mode frequencies are obtained using bisection method.

The rotational restraint T is varied from a minimum value of 0.01 to a maximum of 10^{10} at maximum internal pressure of $P=18.233\text{Pa}$. It is assumed that there is equal rotations on either ends i.e. $T=T_1=T_2$.

Now the spectral response of the bellows to a seismic excitation in the lateral direction is calculated by using the modal expansion technique. Applying this technique to equation (1), the equation of motion in modal space is given by equation (5). From equation (5) the maximum response lateral displacement of any arbitrary section of bellow to a response spectrum is given by-

$$y_{\max} = \beta_b \frac{S_a}{(2\pi f)^2} \cdot \frac{D_p}{2 \cdot N \cdot p} y(x) \quad (26)$$

$\beta_b=1.0$,

Where S_a is the spectral gravitational acceleration at frequency ' f ' and has units of mm/s^2 .

$$y(x) = \frac{\alpha}{y} \{(\psi(n+1) - \psi(n))\} \quad (27)$$

Where ' n ' is convolution number and is equal to $N-1$. Here in this case it is 19 as $N=20$ convolutions.

$$\frac{\alpha}{y} = 1$$

Results and Discussion

Table 1 gives a comparison of the exact frequencies obtained using the bisection method for a single bellows that are elastically restrained at both ends vis-à-vis to the fixed-fixed end results presented by Morishita et al. [5].

Table 1 Comparison of Frequencies at $T=\infty$

Mode #	Morishita [5] f, Hz	Exact f, Hz	Error, %
1	27.7	23.6	15
2	54.2	36.3	53

It is seen that the frequencies obtained by considering the ends as elastically restrained are lower than that was found out by Morishita et al. Therefore, it can be concluded that the seismic response by the present method is exact and not an over prediction.

Table 2 presents the first two mode frequencies at $T_1=T_2$, the time period for the fundamental mode frequency and the spectral acceleration.

Table2: Fundamental Frequency for various values of restraint parameter $T=0.01$ to ∞

T	f (Hz)	t (sec)	Sa (mm/s^2)
0.01	14.8635	0.0672	206.9
0.1	14.9301	0.0669	206.9
1.0	15.501	0.065	413.8
10	17.6262	0.0567	551.7
10^2	20.502	0.0487	655.2
10^3	23.1246	0.0432	603.5
10^4	23.5662	0.0424	569.0
10^5	23.614	0.0423	567.3
10^6	23.619	0.0423	567.3
10^7	23.619	0.0423	567.3
10^8	23.619	0.0423	567.3
10^9	23.619	0.0423	567.3
10^{10}	23.619	0.0423	567.3

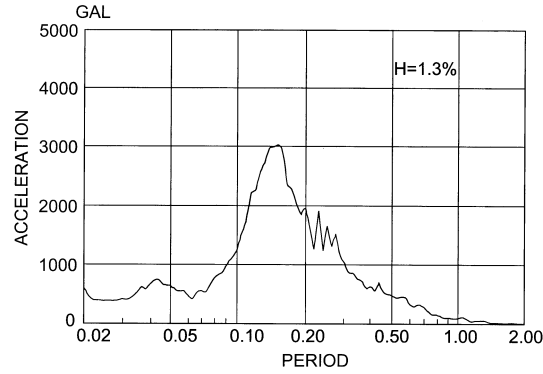


Fig 1:Time History Curve of Seismic Response

It is observed that for $N=1$ and at $T=0.01$ the time period found out is 0.0672sec, while at $T=\infty$, the time period is 0.0423sec. It is seen that as rotational stiffness increases and approaches infinity, the time period of vibration decreases. A standard time history graph of seismic wave and its acceleration response is used for obtaining the seismic accelerations (S_a) at various frequencies as shown in Fig 1.

Table 3 gives the maximum displacement, y_{\max} and bending stress σ_b values for varying rotational restraint parameter T .

Table 3: Response of bellows to lateral seismic excitation

T	$y_{\max}(\text{mm})$	$\sigma_b(\text{kg/mm}^2)$
0.01	0.0136	0.035
0.1	0.0135	0.034
1.0	0.0251	0.065
10	0.0259	0.067
10^2	0.0227	0.058
10^3	0.0165	0.043
10^4	0.015	0.039
10^5	0.0148	0.038
10^6	0.0148	0.038
10^7	0.0148	0.038
10^8	0.0148	0.038

10^9	0.0148	0.038
10^{10}	0.0148	0.038

The seismic gravitational acceleration obtained at $T=\infty$ and time period of $t=0.042\text{sec}$ is 620.68mm/s^2 . Substituting this value in equation (26), the maximum lateral displacement is obtained as $y_{\max} = 0.016\text{mm}$ compared to 0.84mm by Morishita et al [5].

Conclusions

The exact method is developed in present study to calculate the dynamic characteristics and seismic response of bellows for its lateral vibrations. The theoretical formulations are based on the equations of an equivalent Timoshenko beam, and the bending stress due to these vibrations is estimated. In case of lateral vibrations it is found that the influence of elastically rotational restraint at either ends to its natural frequencies is significant.

References

1. EJMA – “The Standards of the Expansion joint Manufacturers Association Inc”. New York, ASME, 1984, p221.
2. Jakubauskas V.F, “Practical Predictions of Natural Frequencies of Transverse Vibrations of Bellows Expansion Joints”, Mechanika- Kaunas, Technologija, 1998, No.3 (14), p47-52.
3. Jakubauskas.V.F, “Transverse Vibrations of bellows Expansion Joints”- PhD. Thesis – Hamilton, Ontario, Canada: McMaster University, 1995, PP145-150.

4. Kameswara Rao.C and Radhakrishna.M,
“Transverse Vibrations of Single Bellows
Expansion Joint Restrained against
Rotation”, Proceedings of Tenth
International Conference on Nuclear
Engineering, USA, Paper # 22090, April 14-
18,2002.
5. Morishita.M. et al., “Dynamic Analysis
Methods of Bellows Including Fluid
Structure Interaction", ASME Pressure
Vessels and Piping Conference, Hawaii,
July 23-27, 1989, P149-157.

Axial vibrations of U-shaped bellows with elastically restrained end conditions

M. Radhakrishna^a, C. Kameswara Rao^{b,*}

^a Design Engineering Group, Indian Institute of Chemical Technology, Hyderabad, India

^b Intellectual Property Management Group, Corporate R & D, Bharat Heavy Electricals Limited, Vikasnagar, Hyderabad 500 093, India

Received 10 June 2003; received in revised form 19 June 2003; accepted 4 July 2003

Abstract

Previous work by Li et al. in the area of axial vibrations of bellows dealt with fixed end conditions. However, it is seen on several occasions that bellow ends are welded to a small pipe spool that has a lumped mass such as a valve or an instrument. Hence, the present paper aims at finding out the effect of elastically restrained ends on the axial natural frequencies. The analysis considers finite stiffness axial restraints on the bellows, i.e. solving the set of equations with non-homogeneous boundary conditions. Two bellow specimens are considered for comparison having the same dimensions as taken by Li in his analysis. The transcendental frequency equation deduced is accurate as the first, second and third mode frequencies computed are in close agreement to the ones obtained by Li.

© 2003 Elsevier Ltd. All rights reserved.

Keywords: Bellow vibration; Single bellows; Axial frequency and elastic restraint

1. Introduction

Gerlach [1] was the first to have developed a simplified method of computing the natural frequencies of bellows. He represented a bellow having ' N ' convolutions by a system consisting of $2N - 1$ identical masses and connected to a $2N$ identical springs. By calculating the elemental mass, added mass and elemental stiffness, the axial natural frequencies of bellows were determined. It is reported that very good predictions were observed for the lowest vibration modes. EJMA [2] also provides

* Corresponding author. Fax: +91-40-3776320.

E-mail address: ckrao_52@yahoo.com (C. Kameswara Rao).

a method for calculating the axial natural frequency of single and double bellows by assuming the bellows as a continuous elastic rod. However, the method does not take into account the mass resulting from simple translation of the fluid between undeformed convolutions.

Jakubauskas derived an expression for the axial natural frequency of bellows. He assumes the total fluid mass, m_f , per unit length to comprise three components—rigid convolution motion in axial direction, m_{f1} , convolution distortion component, m_{f2} , and the third component associated with the motion in return flow in central area of cross-section of bellows, m_{f3} . The distortion component for a half-convolution was determined using finite element analysis. The percentage error in frequency obtained by the EJMA modified method was compared with the results of experiments and was found to be far less than the percentage error in frequency obtained either from standard EJMA or Gerlach methods [3].

The paper contributed by Li et al. [4] presents equations to calculate the axial and lateral natural frequencies of single bellows with three types of end conditions—one end fixed and other end free, one end fixed and other end attached to weight and both ends of the bellows are fixed. The theoretical results were then compared with the experiments performed on bellow specimens having different geometrical parameters. Though the error corresponding to the experimental value was found to be reasonably close to theoretical value, the end conditions represented by Li do not represent most of the practical situations.

It is seen on several occasions that bellow ends are welded to a small pipe spool that has a lumped mass such as a valve or an instrument. Hence, the present paper aims at finding out the effect of elastically restrained ends on the axial natural frequencies of a physical system as shown in Fig. 1. A weight, W_0 , is attached as

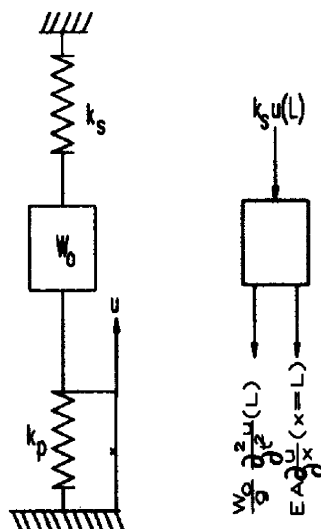


Fig. 1. Pipe with end condition.

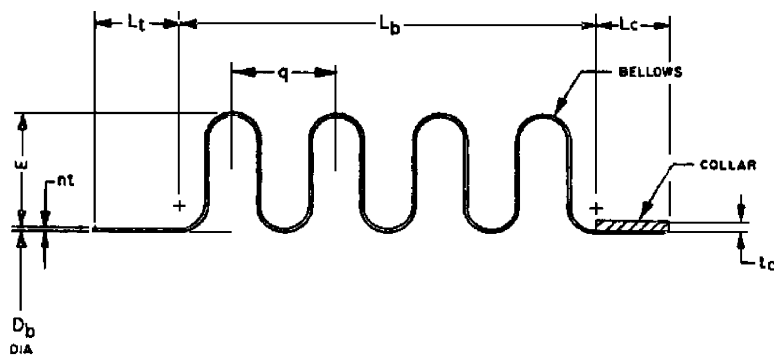


Fig. 2. Dimension of below.

shown and is connected to a spring of stiffness, k_s . It is assumed that a straight pipe is partially fixed at the bottom and connected to a spring of stiffness, k_p . Fig. 2 depicts the various geometrical parameters of the U-shaped bellows used in the analysis.

2. Axial natural frequency of bellows

The differential equation to express the axial vibration for the straight pipe is given by [4]:

$$\frac{\partial^2 u}{\partial t^2} = a^2 \frac{\partial^2 u}{\partial x^2} \quad (1)$$

where ‘ u ’ is the axial displacement of the pipe (mm), ‘ T ’ is the time (s), E is the elastic modulus of bellow material (MPa), g is the gravitational acceleration (9806.65 mm/s^2), v is the weight per unit volume of the bellow material (N/mm^3) and $a = \sqrt{Eg/v}$, respectively.

3. Formulation and analysis

When considering the axial vibrations of a single bellow expansion joint, the boundary conditions for the system are given by

$$AE \frac{\partial u(x)}{\partial x} = k_p \cdot u \quad (2)$$

$$AE \frac{\partial u}{\partial x} + \frac{W_0}{g} \frac{\partial^2 u}{\partial t^2} + k_s \cdot u(x) = 0 \quad (3)$$

The exact solution of the differential equation is written as follows

$$u(x, T) = [C \sin \beta + D \cos \beta x] \cdot e^{i\omega T} \quad (4)$$

where

$$\beta = \omega_i/a \quad (5)$$

and ω_i is the angular frequency in radian/s, C and D are the integration constants. Now applying the boundary conditions and substituting $T = 0$, we get

$$u(x) = C\sin\beta x + D\cos\beta x \quad (6)$$

$$\frac{\partial u(x)}{\partial x} = \beta\{C\cos\beta x - D\sin\beta x\} \quad (7)$$

Substituting for $\partial u/\partial x$ and $u(x)$ in Eq. (2), we get

$$AE \times \beta\{C\cos\beta x - D\sin\beta x\} = k_p\{C\sin\beta x + D\cos\beta x\} \quad (8)$$

Applying $x = 0$ in Eq. (8), we get

$$C = \{k_p/\beta \times AE\}D \quad (9)$$

We know

$$u(x, T) = u(x) \cdot e^{i\omega T} \quad (10)$$

Now substituting for $u(x)$, $\partial u/\partial x$ and $\partial^2 u/\partial t^2$ in Eq. (3)

$$AE\{\beta(C\cos\beta x - D\sin\beta x)\} + \{(k_s - W_0 \cdot \omega^2/g) \times (C\sin\beta x + D\cos\beta x)\} = 0 \quad (11)$$

Applying $x = L$ in Eq. (8), where L is the bellow length, we get

$$AE\{\beta(C\cos\beta L - D\sin\beta L)\} + \{(k_s - W_0 \cdot \omega^2/g) \times (C\sin\beta L + D\cos\beta L)\} = 0 \quad (12)$$

Rearranging the terms in Eq. (12), we get

$$C\{AE \cdot \beta\cos\beta L + (k_s - W_0 \cdot \omega^2/g)\sin\beta L\} = D\{AE \cdot \beta\sin\beta L - (k_s - W_0 \cdot \omega^2/g)\cos\beta L\} \quad (13)$$

Substituting the value of C in (13)

$$\tan\beta L = \frac{AE\beta(k_p + k_s - W_0 \times \omega^2/g)}{(\beta AE)^2 + k_p(k_s - W_0 \times \omega^2/g)} \quad (14)$$

Dividing (13) through out by AE and multiplying by L , we get

$$\tan\beta L = \frac{\beta(k_p L/AE + k_s L/AE - W_0 L\omega^2/gAE)}{(\beta L)^2 + k_p L/AE(k_s L/AE - W_0 L\omega^2/gAE)} \quad (15)$$

Let

$$T_p = k_p L/AE \quad (16)$$

where T_p is physically the ratio of the axial pipe stiffness to the effective bellow stiffness

$$T_s = k_s L / AE \quad (17)$$

$$a = \sqrt{(Eg)/v} \quad (18)$$

$$1/\alpha = W_0/G \quad (19)$$

where α is the ratio of bellow mass to the end mass

$$\beta L = \omega_i(L/a) \quad (20)$$

Now, substituting for the value of ‘ a ’ in Eq. (20), we get

$$\beta L = \omega_i \sqrt{G/(g \cdot k_n)} \quad (21)$$

where $G = LA v$, A is the effective area of cross-section of bellow in mm^2 and k_n is the theoretical stiffness of bellows obtained using the equation given in EJMA.

Assuming the exact equation as

$$u(x, T) = \{C \sin \omega_i x / a + D \cos \omega_i x / a\} e^{i\omega T} \quad (22)$$

Applying the boundary conditions as mentioned above and repeating the procedure, the final frequency equation is obtained as follows

$$\tan \beta_i = \frac{\beta_i \{ \alpha (1 + T_s / T_p - \beta_i^2 / T_p) \}}{\alpha (1 / T_p - T_s) + \beta_i^2} \quad (23)$$

4. Different end conditions

4.1. Case 1

One end of the bellows is fixed and the other end is free ($k_s = 0$, $T_s = 0$, $W_0 = 0$ and $T_p = \infty$): substituting the above conditions in Eq. (23), the resulting frequency equation is written as Eq. (27)

$$\beta_i \tan \beta_i = \alpha \quad (24)$$

$$\tan \beta_i = \frac{\beta_i \{ (\alpha (T_s + T_p) - \beta_i^2) \}}{\{ \alpha (1 - T_s T_p) + T_p \beta_i^2 \}} \quad (25)$$

We know

$$f_i = \omega_i / 2\pi \quad (26)$$

therefore

$$f_i = 49.5(i - 0.5) \times \sqrt{k_n / G} \quad (27)$$

Table 1

T_p	$\beta_i, N = 1$	$\beta_i, N = 2$	$\beta_i, N = 3$
0.01	1.502	3.17331	6.3465
0.1	1.5023	3.4761	6.8862
1.0	1.5022	4.4934	7.7725
10.0	1.5044	4.6910	7.8412
10^2	1.5644	4.71026	7.8527
10^3	1.5701	4.71217	7.853
10^4	1.5707	4.71236	7.8539
10^5	1.5707	4.71238	7.8539
10^6	1.5707	4.71238	7.8539
10^7	1.5707	4.71238	7.8539
10^8	1.5707	4.71238	7.85398
10^9	1.5707	4.7123	7.8539

A computer code in FORTRAN is developed to find the solution of the frequency equation ((23) and (25)) and compute the value of β_i . The values of β_i for the modes $N = 1, 2$ and 3 and increasing order of T_p are given in Table 1.

By considering one end of the bellows to be fixed and the other end free, the value of β_i for $T_p \Rightarrow \alpha$ is 1.5707 for $N = 1$, 4.7123 for $N = 2$ and 7.8539 for $N = 3$, respectively. The weight of the bellow $W_0 = 0$, $\alpha = 0$ and k_s and $T_s = 0$. It is seen that as the value of elastic restraint T_p of the pipe increases from 0.01 to 10^8 , the frequencies tend to increase for all the mode numbers. As the stiffness value $T \rightarrow \infty$, the frequency value increases by about 54% for $N = 1$, $P = 0$ MPa and by 69% for $N = 1$ and $P = 166$ MPa. However, it is observed that there is no change in frequency and it becomes constant from $T = 10^4$ onwards. The same is reflected in Figs. 3 and 4, respectively.

4.2. Case II

If both ends of the bellows are fixed ($W_0 = 0$ and $k_s = \infty$), the frequency equation is written as

$$\tan \beta_i = \frac{\beta_i \{ ((1/T_s + 1/T_p) - \beta_i^2) / \alpha (T_s \times T_p) \}}{\{ [1/(T_s \times T_p) - 1] + (\beta_i^2/T_s \times \alpha) \}} \quad (28)$$

$$f_i = 49.5i \times \sqrt{k_n/G} \quad (29)$$

where ' i ' is the order number of frequency, $i = 1, 2, 3$, etc. The values of β_i for the mode numbers $N = 1, 2$ and 3 and different values of T_p are given in Table 2.

The value of β_i for clamped-clamped condition for $T_p \Rightarrow \infty$ is 3.1415 for $N = 1$, 6.2831 for $N = 2$ and 9.4247 for $N = 3$, respectively. The weight $W_0 = 0$, $\alpha = \infty$ and k_s and $T_s = \infty$.

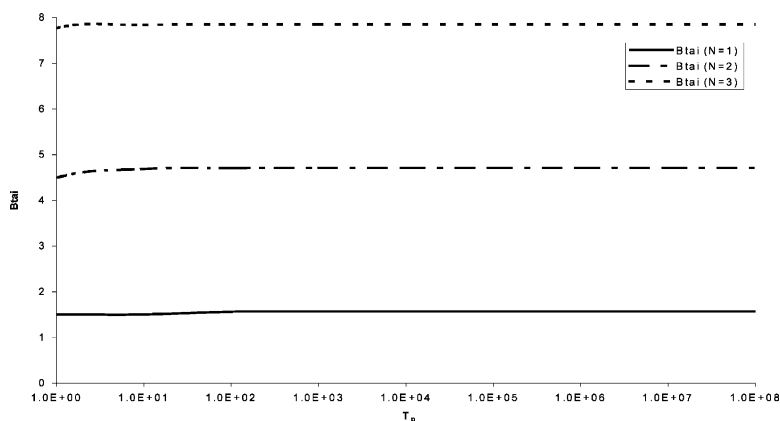


Fig. 3. Axial vibrations of single bellow expansion joint (one end fixed and other free) (β_i for $N = 1, 2$ and 3 , $W_0 = 0$, $T_s = 0$ and $\alpha = \infty$).

4.3. Case III

This represents a practical situation where one end of the bellows is welded to a pipe and the other end is attached to a lumped weight, W_0 ($W_0 \neq 0$ and $k_s = 0$). It is commonly noticed that in a pipeline having a bellow, also has a valve for controlling the flow or an instrument for measuring the flow. Therefore, the values of β_i for this type of end condition are different from the other two cases and are obtained by varying T_p and keeping $1/\alpha$ (0.1, 1, 100 and 1000) a constant value. It depends on the value of α . The same is computed and given in Tables 3–6, respectively. We know that $\alpha = G/W_0$ or $1/\alpha = W_0/G$ where $G = G_1 + G_2$, where G_1 is the weight of the bellow material and G_2 is the weight of liquid.

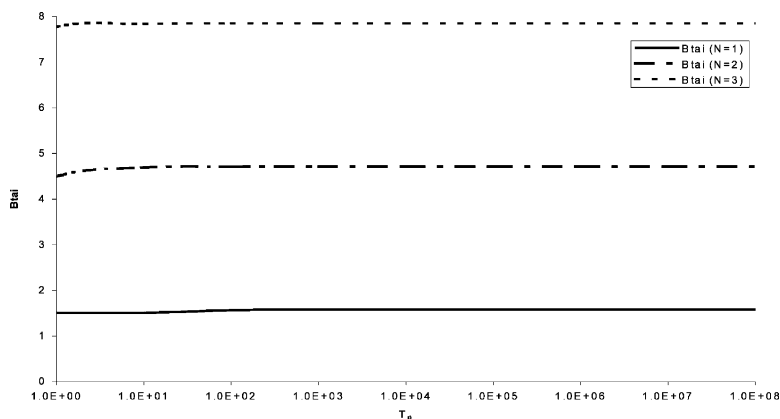


Fig. 4. Axial vibrations of single bellow expansion joint (both ends fixed) (β_i for $N = 1, 2$ and 3 , $W_0 = 0$, T_s and $\alpha = \infty$).

Table 2

T_p	$\beta_i, N = 1$	$\beta_i, N = 2$	$\beta_i, N = 3$
0.01	1.57713	4.71451	7.85525
0.1	1.63199	4.733518	7.86669
1.0	2.02875	4.91318	7.97866
10.0	2.86277	5.76055	8.70831
10^2	3.11049	6.22105	9.33172
10^3	3.13845	6.27690	9.41536
10^4	3.14127	6.28257	9.42383
10^5	3.14156	6.28312	9.42468
10^6	3.14158	6.28317	9.42476
10^7	3.14159	6.28318	9.42477
10^8	3.14159	6.28318	9.42477
10^9	3.14159	6.28318	9.42477

Table 3

 $1/\alpha = 0.1$ and $T_s = \infty$

T_p	$\beta_i, N = 1$	$\beta_i, N = 2$	$\beta_i, N = 3$
0.01	1.435	4.3076	7.2289
0.1	1.4899	4.3239	7.2366
1.0	1.8964	4.4899	7.3172
10.0	2.8417	5.5990	8.228
10^2	3.1101	6.2185	9.323
10^3	3.13845	6.2768	9.4152
10^4	3.14127	6.2825	9.4238
10^5	3.14156	6.28312	9.4246
10^6	3.14158	6.28317	9.4247
10^7	3.14159	6.28318	9.4247
10^8	3.14159	6.28318	9.4247

Table 4

 $1/\alpha = 1.0$ and $T_s = \infty$

T_p	$\beta_i, N = 1$	$\beta_i, N = 2$	$\beta_i, N = 3$
0.01	0.8645	3.42583	6.43733
0.1	0.9014	3.42775	6.43765
1.0	1.2077	3.44823	6.44095
10.0	2.5293	3.82916	6.48289
10^2	3.1072	6.18340	8.98748
10^3	3.1384	6.27665	9.42382
10^4	3.14127	6.28312	9.42468
10^5	3.14156	6.28317	9.42468
10^6	3.14158	6.28317	9.42476
10^7	3.14159	6.28318	9.42477
10^8	3.14159	6.28318	9.42477

Table 5
 $1/\alpha = 100$ and $T_s = \infty$

T_p	$\beta_i, N = 1$	$\beta_i, N = 2$	$\beta_i, N = 3$
0.01	0.1003	3.14477	6.28477
0.1	0.1047	3.14477	6.28477
1.0	0.1411	3.14477	6.28477
10.0	0.3311	3.14480	6.28478
10^2	1.0031	3.1455	6.28481
10^3	3.0809	3.2236	6.285316
10^4	3.1412	3.14124	6.283119
10^5	3.1415	3.14156	6.283119
10^6	3.14158	3.14158	6.283178
10^7	3.14159	3.14159	6.28318
10^8	3.14159	3.14159	6.28318

Table 6
 $1/\alpha = 1000$ and $T_s = \infty$

T_p	$\beta_i, N = 1$	$\beta_i, N = 2$	$\beta_i, N = 3$
0.01	0.0317	3.1419	6.28334
0.1	0.0331	3.14190	6.28334
1.0	0.0447	3.14190	6.28334
10.0	0.1048	3.14190	6.28334
10^2	0.3177	3.14191	6.28334
10^3	1.0003	3.14191	6.28339
10^4	1.1123	3.14151	6.28308
10^5	1.3112	3.14155	6.28317
10^6	1.4234	3.14158	6.28318
10^8	1.5671	3.14159	6.28318

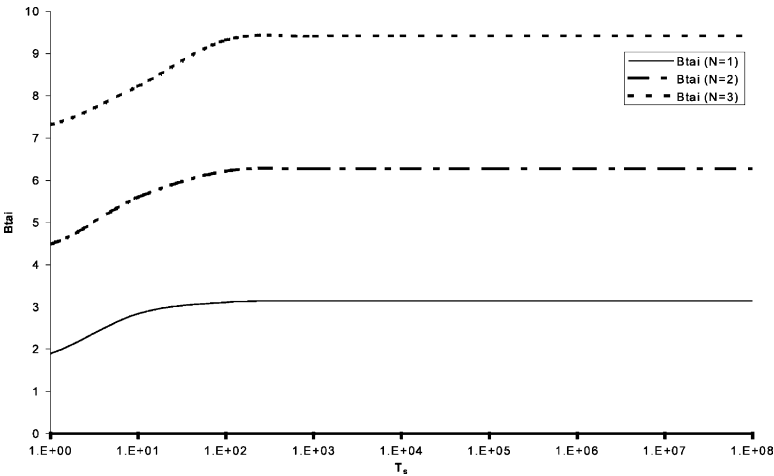


Fig. 5. Axial vibrations of single bellows expansion joint (one end of the bellows fixed and other end attached to weight) (β_i for $N = 1, 2$ and 3 and $\alpha = 10$).

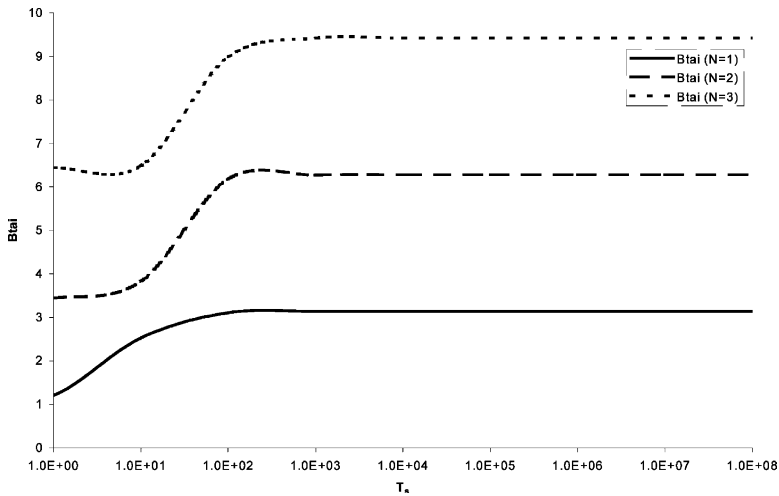


Fig. 6. Axial vibrations of single bellow expansion joint (one end fixed and other end attached to weight) (β_i for $N = 1, 2$ and 3 and $\alpha = 1.0$).

Tables 3 and 4 present β_i values for $1/\alpha$ of 0.1 and 1.0, respectively. It is seen from Figs. 5 and 6 that the values of β_i in both the cases tend to be constant from $T_p = 10^5$ onwards. However, for lower values of $1/\alpha$ of 0.01 and 0.001, which means the bellow weight is greater than the weight attached ($G > W_0$), the values of β_i are almost constant for $N = 1$ and 2 and vary for $N = 1$ only. The same is shown in Figs. 7 and 8, respectively.

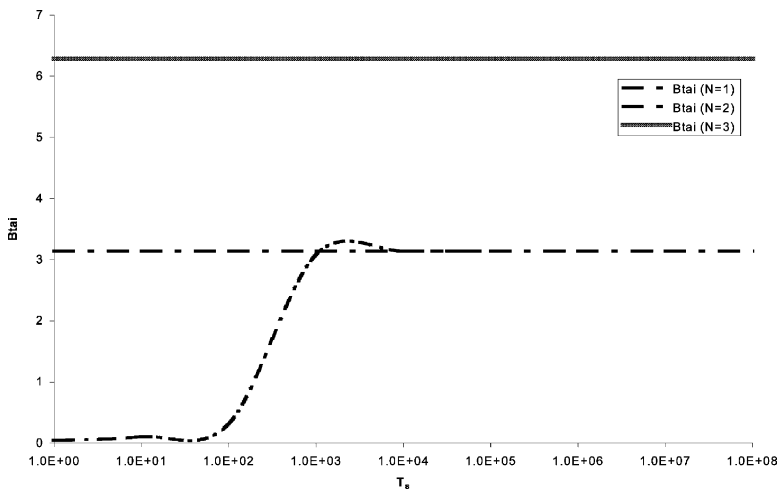


Fig. 7. Axial vibrations of single bellow expansion joint (one end fixed and other attached to a weight) (β_i for $N = 1, 2$ and 3 and $\alpha = 0.01$).

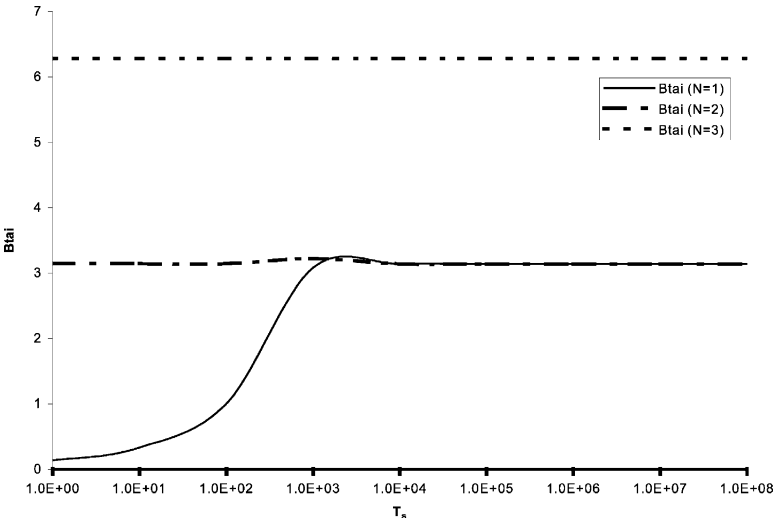


Fig. 8. Axial vibrations of single bellow expansion joint (one end fixed and other end attached to a weight) (β_i for $N = 1, 2$ and 3 and $\alpha = 0.001$).

5. Theoretical verification

Five numbers of U-shaped bellow specimens are used that have the same geometrical dimensions as considered by Li et al. [4] and are given in Table 7. The two specimens have austenitic stainless steel as the material of construction. D_b represents the inside diameter of cylindrical tangent, w is the convolution depth, q is the convolution pitch, n is the number of plies and t is the nominal thickness of the bellow material before forming.

Table 7
Geometrical dimensions of bellows (in mm)

SP	D_b	w	q	n	t	\check{N}
1	322.5	24.5	22.4	1	0.49	9
6	192	26	22	1	0.5	9

SP, specimen number.

Table 8

SP	EXP	Li	Mod	%Error
Air				
1	37.5	40.4	40.5	0.27
6	40.0	38.6	39.8	0.45
Water				
1	27.5	27.5	25.5	7.0

Table 8 presents the frequencies obtained by the present modified for single bellows expansion joint. The frequencies are in close agreement to the experimental and theoretical results of Li for air and water, respectively.

6. Conclusions

A theoretical model has been developed for determining the axial frequencies. The effect of considering the pipe as elastic and partially restrained and the influence of elastic restraints on axial frequencies has not been previously dealt. It is found that the axial frequencies obtained from the present analysis are in close agreement to the ones determined by Li both by theoretical formulations and experiments. The percentage error is 0.27% and 0.45% for specimen numbers 1 and 6 in air and 7% in water.

References

- [1] Gerlach CR. Flow induced vibrations of metal bellows. *ASME J Eng Ind* 1969;91:1196–202.
- [2] EJMA. The Standards of the Expansion Joint Manufacturers Association, Inc. 6th ed. 1995.
- [3] Jakubauskas VF. Added fluid mass for bellows expansion joints in axial vibrations. *ASME J Pressure Vessel Technol* 1999;121:216–9.
- [4] Li T-X, et al. Natural frequencies of U-shaped bellows. *Int J Pressure Vessel Piping* 1990;42:61–74.

See discussions, stats, and author profiles for this publication at: <https://www.researchgate.net/publication/228573555>

Free vibration of thin walled beams

Article in *Periodica Polytechnica, Mechanical Engineering* · January 2004

CITATIONS

8

READS

589

1 author:



Gabor Vörös

Budapest University of Technology and Economics

21 PUBLICATIONS 208 CITATIONS

SEE PROFILE

FREE VIBRATION OF THIN WALLED BEAMS

Gábor M. Vörös

Department of Applied Mechanics, Budapest University of Technology and Economics
H-1512. Budapest, Hungary. e-mail: voros@mm.bme.hu

Abstract

Consistent and simple lumped mass matrices are formulated for the dynamic analysis of beams with arbitrary cross section. The development is based on a general beam theory which includes the effect of flexural-torsion coupling, the constrained torsion warping and the shear centre location. Numerical test are presented to demonstrate the importance of torsion warping constraints and the acceptable accuracy of the lumped mass matrix formulation.

Keywords: torsion, thin walled beam, mass matrix, free vibration

1. Introduction

During the torsion of bars an out of section plane, axial warping displacement takes place which is assumed to depend on the change of the angle of twist. The torsional warping has no effect on stresses if the measure of warping is the same in each section including the ends. This implies that the torsional rotation is a linear function along the beam axis. If the torsional rotation is far from the linear distribution, as it is in torsional vibration modes, or the beam ends are constrained, the torsional warping may have an important effect on the static or dynamic response of the beam structure. In addition to the torsion warping effect, the coupling between the bending and the torsional free vibration modes occurs when the centroid (mass centre) and the shear centre (centre of twist) of the beam section are non-coincident.

The thin-walled beam theory was established by Vlasov [1] and Timoshenko and Gere [2]. Among others coupled bending-torsional vibrations of beams has been investigated in recent years by Friberg [3] and Banerje [4]. Trahair and Pi [5] summarized a series of investigations on this field. A consistent finite element formulation for the free vibration was presented by Kim [6]. In this paper an exactly integrated consistent and a lumped mass matrix are presented for the 7 DOF finite element beam model. The formulation includes the flexure-torsion coupling and the constrained warping effects.

The equation for free vibration of an elastic system undergoing small deformations and displacements can be expressed in the form

$$\underline{\underline{\mathbf{K}}} \underline{\underline{\mathbf{U}}} + \underline{\underline{\mathbf{M}}} \ddot{\underline{\underline{\mathbf{U}}}} = \underline{\underline{\mathbf{0}}},$$

where $\underline{\underline{\mathbf{K}}}$ and $\underline{\underline{\mathbf{M}}}$ are the assembled elastic stiffness and mass matrices, respectively, and $\underline{\underline{\mathbf{U}}}(t)$ is the set of nodal displacements. The dot represents the time derivative.

2. Kinematics of beam

Figure 1. shows the basic systems and notations. The local x axis of the right hand orthogonal system is parallel to the beam straight axis and passes trough the N_1 , N_2 element nodes of the finite element mesh. The axes y and z are parallel to the principal axes, signed as r and s . The position of the centroid C and shear centre T relative to the node N in the plane of the section are given by the co-ordinates y_{NC} , y_{CT} , and z_{NC} , z_{CT} .

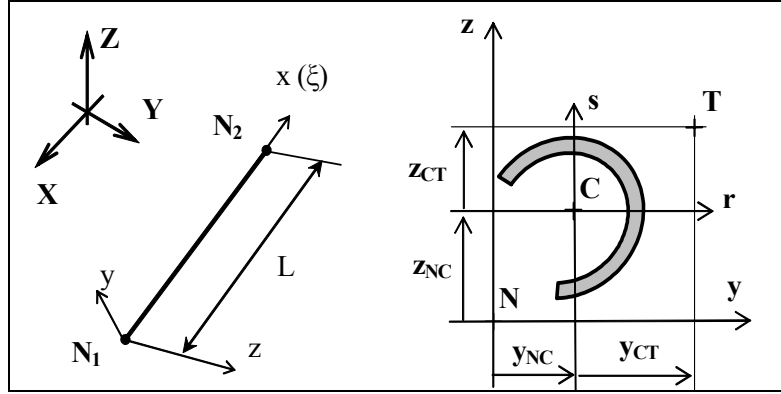


Fig 1.

The linear kinematics of an initially straight, prismatic beam element can be described on the assumption, that the cross section undergoes a rigid body like motion in the plane normal to the centroidal axis. Accordingly, the in plane displacements of a point can be expressed by three parameters, the angle of twist θ_x^T about the longitudinal axis passing trough the T shear centre and the two u_y^T and u_z^T displacement components of point T . The axial displacement is the sum of the u_x^C axial displacement of the C centroid, the θ_y^C , θ_z^C rotations of planar section about the axes r and s , and the out of plane torsion warping displacement. Accordingly, the displacement vector is

$$\mathbf{u}(x, r, s, t) = \begin{bmatrix} u_x \\ u_y \\ u_z \end{bmatrix} = \begin{bmatrix} u_x^C + \Theta_y^C s - \Theta_z^C r - \vartheta \omega^T \\ u_y^T - \Theta_x^T (s - z_{CT}) \\ u_z^T + \Theta_x^T (r - y_{CT}) \end{bmatrix}. \quad (1)$$

where $\vartheta(x, t)$ is the warping parameter and $\omega^T(r, s)$ is the warping function, or – for thin walled sections – the sector area co-ordinate.

The geometric properties of the cross section are

$$\begin{aligned} I_r &= \int_A s^2 dA, \quad I_s = \int_A r^2 dA, \quad I_\omega = \int_A \omega^{T^2} dA, \\ y_{CT} &= -\frac{1}{I_r} \int_A s \omega^T dA, \quad z_{CT} = \frac{1}{I_s} \int_A r \omega^T dA, \quad J = I_r + I_s + \int_A \left(s \frac{\partial \omega^T}{\partial r} - r \frac{\partial \omega^T}{\partial s} \right) dA, \\ I_P &= \int_A \left[(r - y_{CT})^2 + (s - z_{CT})^2 \right] dA = I_s + I_r + A(y_{CT}^2 + z_{CT}^2) \end{aligned} \quad (2)$$

and the principal r , s co-ordinates on Fig. 1 were chosen such that the following integrals are zero:

$$\int_A \mathbf{r} dA = 0, \quad \int_A \mathbf{s} dA = 0, \quad \int_A \mathbf{r} \mathbf{s} dA = 0, \quad \int_A \boldsymbol{\omega}^T dA = 0, \quad \int_A \mathbf{r} \boldsymbol{\omega}^T dA = 0, \quad \int_A \mathbf{s} \boldsymbol{\omega}^T dA = 0.$$

By using the displacement (1) and the *Vlasov* and *Bernoulli* [7] constraints as

$$\Theta_y^C(\mathbf{x}, t) = -\frac{d\mathbf{u}_z^T}{dx} = -\mathbf{u}_z'^T, \quad \Theta_z^C(\mathbf{x}, t) = \frac{d\mathbf{u}_y^T}{dx} = \mathbf{u}_y'^T, \quad \mathcal{G}(\mathbf{x}, t) = \frac{d\Theta_x^T}{dx} = \Theta_x'^T, \quad (3)$$

the U strain and K kinetic energy stored in a linear elastic beam element of length L are:

$$U = \frac{1}{2} \int_0^L \left[E A \mathbf{u}_x'^{C2} + E I_r \mathbf{u}_z''^{T2} + E I_s \mathbf{u}_y''^{T2} + G J \Theta_x'^{T2} + E I_\omega \Theta_x''^{T2} \right] dx, \quad (4)$$

$$K = \frac{1}{2} \int_0^L \left[\dot{\mathbf{u}}_x^{C2} + \dot{\mathbf{u}}_y^{T2} + \dot{\mathbf{u}}_z^{T2} + \frac{I_r}{A} \dot{\mathbf{u}}_z'^{T2} + \frac{I_s}{A} \dot{\mathbf{u}}_y'^{T2} + \frac{I_\omega}{A} \dot{\Theta}_x'^{T2} + \frac{I_p}{A} \dot{\Theta}_x'^{T2} + 2 \left(z_{CT} \dot{\mathbf{u}}_y^T \dot{\Theta}_x^T - y_{CT} \dot{\mathbf{u}}_z^T \dot{\Theta}_x^T \right) \right] \rho A dx$$

where E , G are the properties of isotropic elastic material and ρ is the mass density. The assumptions (3) imply that the shear deformations are neglected. A more detailed description of deformation including the shear effect can be found in [6] or [9].

3. Element Matrices

The derivation of element matrices is based on the assumed displacement field. A linear interpolation is adopted for the axial displacement and a cubic for the lateral deflections and the twist:

$$\begin{aligned} \mathbf{u}_x^C &= \mathbf{u}_{x1}^C (1 - \xi) + \mathbf{u}_{x2}^C \xi, \\ \mathbf{u}_y^T(\xi) &= \mathbf{u}_{y1}^T N_1(\xi) + \Theta_{z1}^C L N_2(\xi) + \mathbf{u}_{y2}^T N_3(\xi) + \Theta_{z2}^C L N_4(\xi), \\ \mathbf{u}_z^T(\xi) &= \mathbf{u}_{z1}^T N_1(\xi) - \Theta_{y1}^C L N_2(\xi) + \mathbf{u}_{z2}^T N_3(\xi) - \Theta_{y2}^C L N_4(\xi), \\ \Theta_x^T(\xi) &= \Theta_{x1}^T N_1(\xi) + \mathfrak{g}_1 L N_2(\xi) + \Theta_{x2}^T N_3(\xi) + \mathfrak{g}_2 L N_4(\xi), \end{aligned} \quad (5)$$

in which:

$$N_1 = 1 - 3\xi^2 + 2\xi^3, \quad N_2 = \xi - 2\xi^2 + \xi^3, \quad N_3 = 3\xi^2 - 2\xi^3, \quad N_4 = \xi^3 - \xi^2, \quad \xi = \frac{x}{L}.$$

Define the order of the element $2 \times 7 = 14$ local displacements at the two ends as

$$\underline{\mathbf{U}}^C(t) = \left[\mathbf{u}_{x1}^C, \mathbf{u}_{y1}^T, \mathbf{u}_{z1}^T, \Theta_{x1}^T, \Theta_{y1}^C, \Theta_{z1}^C, \mathfrak{g}_1, \mathbf{u}_{x2}^C, \mathbf{u}_{y2}^T, \mathbf{u}_{z2}^T, \Theta_{x2}^T, \Theta_{y2}^C, \Theta_{z2}^C, \mathfrak{g}_2 \right]^T. \quad (6)$$

Substituting interpolation (5) into (4) the expression for the potential and kinetic energy may be defined in terms of (6) local variables as

$$U = \frac{1}{2} \underline{\mathbf{U}}^{CT} \underline{\mathbf{k}}^C \underline{\mathbf{U}}^C, \quad K = \frac{1}{2} \dot{\underline{\mathbf{U}}}^{CT} \underline{\mathbf{m}}^C \dot{\underline{\mathbf{U}}}^C.$$

The explicit – exactly integrated - stiffness and consistent mass matrices, \mathbf{k}^C and \mathbf{m}^C are given in *Appendices A* and *B*, respectively. The stiffness matrix – apart from sign conventions – is identical to the matrix published in [10], page 89.

The lumped mass matrix can be derived from the kinetic energy expression for an element which undergoes a rigid body like motion and rotation. The element lumped mass matrix is given in *Appendix C*. Here the lumped mass, due to the shear centre location, is not a diagonal matrix. Nevertheless, it is computationally much more economical than the corresponding consistent mass detailed in *Appendix B*.

4. Transformation from local to nodal variables

The transformation which relates the (6) local variables to nodal displacements are:

$$\begin{bmatrix} u_x^C \\ u_y^T \\ u_z^T \\ \Theta_x^T \\ \Theta_y^C \\ \Theta_z^C \\ \mathcal{G} \end{bmatrix} = \begin{bmatrix} 1 & 0 & 0 & 0 & z_{NC} & -y_{NC} & 0 \\ 0 & 1 & 0 & -(z_{NC} + z_{CT}) & 0 & 0 & 0 \\ 0 & 0 & 0 & (y_{NC} + y_{CT}) & 0 & 0 & 0 \\ 0 & 0 & 0 & 1 & 0 & 0 & 0 \\ 0 & 0 & 0 & 0 & 1 & 0 & 0 \\ 0 & 0 & 0 & 0 & 0 & 0 & 0 \\ 0 & 0 & 0 & 0 & 0 & 0 & 1 \end{bmatrix} \begin{bmatrix} u_x^N \\ u_y^N \\ u_z^N \\ \Theta_x^N \\ \Theta_y^N \\ \Theta_z^N \\ \mathcal{G} \end{bmatrix} \quad (7)$$

Using the above transformation at each node the stiffness and mass matrix can be transformed to the local x, y, z system in the corresponding mesh node. Finally, the element stiffness and mass matrices evaluated in the local x, y, z system, are transformed to the global X, Y, Z structural system in a usual manner. A detailed description of the (7) transformation process can be found in [8].

5. Numerical examples

In order to examine the validity and accuracy of the lumped mass formulation the vibration analysis of a simply supported and a cantilever beam are conducted. Numerical solutions of the present study are compared with the analytical and COSMOS/M shell element results.

5.1 Simply supported beam

Material and sectional properties used in this example are listed on Fig. 2. Closed form solution for the torsional vibration with free end warping is known as [1]:

$$\alpha_n = \frac{n}{2L} \sqrt{\frac{GJ}{\rho(I_r + I_s)}} \sqrt{\frac{1 + n^2 \frac{\pi^2 EI_\omega}{L^2 GJ}}{1 + n^2 \frac{\pi^2 I_\omega}{L^2 (I_r + I_s)}}}, \quad n=1, 2, \dots \quad (8)$$

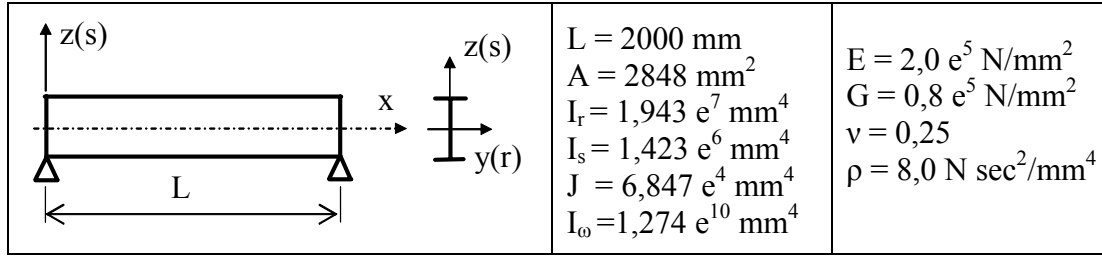


Fig 2. Simply supported beam with doubly symmetric section.

The beam was analysed with different m number of elements. At the end nodes ($x = 0, L$) in addition to the normal hinged support conditions the 7-th warping parameter was left free. Tables 1a and 1b show that the torsional frequencies – even for a coarse mesh and lumped mass – are in good agreement with the (8) analytical solution. As the convergence study shows that $m = 20$ element number is sufficient to get a reasonable accuracy and number of modes, this mesh is used in the subsequent problems.

n	m = 2	m = 4	m = 8	m = 16	m = 20	analytical
1	66,485	66,349	66,340	66,339	66,339	66,339
2		214,29	213,63	213,59	213,59	213,59
3		462,00	454,91	454,41	454,39	454,37
4			790,89	788,13	788,01	787,93
5			1222,5	1212,4	1212,0	1211,6

Table 1a. Convergence of torsional frequencies (Hz), with *consistent* mass matrix.
7 DOF results with free end warping

	m = 2	m = 4	m = 8	m = 16	m = 20	analytical
1	65,601	66,309	66,338	66,339	66,339	66,339
2		211,83	213,51	213,58	213,59	213,59
3		425,59	453,54	454,33	454,36	454,37
4			782,73	787,71	787,84	787,93
5			1187,8	1210,8	1211,3	1211,6

Table 1b. Convergence of torsional frequencies (Hz), with *lumped* mass matrix.
7 DOF results with free end warping

5.2 Cantilever

To illustrate the importance of internal and external warping constraint and the performance of the lumped mass matrix, the results of two test problems with the same material properties are detailed herein: a straight cantilever with (1) a double symmetric I and (2) with U section. In each case the beam structure was analysed with a 20 element mesh. A comparison was made with the classical – neglected warping effect - beam frequency solutions (columns A in tables 2.,3a.):

$$\text{bending: } \alpha_n = \frac{\Gamma_n}{2\pi L^2} \sqrt{\frac{IE}{A\rho}}, \quad \Gamma_1 = 1,875^2, \quad \Gamma_2 = 4,694^2, \quad \Gamma_3 = 7,855^2, \quad (9a)$$

$$\text{torsion: } \alpha_n = \frac{2n-1}{4L} \sqrt{\frac{GJ}{\rho(I_r + I_s)}}, \quad n = 1, 2, \dots \quad (9b)$$

and the results of 6 DOF beam element model (columns B in tables 2.,3a.). Moreover, the frequencies of the beam like torsional modes obtained by COSMOS/M thick shell finite element model are listed in “SHELL” columns in tables 2 and 3b. In this case the cantilevers were modelled by using 1280 (U section) and 1600 (I section) four-noded thick shell elements.

(1) *I section*

	IPE 200 $L = 2000 \text{ mm}$ $A = 2848 \text{ mm}^2$ $I_r = 1,943 \text{ e}^7 \text{ mm}^4$ $I_s = 1,423 \text{ e}^6 \text{ mm}^4$ $J = 6,847 \text{ e}^4 \text{ mm}^4$ $I_\omega = 1,274 \text{ e}^{10} \text{ mm}^4$	$E = 2,0 \text{ e}^5 \text{ N/mm}^2$ $G = 0,8 \text{ e}^5 \text{ N/mm}^2$ $\nu = 0,25$ $\rho = 8,0 \text{ e}^{-9} \text{ N sec}^2/\text{mm}^4$
--	--	---

Fig 3. Cantilever with doubly symmetric section.

	A	B(cons)	<i>B(lump)</i>	C(cons)	<i>C(lump)</i>	D(cons)	<i>D(lump)</i>	SHELL
1	22,650	22,650	22,650	23,889	23,881	33,516	33,494	30,29
2	67,951	67,951	67,938	105,91	105,62	135,03	134,55	127,4
3	113,25	113,25	113,17	272,59	271,05	326,85	324,78	317,3
4	158,55	158,55	158,26	533,82	532,74	612,39	606,89	
5	203,85	203,85	203,05	887,57	878,31	989,69	978,28	
6	249,15	249,16	247,31	1330,6	1312,7	1455,5	1435,0	

Table 2. Test problem 1, torsional frequencies (Hz), 6 DOF results (B) and 7 DOF results with free end warping (C) and constrained end warping (D).

The comparison of results in columns A, B with others in C, D shows the significant effect of warping inertia and internal (C) and external (D) warping constrains on torsional vibration.

(2) *U section*

	U 200 $L = 2000 \text{ mm}$ $A = 3157 \text{ mm}^2$ $I_r = 1,972 \text{ e}^7 \text{ mm}^4$ $I_s = 1,955 \text{ e}^6 \text{ mm}^4$ $J = 1,025 \text{ e}^5 \text{ mm}^4$ $I_\omega = 1,227 \text{ e}^{10} \text{ mm}^4$ $y_{CT} = -48,7 \text{ mm}$
--	---

Fig 4. Cantilever with a channel section.

n	mode	A	B (cons)	<i>B (lump)</i>
1	by1	17,379	17,375	<i>17,355</i>
2	t1	26,635	26,635	<i>26,635</i>
3	bz1	54,720	54,533	<i>54,471</i>
4	t2	79,906	79,906	<i>79,891</i>
5	by2	108,92	108,66	<i>108,23</i>
6	t3	133,18	133,18	<i>133,08</i>
7	t4	186,45	186,45	<i>186,11</i>
8	t5	239,72	239,72	<i>238,78</i>
9	t6	292,99	292,99	<i>290,82</i>
10	by3	305,02	303,02	<i>301,25</i>
19	a1	625,00	625,16	<i>624,84</i>

Table 3a. Test problem 2, frequencies (Hz), 6 DOF results (B).
by_i, bz_i bending, t_i torsion, a_i longitudinal modes.

	mode	C(cons)	<i>C(lump)</i>	mode	D(cons)	<i>D(lump)</i>	mode	SHELL
1	by1	17,375	<i>17,355</i>	by1	17,375	<i>17,355</i>	by1	17,31
2	bz+t1	23,314	<i>23,306</i>	bz+t1	30,198	<i>30,182</i>	bz+t1	29,57
3	bz+t2	63,876	<i>63,791</i>	bz+t2	66,630	<i>66,535</i>	bz+t2	65,34
4	bz+t3	98,621	<i>98,324</i>	by2	108,66	<i>108,23</i>	by2	105,83
5	by2	108,66	<i>108,23</i>	bz+t3	119,90	<i>119,45</i>	bz+t3	116,14
6	bz+t4	234,78	<i>233,44</i>	bz+t4	279,27	<i>277,40</i>	bz+t4	269,83
7	by3	303,20	<i>301,25</i>	by3	303,20	<i>301,25</i>		
8	bz+t5	391,58	<i>390,43</i>	bz+t5	392,24	<i>391,44</i>		
9	bz+t6	453,22	<i>494,43</i>	bz+t6	517,44	<i>512,14</i>		
10	by4	591,23	<i>585,93</i>	by4	591,23	<i>585,93</i>		
11	a1	625,16	<i>624,84</i>	a1	625,16	<i>624,84</i>		

Table 3b. Test problem 2, frequencies (Hz), 7 DOF results with free end warping (C) and constrained end warping (D). by_i, bz_i bending, t_i torsion, a_i longitudinal modes.

The modes – except the by_i bending modes – in consequence of the eccentric position of the shear centre exhibit strong flexural bending coupling. This coupling phenomenon cannot be predicted by the classical 6 DOF finite element model.

All the numerical results prove the good accuracy of the simple lumped mass matrix.

Acknowledgements: The present research was supported by Széchenyi-NKFP (Hungarian National Research and Development Found) Grant no: 2002/16.

References

- [1] VLASOV, V.Z., Thin walled elastic beams, 2nd ed. Israel Program for Scientific Transactions, Jerusalem, 1961.
- [2] TIMOSHENKO, S.P.-GERE, J.M., Theory of elastic stability, 2nd ed. McGraw Hill, New-York, 1961.
- [3] FRIBERG, P.O., Coupled vibration of beams – an exact dynamic element stiffness matrix. *Int.J.Numerical Methods in Engng.* **19** (1993) pp.479-493.
- [4] BANERJEE, J.R.-GUO, S.-HOWSON, W.P., Exact dynamic stiffness matrix of a bending-torsion coupled beam including warping, *Computers and Structures*. **59** (1996) pp.613-621.
- [5] TRAHAIR, N.S.-PI, Y-L., Torsion, bending and buckling of steel beams, *Engineering Structures*. **19** (1997) pp.372-377.
- [6] KIM, S.B.-KIM, M.Y., Improved formulation for spatial stability and free vibration of thin-walled tapered beams and space frames, *Engineering Structures*. **22** (2000) pp.446-458.
- [7] WEMPNER, G., Mechanics of solids with application to thin bodies, Sijthoff Noordhoff, 1981.
- [8] KISS, F., A new aspects for the use of thin walled beams as shell stiffeners as spacecraft structures, *Proc.of conf. on Spacecraft Structures and Mechanical Testing*, Noordwijk, The Netherlands, Oct. 19-21.1987. pp.455-459.
- [9] VÖRÖS, G.M., A special purpose element for shell-beam systems, *Computers and Structures*. **29** (1988) pp.301-308.
- [10] KITIPORNCHAI, S.- CHAN, S.L. Stability and non-linear finite element analysis of thin walled structures, in *Finite element applications to thin-walled structures*, ed. Bull, J.W. Elsevier. 1989.
- [11] KOUHIA, R.- TUOMALA, M., Static and dynamic analysis of space frames using simple Timoshenko type elements, *Int.J.Numerical Methods in Engng.* **36** (1993) pp.1189-1221.

Appendix A: The 14x14 linear stiffness matrix $\underline{\mathbf{k}}^C$ is symmetric. Only the upper triangle is given here.

$$\underline{\mathbf{k}}^C = \left[\begin{array}{cccccc|cccccc} a & 0 & 0 & 0 & 0 & 0 & -a & 0 & 0 & 0 & 0 & 0 \\ & b & 0 & 0 & 0 & c & 0 & 0 & -b & 0 & 0 & c \\ & & d & 0 & -e & 0 & 0 & 0 & 0 & -d & 0 & -e \\ & & & f & 0 & 0 & g & 0 & 0 & 0 & -f & 0 \\ & & & & 2h & 0 & 0 & 0 & 0 & e & 0 & h \\ & & & & & 2i & 0 & 0 & -c & 0 & 0 & i \\ & & & & & & j & 0 & 0 & 0 & -g & 0 \\ \hline & & & & & & & a & 0 & 0 & 0 & 0 \\ & & & & & & & & b & 0 & 0 & -c \\ & & & & & & & & & d & 0 & e \\ & & & & & & & & & & f & 0 \\ & & & & & & & & & & & 2h \\ & & & & & & & & & & & 2i \\ & & & & & & & & & & & & j \end{array} \right]$$

$$a = \frac{EA}{L}, \quad b = \frac{12EI_s}{L^3}, \quad c = \frac{6EI_s}{L^2}, \quad d = \frac{12EI_r}{L^3}, \quad e = \frac{6EI_r}{L^2}, \quad f = \frac{6GJ}{5L} + \frac{12EI_\omega}{L^3},$$

$$g = \frac{GJ}{10} + \frac{6EI_\omega}{L^2}, \quad h = \frac{2EI_r}{L}, \quad i = \frac{2EI_s}{L}, \quad j = \frac{2GJL}{15} + \frac{4EI_\omega}{L}, \quad k = -\frac{GJL}{30} + \frac{2EI_\omega}{L}.$$

Appendix B: The 14x14 *consistent* mass matrix. $\underline{\mathbf{m}}_{(14,14)}^C = \rho AL \begin{bmatrix} \underline{\mathbf{m}}_1 & \underline{\mathbf{m}}_{12} \\ \underline{\mathbf{m}}_{12}^T & \underline{\mathbf{m}}_2 \end{bmatrix},$

$$\underline{\mathbf{m}}_{(7,7)} = \left[\begin{array}{ccc|ccc|c} 2a & 0 & 0 & 0 & 0 & 0 & 0 \\ & b + k i_s^2 & 0 & b z_{CT} & 0 & f + m i_s^2 & f z_{CT} \\ & & b + k i_r^2 & -b y_{CT} & -f - m i_r^2 & 0 & f y_{CT} \\ \hline & & & b i_p^2 + k i_\omega^4 & -f y_{CT} & f z_{CT} & f i_p^2 + m i_\omega^4 \\ & & & & h + 4e i_r^2 & 0 & h y_{CT} \\ & & & & & h + 4e i_s^2 & h z_{CT} \\ \hline & & & & & & h i_p^2 + 4e i_\omega^4 \end{array} \right]$$

$$\underline{\mathbf{m}}_{2(7,7)} = \left[\begin{array}{ccc|ccc|c} 2a & 0 & 0 & 0 & 0 & 0 & 0 \\ & b + k i_s^2 & 0 & b z_{CT} & 0 & -f - m i_s^2 & -f z_{CT} \\ & & b + k i_r^2 & -b y_{CT} & f + m i_r^2 & 0 & -f y_{CT} \\ \hline & & & b i_p^2 + k i_\omega^4 & f y_{CT} & -f z_{CT} & -f i_p^2 - m i_\omega^4 \\ & & & & h + 4e i_r^2 & 0 & h y_{CT} \\ & & & & & h + 4e i_s^2 & h z_{CT} \\ \hline & & & & & & h i_p^2 + 4e i_\omega^4 \end{array} \right]$$

$$\underline{\mathbf{m}}_{12(7,7)} = \left[\begin{array}{ccc|ccc|c} a & 0 & 0 & 0 & 0 & 0 & 0 \\ 0 & c - k i_s^2 & 0 & c z_{CT} & 0 & -g + m i_s^2 & -g z_{CT} \\ 0 & 0 & c - k i_r^2 & -c y_{CT} & g - j i_r^2 & 0 & -g y_{CT} \\ \hline 0 & c z_{CT} & -c y_{CT} & c i_p^2 - k i_\omega^4 & g y_{CT} & -g z_{CT} & -g i_p^2 + m i_\omega^4 \\ 0 & 0 & -g + m i_r^2 & -g y_{CT} & -j - e i_r^2 & 0 & -j y_{CT} \\ 0 & g - m i_s^2 & 0 & g z_{CT} & 0 & -j - e i_s^2 & -j z_{CT} \\ \hline 0 & g z_{CT} & g y_{CT} & g i_p^2 - m i_\omega^4 & -j y_{CT} & -j z_{CT} & -j i_p^2 - e i_\omega^4 \end{array} \right]$$

$$a = \frac{1}{6}, \quad b = \frac{13}{35}, \quad c = \frac{9}{70}, \quad e = \frac{1}{30},$$

$$f = \frac{11L}{210}, \quad g = \frac{13L}{420}, \quad h = \frac{L^2}{105}, \quad j = \frac{L^2}{140}, \quad k = \frac{6}{5L^2}, \quad m = \frac{1}{10L}.$$

$$i_r^2 = \frac{I_r}{A}, \quad i_s^2 = \frac{I_s}{A}, \quad i_p^2 = i_r^2 + i_s^2 + y_{CT}^2 + z_{CT}^2, \quad i_\omega^4 = \frac{I_\omega}{A}.$$

Appendix C: The 14x14 *lumped* mass matrix.

$$\underline{\mathbf{m}}_{(14,14)}^C = \begin{bmatrix} \underline{\mathbf{m}} & \underline{\mathbf{0}} \\ \underline{\mathbf{0}} & \underline{\mathbf{m}} \end{bmatrix}, \quad \underline{\mathbf{m}}_{(7,7)} = \frac{\rho AL}{2} \left[\begin{array}{ccc|ccc|c} 1 & 0 & 0 & 0 & 0 & 0 & 0 \\ & 1 & 0 & z_{CT} & 0 & 0 & 0 \\ & & 1 & -y_{CT} & 0 & 0 & 0 \\ \hline & & & i_p^2 & 0 & 0 & 0 \\ & & & & i_r^2 & 0 & 0 \\ & & & & & i_s^2 & 0 \\ \hline & & & & & & i_\omega^4 \end{array} \right]$$

CRITICAL VELOCITY OF FLUID CONVEYING PIPES RESTING ON TWO-PARAMETER FOUNDATION

Kameswara Rao Chellapilla

Professor, Mechanical Engineering Department
Muffakham Jah College of Engineering & Technology
Hyderabad, India
Phone: 91-040-23811623
Email: ckrao_52@yahoo.com

H. Simha

Scientist, Design & Engineering Division
Indian Institute of Chemical Technology
Hyderabad, India
Phone: 91-040-27193229
Email: simha@iictnet.org

Abstract

Pipelines are used extensively for transportation of fluids. The velocity of the fluid in the pipeline imparts energy to the pipeline making it to vibrate. It is well established from published literature that there exists a critical velocity of the fluid near which the natural frequency of the pipeline tends to zero. This is the required condition for buckling of the pipeline. Literature abounds with analyses, which give information on the influence of boundary conditions on the stability of fluid conveying pipes. However, much of these studies have been carried out for pipelines resting on Winkler type foundations. This has provided the motivation for studying the influence of non-Winkler type foundation on the critical velocities of a fluid-conveying pipe. The foundation considered in this study is a two-parameter foundation model, such as the Pasternak foundation. Expressions are derived for the critical flow velocity by utilizing Fourier series and Galerkin method for three simple boundary conditions, namely: Pinned-Pinned, Pinned-Fixed and Fixed-Fixed. Results are presented for varying values of the foundation stiffness parameter and interesting conclusions are drawn on the effect of the foundation parameters on the critical flow velocity of the pipeline.

Introduction

The technology of transporting fluids, especially petroleum liquids, through long pipelines which cover different types of terrain, has evolved over the years. Interest in studying the dynamic behaviour of such fluid conveying pipes was stimulated when excessive transverse vibrations were observed and subsequently analyzed first by Ashley and Haviland in 1950 [1] and later by Housner in 1952 [2]. Housner considered a simply supported beam model for the pipeline and analyzed it using a series solution approach and showed the existence of a critical flow velocity for a pipeline which could cause buckling. In 1955, Long [3] studied the influence of fixed-fixed and fixed-pinned boundary conditions on the critical velocity. In 1966, Gregory & Paidoussis [4] presented results on the dynamic behaviour of a cantilevered pipe conveying fluid. All the above studies did not consider elastic support conditions.

When a pipeline rests on an elastic medium such as a soil, a model of the soil medium must be included in the governing differential equation. A very common structural model of the soil medium is the Winkler model, in which soil is represented by a series of constant stiffness, closely spaced linear springs. In 1970, Stein & Tobriner [5] studied the vibrations of a fluid conveying pipe resting on an elastic foundation. Lottati and Kornecki, in 1986 [6], studied the influence of the elastic foundation on the stability of the pipeline. Later, in 1992, Dermendjian-Ivanova [7] investigated the behaviour of a fluid conveying pipe resting on an elastic foundation and obtained the critical fluid velocity. In 1993, Chary [8] presented a detailed analysis of fluid conveying pipes resting on elastic foundation. He also considered the inertia of the foundation and analyzed the seismic response of such pipelines. All these studies modeled the elastic foundation as a Winkler model. In this paper, the work of Chary has been extended to study the influence of a two-parameter foundation model on the critical flow velocity. Results are presented for various values of the foundation stiffness parameters.

Equation of motion

The differential equation of motion for lateral displacement $w(x,t)$ of a uniform fluid conveying pipe resting on a Winkler type elastic foundation is given by [8]:

$$EI \frac{\partial^4 w}{\partial x^4} + M \frac{\partial^2 w}{\partial t^2} + rAv^2 \frac{\partial^2 w}{\partial x^2} + 2rAv \frac{\partial^2 w}{\partial x \partial t} + k_1 w = 0 \quad (1)$$

In the above equation, E denotes the modulus of elasticity, I is the moment of inertia of the pipe section, $M(=m+rA)$ is the total mass of the pipe per unit length, m is the mass of the pipe alone per unit length, rA is the mass of the fluid per unit length, v is the steady flow velocity and k_1 is the stiffness of the elastic medium per unit length of the pipe. In this equation, the elastic medium is modeled on the Winkler type foundation. Following the method given by Pantelides [9], The equation of motion for a fluid conveying pipe resting on a two-parameter foundation becomes:

$$EI \frac{\partial^4 w}{\partial x^4} + M \frac{\partial^2 w}{\partial t^2} + (rAv^2 - k_2) \frac{\partial^2 w}{\partial x^2} + 2rAv \frac{\partial^2 w}{\partial x \partial t} + k_1 w = 0 \quad (2)$$

In equation (2) above, k_2 represents the additional parameter defining the foundation, usually termed as the shear constant of the foundation. The model is shown in figure 1. Equation (2) is now solved for three simple boundary conditions.

Pinned-pinned pipe

The boundary conditions for a pinned-pinned pipe are

$$\begin{aligned} w(0,t) &= w(L,t) = 0 \\ \frac{\partial^2 w(0,t)}{\partial x^2} &= \frac{\partial^2 w(L,t)}{\partial x^2} = 0 \end{aligned} \quad (3)$$

Taking the solution of equation (2) which satisfies the boundary conditions (3) as

$$w(x,t) = \sum_{n=1,3,5,\dots} a_n \sin \frac{n\pi x}{L} \sin \omega_j t + \sum_{n=2,4,6,\dots} a_n \sin \frac{n\pi x}{L} \cos \omega_j t, \quad j=1,2,3,\dots \quad (4)$$

Where ω_j represents the natural frequency of the j^{th} mode of vibration. Substitution of equation (4) in (2) and expanding in a Fourier series we have an equation of the form:

$$[\mathbf{K} - \omega_j^2 \mathbf{M}]\{\mathbf{a}\} = 0 \quad (5)$$

where \mathbf{K} is the stiffness matrix whose elements are enumerated in [8] and will not be repeated here, \mathbf{I} is the identity matrix and $\mathbf{a}^T = \{a_1, a_2, \dots, a_n\}$. Retaining the first two terms of the above equation, and setting the determinant equal to zero, we get

$$\begin{aligned} \Omega_j^4 - \left[\left(\frac{256}{9} \mathbf{b} - 5\mathbf{p}^2 \right) (\mathbf{V}^2 - \mathbf{g}_2) + 17\mathbf{p}^4 + 2\mathbf{g}_1 \right] \Omega_j^2 + \\ \left[4\mathbf{p}^4 (\mathbf{V}^2 - \mathbf{g}_2)^2 - (\mathbf{V}^2 - \mathbf{g}_2) (5\mathbf{p}^2 \mathbf{g}_1 + 20\mathbf{p}^6) + (16\mathbf{p}^8 + 17\mathbf{p}^4 \mathbf{g}_1 + \mathbf{g}_1^2) \right] = 0 \end{aligned} \quad (6)$$

In equation (6), the following non-dimensional parameters have been used:

$$\mathbf{b} = \frac{\mathbf{r}A}{M}; \Omega_j = \mathbf{w}_j L^2 \sqrt{\frac{M}{EI}}, j = 1, 2, 3, \dots; V = vL \sqrt{\frac{\mathbf{r}A}{EI}}; \mathbf{g}_1 = \frac{k_1 L^4}{EI}; \mathbf{g}_2 = \frac{k_2 L^2}{EI}$$

When the fluid velocity reaches a certain value V_{cr} , the fundamental natural frequency becomes zero. Hence, setting $\Omega_j = 0$ in equation (8), we obtain:

$$\left[4\mathbf{p}^4 (\mathbf{V}^2 - \mathbf{g}_2)^2 - (\mathbf{V}^2 - \mathbf{g}_2) (5\mathbf{p}^2 \mathbf{g}_1 + 20\mathbf{p}^6) + (16\mathbf{p}^8 + 17\mathbf{p}^4 \mathbf{g}_1 + \mathbf{g}_1^2) \right] = 0 \quad (7)$$

Solving equation (7) for V , we obtain the critical flow velocity for the pinned-pinned case.

Pinned-fixed and fixed-fixed pipe

The boundary conditions for a pinned-fixed pipe are

$$\begin{aligned} w(0, t) &= w(L, t) = 0 \\ \frac{\partial w(0, t)}{\partial x} &= \frac{\partial^2 w(L, t)}{\partial x^2} = 0 \end{aligned} \quad (8)$$

And those for a fixed-fixed pipe are

$$\begin{aligned} w(0, t) &= w(L, t) = 0 \\ \frac{\partial w(0, t)}{\partial x} &= \frac{\partial w(L, t)}{\partial x} = 0 \end{aligned} \quad (9)$$

We assume the deflection of the pipe to be of the form

$$w(x, t) = \Re \left[\mathbf{f}_n \left(\frac{x}{L} \right) e^{i\mathbf{w}t} \right] \quad (10)$$

In equation (10), \Re denotes the real part, $\mathbf{f}_n \left(\frac{x}{L} \right)$ is a series of beam eigen-functions $\mathbf{y}_r(\mathbf{x})$ given by:

$$\begin{aligned} \mathbf{y}_r(\mathbf{x}) &= \cosh(\mathbf{I}_r \mathbf{x}) - \cos(\mathbf{I}_r \mathbf{x}) - \mathbf{s}_r (\sinh(\mathbf{I}_r \mathbf{x}) - \sin(\mathbf{I}_r \mathbf{x})), r = 1, 2, 3, \dots, n; \mathbf{x} = \left(\frac{x}{L} \right) \\ \mathbf{s}_r &= \frac{\cosh \mathbf{I}_r - \cos \mathbf{I}_r}{\sinh \mathbf{I}_r - \sin \mathbf{I}_r} \end{aligned} \quad (11)$$

In the above equation, \mathbf{I}_r is the frequency parameter of the pipe without fluid flow, which is considered as a beam, and its values are [10]

$\mathbf{I}_1 = 3.926602$ and $\mathbf{I}_2 = 7.068583$ for the pinned-fixed case and
 $\mathbf{I}_1 = 4.730041$ and $\mathbf{I}_2 = 7.853205$ for the fixed-fixed case

Substituting equation (10) in the equation of motion (2) gives

$$L_n = EI \frac{\partial^4 \mathbf{f}}{\partial x^4} + (\mathbf{r} A v^2 - k_2) \frac{\partial^2 \mathbf{w}}{\partial x^2} + 2i \mathbf{w} \mathbf{r} A v \frac{\partial \mathbf{f}}{\partial x} + (k_1 - M \mathbf{w}^2) \mathbf{f} = 0 \quad (12)$$

Following the method given in [8], using Galerkin's method and minimizing the mean square of the residual L_n over the length of the pipe, we have the following equations in V .

For the pinned-fixed case:

$$(C_{11}C_{22} - C_{12}C_{21})(V^2 - \mathbf{g}_2)^2 + (V^2 - \mathbf{g}_2) \left[(I_1^4 + \mathbf{g}_1)C_{22} + (I_2^4 + \mathbf{g}_1)C_{11} \right] + \left[(I_1^4 + \mathbf{g}_1)(I_2^4 + \mathbf{g}_1) \right] = 0 \quad (13)$$

For the fixed-fixed case:

$$(C_{11}C_{22})(V^2 - \mathbf{g}_2)^2 + (V^2 - \mathbf{g}_2) \left[(I_1^4 + \mathbf{g}_1)C_{22} + (I_2^4 + \mathbf{g}_1)C_{11} \right] + \left[(I_1^4 + \mathbf{g}_1)(I_2^4 + \mathbf{g}_1) \right] = 0 \quad (14)$$

In equations (13) and (14), the constants C_{11} etc. are integral values which are enumerated in [8].

Results

Table 1 gives the numerical values of the critical velocity parameter. The two foundation parameters are varied from 1.0E-06 to 1.0E+4. The first value is equivalent to no foundation while the last value represents a very stiff foundation. The results are tabulated for all the three boundary conditions.

In figures 2 3 & 4, the influence of γ_2 on the critical velocity parameter of the pipe for a pinned-pinned boundary condition is shown for various values of γ_1 . The results for the other two cases of pinned-fixed and fixed-fixed follow a similar trend.

Figure 5 shows the variation of the critical velocity parameter with γ_2 for various values of γ_1 . Finally, a comparison of the individual effects of each of the two foundation parameters, when the other is equivalent to zero, on the critical velocity parameter is shown in figure 6.

Conclusions

It is seen from figure 2 that there is not any perceptible change in the dynamic behaviour of the pipe until the shear constant of the two-parameter foundation γ_2 takes a value of 10.0. The critical velocity increases slightly for the value of γ_2 of 10.0. For a value of γ_2 of 100.0, there is a sharp jump in the value of the critical velocity parameter and this trend continues for increasing values of γ_2 , as shown in figures 3 and 4. Another observation from these plots is that, for lower values of γ_2 , there is a sharp increase in the value of critical velocity for the Winkler foundation constant γ_1 values greater than 10.0. The critical velocity does not seem to be effected by the value of the Winkler constant γ_1 for higher values of γ_2 .

This is shown in another way in figure 5. It can be seen that the Winkler constant γ_1 has little effect on the critical velocity especially for values of γ_2 greater than about 100.0.

In figure 6, a comparison between the relative effects of each of the two foundation parameters is shown. The top curve shows that there is a sharp increase in the critical velocity when there is a progressive increase in the value of γ_2 beyond 100.0. This curve represents the case where γ_1 is near zero. The bottom curve shows the variation of critical velocity with γ_1 when γ_2 is near zero. It can be observed that the influence of the shear constant of the two-parameter foundation is more than that of the Winkler constant on the critical velocity.

References

1. Ashley, H. and Haviland, G., (1950), "Bending Vibrations of a Pipe Line Containing Flowing Fluid", *J. Appl. Mech., Trans. ASME*, September, pp. 229-232.
2. Housner, G. W., (1952), "Bending Vibrations of a Pipe Line Containing Flowing Fluid", *J. Appl. Mech., Trans. ASME*, June, pp. 205-208.
3. Long, Jr., R. H., (1955), "Experimental and Theoretical Study of Transverse Vibration of a Tube Containing Flowing Fluid", *J. Appl. Mech., Trans. ASME*, March, pp. 65-68.
4. Gregory, R. W. and Paidoussis, M. P., (1966), "Unstable Oscillations of Tubular Cantilevers Conveying Fluid *Proc. Roy. Soc (London)*, **293A**, pp. 512-542.
5. Stein, R. A. and Tobriner, M. W., (1970), "Vibration of Pipes Containing Flowing Fluids", *J. Appl. Mech., Trans. ASME*, December, pp. 906-916.
6. Lottati, I. And Kornecki, A., (1986), "The effect of an Elastic Foundation and of Dissipative Forces on the Stability of Fluid-Conveying Pipes", *J. Sound Vibration*, **109**(2), pp. 327-338.
7. Dermendjian-Ivanova, D. S., (1992), "Critical Flow Velocities of a Simply Supported Pipeline on an Elastic Foundation", *J. Sound Vibration*, **157**(2), pp. 370-374.
8. Chary, S. R., (1993), "Vibrations of Pipes Resting on Soil Medium", *M.S. Thesis, Indian Institute of Science*, Bangalore.
9. Pantelides, C. P., (1992), "Stability of Columns on Biparametric Foundations", *Comp. Str.*, **42**(1), pp. 21-29.
10. Rao, S. S., (1986), "Mechanical Vibrations, *Addison Wesley Publishing Company*, Massachusetts, p.386.

Table 1 – Values of the critical velocity parameter for various values of g_1 and g_2 for the three boundary conditions

Pinned-pinned pipe			Pinned-fixed Pipe			Fixed-fixed pipe		
γ_1	γ_2	V_{Cr}	γ_1	γ_2	V_{Cr}	γ_1	γ_2	V_{Cr}
1.00E-06	1.00E-06	3.14159	1.00E-06	1.00E-06	4.49975	1.00E-06	1.00E-06	5.43433
1.00E-05	1.00E-06	3.14159	1.00E-05	1.00E-06	4.49975	1.00E-05	1.00E-06	5.43433
1.00E+02	1.00E-06	4.47233	1.00E+02	1.00E-06	5.32942	1.00E+02	1.00E-06	5.95246
1.00E+03	1.00E-06	8.05039	1.00E+03	1.00E-06	8.66386	1.00E+03	1.00E-06	9.40901
1.00E+04	1.00E-06	17.11086	1.00E+04	1.00E-06	16.91955	1.00E+04	1.00E-06	16.00158
1.00E-06	1.00E-05	3.14159	1.00E-06	1.00E-05	4.49975	1.00E-06	1.00E-05	5.43433
1.00E-05	1.00E-05	3.14159	1.00E-05	1.00E-05	4.49975	1.00E-05	1.00E-05	5.43433
1.00E+02	1.00E-05	4.47233	1.00E+02	1.00E-05	5.32942	1.00E+02	1.00E-05	5.95246
1.00E+03	1.00E-05	8.05039	1.00E+03	1.00E-05	8.66386	1.00E+03	1.00E-05	9.40901
1.00E+04	1.00E-05	17.11086	1.00E+04	1.00E-05	16.91955	1.00E+04	1.00E-05	16.00158
1.00E-06	1.00E+01	4.45753	1.00E-06	1.00E+01	5.4998	1.00E-06	1.00E+01	6.28745
1.00E-05	1.00E+01	4.45753	1.00E-05	1.00E+01	5.4998	1.00E-05	1.00E+01	6.28745
1.00E+02	1.00E+01	5.47738	1.00E+02	1.00E+01	6.19699	1.00E+02	1.00E+01	6.74031
1.00E+03	1.00E+01	8.6492	1.00E+03	1.00E+01	9.22293	1.00E+03	1.00E+01	9.9262
1.00E+04	1.00E+01	17.40061	1.00E+04	1.00E+01	17.21253	1.00E+04	1.00E+01	16.31105
1.00E-06	1.00E+02	10.48187	1.00E-06	1.00E+02	10.96575	1.00E-06	1.00E+02	11.38121
1.00E-05	1.00E+02	10.48187	1.00E-05	1.00E+02	10.96575	1.00E-05	1.00E+02	11.38121
1.00E+02	1.00E+02	10.95453	1.00E+02	1.00E+02	11.33149	1.00E+02	1.00E+02	11.63751
1.00E+03	1.00E+02	12.83778	1.00E+03	1.00E+02	13.23111	1.00E+03	1.00E+02	13.7306
1.00E+04	1.00E+02	19.81871	1.00E+04	1.00E+02	19.65379	1.00E+04	1.00E+02	18.8693
1.00E-06	1.00E+03	31.77845	1.00E-06	1.00E+03	31.94132	1.00E-06	1.00E+03	32.08632
1.00E-05	1.00E+03	31.77845	1.00E-05	1.00E+03	31.94132	1.00E-05	1.00E+03	32.08632
1.00E+02	1.00E+03	31.93747	1.00E+02	1.00E+03	32.06872	1.00E+02	1.00E+03	32.17812
1.00E+03	1.00E+03	32.63141	1.00E+03	1.00E+03	32.78814	1.00E+03	1.00E+03	32.99287
1.00E+04	1.00E+03	35.95527	1.00E+04	1.00E+03	35.86462	1.00E+04	1.00E+03	35.4408
1.00E-06	5.00E+03	70.78043	1.00E-06	5.00E+03	70.85371	1.00E-06	5.00E+03	70.91919
1.00E-05	5.00E+03	70.78043	1.00E-05	5.00E+03	70.85371	1.00E-05	5.00E+03	70.91919
1.00E+02	5.00E+03	70.85197	1.00E+02	5.00E+03	70.91123	1.00E+02	5.00E+03	70.96078
1.00E+03	5.00E+03	71.16747	1.00E+03	5.00E+03	71.23947	1.00E+03	5.00E+03	71.33393
1.00E+04	5.00E+03	72.7515	1.00E+04	5.00E+03	72.70675	1.00E+04	5.00E+03	72.49862
1.00E-06	8.00E+03	89.49787	1.00E-06	8.00E+03	89.55584	1.00E-06	8.00E+03	89.60766
1.00E-05	8.00E+03	89.49787	1.00E-05	8.00E+03	89.55584	1.00E-05	8.00E+03	89.60766
1.00E+02	8.00E+03	89.55446	1.00E+02	8.00E+03	89.60135	1.00E+02	8.00E+03	89.64057
1.00E+03	8.00E+03	89.80428	1.00E+03	8.00E+03	89.86135	1.00E+03	8.00E+03	89.93625
1.00E+04	8.00E+03	91.06471	1.00E+04	8.00E+03	91.02896	1.00E+04	8.00E+03	90.86281
1.00E-06	1.00E+04	100.0493	1.00E-06	1.00E+04	100.1012	1.00E-06	1.00E+04	100.1476
1.00E-05	1.00E+04	100.0493	1.00E-05	1.00E+04	100.1012	1.00E-05	1.00E+04	100.1476
1.00E+02	1.00E+04	100.1	1.00E+02	1.00E+04	100.1419	1.00E+02	1.00E+04	100.177
1.00E+03	1.00E+04	100.3235	1.00E+03	1.00E+04	100.3746	1.00E+03	1.00E+04	100.4417
1.00E+04	1.00E+04	101.4534	1.00E+04	1.00E+04	101.4213	1.00E+04	1.00E+04	101.2722

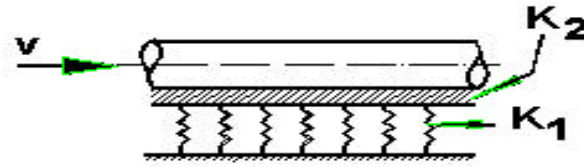


Figure 1 – Model of a pipe fluid conveying pipe resting on a two-parameter foundation

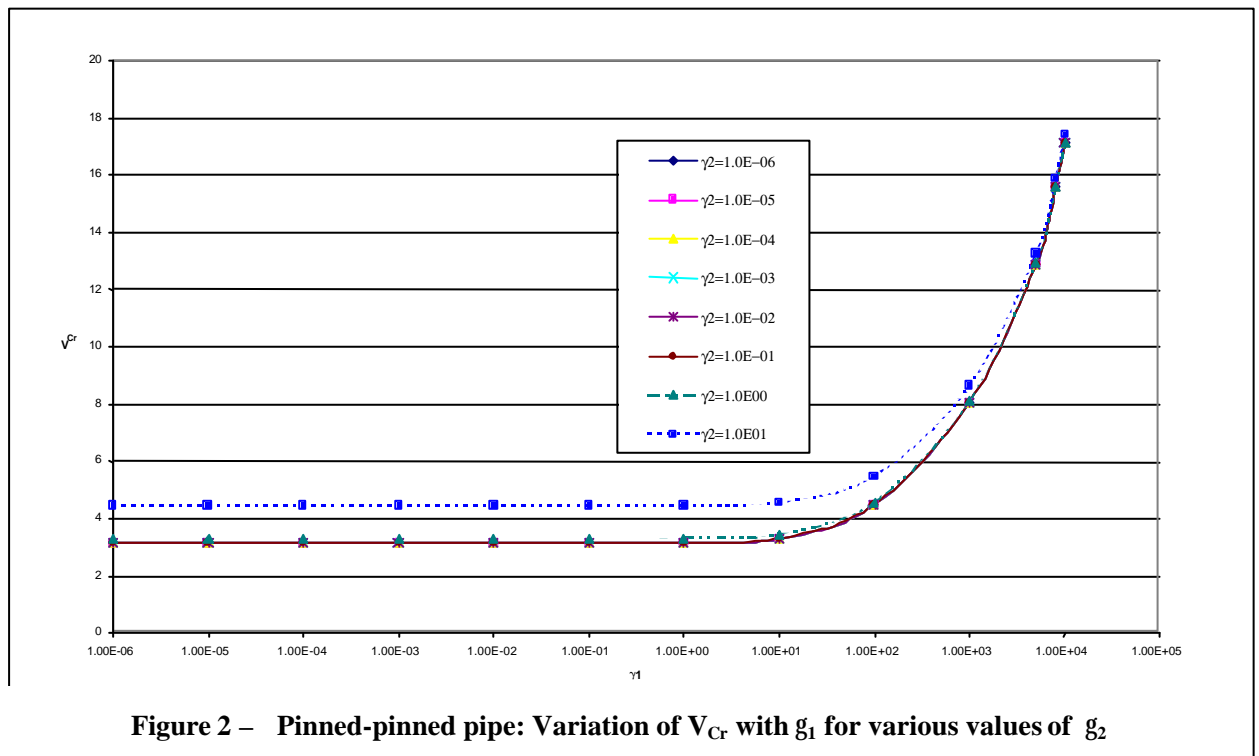


Figure 2 – Pinned-pinned pipe: Variation of V_{Cr} with g_1 for various values of g_2

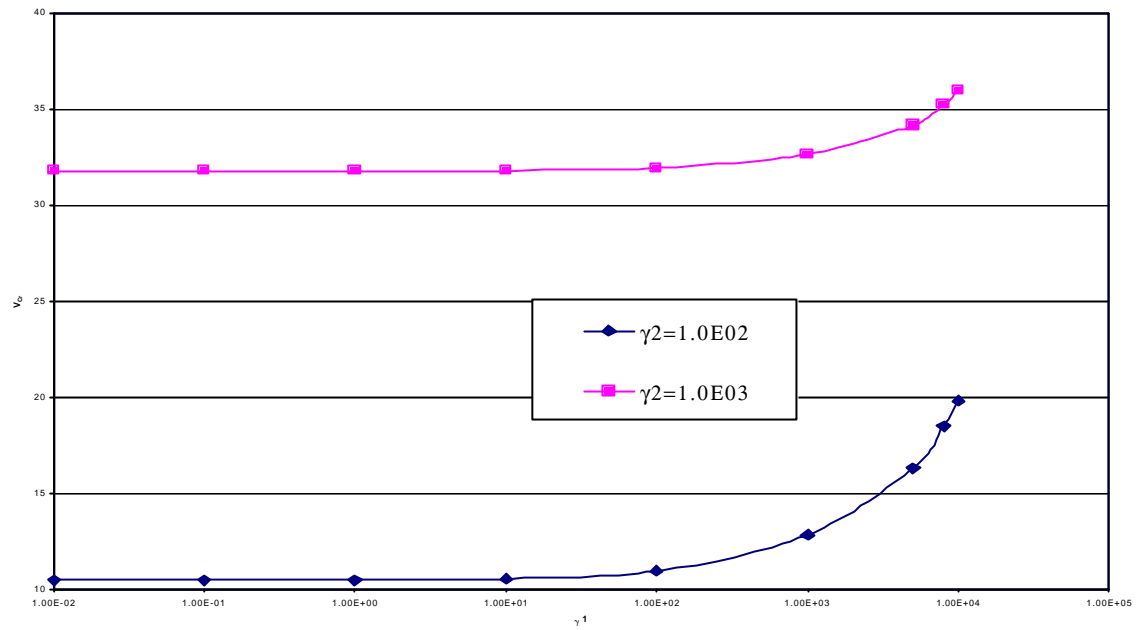


Figure 3 – Pinned-pinned pipe: Variation of V_{Cr} with g_1 for various values of g_2 – contd.

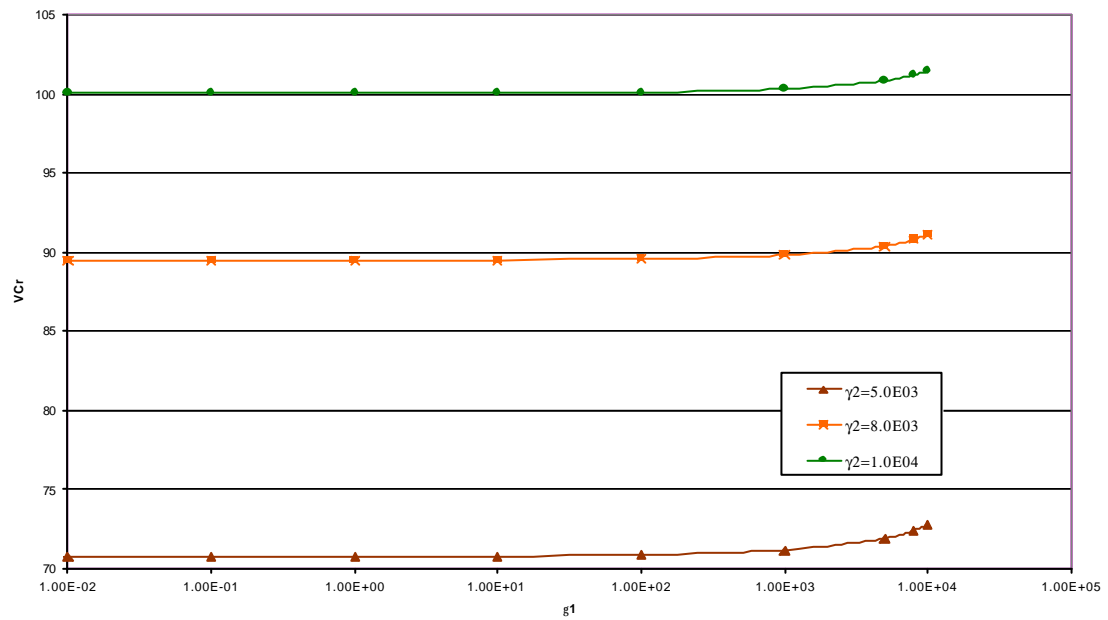


Figure 4 – Pinned-pinned pipe: Variation of V_{Cr} with g_1 for various values of g_2 – contd.

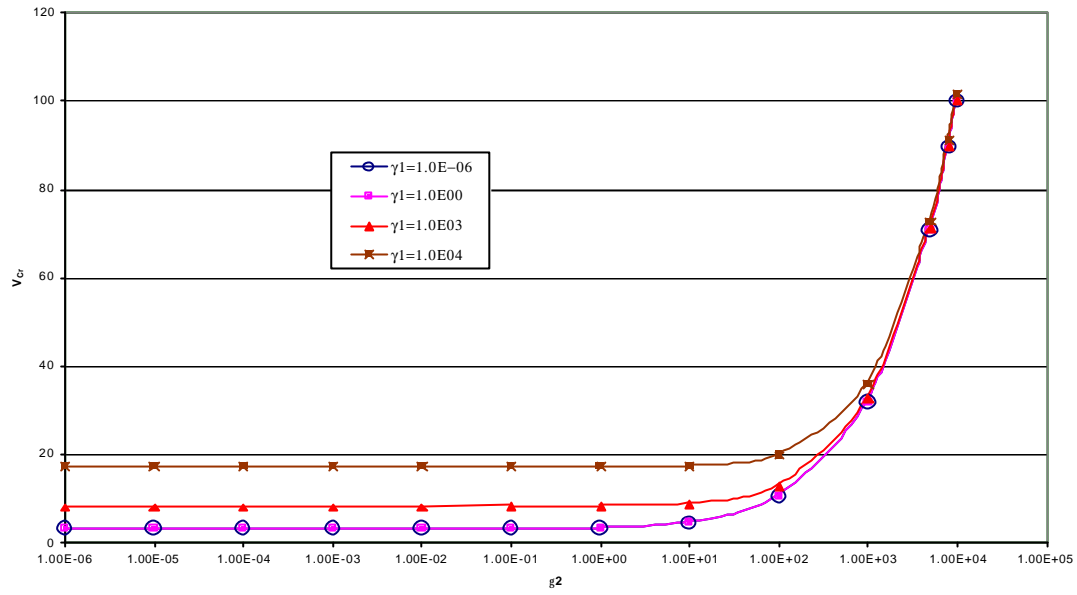


Figure 5 – Pinned-pinned pipe: Influence of g_2 on V_{Cr} for various values of g_1

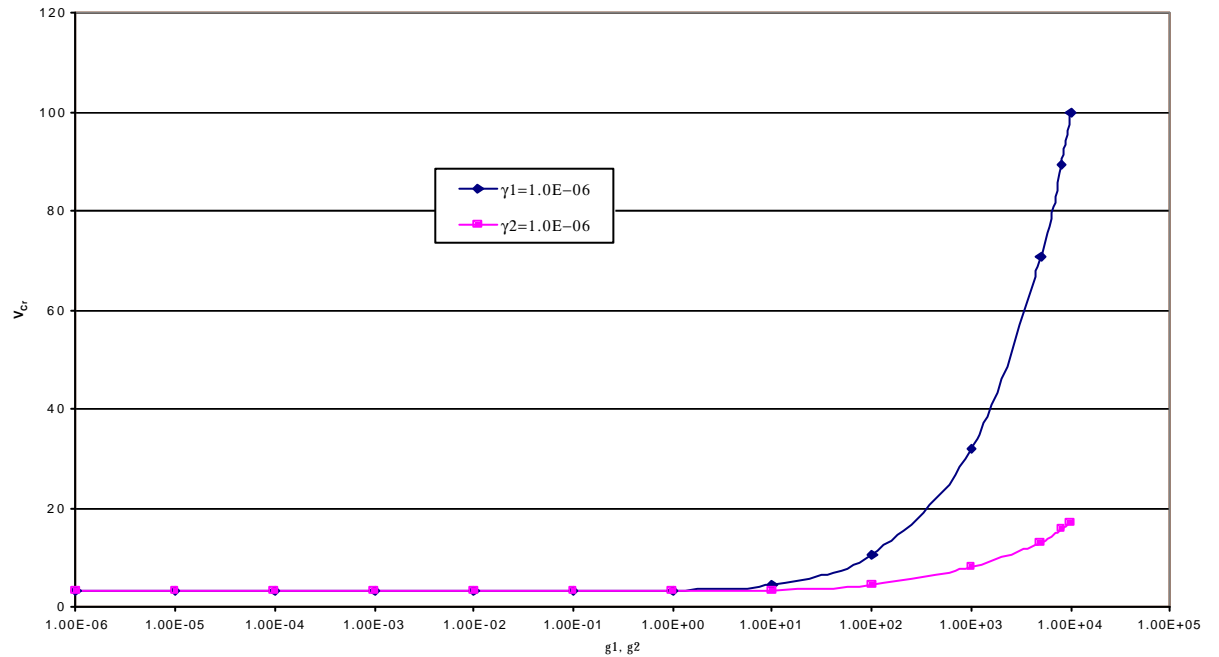


Figure 6 – Pinned-pinned pipe: Comparison of the effect of g_1 and g_2 on V_{Cr}

DYNAMICS OF MULTIPLY EXPANSION BELLOWS WITH ELASTICALLY RESTRAINED ENDS

KAMESWARA RAO.C

*Professor, Mechanical Engineering
Department, Muffakham Jah College
of Engineering & Technology
Hyderabad, India
Phone: 91 040 23811623
email: ckrao_52@yahoo.com*

RADHAKRISHNA .M

*Scientist, Design Engineering Division
Indian Institute of Chemical Technology
Hyderabad, India
Phone: 91 040 27193229
email: madabhushirk@yahoo.com*

Keywords

Multiply, bellows, elastic restraint, transverse, vibration

Abstract

The paper presents study of the dynamic aspects of the multiply bellows with elastically restrained ends and under rotatory inertia. The influence of rotational restraint and internal pressure loading on dynamic response of such bellows configuration has been attempted here.

An attempt has been made here to establish relations that are simple and compatible in computing the frequency of bellows. The "Rayleigh Quotient", method is used for this purpose. The coupled responses obtained are compared with exact analysis for multiply configuration. Two cases are considered – bellows having same material and different materials for plies.

1. Introduction

Multiply bellows are generally used in applications where higher-pressure capacity is

Required than a single-ply construction. The multiply construction increases the overall stiffness of the system and reduces deflection. These bellows are manufactured as multi-layered tubes of plies generally ranging in number from 2 to 20 depending on diameter and operating pressure.

Each thin layer acts as a nearly neutral fiber that offers significantly lower resistance to movement in the piping system than a single wall bellow. Therefore, less force is required for actuating multiply bellows. The stresses induced on the individual layers of bellows are a fraction of the stresses induced in the single wall bellows of equal thickness. This results in highest possible service life of bellows.

The multiply design results in lower spring rates for a given pressure capacity. Also the effective cross sectional area of multiply bellows is less compared to single-ply bellows

□ email: ckrao_52@yahoo.com

to accommodate a given movement. These two reductions would result in lower forces and moments on the anchors, equipment and guides supporting the piping system. The anchors and guides of the system can be dimensioned significantly smaller and more economically. The life of the connected equipment is improved and also raises the reliability of the overall piping system.

This type of construction is well suited for applications with vibratory or rapid cyclic motion because of the inherent damping that is provided by the relative inter-ply movement.

Fig. 1 shows a typical cross-sectional view of the bellows with number of plies and geometrical dimensions.

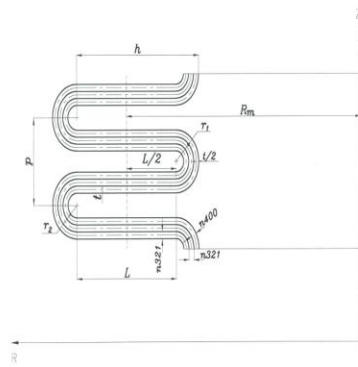


Fig.1 : Geometrical Dimensions of Multiply Bellows

2. Theoretical Development

An attempt has been made here to establish relations that are simple and compatible in computing the frequency of bellows. The "Rayleigh Quotient", method is used for this purpose. Multiply bellows with multiple or same materials of construction for plies are considered.

One such case is to have the innermost ply of Alloy 400, which is in contact with the fluid and outer two plies of austenitic steel of 321, to take care of the pressure capacity.

A literature search on multiply bellows shows relatively little work carried out on the subject and hence has led the authors to take up the work. The works contributed by Li Ting-Xin on axial vibration of single-ply bellows, Jakubauskas. V.F et al. [2] on transverse vibrations for a set of classical fixed-fixed boundary conditions and Rao.C.K et al. [3] for rotationally restrained ends reflect the same.

The paper deals with flexural vibration characteristics of multiply bellows subjected to an internal pressure loading and by considering the ends of bellows elastically restrained against rotation. It is assumed that inter-ply interaction is neglected and the plies considered to be closely fit.

The derivation of transcendental frequency equation of transverse vibrations for multiply bellows has been thoroughly dealt by the authors [4]. Two cases were considered- Case I - a multiply bellow that has same material of construction for all the three plies and Case II - a multiply bellow of different materials of construction. Results of the exact analysis would serve here for comparison purpose.

Bellows having same dimensions as in [6], and having 3 numbers of plies of equal thickness are considered. The maximum critical

pressure and spring rate are calculated using the formulae given [3].

3. The Differential Equation

The fundamental equation of motion of the equivalent Timoshenko beam [5] is given by-

$$EI \frac{\partial^4 w}{\partial x^4} + P \pi R_m^2 \frac{\partial^2 w}{\partial x^2} \rho A - J \frac{\partial^4 w}{\partial x^2 \partial t^2} + m_{tot} \frac{\partial^2 w}{\partial t^2} = 0 \quad (1)$$

Where EI represents bending stiffness, P- internal pressure in bellows, J – rotatory inertia per unit length, w –lateral deflection x-axial coordinate, R_m –mean radius of bellows, m_{tot} is the total mass of bellows per unit length includes mass of bellows and fluid mass and t-time [4].

Using the separation of variables approach by expressing the lateral deflection, w as the product of a function X (t) and harmonic function T (t) as-

$$w(x, t) = X(x) \cdot T(t) \quad (2)$$

$$T(t) = X(x) e^{i\omega t} \quad (3)$$

Where ‘ ω ’ is natural frequency

Substitution of equation (2) into equation (1), we get the ordinary differential equation-

$$\frac{d^4 X}{dx^4} + \frac{(P \pi R_m^2 + J \omega^2)}{EI} \frac{d^2 X}{dx^2} - \omega^2 \frac{m_{tot}}{EI} X = 0 \quad (4)$$

At the ends ‘A and B’, the bellows are welded to short pipe nipples and so do not represent a classical case. The present set of boundary

conditions considered to have a rotational stiffness of R_1 and R_2 depicts the best of the practical situation.

4. Approximate Analytical Solution (Rayleigh’s method)

Multiplying both sides of the differential equation (4) by X and integrate the domain of the bellows, according to Volterra and Zachmanoglou (1965).

$$EI \int_0^l \frac{d^4 X}{dx^4} X \cdot dx + P \pi R_m^2 \int_0^l \frac{d^2 X}{dx^2} X \cdot dx + J \omega^2 \int_0^l \frac{d^2 X}{dx^2} X \cdot dx - \omega^2 m_{tot} \int_0^l X^2 \cdot dx = 0 \quad (5)$$

Integrating the first integral by parts with respect to coordinate twice, and the second and third just once, we get-

$$EI \left[\frac{d^3 X}{dx^3} X - \frac{d^2 X}{dx^2} \frac{dX}{dx} \right]_0^l + \int_0^l \left(\frac{d^2 X}{dx^2} \right)^2 \cdot dx + P \pi R_m^2 \left[\frac{dX}{dx} X \right]_0^l - \int_0^l \left(\frac{dX}{dx} \right)^2 \cdot dx + J \omega^2 \left[\frac{dX}{dx} X - \int_0^l \left(\frac{dX}{dx} X \right)^2 \cdot dx \right] - \omega^2 m_{tot} \int_0^l X^2 \cdot dx = 0 \quad (6)$$

After substitution of bounds -

$$\begin{aligned}
& EI \left(\frac{d^3 X(l)}{dx^3} X(l) - \frac{d^3 X(0)}{dx^3} X(0) - \right. \\
& \frac{d^2 X(l)}{dx^2} \frac{dX(l)}{dx} + \frac{d^2 X(0)}{dx^2} \frac{dX(0)}{dx} + \\
& \left. \int_0^l \left(\frac{d^2 X}{dx^2} \right)^2 dx \right] + P \pi R_m^2 \left[\frac{dX(l)}{dx} X(l) \right. \\
& + J \omega^2 \left[\frac{dX(l)}{dx} X(l) - \frac{dX(0)}{dx} X(0) \right. \\
& \left. \left. - \int_0^l \left(\frac{dX}{dx} \right)^2 dx \right] - \omega^2 m_{tot} \int_0^l X^2 dx = 0 \right. \\
& \quad \quad \quad (7)
\end{aligned}$$

The above expression yields ω^2 -

$$\begin{aligned}
& EI \int_0^l \frac{d^2 X}{dx^2} X dx - P \pi R_m^2 \int_0^l \left(\frac{dX}{dx} \right)^2 X dx + \\
& J \omega^2 \int_0^l \left(\frac{dX}{dx} \right)^2 X dx - \omega^2 m_{tot} \int_0^l X^2 dx = 0 \\
& \quad \quad \quad (8) \\
& \omega^2 = \frac{EI \int_0^l \frac{d^2 X}{dx^2} X dx - P \pi R_m^2 \int_0^l \left(\frac{dX}{dx} \right)^2 X dx}{J \int_0^l \left(\frac{dX}{dx} \right)^2 X dx + m_{tot} \int_0^l X^2 dx} \\
& \quad \quad \quad (9)
\end{aligned}$$

The above expression is the “Rayleigh Quotient”, applied to the fixed-fixed ends of bellows. To find the value of ω^2 a certain deflection or mode shape function for $w(x)$ that satisfies the geometric boundary conditions is assumed and given in equation (10). Since the exact eigenfunction in the quotient is not known, the approximate function X is assumed that reasonably resembles the particular mode shape and satisfies the boundary conditions.

$$X = A(x^4 + Bx^3 + Cx^2 + Dx + E) \quad (10)$$

$$X = x^4 + Ax^3 + Bx^2 + Cx + D \quad (11)$$

Differentiation of the above expression (11)

twice, we get

$$X' = 4x^3 + 3Ax^2 + 2Bx + C \quad (12)$$

$$X'' = 12x^2 + 6Ax + 2B \quad (13)$$

Substitution of boundary conditions (14) to (17) into the above expression (10) and applying the limits the constants A , B , C and D are determined.

At $x=0$, the B.C are

$$X(x=0) = 0 \text{ and} \quad (14)$$

$$EI \frac{\partial^2 X(0)}{\partial x^2} = -T_1 \frac{\partial X(0)}{\partial x} \quad (15)$$

At $x=l$, the B.C. are

$$X(x=l) = 0 \text{ and} \quad (16)$$

$$EI \frac{\partial^2 X(l)}{\partial x^2} = -T_2 \frac{\partial X(l)}{\partial x} \quad (17)$$

$$\text{Where } T_1 = \frac{R_1 l}{EI} \text{ and } T_2 = \frac{R_2 l}{EI} \quad (18)$$

$$A = \frac{-R_1 - B(R_1 + 2)}{R_1} \quad (19)$$

$$B = \frac{R_1 R_2 + 6R_1}{12 + 4R_1 + 4R_2 + R_1 R_2} \quad (20)$$

$$C = \frac{2B}{R_1} \quad (21)$$

$$D = 0 \quad (22)$$

$$\text{Integrals } \int_0^l \frac{d^2 X}{dx^2} X dx, \int_0^l \left(\frac{dX}{dx} \right)^2 X dx \text{ and } X^2 dx$$

are evaluated in form of non-dimensional

coefficients A_1 , A_2 , A_3 and A_4 , that are written in terms of B , R_1 and R_2 for convenience and given in equations (23) to (26) respectively.

$$A_1 = \frac{144}{5} + 3[R_1 + B(R_1 + 2)]^2 - 18[R_1 + B(R_1 + 2)] + 16B - 6B[R_1 + B(R_1 + 2)]^2 \quad (23)$$

$$A_2 = \frac{16}{7} - 2[R_1 + B(R_1 + 2)] + \frac{5}{4}[R_1 + B(R_1 + 2)]^2 + 5\left\{\frac{2B}{R_1} - \frac{B}{2}[R_1 + B(R_1 + 2)]\right\} - \frac{2B}{R_1}[R_1 + B(R_1 + 2)] + \frac{4B^2}{R_1} + \frac{8B^3}{R_1} + \frac{4B^2}{R_1^2} \quad (24)$$

$$A_3 = \frac{1}{9} - \frac{1}{8}[R_1 + B(R_1 + 2)] + \frac{2}{7}B + \frac{1}{4}[R_1 + B(R_1 + 2)]^2 + \frac{B}{3}\left[\frac{2}{R_1} - \frac{1}{2}[R_1 + B(R_1 + 2)]\right] - \frac{2B}{5R_1}[R_1 + B(R_1 + 2)] + \frac{B^2}{R_1} + \frac{4}{3}\frac{B^2}{R_1^2} \quad (25)$$

$$A_4 = \frac{16}{7} - 2[R_1 + B(R_1 + 2)] + \frac{5}{4}[R_1 + B(R_1 + 2)]^2 + 5\left\{\frac{2B}{R_1} - \frac{B}{2}[R_1 + B(R_1 + 2)]\right\} - \frac{2B}{R_1}[R_1 + B(R_1 + 2)] + \frac{4B^2}{R_1} + \frac{8B^3}{R_1} + \frac{4B^2}{R_1^2} \quad (26)$$

Now by substitution of the non-dimensional coefficients into equation (9), will result in obtaining the eigenvalue, ω .

$$\omega^2 = \frac{EI.(A_1) - P\pi R_m^2.(A_2)}{m_{tot}.(A_3) + J.(A_4)} \quad (24)$$

The final frequency expression for the natural frequency of transverse vibration of a multiply expansion joint in lateral modes is derived as –

$$f_k = \frac{1}{2\pi} \sqrt{\frac{EI.A_1 - P\pi R_m^2.A_2}{m_{tot}.A_3 + J.A_4}} \quad (25)$$

5. Bellows Dimensions

The various dimensional parameters of U-shaped bellows are assumed same as those considered by Jakubauskas [3] for comparison purpose.

Mean diameter (D_m) –69.3mm, convolution height, $h=5.71$ mm; convolution pitch, $q=5$ mm; bellows thickness after forming, $t_p=0.28$ mm; number of convolutions, $N=9$; pitch diameter of bellows, $D_b=62.8$ mm: E_{400} at 400 deg F $=2.03 \times 10^{11}$ N/m²; $E_{321}=1.82 \times 10^{11}$ N/m²; operating pressure, $P=166 \times 10^6$ N/m² (Pa) and bellows length, $L = 0.0693$ m respectively.

Case I: bellows having SS-321 as material of construction for all the three plies

Case II: bellows having inner ply as Alloy 400 and two outer plies as SS-321

The axial stiffness of bellows is computed by using the expressions given below-

$$k_1 = 4R_m E_{321} \left(\frac{t_p}{h}\right)^3 n_{321} \quad (26)$$

$$k_2 = 4R_m [E_{400} n_{400} + E_{321} n_{321}] \left(\frac{t_p}{h}\right)^3 \quad (27)$$

Where, n_{321} and n_{400} represent number of plies of 321 and alloy 400 respectively. According to

equations (26) and (27), $k_1=8.92 \times 10^6 \text{ N/m}$ and $k_2=9.26 \times 10^6 \text{ N/m}$.

The maximum critical pressure of bellows that can withstand without buckling and bending stiffness are given by the expressions -

$$P_{\max} = \frac{\pi k_{1,2} \cdot q}{6.66 l^2} \quad (28)$$

$$EI = \frac{1}{4} k \cdot q \cdot R_m^2 \quad (29)$$

Substituting the values for $k_{1,2}$, q , l and R_m , we get the values for critical pressure and bending stiffness. m_{tot} , total mass of bellows per unit length. m_{tot} for both the cases is obtained.

$$EI_{(1)} = 26.77 \text{ Nm}^2:$$

$$EI_{(2)} = 27.8 \text{ Nm}^2:$$

$$m_{\text{tot}} = 3.84 \text{ kg/m}$$

Also, the rotatory inertia (J) of bellows per unit length is $J = 0.00826354 \text{ kgm}$. The influence of rotational restraint (T) on natural frequency is observed by varying from 0.01 to 10^{10} at 0.0MPa, 10MPa and up to critical pressure of 166MPa. Equal rotations are assumed on either ends, so $T=T_1=T_2$.

6. Results and Discussion

Tables 1 and 2, gives a comparison of the first mode frequencies obtained using the approximate Rayleigh-Ritz method for multiply bellows and compared with the exact frequencies.

Table 1: Comparison of Transverse Frequencies $T_1=T_2=T=1 \times 10^{10}$, $P=166.0 \text{ MPa}$ & $n=3$

Mode No. \tilde{N}	Exact n_{321} Rao.C.K [5] ω , radian/s	Exact n_{400} Rao.C.K. [5] ω , radian/s	Rayleigh n_{321} ω , radian/s	Rayleigh n_{400} ω , radian/s
1	7036.1	4726.8	6212.1	6212.1

The error of frequency obtained by the Rayleigh quotient method is about 33% or less for case 1 and 20% in case 2 for first mode respectively. Therefore, the approximate Rayleigh quotient formula has to be judiciously used for multiply bellows. However, in case of single ply bellows the percent error is less than half and so can be treated precise enough to use for the natural frequency estimation.

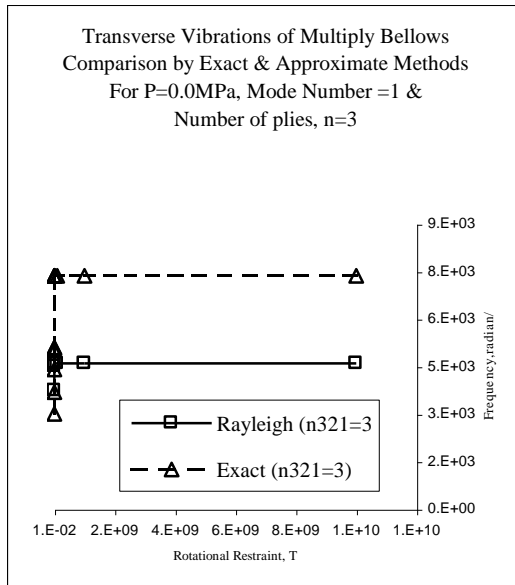
Table 2: Comparison of Transverse Frequencies $T_1=T_2=T=1 \times 10^{10}$, $P=166.0 \text{ MPa}$ & $n=1$

Mode No. \tilde{N}	Exact $n_{321}=1$ Rao.C.K [5] ω , radian/s	Rayleigh $n_{321}=1$ ω , radian/s
1	3400.1	3973.2

Table 3 shows the influence of rotational restraint parameter T on the natural frequency. It is found that the percent variation in frequency is less than 10% than that obtained by exact method at the critical pressure. Also, for the conditions and bellows dimensions assumed there is absolutely no change in the frequency for plies of 321 and combination of alloy 400 and 321 respectively. Frequency values are obtained for internal pressures of 0.0MPa and critical pressure 166MPa respectively.

7. Conclusions

It is found that vibrations related to multiply bellows has not been dealt by previous authors. The approximate natural frequency for multiply bellows is derived using the Rayleigh-Ritz method. The same problem that was dealt by the authors [5] to determine the exact frequencies is considered here to compare the frequencies obtained using the approximate solution.



The influence of rotational restraint at either end is studied and the results are presented in Table 3. It is found that the first mode frequency of multiply bellows is nearly 50% away than the exact and is supposed to be quite significant. Though, the method can be used as first approximation by the designers, it is found that it is not a reliable one in comparison with the exact method. It is found that the frequency of multiply bellows of for n_{321} and n_{400} for the plies is same.

References

1. EJMA – “The Standards of the Expansion joint Manufacturers Association Inc”. New York, ASME, 1984, p221.
2. Jakubauskas V.F, “Practical Predictions of Natural Frequencies of Transverse Vibrations of Bellows Expansion Joints”, Mechanika- Kaunas, Technologija, 1998, No.3 (14), p47-52.
3. Jakubauskas.V.F, “Transverse Vibrations of bellows Expansion Joints”- PhD. Thesis – Hamilton, Ontario, Canada: McMaster University, 1995, PP145-150.
4. Kameswara Rao.C and Radhakrishna.M, “Transverse Vibrations of Single Bellows Expansion Joint Restrained against Rotation”, Proceedings of Tenth International Conference on Nuclear Engineering, USA, Paper # 22090, April 14-18,2002.
5. Morishita.M. et al., “Dynamic Analysis Methods of Bellows Including Fluid Structure Interaction”, ASME Pressure Vessels and Piping Conference, Hawaii, July 23-27, 1989, P149-157.
6. Radhakrishna.M, “Vibrations and Stability of Elastically Restrained Expansion Bellows in Pipelines”- PhD. Thesis –Hyderabad, India, Osmania University, 2003.

Table 3: Transverse Frequencies for varying T (0.01 to 10^{10}), Internal Pressure (P=0.0 MPa, 10 MPa & 166 MPa), Mode number $\tilde{N}=1$ & Number of plies, n=3

	P=0.0 MPa Exact n ₃₂₁ ω, rad/s	P=0.0 MPa Rayleigh n ₃₂₁ ω, rad/s	P=0.0 MPa Exact n ₄₀₀ ω, rad/s	P=0.0 MPa Rayleigh n ₄₀₀ ω, rad/s	P=166 MPa Exact n ₃₂₁ ω, rad/s	P=166 MPa Rayleigh n ₃₂₁ ω, rad/s	P=166 MPa Exact n ₄₀₀ ω, rad/s	P=166 MPa Rayleigh n ₄₀₀ ω, rad/s
T								
0.01	3004.5	3743.5	3063.08	3778.0	2098.8	4451.2	2158.9	4491.4
0.1	3690.9	4497.1	3762.9	4500.6	2999.7	5905.1	3071.7	5915.4
1.0	4407.9	4586.2	4494.0	4586.6	3847.6	6178.5	3933.2	6179.7
10	5002.5	4595.8	5100.3	4595.8	4515.5	6208.7	4612.7	6208.8
10 ²	5093.8	4596.7	5193.5	4596.7	4616.0	6211.7	4715.6	6211.7
10 ³	5103.3	4596.8	5203.0	4596.8	4626.3	6212.1	4725.6	6212.0
10 ⁴	7364.6	4596.8	5204.0	4596.8	7036.8	6212.0	4726.7	6212.0
10 ⁵	7364.8	4596.8	5204.15	4596.8	7036.9	6212.0	4726.8	6212.0
10 ⁶	7364.9	4596.8	5204.16	4596.8	7036.9	6212.0	4726.8	6212.0
10 ⁷	7364.9	4596.8	5204.17	4596.8	7036.9	6212.0	4726.8	6212.0
10 ⁸	7364.9	4596.8	5204.17	4596.8	7036.9	6212.0	4726.8	6212.0
10 ⁹	7364.9	4596.8	5204.17	4596.8	7036.9	6212.0	4726.8	6212.0
10 ¹⁰	7364.9	4596.8	5204.17	4596.8	7036.9	6212.0	4726.8	6212.0

TRANSVERSE VIBRATIONS OF MULTIPLY BELLOWS EXPANSION JOINT ELASTICALLY RESTRAINED AGAINST ROTATION

KAMESWARA RAO.C

*Professor, Mechanical Engineering
Department, Muffakham Jah College
of Engineering & Technology
Hyderabad, India
Phone: 91 040 23811623
email: ckrao_52@yahoo.com*

RADHAKRISHNA .M

*Scientist, Design Engineering Division
Indian Institute of Chemical Technology
Hyderabad, India
Phone: 91 040 27193229
email: madabhushirk@yahoo.com*

Keywords: Multiply bellows, elastic restraint, transverse and vibration

Abstract

This paper presents the study of dynamic aspects of the multiply bellows with elastically restrained ends and under rotatory inertia. The effect of rotational restraint and internal pressure load on response of such bellows configuration is attempted. The coupled response obtained is compared with single ply configuration. Two cases are considered –bellows having same material and different materials for plies.

1. Introduction

Multiply bellows are generally used in applications where higher-pressure capacity is required than a single-ply construction. The multiply construction increases the overall stiffness of the system and reduces deflection. These bellows are manufactured as multi-layered tubes of plies generally ranging in number from 2 to 20 depending on diameter and operating pressure. Each of the thin-

layer acts as a nearly neutral fiber that offers significantly lower resistance to movement in the piping system than a single wall bellow. Therefore, less force is required for actuating multiply bellows. The stresses induced on the individual layers of bellows are a fraction of the stresses induced in the single wall bellows of equal thickness. This results in highest possible service life of bellows.

The multiply design results in lower spring rates for a given pressure capacity. Also the effective cross sectional areas of multiply bellows is less compared to conventional bellows to accommodate a given movement. These two reductions result in lower forces and moments on the anchors, equipment and guides supporting the piping system. The anchors and guides of the system can be dimensioned significantly smaller and more economically. This increases the life of the connected equipment and raises the reliability of the overall piping system.

This type of construction is well suited for applications with vibration or rapid cyclic motion because of the inherent damping provided by the relative inter-ply movement. Fig. 1, shows number of plies and geometrical dimensions of multiply bellows.

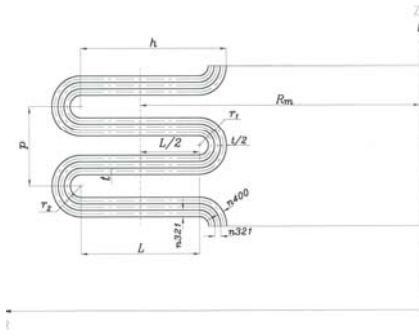


Fig. 1 : Geometrical Dimensions of Multiply Bellows

2. Theoretical Development

An attempt has been made here to derive the transcendental frequency equation for transverse vibrations of multiply bellows with multiple materials of construction for plies. The innermost ply that is in contact with the fluid is of Alloy 400 and compatible to the fluid to resist corrosion and other subsequent two plies are of austenitic stainless steel - type 321 to take care of the pressure capacity.

A literature search shows relatively little work was carried out in predicting the dynamic response of multiply bellows. The previous works contributed by Li Ting-Xin and Jakubauskas. V.F et al. [2] studied the effect of classical fixed-fixed type of boundary conditions for single ply bellows and obtained axial and transverse frequencies there on [3].

Therefore, the paper is an attempt to obtain the flexural vibration characteristics of multiply bellows subjected to an internal pressure and

considers the ends of bellows as elastically restrained against rotation. The inter-ply interaction is not considered here and the plies are considered closely fit.

It is also seen that no provision has been made to this effect in the expansion bellows [EJMA 1] code.

The equations for the transverse vibrations of multiply bellows are derived. Case I considers a multiply bellow that have same material of construction for all the three plies and Case II considers a multiply bellow having different materials of construction. Results are obtained to observe the effect of varying the rotational spring stiffness parameter T from 10 to 10^{10} on natural frequencies.

Bellows having same dimensions as in thesis [6], and having 3 numbers of plies of equal thickness are considered here for comparison purpose. The maximum critical pressure and spring rate are calculated using the formulae given [3].

3. The Differential Equation

The fundamental equation of motion of the equivalent Timoshenko beam [5] is given by-

$$EI \frac{\partial^4 w}{\partial x^4} + P \pi R_m^2 \frac{\partial^2 w}{\partial x^2} - J \frac{\partial^4 w}{\partial x^2 \partial t^2} + m_{tot} \frac{\partial^2 w}{\partial t^2} = 0 \quad (1)$$

Where EI is bending stiffness, P- internal pressure in bellows, J – rotatory inertia per unit length, w –lateral deflection x-axial coordinate, R_m –mean radius of

bellows, m_{tot} is the total mass of bellows per unit length includes mass of bellows and fluid mass and time [4].

Using the technique of Separation of variables, the lateral deflection of the bellows axis 'w' is expressed as-

$$w(x, t) = X(x) \cdot T(t) \quad (2)$$

Where $w(t)$ is a parameter of 'x' and $T(t)$ is the time harmonic function -

$$T(t) = X(x) e^{i\omega t} \quad (3)$$

' ω ' is natural frequency

Differentiating the above equation (Eq.2) and substituting in the differential equation (Eq.1), we get-

$$\frac{\partial^4 X}{\partial x^4} + \frac{(P\pi R_m^2 + J\omega^2)}{EI} \frac{\partial^2 X}{\partial x^2} - \omega^2 \frac{m_{tot}}{EI} X = 0 \quad (4)$$

$$\text{If } c = \sqrt{\frac{(P\pi R_m^2 + J\omega^2)}{2EI}} \quad (5)$$

Then equation (Eq.4) can be written as-

$$\frac{d^4 X}{dx^4} + 2c^2 \frac{d^2 X}{dx^2} - \lambda^4 X = 0 \quad (6)$$

The general solution of equation (6) is given by

$$X(x) = A \sinh \alpha x + B \cosh \alpha x + C \sin \beta x + D \cos \beta x \quad (7)$$

Where A, B, C & D are arbitrary constants respectively. The first two derivatives of equation (Eq.7) are as follows-

$$\begin{aligned} \frac{dX(x)}{dx} &= A\alpha \cosh \alpha x + B\sinh \alpha x + C\beta \cos \beta x \\ &+ D\beta \sin \beta x \end{aligned} \quad (8)$$

$$\begin{aligned} \frac{dX(x)^2}{dX^2} &= A\alpha^2 \sinh \alpha x + B\alpha^2 \cosh \alpha x - \\ &C\beta^2 \sin \beta x - D\beta^2 \cos \beta x \end{aligned} \quad (9)$$

Let the roots of the equation be α & β

$$\begin{aligned} \alpha &= \sqrt{-c^2 + \sqrt{c^4 + \lambda^4}} \\ \beta &= \sqrt{c^2 + \sqrt{c^4 + \lambda^4}} \end{aligned} \quad (10)$$

And

$$\lambda^4 = \sqrt[4]{\frac{m_{tot} \cdot \omega^2}{EI}} \quad (11)$$

At the ends 'A and B', the bellows are connected to short pipe nipples and so are considered to have a rotational stiffness of R_1 and R_2 respectively.

At $x=0$, the boundary conditions are

$$\begin{aligned} X(0) &= 0 \\ EI \frac{\partial^2 X(0)}{\partial x^2} &= -T_1 \frac{\partial X(0)}{\partial x} \end{aligned} \quad (12)$$

At $x=L$, the boundary conditions are

$$\begin{aligned} X(L) &= 0 \\ EI \frac{\partial^2 X(L)}{\partial x^2} &= -T_2 \frac{\partial X(L)}{\partial x} \end{aligned} \quad (13)$$

$$\text{Where } T_1 = \frac{R_1 L}{EI} \text{ and } T_2 = \frac{R_2 L}{EI}$$

Applying the boundary conditions we get-

$$B+D=0 \quad (14)$$

$$EI[B(\alpha L)^2 - D(\beta L)^2] = T_1[A(\alpha L) + C(\beta L)] \quad (15)$$

$$\begin{aligned} A \sinh \alpha L + B \cosh \alpha L + C \sin \beta L \\ + D \cos \beta L = 0 \end{aligned} \quad (16)$$

$$\begin{aligned}
& A\{(\alpha L)(\alpha L \sinh \alpha L + T_2 \cosh \alpha L)\} + \\
& B\{(\alpha L)(\alpha L \cosh \alpha L + T_2 \sinh \alpha L)\} + \\
& C\{(\beta L)(T_2 \cosh \beta L - \beta L \sin \beta L)\} - \\
& D(\beta L)(T_2 \sin \beta L + \beta L \cos \beta L) = 0
\end{aligned} \tag{17}$$

The above set of equations can be written in matrix form.

$$\begin{bmatrix} 0 & 1 & 1 & 1 \\ T_1 \alpha L & -\alpha L^2 & T_1 \beta L & \beta L^2 \\ \sinh \alpha L & \cosh \alpha L & \sin \beta L & \cos \beta L \\ c_1 & c_2 & c_3 & -c_4 \end{bmatrix} \begin{Bmatrix} A \\ B \\ C \\ D \end{Bmatrix} = 0 \tag{18}$$

$$\begin{aligned}
c_1 &= (\alpha L)(\alpha L \sinh \alpha L + T_2 \cosh \alpha L) \\
c_2 &= (\alpha L)(\alpha L \cosh \alpha L + T_2 \sinh \alpha L) \\
c_3 &= (\beta L)(T_2 \cos \beta L + \beta L \sin \beta L) \\
c_4 &= (\beta L)(T_2 \sin \beta L + \beta L \cos \beta L)
\end{aligned} \tag{19}$$

Expanding the matrix and substituting for c_1, c_2, c_3 & c_4 and on simplification, we get the final frequency equation as follows-

$$\begin{aligned}
& \left\{ ((\alpha L)^2 - (\beta L)^2) + \frac{1}{T_1 T_2} (\alpha L)^2 + (\beta L)^2 \right\} \\
& \sinh \alpha L \sin \beta L + 2\alpha L \cdot \beta L (1 - \cosh \alpha L \cos \beta L) + \\
& \left(\frac{1}{T_1} + \frac{1}{T_2} \right) [(\alpha L)^2 + (\beta L)^2] \\
& [(\alpha L) \cosh \alpha L \sin \beta L - (\beta L) \sinh \beta L \cos \beta L] = 0
\end{aligned} \tag{20}$$

The frequency equation is same for Case I and II respectively.

4. Exact Analysis

The various dimensional parameters of U-shaped bellows are same as those that have been considered by Jakubauskas [3].

Mean diameter (D_m) –69.3mm, convolution height, $h=5.71$ mm; convolution pitch, $q=5$ mm; bellows thickness after forming, $t_p=0.28$ mm; number of convolutions, $N=9$; pitch diameter of bellows, $D_b=62.8$ mm; E_{400} at 400 deg F $=2.03 \times 10^{11}$ N/m²; $E_{321}=1.82 \times 10^{11}$ N/m²; operating pressure, $P=0.862 \times 10^6$ N/m² and bellows length, $L = 0.045$ m respectively.

Case I: bellows have SS-321 as same material of construction for all the three plies.

Case II: bellows have first inner ply as Alloy 400 and subsequent two plies as SS-321.

The axial stiffness of bellows is computed by using the expression given below-

$$k_1 = 4R_m E_{321} \left(\frac{t_p}{h} \right)^3 n_{321} \tag{21}$$

$$k_2 = 4R_m [E_{400} n_{400} + E_{321} n_{321}] \left(\frac{t_p}{h} \right)^3 \tag{22}$$

Where, n_{321} and n_{400} represent number of plies of respective material of construction. According to equations (21) and (22), $k_1=8.92 \times 10^6$ N/m and $k_2=9.26 \times 10^6$ N/m.

The maximum critical pressure bellows can withstand and bending stiffness are given by the expressions -

$$P_{\max} = \frac{\pi k_{1,2} q}{6.66 L^2} \tag{23}$$

$$EI = \frac{1}{4} k \cdot q \cdot R_m^2 \tag{24}$$

Substituting the values for $k_{1,2}$, q , L and R_m , we get the values for maximum critical pressure, bending stiffness and m_{tot} , total mass of bellows per unit length. m_{tot} for both the cases is same as the thickness of ply assumed is same.

$$EI_{(1)} = 26.77 \text{ Nm}^2:$$

$$EI_{(2)} = 27.8 \text{ Nm}^2:$$

$$m_{\text{tot}} = 3.84 \text{ kg/m}$$

Also the rotatory inertia (J) of bellows per unit length are found out as $J = 0.00826354 \text{ kgm}$

Substituting the above values in equation (Eq.5) and (Eq.11) we get the values of c and λ for Case I & II respectively.

$$c^2_{(1)} = 732 + 0.000154.\omega^2 \quad (25)$$

$$\lambda^2_{(1)} = 0.3788.\omega \quad (26)$$

$$c^2_{(2)} = 720 + 0.000148.\omega^2 \quad (27)$$

$$\lambda^2_{(2)} = 0.5127.\omega \quad (28)$$

The first lateral mode fundamental frequency is obtained by using bisection method. The rotational restraint T is varied from a minimum value of 0.1 to a maximum of 10^{10} at maximum and minimum internal pressure as calculated. Equal rotations are assumed on either ends and hence $T=T_1=T_2$.

5. Results and Discussion

Table 1 gives a comparison of the frequencies obtained using the bisection method for multiply bellows vis-à-vis to the single ply bellows having elastically restrained ends presented by Rao.C.K et al. [5].

Table 1 Comparison of Frequencies at $T_1=T_2=T=\infty$

Mode	Pressure P, MPa	Rao.C. K. [5] n=1, ω , Radian/s	$n_{321}=3$ ω , Radian/s	$n_{400}=3$ ω , Radian/s
1	0.0	3684.1	7364.8	5204.1
1	10.0	3400.16	7036.9	4726.8

It is seen that the frequencies obtained by considering the ends as elastically restrained are higher than that were found out for single ply bellows. Table 1

presents frequencies obtained for n_{321} and n_{400} respectively.

Table 2 presents the first mode frequencies by varying the rotational restraint parameter T .

Table2: First Mode Frequency for various values of T and at $P=0.0 \text{ Mpa}$

T, Rotational Restraint	ω , Radian/s, $n_{321}=3$	ω , Radian/s, $\tilde{N}=1$, $n_{400}=3$
0.01	3004.5	3063.08
1.0	3690.9	3762.9
10	4407.9	4494.0
10^2	5002.5	5100.3
10^3	5093.8	5193.5
10^4	5103.3	5203.0
10^5	7364.6	5204.0
10^6	7364.8	5204.15
10^7	7364.9	5204.16
10^8	7364.9	5204.17
10^9	7364.9	5204.17
10^{10}	7364.9	5204.17

Fig 2: Transverse Vibrations of Multiply bellows at $P=0.0 \text{ MPa}$

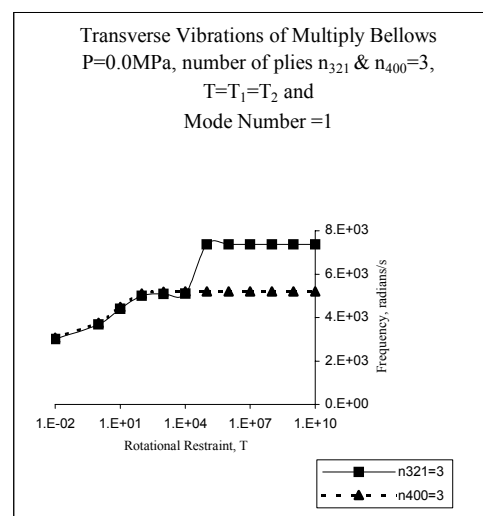


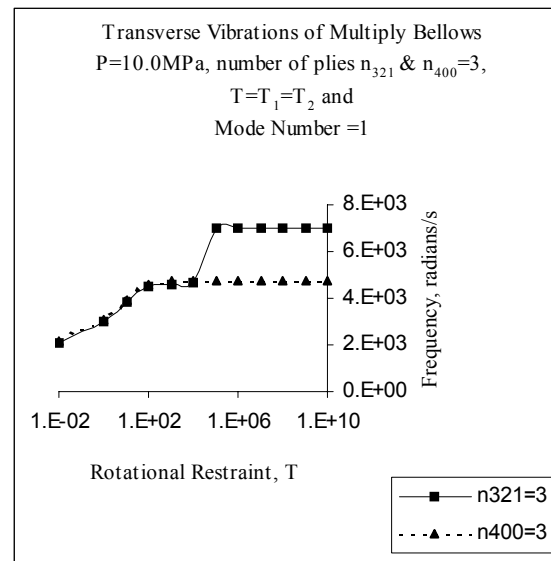
Table 3 presents the first mode frequencies by varying the rotational restraint parameter T .

Table 3: First Mode Frequency for various values of T and at $P=10\text{MPa}$

T , Rotational Restraint	ω , Radian/s, $n_{321}=3$	ω , Radian/s, $\tilde{N}=1$ $n_{400}=3$
0.01	2098.8	2158.9
1.0	2999.7	3071.7
10	3847.6	3933.2
10^2	4515.5	4612.7
10^3	4616.0	4715.6
10^4	4626.3	4725.6
10^5	7036.8	4726.7
10^6	7036.9	4726.8
10^7	7036.9	4726.8
10^8	7036.9	4726.8
10^9	7036.9	4726.8
10^{10}	7036.9	4726.8

It is seen that as rotational stiffness, T increases and approaches infinity, the lateral frequencies increases in both the cases. It is interesting to note that the transverse frequencies of multiply bellows having different materials of construction for plies lie midway between single-ply and multiply bellows with same materials of construction for plies.

Fig 3: Transverse Vibrations of Multiply Bellows at $P=10\text{MPa}$



6. Conclusions

The exact method developed would determine the dynamic characteristics of multiply bellows for its lateral vibrations. The theoretical formulations are based on the equations of an equivalent Timoshenko beam. The influence of elastically rotational restraint at either end is considered and the first fundamental mode frequency is quite significant.

References

1. EJMA – “The Standards of the Expansion joint Manufacturers Association Inc”. New York, ASME, 1984, p221.
2. Jakubauskas V.F, “Practical Predictions of Natural Frequencies of Transverse Vibrations of Bellows Expansion Joints”, Mechanika- Kaunas, Technologija, 1998, No.3 (14), p47-52.
3. Jakubauskas.V.F, “Transverse Vibrations of bellows Expansion Joints”- PhD. Thesis – Hamilton, Ontario, Canada: McMaster University, 1995, PP145-150.
4. Kameswara Rao.C and Radhakrishna.M, “Transverse Vibrations of Single Bellows

Expansion Joint Restrained against Rotation”,
Proceedings of Tenth International Conference
on Nuclear Engineering, USA, Paper # 22090,
April 14-18,2002.

5. Morishita.M. et al., “Dynamic Analysis Methods of Bellows Including Fluid Structure Interaction”, ASME Pressure Vessels and Piping Conference, Hawaii, July 23-27, 1989, P149-157.
6. Radhakrishna.M, “Vibrations and Stability of Elastically Restrained Expansion Bellows in Pipelines”- PhD. Thesis –Hyderabad, India, Osmania University, 2003.

VIBRATION OF DOUBLE BELLAWS TYPE EXPANSION JOINT IN LATERAL AND ROCKING MODES

M. RADHAKRISHNA^a and C.KAMESWARA RAO^b

^a *Design Engineering Division,
Indian Institute of Chemical Technology,
Hyderabad, India
Tel: +90-40-2719 3229
madabhushirk@yahoo.com*

^b *Client Manager,
SciTech Patent Art Services Private Limited,
604A, Aditya Trade Center
Hyderabad, India
Tel: +90-40-2381 1623
ckrao_52@yahoo.com
ckrao@patent-art.com*

Abstract

In this paper the exact frequency and mode shape expressions are derived for universal bellows type of expansion joint in lateral and rocking modes of vibration. The effect of equivalent support stiffness and mass on the natural frequencies and mode shapes are studied in detail and the results for a range of non-dimensional parameters are presented in graphical forms which should be useful for piping and bellows designers.

Keywords: Double bellows, elastic restraint, lateral, rocking, vibration

1. Introduction

A universal double bellows type of expansion joint has two single bellows in series and is joined by a short pipe spool piece. The primary purpose of this kind of an arrangement is to have a unit that will accept large amounts of lateral deflection. The amount of lateral deflection that it can accept is a function of the amount of angulations of each bellows can absorb and the distance between the bellows. So, for a given bellows element, the amount of lateral deflection capability can be increased or decreased by simply changing the length of the center spool [1-2].

Most of the previous studies on transverse vibration of double bellows consider the classical fixed-fixed end condition [3-4]. In an earlier publication by the authors and others, axial vibrations of elastically restrained U-shaped single bellows were analyzed [5-6]. However, based on practical experience the bellows expansion joint is generally subjected to equal

^b Corresponding Author

or unequal rotations at the ends. Therefore, the study focuses in investigation of the effect of elastically restrained ends on vibrations of double bellows expansion joint in lateral and rocking modes. Universal expansion joint has two single bellows joined by a connector pipe and generally installed to absorb combination of the three basic movements i.e. axial, lateral and angular. However, there are different types of expansion joints, specifically designed and developed to meet the desired end functionality.

The design analysis of an expansion bellow is quite complex because it is stressed due to operating pressure and axial deflection. At the same time the bellows have to be stable and work-up to the designed fatigue life. Any assumed bellows geometry which is defined by diameter, depth of convolution, pitch, number of convolutions, thickness and number of plies for a given material of construction and manufacturing technique has to satisfy the above criteria. All the factors are interdependent and so the overall bellows design is affected if any one of the variables changes [7-9].

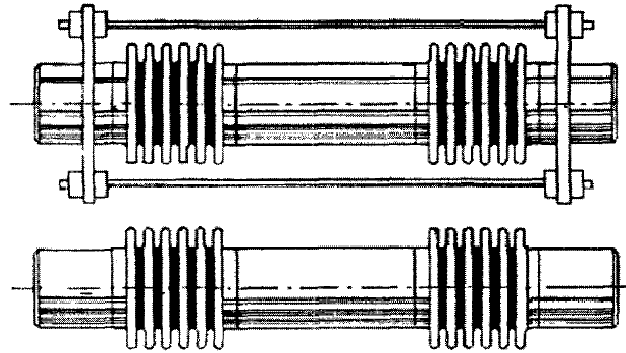


Fig 1: Universal Double Bellows

2. Modeling of Problem

Figure 2 shows a mathematical model that depicts the vibration problem of double bellows type expansion joint. It comprises of an expansion joint of length ' L ' for the bellow, a short pipe connector piece of length ' a ' and elastic rotational restraints at the ends

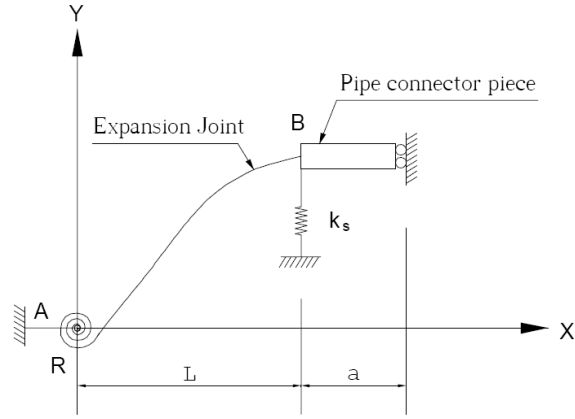


Fig 2: Mathematical Model of Double Bellows in Lateral Mode

3. Governing Differential Equation and Solution Method

The effect of rotatory inertia is considered here in the present study, while the effect of transverse shear deformation is neglected. 1. Since the transverse vibration of a bellows is being modeled as a relatively short beam in bending, only rotary inertia is considered to be important and so Timoshenko Beam Theory is used. For short beams in bending, the effect of shear deformation is either equal or greater than the rotary inertia. Also, it was shown by Morishita et al, [10] that the effect of shear deformation on bending of bellows was negligibly small. The calculation of ratio of shear to rotary inertia, was shown to be of the order of 10^{-3} by Jakubauskas, 1996 [11], confirmed further that the effect of shear deformation is negligible and hence, the shear term in the equation below is neglected

The general form of equation of motion is

$$EI \frac{\partial^4 w}{\partial x^4} + m_{tot} \frac{\partial^2 w}{\partial t^2} - \left(\rho I + \rho \frac{EI}{Gk'} \right) \frac{\partial^4 w}{\partial x^2 \partial t^2} + \frac{\rho^2 I}{Gk'} \frac{\partial^4 w}{\partial t^4} + 2\rho_f A_{min} V \frac{\partial^2}{\partial t \partial x} + \left(P\pi R_m^2 + \rho_f A_{min} V^2 \right) \frac{\partial^2 w}{\partial x^2} = 0 \quad (I)$$

Where EI is the effective bending stiffness of bellows, m_{tot} is the mass per unit length of the bellows, ρI in the third term is effective rotary inertia of bellows and contained fluid.

The terms containing Gk' accounts for shear and the fifth term is the coriolis force and the sixth term accounts for the curvature effects of pressure and centrifugal forces. Additionally, since the research was motivated by bellows vibrations excited by internal fluid flow, the beam is represented by a pipe conveying fluid of density, velocity V , pressure P and net flow area A_{min} .

The influence of variation of rotational restraint T on the natural frequency and mode shape is discussed. The variable separable method is used in computation of the natural frequencies. The frequencies are obtained by exact analysis and compared with the approximate methods considered by the previous authors on the subject.

The differential equation of vibration of bellows for double bellows expansion joint after neglecting the shear and coriolis terms in Eq. (I) is given by (11)

$$EI \frac{\partial^4 w}{\partial x^4} + P\pi R_m^2 \frac{\partial^2 w}{\partial x^2} - J \frac{\partial^4 w}{\partial x^2 \partial t^2} + m_{tot} \frac{\partial^2 w}{\partial t^2} = 0 \quad (1)$$

Where EI is the bending stiffness; P internal pressure; J is the mass moment of inertia per unit length; m_{tot} the total mass of bellows per unit length including bellows mass and fluid mass; x is axial coordinate; R_m is mean radius of bellow; w is the deflection and t the time. Using the variable separable method, the lateral deflection of the bellows axis 'w' can be expressed as

$$w(x,t) = X(x).e^{i\omega t} \quad (2)$$

By differentiating Eq. (2) and substituting into Eq. (1), we get

$$\frac{\partial^4 X}{\partial x^4} + \frac{(P\pi R_m^2 + J.\omega^2)}{EI} \frac{\partial^2 X}{\partial x^2} - \omega^2 \frac{m_{tot}}{EI} X = 0 \quad (3)$$

By introducing the following non-dimensional parameters

$$c = \frac{P\pi R_m^2 + J\omega^2}{2EI} \text{ and } \lambda = \sqrt[4]{\frac{m_{tot} \omega^2}{EI}} \quad (4)$$

Eq. (3) may be expressed as

$$\frac{d^4 X}{dx^4} + 2c^2 \frac{d^2 X}{dx^2} - \lambda^4 X = 0 \quad (5)$$

The general solution of Eq. (5) is given by

$$X(x) = A \sinh \alpha x + B \cosh \alpha x + C \sin \beta x + D \cos \beta x \quad (6)$$

Where A, B, C and D are constants and α, β are roots of Eq. (6) and are given by

$$\alpha = \sqrt{-c^2 + \sqrt{c^4 + \lambda^4}} \quad (7)$$

$$\beta = \sqrt{c^2 + \sqrt{c^4 + \lambda^4}} \quad (8)$$

4. Lateral Mode of Vibration

The pipe that connects the two bellows undergoes a pure translation motion due to the geometry and physical symmetry of the system. The coriolis component of the force acting on the bellows from the fluid flowing inside is neglected. A simple mathematical model is developed. It depicts a bellow connected to a short pipe spool. Now by considering one half of the system, where the left end of bellows has a rotational spring of stiffness 'R' and right end is fixed to vertical rollers.

4.1 Derivation of Frequency Equation

The boundary conditions for such a system are given by

$$w(0,t) = 0; atx = 0 \quad (9)$$

$$EI \frac{\partial^2 X}{\partial x^2} = R \frac{\partial X}{\partial x} \quad (10)$$

$$\text{Let } T = \frac{R}{EI}; \text{ then Eq. (10) is written as } \frac{\partial^2 X}{\partial x^2} = T \frac{\partial X}{\partial x}$$

$$\text{As end B does not rotate, we have } \frac{\partial w(L,t)}{\partial x} = 0 \text{ as the third boundary condition} \quad (11)$$

The fourth boundary condition at B, is the shear force Q (L, t) of the bellows

$$\frac{d^3 w(L)}{dx^3} = \frac{-w^2 \{M_s + (m_p + m_{f3})a\}}{EI} \cdot X(L) + \frac{k_s}{EI} (L) \quad (12)$$

$$\text{Let } b = \frac{-w^2 \{M_s + (m_p + m_{f3})a\}}{EI} - \frac{k_s X(L)}{EI} \quad (13)$$

Where M_s is equivalent lateral support mass, k_s is equivalent spring stiffness of lateral support, m_p is the mass per unit length of the connecting pipe of length 'a' and m_{f3} the mass of the fluid per unit length in the pipe

Substitution of Eq.6 and derivatives into boundary condition expressions (9) to (12), would yield a set of linear equations with respect to the constants A, B, C and D

$$B + D = 0 \quad (14)$$

$$\{B(\alpha L)^2 - D(\beta L)^2 - T(A\alpha L + C\beta L)\} = 0 \quad (15)$$

$$A\alpha \cosh \alpha L + B\alpha \sinh \alpha L + C\beta \cos \beta L - D\beta \sin \beta L = 0 \quad (16)$$

$$c_1 A + c_2 B - c_3 C + c_4 D = 0 \quad (17)$$

Where

$$c_1 = \alpha^3 \cosh \alpha L + b \sinh \alpha L \quad (18)$$

$$c_2 = \alpha^3 \sinh \alpha L + b \cosh \alpha L \quad (19)$$

$$c_3 = \beta^3 \cos \beta L - b \sin \beta L \quad (20)$$

$$c_4 = \beta^3 \sin \beta L + b \cos \beta L \quad (21)$$

Equations (14 to 17) can be expressed in matrix form as

$$\begin{bmatrix} 0 & 1 & 0 & 1 \\ +T\alpha & \alpha^2 & +T\beta & \beta^2 \\ \alpha \cosh(\alpha L) & \alpha \sinh(\alpha L) & \beta \cos \beta L & -\beta \sin \beta L \\ c_1 & c_2 & c_3 & c_4 \end{bmatrix} \begin{Bmatrix} A \\ B \\ C \\ D \end{Bmatrix} = \begin{Bmatrix} 0 \\ 0 \\ 0 \\ 0 \end{Bmatrix} \quad (22)$$

For a non-trivial solution, the determinant is formed by the coefficients of algebraic equations and is equal to zero. By expanding the determinant and equating it to zero can obtain the frequency equation of double bellows in lateral mode.

$$\begin{aligned} T \{ & b [(\alpha^2 - \beta^2) \sin \beta L \sinh \alpha L + 2\alpha\beta (1 - \cos \beta L \cosh \alpha L)] - \alpha\beta (\alpha^2 + \beta^2) (\alpha \cos \beta L \sinh \alpha L + \\ & \beta \sin \beta L \cosh \alpha L) \} + b (\alpha^2 + \beta^2) (\alpha \sin \beta L \cosh \alpha L - \beta \cos \beta L \sinh \alpha L) \} - \alpha\beta (\alpha^2 + \beta^2) \\ & \cos \beta L \cosh \beta L = 0 \end{aligned} \quad (23)$$

4.2 Results

A double bellows having dimensions similar to the one considered by Jakubauskas is considered for comparison purpose. The bellow length $L = 0.0693\text{m}$; the mass moment of inertia per unit length, $J = 0.001153\text{kgm}$; the bending stiffness $EI = 5.078 \text{ Nm}^2$; the total mass of bellows $m_{\text{tot}} = 5.13\text{kg/m}$; the total connecting pipe mass, $m_p + m_{f3} = 5.0\text{kg/m}$; and $a = L$ is assumed.

The maximum allowable pressure [5] in bellow is

$$P_{\max} = \frac{\pi k P}{6.666 L^2} \quad (24)$$

Where k is the equivalent axial stiffness of bellows. Substitution of numerical values in Eq. (8) yields

$$c = \sqrt{616.49 + 0.0001135 \omega^2} \quad (25)$$

$$\lambda = 1.0029 \sqrt{\omega} \quad (26)$$

$$b = 0.10235 \omega^2 \quad (27)$$

The frequency Eq. (23) is solved by using the bisection method and results presented in Tables 1 and 2 respectively.

Table 1: Exact Frequencies for $T=\infty$; Mode number $\check{N}=1, 2$; $M_s=0$ and Variable Support Stiffness k_s

Spring Support Stiffness k_s	Frequency, rad/s $\check{N}=1$	Frequency. rad/s $\check{N}=2$
10^2	331.40	3500.68
10^3	333.41	3500.69
10^4	35 2.87	3500.81
10^5	507.89	3501.97
10^6	1256.95	3515.09
10^7	3204.51	4195.03
10^8	3392.10	6856.60
10^9	3399.40	13673.99
10^{10}	3400.15	13678.91

Table 2: Exact Frequencies for mode numbers $\tilde{N}=1, 2$; $T=\infty$; $k_s=0$ and Variable Support Mass M_s

Support mass M_s	Frequency, rad/s $\tilde{N}=1$	Frequency, rad/s $\tilde{N}=2$
1	210.10	3439.57
10	83.18	3406.24
20	59.77	3403.29
30	49.07	3402.27
40	42.61	3401.75
50	38.89	3401.14
60	34.89	3401.12
70	32.32	3401.07
80	30.25	3400.96
90	28.54	3400.87
100	27.08	3400.80

Table 2 presents frequencies obtained by varying the support stiffness k_s for first and second modes of vibration, $\tilde{N}=1$ and $\tilde{N}=2$. It is seen that as stiffness increases from 10^2 to 10^{10} , the frequency increases from 331.40rad/s to 3400.15rad/s, which is a steep rise of almost 90%. It is found that the transverse frequency of the bellows remains constant from stiffness of 10^8 onwards.

The effect of varying the support mass on the frequency of vibration is studied and the results presented in Table 3. By varying the support mass, it is found that there is a steep drop in the frequency by about 87% as the mass increases from 1 to 100 for the first mode of vibration, $\tilde{N}=1$. For the second mode of vibration i.e. $\tilde{N}=2$., the frequency drops to about 1%.

4.3 Mode Shape

As given above, we know the boundary conditions of double bellows subjected to transverse mode of vibration

At $x = L$

$$\frac{dX(x=L)}{dx} = 0 \quad (28)$$

Differentiation of Eq. (6) gives

$$A\alpha \cosh \alpha L + B\alpha \sinh \alpha L + C\beta \cos \beta L - D\beta \sin \beta L = 0 \quad (29)$$

Substitution of boundary conditions in Eq. (29)

$$\frac{d^3 X}{dX^3} = 0 \quad (30)$$

We know

$$\alpha^3 (\cosh \alpha L + b \sinh \alpha L) A + (\alpha^3 \sinh \alpha L + b \cosh \alpha L) B - (\beta^3 \cos \beta L - b \sin \beta L) C + (\beta^3 \sin \beta L + b \cos \beta L) D = 0, \quad (31)$$

Where c_1 , c_2 , c_3 and c_4 have already been defined

$$L^2 (B\alpha^2 - D\beta^2) = \frac{R_1 L}{EI} (\alpha L A + CL\beta) \quad (32)$$

$$B(\alpha L)^2 - D(\beta L)^2 - T_1 (A\alpha L + CL\beta) \quad (33)$$

Substitution of $B = -D$ in Eq. (33)

$$-T_1 (A\alpha L + CL\beta) = D \{ (\alpha L)^2 + (\beta L)^2 \} \quad (34)$$

We know,

$$A\alpha \cosh \alpha L + B\alpha \sinh \alpha L + C\beta \cos \beta L - D\beta \sin \beta L = 0 \quad (35)$$

Substitution of $B = -D$ in Eq. (35)

$$A\alpha \cosh \alpha L - D\alpha \sinh \alpha L + C\beta \cos \beta L - D\beta \sin \beta L = 0 \quad (36)$$

$$A\alpha \cosh \alpha L + C\beta \cos \beta L = D [\alpha \sinh \alpha L + \beta \sin \beta L] \quad (37)$$

Multiplying Eq. (34) by $\cosh \alpha L$ and Eq. (37) by $T_1 L$ and cancellation of like terms A and

C , the ratios $\frac{C}{D}$ and $\frac{A}{D}$ are obtained

$$C' = \frac{C}{D} = \left\{ \frac{[(\alpha L)^2 \cosh \alpha L + (\beta L)^2 \cosh \alpha L] - [\alpha \sinh \alpha L + \beta \sinh \beta L] T_1}{\beta L (\cosh \alpha L + T_1 \cos \beta L)} \right\} \quad (38)$$

$$A' = \frac{A}{D} = \left\{ \frac{[(\alpha L)^2 \cos \beta L + (\beta L)^2 \cos \beta L] - [\alpha \sinh \alpha L + \beta \sinh \beta L]}{(T_1 \alpha L \cos \beta L + \alpha L \cosh \alpha L)} \right\} \quad (39)$$

$$\text{Substitution } \frac{B}{D} = -1$$

$$y_{\max} = D \left[\frac{A}{D} \alpha \cosh \alpha L \xi + \frac{B}{D} \alpha \sinh \alpha L \xi + \frac{C}{D} \beta \cos \beta L \xi - \beta \sin \beta L \xi \right] \quad (40)$$

$$\text{where } \xi = \frac{C}{L}$$

$$\frac{y_{\max}}{D} = A' \alpha \cosh \alpha L \xi - \alpha \sinh \alpha L \xi + C' \beta \cos \beta L \xi - \beta \sin \beta L \xi \quad (41)$$

$$A' = \frac{A}{D} = \left\{ \frac{\{(\alpha L)^2 \cos \beta L + (\beta L)^2 \cos \beta L\} - \{\alpha L \sinh \alpha L + \beta L \sin \beta L\}}{(T_1 \alpha L \cos \beta L + \alpha L \cosh \alpha L)} \right\} \quad (42)$$

$$C' = \frac{C}{D} = \left\{ \frac{\{(\alpha L)^2 \cosh \alpha L + (\beta L)^2 \cosh \alpha L\} + T_1 \{\alpha L \sinh \alpha L + \beta L \sin \beta L\}}{\beta L (\cosh \alpha L + T_1 \cos \beta L)} \right\} \quad (43)$$

Therefore, the final mode shape equation is

$$\frac{y}{D} = A' \alpha \cosh \alpha L \xi - \alpha \sinh \alpha L \xi + C' \beta \cos \beta L \xi - \beta \sin \beta L \xi \quad (44)$$

Figures 3 and 4, are mode shapes of double bellows obtained with support stiffness of $k_s=100$ and $k_s=\infty$. The support mass $M_s=0$ and rotational restraint parameter, $T=\infty$. The values y/D are obtained for two modes of vibration, $\tilde{N}=1$ and $\tilde{N}=2$. The ordinate in Figures 3 & 4 is ratio of minimum to maximum values of y/D and are plotted for ξ ranging from 0 to 0.5 for half mode shape. It is found that as ξ varies between 0 to 1 and support stiffness increases, the mode shape follows an upward trend with slight drop and rise at $\xi=0.2$ and 0.3 and then remains constant approaching infinity. This feature is observed for both the modes of vibration $\tilde{N}=1$ and $\tilde{N}=2$. Figure 5, is mode shape of double bellows obtained by varying rotational restraint T from 0.01 to 100. The support

stiffness $k_s = 100$ and support mass $M_s = 0$. It is found that as T increases the ratio y/D decreases. It is observed that there is a sharp rise in y/D at $T=100$, and $\xi=0.1$. Further, there is no significant change in y/D by varying T from 0.01 to 10.

Table 3: y/D at $T=\infty$, $M_s=0$ and $N=1$

ξ	$y/D, k_s=100$	$y/D, k_s=\infty$
0.1	0.9×10^{-8}	-0.14×10^{-6}
0.2	0.18×10^{-7}	-0.27×10^{-6}
0.3	0.4×10^{-7}	-0.39×10^{-6}
0.4	0.37×10^{-7}	-0.55×10^{-6}
0.5	0.66×10^{-7}	-0.72×10^{-6}

Table 4: y/D at $T=\infty$, $M_s=0$ and $N=2$

ξ	$y/D, k_s=100$	$y/D, k_s=\infty$
0.1	0.83×10^{-8}	0.17×10^{-5}
0.2	0.16×10^{-7}	0.34×10^{-5}
0.3	0.23×10^{-7}	0.51×10^{-5}
0.4	0.33×10^{-7}	0.68×10^{-5}
0.5	0.43×10^{-7}	0.85×10^{-5}

Table 5: y/D for $T=0.01$ to 100

ξ	$y/D, T=0.01$	$y/D, T=0.1$	$y/D, T=1.0$	$y/D, T=10$	$y/D, T=100$
0	0	0	0	0	0
0.1	-4.73	-4.73	-4.98	-7.74	-1.04
0.2	-9.42	-9.47	-9.97	-15.5	-2.08
0.3	-14.1	-14.9	-14.9	-21.2	-3.13
0.4	-18.8	-18.9	-19.9	-30.9	-4.17
0.5	-23.5	-23.6	-24.9	-39.74	-5.21
0.6	-18.8	-18.9	-19.9	-30.9	-4.17
0.7	-14.1	-14.9	-14.9	-21.2	-3.13
0.8	-9.42	-9.47	-9.97	-15.5	-2.08
0.9	-4.73	-4.73	-4.98	-7.74	-1.04
1	0	0	0	0	0

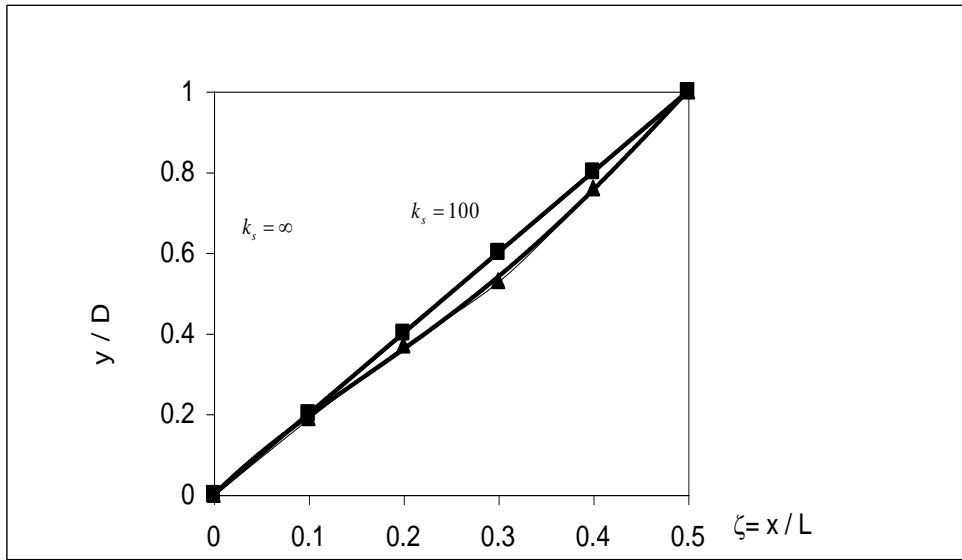


Fig. 3: Mode Shape at $T = \infty$; $k_s = 100$ and $k_s = \infty$; $M_s = 0$ and $\tilde{N} = 1$

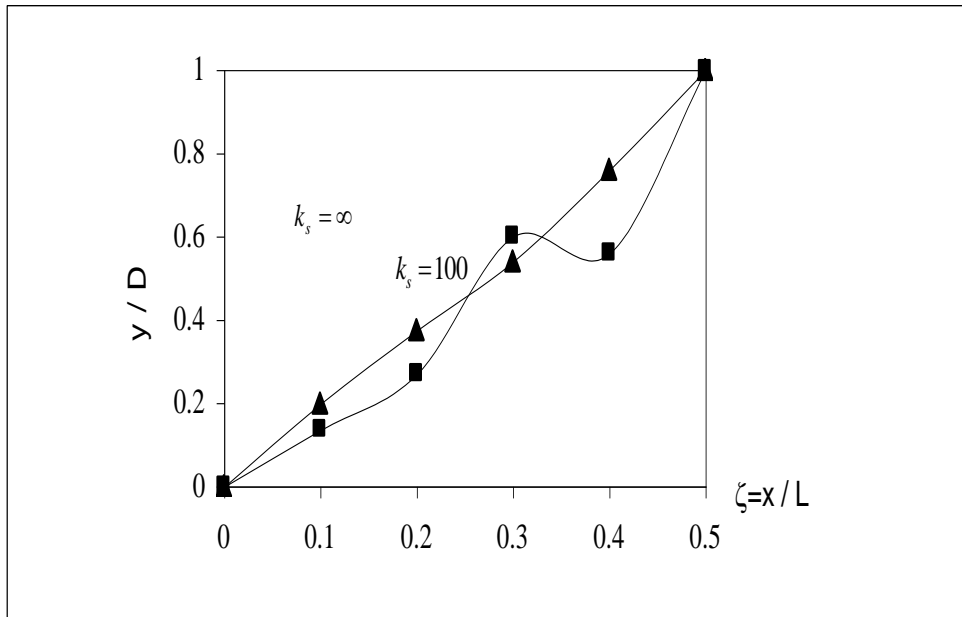


Fig. 4: Mode Shape at $T = \infty$; $k_s = 100$ and $k_s = \infty$; $M_s = 0$ and $\tilde{N} = 2$

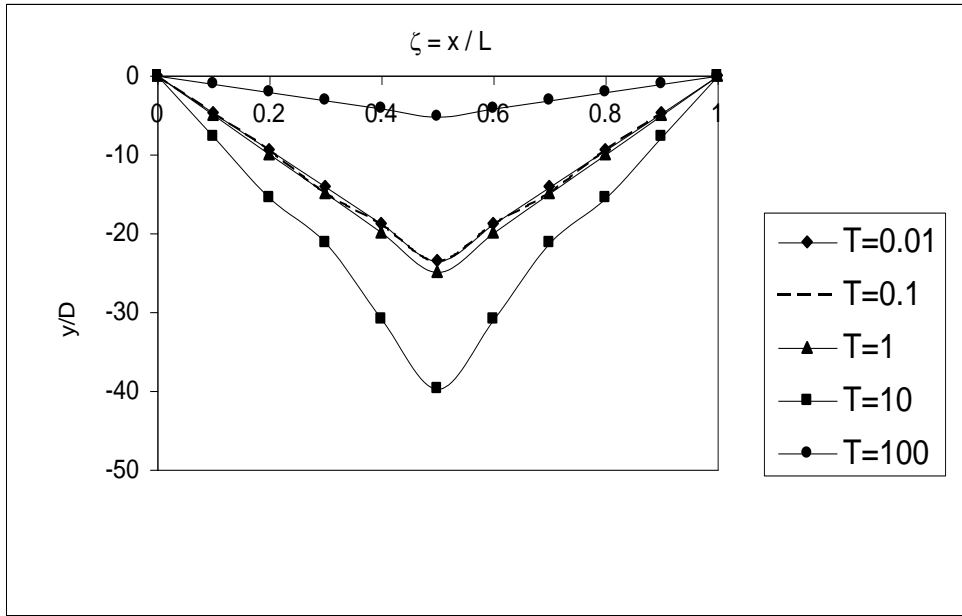


Fig: 5 Mode Shape for T varying from 0.01 to 100; $k_s=100$ $M_s=0$

5. Rocking Mode of Vibration

The physical representation of the model of bellows subjected to vibrations and in rocking mode is shown in Fig.6. The mid point of the connecting pipe does not translate because of the geometrical symmetry of the system with respect to the imaginary vertical axis. Therefore, the system at left end 'A' is elastically restrained having a rotational stiffness 'R' while the right end 'B' is simply supported and held at the midway of the connecting pipe. The coriolis forces acting on the bellows due to the fluid forces are neglected.

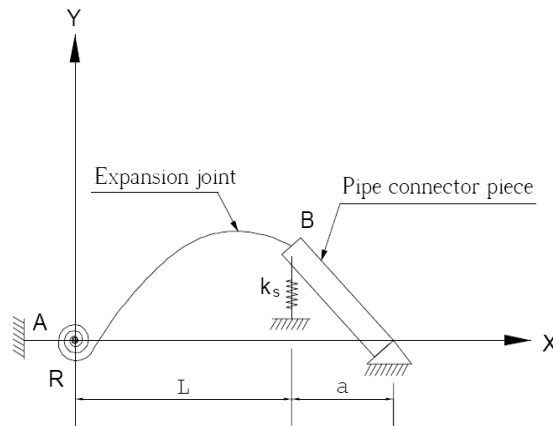


Fig 6. Mathematical Model of Double Bellows in Rocking Mode

5.1 Derivation of Frequency Equation

As shown in Fig. 6 the boundary conditions at ends ‘A’ and ‘B’ are given by

$$\frac{dX(L)}{dx} = -\frac{X(L)}{a} \quad (45)$$

$$\frac{d^3 X(L)}{d x^3} = -\frac{d^2 X(L)}{d x^2} \frac{L}{a} - \frac{P \pi R_m^2}{EI} \frac{dX(L)}{dx} - \frac{J \omega^2}{EI} \frac{dX(L)}{dx} - \omega^2 \frac{J_{tot}}{EI_a^2} X(L) + \frac{k_s}{EI} X(L) \quad (46)$$

$$w(0, t) = 0 \text{ at } x = 0$$

$$B + D = 0 \quad (47)$$

$$EI (B\alpha^2 - D\beta^2) = T_1 (A\alpha - C\beta) \quad (48)$$

$$\frac{\partial w(L, t)}{\partial x} = \frac{1}{a} w(L, t) \quad (49)$$

$$a [A\alpha \cosh\alpha L + B\alpha \sinh\alpha L + C\beta \cos\beta L - D\beta \sin\beta L] + [A \sinh\alpha L + B \cosh\alpha L + C \sin\beta L + D \cos\beta L] = 0 \quad (50)$$

$$d_1 A + d_2 B + d_3 C - d_4 D = 0 \quad (51)$$

Where

$$d_1 = (\alpha a \cosh\alpha L + \sinh\alpha L) \quad (52)$$

$$d_2 = (\alpha a \sinh\alpha L + \cosh\alpha L) \quad (53)$$

$$d_3 = (\beta a \cos\beta L + \sin\beta L) \quad (54)$$

$$d_4 = (\beta a \sin\beta L - \cos\beta L) \quad (55)$$

The other boundary condition at end ‘B’ is derived from the differential equation for one-half of the pipe OB.

$$\frac{\partial^3 w(L, t)}{\partial x^3} = \frac{\partial^3 w(L, t)}{\partial x^2} \frac{1}{a} - \frac{P\pi R_m^2}{EI} \frac{\partial w(L, t)}{\partial x} + \frac{k_b w(L, t)}{EI} + \frac{J \partial^3 \omega(L, t)}{EI \cdot \partial x \partial t^2} + \frac{J_{tot} \partial^2 \omega(L, t)}{EI \cdot a^2 \partial t^2} \quad (56)$$

The total mass moment of inertia of fluid and bellows (of one-half of the connecting pipe) about the point of rotation 'O', including the inertia of lateral supports is expressed as

$$J_{tot} = \frac{m_p + m_{f3}}{3} a^3 + \frac{2m_p + m_{f3}}{4} a R^2 + M_s a^2 \quad (57)$$

By eliminating the time harmonic function and rewriting the expression

$$X(0) = 0 \quad (58)$$

$$\frac{d^3 X(L)}{dx^3} = -\frac{1}{a} \frac{d^2 X(L)}{dx^2} - 2c^2 \frac{d X(L)}{dx} - b X(L) \quad (59)$$

Where 'c' and 'λ' are defined in equations (7) & (8) and b is given by

$$b = \omega^2 \left(\frac{J_{tot}}{EI a^2} - \frac{k_s}{EI} \right)$$

Eq. (59) is written as

$$\{\alpha^3 \cosh \alpha L + (\alpha^2/a) \sinh \alpha L + 2c^2 \cosh \alpha L + b \sinh \alpha L\} A + \{\alpha^3 \sinh \alpha L + (\alpha^2/a) \cosh \alpha L + 2c^2 \alpha \sinh \alpha L + b \cosh \alpha L\} B - \{\beta^3 \cos \beta L + (\beta^2/a) \sin \beta L - 2c^2 \beta \cos \beta L - b \sin \beta L\} C + \{\beta^3 \sin \beta L + (\beta^2/a) \cos \beta L - 2c^2 \beta \sin \beta L + b \cos \beta L\} D = 0 \quad (60)$$

Grouping all like terms and rewriting

$$\{\alpha(\alpha^2 + c^2) \cos \alpha L + (\alpha^2/a + b) \sin \alpha L\} A + \{\alpha(\alpha^2 + 2c^2) \sin \alpha L + (\alpha^2/a + b) \cosh \beta L\} B - \{\beta(\beta^2 - 2c^2) \cos \beta L + (\beta^2/a - b) \sin \beta L\} C + \{\beta(\beta^2 - 2c^2) \sin \beta L - (\beta^2/a - b) \cos \beta L\} D = 0 \quad (61)$$

If

$$a_1 = \frac{\alpha^2}{a+b} \quad (62)$$

$$a_2 = \alpha(\alpha^2 + 2c^2) \quad (63)$$

$$b_1 = \frac{\beta^2}{a-b} \quad (64)$$

$$b_2 = \beta(\beta^2 - 2c^2) \quad (65)$$

$$c_1 = a_1 \sinh \alpha L + a_2 \cosh \alpha L \quad (66)$$

$$c_2 = a_1 \cosh \alpha L + a_2 \sinh \alpha L \quad (67)$$

$$c_4 = b_2 \sin \beta L - b_1 \cos \beta L \quad (68)$$

Eq. (61) is written as

$$c_1 A + c_2 B - c_3 C + c_4 D = 0 \quad (69)$$

The determinant formed by the coefficients of this system of algebraic equations is set equal to zero

$$\begin{Bmatrix} 0 & 1 & 0 & 1 \\ +T_1(\alpha L) & (\alpha L)^2 & +T_1(\beta L) & -(\beta L)^2 \\ d_1 & d_2 & d_3 & d_4 \\ c_1 & c_2 & c_3 & c_4 \end{Bmatrix} \begin{Bmatrix} A \\ B \\ C \\ D \end{Bmatrix} = 0 \quad (70)$$

Expanding the above matrix, we get the final frequency equation of double bellows in rocking mode

$$\left\{ \begin{aligned} &(-\alpha\beta ab_1 - \beta a_2 + \alpha\beta aa_1 + \alpha b_2)(1 - \cosh \alpha L \cos \beta L) - (-\beta_2 aa_1 - \beta b_2 + \alpha_2 ab_1 + \alpha a_2) \\ &(\sin \beta L \sinh \alpha L) + (\alpha\beta ab_2 + \alpha\beta^2 a_2 + \alpha a_1 + \alpha b_1)(\cosh \alpha L \sin \beta L) + \\ &(\beta a_1 + \beta b_1 - a\alpha^2 b_2 + \alpha\beta a_2 a) \sinh \alpha L \cos \beta L \end{aligned} \right\} = 0 \quad (71)$$

5.2 Mode Shape in Rocking Mode

Boundary conditions are

$$X(0) = 0 \quad (72)$$

$$EI \frac{\partial^2 X(0)}{\partial x^2} = R_1 \frac{\partial X(0)}{\partial x} \text{ at end A} \quad (73)$$

$$\frac{\partial X(L)}{\partial x} = -\frac{1}{a} X(L) \text{ at end B} \quad (74)$$

$$\begin{aligned} \frac{\partial^3 w(L,t)}{\partial x^3} = & -\frac{\partial^2 w(L,t)}{\partial x^2} \frac{1}{a} - \frac{P\pi R_m^2}{EI} \frac{\partial^2 w(L,t)}{\partial x^2} + \frac{k_s}{EI} w(L,t) + \frac{J}{EI} \frac{\partial^2 w(L,t)}{\partial x^2 \partial t^2} \\ & + \frac{J}{EI a^2} \frac{\partial^2 w(L,t)}{\partial t^2} \end{aligned} \quad (75)$$

Eq. (75) can be written as

$$\frac{d^3 X(L)}{dx^3} = -\frac{1}{a} \frac{d^2 X(L)}{dx^2} - 2c^2 \frac{dX(L)}{dx} - bX(L) \quad (76)$$

$$\text{Assuming } X(L) = A \sinh \alpha L + B \cosh \alpha L + C \sin \beta L + D \cos \beta L \quad (77)$$

Substitution of $X(0) = 0$ and differentiation of Eq. (77) we get

$$B + D = 0$$

$$R_1 \frac{dX(0)}{dx} = R_1 (A\alpha + C\beta) \quad (78)$$

$$EI \frac{d^2 X(0)}{dx^2} = B\alpha^2 - D\beta^2 \quad (79)$$

Equating Eq. (78) and (79), multiplying both sides by L and substitution of $T_1 = \frac{R_1 L}{EI}$ &

$B = -D$, we get

$$-D[(\alpha L)^2 - D(\beta L)^2] - T_1 (A\alpha + C\beta) = 0 \quad (80)$$

We know,

$$\frac{d X(L)}{d x} = A \alpha \cosh \alpha L + B \alpha \sinh \alpha L + C \beta \cos \beta L - D \beta \sin \beta L \quad (81)$$

And $-\frac{1}{a} X(L)$ is written as

$$-\frac{1}{a}(A \sinh \alpha L + B \cosh \alpha L + C \sin \beta L + D \cos \beta L) \quad (82)$$

$$a(\alpha \cosh \alpha L + B \alpha \sinh \alpha L + C \beta \cosh \alpha L + \sin \beta L) + (A \sinh \alpha L + B \cosh \alpha L + C \sin \beta L + D \cos \beta L) = 0 \quad (83)$$

$$A(\alpha \cosh \alpha L + \sinh \alpha L) + B(\alpha \sinh \alpha L + \cosh \alpha L) + C(a \beta \cos \beta L + \sin \beta L) - D(a \beta \sin \beta L - \cos \beta L) = 0 \quad (84)$$

Writing $B = -D$, and $-T_1(A \alpha + C \beta) = D[(\alpha L)^2 + (\beta L)^2]$, we get

$$A(\alpha \cosh \alpha L + \sinh \alpha L) + C(a \beta \cos \beta L + \sin \beta L) = D(\alpha \sinh \alpha L + \cosh \alpha L + a \beta \sin \beta L - \cos \beta L) \quad (85)$$

Multiplying left hand side of Eq. (85) by $(\alpha \cosh \alpha L + \sinh \alpha L)$ and right hand side of Eq.

(85) by $(T_1 A a)$ and cancellation of 'A' terms to get the ratio $\frac{C}{D}$

$$\frac{C}{D} = \left\{ \frac{T_1 \beta (a \alpha \cosh \alpha L + \sinh \alpha L) + T_1 a (a \beta \cos \beta L + \sin \beta L)}{(a \alpha \cosh \alpha L + \sinh \alpha L)[(\alpha L)^2 + (\beta L)^2] - T_1 a [\alpha \sinh \alpha L + \cosh \alpha L + a \beta \sin \beta L - \cos \beta L]} \right\} \quad (86)$$

Cancellation of 'C' terms to obtain the ratio $\frac{A}{D}$

$$\therefore \frac{A}{D} = \left\{ \frac{T_1 \alpha (a \beta \cosh \beta L + \sin \beta L) + \beta (\alpha \cosh \alpha L - \sinh \alpha L)}{(\alpha \beta a^2 \sinh \alpha L \cosh \beta L + a \beta \cos \beta L \cosh \alpha L + \cos \beta L \sin \beta L (a^2 - 1) - a \beta + \alpha a \sin \beta \sinh \alpha L + \cosh \alpha L \sin \beta L) + \beta [\alpha \sinh \alpha L + \cosh \alpha L + a \beta \sin \beta L - \cos \beta L]} \right\}$$

(87)

If

$$\left. \begin{aligned} A' &= \frac{A}{D} \\ C' &= \frac{C}{D} \\ \frac{B}{D} &= -1 \end{aligned} \right\}$$

(88)

The final mode shape expression is

$$\frac{y(\xi)}{D} = A' \sinh \alpha L - B \cosh \alpha L + C' \sin \beta L + D \cos \beta L$$

(89)

5.3 Results

The fundamental frequencies are obtained for the rocking mode of vibration by varying the support stiffness k_s and support mass M_s and are presented in Tables 6 and 7. It is seen that as support stiffness increases from 10^2 to 10^{15} , the frequency increases from 936.10rad/s to 3856.172rad/s by about 75%.

Results are also obtained by varying the support mass and frequencies of vibration are presented in Table 8. It is found that the frequency drops by 87% as the support mass increases from 1 to 100 for $\tilde{N} = 1$ and by 2% for $\tilde{N} = 2$. The frequencies obtained by the exact method are compared with the work of previous authors and we found that at $k_s=100$ the percentage error is as low as 0.01%, given in Table 8.

Table 6: Rocking mode frequency for $\tilde{N}=1,2$; $T=\infty$ and $M_s=0$

Support Stiffness, k_s	Exact frequency (rad/s) $\tilde{N}=1$	Exact frequency (rad/s) $\tilde{N}=2$
10^2	936.10	3856.17
10^3	937.54	3856.27
10^4	951.83	3857.30
10^5	1083.43	3867.81
10^6	1904.56	3993.81
10^7	3232.53	5950.79
10^8	3386.14	6849.09
10^9	3390.12	6886.40
10^{10}	3400.02	6889.80
10^{15}	3856.17	6889.80

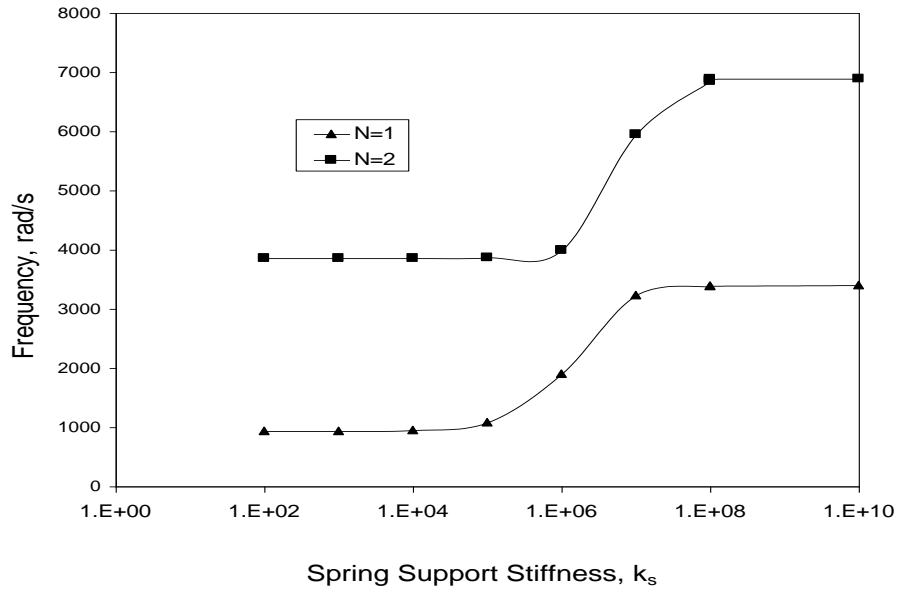


Fig 7: Frequency for $\tilde{N}=1, 2$; $T=\infty$ and $M_s=0$

Table 7: Rocking mode frequency for $\tilde{N}=1, 2$ and $T=\infty$ & $k_s=0$

Support Mass, M_s	Exact frequency (rad/s) $\tilde{N}=1$	Exact frequency (rad/s) $\tilde{N}=2$
1	429.17	3480.08
10	164.62	3411.48
20	117.96	3405.95
30	96.75	3404.05
40	83.97	3403.09
50	75.21	3402.51
60	68.72	3402.12
70	63.66	3401.84
80	59.56	3401.63
90	56.19	3401.47
100	53.33	3401.34

Table 8: Comparison of Frequencies at $T=\infty$

Mode number \tilde{N}	[3] ω , rad/s $k_s=100$	Exact method ω , rad/s $k_s = 100$	Percentage Error
1	935.69	936.10	0.01
2	3855.93	3856.17	0.01

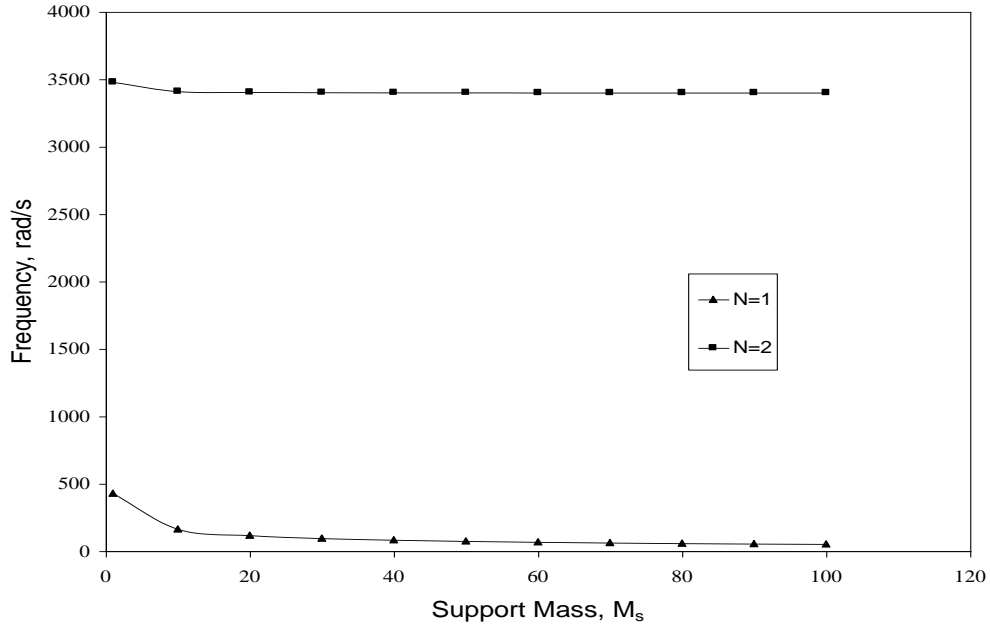


Fig 8: Frequency for $\tilde{N}=1,2; T=\infty$ and $k_s=0$

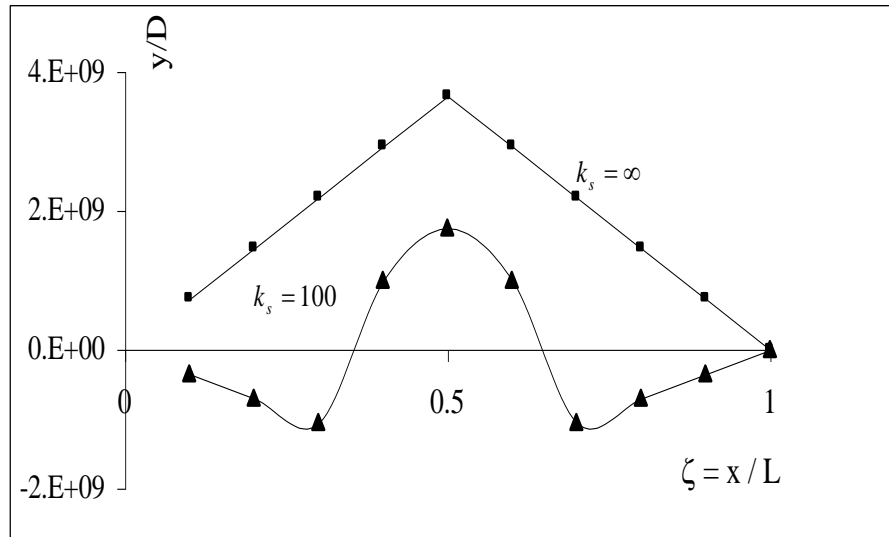


Fig 9: Mode Shape in Rocking Mode for $M_s=0$ & $\tilde{N}=1, T=\infty$

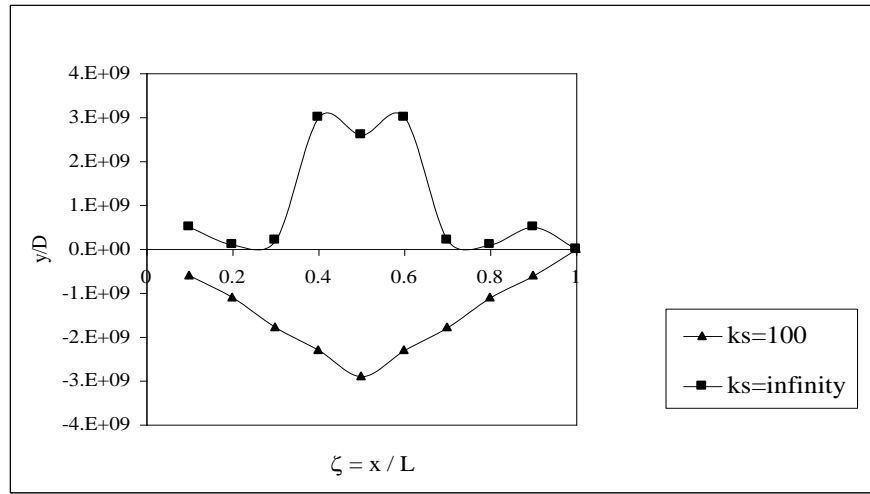


Fig 10: Mode Shape in Rocking Mode for $M_s=0$, $T=\infty$ and $\tilde{N}=2$

The first and second mode shapes of double bellows in rocking mode are shown in Fig 9 and Fig.10 respectively. By varying the value of ξ from 0 to 1 for full cycle, the response is observed at $T=\infty$; $k_s=100$ and $k_s=\infty$. It is found that as support stiffness k_s increases the response is negative.

6. Concluding Remarks

Exact expressions for frequency and mode shapes of double bellows expansion joints in transverse and rocking modes are derived. It is found that the support stiffness and support mass play a vital role in the response of bellows. It is found that the percentage error in the frequency of bellows with lateral supports is very small in comparison to a bellow without lateral supports. This could be a possible method of controlling vibration of bellows expansion joints by suitably altering the stiffness of the supports.

References

1. Kameswara Rao,C., and Radhakrishna,M, “Transverse Vibrations of Double Bellows Expansion Joint Restrained against Rotation”, Proceedings of Tenth International Conference on Nuclear Engineering, USA, ICONE 22092, April 14-18,2002
2. Radhakrishna. M and Kameswara Rao. C. “Vibrations of Fluid Filled Bellows – A-State-of-the-Art”, Proceedings of the National Symposium on Advances in Structural Dynamics and Design, Jan 9-11, 2001

3. Jakubauskas, V.F, "Exact Solution of Natural Frequencies of Double Bellows Expansion Joint", ISSN 1392-1207, Mechanika 1999 No.3 (18)
4. Jakubauskas, V.F., "Transverse Vibrations of bellows Expansion Joints"- PhD. Thesis –Hamilton, Ontario, Canada: Mc Master University, 1995, PP145-150
5. Radhakrishna, M., Kameswara Rao, C., "Axial Vibrations of U-shaped Bellows with Elastically Restrained End Conditions", Thin-walled Structures, 2004, Vol. 42, PP 415
6. Jakubauskas, V.F. & David. S. Weaver, "Axial Vibrations of Fluid Filled Bellows Expansion Joints", Transactions of ASME, Journal of Pressure Vessel Technology, Vol. 118, Nov 1986, P484-490
7. Gerlach, C.R., "Flow Induced Vibrations of Metal Bellows," ASME Journal of Engineering for Industry, Vol. 91, 1969, pp. 1196-1202
8. Jakubauskas, V.F., Weaver, D.S., "Natural Vibrations of Fluid Filled Bellows," ASME PVP Vol. 244, 1992, pp. 145-158.
9. Jakubauskas, V.F., Weaver, D.S., "Transverse Vibrations of Fluid Filled Bellows expansion joints," ASME AD Vol. 53-2, 1997, pp. 463-471
10. Morishita C., Ikahanta N., Kitamura S, "Dynamic Analysis Methods of Bellows Including Fluid-Structure Interaction', PVP-Vol.168. 1989, pp.149-157, New York:ASME
11. Radhakrishna, M., "Vibrations and Stability of Elastically Restrained Expansion Bellows in Pipelines"- PhD. Thesis, Osmania University, Hyderabad, India, Oct 2004, PP142-158
12. Jakubauskas, V.F. & Weaver, D.S, "Transverse Vibrations of Bellows Expansion Joints Part-II: Beam Model Development & Experimental Verification"
13. Jakubauskas, V.F. & Weaver, D.S, "Transverse Vibrations of Bellows Expansion Joints Part-II; Beam Model Development & Experimental Verification"- Journal of Fluids and Structures, 1998, 12, p457-473
14. C. Becht IV, "Predicting Bellows Response by Numerical and Theoretical Methods," Journal of Pressure Vessel Technology, Vol.108, Aug 1986, P334-341
15. Jakubauskas, V.F, "Practical Prediction of Natural Frequencies of Transverse Vibrations of Bellows Expansion Joint", ISSN 1329-1207, Mechanika 1998 No.3 (14)
16. EJMA – "The Standards of the Expansion joint Manufacturers Association Inc". New York, ASME, 1984, P221

BUCKLING OF CIRCULAR PLATES WITH AN *INTERNAL RING* SUPPORT AND ELASTICALLY RESTRAINED EDGE

Lokavarapu Bhaskara Rao ¹, Dr. Chellapilla Kameswara Rao ²

¹ *Assoc. Professor, Department of Mechanical Engineering, DRK College Of Science & Technology, Hyderabad-500043, India, E-mail: bhaskarbabu_20@yahoo.com*

² *Client Manager (Mechanical), Sci-Tech Patent Art (P) Ltd, #604, ATC, Hyderabad-500038, India, E-mail: ckr_52@yahoo.com*

ABSTRACT: Circular plates are commonly used as Structural elements in many Aeronautical, Civil, Mechanical and Naval applications. It is worth noting that these find applications in modeling various fluid-structure interaction problems. Even though the circular symmetry of the problem allows for its significant simplification, additional difficulties often arise due to uncertainty of boundary conditions. This uncertainty occurs because, in many practical applications, the edge of the plate is not free, simply supported or clamped. When the plate's boundary conditions depart from the classical cases, elastic translational constraint should be considered. This paper is concerned with the elastic buckling of circular plates with an *internal ring* support and elastically restrained guided edge against translation. The classical plate theory is used to derive the governing differential equation for circular plate with *internal ring* support and guided elastic edge support system. This work presents the existence of buckling mode switching with respect to the radius of *internal ring* support. The buckling mode may not be *axisymmetric* as previously assumed. The plate may buckle in an *axisymmetric* mode in general, but when the radius of the ring support becomes small, the plate may buckle in an *asymmetric* mode. The optimum radius of the *internal ring* support is also determined. Extensive data is tabulated so that pertinent conclusions can be arrived at on the influence of translational restraint, Poisson's ratio, and other boundary conditions on the buckling of uniform isotropic circular plates. The numerical results obtained are in good agreement with the previously published data.

Keywords: Buckling; Circular Plates; Ring Support; Elastically Restrained Edge; Guided Edge; Mode Switching; Translational Spring Stiffness.

1. INTRODUCTION

Buckling of plates is an important topic in structural engineering. The prediction of buckling of structural members restrained laterally is important in the design of various engineering components. In particular, circular plates with *internal ring* supports find applications in aeronautical (instrument mounting bases for space vehicles), rocket launching pads, aircrafts and naval vessels (instrument mounting bases). Based on the

Kirchhoff's theory, the elastic buckling of thin circular plates has been extensively studied by many authors after the pioneering work published by Bryan [1]. Since then, there have been extensive studies on the subject covering various aspects such as different materials, boundary and loading conditions. Also the buckling of circular plates was studied by different authors [2, 3]. However, these sources only considered axisymmetric case, which may not lead to the correct buckling load. The elastic buckling capacity of in-plane loaded circular plates may be increased significantly by introducing an *internal ring* supports. Laura et al. [4] investigated the elastic buckling problem of the aforesaid type of circular plates, who modeled the plate using the classical thin plate theory. In their study only axisymmetric modes are considered. It is an accepted fact that the condition on a periphery often tends to be in between the classical boundary conditions (free, clamped and simply supported) and may correspond more closely to some form of elastic restraints [5 – 7]. In a recent study, Wang and Wang [8] showed that when the ring support has a small radius, the buckling mode takes the asymmetric form. But they have studied only the circular plate with elastically restrained edge against rotation. The purpose of the present work is to complete the results of the buckling of circular plates with an *internal ring* support and elastically restrained guided edge against translation by including the asymmetric modes, thus correctly determining the buckling loads.

2. DEFINITION OF THE PROBLEM

Consider a thin circular plate of radius R , uniform thickness h , Young's modulus E and Poisson's ratio ν and subjected to a uniform in-plane load N along its boundary, as shown in Fig. 1. Circular plate is assumed to be made of linearly elastic, homogeneous and isotropic material and the effects of shear deformation and rotary inertia are neglected. The edge of the circular plate is guided and elastically restrained against translation and supported by an *internal ring* support, as shown in Fig. 1. The problem at hand is to determine the elastic buckling load of a circular plate with an *internal ring* support and the edge is guided and elastically restrained against translation.

3. FORMULATION OF THE SYSTEM

The plate is elastically restrained against translation on the guided edge of radius R and supported on a ring of smaller radius bR as shown in Fig. 1. Let subscript I denote the inner region $0 \leq \bar{r} \leq b$ and the subscript II denote the outer region $b \leq \bar{r} \leq 1$. Here, all

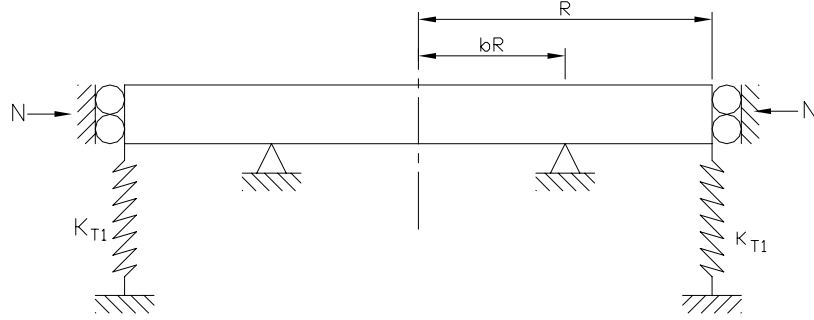


Fig. 1. Buckling of a Circular plate with an Internal *ring* Support and Elastically Restrained Guided edge against Translation

lengths are normalized by R . Using classical (Kirchhoff's) plate theory, the following fourth order differential equation for buckling in polar coordinates (r, θ) .

$$D\nabla^4 w + N\nabla^2 w = 0 \quad (1)$$

Where w is the lateral displacement, N is the uniform compressive load at the edge.

After normalizing the lengths by the radius of the plate R , Eq. (1) can be written as

$$D\nabla^4 \bar{w} + k^2 \nabla^2 \bar{w} = 0 \quad (2)$$

Where $\nabla^2 = \frac{\partial^2}{\partial \bar{r}^2} + \frac{1}{\bar{r}} \frac{\partial}{\partial \bar{r}} + \frac{1}{\bar{r}^2} \frac{\partial^2}{\partial \theta^2}$ is the Laplace operator in the polar coordinates r and θ .

Where \bar{r} is the radial distance normalized by R . $\bar{D} = Eh^3 / 12(1 - \nu^2)$ is the flexural rigidity, $\bar{w} = w / R$, is normalized transverse displacement of the plate. $k^2 = R^2 N / \bar{D}$ is non-dimensional load parameter. Suppose there are n nodal diameters. In polar coordinates (r, θ) set

$$\bar{w}(\bar{r}, \theta) = \bar{u}(\bar{r}) \cos(n\theta) \quad (3)$$

The general solution [9] to Eq. (2) is

$$\bar{u}(r) = C_1 J_n(k\bar{r}) + C_2 Y_n(k\bar{r}) + C_3 \bar{r}^n + C_4 \left\{ \log \bar{r} \right\} \bar{r}^{-n} \quad (4)$$

Where top form of the Eq. (4) is used for $n = 0$ and the bottom form is used for $n \neq 0$, C_1, C_2, C_3 & C_4 are constants, $J_n(.)$ & $Y_n(.)$ are the Bessel functions of the first and seconds of order n , respectively. Substituting Eq. (4) into Eq. (3) yields the following

$$\bar{w}(\bar{r}, \theta) = \left[C_1 J_n(k\bar{r}) + C_2 Y_n(k\bar{r}) + C_3 \bar{r}^n + C_4 \left\{ \log \bar{r} \right\} \bar{r}^{-n} \right] \cos(n\theta) \quad (5)$$

The boundary conditions at outer region of the circular plate in terms of slope and translational stiffness (K_{T1}) is given by the following expressions

$$\frac{\partial \bar{w}_I(\bar{r}, \theta)}{\partial \bar{r}} = 0 \quad (6)$$

$$V_r(\bar{r}, \theta) = -K_{T1} \bar{w}_I(\bar{r}, \theta) \quad (7)$$

The radial Kirchhoff shear at outer edge is defined as follows

$$V_r(\bar{r}, \theta) = -\frac{D}{R^3} \left[\frac{\partial}{\partial \bar{r}} \nabla^2 \bar{w}_I(\bar{r}, \theta) + (1-\nu) \frac{1}{\bar{r}} \frac{\partial}{\partial \theta} \left(\frac{1}{\bar{r}} \frac{\partial^2 \bar{w}_I(\bar{r}, \theta)}{\partial \bar{r} \partial \theta} - \frac{1}{\bar{r}^2} \frac{\partial \bar{w}_I(\bar{r}, \theta)}{\partial \theta} \right) \right] \quad (8)$$

From Eq. (6),

$$\frac{\partial \bar{w}_I(\bar{r}, \theta)}{\partial \bar{r}} = 0 \quad (9)$$

From Eqs. (7) and (8) yields the following

$$\left[\frac{\partial}{\partial \bar{r}} \nabla^2 \bar{w}_I(\bar{r}, \theta) + (1-\nu) \frac{1}{\bar{r}} \frac{\partial}{\partial \theta} \left(\frac{1}{\bar{r}} \frac{\partial^2 \bar{w}_I(\bar{r}, \theta)}{\partial \bar{r} \partial \theta} - \frac{1}{\bar{r}^2} \frac{\partial \bar{w}_I(\bar{r}, \theta)}{\partial \theta} \right) \right] = \frac{K_{T1} R^3}{D} \bar{w}_I(\bar{r}, \theta) \quad (10)$$

Apart from the elastically restrained guided edge against translation, there is an internal elastic ring support constraint and the continuity requirements of slope and curvature at the support, i.e. at $\bar{r} = b$

$$\bar{w}_I(b, \theta) = 0 \quad (11)$$

$$\bar{w}_{II}(b, \theta) = 0 \quad (12)$$

$$\bar{w}'_I(b, \theta) = \bar{w}'(b, \theta) \quad (13)$$

$$\bar{w}''_I(b, \theta) = \bar{w}''_{II}(b, \theta) \quad (14)$$

Where ' denotes the differentiation with respect to \bar{r} . The non-trivial solutions to Eqs. (9), (10), (11)-(14) are sought. The lowest value of k is the square root of the normalized buckling load. From Eqs. (5), (9), (10) and (11)-(14), we get the following equations.

$$\left[\frac{k}{2}P_1\right]C_1 + \left[\frac{k}{2}Q_1\right]C_2 + [n]C_3 + \left\{\frac{1}{-n}\right\}C_4 = 0 \quad (15)$$

$$\begin{aligned} &\left[\frac{k^3}{8}P_3 + \frac{k^2}{4}P_2 - \frac{k}{2}\left(\frac{3}{4}k^2 + n^2(2-\nu)+1\right)P_1 + \left(n^2(3-\nu) - \frac{k^2}{2} - T_{11}\right)J_n(k)\right]C_1 + \\ &\left[\frac{k^3}{8}Q_3 + \frac{k^2}{4}Q_2 - \frac{k}{2}\left(\frac{3}{4}k^2 + n^2(2-\nu)+1\right)Q_1 + \left(n^2(3-\nu) - \frac{k^2}{2} - T_{11}\right)Y_n(k)\right]C_2 + \\ &\left[n^2(n-1)\nu - n^3 - T_{11}\right]C_3 - \left\{\frac{n^2(2-\nu)}{-n^2(n+1)\nu + n^3 - T_{11}}\right\}C_4 = 0 \end{aligned} \quad (16)$$

$$J_n(kb)C_1 + Y_n(kb)C_2 + b^n C_3 + \left\{\frac{\log b}{b^{-n}}\right\}C_4 = 0 \quad (17)$$

$$J_n(kb)C_5 + b^n C_6 \quad (18)$$

$$\frac{k}{2}P_1' C_1 + \frac{k}{2}Q_1' C_2 + nb^{n-1}C_3 + \left\{\frac{1}{b}\right\}C_4 \quad (19)$$

$$-\frac{k}{2}P_1' C_5 - nb^{n-1}C_6 = 0$$

$$\begin{aligned} &\frac{k^2}{4}(P_2' - 2J_n(kb))C_1 + \frac{k^2}{4}(Q_2' - 2Y_n(kb))C_2 \\ &+ n(n-1)b^{n-2}C_3 - \left\{\frac{1}{b^2}\right\}C_4 \\ &-\frac{k^2}{4}(P_2' - 2J_n(kb))C_5 \\ &- n(n-1)b^{n-2}C_6 = 0 \end{aligned} \quad (20)$$

Where, $T_{11} = \frac{K_{T1}R^3}{D}$; C_1, C_2, C_3, C_4, C_5 & C_6 are constants.

$$P_1 = J_{n-1}(k) - J_{n+1}(k); P_2 = J_{n-2}(k) + J_{n+2}(k); P_3 = J_{n-3}(k) - J_{n+3}(k);$$

$$Q_1 = Y_{n-1}(k) - Y_{n+1}(k); Q_2 = Y_{n-2}(k) + Y_{n+2}(k); Q_3 = Y_{n-3}(k) - Y_{n+3}(k);$$

$$P_1' = J_{n-1}(kb) - J_{n+1}(kb); P_2' = J_{n-2}(kb) + J_{n+2}(kb);$$

$$Q_1' = Y_{n-1}(kb) - Y_{n+1}(kb); Q_2' = Y_{n-2}(kb) + Y_{n+2}(kb);$$

The top form of Eqs. (17)-(20) are used for $n = 0$ (axisymmetric buckling) and the bottom form is used for $n \neq 0$ (asymmetric buckling).

4. SOLUTION

For the given values of n, ν, b & T_{11} the above set of equations, gives an exact characteristic equation for non-trivial solutions of the coefficients C_1, C_2, C_3, C_4, C_5 & C_6 . For non-trivial solution, the determinant of $[C]_{6 \times 6}$ must vanish. Mathematica, computer software with symbolic capabilities is used to solve the buckling load parameter k by a simple root search method.

5. RESULTS & DISCUSSIONS

There is a lot of flexibility of the code developed in Mathematica. It is used to determine the buckling load parameter for any range of translational constraints. This code is also implanted for various plate materials by adjusting Poisson's ratio. Since Poisson's ratio occurs as a parameter in most of the equations, the effect of this ratio on the roots of the equations is also considered. The findings are presented in both tabular and graphical form. The buckling loads are calculated for various *internal ring* support radii b , and translational spring stiffness parameter. Poisson's ratio adopted in the present work is 0.3.

Figures. 2 – 4 shows the variations of buckling load parameter, k with respect to the internal *ring* support radius, b for various values of translational spring stiffness parameters. It is observed from Figures 2 - 4 that for a given value of translational spring stiffness parameters, the curve in each case is composed of two segments. This is due to the switching of buckling modes. For a smaller internal *ring* support radius b , the plate buckles in an asymmetric mode (i.e. $n \neq 0$). In this segment (as shown by dotted lines in Figures 2 - 4) the buckling load decreases as b decreases in value. For a larger internal *ring* support radius b , the plate buckles in an axisymmetric mode (i.e. $n = 0$). In this segment (as shown by continuous lines in all the Figures) the buckling load increases as b decreases up to a peak point corresponds to maximum buckling load and thereafter decreases as b decreases in value as shown in Figures. 2 - 4. As $T_{11} \rightarrow \infty$, the edge of the plate becomes clamped and as $b \rightarrow 1$, the buckling solution for this case is 3.83163. This is in good agreement with that of Wang and Wang [8]. It is also observed from the Figures 2 – 4, all curves converge to $k = 3.83163$ as $b \rightarrow 1$.

Fig. 2, shows the variations of buckling load parameter k , with respect to the internal *ring* support radius b , for translational spring stiffness parameter $T_{11}=1000$. The cross over radius in this case is $b=0.1514$. Fig. 3, shows the variations of buckling load parameter k , with respect to the internal *ring* support radius b , for translational spring stiffness parameter $T_{11}=100000$. The cross over radius in this case is $b=0.15226$. Fig. 4, shows the variations of buckling load parameter k , with respect to the internal *ring* support radius b , for translational spring stiffness parameter $T_{11}=\infty$. The cross over radius in this case is $b=0.1532$. Of interest in the design of supported circular plates is the optimal location of the internal *ring* support for maximum buckling load. The optimal solutions for this case are presented in Table 1, for various translational spring stiffness parameters ($T_{11} = 1000, 100000 \& \infty$).

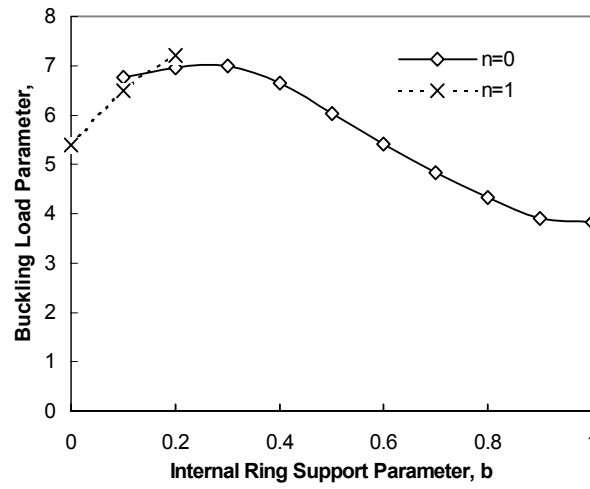


Fig. 2. Buckling Load Parameter, k versus Internal *ring* Support Radius, b for $T_{11} = 1000$

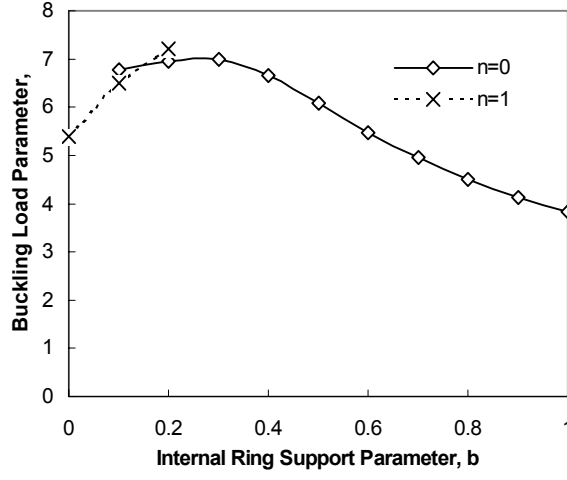


Fig. 3. Buckling Load Parameter, k versus Internal *ring* Support Radius, b for $T_{11} = 100000$

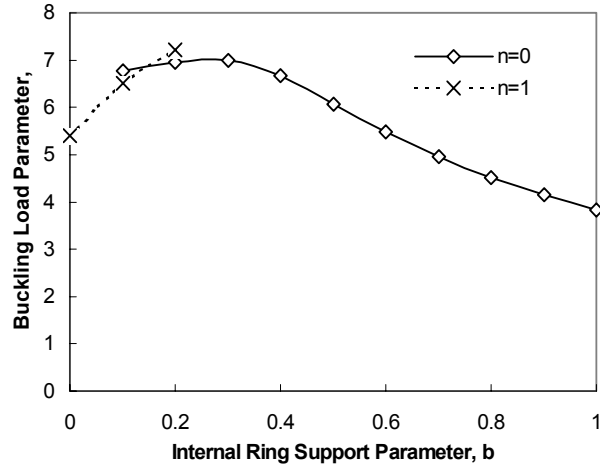


Fig. 4. Buckling Load Parameter, k versus Internal *ring* Support Radius, b for $T_{11} = \infty$

The optimal internal *ring* support radius is found to be independent of the Poisson's ratio and it is affected by the translational spring stiffness parameter. There is no influence of Poisson's ratio on buckling load parameters, for a given values of translational spring stiffness parameters and internal *ring* support radius parameter, as shown in Fig. 5.

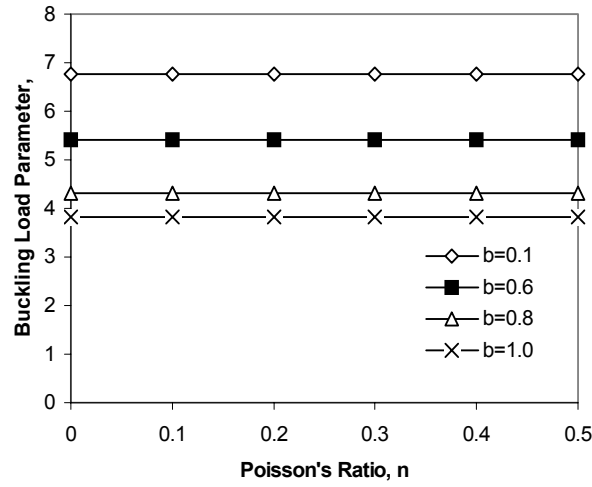


Fig. 5. Buckling Load Parameter, k versus Poisson's Ratio, ν , for $T_{11} = 1000$ and internal ring support radius parameter, b

However, it is observed from the Figures 2 - 4, that the affect of translational spring stiffness parameters, on buckling load parameter is less as compared to rotational spring stiffness parameter [12]. The results of this kind were scarce in the literature. However, the results are compared with the following cases. The buckling load parameters k , for clamped and simply supported edges are compared with those obtained by Wang et al. [10] and Wang et al. [11] as shown in Tables 2. and 3 respectively.

Table 1. Optimum location of the ring support and the corresponding buckling load parameters

T_{11}	1000	100000	∞
b_{opt}	0.3001	0.2995	0.2994
k_{opt}	6.994	6.995	6.996

Table 2. Comparison of Buckling Load Parameter k , with Wang et al. [10] and Wang et al [11] for Clamped Edge for $\nu = 0.3$

Ring support radius, b	Wang et al (1993)	Wang et al (2005)	Present
0.1	----	6.5009*	6.50095*
0.2	6.9559	6.9558	6.95582
0.3	6.9948	6.9947	6.99475
0.4	6.6627	6.6625	6.66248

0.5	6.0749	6.0745	6.07454
0.6	5.476	5.4755	5.4755
0.7	4.9532	4.9526	4.95263
0.8	4.5134	4.5127	4.51266
0.9	4.1448	4.1436	4.1436
0.99	3.8667	3.8604	3.86061

* Asymmetric buckling load parameters

Table 3. Comparison of Buckling Load Parameter k , with Wang et al. [10] and Wang et al [11] for Simply Supported Edge for $\nu = 0.3$

Ring support radius, b	Wang et al (1993)	Wang et al (2005)	Present
0.1	----	4.5235	4.52341
0.2	4.7703	4.7702	4.77018
0.3	5.0711	5.071	5.07091
0.4	5.3297	5.3296	5.32964
0.5	5.3667	5.3666	5.36659
0.6	5.1264	5.1261	5.12606
0.7	4.773	4.7727	4.77266
0.8	4.4219	4.4215	4.42141
0.9	4.1069	4.1063	4.10629
0.99	3.8603	3.8573	3.85742

6. CONCLUSIONS

The paper introduced a Mathematica code for calculation of buckling load. The buckling problem of thin circular plates with an internal *ring* support and elastically restrained guided edge against translation has been solved analytically. Also the buckling loads are given for various translational spring stiffness parameters $[T_{11}]$ at the edges that simulate the translational restraints where $T_{11} \rightarrow \infty$, represents a clamped edge. It has been observed that the buckling mode switches from an asymmetric mode to an axisymmetric mode at a particular ring support radius parameter. This cross over radius depends on the translational spring stiffness parameter. The cross - over radius varies from $b=0.1514$ for $T_{11}=1000$ to $b=0.1532$ for $T_{11}=\infty$. The optimal internal *ring* support varies from $b_{opt}=0.3001$ for $T_{11}=1000$ to $b_{opt}=0.2994$ for $T_{11}=\infty$. Two-dimensional plots are drawn for a wide range of translational constraints. In this paper the characteristic equations are exact, therefore the results can be calculated to any accuracy. These exact solutions can be used to check numerical or approximate results. Comparison of studies demonstrates the accuracy and stability of the present work. The effect of various parameters such as translational stiffness parameters on buckling loads of circular plate - *internal ring*

support - elastic guided edge system is studied in detail. The tabulated buckling results are useful to designers in vibration control, structural design and related industrial applications.

NOMENCLATURE

$w(r, \theta)$	Transverse deflection of the plate
h	Thickness of a plate
R	Radius of a plate
b	Non-dimensional radius of ring support
ν	Poisson's ratio
E	Young's modulus of a material
D	Flexural rigidity of a material
K_{T1}	Translational spring stiffness
T_{11}	Non-dimensional translational Flexibility parameter
N	Uniform in - plane load
k	Non-dimensional Buckling Load Parameter

REFERENCES

- [1] Bryan, G. H. 1891, "On the Stability of a Plane Plate under Thrust in its own Plane with Application to the Buckling of the Side of a Ship." Proceedings, London Math Society, 22, pp. 54-67.
- [2] Wolkowisky, J. H., 1969, "Buckling of the Circular Plate Embedded in Elastic Springs, an Application to Geophysics," Communicated Pure Appl. Math, 22, pp.367-667.
- [3] Brush, D. O., and Almroth, B. O. 1975, Buckling of Bars, Plates and Shells, McGraw-Hill, New York.
- [4] Laura, P. A. A., Gutierrez, R. H., Sanzi, H. C., and Elvira, G. 2000, "Buckling of Circular, Solid and Annular Plates with an Intermediate Circular Support." Ocean Engineering., 27, pp. 749-755.
- [5] Kim, C. S. and Dickinson, S. M., 1990, "The Flexural Vibration of the Isotropic and Polar Orthotropic Annular and Circular Plates with Elastically Restrained Peripheries," Journal of Sound and Vibration, 143, pp. 171-179.
- [6] Reismann, H, 1952, "Bending and Buckling of an Elastically Restrained Circular Plate." Journal of Applied Mechanics, 19, pp 167-172.
- [7] Thevendran V, Wang, C. M, 1996, Buckling of Annular Plates Elastically Restrained Against Rotation Along Edges," Thin Walled Structures, 25, pp 231-246.
- [8] Wang, C. Y., and Wang, C. M. 2001, "Buckling of Circular Plates with an *Internal ring* Support and Elastically Restrained Edges." Thin-Walled Structures, 39, pp. 821-825.
- [9] Yamaki, N. 1958, "Buckling of a Thin Annular Plate under Uniform Compression." Journal of Applied Mechanics, 25, pp. 267-273.
- [10] Wang, C. M., Xiang, Y., Kitipornchai, S., and Liew, K. M. 1993, "Axisymmetric Buckling of Circular Mindlin Plates with Ring Supports." Journal of Structural Engineering, 119(3), pp. 782-793.
- [11] Wang, C. M., and Tun Myint Aung, 2005, "Buckling of Circular Mindlin Plates with an *Internal ring* Support and Elastically Restrained Edge," 131, pp. 359-366.
- [12] Bhaskara Rao, L., and Kameswara Rao, C., 2007, "Buckling of Circular Plates with an *Internal ring* Support and Elastically Restrained Edge Against Rotation and Translation," 15th International Conference on Nuclear Engineering, Japan [ICONE15], April 22-26, 2007.

Short Communication

Critical velocity of fluid-conveying pipes resting on two-parameter foundation

Kameswara Rao Chellapilla^{a,*}, H.S. Simha^b^a*SciTech Patent Art Services Private Limited, 604A, Aditya Trade Centre, Ameerpet, S.R. Nagar P.O., Hyderabad 500038, India*^b*Design & Engineering Division, Indian Institute of Chemical Technology, Hyderabad, India*

Received 11 July 2006; received in revised form 13 November 2006; accepted 19 November 2006

Available online 16 January 2007

Abstract

Analytical expressions are derived for computation of critical velocity of a fluid flowing in a pipeline and resting on a two-parameter foundation like the Pasternak foundation. Fourier series and Galerkin methods have been utilized in computing the results for three simple boundary conditions, namely: pinned–pinned, pinned–clamped and clamped–clamped. Results are presented for varying values of both the foundation stiffness parameters and comparison is made with available literature for the case of the second parameter equal to zero, and new results are presented for varying values of the second foundation parameter. Interesting conclusions are drawn on the effect of the foundation parameters on the critical flow velocity of the pipeline.

© 2006 Elsevier Ltd. All rights reserved.

1. Introduction

The technology of transporting fluids, especially petroleum liquids, through long pipelines, which cover different types of terrain, has evolved over the years. The velocity of the fluid in a pipeline transporting fluids imparts energy to the pipeline making it to vibrate. It is well established from published literature that there exists a critical velocity of the fluid near which the natural frequency of the pipeline tends to zero. This is the required condition for buckling of the pipeline. Literature abounds with analyses, which give information on the influence of boundary conditions on the stability of fluid conveying pipes. Interest in studying the dynamic behaviour of such fluid conveying pipes was stimulated when excessive transverse vibrations were observed and subsequently analysed first by Ashley and Haviland in 1950 [1] and later by Housner in 1952 [2]. Housner considered a simply supported beam model for the pipeline and analysed it using a series solution approach and showed the existence of a critical flow velocity for a pipeline, which could cause buckling. In 1955, Long [3] studied the influence of clamped–clamped and clamped–pinned boundary conditions on the critical velocity. In 1966, Gregory and Paidoussis [4] presented results on the dynamic behaviour of a cantilevered pipe conveying fluid. All the above studies did not consider elastic support conditions.

*Corresponding author. Tel.: +91 40 2373 2194; fax: +91 40 2373 2394.

E-mail addresses: ckrao@patent-art.com (K.R. Chellapilla), simha@iictnet.org (H.S. Simha).

Nomenclature

$A\rho$	mass of pipe/unit length	<i>Greek symbols</i>	
C_{ij}	integration constants		
E	modulus of elasticity	β	non-dimensional mass-ratio parameter
I	moment of inertia	γ_1	non-dimensional Winkler foundation parameter
k_1	winkler foundation stiffness/unit length	γ_2	non-dimensional shear foundation parameter
k_2	shear foundation constant/unit length	λ_r	beam frequency parameter
L	length of the pipe	ψ_r	beam eigenfunctions
m	mass of pipe/unit length	σ_r	frequency function
M	total mass of pipe plus fluid/unit length	ω_j	j th mode of vibration
v	steady flow velocity of fluid	Ω	non-dimensional frequency parameter
V	non-dimensional flow velocity parameter		
V_{cr}	critical velocity parameter		
w	lateral displacement of the pipe		
x	dimension along the length of pipe		

When a pipeline rests on an elastic medium such as a soil, a model of the soil medium must be included in the governing differential equation. A very common structural model of the soil medium is the Winkler model, in which soil is represented by a series of constant stiffness, closely spaced linear springs. This model is extensively used in engineering analysis because of its simplicity and also because it is possible to obtain closed-form solutions for uniform stiffness. In 1970, Stein and Tobriner [5] studied the vibrations of a fluid-conveying pipe resting on an elastic foundation. Lottati and Kornecki, in 1986 [6], studied the influence of the elastic foundation on the stability of the pipeline. Later, in 1992, Dermendjian-Ivanova [7] investigated the behaviour of a fluid conveying pipe resting on an elastic foundation and obtained the critical fluid velocity. In 1993, Raghava Chary et al. [8] presented a detailed analysis of fluid conveying pipes resting on elastic foundation. In a recent paper, Doaré and de Langre [9] studied instability of fluid conveying pipes on Winkler-type foundation. The focus in their paper was on instability of infinitely long fluid conveying pipes using wave propagation approach, wherein results are interpreted in terms static neutrality as criteria for pinned–pinned, clamped–clamped ends and dynamic neutrality for clamped–free ends. All these studies modelled the elastic foundation as a Winkler model.

A real soil medium, however is more complex in its elastic behaviour than what the above model considers. The Winkler model assumes that the deformation of the foundation is only in the loaded region and hence implies a deformation discontinuity between the loaded and unloaded parts. Also, this model is inadequate when a lift-off takes place between the soil and the structure. To address such deficiencies, many researchers suggested an interaction between the springs of the Winkler model to obtain a more realistic model of the soil. Hence, two-parameter foundation models were developed, of which, the Pasternak model is considered closer to the soil behaviour than other models—for example, see Dutta and Roy [10]. In the Pasternak model, an incompressible shear layer is introduced between the Winkler springs and the pipe surface. The springs are connected to this shear layer, which is capable of resisting only transverse shear, thus allowing for “shear interaction” between the Winkler springs. Pipelines, especially those carrying petroleum products, traverse varied terrains like sand, gravel, mud and rock. The Pasternak model is considered to be closer to these real media. Analysis of fluid conveying pipes has been extensively performed for the case of one-parameter elastic foundation models like the Winkler model, and there is a good amount of literature on the behaviour of beams on two-parameter foundations. However, to the best of authors’ knowledge, no study has been published dealing with the behaviour of fluid-conveying pipes resting on a two-parameter elastic foundation. It is therefore felt necessary to study the dynamics and stability of fluid conveying pipes resting on two-parameter foundation such as Pasternak foundation for pinned–pinned, clamped–clamped and clamped–pinned ends.

In this paper, the work of previous authors [5–8] has been extended suitably to include the influence of a two-parameter foundation model on the vibration and stability characteristics of the fluid conveying pipes. Results are presented showing the variation for various values of the foundation stiffness parameters.

2. Equation of motion

The differential equation of motion for lateral displacement $w(x, t)$ of a uniform fluid-conveying pipe resting on a Winkler-type elastic foundation is given by

$$EI \frac{\partial^4 w}{\partial x^4} + M \frac{\partial^2 w}{\partial t^2} + \rho A v^2 \frac{\partial^2 w}{\partial x^2} + 2\rho A v \frac{\partial^2 w}{\partial x \partial t} + k_1 w = 0. \quad (1)$$

The symbols in the above equation are defined in the nomenclature. In this equation, the elastic medium is modelled on the Winkler-type foundation. The equation of motion for a fluid-conveying pipe resting on a two-parameter foundation becomes:

$$EI \frac{\partial^4 w}{\partial x^4} + M \frac{\partial^2 w}{\partial t^2} + (\rho A v^2 - k_2) \frac{\partial^2 w}{\partial x^2} + 2\rho A v \frac{\partial^2 w}{\partial x \partial t} + k_1 w = 0. \quad (2)$$

In Eq. (2) above, k_2 represents the additional parameter defining the foundation, usually termed as the shear constant of the foundation. The model is shown in Fig. 1. Eq. (2) is now solved for three simple boundary conditions.

2.1. Pinned–pinned pipe

The boundary conditions for a pinned–pinned pipe are

$$\begin{aligned} w(0, t) = w(L, t) &= 0, \\ \frac{\partial^2 w(0, t)}{\partial x^2} = \frac{\partial^2 w(L, t)}{\partial x^2} &= 0. \end{aligned} \quad (3)$$

Taking the solution of Eq. (2) which satisfies the boundary conditions Eq. (3) as

$$w(x, t) = \sum_{n=1,3,5,\dots} a_n \sin \frac{n\pi x}{L} \sin \omega_j t + \sum_{n=2,4,6,\dots} a_n \sin \frac{n\pi x}{L} \cos \omega_j t, \quad j = 1, 2, 3, \dots, \quad (4)$$

where ω_j represents the natural frequency of the j th mode of vibration. Substitution of Eq. (4) into Eq. (2) and expanding in a Fourier series we have an equation of the form:

$$[\mathbf{K} - \omega_j^2 \mathbf{M}] \{\mathbf{a}\} = 0, \quad (5)$$

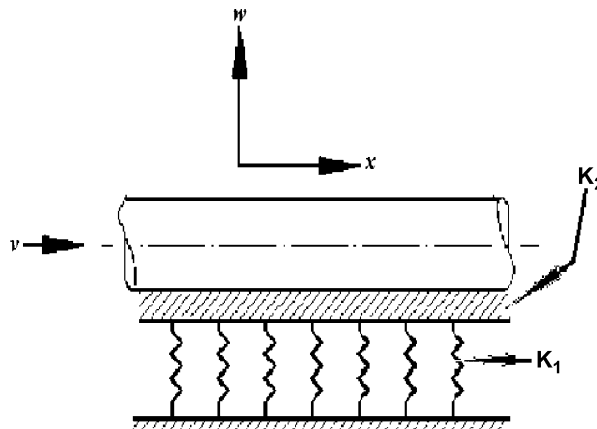


Fig. 1. Model of a fluid-conveying pipe resting on a two-parameter foundation.

where \mathbf{K} is the stiffness matrix whose elements are enumerated in Ref. [8] and will not be repeated here, \mathbf{I} is the identity matrix and $\mathbf{a}^T = \{a_1, a_2, \dots, a_n\}$. Retaining the first two terms of the above equation, and setting the determinant equal to zero, we get

$$\Omega_j^4 - \left[\left(\frac{256}{9} \beta - 5\pi^2 \right) (V^2 - \gamma_2) + 17\pi^4 + 2\gamma_1 \right] \Omega_j^2 + [4\pi^4 (V^2 - \gamma_2)^2 - (V^2 - \gamma_2) (5\pi^2 \gamma_1 + 20\pi^6) + (16\pi^8 + 17\pi^4 \gamma_1 + \gamma_1^2)] = 0. \quad (6)$$

In Eq. (6), the following non-dimensional parameters have been used:

$$\beta = \frac{\rho A}{M}; \quad \Omega_j = \omega_j L^2 \sqrt{\frac{M}{EI}}, \quad j = 1, 2, 3, \dots; \quad V = vL \sqrt{\frac{\rho A}{EI}}; \quad \gamma_1 = \frac{k_1 L^4}{EI}; \quad \gamma_2 = \frac{k_2 L^2}{EI}.$$

When the fluid velocity reaches a certain value V_{cr} , the fundamental natural frequency becomes zero. Hence, setting $\Omega_j = 0$ in Eq. (6), we obtain

$$[4\pi^4 (V^2 - \gamma_2)^2 - (V^2 - \gamma_2) (5\pi^2 \gamma_1 + 20\pi^6) + (16\pi^8 + 17\pi^4 \gamma_1 + \gamma_1^2)] = 0. \quad (7)$$

Solving Eq. (7) for V , we obtain the critical flow velocity for the pinned–pinned case. Doaré and de Langre [9], have used Eq. (8) below, for computing the critical velocity, considering only the Winkler foundation. This equation is based on the relations for a column under compressive load [11]

$$V_{cr} = N\pi \left(1 + \frac{\gamma_1}{(N\pi)^4} \right)^{1/2}, \quad (8)$$

where N is the smallest integer satisfying $N^2(N+1)^2 \geq \gamma_1/\pi^4$.

2.2. Pinned–clamped and clamped–clamped pipe

The boundary conditions for a pinned–clamped pipe are

$$\begin{aligned} w(0, t) &= w(L, t) = 0, \\ \frac{\partial w(0, t)}{\partial x} &= \frac{\partial^2 w(L, t)}{\partial x^2} = 0. \end{aligned} \quad (9)$$

And those for a clamped–clamped pipe are

$$\begin{aligned} w(0, t) &= w(L, t) = 0, \\ \frac{\partial w(0, t)}{\partial x} &= \frac{\partial w(L, t)}{\partial x} = 0. \end{aligned} \quad (10)$$

We assume the deflection of the pipe to be of the form

$$w(x, t) = \Re \left[\phi_n \left(\frac{x}{L} \right) e^{i\omega t} \right]. \quad (11)$$

In Eq. (11), \Re denotes the real part, $\phi_n(x/L)$ is a series of beam eigenfunctions $\psi_r(\xi)$ given by

$$\begin{aligned} \psi_r(\xi) &= \cosh(\lambda_r \xi) - \cos(\lambda_r \xi) - \sigma_r (\sinh(\lambda_r \xi) - \sin(\lambda_r \xi)), \\ r &= 1, 2, 3, \dots, n; \quad \xi = \left(\frac{x}{L} \right), \\ \sigma_r &= \frac{\cosh \lambda_r - \cos \lambda_r}{\sinh \lambda_r - \sin \lambda_r}. \end{aligned} \quad (12)$$

In the above equation, λ_r is the frequency parameter of the pipe without fluid flow, which is considered as a beam, and its values [12] are:

$\lambda_1 = 3.926602$ and $\lambda_2 = 7.068583$ for the pinned–clamped case and $\lambda_1 = 4.730041$ and $\lambda_2 = 7.853205$ for the clamped–clamped case.

Substituting Eq. (11) in the equation of motion Eq. (2) gives

$$L_n = EI \frac{\partial^4 \phi}{\partial x^4} + (\rho A v^2 - k_2) \frac{\partial^2 w}{\partial x^2} + 2i\omega \rho A v \frac{\partial \phi}{\partial x} + (k_1 - M\omega^2)\phi = 0. \quad (13)$$

Following the method given in Ref. [8], using Galerkin's method and minimizing the mean square of the residual L_n over the length of the pipe and using only the first two terms, we have the following equations in V .

For the pinned–clamped case:

$$(C_{11}C_{12} - C_{12}C_{21})(V^2 - \gamma_2)^2 + (V^2 - \gamma_2) \times [(\lambda_1^4 + \gamma_1)C_{22} + (\lambda_2^4 + \gamma_1)C_{11}] + [(\lambda_1^4 + \gamma_1)(\lambda_2^4 + \gamma_1)] = 0. \quad (14)$$

For the clamped–clamped case:

$$(C_{11}C_{12})(V^2 - \gamma_2)^2 + (V^2 - \gamma_2)[(\lambda_1^4 + \gamma_1)C_{22} + (\lambda_2^4 + \gamma_1)C_{11}] + [(\lambda_1^4 + \gamma_1)(\lambda_2^4 + \gamma_1)] = 0. \quad (15)$$

In Eqs. (14) and (15), the constants C_{11} , etc., are integral values, which are enumerated in Ref. [8]. Solving the above equations for V , we obtain the critical flow velocities for the pinned–clamped and clamped–clamped cases, respectively. In Doaré and de Langre [9], Eqs. (16) and (17) below have been used for obtaining the critical flow velocity for the clamped–clamped boundary conditions, considering the Winkler foundation model only

$$V_{cr} = 2\pi \left(1 + \frac{3\gamma_1}{(2\pi)^4} \right)^{1/2}. \quad (16)$$

Eq. (16) is used for $\gamma_1 \leq (84/11)\pi^4$, and Eq. (17) below,

$$V_{cr} = \pi \left(\frac{N^4 + 6N^2 + 1}{N^2 + 1} + \frac{\gamma_1}{\pi^4(N^2 + 1)} \right)^{1/2} \quad (17)$$

otherwise. Here, N is the smallest integer satisfying $N^4 + 2N^3 + 3N^2 + 2N + 6 \geq \gamma_1/\pi^4$.

3. Results and discussion

In the present work, for the pinned–pinned case, the first two terms of the equation resulting from using Fourier series have been considered in obtaining the numerical results. For the clamped–clamped case, the present work has used the assumed modes in the Galerkin method, again retaining the first two terms while Doaré and de Langre [9], have used Eq. (8) for the pinned–pinned case and Eqs. (16) and (17) for the clamped–clamped case. For both the boundary conditions, they have considered the Winkler foundation model only. Since the mode shapes of the pipe will not appreciably change with fluid flow, the modes that are assumed in the present work are for a pipe or beam without fluid flow.

3.1. Case I: $\gamma_2 = 0$, γ_1 varying

It is useful to compare the results of the present work for the condition where $\gamma_2 = 0$, which represents the Winkler foundation model, with those of Doaré and de Langre [9]. Tables 1 and 2 show the comparison. It is seen that for all the boundary conditions, the variation in the results is not significant, especially for lower values of the Winkler parameter, even though only the first two terms of the respective equations have been considered.

In Figs. 2 and 3, here, a comparison is made with Fig. 3 of Doaré and de Langre [9], for the pinned–pinned and the clamped–clamped boundary conditions, respectively, for the condition where the parameter γ_2 equals zero. Eq. (8) has been used for pinned–pinned case and Eqs. (16) and (17) for the clamped–clamped case. As shown in Fig. 2, for the value of the shear parameter γ_2 equal to zero, there is very good agreement with the curve given in Fig. 3 of Doaré and de Langre [9] for the pinned–pinned case, up to a value of $\gamma_1 = 4500$. Higher values of γ_1 give higher values of critical velocity as compared to the work of Doaré and de Langre [9]. This deviation could be attributed to the use of only the first two terms of Eq. (5). As the value of γ_1 is

Table 1

Values of the critical velocity parameter for various values of γ_1 with $\gamma_2 = 0.0$ for the pinned–pinned case

γ_1	Doaré and de Langre [9]	Present work	% Variation
1.00E+00	3.1577	3.15768	0.0
1.00E+01	3.2989	3.29891	0.0
1.00E+02	4.4723	4.47233	0.0
2.00E+02	5.4894	5.48943	0.0
3.00E+02	6.3455	6.34555	0.0
4.00E+02	7.0435	7.04347	0.0
5.00E+02	7.2211	7.22105	0.0
6.00E+02	7.3944	7.39436	0.0
7.00E+02	7.5637	7.5637	0.0
8.00E+02	7.7293	7.72934	0.0
9.00E+02	7.8915	7.89149	0.0
1.00E+03	8.0504	8.05039	0.0
1.10E+03	8.2062	8.2062	0.0
1.30E+03	8.5093	8.50928	0.0
1.50E+03	8.8019	8.80192	0.0
1.70E+03	9.0851	9.08515	0.0
2.00E+03	9.4942	9.49416	0.0
2.50E+03	10.1392	10.13924	0.0
3.00E+03	10.7457	10.74566	0.0
3.50E+03	11.3196	11.31965	0.0
4.00E+03	11.5697	11.8659	2.6
4.50E+03	11.8105	12.38809	4.9
5.00E+03	12.0464	12.88914	7.0
5.50E+03	12.2778	13.37143	8.9
6.00E+03	12.505	13.83691	10.7
7.00E+03	12.9473	14.72381	13.7

increased, more and more modes should be taken into consideration [13]. Fig. 3 shows the comparison for the clamped–clamped case. In this case also, for higher values of γ_1 there is a deviation in the results obtained here, due to the same reason.

3.2. Case 2: γ_1, γ_2 varying

In Tables 3–5, the effect of the shear parameter γ_2 on the critical velocity is clearly brought out. The comparison is made for two values of the Winkler parameter $\gamma_1 = 10.0$ and $1.0E4$. It is seen that, percentage-wise, compared to the value of $\gamma_2 = 0.0$, there is a very high increase in the value of V_{cr} for increasing values of γ_2 . This increase is somewhat lower for the pinned–clamped and the clamped–clamped conditions. In Figs. 4–6, the influence of γ_2 on the critical velocity parameter of the pipe for the three boundary conditions is shown for various values of γ_1 . There is not any perceptible change in the behaviour of the pipe until the shear constant of the two-parameter foundation γ_2 takes a value of 10.0. The critical velocity increases slightly for the value of γ_2 of 10.0. For a value of γ_2 of 100.0, there is a sharp jump in the value of the critical velocity parameter and this trend continues for increasing values of γ_2 , as shown in the figures. Another observation from these plots is that, for lower values of γ_2 , there is a sharp increase in the value of critical velocity for the Winkler foundation constant γ_1 values greater than 10.0. The critical velocity does not seem to be effected by the value of the Winkler constant γ_1 for higher values of γ_2 .

3.3. Case 3: $\gamma_1 = 0.0, \gamma_2$ varying and $\gamma_2 = 0.0, \gamma_1$ varying

Finally, a comparison of the individual effects of each of the two foundation parameters on the critical velocity parameter, when the other is equivalent to zero, is shown in Fig. 7, for the pinned–pinned case.

Table 2

Values of the critical velocity parameter for various values of γ_1 with $\gamma_2 = 0.0$ for the clamped–clamped case

γ_1	Doaré and de Langre [9]	Present work	% Variation
1.00E+00	6.2892	6.38505	1.5
1.00E+01	6.3434	6.44208	1.6
1.00E+02	6.8613	6.98684	1.8
2.00E+02	7.3944	7.54614	2.1
3.00E+02	7.8915	8.06676	2.2
4.00E+02	8.3591	8.55576	2.4
5.00E+02	8.8019	9.01828	2.5
6.00E+02	9.2235	9.45821	2.5
7.00E+02	9.6266	9.87856	2.6
8.00E+02	8.9447	9.9984	11.8
9.00E+02	9.2235	10.10641	9.6
1.00E+03	9.4942	10.21328	7.6
1.10E+03	9.7573	10.31904	5.8
1.30E+03	10.2634	10.52738	2.6
1.50E+03	10.5512	10.73167	1.7
1.70E+03	10.7415	10.93215	1.8
2.00E+03	11.0209	11.22615	1.9
2.50E+03	11.4713	11.69976	2.0
3.00E+03	11.9048	12.15492	2.1
3.50E+03	12.323	12.59364	2.2
4.00E+03	12.7274	13.01758	2.3
4.50E+03	13.1194	13.42815	2.4
5.00E+03	13.5001	13.82653	2.4
5.50E+03	13.7824	14.21375	3.1
6.00E+03	13.9649	14.5907	4.5
7.00E+03	14.3231	15.31678	6.9

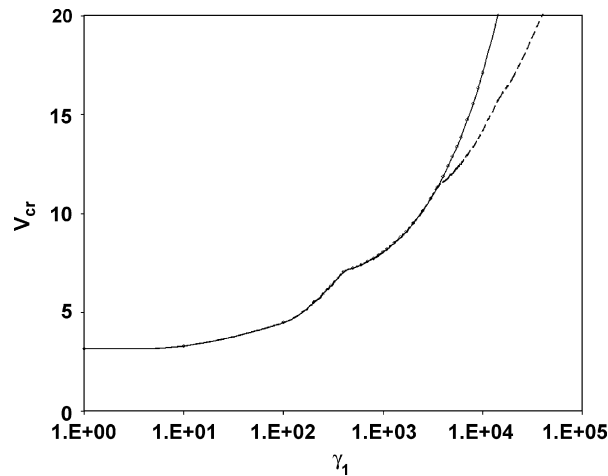


Fig. 2. Comparison of results for $\gamma_2 = 0.0$, with Fig. 3. of Doaré and de Langre [9] —○—, pinned–pinned pipe (present work); ---, pinned–pinned pipe [9].

The top curve shows that there is a sharp increase in the critical velocity when there is a progressive increase in the value of γ_2 beyond 100.0. This curve represents the case where γ_1 is near zero. The bottom curve shows the variation of critical velocity with γ_1 when γ_2 is near zero. It can be observed that the influence of the shear constant of the two-parameter foundation is more than that of the Winkler constant on the critical velocity.

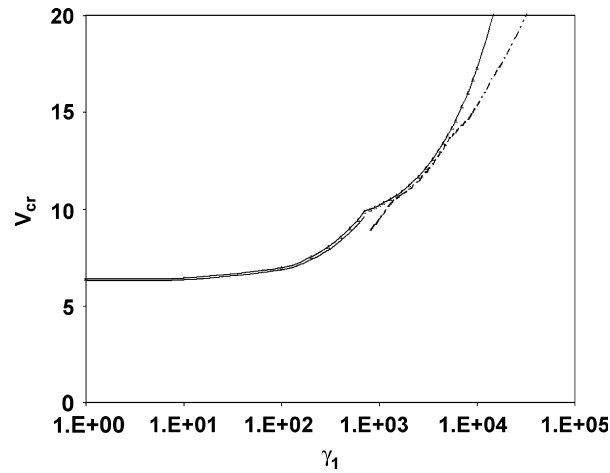


Fig. 3. Comparison of results for $\gamma_2 = 0.0$, with Fig. 3 of Doaré and de Langre [9] — \triangle —, clamped-clamped pipe (present work); —, clamped-clamped pipe—Eq. (16); — · —, clamped-clamped pipe—Eq. (17).

Table 3

Pinned–pinned case: Variation in V_{cr} for $\gamma_1 = 10.0$ and $1.0E4$

γ_2	$V_{cr-10.0}$	% Variation	$V_{cr-1.0E4}$	% Variation
$1.0E-06$	3.2989	0.0	17.1108	0.0
$1.0E-04$	3.2989	0.0	17.1108	0.0
$1.0E+01$	4.4586	35.2	17.4006	1.7
$1.0E+02$	10.4823	217.8	19.8187	15.8
$1.0E+03$	31.7786	863.3	35.9552	110.1
$5.0E+03$	70.7875	2045.8	72.751	325.2
$1.0E+04$	100.054	2933.0	101.4533	492.9

Table 4

Pinned–clamped case: variation in V_{cr} for $\gamma_1 = 10.0$ and $1.0E4$

γ_2	$V_{cr-10.0}$	% Var.	$V_{cr-1.0E4}$	% Var.
$1.0E-06$	4.5908	0.0	16.9195	0.0
$1.0E-04$	4.5908	0.0	16.9195	0.0
$1.0E+01$	5.5745	21.4	17.2125	1.7
$1.0E+02$	11.0034	139.7	19.6537	16.2
$1.0E+03$	31.9542	596.0	35.8646	112.0
$5.0E+03$	70.8595	1443.5	72.7067	329.7
$1.0E+04$	100.105	2080.5	101.4213	499.4

Table 5

Clamped–clamped case: variation in V_{cr} for $\gamma_1 = 10.0$ and $1.0E4$

γ_2	$V_{cr-10.0}$	% Var.	$V_{cr-1.0E4}$	% Var.
$1.0E-06$	6.4420	0.0	17.3133	0.0
$1.0E-04$	6.4420	0.0	17.3133	0.0
$1.0E+01$	7.1763	11.4	17.5997	1.7
$1.0E+02$	11.895	84.7	19.9937	15.5
$1.0E+03$	32.2722	401.0	36.0520	108.2
$5.0E+03$	71.0035	1002.2	72.7993	320.5
$1.0E+04$	100.207	1455.5	101.487	486.2

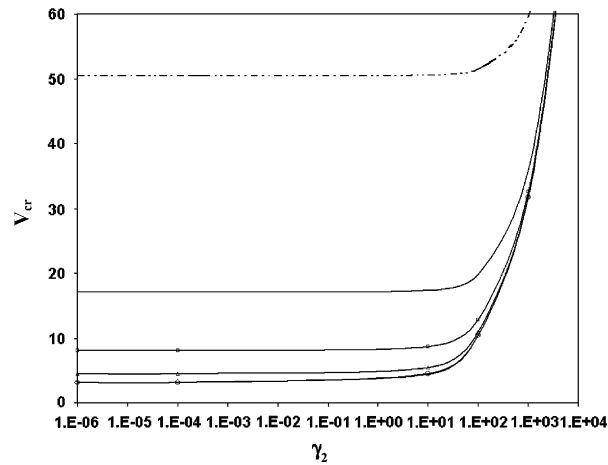


Fig. 4. Pinned–pinned pipe: Variation of V_{cr} with γ_2 for various values of γ_1 ; — \times —, $\gamma_1 = 0$; — \circ —, $\gamma_1 = 1.0$; — \triangle —, $\gamma_1 = 100.0$; — \square —, $\gamma_1 = 1000.0$; —, $\gamma_1 = 10000.0$; — $\cdot\cdot\cdot$ —, $\gamma_1 = 9.9E+4$.

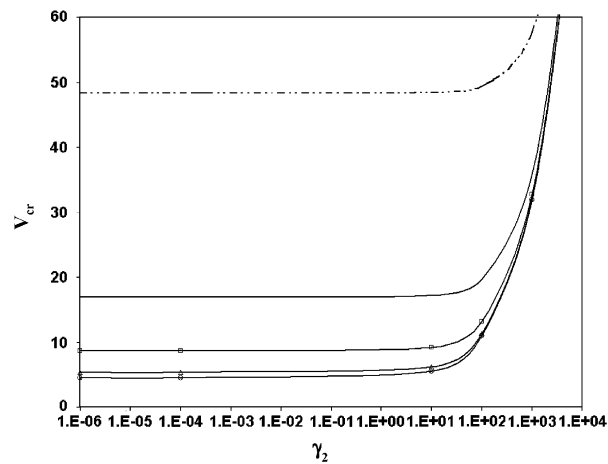


Fig. 5. Pinned–clamped pipe: Variation of V_{cr} with γ_2 for various values of γ_1 ; — \times —, $\gamma_1 = 0$; — \circ —, $\gamma_1 = 1.0$; — \triangle —, $\gamma_1 = 100.0$; — \square —, $\gamma_1 = 1000.0$; —, $\gamma_1 = 10000.0$; — $\cdot\cdot\cdot$ —, $\gamma_1 = 9.9E+4$.

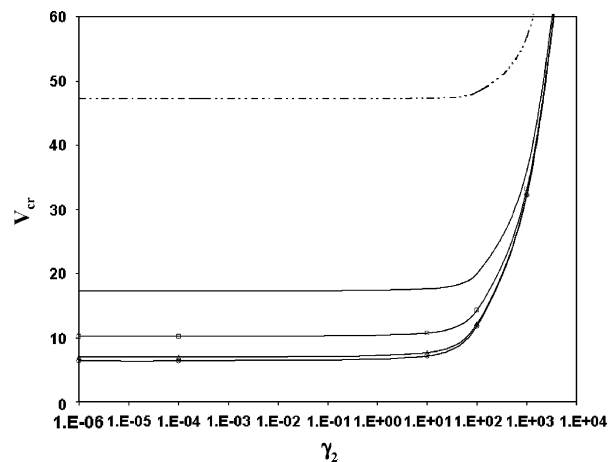


Fig. 6. Clamped–clamped pipe: Variation of V_{cr} with γ_2 for various values of γ_1 ; — \times —, $\gamma_1 = 0$; — \circ —, $\gamma_1 = 1.0$; — \triangle —, $\gamma_1 = 100.0$; — \square —, $\gamma_1 = 1000.0$; —, $\gamma_1 = 10000.0$; — $\cdot\cdot\cdot$ —, $\gamma_1 = 9.9E+4$.

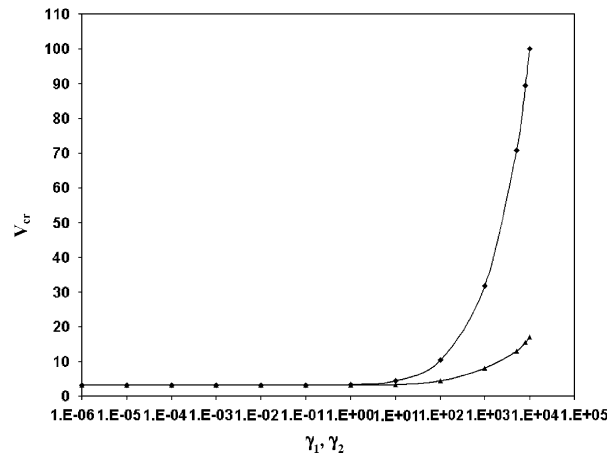


Fig. 7. Pinned–pinned pipe: Comparison of the effect of γ_1 and γ_2 on V_{cr} ; —◆—, $\gamma_1 = 0.0$, —▲—, $\gamma_2 = 0.0$.

4. Conclusions

The critical flow velocity of fluid-conveying pipes has been computed for three simple boundary conditions—pinned–pinned, pinned–clamped and clamped–clamped, when such a pipe is resting on a two-parameter elastic medium like the Pasternak foundation. Results have been presented for varying values of both the foundation parameters. From the foregoing discussion, we can conclude the following:

- A comparison shows that the results from the present study are satisfactorily close to the results obtained by earlier researchers Doaré and de Langre [9], for the case where γ_2 , the shear foundation parameter, equals zero, even though only two terms are considered for the computations. They have given results for pinned–pinned and clamped–clamped boundary conditions. In the present work, a single expression for the critical flow velocity is used to cover the entire range of foundation parameter values, while Doaré and de Langre [9] have used two equations to compute the critical flow velocity parameter for different ranges of the foundation parameter γ_1 , for the clamped–clamped conditions.
- Results are also given for the pinned–clamped boundary condition. From the expressions for critical flow velocity parameter, one can compute the values of the parameter for conditions like $\gamma_2 = 0.0$ (only Winkler foundation), $\gamma_1 = 0.0$ (absence of Winkler foundation) and both γ_1 and γ_2 varying.
- New results are presented for a fluid-conveying pipe resting on a two-parameter foundation. The effect of the second parameter on the critical flow velocity is investigated. The results show that the influence of the shear parameter γ_2 , cannot be ignored. The variation in the critical flow velocity is higher in the presence of γ_2 .

References

- [1] H. Ashley, G. Haviland, Bending vibrations of a pipe line containing flowing fluid, *Transactions of the ASME-Journal of the Applied Mechanics* September (1950) 229–232.
- [2] G.W. Housner, Bending vibrations of a pipe line containing flowing fluid, *Transactions of the ASME-Journal of the Applied Mechanics* June (1952) 205–208.
- [3] R.H. Long Jr., Experimental and theoretical study of transverse vibration of a tube containing flowing fluid, *Transactions of the ASME-Journal of the Applied Mechanics* March (1955) 65–68.
- [4] R.W. Gregory, M.P. Paidoussis, Unstable oscillations of tubular cantilevers conveying fluid—Parts I & II, *Proceedings of the Royal Society (London) A* 293 (1966) 512–542.
- [5] R.A. Stein, M.W. Tobriner, Vibration of pipes containing flowing fluids, *Transactions of the ASME-Journal of the Applied Mechanics* December (1970) 906–916.

- [6] I. Lottati, A. Kornecki, The effect of an elastic foundation and of dissipative forces on the stability of fluid-conveying pipes, *Journal of Sound and Vibration* 109 (1986) 327–338.
- [7] D.S. Dermendjian-Ivanova, Critical flow velocities of a simply supported pipeline on an elastic foundation, *Journal of Sound and Vibration* 157 (2) (1992) 370–374.
- [8] S.R. Chary, C.K. Rao, R.N. Iyengar, Vibration of fluid conveying pipe on Winkler Foundation, *Proceedings of the Eighth National Convention of Aerospace Engineers on Aeroelasticity, Hydroelasticity and other Fluid-Structure Interaction Problems*, IIT Kharagpur, India, 1993, pp. 266–287.
- [9] O. Doaré, E. de Langre, Local and global instability of fluid conveying pipes on elastic foundation, *Journal of Fluids and Structures* 16 (2002) 1–14.
- [10] S.C. Dutta, R. Roy, A critical review on idealization and modelling for interaction among soil foundation-structure system, *Computers and Structures* 80 (2002) 1579–1594.
- [11] S.P. Timoshenko, J.M. Gere, *Theory of Elastic Stability*, McGraw-Hill, New York, 1961.
- [12] S.S. Rao, *Mechanical Vibrations*, Addison-Wesley Publishing Company, Reading, MA, 1986, p. 386.
- [13] O. Doaré, Personal communication, 2006.

Vibration Engineering & Technology of Machinery (VETOMAC-IV),
17 – 19, December 2007, Osmania University, Hyderabad
**VIBRATIONS OF CIRCULAR PLATES ON ELASTIC
FOUNDATION WITH INTERNAL ELASTIC RING SUPPORT
AND ELASTICALLY RESTRAINED OUTER EDGE**

L. Bhaskara Rao ¹, Dr. Chellapilla Kameswara Rao ²

¹ Department of Mechanical Engineering, DRK College Of Science & Technology,
Hyderabad-501401, India. E-mail: bhaskarbabu_20@yahoo.com

² Sci-Tech Patent Art (Pvt) Limited, Hyderabad-500016, India.
E-mail: ckr_52@yahoo.com

ABSTRACT: Circular plates mounted on intermediate ring supports are commonly observed in structures such as ships, submarines, pressure vessels and boilers. Structures resting on elastic foundations have wide applications in modern engineering practices, such as highway pavements, base plates and continuously supported pipelines. Many structural components in aerospace, mechanical, marine and civil engineering are supported on elastic medium. The vibration characteristics of plates resting on an elastic medium are different from those of the plates supported only on the boundary. This paper describes a study of vibration characteristics of circular plates on *elastic foundation* with internal, concentric, *elastic ring* support and elastically restrained edge against rotation. The Winkler model describes the foundation. The classical plate theory is used to derive the frequency equation of the plate - elastic foundation – internal elastic ring - elastic edge support system. The solutions are obtained in terms of Bessel functions for the complete plate - elastic foundation - internal elastic ring - elastic edge support system. Parametric investigations on the behavior of circular plates with internal elastic ring support, elastic foundation and flexible edge conditions have been carried out with respect to various rotational stiffness, translational stiffness of internal ring, foundation modulus and various boundary conditions. Extensive data is tabulated so that pertinent conclusions can be drawn on the influence of an internal elastic ring support, foundation modulus, and rotational edge restraints on the vibration of uniform isotropic circular plates.

Keywords: Vibrations; Circular plate; Flexible edge; Elastic ring support; Rotational stiffness; Elastic foundation.

1. INTRODUCTION

Circular plates are widely used in modern aerospace technology, naval structural engineering and aircraft structures. Circular plates with internal *elastic ring* supports find applications in aircrafts, rocket launching pads, and instrument mounting bases for space vehicles. A few authors considered the problem circular plates with *rigid* internal ring supports, which add to stabilize or to increase the frequency. But, in many cases the supports are not entirely rigid, such as those made of rubber. Vibrations of circular plates have been of practical and academic interest for at least a century and half [1, 2]. A lot of literature exists for the free vibrations of circular plates. But, the majority of literature deals with classical boundary conditions representing Clamped and Simply supported or free edges, and only a small number deals with edges which are restrained against rotation or/and translation, or with other non- classical boundary conditions. Earlier published investigations in this area were mainly confined to the determination of frequency of circular plates with various edge conditions [3, 4]. Kunukkasseril and Swamidass [5] are probably the first to consider internal *ring* support. They have presented only the case of a circular plate with a free edge. Chou and Wang [6] also studied vibration of circular plates with internal *ring* support with classical boundary conditions. The problems of circular plates on *elastic foundation* in general are important in engineering design. The response of circular plates supported by a Winkler foundation has been studied widely by assuming that the foundation reacts in compression as well as in tension. The vibration of a circular plate supported laterally by an *elastic foundation* was discussed by Leissa [7]. Leissa deduced that the effect of a Winkler foundation merely increases the square of the natural frequency of the plate by a constant. The same conclusion was considered by Laura et al [8], in which case a simple frequency relation no longer holds. The most general soil model used in practical applications is the Winkler model [9] in which the soil layer is represented by unconnected closely spaced elastic springs. The effect of the rotational stiffness, foundation stiffness and various boundary conditions on the plate natural frequency is studied in detail. The purpose of this paper is to present accurate and extensive numerical results for the case of an elastic plate with

internal, concentric, elastic *ring* support and *partial elastic foundation*, which are useful to both designers and researchers.

2. DEFINITION OF THE PROBLEM

Consider a thin circular isotropic plate of radius R , uniform thickness h , Young's modulus E , density ρ and Poisson's ratio ν as shown in Fig.1. The plate is elastically restrained against rotation with an internal, concentric, *elastic ring* support and *partial elastic foundation* at a smaller radius of bR as shown in Fig.1. The present problem is to determine the frequencies of this plate with flexible edge conditions.

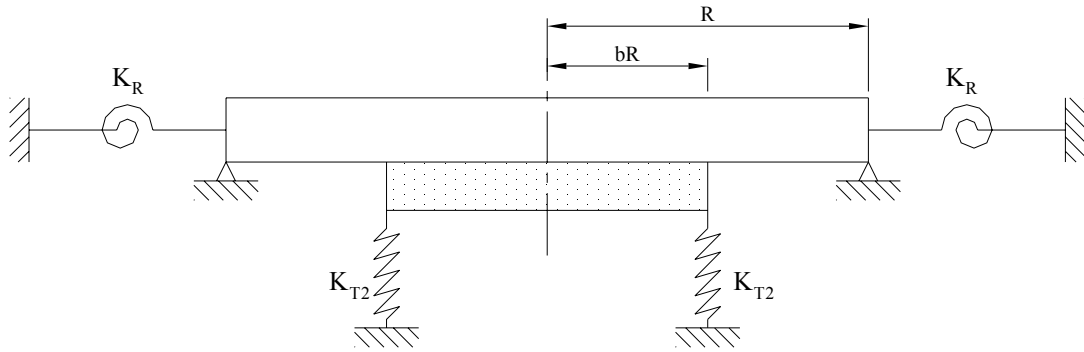


Fig. 1. A Circular Plate with Elastically Restrained Edge Against Rotation and Simply Supported and Supported on Internal Elastic Ring and Elastic Foundation

3. MATHEMATICAL FORMULATION OF THE SYSTEM

Here, all lengths are normalized by R . The normalized outer and inner radii are 1 and b respectively. Let the subscript **I** denote the outer region $b \leq \tilde{r} \leq 1$ and the subscript **II** denote the inner region $0 \leq \tilde{r} \leq b$. In the classical plate theory [3] the following fourth order differential equation describes free flexural vibrations of a thin circular uniform plate for region **I** is

$$\nabla^4 \tilde{w}_I(\tilde{r}, \theta) - k^4 \tilde{w}_I(\tilde{r}, \theta) = 0 \quad (1)$$

Where $\tilde{w} = w/R$; r, θ are polar co-ordinates, w is the transverse displacement.

$k^4 = R^4 \omega^2 \rho / D$ is a parameter representing the frequency, ω ; $D = Eh^3 / 12(1-\nu)$ is flexural rigidity of the plate.

The plate equation [10] for region II is

$$\nabla^4 \tilde{w}_{II}(\tilde{r}, \theta) - k^4 \tilde{w}_{II}(\tilde{r}, \theta) + \xi^4 \tilde{w}_{II}(\tilde{r}, \theta) = 0 \quad (2)$$

Where $\xi^2 = R^4 K_w / D$ represents the stiffness K_w of the foundation.

$$\text{Let } \tilde{w}(\tilde{r}, \theta) = u(\tilde{r}) \cos(n\theta) \quad (3)$$

Where r is the radius normalized by R , n is the number of nodal diameters. The general solution to equation (1) is a linear combination of the Bessel functions

$$J_n(k\tilde{r}), Y_n(k\tilde{r}), I_n(k\tilde{r}) \& K_n(k\tilde{r}).$$

$$u_I(r) = C_1 J_n(k\tilde{r}) + C_2 Y_n(k\tilde{r}) + C_3 I_n(k\tilde{r}) + C_4 K_n(k\tilde{r}) \quad (4)$$

Where C_1, C_2, C_3 & C_4 are constants.

$J_n(.)$ and $Y_n(.)$ are the Bessel functions of the first and second kinds of order n respectively.

$I_n(.)$ and $K_n(.)$ are the modified Bessel functions of the first and second kinds of order n respectively.

Substituting equation (4) into equation (3) yields the following

$$\tilde{w}_I(\tilde{r}, \theta) = [C_1 J_n(k\tilde{r}) + C_2 Y_n(k\tilde{r}) + C_3 I_n(k\tilde{r}) + C_4 K_n(k\tilde{r})] \cos(n\theta) \quad (5)$$

The general solution to equation (2) is given by

$$u_{II}(\tilde{r}) = C_5 J_n(k^* \tilde{r}) + C_6 I_n(k^* \tilde{r}) \quad (6)$$

$$\text{Where } k^* = (k^4 + \xi^2)^{\frac{1}{4}} \quad (7)$$

Substituting equation (6) into equation (3) yields the following

$$\tilde{w}_{II}(\tilde{r}, \theta) = [C_5 J_n(k^* \tilde{r}) + C_6 I_n(k^* \tilde{r})] \cos(n\theta) \quad (8)$$

The boundary conditions at the edge of the plate is given by the following expressions

$$\tilde{w}_I(\tilde{r}, \theta) = 0 \quad (9)$$

$$M_r(\tilde{r}, \theta) = K_{R1} \frac{\partial \tilde{w}}{\partial \tilde{r}}(\tilde{r}, \theta) \quad (10)$$

Where the bending moment is defined as follows

$$M_r(\tilde{r}, \theta) = -\frac{D}{R^2} \left[\frac{\partial^2 \tilde{w}_I(\tilde{r}, \theta)}{\partial \tilde{r}^2} + \nu \left(\frac{1}{\tilde{r}} \frac{\partial \tilde{w}_I(\tilde{r}, \theta)}{\partial \tilde{r}} + \frac{1}{\tilde{r}^2} \frac{\partial^2 \tilde{w}_I(\tilde{r}, \theta)}{\partial \theta^2} \right) \right] \quad (11)$$

From equations (9), (10) & (11) we get the following

$$\left[\frac{\partial^2 \tilde{w}_I(\tilde{r}, \theta)}{\partial \tilde{r}^2} + \nu \left(\frac{1}{\tilde{r}} \frac{\partial \tilde{w}_I(\tilde{r}, \theta)}{\partial \tilde{r}} + \frac{1}{\tilde{r}^2} \frac{\partial^2 \tilde{w}_I(\tilde{r}, \theta)}{\partial \theta^2} \right) \right] = -\frac{K_{R1} R^2}{D} \frac{\partial \tilde{w}}{\partial \tilde{r}}(\tilde{r}, \theta) \quad (12)$$

The plate is continuous in terms of displacement, slope and moment at $\tilde{r} = b$ for which the boundary conditions are

$$\tilde{w}_I(b) = \tilde{w}_{II}(b) \quad (13)$$

$$\tilde{w}'_I(b) = \tilde{w}'_{II}(b) \quad (14)$$

$$\tilde{w}''_I(b) = \tilde{w}''_{II}(b) \quad (15)$$

$$\tilde{w}''_I(b) = \tilde{w}'''_{II}(b) - T_{22} \tilde{w}_{II}(b) \quad (16)$$

From equations (5), (9) and (12) we obtained the following equations at $\tilde{r} = 1$

$$\left[\frac{k^2}{4} P_2 + \frac{k}{2} (\nu + R_{11}) P_1 - \left(\frac{k^2}{2} + \nu m^2 \right) J_n(k) \right] C_1 + \left[\frac{k^2}{4} Q_2 + \frac{k}{2} (\nu + R_{11}) Q_1 - \left(\frac{k^2}{2} + \nu m^2 \right) Y_n(k) \right] C_2 + \quad (17)$$

$$\left[\frac{k^2}{4} R_2 + \frac{k}{2} (\nu + R_{11}) R_1 + \left(\frac{k^2}{2} - \nu m^2 \right) I_n(k) \right] C_3 + \left[\frac{k^2}{4} S_2 - \frac{k}{2} (\nu + R_{11}) S_1 + \left(\frac{k^2}{2} - \nu m^2 \right) K_n(k) \right] C_4 = 0$$

$$[J_n(k)]C_1 + [Y_n(k)]C_2 + [I_n(k)]C_3 + [K_n(k)]C_4 = 0 \quad (18)$$

$$\text{Where, } R_{11} = \frac{K_{R1} R}{D}; T_{22} = \frac{K_{T2} R^3}{D} \quad (19)$$

$$\begin{aligned} P_1 &= J_{n-1}(k) - J_{n+1}(k); P_2 = J_{n-2}(k) + J_{n+2}(k); P_3 = J_{n-3}(k) - J_{n+3}(k); \\ Q_1 &= Y_{n-1}(k) - Y_{n+1}(k); Q_2 = Y_{n-2}(k) + Y_{n+2}(k); Q_3 = Y_{n-3}(k) - Y_{n+3}(k); \\ R_1 &= I_{n-1}(k) + I_{n+1}(k); R_2 = I_{n-2}(k) + I_{n+2}(k); R_3 = I_{n-3}(k) + I_{n+3}(k); \\ S_1 &= K_{n-1}(k) + K_{n+1}(k); S_2 = K_{n-2}(k) + K_{n+2}(k); S_3 = K_{n-3}(k) + K_{n+3}(k); \end{aligned} \quad (20)$$

Equations (8), (13), (14), (15) and (16) yield the following expressions

$$J_n(kb)C_1 + Y_n(kb)C_2 + I_n(kb)C_3 + K_n(kb)C_4 - J_n(k^*b)C_5 - I_n(k^*b)C_6 = 0 \quad (21)$$

$$\frac{k}{2} P'_1 C_1 + \frac{k}{2} Q'_1 C_2 + \frac{k}{2} R'_1 C_3 - \frac{k}{2} S'_1 C_4 - \frac{k^*}{2} P'_{11} C_5 - \frac{k^*}{2} R'_{11} C_6 = 0 \quad (22)$$

$$\begin{aligned} \frac{k^2}{4} (P'_2 - 2J_n(kb))C_1 + \frac{k^2}{4} (Q'_2 - 2Y_n(kb))C_2 + \frac{k^2}{4} (R'_2 + 2I_n(kb))C_3 + \\ \frac{k^2}{4} (S'_2 + 2K_n(kb))C_4 - \frac{k^{*2}}{4} (P'_{22} - 2J_n(k^*b))C_5 - \frac{k^{*2}}{4} (R'_{22} + 2I_n(k^*b))C_6 = 0 \end{aligned} \quad (23)$$

$$\begin{aligned} & \frac{k^3}{8}(P'_3 - 3P'_1)C_1 + \frac{k^3}{8}(Q'_3 - 3Q'_1)C_2 + \frac{k^3}{8}(R'_3 + 3R'_1)C_3 - \frac{k^3}{8}(S'_3 + 3S'_1)C_4 - \\ & \left[\frac{k^{*3}}{8}(P'_{33} - 3P'_{11}) - T_{22}J_n(k^*b) \right] C_5 - \left[\frac{k^{*3}}{8}(R'_{33} + 3R'_{11}) - T_{22}I_n(k^*b) \right] C_6 = 0 \end{aligned} \quad (24)$$

Where,

$$\begin{aligned} P'_1 &= J_{n-1}(kb) - J_{n+1}(kb); P'_2 = J_{n-2}(kb) + J_{n+2}(kb); P'_3 = J_{n-3}(kb) - J_{n+3}(kb); \\ Q'_1 &= Y_{n-1}(kb) - Y_{n+1}(kb); Q'_2 = Y_{n-2}(kb) + Y_{n+2}(kb); Q'_3 = Y_{n-3}(kb) - Y_{n+3}(kb); \\ R'_1 &= I_{n-1}(kb) + I_{n+1}(kb); R'_2 = I_{n-2}(kb) + I_{n+2}(kb); R'_3 = I_{n-3}(kb) + I_{n+3}(kb); \\ S'_1 &= K_{n-1}(kb) + K_{n+1}(kb); S'_2 = K_{n-2}(kb) + K_{n+2}(kb); S'_3 = K_{n-3}(kb) + K_{n+3}(kb); \\ P'_{11} &= J_{n-1}(k^*b) - J_{n+1}(k^*b); P'_{22} = J_{n-2}(k^*b) + J_{n+2}(k^*b); P'_{33} = J_{n-3}(k^*b) - J_{n+3}(k^*b); \\ R'_{11} &= I_{n-1}(k^*b) + I_{n+1}(k^*b); R'_{22} = I_{n-2}(k^*b) + I_{n+2}(k^*b); R'_{33} = I_{n-3}(k^*b) + I_{n+3}(k^*b); \end{aligned} \quad (25)$$

4. SOLUTION

For the given values of $n, \nu, b, R_{11}, T_{22}$ and ξ , the above set of equations, gives an exact characteristic equation for non-trivial solutions of the coefficients $C_1, C_2, C_3, C_4, C_5, C_6$. For non-trivial solution, the determinant of $[C]_{6 \times 6}$ must vanish. A simple bisection algorithm finds the roots. The problem is solved using Mathematica computer software with symbolic capabilities.

5. RESULTS & DISCUSSIONS

The frequency values for the plate with elastically restrained edge against rotation and supported on an internal *elastic ring* and elastic foundation, at various values of the rotational stiffness parameter, R_{11} and for constant T_{22} & ξ , have been calculated and the results are shown in the Table 1. As observed from the data, the frequency parameter increases with rotational stiffness parameter, R_{11} . The variation of frequency parameter with ring support is shown in the Figure. 2. It is found that the fundamental frequency parameter is completely governed by the axisymmetric mode, i.e., $n = 0$. For other values of R_{11} , the fundamental frequencies are shown in the Table 1. The variation of frequency parameter with internal elastic ring support radius for $R_{11} = 0.2$ & ∞ by keeping $T_{22} = \xi = 10$ is shown in Figures 2 and 3. The frequencies at various values of foundation stiffness parameter, ξ and for constant R_{11} & T_{22} , have been calculated and the results are shown in the Table 2. As observed from the data, the frequency parameter increases with

increase in value of foundation stiffness parameter at higher values of ring support radius. It is also observed from the data, that the frequency increases with ring support radius up to certain extent and thereafter decreases. The variation of frequency with internal elastic ring support radius for $\xi = 0.2$ & ∞ by keeping $R_{11} = 10$ is shown in Figures 4 and 5. It is found that the fundamental frequency parameter is completely governed by the axisymmetric mode, i.e., $n = 0$. For lower values of foundation parameter, the frequency increases up to certain extent and thereafter decreases with ring support radius as shown in Figure 4. For higher values of foundation parameter, the frequency increases with increase in ring support radius as shown in Figure. 5. For other values of ξ , the fundamental frequencies are shown in the Table 2.

Table 1. Frequency Parameter for different Rotational stiffness Parameter R_{11} when $T_{22} = \xi = 10$ & $\nu = 0.3$

b	$R_{11} = 0.2$	$R_{11} = 10$	$R_{11} = 100$	$R_{11} = 1000$	$R_{11} = \infty$
0.0	2.28322	2.95841	3.16535	3.19308	3.19627
0.1	2.35119	3.00028	3.20383	3.23117	3.23436
0.2	2.26638	2.94435	3.15089	3.17852	3.18171
0.3	1.95864	2.78075	3.00312	3.03234	3.03574
0.4	5.40619	2.49326	2.76454	2.79894	2.80283
0.5	5.40865	2.0323	2.44952	2.49667	2.50195
0.6	5.41273	5.89256	2.07327	2.1509	2.15947
0.7	5.39667	5.87065	1.64827	1.80072	1.81627
0.8	5.3605	5.8383	1.19924	1.52742	1.55432
0.9	5.32563	5.81624	0.849963	1.41872	1.45349
1.0	5.31285	5.81115	0.787793	1.40955	1.44522

Table 2. Frequency Parameter for different Elastic Foundation Stiffness Parameter, ξ when $R_{11} = T_{22} = 10$ & $\nu = 0.3$

b	$\xi = 0.2$	$\xi = 10$	$\xi = 100$	$\xi = 1000$	$\xi = \infty$
0.0	2.95838	2.95841	2.95841	2.9579	4.45181
0.1	3.04141	3.00028	5.11984	3.90296	4.85243
0.2	3.10142	2.94435	4.90024	4.14212	5.43559
0.3	3.13161	2.78075	4.71527	4.55186	6.18388
0.4	3.12922	2.49326	7.60098	5.11977	7.1723
0.5	3.09962	2.0323	7.3758	5.9337	8.54229
0.6	3.05507	5.89256	7.14134	7.15464	10.5768
0.7	3.01051	5.87065	5.13314	9.05963	13.9339
0.8	2.97772	5.8383	10.8454	12.0551	20.5821
0.9	2.96137	5.81624	10.4075	16.3459	40.3462
1.0	2.95789	5.81115	10.2815	23.7849	696.957

Table3.Frequency Parameter for different Elastic Ring stiffness Parameter T_{22} when $R_{11} = \xi = 10$ & $\nu = 0.3$

b	$T_{22} = 0.2$	$T_{22} = 10$	$T_{22} = 100$	$T_{22} = 1000$	$T_{22} = \infty$
0.0	2.95831	2.95841	2.95921	2.96738	4.45182
0.1	5.1124	5.11984	5.19826	4.20749	4.64494
0.2	4.90023	4.90024	4.90018	4.90042	4.90001
0.3	4.7082	4.71527	4.77722	5.21827	6.26752
0.4	7.59484	7.60098	7.65954	5.5423	6.72788
0.5	7.37578	7.3758	7.37584	7.37582	7.37572
0.6	7.13414	7.14134	7.20758	7.81146	9.88581
0.7	5.08738	5.13314	5.50829	7.57724	10.953
0.8	10.8414	10.8454	10.8829	3.64841	8.91977
0.9	10.4043	10.4075	10.437	10.7068	5.51368
1.0	10.2815	10.2815	10.2815	10.2815	11.0721

Table 4. Frequency Parameter for different Three Elastic Stiffness Parameters, $R_{11}\xi$ & T_{22} when $\nu = 0.3$

b	$R_{11} = \xi = T_{22} = 0.2$	$R_{11} = \xi = T_{22} = 10$	$R_{11} = \xi = T_{22} = 100$	$R_{11} = \xi = T_{22} = 1000$	$R_{11} = \xi = T_{22} = \infty$
0.0	2.28306	2.95841	3.16608	3.20092	4.76824
0.1	2.28595	3.00028	5.55784	4.31689	5.22303
0.2	2.28834	2.94435	5.23702	4.67256	5.88294
0.3	2.28974	2.78075	5.11466	5.20658	6.73387
0.4	2.29023	2.49326	8.13405	5.92596	7.86585
0.5	2.28954	2.0323	7.91249	6.92951	9.4472
0.6	2.28804	5.89256	7.71051	8.39387	11.816
0.7	2.28615	5.87065	6.21319	10.6031	15.7608
0.8	2.28416	5.8383	11.3494	13.8306	23.6466
0.9	2.28276	5.81624	10.9788	18.0775	47.2988
1.0	2.28226	5.81115	10.9065	25.4765	695.6

The frequencies at various values of internal ring spring stiffness ratios, T_{22} and for constant R_{11} & ξ , have been calculated and the results are shown in the Table 3. It is observed from the data that the frequency increases with ring support radius up to certain extent and thereafter decreases. The variation of frequency with internal elastic ring support radius for $T_{22} = 0.2$ & ∞ by keeping R_{11} & $\xi = 10$ is shown in Figures 6 and 7. It is found that the fundamental frequency is completely governed by the axisymmetric mode, i.e., $n = 0$. For lower values of foundation parameter, the frequency increases up to certain extent and thereafter decreases with ring support radius as shown in Figure 6. For higher values of foundation parameter, the frequency increases with increase in ring support radius as shown in Figure 7. For other values of T_{22} , the fundamental frequencies are shown in the Table 2.

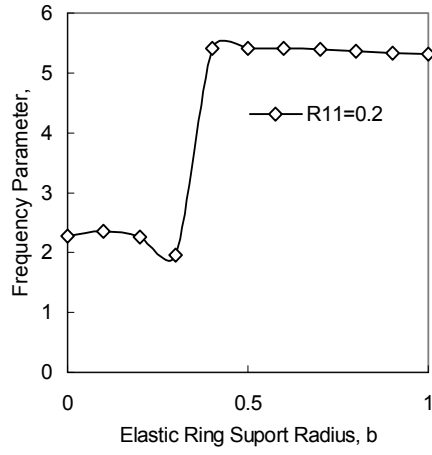


Fig. 2 Effect of Rotational Stiffness Parameter, R_{11} , on Natural Frequency Parameter, k when $\xi = T_{22} = 10$

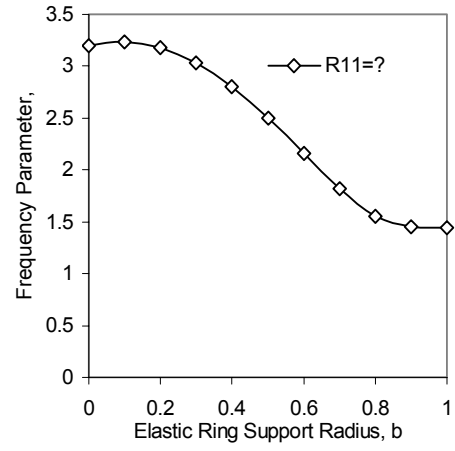


Fig. 3 Effect of Rotational Stiffness Parameter, R_{11} , on Natural Frequency Parameter, k when $\xi = T_{22} = 10$

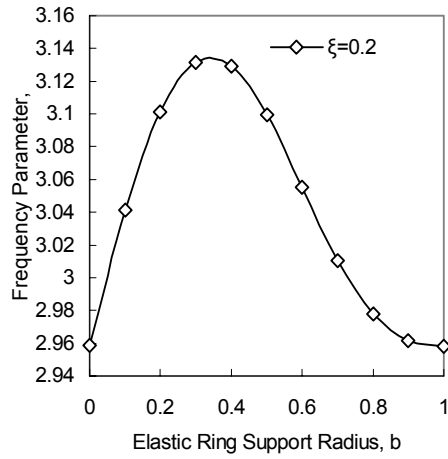


Fig. 4 Effect of Foundation Stiffness Parameter, ξ on Natural Frequency Parameter, k when $R_{11} = T_{22} = 10$

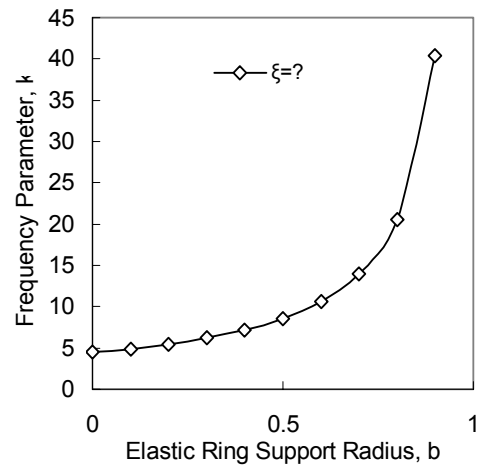


Fig. 5 Effect of Foundation stiffness Parameter, ξ on Natural Frequency Parameter, k when $R_{11} = T_{22} = 10$

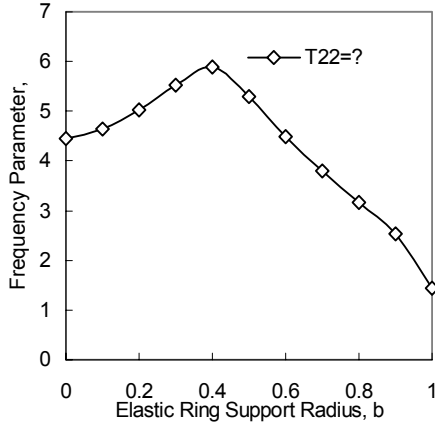


Fig. 6 Effect of Translational Stiffness Parameter, T_{22} on Natural Frequency Parameter, k when $R_{11} = \xi = 10$

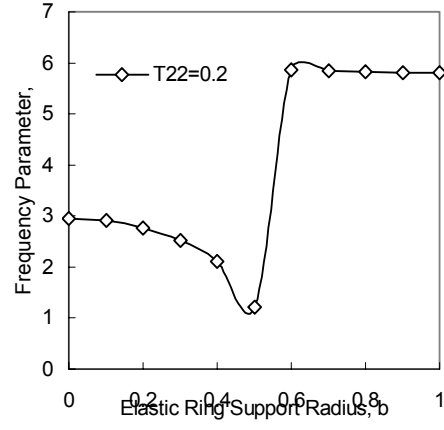


Fig. 7 Effect of Translational Stiffness Parameter, T_{22} on Natural Frequency Parameter, k when $R_{11} = \xi = 10$

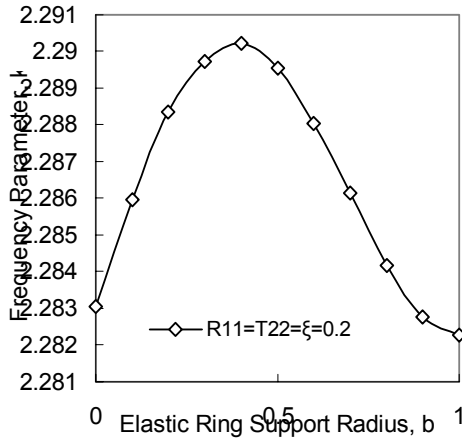


Fig. 8 Effect of Rotational Stiffness Parameter, R_{11} , Translational Stiffness Parameter, T_{22} and Foundation Stiffness parameter, ξ on Natural Frequency Parameter, k when $R_{11} = \xi = 10$

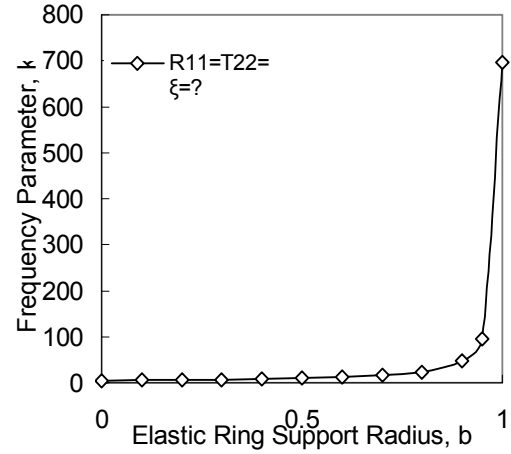


Fig. 9 Effect of Rotational Stiffness Parameter, R_{11} , Translational Stiffness Parameter, T_{22} and Foundation Stiffness parameter, ξ on Natural Frequency Parameter, k when $R_{11} = \xi = 10$

The frequencies at various values of rotational spring stiffness Parameter, R_{11} internal ring spring stiffness Parameter, T_{22} and foundation stiffness parameter, have been calculated and the results are shown in the Table 4. It is observed from the data that the frequency Parameter increases with ring support radius up to certain extent and thereafter decreases. The variation of frequency Parameter with internal elastic ring support radius for $R_{22} = \xi = T_{22} = 0.2 \text{ \& } \infty$ is shown in Figures 8 and 9. It is found that the fundamental frequency is completely governed by the axisymmetric mode, i.e., $n = 0$. For lower values these parameters, the frequency Parameter increases up to certain extent and thereafter decreases with ring support radius as shown in Figure 8. For higher values, the frequency increases with increase in ring support radius as shown in Figure 9. For other values, the fundamental frequencies are shown in the Table 4. The results of this kind are scarce in the literature. However the results are compared with the following cases. (i) The Clamped boundary conditions could be accounted for by setting $K_{R1} \rightarrow \infty \text{ \& } \xi = 0$ as shown in Fig. 10. When b is zero or one the fundamental frequency Parameter in this case is 3.1962 and this is in good agreement the results published by C. Y. Wang and C. M. Wang [11]. Also the comparisons of the present exact results and those of C. Y. Wang and C. M. Wang [11], S. Azimi [12], Z. Ding [13] and Bhaskara Rao and Kameswara Rao [14, 15] and for Clamped plate are presented in Table 5. However, present results denote by substituting $\xi = 0$ and the results from the References [12] and [13] are approximate.

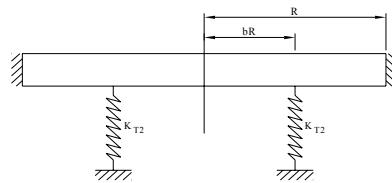


Fig. 10. A Circular Plate with Clamped Edge and Internal Ring Support

(ii) Simply supported boundary conditions could be accounted for by setting $K_{R1} \rightarrow 0$ as shown in Fig. 11. When b is zero or one the fundamental frequency in this case is

2.22151 and this is in good agreement [2.2215] with the results published by C. Y. Wang and C. M. Wang [11]. Also the comparisons of the present exact results and those of C. Y. Wang and C. M. Wang [11], S. Azimi [12] and Bhaskara Rao and Kameswara Rao [14] & [15] for simply supported plate are presented in Table 6. However, present results denote by substituting $\xi = 0$. The present results are in excellent agreement with those earlier published results.

Table 5. Comparison of results with those of Ref. 11, 12, 13 & 14 for the Clamped plate

T_{22}	$b = 0.2$	$b = 0.4$	$b = 0.6$	$b = 0.8$
10	3.3255*	3.3383*	3.2621*	3.2040*
	3.3256[11]	3.3384[11]	3.2622[11]	3.2041[11]
	3.326[12]	3.338[12]	3.262[12]	3.199[12]
	3.322[13]	3.334[13]	3.262[13]	3.204[13]
	3.32555[14]	3.33835[14]	3.26218[14]	3.20406[14]
	3.32555[15]	3.33835[15]	3.26218[15]	3.20406[15]
1000	5.17567*	6.11075*	4.50325*	3.53919*
	5.1757[11]	6.1108[11]	4.5033[11]	3.5392[11]
	5.187[12]	6.129[12]	4.512[12]	3.547[12]
	4.929[13]	6.114[13]	4.492[13]	3.547[13]
	5.17567[14]	6.11075[14]	4.50325[14]	3.53919[14]
	5.17567[15]	6.11075[15]	4.50325[15]	3.53919[15]

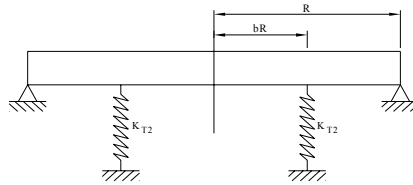


Fig. 11. A Circular Plate with Simply Supported Edge and Internal Ring Support

Table 6. Comparison of results with those of Wang and Wang [11], Azimi [12] and Bhaskara Rao and Kameswara Rao [14] for Simply Supported plate

T_{22}	$b = 0.2$	$b = 0.4$	$b = 0.6$	$b = 0.8$
10	2.46063*	2.54709*	2.47884*	2.32102*
	2.4607[11]	2.5472[11]	2.4788[11]	2.3211[11]
	2.461[12]	2.547[12]	2.479[12]	2.321[12]
	2.46063[14]	2.54709[14]	2.47884[14]	2.32102[14]
	2.46063[15]	2.54709[15]	2.47884[15]	2.32102[15]
	4.20239*	5.27635*	4.47991*	3.5321*
1000	4.2025[11]	5.2764[11]	4.4799[11]	3.5323[11]
	4.2108[12]	5.282[12]	4.486[12]	3.537[12]
	4.20239[14]	5.27635[14]	4.47991[14]	3.5321[14]
	4.20239[15]	5.27635[15]	4.47991[15]	3.5321[15]

* Denote the present results

(iii). Also the results are in good agreement with the results published by Bhaskara Rao and Kameswara Rao [15] for different values of Rotational spring stiffness ratio, R_{11} and elastic ring stiffness parameter, T_{22} .

6. CONCLUSIONS

In this paper, a detailed study on the effect of various parameters such as rotational stiffness ratio, Foundation stiffness parameter, and internal spring stiffness ratio on the frequency has been done. Frequencies are given for various rotational spring stiffness parameters $[R_{11}]$ at the edges that simulate the rotational restraints where $R_{11} \rightarrow \infty$, represents a clamped edge and $R_{11} \rightarrow 0$, represents a simply supported edge. Two-dimensional plots of frequency values are drawn for wide range of elastic edge constraints and internal spring stiffness ratio. It is observed that the influence of internal spring stiffness ratio on frequency is much more predominant than that of rotational stiffness ratio. It is also observed that the influence of foundation stiffness parameter on frequency is more at higher ring support radius and foundation parameter. In this paper the characteristic equations are exact, therefore the results can be calculated to any accuracy. These exact solutions can be used to check numerical or approximate results. The tabulated results are useful to designers in vibration control and structural design. All comparisons produced an excellent agreement with that of earlier published results.

NOTATION

h	Thickness of a plate
R	Radius of a plate
ν	Poisson's ratio
E	Young's modulus of a material
ρ	Density of a material
ω	Angular frequency
D	Flexural rigidity of a material
K_{R1}	Rotational spring stiffness at outer edge
K_{T2}	Translational spring stiffness of internal elastic ring
R_{11}	Non-dimensional rotational flexibility parameter at outer edge
T_{22}	Non-dimensional translational flexibility parameter of internal ring support or ring support parameter
K_w	Elastic Foundation Stiffness Constant
ξ	Non-dimensional Foundation Stiffness parameter
k	Non-dimensional frequency parameter

k^* Non-dimensional frequency parameter with foundation

REFERENCES

1. E. F. F. Chladni 1803 *Die Akustik. Leipzig*
2. S. D. Poisson 1829 *Memorires del l' Academie Royales des Sciences de l' Institut de la France*, ser. 28, 357. L' Equilibre et le mouvement des corps elastiques.
3. A.W. Leissa, *Vibration of Plates*, NASA SP-160, 1969.
4. G.N.Weissensel, "Natural frequency information for circular and annular plates", *Journal of Sound and Vibration* 133(1989) 129-134
5. V.X.Kunukkasseril, A.S.J. Swanidas, "Vibration of continuous circular plates", *International Journal of Solids and Structures* 10(1974)603-619.
6. F. S. Chou, C. M. Wang, G. D. Cheng, N. Olhoff, "Optimal design of internal ring support for vibrating Circular plates", *Journal of Sound and Vibration* 1999; 219 (3): 525-37.
7. A. W. Leissa, *Vibration of Plates*, Acoustical Society Of America, Sewickley. PA, 1993.
8. P.A.A.Laura, R.H. Gutierrez, H. C.Sanzi, G.Elaira, The lowest axi-symmetrical frequency of Vibration of a circular plate Partially embedded in a Winkler foundation, *Journal of Sound and Vibration* 185 (1995) 915-919.
9. E. Winkler, *Die Lehre von der Elasticitaet and Festigkeit*, Prag. Dominicus, 1867.
10. A. W. Leissa, *Vibration of Plates*, Acoustical Society Of America, Sewickley. PA, 1993.
11. C. Y. Wang, C. M. Wang "Fundamental frequencies of circular plates with internal ring support", *Journal of Sound and Vibration*.236 (2003) 1071-1078
12. S. Azimi, Free vibration of circular plates with elastic or rigid interior support, *Journal of Sound and Vibration* 120(1998) 37-52.
13. Z. Ding, Free vibration of arbitrarily shaped plates with concentric ring elastic and/or rigid supports, *Computers and Structures* 50 (1992).
14. Bhaskara Rao, L and Kameswara Rao, C. 2007. "Vibrations of Circular Plates with an Internal Ring Support and Flexible Edge Conditions", Proc. Of International Conference on Advances in Machine Design and Industry Automation (ICAMDIA-2007), COE, Pune, India, (2007) 182-186.
15. Bhaskara Rao, L and Kameswara Rao, C. 2007. "Frequency Analysis of Circular Plates with an Internal Elastic Ring Support and Flexible Edge Against Rotation and Simply Supported", International Conference on Computer Aided Engineering 2007 (CAE 2007), IIT, Chennai, India.

This article was downloaded by: [University of Connecticut]

On: 09 October 2014, At: 05:33

Publisher: Taylor & Francis

Informa Ltd Registered in England and Wales Registered Number: 1072954 Registered office: Mortimer House, 37-41 Mortimer Street, London W1T 3JH, UK



Mechanics Based Design of Structures and Machines: An International Journal

Publication details, including instructions for authors and subscription information:

<http://www.tandfonline.com/loi/lmbd20>

Buckling of Circular Plates with an Internal Elastic Ring Support and Elastically Restrained Guided Edge Against Translation

L. Bhaskara Rao^a & C. Kameswara Rao^b

^a Department of Mechanical Engineering , DRK Institute of Science and Technology , Hyderabad, India

^b Sci-Tech Patent Art (Pvt) Limited , Hyderabad, India

Published online: 06 Mar 2009.

To cite this article: L. Bhaskara Rao & C. Kameswara Rao (2009) Buckling of Circular Plates with an Internal Elastic Ring Support and Elastically Restrained Guided Edge Against Translation , Mechanics Based Design of Structures and Machines: An International Journal, 37:1, 60-72, DOI: [10.1080/15397730802706672](https://doi.org/10.1080/15397730802706672)

To link to this article: <http://dx.doi.org/10.1080/15397730802706672>

PLEASE SCROLL DOWN FOR ARTICLE

Taylor & Francis makes every effort to ensure the accuracy of all the information (the "Content") contained in the publications on our platform. However, Taylor & Francis, our agents, and our licensors make no representations or warranties whatsoever as to the accuracy, completeness, or suitability for any purpose of the Content. Any opinions and views expressed in this publication are the opinions and views of the authors, and are not the views of or endorsed by Taylor & Francis. The accuracy of the Content should not be relied upon and should be independently verified with primary sources of information. Taylor and Francis shall not be liable for any losses, actions, claims, proceedings, demands, costs, expenses, damages, and other liabilities whatsoever or howsoever caused arising directly or indirectly in connection with, in relation to or arising out of the use of the Content.

This article may be used for research, teaching, and private study purposes. Any substantial or systematic reproduction, redistribution, reselling, loan, sub-licensing, systematic supply, or distribution in any form to anyone is expressly forbidden. Terms & Conditions of access and use can be found at <http://www.tandfonline.com/page/terms-and-conditions>

Buckling of Circular Plates with an Internal Elastic Ring Support and Elastically Restrained Guided Edge Against Translation[#]

L. Bhaskara Rao¹ and C. Kameswara Rao²

¹Department of Mechanical Engineering, DRK Institute of Science and Technology, Hyderabad, India

²Sci-Tech Patent Art (Pvt) Limited, Hyderabad, India

Abstract: This article is concerned with the elastic buckling of circular plates with a support and elastically restrained *guided edge* against translation. The classical plate theory is used to derive the governing differential equation for circular plate with internal *elastic ring* support and elastically restrained guided edge support system. This work presents the existence of buckling mode switching with respect to the radius of internal *elastic ring* support. The buckling mode may not be *axisymmetric* as previously assumed. In general, the plate may buckle in an *axisymmetric* mode, but when the radius of the ring support becomes small, the plate may buckle in an *asymmetric* mode. The optimum radius of the internal *elastic ring* support is also determined. Extensive data is tabulated so that pertinent conclusions can be arrived at on the influence of translational restraint, Poisson's ratio and other boundary conditions on the buckling of uniform isotropic circular plates. The numerical results obtained are in good agreement with the previously published data.

Keywords: Buckling; Circular plate; Elastic edge; *Elastic ring* support; *Guided edge*; Mode switching; Translational spring stiffness.

Received August 25, 2007; Accepted March 3, 2008

[#]Communicated by I. Elishakoff.

Correspondence: L. Bhaskara Rao, Department of Mechanical Engineering, DRK Institute of Science and Technology, Bowrampet (V), Hyderabad 500043, India; E-mail: bhaskarbabu_20@yahoo.com

1. INTRODUCTION

Buckling of plates is an important topic in structural engineering. The prediction of buckling of structural members restrained laterally is important in the design of various engineering components. In particular, circular plates with internal elastic ring supports find applications in aeronautics (instrument mounting bases for space vehicles), rocket launching pads, aircrafts and naval vessels (instrument mounting bases). Based on Kirchhoff's theory, the elastic buckling of thin circular plates has been extensively studied by many authors after the pioneering work published by Bryan (1891). Since then, there have been extensive studies on the subject covering various aspects such as different materials, boundary and loading conditions. Also, the buckling of circular plates was studied by different authors (Brushes and Almroth, 1975; Wolkowsky, 1969). However, these sources only considered an *axisymmetric* case, which may not lead to the correct buckling load. Introducing internal *elastic ring* supports may increase the elastic buckling capacity of in-plane loaded circular plates significantly. Laura et al. (2000) investigated the elastic buckling problem of the aforesaid type of circular plates, and modeled the plate using the classical thin plate theory. In their study only *axisymmetric* modes are considered. Kunukkasseril and Swamidas (1974) are probably the first to consider elastic ring supports. They formulated the equations in general, but presented only the case of circular plate with a free edge. Although the circular symmetry of the problem allows for its significant simplification, many difficulties very often arise due to complexity and uncertainty of boundary conditions. This uncertainty could be due to practical engineering applications where the edge of the plate does not fall into the classical boundary conditions. It is an accepted fact that the condition on a periphery often tends to be in between the classical boundary conditions (free, clamped and simply supported) and may correspond more closely to some form of rotational and translational elastic restraints (Kim and Dickinson, 1990; Wang and Wang, 2001; Yamaki, 1958). In a recent study, Wang and Wang (2001) showed that when the ring support has a small radius, the buckling mode takes the asymmetric form. But they have studied only the circular plate with *rigid ring* support and elastically restrained edge against rotation and showed that the *axisymmetric* mode assumed by the previous authors might not yield the correct buckling load. In certain cases, an *asymmetric* mode would yield a lower buckling load. Recently, Wang (2003) studied the buckling of a circular plate with internal elastic ring support by considering only the classical boundary conditions. The purpose of the present work is to complete the results of the buckling of circular plates with an internal *elastic ring* support and elastically restrained

guided edge against translation by including the *asymmetric* modes, thus correctly determining the buckling loads.

2. DEFINITION OF THE PROBLEM

Consider a thin circular plate of radius R , uniform thickness h , Young's modulus E and Poisson's ratio ν and subjected to a uniform in-plane load, N along its boundary, as shown in Fig. 1. The circular plate is also assumed to be made of linearly elastic, homogeneous and isotropic material. The edge of the circular plate is elastically restrained guided edge against translation and supported by an internal elastic ring support, as shown in Fig. 1. The problem at hand is to determine the elastic critical buckling load of a circular plate with an internal elastic ring support and elastically restrained guided edge against translation.

3. ANALYTICAL FORMULATION OF THE SYSTEM

The plate is elastically restrained against translation and guided at the edge of radius R and supported on an internal elastic ring of smaller radius bR as shown in Fig. 1. Let subscript I denote the outer region $b \leq \bar{r} \leq 1$ and subscript II denote the inner region $0 \leq \bar{r} \leq b$. Here, all lengths are normalized by R . Using classical (Kirchhoff's) plate theory, the following fourth order differential equation is for buckling in polar coordinates (r, θ)

$$D\nabla^4 w + N\nabla^2 w = 0 \quad (1)$$

where w is the lateral displacement, N is the uniform compressive load at the edge. After normalizing the lengths by the radius of the plate R , Eq. (1) can be written as

$$D\nabla^4 \bar{w} + k^2 \nabla^2 \bar{w} = 0 \quad (2)$$

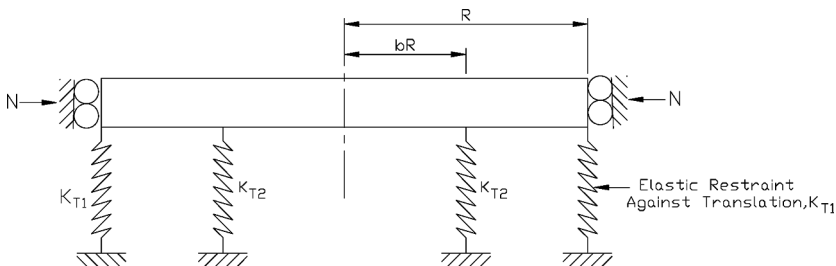


Figure 1. Buckling of a circular plate with an internal elastic ring support and elastically restrained guided edge against translation.

where $\nabla^2 = \frac{\partial^2}{\partial \bar{r}^2} + \frac{1}{\bar{r}} \frac{\partial}{\partial \bar{r}} + \frac{1}{\bar{r}^2} \frac{\partial^2}{\partial \theta^2}$ is the Laplace operator in the polar coordinates r and θ , where \bar{r} is the radial distance normalized by R . $\bar{D} = Eh^3/12(1 - \nu^2)$ is the flexural rigidity, $\bar{w} = w/R$, is normalized transverse displacement of the plate. $k^2 = R^2 N/\bar{D}$ is the nondimensional load parameter. Suppose there are n nodal diameters. In polar coordinates (r, θ) set

$$\bar{w}(\bar{r}, \theta) = \bar{u}(\bar{r}) \cos(n\theta) \quad (3)$$

General solution for the two regions are

$$\bar{u}_I(r) = C_1 J_n(k\bar{r}) + C_2 Y_n(k\bar{r}) + C_3 \bar{r}^n + C_4 \left\{ \frac{\log \bar{r}}{\bar{r}^{-n}} \right\} \quad (4)$$

$$\bar{u}_{II}(r) = C_5 J_n(k\bar{r}) + C_6 \bar{r}^n \quad (5)$$

where the top form of Eq. (4) is used for $n = 0$ and the bottom form is used for $n \neq 0$, C_1, C_2, C_3, C_4, C_5 and C_6 are constants, $J_n(\cdot)$ and $Y_n(\cdot)$ are the Bessel functions of the first and seconds of order n , respectively. Substituting Eqs. (4) and (5) into Eq. (3) gives the following:

$$\bar{w}_I(\bar{r}, \theta) = \left[C_1 J_n(k\bar{r}) + C_2 Y_n(k\bar{r}) + C_3 \bar{r}^n + C_4 \left\{ \frac{\log \bar{r}}{\bar{r}^{-n}} \right\} \right] \cos(n\theta) \quad (6)$$

$$\bar{w}_{II}(\bar{r}, \theta) = [C_5 J_n(k\bar{r}) + C_6 \bar{r}^n] \cos(n\theta) \quad (7)$$

The boundary conditions at outer regions of the circular plate in terms of slope and translational stiffness (K_{T1}) is given by the following expressions

$$\frac{\partial \bar{w}_I(\bar{r}, \theta)}{\partial \bar{r}} = 0 \quad (8)$$

$$V_r(\bar{r}) = -K_{T1} \bar{w}_I(\bar{r}, \theta) \quad (9)$$

The radial Kirchhoff's shear at outer edge is defined as follows:

$$V_r(\bar{r}) = -\frac{D}{R^3} \left[\frac{\partial}{\partial \bar{r}} \nabla^2 \bar{u}_I(\bar{r}) + (1 - \nu) \frac{1}{\bar{r}} \frac{\partial}{\partial \theta} \left(\frac{1}{\bar{r}} \frac{\partial^2 \bar{w}_I(\bar{r}, \theta)}{\partial \bar{r} \partial \theta} - \frac{1}{\bar{r}^2} \frac{\partial \bar{w}_I(\bar{r}, \theta)}{\partial \theta} \right) \right] \quad (10)$$

From Eqs. (9) and (10) we derive the following expressions:

$$\begin{aligned} & \left[\frac{\partial}{\partial \bar{r}} \nabla^2 \bar{w}_I(\bar{r}, \theta) + (1 - \nu) \frac{1}{\bar{r}} \frac{\partial}{\partial \theta} \left(\frac{1}{\bar{r}} \frac{\partial^2 \bar{w}_I(\bar{r}, \theta)}{\partial \bar{r} \partial \theta} - \frac{1}{\bar{r}^2} \frac{\partial \bar{w}_I(\bar{r}, \theta)}{\partial \theta} \right) \right] \\ & = \frac{K_{T1} R^3}{D} \bar{w}_I(\bar{r}, \theta) \end{aligned} \quad (11)$$

Apart from the elastically restrained guided edge against translation, there is an internal elastic ring support constraint and the continuity requirements of slope and curvature at the support (i.e., at $\bar{r} = b$)

$$\bar{u}_I(b) = \bar{u}_{II}(b) \quad (12)$$

$$\bar{u}'_I(b) = \bar{u}'_{II}(b) \quad (13)$$

$$\bar{u}''_I(b) = \bar{u}''_{II}(b) \quad (14)$$

$$\bar{u}'''_I(b) = \bar{u}'''_{II}(b) - T_{22}\bar{u}_{II}(b) \quad (15)$$

The nontrivial solutions to Eqs. (8), (11), and (12)–(15) are sought. The lowest value of k is the square root of the normalized buckling load. From Eqs. (6)–(8), (11), and (12)–(15) we derive the following equations:

$$\left[\frac{k}{2}P_1\right]C_1 + \left[\frac{k}{2}Q_1\right]C_2 + [n]C_3 + \left\{\begin{matrix} 1 \\ -n \end{matrix}\right\}C_4 = 0 \quad (16)$$

$$\begin{aligned} &\left[\frac{k^3}{8}P_3 + \frac{k^2}{4}P_2 - \frac{k}{2}\left(\frac{3}{4}k^2 + n^2(2-v) + 1\right)P_1\right. \\ &\quad \left.+ \left(n^2(3-v) - \frac{k^2}{2} - T_{11}\right)J_n(k)\right]C_1 \\ &\quad + \left[\frac{k^3}{8}Q_3 + \frac{k^2}{4}Q_2 - \frac{k}{2}\left(\frac{3}{4}k^2 + n^2(2-v) + 1\right)Q_1\right. \\ &\quad \left.+ \left(n^2(3-v) - \frac{k^2}{2} - T_{11}\right)Y_n(k)\right]C_2 + [n^2(n-1)v - n^3 - T_{11}]C_1 \\ &\quad - \left\{\begin{matrix} n^2(2-v) \\ -n^2(n+1)v + n^3 - T_{11} \end{matrix}\right\}C_4 = 0 \end{aligned} \quad (17)$$

$$J_n(kb)C_1 + Y_n(kb)C_2 + b^n C_3 + \left\{\begin{matrix} \log b \\ b^{-n} \end{matrix}\right\}C_4 - J_n(kb)C_5 - b^n C_6 = 0 \quad (18)$$

$$\begin{aligned} &\frac{k}{2}P'_1C_1 + \frac{k}{2}Q'_1C_2 + nb^{n-1}C_3 + \left\{\begin{matrix} \frac{1}{b} \\ -nb^{-n-1} \end{matrix}\right\}C_4 \\ &\quad - \frac{k}{2}P'_1C_5 - nb^{n-1}C_6 = 0 \end{aligned} \quad (19)$$

$$\begin{aligned} &\frac{k^2}{4}(P'_2 - 2J_n(kb))C_1 + \frac{k^2}{4}(Q'_2 - 2Y_n(kb))C_2 + n(n-1)b^{n-2}C_3 \\ &\quad + \left\{\begin{matrix} -\frac{1}{b^2} \\ n(n+1)b^{-n-2} \end{matrix}\right\}C_4 - \frac{k^2}{4}(P'_2 - 2J_n(kb))C_5 - n(n-1)b^{n-2}C_6 = 0 \end{aligned} \quad (20)$$

$$\begin{aligned}
& \frac{k^2}{8}(P'_3 - 3P'_1)C_1 + \frac{k^2}{8}(Q'_3 - Q'_1)C_2 + n(n-1)(n-2)b^{n-3}C_3 \\
& + \left\{ \frac{2}{b^3} \right. \\
& \quad \left. - n(n+1)(n+2)b^{-n-3} \right\} C_4 - \left[\frac{k^2}{8}(P'_3 - 3P'_1) - T_{22}J_n(kb) \right] C_5 \\
& - [n(n-1)(n-2)b^{n-3} - T_{22}b^n]C_6 = 0
\end{aligned} \tag{21}$$

where $T_{11} = \frac{K_{T1}R^3}{D}$, $T_{22} = \frac{K_{T2}R}{D}$;

$$P_1 = J_{n-1}(k) - J_{n+1}(k); \quad P_2 = J_{n-2}(k) + J_{n+2}(k);$$

$$P_3 = J_{n-3}(k) - J_{n+3}(k);$$

$$Q_1 = Y_{n-1}(k) - Y_{n+1}(k); \quad Q_2 = Y_{n-2}(k) + Y_{n+2}(k);$$

$$Q_3 = Y_{n-3}(k) - Y_{n+3}(k);$$

$$P'_1 = J_{n-1}(kb) - J_{n+1}(kb); \quad P'_2 = J_{n-2}(kb) + J_{n+2}(kb);$$

$$P'_3 = J_{n-3}(kb) - J_{n+3}(kb);$$

$$Q'_1 = Y_{n-1}(kb) - Y_{n+1}(kb); \quad Q'_2 = Y_{n-2}(kb) + Y_{n+2}(kb);$$

$$Q'_3 = Y_{n-3}(kb) - Y_{n+3}(kb);$$

The top forms of Eqs. (17)–(21) are used for $n = 0$ (*axisymmetric* buckling) and the bottom forms are used for $n \neq 0$ (*asymmetric* buckling).

4. SOLUTION

For the given values of n , v , T_{11} , T_{22} and b , the above set of equations gives an exact characteristic equation for nontrivial solutions of the coefficients C_1, C_2, C_3, C_4, C_5 and C_6 . For a nontrivial solution, the determinant of $[C]_{6 \times 6}$ must be factored out. The value of k is calculated from the characteristic equation by a simple root search. Using Mathematica, computer software with symbolic capabilities, solves this problem.

5. RESULTS AND DISCUSSIONS

There is a lot of flexibility of the code developed in Mathematica. It is used to determine the buckling load parameter for any range of translational constraints and also various translational spring stiffness constraints of an internal elastic ring support. This code is also implanted for various plate materials by adjusting Poisson's ratio. Since Poisson's ratio occurs as a parameter in most of the equations, the effect of this ratio on the roots of

the equations is also considered. The findings are presented in both tabular and graphical form. The buckling loads are calculated for various internal elastic ring support radii b , translational spring stiffness parameter and translational spring stiffness parameters of an internal elastic ring support. Poisson's ratio used in these calculations is 0.3.

Figures 2 and 3 show the variations of buckling load parameter k , with respect to the internal elastic ring support radius b , for various values of translational spring stiffness parameters and for a given translational spring stiffness parameters of an elastic ring support. It is observed from Figs. 2 and 3, that for a given value of T_{11} and T_{22} , the curve is composed of two segments. This is due to the switching of buckling modes. For a smaller internal elastic ring support radius b , the plate buckles in an asymmetric mode (i.e., $n = 1$). In this segment (as shown by dotted lines in Figs. 2 and 3) the buckling load decreases as b decreases in value. For larger internal elastic ring support radius b , the plate buckles in an axisymmetric mode (i.e., $n = 0$). In this segment (as shown by continuous lines in Figs. 2 and 3) the buckling load increases as b decreases up to a peak point corresponds to maximum buckling load and thereafter decrease as b decreases in value as shown in Figs. 2 and 3.

Figures 2 and 3 show the variations of buckling load parameter k , with respect to the internal elastic ring support radius b , for various values of translational spring stiffness parameters ($T_{11} = 1000$ and ∞) and keeping translational spring stiffness parameter of an internal elastic ring support constant ($T_{22} = 1000$). The cross-over radius varies from $b = 0.23134$ for $T_{11} = 1000$ and $T_{22} = 1000$ to $b = 0.23283$ for $T_{11} = \infty$ and $T_{22} = 1000$ as shown in Figs. 2 and 3. Note that when $b \rightarrow 1$, all

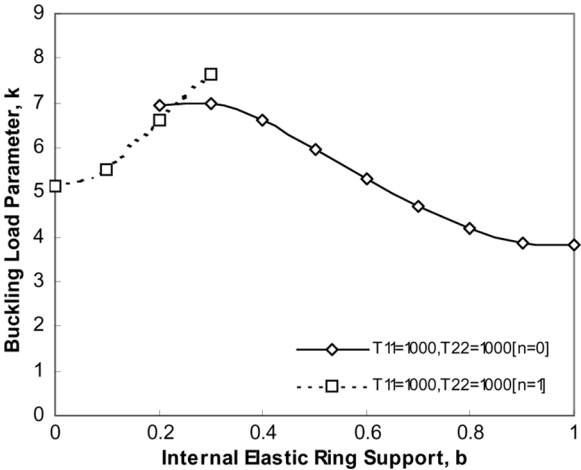


Figure 2. Buckling load parameter k , versus internal elastic ring support radius b , for various values of $T_{11} = T_{22} = 1000$.

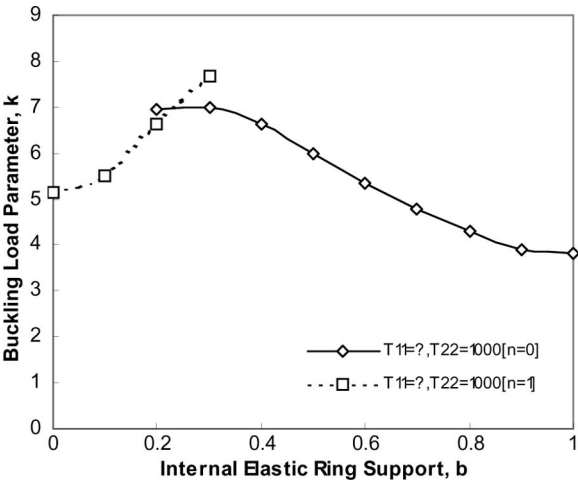


Figure 3. Buckling load parameter k , versus internal *elastic ring* support radius b , for various values of $T_{11} = \infty$ and $T_{22} = 1000$.

curves (as shown in Figs. 2 and 3) converge to $k = 3.83163$, which is the first root of $J_1(k) = 0$ of the clamped plate (i.e., the buckling solution approaches that of a clamped plate without any internal ring support, $k = 3.83163$). This is in well agreement with those of Wang et al. (2005). Of interest in the design of supported circular plates is the optimal location of the internal elastic ring support for maximum buckling load. The optimal solutions for this case are presented in Table 1. Analysis of asymmetric modes of buckling (various values of n) are also determined; however, it is observed that the fundamental buckling load corresponds to asymmetric mode of $n = 1$.

Figures 4 and 5 show the variations of buckling load parameter k , with respect to the internal elastic ring support radius b , for various values of translational spring stiffness parameters of an elastic ring support and for a given value of translational spring stiffness parameters. It is observed from Figs. 4 and 5, which for a given value of T_{11} and T_{22} , the curve is composed of two segments. This is due to the switching

Table 1. Optimal location of an internal *elastic ring* support b_{opt} and the corresponding buckling load parameter k_{opt}

$T_{22} = 1000$		
T_{11}	1000	∞
b_{opt}	0.300	0.2993
k_{opt}	6.991	6.99308

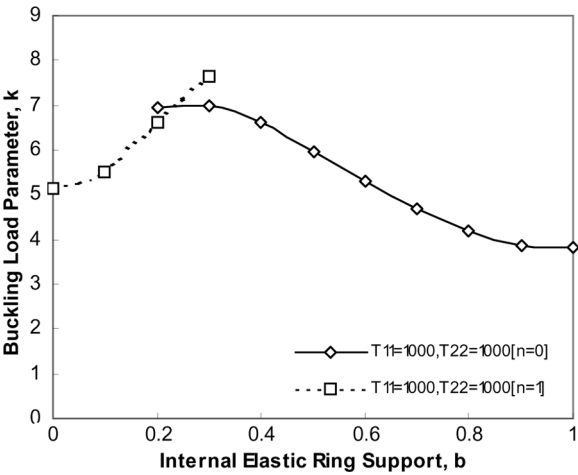


Figure 4. Buckling load parameter k , versus internal *elastic ring* support radius b , for various values of $T_{11} = T_{22} = 1000$.

of buckling modes. For a smaller internal elastic ring support radius b , the plate buckles in an asymmetric mode (i.e., $n = 1$). In this segment (as shown by dotted lines in Figs. 4 and 5), the buckling load decreases as b decreases in value. For larger internal elastic ring support radius b , the plate buckles in an axisymmetric mode (i.e., $n = 0$). In this segment (as shown by continuous lines in Figs. 4 and 5), the buckling load increases as b decreases up to a peak point corresponds to maximum

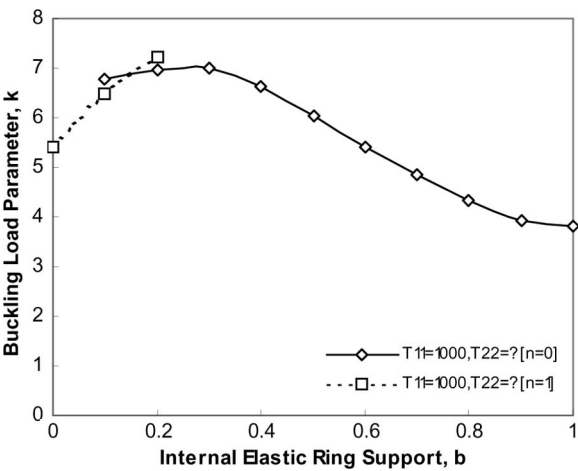


Figure 5. Buckling load parameter k , versus internal *elastic ring* support radius b , for various values of $T_{11} = 1000$ and $T_{22} = \infty$.

buckling load and thereafter decrease as b decreases in value as shown in Figs. 4 and 5. Analysis of asymmetric modes of buckling (various values of n) is also determined, however it is observed that the fundamental buckling load is corresponding to asymmetric mode of $n = 1$.

Figures 4 and 5 show the variations of buckling load parameter k , with respect to the internal elastic ring support radius b , for various values of translational spring stiffness parameters of an internal elastic ring support ($T_{22} = 1000$ and ∞) and keeping translational spring stiffness parameters constant ($T_{11} = 1000$). The cross-over radius varies from $b = 0.23134$ for $T_{22} = 1000$ and $T_{11} = 1000$ to $b = 0.1522$ for $T_{22} = \infty$ and $T_{11} = 1000$ as shown in Figs. 4 and 5. Note that when $b \rightarrow 1$, all curves (as shown in Figs. 4 and 5) converge to $k = 3.83163$, which is the first root of $J_1(k) = 0$ of the clamped plate (i.e., the buckling solution approaches that of a clamped plate without any internal ring support; $k = 3.83163$). This is in well agreement with those of Wang et al. (2005). Of interest in the design of supported circular plates is the optimal location of the internal elastic ring support for maximum buckling load. The optimal solutions for this case are presented in Table 2. Results of this kind were scarce in the literature. However, the results are compared with the following cases:

- (i) The buckling load parameters k , for clamped edges (by considering $T_{11} = 10^5$ and $T_{22} \rightarrow \infty$, i.e., circular plate with clamped edge and internal concentric *rigid ring* support) are compared with those obtained by Wang et al. (1993, 2005) and Bhaskara Rao and Kameswara Rao (2007) as shown in Table 3. Wang et al. (1993) is considered because the plate can be considered as thin for $\tau = 0.001$.
- (ii) When T_{11} and $T_{22} \rightarrow \infty$, or rigid support, the optimum location is at a radius of $b = 0.2663$, with a buckling load of $k = 7.01554$ and that agrees with the results of Wang and Wang (2001).
- (iii) $T_{11} \rightarrow \infty$ and $T_{22} = 1$, or rigid support with internal *elastic ring* support, the optimum location is at a radius of $b = 0.290$, with a buckling load of $k = 3.8711$ and that agrees with the results of Wang (2003).

Table 2. Optimal locations of an internal *elastic ring* support b_{opt} and the corresponding buckling load parameter k_{opt}

$T_{11} = 1000$		
T_{22}	1000	∞
b_{opt}	0.3	0.2993
k_{opt}	6.991	6.995

Table 3. Comparison of buckling load parameter k , with Wang et al. (1993, 2005) and Bhaskara Rao and Kameswara Rao (2007) for clamped edge for rotational stiffness parameter $R_{11} = 10^5$ and $\nu = 0.3$

Ring support radius, b	Wang et al. (1993)	Wang et al. (2005)	Bhaskara Rao and Kameswara Rao (2007)	Present
0.1	—	6.5009*	6.50095*	6.50095*
0.2	6.9559	6.9558	6.95582	6.95582
0.3	6.9948	6.9947	6.99475	6.99475
0.4	6.6627	6.6625	6.66248	6.66248
0.5	6.0749	6.0745	6.07454	6.07454
0.6	5.476	5.4755	5.4755	5.4755
0.7	4.9532	4.9526	4.95263	4.95263
0.8	4.5134	4.5127	4.51266	4.51266
0.9	4.1448	4.1436	4.14357	4.14357
0.99	3.8667	3.8604	3.86061	3.86061

*Asymmetric buckling load parameters.

- (iv) When $T_{11} = 0$ and $T_{22} = 100$, or guided edge with internal *elastic ring* support, the optimum location is at a radius of $b = 0.4740$, with a buckling load of $k = 3.83163$ and that agrees with the results of Wang (2003).

6. CONCLUSIONS

The buckling of thin circular plates with an internal *elastic ring* support and elastically restrained guided edge against translation has been solved. Also the buckling loads are given for various spring stiffness parameter $[T_{11}]$ at the edges that simulate the translational restraints where $T_{11} \rightarrow \infty$, represents a clamped edge. Also the buckling loads are given for various translational spring stiffness parameters of an internal *elastic ring* support $[T_{22}]$. Two-dimensional plots are drawn for a wide range of translational constraints and translational constraints of an internal *elastic ring* support. It is observed that the buckling mode switches from an *asymmetric* mode to an *axisymmetric* mode at a particular internal *elastic ring* support radius. The cross-over radius is determined for different values of translational constraints and translational constraints of *elastic ring*. The optimal internal *elastic ring* support is affected by the translational stiffness parameters and translational spring stiffness parameters of an internal *elastic ring* support. However, it is observed that the influence of translational spring stiffness parameters on buckling load is not much more predominant than that of rotational spring stiffness parameters and elastic ring

support constraints (Bhaskara Rao and Kameswara Rao, 2007). Also, it is observed that for $T_{11} = 0$, the symmetric buckling mode is independent of the internal elastic ring support and gives a constant buckling load. In this paper the characteristic equations are exact; therefore the results can be calculated to any accuracy. These exact solutions can be used to check numerical or approximate results. A comparison of studies demonstrates the accuracy and stability of the present work. The effect of various parameters, such as translational stiffness parameters and translational spring stiffness parameters of an internal *elastic ring* support, on buckling loads of circular plates with internal elastic ring support and an elastically restrained guided edge system were studied in detail. The tabulated buckling results are useful to designers in vibration control, structural design and related industrial applications.

NOMENCLATURE

$w(r, \theta)$	Transverse deflection of the plate
h	Thickness of a plate
R	Radius of a plate
b	Nondimensional radius of ring support
ν	Poisson's ratio
E	Young's modulus of a material
D	Flexural rigidity of a material
K_{T1}	Translational spring stiffness
K_{T2}	Translational spring stiffness of internal elastic ring
T_{11}	Nondimensional translational flexibility parameter
T_{22}	Nondimensional translational flexibility parameter of internal elastic ring
N	Uniform in-plane compressive load
k	Nondimensional buckling load parameter

REFERENCES

Bhaskara Rao, L., Kameswara Rao, C. (2007). Buckling of circular plates with an internal ring support and elastically restrained edge against rotation and translation. Fifteenth International Conference on Nuclear Engineering (ICONE 15). ICONE-10864. Japan, April 22–26.

Brushes, D. O., Almroth, B. O. (1975). *Buckling of Bars, Plates and Shells*. New York: McGraw-Hill.

Bryan, G. H. (1891). On the stability of a plane plate under thrust in its own plane with application to the buckling of the side of a ship. *Proceedings, London Math Society* 22:54–67.

- Kim, C. S., Dickinson, S. M. (1990). The flexural vibration of the isotropic and polar orthotropic annular and circular plates with elastically restrained peripheries. *Journal of Sound and Vibration* 143:171–179.
- Kunukkasseril, V. X., Swamidas, A. S. J. (1974). Vibration of continuous circular plates. *International Journal of Solids and Structures* 10:603–619.
- Laura, P. A. A., Gutierrez, R. H., Sanzi, H. C., Elvira, G. (2000). Buckling of circular, solid and annular plates with an intermediate circular support. *Ocean Engineering* 27:749–755.
- Wang, C. Y. (2003). Buckling of a circular plate with internal elastic ring support. *Mechanics Based Design of Structures and Machines* 31(1):93–102.
- Wang, C. Y., Wang, C. M. (2001). Buckling of circular plates with an internal ring support and elastically restrained edges. *Thin-Walled Structures* 39:821–825.
- Wang, C. M., Aung, T. M. (2005). Buckling of circular mindlin plates with an internal ring support and elastically restrained edge. *Journal of Engineering Mechanics* 131(4):359–366.
- Wang, C. M., Xiang, Y., Kitipornchai, S., Liew, K. M. (1993). Axisymmetric buckling of circular mindlin plates with ring supports. *Journal of Structural Engineering* 119(3):782–793.
- Wang, C. M., Wang, C. Y., Reddy, J. N. (2005). *Exact Solutions for Buckling of Structural Members*. Boca Raton, FL: CRC Press.
- Wolkowisky, J. H. (1969). Buckling of the circular plate embedded in elastic springs, an application to geophysics. *Communications on Pure and Applied Mathematics* 22:367–667.
- Yamaki, N. (1958). Buckling of a thin annular plate under uniform compression. *Journal of Applied Mechanics* 25:267–273.

Vibrations of Elastically Restrained Circular Plates Resting on Partial Winkler Foundation

Chellapilla Kameswara Rao^{*,1} and Lokavarapu Bhaskara Rao²

¹Hitech College of Engineering & Technology, Gandipet-Himayatnagar, Hydreabad-500075, India

²Deapartment of Mechanical Engineering, D.R.K. College of Engineering and Technology, Hyderabad, Andhra Pradesh, India

Abstract: This work describes a study of vibration characteristics of thin circular plates with elastic edge support and resting on partial Winkler-type elastic foundation. The foundation is described by the Winkler model, which is called as single parameter foundation. The exact analytical method is used to derive the frequency equation of the circular plate with elastic edge support-conditions and resting on partial elastic foundation system. Parametric investigations on the behavior of circular plates with elastic edge support and resting on partial elastic foundation have been carried out with respect to various values of transverse stiffness parameter, foundation parameter for a variety of boundary conditions. Extensive data is tabulated so that pertinent conclusions can be arrived at on the influence of translational edge restraint, and the foundation modulus parameters of the Winkler foundation on the natural frequencies of uniform isotropic circular plates. A comparison of the results obtained here in this paper with those available in the literature shows an excellent agreement.

Keywords: Circular plate, restrained edge, translational spring stiffness, elastic foundation.

1. INTRODUCTION

The structural behavior of circular plates on elastic foundation is of great interest for the design on many engineering problems. Such plate systems can be found in many engineering applications, ranging from more conventional civil engineering, mechanical engineering and marine engineering to an aerospace engineering. Research work in this area has been discussed in a series of papers by Lessia [1, 2] and Bert [3, 4]. The vibration of a circular plate supported laterally by an elastic foundation was studied by Leissa in Ref. [5] from which he deduced that the effect of a Winkler foundation merely increases the square of the natural frequency of the plate by a constant. Laura *et al.* [6], while studying the case of a circular plate partially embedded in a Winkler foundation, found that a simple frequency relation like the above no longer holds good, and thus reached a similar conclusion. The most general soil model used in practical applications is the Winkler model [7] in which the soil layer is represented by unconnected closely spaced elastic springs.

The present study of circular plates on elastic foundations with elastic edge support finds useful applications in foundation designs of large storage tanks, deep-sea pressure vessels and heavy machines [8].

However, studies of the vibration of plates considering the combined effects of elastic foundations and elastic

constraints are relatively scarce in the literature [9]. The vibration characteristics of plates resting on an elastic medium are different from those of the plates supported only on the boundary. There are many difficulties which very often arise due to complexity and uncertainty of boundary conditions. This uncertainty could be due to practical engineering applications where the edge of the plate does not fall into the classical boundary conditions. The accepted fact is that the condition on a periphery often tends to be part away between the classical boundary conditions (simply supported, free, pinned) and non-classical boundary conditions (elastic edge restraints) [10]. Therefore, when the boundary conditions of the plate deviate from classical cases, elastic edge restraints need to be considered. The present study considers the problem of vibrations of circular plates elastically restrained against translation and resting on partial elastic foundation i.e. on partial Winkler foundation. In this paper, exact solutions for first Eigen-frequencies of thin circular plates for various values of non-dimensional parameters are presented in graphical and tabular form, which may be useful for engineers in practice as well as to researchers as benchmark results for checking the relative accuracy of the approximate results obtained through alternate methods of solution.

2. DEFINITION OF THE PROBLEM

Consider a thin isotropic, circular plate of radius R , uniform thickness h , Young's modulus E , flexural rigidity D and Poisson's ratio ν as shown in Fig. (1). The plate edge is considered to be elastically restrained in translation and partially supported on Winkler foundation. The plate is also assumed to be made of linearly elastic, homogeneous and isotropic material. However, the effects of shear

*Address correspondence to this author at the Hitech College of Engineering & Technology, Gandipet-Himayatnagar, Hydreabad-500075, India; E-mail: chellapilla95@gmail.com

deformation and rotary inertia are neglected in the present paper as the plate considered is quite thin. The problem at hand is to determine the frequencies of a circular plate with elastically restrained edge and resting on partial elastic foundation.

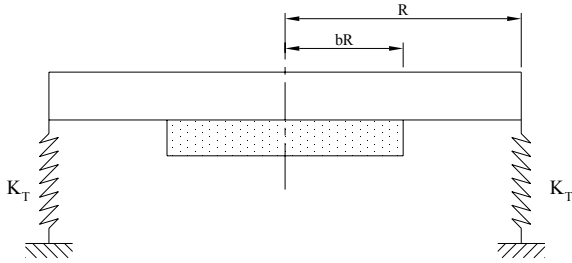


Fig. (1). A thin circular plate with rotational K_R and translational K_T elastic edge constraints and supported on partial elastic foundation.

3. MATHEMATICAL FORMULATION

The geometrical and loading configuration of the plate is axi-symmetric and consequently, deflection shape of the plate will be axially symmetric as well. Consider a circular plate of radius R being supported in the interior by a foundation of radius bR as shown in Fig. (1). Let the subscript **I** denote the outer region $b \leq r \leq 1$ and the subscript **II** denote the inner region $0 \leq r \leq b$. Here, all lengths are normalized with respect to R . The non-dimensional radius at the outer edge is 1 and at the inner edge is b . As per the classical Kirchhoff's plate theory [11, 12], the fourth order differential equation describing the free flexural vibrations of a thin circular uniform plate for region **I**, in polar coordinates (r, θ) is given by:

$$\nabla^4 w_I - k^4 w_I = 0 \quad (1)$$

where $k^4 = R^4 \omega^2 \rho / D$ which is the non-dimensional frequency parameter.

The plate Eq. (5) for region **II** is:

$$\nabla^4 w_{II} - k^4 w_{II} + \lambda^4 w_{II} = 0 \quad (2)$$

where $\lambda^4 = R^4 K_w / D$ which represents the no-dimensional foundation stiffness parameter.

Let the solution to the Eq. (1) be represented as:

$$w = u(r) \cos(n\theta) \quad (3)$$

where r is the radius normalized w.r.t R , n is the number of nodal diameters. The function u a linear combination of the Bessel functions $J_n(kr)$, $Y_n(kr)$, $I_n(kr)$ & $K_n(kr)$ is:

$$u_I(r) = C_1 J_n(kr) + C_2 Y_n(kr) + C_3 I_n(kr) + C_4 K_n(kr) \quad (4)$$

where C_1, C_2, C_3 & C_4 are constants.

$J_n(\cdot)$ and $Y_n(\cdot)$ are the Bessel functions of the first and second kinds of order n respectively.

$I_n(\cdot)$ and $K_n(\cdot)$ are the modified Bessel functions of the first and second kinds of order n respectively.

Substituting Eq. (4) in Eq. (3) gives the following:

$$w_I(r, \theta) = \left[C_1 J_n(kr) + C_2 Y_n(kr) + C_3 I_n(kr) + C_4 K_n(kr) \right] \cos(n\theta) \quad (5)$$

Unlike Eq. (1), the general solution to Eq. (2), is more complicated and the following three special cases are considered in this paper.

Case (i) If $k > \lambda$, the solution to Eq. (2) is:

$$u_{II}(r) = C_5 J_n(k_1 r) + C_6 I_n(k_1 r) \quad (6)$$

where $k_1 = (k^4 - \lambda^4)^{\frac{1}{4}}$.

Substituting Eq. (6) in Eq. (3), we get:

$$w_{II}(r, \theta) = \left[C_5 J_n(k_1 r) + C_6 I_n(k_1 r) \right] \cos(n\theta) \quad (7)$$

Case (ii) If $k = \lambda$, the solution to Eq. (2) is given by:

$$u_{II}(r) = C_5 r^n + C_6 r^{n+2} \quad (8)$$

Substitution of Eq. (8) in Eq. (3) gives the following:

$$w_{II}(r, \theta) = \left[C_5 r^n + C_6 r^{n+2} \right] \cos(n\theta) \quad (9)$$

Case (iii) If $k < \lambda$, the solution to Eq. (2) is given by:

$$u_{II}(r) = C_5 \text{Re}[J_n(\sqrt{ik_2} r)] + C_6 \text{Im}[\sqrt{ik_2} r] \quad (10)$$

where $k_2 = (\lambda^4 - k^4)^{\frac{1}{4}}$.

Substitution of Eq. (10) in Eq. (3) gives the following:

$$w_{II}(r, \theta) = \left[C_5 \text{Re}[J_n(\sqrt{ik_2} r)] + C_6 \text{Im}[\sqrt{ik_2} r] \right] \cos(n\theta) \quad (11)$$

For an elastically restrained circular plate, the boundary conditions at the edge of the plate in terms of rotational and translational stiffness are given by the following expressions:

$$v_r(r, \theta) = -K_T w_I(r, \theta) \quad (12)$$

$$M_r(r, \theta) = K_R \frac{\partial w}{\partial r}(r, \theta) \quad (13)$$

where the shearing force and bending moment as per Kelvin-Kirchhoff theory are defined as follows:

$$V_r = -D \left[\frac{\partial}{\partial r} \nabla^2 w + (1-\nu) \frac{1}{r} \frac{\partial}{\partial \theta} \left(\frac{1}{r} \frac{\partial^2 w}{\partial r \partial \theta} - \frac{1}{r^2} \frac{\partial w}{\partial \theta} \right) \right] \quad (14)$$

$$M_r = -D \left[\frac{\partial^2 w}{\partial r^2} + \nu \left(\frac{1}{r} \frac{\partial w}{\partial r} + \frac{1}{r^2} \frac{\partial^2 w}{\partial \theta^2} \right) \right] \quad (15)$$

B.C. A : For a circulate plate with outer edge elastically restrained against rotation only, the Eqs. (12) and (13) become:

$$v_r(r, \theta) = -K_T w_I(r, \theta) \quad (12a)$$

$$M_r(r, \theta) = 0 \quad (13a)$$

From Eqs.(12a) & (14)

$$\left[\frac{\partial}{\partial r} \nabla^2 w_I(r, \theta) + (1-\nu) \frac{1}{r} \frac{\partial}{\partial \theta} \left(\frac{1}{r} \frac{\partial^2 w_I(r, \theta)}{\partial r \partial \theta} - \frac{1}{r^2} \frac{\partial w_I(r, \theta)}{\partial \theta} \right) \right] = \frac{K_T}{D} w_I(r, \theta) \quad (14a)$$

From Eqs.(13a) & (15):

$$\left[\frac{\partial^2 w_l(r, \theta)}{\partial r^2} + v \left(\frac{1}{r} \frac{\partial w_l(r, \theta)}{\partial r} + \frac{1}{r^2} \frac{\partial^2 w_l(r, \theta)}{\partial \theta^2} \right) \right] = 0 \quad (15a)$$

The plate is continuous in terms of displacement, slope and moment at $r = b$. Therefore, the boundary conditions are:

$$w_l(b) = w_{ll}(b) \quad (16)$$

$$w'_l(b) = w'_{ll}(b) \quad (17)$$

$$w''_l(b) = w''_{ll}(b) \quad (18)$$

$$w'''_l(b) = w'''_{ll}(b) \quad (19)$$

Then for region **I**, from Eqs. (5) and (17), we get the following expression:

$$\begin{aligned} & \left[\frac{k^2}{4} J_{m2} + \frac{k v}{2} J_{m1} - \left(\frac{k^2}{2} + v n^2 \right) J_n(k) \right] C_1 \\ & + \left[\frac{k^2}{4} Y_{n2} + \frac{k v}{2} Y_{n1} - \left(\frac{k^2}{2} + v n^2 \right) Y_n(k) \right] C_2 \\ & + \left[\frac{k^2}{4} I_{p2} + \frac{k v}{2} I_{p1} - \left(\frac{k^2}{2} + v n^2 \right) I_n(k) \right] C_3 \\ & + \left[\frac{k^2}{4} k_{q2} - \frac{k v}{2} k_{q1} + \left(\frac{k^2}{2} - v n^2 \right) k_n(k) \right] C_4 = 0 \end{aligned} \quad (20)$$

B.C. B: For a circulate plate with outer edge elastically restrained against translation only, Eqs. (12) and (13) become:

$$v_r(r, \theta) = 0 \quad (12b)$$

$$M_r(r, \theta) = K_R \frac{\partial w}{\partial r}(r, \theta) \quad (13b)$$

Then for region **I**, from Eqs. (5) and (16), we get the following expression:

$$\begin{aligned} & \left[\frac{k^3}{8} J_{m3} + \frac{k^2}{4} J_{m2} - \frac{k}{2} \left(\frac{3}{4} k^2 + n^2 (2 - v) + 1 \right) J_{m1} \right. \\ & \left. + \left(n^2 (2 - v) - \frac{k^2}{2} - \frac{K_r}{D} \right) J_n(k) \right] C_1 + \\ & \left[\frac{k^3}{8} Y_{n3} + \frac{k^2}{4} Y_{n2} - \frac{k}{2} \left(\frac{3}{4} k^2 + n^2 (2 - v) + 1 \right) Y_{n1} \right. \\ & \left. + \left(n^2 (2 - v) - \frac{k^2}{2} - \frac{K_r}{D} \right) Y_n(k) \right] C_2 + \\ & \left[\frac{k^3}{8} I_{p3} + \frac{k^2}{4} I_{p2} + \frac{k}{2} \left(\frac{3}{4} k^2 + n^2 (-2 + v) - 1 \right) I_{p1} \right. \\ & \left. + \left(n^2 (2 - v) + \frac{k^2}{2} - \frac{K_r}{D} \right) I_n(k) \right] C_3 + \\ & \left[\frac{k^3}{8} k_{Q3} + \frac{k^2}{4} K_{Q2} + \frac{k}{2} \left(-\frac{3}{4} k^2 + n^2 (2 - v) + 1 \right) K_{Q1} \right. \\ & \left. + \left(n^2 (2 - v) + \frac{k^2}{2} - \frac{K_r}{D} \right) K_n(k) \right] C_4 = 0 \end{aligned} \quad (21)$$

where

$$\begin{aligned} J_{m1} &= J_{n-1}(k) - J_{n+1}(k); J_{m2} = J_{n-2}(k) + J_{n+2}(k); \\ J_{m3} &= J_{n-3}(k) - J_{n+3}(k); Y_{n1} = Y_{n-1}(k) - Y_{n+1}(k); \\ Y_{n2} &= Y_{n-2}(k) + Y_{n+2}(k); Y_{n3} = Y_{n-3}(k) - Y_{n+3}(k); \\ I_{p1} &= I_{n-1}(k) + I_{n+1}(k); I_{p2} = I_{n-2}(k) + I_{n+2}(k); \\ I_{p3} &= I_{n-3}(k) + I_{n+3}(k); K_{q1} = K_{n-1}(k) + K_{n+1}(k); \\ K_{q2} &= K_{n-2}(k) + K_{n+2}(k); K_{q3} = K_{n-3}(k) + K_{n+3}(k); \end{aligned}$$

Case (i): Considering the case (i) i.e. $k > \lambda$, for the region **(II, n)**, the solution to Eq. (2) is given by Eq.(7) and for this case the boundary conditions, Eqs. (16), (17), (18) and (19) give us the following:

$$J_n(kb)C_1 + Y_n(kb)C_2 + I_n(kb)C_3 + K_n(kb)C_4 - J_n(k1b)C_5 - I_n(k1b)C_6 = 0 \quad (22)$$

$$\frac{k}{2} J'_{m1} C_1 + \frac{k}{2} Y'_{n1} C_2 + \frac{k}{2} I'_{p1} C_3 - \frac{k}{2} K'_{q1} C_4 - \frac{k_1}{2} J'_{m11} C_5 - \frac{k_1}{2} I'_{p11} C_6 = 0 \quad (23)$$

$$\begin{aligned} & \frac{k^2}{4} (J'_{m2} - 2J_n(kb))C_1 + \frac{k^2}{4} (Y'_{n2} - 2Y_n(kb))C_2 + \\ & \frac{k^2}{4} (I'_{p2} + 2I_n(kb))C_3 + \frac{k^2}{4} (K'_{q2} + 2K_n(kb))C_4 \\ & - \frac{k^2_1}{4} (J'_{m22} - 2J_n(k_1b))C_5 - \\ & \frac{k^2_1}{4} (I'_{p22} + 2I_n(k_1b))C_6 = 0 \end{aligned} \quad (24)$$

$$\begin{aligned} & \frac{k^3}{8} [J'_{m3} - 3J'_{m1}]C_1 + \frac{k^3}{8} [Y'_{n3} - 3Y'_{n1}]C_2 + \\ & \frac{k^3}{8} [I'_{p3} + 3I'_{p1}]C_3 - \frac{k^3}{8} [K'_{q3} + 3K'_{q1}]C_4 - \\ & \frac{k^3_1}{8} [J'_{m33} - 3J'_{m11}]C_5 - \\ & \frac{k^3_1}{8} [I'_{p33} + 3I'_{p11}]C_6 = 0 \end{aligned} \quad (25)$$

Case (ii): Considering the case (ii) i.e. $k = \lambda$, for the region **(II, n)**, the solution to Eq. (2) is given by Eq. (9) and for this case the boundary conditions, Eqs. (16), (17), (18) and (19) give us the following:

$$J_n(kb)C_1 + Y_n(kb)C_2 + I_n(kb)C_3 + K_n(kb)C_4 - b^n C_5 - b^{n+2} C_6 = 0 \quad (26)$$

$$\begin{aligned} & \frac{k}{2} J'_{m1} C_1 + \frac{k}{2} Y'_{n1} C_2 + \frac{k}{2} I'_{p1} C_3 - \\ & \frac{k}{2} K'_{q1} C_4 - n b^{n-1} C_5 - (n+2) b^{n+1} C_6 = 0 \end{aligned} \quad (27)$$

$$\begin{aligned} & \frac{k^2}{4} (J'_{m2} - 2J_n(kb))C_1 + \frac{k^2}{4} (Y'_{n2} - 2Y_n(kb))C_2 \\ & + \frac{k^2}{4} (I'_{p2} + 2I_n(kb))C_3 + \frac{k^2}{4} (K'_{q2} + 2K_n(kb))C_4 \\ & - (n(n-1)b^{n-2})C_5 - (n+1)(n+2)b^n C_6 = 0 \end{aligned} \quad (28)$$

$$\begin{aligned} & \frac{k^3}{8} [J'_{m3} - 3J'_{m1}]C_1 + \frac{k^3}{8} [Y'_{n3} - 3Y'_{n1}]C_2 \\ & + \frac{k^3}{8} [I'_{p3} + 3I'_{p1}]C_3 - \frac{k^3}{8} [K'_{q3} + 3K'_{q1}]C_4 - \\ & [n(n-1)(n-2)b^{n-3}]C_5 - [n(n+1)(n+2)b^{n-1}]C_6 = 0 \end{aligned} \quad (29)$$

where

$$\begin{aligned}
J'_{m1} &= J_{n-1}(kb) - J_{n+1}(kb); J'_{m2} = J_{n-2}(kb) + J_{n+2}(kb); \\
J'_{m3} &= J_{n-3}(kb) - J_{n+3}(kb); Y'_{n1} = Y_{n-1}(kb) - Y_{n+1}(kb); \\
Y'_{n2} &= Y_{n-2}(kb) + Y_{n+2}(kb); Y'_{n3} = Y_{n-3}(kb) - Y_{n+3}(kb); \\
I'_{p1} &= I_{n-1}(kb) + I_{n+1}(kb); I'_{p2} = I_{n-2}(kb) + I_{n+2}(kb); \\
I'_{p3} &= I_{n-3}(kb) + I_{n+3}(kb); K'_{q1} = K_{n-1}(kb) + K_{n+1}(kb); \\
K'_{q2} &= K_{n-2}(kb) + K_{n+2}(kb); K'_{q3} = K_{n-3}(kb) + K_{n+3}(kb)
\end{aligned}$$

Case (iii) : Considering the case (iii), for $k < \lambda$, for region (II, n), the solution to Eq. (2) is given by Eq. (11) and for this case the boundary conditions Eqs. (16), (17), (18) and (19) give us the following:

$$J_n(kb)C_1 + Y_n(kb)C_2 + I_n(kb)C_3 + K_n(kb)C_4 - \text{Re}[J_n(\sqrt{ik_2b})]C_5 - \text{Im}[J_n(\sqrt{ik_2b})]C_6 = 0 \quad (30)$$

$$J'_n(kb)C_1 + Y'_n(kb)C_2 + I'_n(kb)C_3 - K'_n(kb)C_4 - \text{Re}[J'_n(\sqrt{ik_2b})]C_5 - \text{Im}[J'_n(\sqrt{ik_2b})]C_6 = 0 \quad (31)$$

$$J''_n(kb)C_1 + Y''_n(kb)C_2 + I''_n(kb)C_3 - K''_n(kb)C_4 - \text{Re}[J''_n(\sqrt{ik_2b})]C_5 - \text{Im}[J''_n(\sqrt{ik_2b})]C_6 = 0 \quad (32)$$

$$J'''_n(kb)C_1 + Y'''_n(kb)C_2 + I'''_n(kb)C_3 - K'''_n(kb)C_4 - \text{Re}[J'''_n(\sqrt{ik_2b})]C_5 - \text{Im}[J'''_n(\sqrt{ik_2b})]C_6 = 0 \quad (33)$$

Therefore, the set of Eqs. (20), (21), (30)-(33), represent for the case $k < \lambda$.

4. SOLUTION

For the given values of $n, \nu, b, T_{11}, R_{11}$ & λ the above set of equations gives an exact characteristic equation for non-trivial solutions of the coefficients C_1, C_2, C_3, C_4, C_5 & C_6 . For non-trivial solution, the determinant of $[C]_{6 \times 6}$ must vanish. This eigenvalue problem was solved using Mathematica computer software with symbolic capabilities.

5. RESULTS & DISCUSSIONS

There is a lot of flexibility in the code developed in Mathematica. It is used to determine the frequency parameter for any range of translational constraints. This code is also implanted for various plate materials by adjusting Poisson's ratio. Since Poisson's ratio occurs as a parameter in most of the equations, the effect of this ratio on the roots of the equations is also considered. The findings are presented in

both tabular and graphical form. The frequencies are calculated for various radius radii b , translational spring stiffness parameter.

The frequency values for the plate with elastically restrained edge against translation and resting on partial foundation, at various values of the translational stiffness parameter, T_{11} and for constant λ , have been calculated and the results are shown in the Table 1 and graphically in Fig. (2). The frequency has increased considerably as increase in translational constraint. The results also listed in Table 2 and graphically in Fig. (3), for different values of foundation constraint (λ) by keeping translational constraint (T_{11}) constant. For large foundation stiffness the curves will be asymptotic in nature. The results are shown in Fig. (4) for different values of Translational and foundation constraints. It is observed that the frequency is increases as two constraints increase simultaneously. It was found that the $n=0$ axisymmetric mode gives the fundamental frequency. When $b=0$, the foundation is absent and the frequency is governed by the elastically restrained edge plate, i.e. $k=2.1834$. When $b=1$, the plate has full foundation support, and the frequency is $k_0=2.1834$. The effect of Translational constraint and Foundation constraint on frequency is shown in Figs. (2, 3) respectively. Also the combined effect of translational and Foundation constraints are shown in Fig. (4).

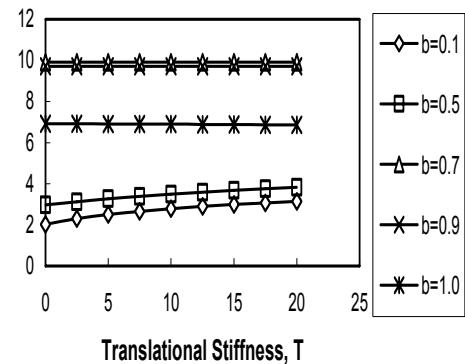


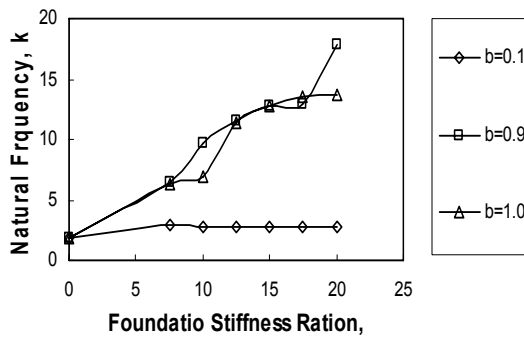
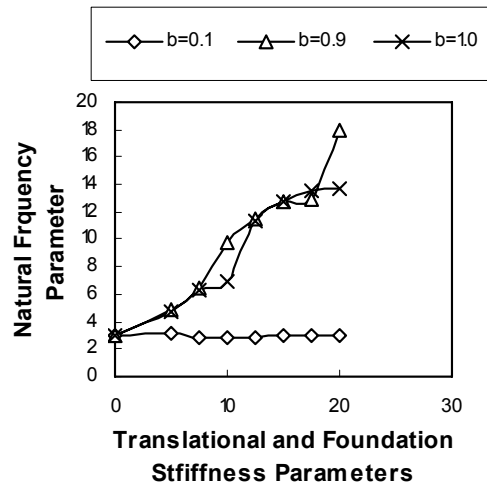
Fig. (2). Effect of translational stiffness parameter, T_{11} on first natural frequency parameter, k for $\lambda = 10$.

Table 1. First Frequency Parameters for Different Translational Stiffness Ratio for $\lambda = 10$ & $\nu = 0.33$

T_{11}	$b = 0.1$	$b = 0.2$	$b = 0.3$	$b = 0.4$	$b = 0.5$	$b = 0.6$	$b = 0.7$	$b = 0.8$	$b = 0.9$	$b = 1$
0	2.02235	2.00269	1.65954	3.17252	2.97074	2.59295	9.91088	9.82665	9.71751	6.9251
2.5	2.30653	2.28733	2.06005	3.32198	3.1293	2.81866	9.91072	9.82583	9.71713	6.91746
5	2.50643	2.48571	2.29898	3.45341	3.26574	2.99905	9.91056	9.82492	9.71666	6.90972
7.5	2.66201	2.63915	2.47235	3.5711	3.38604	3.15054	9.91039	9.824	9.71627	6.90198
10	2.78959	2.7643	2.60887	3.67793	3.49379	3.28191	9.91023	9.82319	9.71579	6.89404
12.5	2.89784	2.86973	2.72118	3.77599	3.59168	3.39823	9.91007	9.82227	9.71541	6.8862
15	2.99165	2.96052	2.81616	3.86678	3.68139	3.5029	9.9099	9.82135	9.71492	6.87817
17.5	3.07421	3.03995	2.89819	3.95139	3.76433	3.5981	9.90974	9.82044	9.71444	6.87013
20	3.1477	3.11033	2.96997	4.03073	3.84139	3.68573	9.90957	9.81952	9.71404	6.86199

Table 2. First Frequency for Different Foundation Stiffness Parameter for T_{11} & $\nu = 0.33$

λ	$b = 0.1$	$b = 0.2$	$b = 0.3$	$b = 0.4$	$b = 0.5$	$b = 0.6$	$b = 0.7$	$b = 0.8$	$b = 0.9$	$b = 1$
0	1.85759	1.85759	1.85759	1.85759	1.85759	1.85759	1.85759	1.85759	1.85759	1.85759
7.5	2.95671	2.82178	2.81512	2.66589	6.00336	4.8109	4.54729	4.3199	6.40789	6.36732
10	2.78959	2.7643	2.60887	3.67793	3.49379	3.28191	9.91023	9.82319	9.71579	6.89404
12.5	2.74279	2.72015	3.46242	3.2138	7.75637	4.58806	4.45195	11.6979	11.5023	11.3633
15	2.72551	2.58	3.0792	2.94435	3.83438	3.65997	6.43791	5.90339	12.7186	12.6973
17.5	2.71662	3.36935	2.9918	3.62631	3.4595	4.69047	4.25264	8.95145	12.9626	13.52
20	2.70984	2.96343	2.83938	3.31891	4.39574	3.9389	5.6791	18.1682	17.9198	13.6294

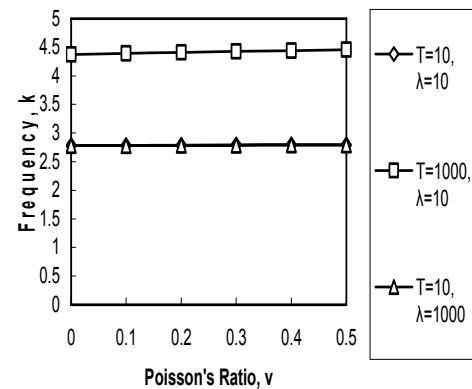
**Fig. (3).** Effect of foundation stiffness parameter, λ on first natural frequency parameter, k for $T_{11} = 10$.**Fig. (4).** Effect of translational stiffness parameter, T_{11} and foundation stiffness parameter λ on natural frequency parameter, k .

The frequencies for different plate materials, for various values of transverse, rotational and foundation parameters are computed and the results are given in Table 3. It is observed that for any value of foundation parameter (λ), frequencies are independent on Poisson ratio, as shown in

Fig. (5). And also it was observed that for any value of T_{11} , frequencies are independent on Poisson ratio.

Table 3. Frequencies for Different Poisson Ratios

ν	$T_{11} = 10, \lambda = 10$	$T_{11} = 1000, \lambda = 10$	$T_{11} = 10, \lambda = 1000$
0	2.77951	4.37181	2.78038
0.1	2.7831	4.39014	2.78338
0.2	2.7865	4.40768	2.78608
0.3	2.78959	4.42472	2.78857
0.4	2.79248	4.44116	2.79087
0.5	2.79517	4.4571	2.79306

**Fig. (5).** Effect of poisson ratio, ν on frequency parameters, k .

The results of this kind are scarce in the literature. However, the results are compared with the following. If $R_{11} \rightarrow 0$ & $T_{11} \rightarrow \infty$, then the problem at hand becomes a simply supported boundary condition as shown in Fig. (6). The results are listed in Table 4. It was found that the $n = 0$ axisymmetric mode gives the fundamental frequency. When $b = 0$, the foundation is absent and the circular simply supported plate governs the frequency, i.e., $k = 2.22152$. When $b = 1$, the plate has full foundation support and the frequency is $k_0 = 2.22152$. Table 5, presents the comparison of frequency parameters k , for the plate with simply

supported edges as shown in Fig. (6) (by setting the translational restraints with $R_{11} \rightarrow 0$ & $T_{11} \rightarrow \infty$), against those obtained by Wang [13] and Laura *et al* [6] by Ritz and finite element methods respectively. Results presented in this paper can be seen to be in excellent agreement with the those results available in the literature.

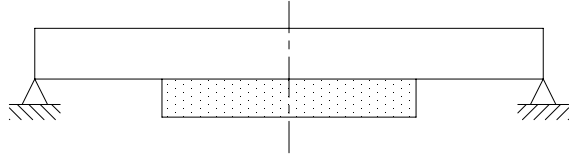


Fig. (6). A thin circular plate with simply supported edge and supported on partial elastic foundation.

Table 4. Frequency for Different Foundation Stiffness Ratio for $\nu = 0.33$

λ	$b = 0.1$	$b = 0.3$	$b = 0.4$	$b = 0.9$
0	2.2215	2.2215	2.2215	2.22152
20	3.9522	4.5808	6.0081	14.6284
50	4.1065	5.1786	6.336	29.1056
100	4.2517	5.3877	6.228	36.7841
500	4.1747	5.4437	6.3845	39.3756
1000	4.2049	5.4673	6.4141	38.8204
2000	4.214	5.3866	6.41	37.7465
5000	4.2186	5.4738	6.4151	39.1173
7500	4.2165	5.4756	6.4103	39.1006
10000	4.2176	5.4708	6.4183	39.0791

Table 5. Comparison of Exact Values with Approximate Values from Ref. [6, 13, 14] for Simply Supported Edge Plate

b	0.3	0.3	0.6	0.6
λ	2.1147	3.1623	2.1147	3.1623
k [Present]	2.33844	2.67264	2.51384	3.17202
k [12]	2.33844	2.67274	2.51304	3.17204
Ritz [6] [*]	2.339	2.677	2.514	3.1724
F.E [6] [*]	2.349	2.702	2.536	3.2249
k [13]	2.33844	2.67264	2.51384	3.17202

* The results are approximate.

If $R_{11} \rightarrow \infty$ & $T_{11} \rightarrow \infty$, then the problem at hand becomes a clamped boundary condition as shown in Fig. (7). The results are listed in Table 6. It was found that the $n=0$ axisymmetric mode gives the fundamental frequency. When $b=0$, the foundation is absent and the circular clamped plate governs frequency, i.e., $k = 3.19622$.

When $b=1$, the plate has full foundation support and the frequency is $k_0 = 3.19622$. Table 7 shows a comparison of our exact values with the values obtained by Wang [13] and

Laura *et al.* [6] by Ritz and finite element methods respectively. Excellent agreement has been found between these results.

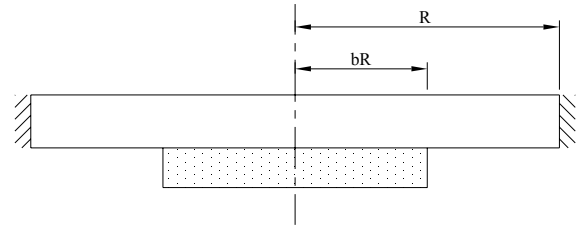


Fig. (7). A thin circular plate with clamped edge and supported on partial elastic foundation.

Table 6. Frequency for Different Foundation Stiffness Ratio for $\nu = 0.33$

λ	$b = 0.3$	$b = 0.4$	$b = 0.8$	$b = 1.0$
0	3.19622	3.19622	3.1962	3.19622
20	5.73303	7.42844	18.151	13.536
50	6.38558	7.77718	21.658	33.8797
100	6.63007	7.64012	22.987	56.2845
500	6.69625	7.82554	23.572	124.841
1000	6.72454	7.86099	23.474	249.707
2000	6.62889	7.85603	23.633	499.426
5000	6.73224	7.86222	23.649	1002.67
10000	6.72868	7.86598	23.636	1200.98
20000	6.73245	7.86527	23.597	1600.78

Table 7. Comparison of Exact Values with Approximate Values from Ref. [6, 12] for Clamped Edge Plate

b	0.3	0.3	0.6	0.6
λ	2.1147	3.1623	2.1147	3.1623
k [Present]	3.25572	3.46125	3.32705	3.73673
k [12]	3.25573	3.46124	3.32706	3.73672
Ritz [6] [*]	3.2558	3.4615	3.3275	3.7367
F.E [6] [*]	3.2558	3.4771	3.1237	3.6576

* The results are approximate.

6. CONCLUSIONS

The flexural vibration behaviour of a circular plate supported along its edge by elastically restrained springs against rotation and translational and supported partially on a Winkler-type foundation has been studied in this paper. Mathematica computer software was used in obtaining the results for first frequency values of this circular plate.

The values of first frequencies are presented in both tabular and graphical form for various values of translational spring stiffness parameters [R_{11} & T_{11}] at the edges that

simulate a clamped edge when $R_{11} \rightarrow \infty$ & $T_{11} \rightarrow \infty$, or a simply supported edge when $R_{11} \rightarrow 0$ & $T_{11} \rightarrow \infty$.

Graphical plots of first frequencies are presented for a wide range of rotational, translational and foundation constraints. The wide range of results provided in this paper could be potentially utilized for vibration control and in structural design. It is observed that the influence of foundation parameter on frequency is more predominant than that of translational parameter or rotational parameter.

Comparison of results obtained here with those available in literature for some special cases, demonstrates excellent accuracy and numerical stability of the present method. In this paper the characteristic equations solved are exact ones and therefore the frequency results can be calculated to any desired accuracy. These exact solutions can be used as benchmark solutions to check numerical or approximate results obtained through other methods of solution.

NOTATIONS

h	= Thickness of a plate
R	= Radius of a plate
b	= Non-dimensional radius of support
ν	= Poisson's ratio
E	= Young's modulus of a material
ρ	= Density of a material
ω	= Angular frequency
D	= Flexural rigidity of a material
K_{R1}	= Rotational spring stiffness at outer edge
K_{T2}	= Translational spring stiffness at outer edge

R_{11}	= Non-dimensional rotational flexibility Parameter at outer edge
T_{22}	= Non-dimensional translational flexibility Parameter at outer edge
λ	= Non-dimensional foundation parameter

REFERENCES

- [1] Leissa AW. Plate vibration research: 1976-1980: complicating effects. Shock Vibration Digest 1981; 13(10): 19-36.
- [2] Leissa AW. Resent research in plate vibrations: 1981-1985 Part II: complicating effects. Shock Vibrations Digest 1987; 19(3): 10-24.
- [3] Bert CW. Research on dynamic behavior of composite and sandwich plates-IV. Shock Vibration Digest 1985; 17(11): 3-25.
- [4] Bert CW. Research on dynamic behavior of composite and sandwich plates-V: Part I. Shock Vibration Digest 1991; 23(6): 3-14.
- [5] Leissa AW. Vibration of Plates, Acoustical Society of America, Sewickley, P. A. 1993.
- [6] Laura PAA, Gutierrez RH, Sanzi HC, Elvira G. The lowest axisymmetrical frequency of vibration of a circular plate partially embedded in a Winkler foundation. J Sound Vibration 1995; 185: 915-9.
- [7] Winkler E. Die Lehre von der Elasticitaet and Festigkeit, Prag. Dominicus 1867.
- [8] Dumir PC. Large deflection axisymmetric analysis of orthotropic annular plates on elastic Foundations. Int J Solids Struct 1988; 24: 777-87.
- [9] Bhaskara Rao L. Study of Static Stability of Circular and Annular Plates on Generalized Elastic Medium, PhD Thesis, Osmania University, Hyderabad, A.P. India 2008.
- [10] Kim CS, Dickinson SM. The flexural vibration of thin isotropic and polar orthotropic annular and circular plates with elastically restrained peripheries. J Sound Vibration 1990; 143: 171-9.
- [11] Amabili M, Pierandrei R. Analysis of vibrating circular plates having non-uniform constraint using the modal properties of free edge plates: Application to bolted plates. J Sound Vibration 1997; 206 (1): 23-38.
- [12] Yu SC, Huang SC. Vibration of three-layered viscoelastic sandwich circular plate. Int J Mech Sci 2001; 43: 2215-36.
- [13] Wang CM. Fundamental frequency of a circular plate supported by a partial elastic foundation. J Sound Vibration 2005; 285: 1203-9.

Received: March 6, 2009

Revised: May 25, 2009

Accepted: May 31, 2009

© Rao and Rao; Licensee Bentham Open.

This is an open access article licensed under the terms of the Creative Commons Attribution Non-Commercial License (<http://creativecommons.org/licenses/by-nc/3.0/>) which permits unrestricted, non-commercial use, distribution and reproduction in any medium, provided the work is properly cited.



Mechanics Based Design of Structures and Machines: An International Journal

Publication details, including instructions for authors and subscription information:

<http://www.tandfonline.com/loi/lmbd20>

Buckling Analysis of Circular Plates with Elastically Restrained Edges and Resting on Internal Elastic Ring Support[#]

L. Bhaskara Rao ^a & C. Kameswara Rao ^b

^a Department of Mechanical Engineering , Gokaraju Rangaraju Institute of Engineering and Technology , Hyderabad, Andhra Pradesh, India

^b Department of Mechanical Engineering , Tirumala Engineering College , Hyderabad, Andhra Pradesh, India

Published online: 09 Nov 2010.

To cite this article: L. Bhaskara Rao & C. Kameswara Rao (2010) Buckling Analysis of Circular Plates with Elastically Restrained Edges and Resting on Internal Elastic Ring Support[#] , Mechanics Based Design of Structures and Machines: An International Journal, 38:4, 440-452, DOI: [10.1080/15397734.2010.485297](https://doi.org/10.1080/15397734.2010.485297)

To link to this article: <http://dx.doi.org/10.1080/15397734.2010.485297>

PLEASE SCROLL DOWN FOR ARTICLE

Taylor & Francis makes every effort to ensure the accuracy of all the information (the "Content") contained in the publications on our platform. However, Taylor & Francis, our agents, and our licensors make no representations or warranties whatsoever as to the accuracy, completeness, or suitability for any purpose of the Content. Any opinions and views expressed in this publication are the opinions and views of the authors, and are not the views of or endorsed by Taylor & Francis. The accuracy of the Content should not be relied upon and should be independently verified with primary sources of information. Taylor and Francis shall not be liable for any losses, actions, claims, proceedings, demands, costs, expenses, damages, and other liabilities whatsoever or howsoever caused arising directly or indirectly in connection with, in relation to or arising out of the use of the Content.

This article may be used for research, teaching, and private study purposes. Any substantial or systematic reproduction, redistribution, reselling, loan, sub-licensing, systematic supply, or distribution in any form to anyone is expressly forbidden. Terms & Conditions of access and use can be found at <http://www.tandfonline.com/page/terms-and-conditions>

BUCKLING ANALYSIS OF CIRCULAR PLATES WITH ELASTICALLY RESTRAINED EDGES AND RESTING ON INTERNAL ELASTIC RING SUPPORT[#]

L. Bhaskara Rao¹ and C. Kameswara Rao²

¹Department of Mechanical Engineering, Gokaraju Rangaraju Institute of Engineering and Technology, Hyderabad, Andhra Pradesh, India

²Department of Mechanical Engineering, Tirumala Engineering College, Hyderabad, Andhra Pradesh, India

This paper is concerned with the elastic buckling of circular plates with internal elastic ring support and elastically restrained edge against rotation and translation. The classical plate theory is used to derive the governing differential equation for circular plate with internal elastic ring support and elastically restrained edges. This work presents the existence of buckling mode switching with respect to the radius of internal elastic ring support. The buckling mode may not be axisymmetric as previously assumed. In general, the plate may buckle in an axisymmetric mode but when the radius of the ring support becomes small, the plate may buckle in an asymmetric mode. The optimum radius of the internal elastic ring support for maximum buckling load is also determined. The percentage of increase in buckling load capacity by introducing concentric elastic ring support is determined for the first time. Extensive data are tabulated so that pertinent conclusions can be arrived at on the influence of rotational and translational restraints, Poisson's ratio, and other boundary conditions on the buckling of uniform isotropic circular plates. The numerical results obtained are in good agreement with the previously published data.

Keywords: Buckling; Circular plates; Elastic ring support; Elastically restrained edges; Mode switching.

INTRODUCTION

Buckling of plates is an important topic in structural engineering. The prediction of buckling of structural members restrained laterally is important in the design of various engineering components. In particular, circular plates with an internal elastic ring support find applications in aeronautical (instrument mounting bases for space vehicles), rocket launching pads, aircrafts, and naval vessels (instrument mounting bases). Based on the Kirchhoff's theory, the elastic buckling of thin circular plates has been extensively studied by many authors

Received January 14, 2009; Accepted July 29, 2009

[#]Communicated by I. Elishakoff.

Correspondence: L. Bhaskara Rao, Department of Mechanical Engineering, Gokaraju Rangaraju Institute of Engineering and Technology, Kukatpally Hyderabad, Andhra Pradesh 500072, India; E-mail: bhaskarababu_20@yahoo.com

after the pioneering work published by Bryan (1891). Since then, there have been extensive studies on the subject covering various aspects such as different materials, boundary, and loading conditions. Also, the buckling of circular plates was studied by different authors (Brushes and Almroth, 1975; Wolkowisky, 1969). However, these sources only considered axisymmetric case, which may not lead to the correct buckling load. Introducing an internal elastic ring support may increase the elastic buckling capacity of in-plane loaded circular plates significantly. Laura et al. (2000) investigated the elastic buckling problem of the aforesaid type of circular plates, who modeled the plate using the classical thin plate theory. In their study only axisymmetric modes are considered. Kunukkasseril and Swamidas (1974) are probably the first to consider elastic ring supports. They formulated the equations in general, but presented only the case of circular plate with a free edge. Although the circular symmetry of the problem allows for its significant simplification, many difficulties very often arise due to complexity and uncertainty of boundary conditions. This uncertainty could be due to practical engineering applications where the edge of the plate does not fall into the classical boundary conditions. It is an accepted fact that the condition on a periphery often tends to be in between the classical boundary conditions (free, clamped, and simply supported) and may correspond more closely to some form of elastic restraints, i.e., rotational and translational restraints (Kim and Dickinson, 1990; Wang and Wang, 2001; Yamaki, 1958). In a recent study, Wang et al. (1993) showed that when the ring support has a small radius, the buckling mode takes the asymmetric form. But they have studied only the circular plate with rigid ring support and elastically restrained edge against rotation. Wang and Wang (2001) showed that the axisymmetric mode assumed by the previous authors might not yield the correct buckling load. In certain cases, an asymmetric mode would yield a lower buckling load. Recently, Wang (2003) studied the buckling of a circular plate with internal elastic ring support by considering only the classical boundary conditions. The purpose of the present work is to complete the results of the buckling of circular plates with an internal elastic ring support and elastically restrained edge against rotation and translation by including the asymmetric modes, thus correctly determining the buckling loads.

PROBLEM DEFINITION

Consider a thin circular plate of radius R , uniform thickness h , Young's modulus E , and Poisson's ratio ν and subjected to a uniform in-plane load, N along its boundary, as shown in Fig. 1. This circular plate is assumed to be made of linearly elastic, homogeneous, and isotropic material. The edge of the circular plate is elastically restrained against rotation and translation and it is also supported by an internal elastic ring support, as shown in Fig. 1. The purpose of the present work is to complete the results of the buckling of circular plates with an internal elastic ring support and elastically restrained edge against rotation and translation by including the asymmetric modes, thus correctly determining the buckling loads.

ANALYTICAL FORMULATION OF THE PROBLEM

The plate is elastically restrained against rotation and translation at the edge of radius, R and supported on an internal elastic ring of smaller radius bR as shown

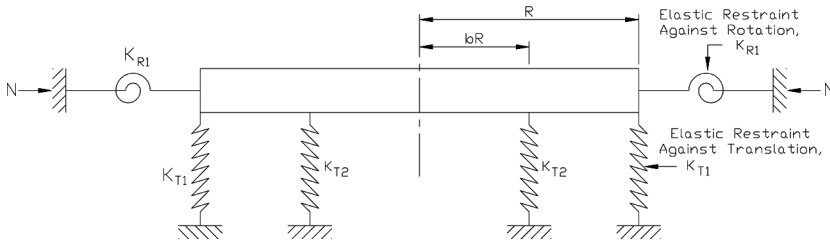


Figure 1 Buckling of a circular plate with elastically restrained edges and resting on internal elastic ring support.

in Fig. 1. Let subscript I denote the inner region $0 \leq \bar{r} \leq b$ and the subscript II denote the outer region $b \leq \bar{r} \leq 1$. Here, all lengths are normalized by R . Using classical (Kirchhoff's) plate theory, the following fourth-order differential equation for buckling in polar coordinates (r, θ) :

$$D\nabla^4 w + N\nabla^2 w = 0, \quad (1)$$

where w is the lateral displacement, N is the uniform compressive load at the edge. After normalizing the lengths by the radius of the plate R , Eq. (1) can be written as

$$D\nabla^4 \bar{w} + k^2 \nabla^2 \bar{w} = 0, \quad (2)$$

where $\nabla^2 = \frac{\partial^2}{\partial \bar{r}^2} + \frac{1}{\bar{r}} \frac{\partial}{\partial \bar{r}} + \frac{1}{\bar{r}^2} \frac{\partial^2}{\partial \theta^2}$ is the Laplace operator in the polar coordinates r and θ , where \bar{r} is the radial distance normalized by R . After normalization, the inner and outer radius parameters are b and 1 , respectively; $\bar{D} = Eh^3/12(1 - \nu^2)$ is the flexural rigidity; $\bar{w} = w/R$, is normalized transverse displacement of the plate; $k^2 = R^2 N / \bar{D}$ is nondimensional load parameter. Suppose there are n nodal diameters. In polar coordinates (r, θ) set

$$\bar{w}(\bar{r}, \theta) = \bar{u}(\bar{r}) \cos(n\theta). \quad (3)$$

Considering the boundness at the origin, the general solution (Yamaki, 1958) for the two regions is

$$\bar{u}_I(r) = C_1 J_n(k\bar{r}) + C_2 Y_n(k\bar{r}) + C_3 \bar{r}^n + C_4 \left\{ \frac{\log \bar{r}}{\bar{r}^{-n}} \right\}, \quad (4)$$

$$\bar{u}_{II}(r) = C_5 J_n(k\bar{r}) + C_6 \bar{r}^n. \quad (5)$$

Where top form of the Eq. (4) is used for $n = 0$ (axisymmetric) and the bottom form is used for $n \neq 0$ (asymmetric), C_1, C_2, C_3, C_4, C_5 , & C_6 are constants, $J_n(\cdot)$ & $Y_n(\cdot)$ are the Bessel functions of the first and second kinds of order n , respectively. Substituting Eq. (4) into Eq. (3), gives the following:

$$\bar{w}_I(\bar{r}, \theta) = \left[C_1 J_n(k\bar{r}) + C_2 Y_n(k\bar{r}) + C_3 \bar{r}^n + C_4 \left\{ \frac{\log \bar{r}}{\bar{r}^{-n}} \right\} \right] \cos(n\theta), \quad (6)$$

$$\bar{w}_H(\bar{r}, \theta) = [C_5 J_n(k\bar{r}) + C_6 \bar{r}^n] \cos(n\theta). \quad (7)$$

The boundary conditions at outer region of the circular plate in terms of rotational stiffness (K_{R1}) and translational stiffness (K_{T1}) is given by the following expressions:

$$M_r(\bar{r}) = K_{R1} \bar{u}'_I(\bar{r}), \quad (8)$$

$$V_r(\bar{r}) = -K_{T1} \bar{u}_I(\bar{r}). \quad (9)$$

The radial moment and the radial Kirchhoff shear at outer edge are defined as follows:

$$M_r(\bar{r}) = -\frac{D}{R^3} [\bar{u}''_I(\bar{r}) + \nu (\bar{u}'_I(\bar{r}) - n^2 \bar{u}_I(\bar{r}))], \quad (10)$$

$$V_r(\bar{r}) = -\frac{D}{R^3} [\bar{u}'''_I(\bar{r}) + \bar{u}''_I(\bar{r}) - \bar{u}'_I(\bar{r})(n^2(2-\nu)) + n^2(1-\nu) \bar{u}_I(\bar{r})]. \quad (11)$$

Equations (8) and (10) yield the following:

$$[\bar{u}''_I(\bar{r}) + \nu (\bar{u}'_I(\bar{r}) - n^2 \bar{u}_I(\bar{r}))] = -\frac{K_{R1} R^2}{D} \bar{u}'_I(\bar{r}), \quad (12)$$

$$[\bar{u}''_I(\bar{r}) + \nu (\bar{u}'_I(\bar{r}) - n^2 \bar{u}_I(\bar{r}))] = -R_{11} \bar{u}'_I(\bar{r}). \quad (13)$$

From Eqs. (9) and (11) we get the following:

$$[\bar{u}'''_I(\bar{r}) + \bar{u}''_I(\bar{r}) - \bar{u}'_I(\bar{r})(n^2(2-\nu)) + n^2(1-\nu) \bar{u}_I(\bar{r})] = \frac{K_{T1} R^3}{D} \bar{u}_I(\bar{r}), \quad (14)$$

$$[\bar{u}'''_I(\bar{r}) + \bar{u}''_I(\bar{r}) - \bar{u}'_I(\bar{r})(n^2(2-\nu)) + n^2(1-\nu) \bar{u}_I(\bar{r})] = T_{11} \bar{u}_I(\bar{r}), \quad (15)$$

where $R_{11} = \frac{K_{R1} R^2}{D}$ and $T_{11} = \frac{K_{T1} R^3}{D}$.

Therefore, the boundary conditions at the outer region are given by Eqs. (13) and (15) at $\bar{r} = 1$. Apart from the elastically restrained edge against rotation and translation, there is an internal elastic ring support constraint and the continuity requirements of slope and curvature at the support, i.e., $\bar{r} = b$.

$$\bar{u}_I(b) = \bar{u}_{II}(b), \quad (16)$$

$$\bar{u}'_I(b) = \bar{u}'_{II}(b), \quad (17)$$

$$\bar{u}''_I(b) = \bar{u}''_{II}(b), \quad (18)$$

$$\bar{u}'''_I(b) = \bar{u}'''_{II}(b) - T_{22} \bar{u}_{II}(b), \quad (19)$$

where $T_{22} = \frac{K_{T2} R^3}{D}$ is the normalized spring constant, K_{T2} of the translational spring.

The nontrivial solutions to Eqs. (13), (15), (16)–(19) are sought. The lowest value of k is the square root of the normalized buckling load. From Eqs. (4), (5), (13), and (15)–(19) yield the following equations:

$$\left[\frac{k^2}{4} P_2 + \frac{k}{2} (\nu + R_{11}) P_1 - \left(\frac{k^2}{2} + \nu n^2 \right) J_n(k) \right] C_1$$

$$\begin{aligned}
& + \left[\frac{k^2}{4} Q_2 + \frac{k}{2} (v + R_{11}) Q_1 - \left(\frac{k^2}{2} + vn^2 \right) Y_n(k) \right] C_2 \\
& + [n((n-1)(1-v) + R_{11})] C_3 + \left\{ \frac{(v + R_{11}) - 1}{n((n+1)(1-v) - R_{11})} \right\} C_4 = 0, \quad (20)
\end{aligned}$$

$$\begin{aligned}
& \left[\frac{k^3}{8} P_3 + \frac{k^2}{4} P_2 - \frac{k}{2} \left(\frac{3}{4} k^2 + n^2(2-v) + 1 \right) P_1 + \left(n^2(3-v) - \frac{k^2}{2} - T_{11} \right) J_n(k) \right] C_1 \\
& + \left[\frac{k^3}{8} Q_3 + \frac{k^2}{4} Q_2 - \frac{k}{2} \left(\frac{3}{4} k^2 + n^2(2-v) + 1 \right) Q_1 + \left(n^2(3-v) - \frac{k^2}{2} - T_{11} \right) Y_n(k) \right] C_2 \\
& + [n^2(n-1)v - n^3 - T_{11}] C_3 - \left\{ \frac{n^2(2-v)}{-n^2(n+1)v + n^3 - T_{11}} \right\} C_4 = 0, \quad (21)
\end{aligned}$$

where

$$\begin{aligned}
P_1 &= J_{n-1}(k) - J_{n+1}(k); \quad P_2 = J_{n-2}(k) + J_{n+2}(k); \quad P_3 = J_{n-3}(k) - J_{n+3}(k); \\
Q_1 &= Y_{n-1}(k) - Y_{n+1}(k); \quad Q_2 = Y_{n-2}(k) + Y_{n+2}(k); \quad Q_3 = Y_{n-3}(k) - Y_{n+3}(k);
\end{aligned}$$

$$J_n(kb)C_1 + Y_n(kb)C_2 + b^n C_3 + \left\{ \frac{\log b}{b^{-n}} \right\} C_4 - J_n(kb)C_5 - b^n C_6 = 0, \quad (22)$$

$$\frac{k}{2} P'_1 C_1 + \frac{k}{2} Q'_1 C_2 + nb^{n-1} C_3 + \left\{ \frac{\frac{1}{b}}{-nb^{-n-1}} \right\} C_4 - \frac{k}{2} P'_1 C_5 - nb^{n-1} C_6 = 0, \quad (23)$$

$$\begin{aligned}
& \frac{k^2}{4} (P'_2 - 2J_n(kb))C_1 + \frac{k^2}{4} (Q'_2 - 2Y_n(kb))C_2 + n(n-1)b^{n-2}C_3 - \left\{ \frac{\frac{1}{b^2}}{n(n+1)b^{-n-2}} \right\} C_4 \\
& - \frac{k^2}{4} (P'_2 - 2J_n(kb))C_5 - n(n-1)b^{n-2}C_6 = 0, \quad (24)
\end{aligned}$$

$$\begin{aligned}
& \frac{k^2}{8} (P'_3 - 3P'_1)C_1 + \frac{k^2}{8} (Q'_3 - 3Q'_1)C_2 + n(n-1)(n-2)b^{n-3}C_3 \\
& + \left\{ \frac{\frac{2}{b^3}}{-n(n+1)(n+2)b^{-n-3}} \right\} C_4 - \left[\frac{k^2}{8} (P'_3 - 3P'_1) - T_{22}J_n(kb) \right] C_5 \\
& - [n(n-1)(n-2)b^{n-3} - T_{22}b^n]C_6 = 0, \quad (25)
\end{aligned}$$

where

$$\begin{aligned}
P'_1 &= J_{n-1}(kb) - J_{n+1}(kb); \quad P'_2 = J_{n-2}(kb) + J_{n+2}(kb); \quad P'_3 = J_{n-3}(kb) - J_{n+3}(kb); \\
Q'_1 &= Y_{n-1}(kb) - Y_{n+1}(kb); \quad Q'_2 = Y_{n-2}(kb) + Y_{n+2}(kb); \quad Q'_3 = Y_{n-3}(kb) - Y_{n+3}(kb).
\end{aligned}$$

The top form of Eqs. (20)–(25) are used for $n = 0$ (axisymmetric buckling) and the bottom form is used for $n \neq 0$ (asymmetric buckling).

SOLUTION

For the given values of n , ν , R_{11} , T_{11} , T_{22} , & b the above set of equations, gives an exact characteristic equation for nontrivial solutions of the coefficients C_1 , C_2 , C_3 , C_4 , C_5 , & C_6 . For nontrivial solution, the determinant of $[C]_{6 \times 6}$ vanishes. The value of k is calculated from the characteristic equation by a simple root search method. Using Mathematica, a computer software with symbolic capabilities, solves this problem.

RESULTS AND DISCUSSIONS

There is a lot of flexibility in the code developed in Mathematica. It is used to determine the buckling load parameter for any range of rotational and translational constraints and also various stiffness constraints of an internal elastic ring support. The findings are presented in both tabular and graphical form. Buckling loads are calculated for various internal elastic ring support radii b , rotational spring stiffness parameter R_{11} , translational spring stiffness parameter T_{11} , and translational spring stiffness parameters of an internal elastic ring support T_{22} . Poisson's ratio used in this work is 0.3.

The buckling load parameters for axisymmetric and asymmetric modes for various values of rotational spring stiffness parameters, R_{11} , by keeping translational spring stiffness parameter, T_{11} and translational spring stiffness parameter, T_{22} constant, are presented in Table 1. It is observed from the Figs. 2–5, for a given value of R_{11} , the curve is composed of two segments. This is due to the switching of buckling modes. For a smaller internal elastic ring support radius b , the plate buckles in an asymmetric mode (i.e., $n = 1$). In this segment (as shown by dotted lines in Figs. 2–5) the buckling load decreases as b decreases in value. For larger internal elastic ring support radius b , the plate buckles in an axisymmetric mode (i.e., $n = 0$). In this segment (as shown by continuous lines in Figs. 2–5) the buckling load increases as b decreases up to a peak point, corresponds to maximum buckling

Table 1 Buckling (for axisymmetric and asymmetric modes) load parameters for different values of rotational stiffness parameters, R_{11} , and constant translational stiffness parameter, T_{11} , and translational stiffness parameter of internal elastic ring, R_{22} ($T_{11} = T_{22} = 1000$), when $\nu = 0.3$

b	$R_{11} = 0.5, T_{11} = T_{22} = 1000$		$R_{11} = 10, T_{11} = T_{22} = 1000$		$R_{11} = \infty, T_{11} = T_{22} = 1000$	
	$n = 0$	$n = 1$	$n = 0$	$n = 1$	$n = 0$	$n = 1$
0	2.34422	3.77555	3.51188	4.70945	3.8531	5.13048
0.1	4.67684	4.0601	6.1039	5.06033	6.69782	5.52023
0.2	4.96006	4.81372	6.32317	6.00965	6.94504	6.61564
0.3	5.25523	5.55305	6.43411	6.88999	6.99121	7.66182
0.4	5.4671	6.29013	6.24905	7.59267	6.60737	8.37771
0.5	5.40957	6.90851	5.7695	7.67119	5.95379	3.12889
0.6	5.0828	6.8419	5.2116	7.03001	5.29611	3.86641
0.7	4.65656	6.27244	4.68264	6.29575	4.70433	4.64511
0.8	4.18204	5.60991	4.18626	5.61847	4.19007	5.09741
0.9	3.46153	4.75036	3.71744	5.01776	3.87304	5.15389
1	2.31723	3.77684	3.4889	4.71475	3.83163	5.13591

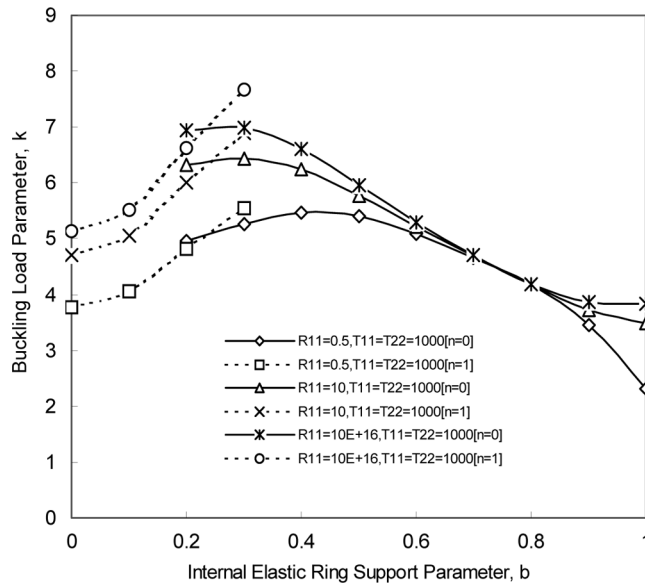


Figure 2 Buckling load parameter k , versus internal elastic ring support radius b , for various values of R_{11} & $T_{11} = T_{22} = 1000$.

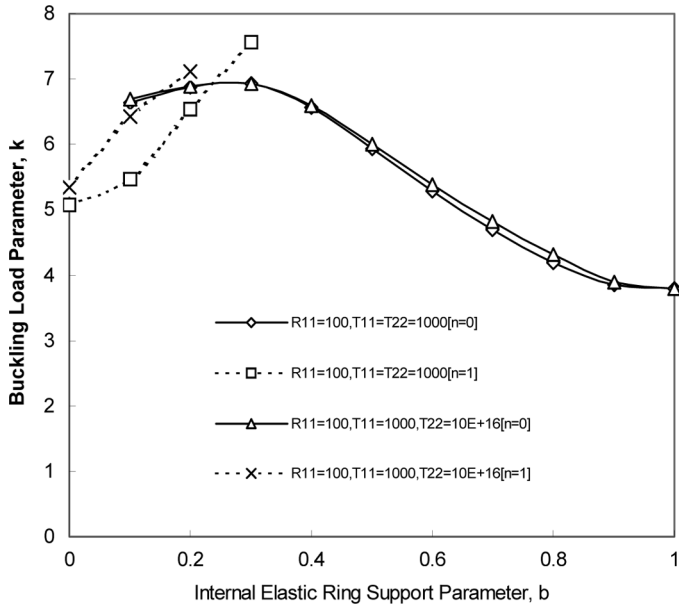


Figure 3 Buckling load parameter k , versus internal elastic ring support radius b , for various values of T_{22} & $R_{11} = T_{11} = 1000$.

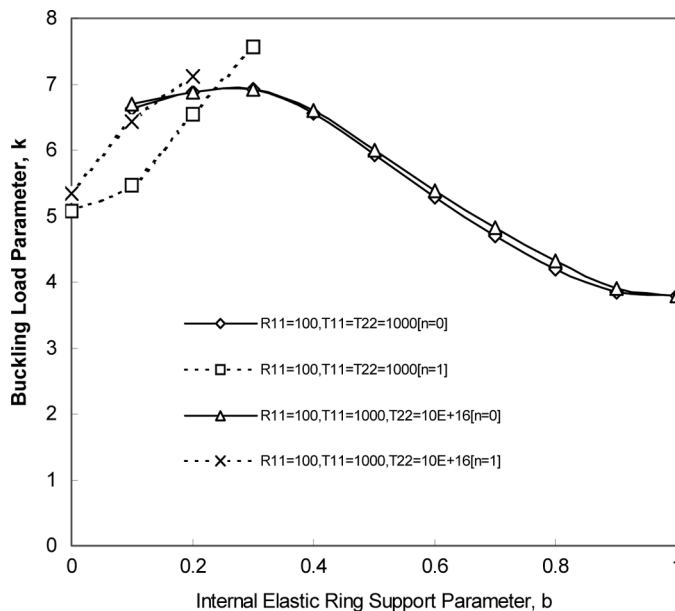


Figure 4 Buckling load parameter k , versus internal elastic ring support radius b , for various values of T_{11} & $R_{11} = T_{22} = 1000$.

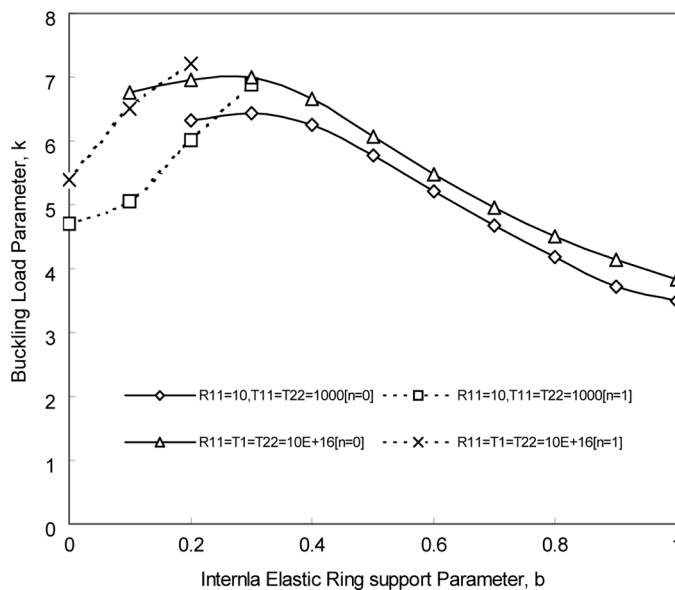


Figure 5 Buckling load parameter k , versus internal elastic ring support radius b , for various values of R_{11} , T_{11} & T_{22} .

Table 2 Optimal locations of an internal elastic ring support b_{opt} ; the corresponding buckling load parameter k_{opt} and the percentage increase in buckling load parameter

$T_{11} = T_{22} = 1000$			
R_{11}	0.5	10	∞
b_{opt}	0.4050	0.3003	0.2340
k_{opt}	5.464	6.434	6.971
%	135.82	84.41	81.93

load, and thereafter decreases as b decreases in value as shown in Figs. 2–5. Figure 2, shows the variation of buckling load parameter k , with respect to the internal elastic ring support radius b , for various values of rotational spring stiffness parameters ($R_{11} = 0.5, 10$ & ∞) and keeping translational spring stiffness parameter and translational spring stiffness parameter of an internal elastic ring support are constant ($T_{11} = T_{22} = 1000$). The cross over radius varies from $b = 0.233$ for $R_{11} = 0.5$ & $T_{11} = T_{22} = 1000$ to $b = 0.234$ for $R_{11} = \infty$ & $T_{11} = T_{22} = 1000$ as shown in Fig. 2. It is observed from the Fig. 2 that the buckling is governed by the asymmetric mode $n = 1$, when $b \leq 0.233$ for $R_{11} = 0.5$ & $T_{11} = T_{22} = 1000$. When b is increased beyond 0.233, the $n = 0$ axisymmetric mode gives the correct lower buckling load. Similarly, the buckling is governed by the asymmetric mode $n = 1$, when $b \leq 0.234$ for $R_{11} = \infty$ & $T_{11} = T_{22} = 1000$. When b is increased beyond 0.234, the $n = 0$ axisymmetric mode gives the correct lower buckling load. Optimal location of internal elastic ring support for maximum buckling load is of interest in the design of supported circular plates. The optimal solutions (optimal location of internal elastic ring support and corresponding buckling loads) for this case are presented in Table 2. It is observed that the optimum-buckling load parameter increases with increase in rotational spring stiffness parameter, R_{11} . Introducing internal elastic ring support, when placed at an optimal position increases the elastic buckling capacity significantly, and the percentage of increase in buckling loads is presented in Table 2. It is observed that the percentage increase in buckling load parameter decreases with increase in R_{11} . This is due to the amount of increase in buckling load without elastic ring support with R_{11} is more than that of increase in buckling load with elastic ring support with R_{11} . The buckling load parameters for axisymmetric and asymmetric modes for various values of translational spring stiffness parameters of an internal elastic ring support ($T_{22} = 1000$ & ∞) by keeping R_{11} and T_{11} constant are presented in Table 3. Figure 3 shows the variation of buckling load parameter k , with respect to the internal elastic ring support radius b , for various values of translational spring stiffness parameters of an internal elastic ring support ($T_{22} = 1000$ & ∞) and $R_{11} = 100$ & $T_{11} = 1000$. The cross over radius (switching of buckling mode) varies from $b = 0.1537$ to 0.2341 as shown in Fig. 3.

It is observed from the Fig. 3 that the buckling is governed by the asymmetric mode $n = 1$, when $b \leq 0.1537$ for $T_{22} = 1000$ & $R_{11} = 100, T_{11} = 1000$. When b is increased beyond 0.1537, the $n = 0$ axisymmetric mode gives the correct lower buckling load. Similarly, the buckling is governed by the asymmetric mode $n = 1$, when $b \leq 0.2341$ for $T_{22} = 10^{16}$ & $R_{11} = 100, T_{11} = 1000$. When b is increased

Table 3 Buckling (for axisymmetric and asymmetric modes) load parameters for different values of translational stiffness parameter of internal elastic ring, T_{22} and constant rotational stiffness parameters, $R_{11} = 100$, and translational stiffness parameter, $T_{11} = 1000$ when $\nu = 0.3$

b	$T_{22} = 1000, R_{11} = 100 \text{ \& } T_{11} = 1000$		$T_{22} = \infty, R_{11} = 100 \text{ \& } T_{11} = 1000$	
	$n = 0$	$n = 1$	$n = 0$	$n = 1$
0	3.81535	5.07899	6.57733	5.34015
0.1	6.6333	5.46437	6.69453	6.42772
0.2	6.87437	6.54262	6.88357	7.12049
0.3	6.92542	7.56651	6.92777	7.80417
0.4	6.56336	8.2795	6.60053	8.29339
0.5	5.92915	7.97692	6.00578	8.0656
0.6	5.28363	7.12069	5.38818	7.31334
0.7	4.70083	6.3111	4.82919	6.53979
0.8	4.18947	5.62491	4.32015	5.83674
0.9	3.85064	5.17693	3.89536	5.25568
1	3.79368	5.08212	3.79368	5.08516

beyond 0.2341, the $n = 0$ axisymmetric mode gives the correct lower buckling load. The optimal solutions (optimal location of internal elastic ring support and corresponding buckling loads) for this case are presented in Table 4. Introducing internal elastic ring support, when placed at an optimal position increases the elastic buckling capacity significantly, and the percentage of increase in buckling loads is presented in Table 4. It is found that the percentage increase in buckling load is negligible due to the fact that there is less influence of T_{22} on buckling load parameter. The buckling load parameters for axisymmetric and asymmetric modes and for various values of translational spring stiffness parameters ($T_{11} = 1000 \text{ \& } \infty$) and keeping rotational spring stiffness parameter, R_{11} and translational spring stiffness parameter of the internal elastic ring support T_{22} constant are presented in Table 5. Figure 4 show the variations of buckling load parameter k , with respect to the internal elastic ring support radius b , for various values of translational spring stiffness parameters ($T_{11} = 1000 \text{ \& } \infty$) and $R_{11} = 100 \text{ \& } T_{22} = 1000$. The optimal solutions (optimal location of internal elastic ring support and corresponding buckling loads) for this case are presented in Table 6. Introducing internal elastic ring support, when placed at an optimal position increases the elastic buckling capacity significantly, and the percentage of increase in buckling loads is presented

Table 4 Optimal locations of internal elastic ring support b_{opt} , the corresponding buckling load parameter k_{opt} , and percentage increase in buckling parameter

T_{22}	$R_{11} = 100 \text{ \& } T_{11} = 1000$	
	1000	∞
b_{opt}	0.2905	0.2824
k_{opt}	6.921	6.928
%	82.43	82.62

Table 5 Buckling (for axisymmetric and asymmetric modes) load parameters for different values of translational stiffness parameter, T_{11} and constant rotational stiffness parameters, $R_{11} = 1000$, and translational stiffness parameter of internal elastic ring, $T_{22} = 1000$, when $\nu = 0.3$

b	$T_{11} = 1000, R_{11} = T_{22} = 1000$		$T_{11} = \infty, R_{11} = T_{22} = 1000$	
	$n = 0$	$n = 1$	$n = 0$	$n = 1$
0	3.84932	5.12531	3.84932	5.13048
0.1	6.69136	5.51456	6.69848	5.51788
0.2	6.93798	6.60828	6.93984	6.60877
0.3	6.98455	7.65218	6.98562	7.65225
0.4	6.60289	8.3678	6.6202	8.37255
0.5	5.9513	8.01422	5.99288	8.05125
0.6	5.29481	7.13382	5.36053	7.20067
0.7	4.70393	6.31373	4.7949	6.40582
0.8	4.19007	5.62602	4.28826	5.718
0.9	3.87065	5.20212	3.90033	5.22168
1	3.82784	5.12785	3.82784	5.13048

in Table 6. It is observed that the percentage increase in buckling load is negligible; this is due to the minute influence of T_{22} on buckling load parameter.

The buckling load parameters for axisymmetric and asymmetric modes and for various values of three spring stiffness parameters R_{11} , T_{11} , and T_{22} are presented in Table 7. Figure 5 shows the variations of buckling load parameter k , with respect to the internal elastic ring support radius b , for various values of translational spring stiffness parameters ($T_{11} = 1000$ & ∞) and keeping rotational spring stiffness parameters ($R_{11} = 10$ & ∞), translational spring stiffness parameters of the internal ring elastic support ($T_{22} = 1000$ & ∞). The cross over radius (switching of mode) varies from $b = 0.1514$ to 0.2414 as shown in Fig. 5. The optimal solutions for this case are presented in Table 8. Introducing internal elastic ring support, when placed at an optimal position increases the elastic buckling capacity significantly, and the percentage of increase in buckling loads is presented in Table 8. The results of this kind were scarce in the literature. However, the results are compared with the following case. Table 9, presents the buckling load parameters k , for a circular plate with simply supported edge and rotational restraint (by setting $T_{11} \rightarrow \infty$ & $T_{22} \rightarrow \infty$ to the present problem), against those obtained by Wang and Tun (2005).

Table 6 Optimal locations of internal elastic ring support b_{opt} , the corresponding buckling load parameter k_{opt} , and percentage increase in buckling load parameter

$R_{11} = 100$ & $T_{22} = 1000$		
T_{11}	1000	∞
b_{opt}	0.3011	0.2893
k_{opt}	6.98	6.984
%	82.35	82.45

Table 7 Buckling (for axisymmetric and asymmetric modes) load parameters for different values of rotational stiffness parameters, R_{11} , translational stiffness parameter, T_{11} , and translational stiffness parameter of internal elastic ring, T_{22} , when $\nu = 0.3$

b	$R_{11} = 10, T_{11} = T_{22} = 1000$		$R_{11} = T_{11} = T_{22} = \infty$	
	$n = 0$	$n = 1$	$n = 0$	$n = 1$
0	3.51188	4.70945	6.64780	5.39854
0.1	6.1039	5.06033	6.76632	6.50105
0.2	6.32317	6.00965	6.95592	7.20716
0.3	6.43411	6.88999	6.99485	7.90409
0.4	6.24905	7.59267	6.66257	8.39426
0.5	5.76950	7.67119	6.07454	8.15012
0.6	5.21160	7.03001	5.47550	7.40994
0.7	4.68264	6.29575	4.95263	6.68062
0.8	4.18626	5.61847	4.51266	6.06546
0.9	3.71744	5.01776	4.14357	5.55732
1	3.48890	4.71475	3.83194	5.13594

Table 8 Optimal locations of internal elastic ring support, b_{opt} , the corresponding buckling load parameter, k_{opt} , and percentage increase in buckling load parameter

T_{22}	$R_{11} = 10, T_{11} = 1000 = T_{11} = 1000$	$R_{11} = T_{11} = T_{11} = \infty$
b_{opt}	0.3003	0.2801
k_{opt}	6.434	6.987
%	84.41	82.35

Table 9 Comparison of buckling load parameter k , with Wang et al. (2005) for various rotational stiffness parameters R_{11} , and Poisson's ratio = 0.3

R_{11}	0	0.1	5	10	100	∞
Wang and Tun (2005)	4.198	4.449	10.462	12.173	14.392	14.682
Bhaskara Rao (2008)	4.1976	4.4486	10.4613	12.1724	14.392	14.6813
Present	4.19766	4.44864	10.46134	12.17242	14.392	14.6813

CONCLUSIONS

The buckling of thin circular plates with an internal elastic ring support and elastically restrained edges against rotation and translation has been solved. Also the buckling loads are given for various spring stiffness parameters [R_{11} & T_{11}] at the edges that simulate the rotational and translational restraints where $R_{11} \rightarrow \infty$ & $T_{11} \rightarrow \infty$, represents a clamped edge. Also the buckling loads are given for various translational spring stiffness parameters of an internal elastic ring support [T_{22}]. Two-dimensional plots are drawn for a wide range of rotational and translational constraints and translational constraints of an internal elastic ring support. It is observed that the buckling mode switches from an asymmetric mode to an axisymmetric mode at a particular internal elastic ring support radius. The cross over radius (switching of mode) is determined for different values of rotational,

translational constraints, and translational constraints of elastic ring. The optimal radius for the internal elastic ring support for maximum buckling load is found at the nodal circle of the higher buckling mode of a corresponding circular plate without any internal ring support where the buckling mode is always axisymmetric mode. The percentage of increase in buckling load capacity by introducing internal elastic ring support, when it is placed at an optimal position is also determined for the first time. In this paper the characteristic equations are exact; therefore the results can be calculated to any accuracy (Wang et al., 2005). These exact solutions can be used to check numerical or approximate results. Comparison of studies demonstrates the accuracy and stability of the present work. The tabulated buckling results are useful to designers in vibration control, structural design, and other related industrial applications.

REFERENCES

- Bhaskara Rao, L. (2008). Study of static stability and vibrations of circular and annular plates on generalized elastic medium. PhD Thesis, Osmania University, India.
- Brushes, D. O., Almroth, B. O. (1975). *Buckling of Bars, Plates and Shells*. New York: McGraw-Hill.
- Bryan, G. H. (1891). On the stability of a plane plate under thrust in its own plane with application to the buckling of the side of a ship. *Proceedings, London Math Society* 22:54–67.
- Kim, C. S., Dickinson, S. M. (1990). The flexural vibration of the isotropic and polar orthotropic annular and circular plates with elastically restrained peripheries. *Journal of Sound and Vibration* 143:171–179.
- Kunukkasseril, V. X., Swamidass, A. S. J. (1974). Vibration of continuous circular plates. *International Journal of Solids and Structures* 10:603–619.
- Laura, P. A. A., Gutierrez, R. H., Sanzi, H. C., Elvira, G. (2000). Buckling of circular, solid and annular plates with an intermediate circular support. *Ocean Engineering* 27:749–755.
- Wang, C. Y. (2003). Buckling of a circular plate with internal elastic ring support. *Mechanics Based Design of Structures and Machines* 31:93–102.
- Wang, C. M., Tun, M. A. (2005). Buckling of circular mindlin plates with an internal ring support and elastically restrained edge. *Journal of Engineering Mechanics* 131:359–366.
- Wang, C. Y., Wang, C. M. (2001). Buckling of circular plates with an internal ring support and elastically restrained edges. *Thin Walled Structures* 39:821–825.
- Wang, C. M., Wang, C. Y., Reddy, J. N. (2005). *Exact Solutions for Buckling of Structural Members*. Boca Raton, FL: CRC Press.
- Wang, C. M., Xiang, Y., Kitipornchai, S., Liew, K. M. (1993). Axisymmetric buckling of circular mindlin plates with ring supports. *Journal of Structural Engineering* 119:782–793.
- Wolkowisky, J. H. (1969). Buckling of the circular plate embedded in elastic springs, an application to geophysics. *Communications on Pure and Applied Mathematics* 22:367–667.
- Yamaki, N. (1958). Buckling of a thin annular plate under uniform compression. *Journal of Applied Mechanics* 25:267–273.

Vibrations of Circular Plates with Guided Edge and Resting on Elastic Foundation

L. B. Rao ^{1,*}, C. K. Rao ²

¹*School of Mechanical and Building Sciences, VIT University, Chennai Campus, Vandalur-Kelambakkam Road, Chennai-600127, Tamil Nadu, India*

²*Department of Mechanical Engineering, Gurnanak Institutions and Technical Campus, Ibrahimpatnam, R.R. District, Hyderabad-505450, A.P., India*

Received 26 August 2012; accepted xxx xxx 2012

ABSTRACT

In this paper, transverse vibrations of thin circular plates with guided edge and resting on Winkler foundation have been studied on the basis of Classical Plate Theory. Parametric investigations on the vibration of circular plates resting on elastic foundation have been carried out with respect to various foundation stiffness parameters. Twelve vibration modes are presented. The location of the stepped region with respect to foundation stiffness parameter is presented.

© 2012 IAU, Arak Branch. All rights reserved.

Keywords : Plate; Frequency; Guided edge; Elastic foundation.

1 INTRODUCTION

CIRCULAR plate systems [1-4] have wide applications in various fields of engineering; they are used as structural elements resting on foundations. The problems of plates on elastic foundation are important in engineering design and have been the focus of attention of many researchers. Some of the recent studies have reestablished the efficiency of the classical approach in analyzing the vibrations of variety of structures. Although the circular symmetry of the problem allows for its significant simplification, many difficulties very often arise due to complexity and uncertainty of boundary conditions. This uncertainty could be due to practical engineering applications where the edge of the plate does not fall into the classical boundary conditions such as Clamped, simply supported or free. When the boundary conditions of the plate deviate from classical cases, elastic translational restraints should be considered. A recent survey of literature shows that very few studies exist on the study of circular plates resting on elastic foundation. Wang and Wang [5], who observed the switching between axisymmetric and asymmetric vibration modes, recently investigated the effect of internal elastic translational supports.

The vibration characteristics of plates resting on an elastic medium are different from those of the plates supported only on the boundary. Leissa [3] discussed the vibration of a plate supported laterally by an elastic foundation. Leissa deduced that the effect of Winkler foundation merely increases the square of the natural frequency of the plate by a constant. Salari et al. [4] speculated the same conclusion. Ascione and Grimaldi [5] studied unilateral frictionless contact between a circular plate and a Winkler foundation using a variational

*Corresponding author. Tel.: +91 44 3993 1276.

E-mail address: bhaskarbabu_20@yahoo.com (L.B. Rao).

formulation. One of the earliest formulations of this problem was presented by Leissa [6], who tabulated values of frequency parameter for four vibration modes of simply supported circular plate with varying rotational stiffness.

Kang and Kim [9] presented an extensive review of the modal properties of the elastically restrained beams and plates. Zheng and Zhou [10] studied the large deflection of a circular plate resting on Winkler foundation. Ghosh [11] studied the free and forced vibration of circular plates on Winkler foundation by exact analytical method. The most general soil model used in practical applications is the Winkler [12] model in which the elastic medium below a structure is represented by a system of identical but mutually independent elastic linear springs. Recent investigations have reiterated the efficiency of the classical approach [13] in analyzing the behavior of structures under vibrations. There are other papers [Weisman [14], Dempsey et al. [15], Celep et al. [16]] dealing with the study of plates on a Winkler foundation. In general, papers dealing with vibrating plates, shells and beams are concerned primarily with the determination of eigenvalues and mode shapes [1-4]. The present study deals with obtaining exact solutions to the most important practical case of transverse vibrations of circular plates resting on Winkler foundation with guided edge conditions at the periphery of the plate. The results are presented for the non-dimensional frequency parameter of the plate for a wide range of values of Winkler foundation modulus parameter for use in design of such systems in micro or macro electro-mechanical devices.

2 MATHEMATICAL FORMULATION OF THE SYSTEM

The considered elastic thin circular plate is supported on a Winkler foundation as shown in Fig. 1. In the classical plate theory [1-4], the following fourth order differential equation describes free flexural vibrations of a thin circular uniform plate.

$$D\nabla^4 w(r, \theta, t) + \rho h \partial^2 w(r, \theta, t) / \partial t^2 = 0 \quad (1)$$

where $D = Eh^3 / 12(1 - \nu^2)$ is the flexural rigidity of a plate and a, h, ρ, E, ν are the plate's radiuses, thickness, density, Young's modulus and Poisson ratio's respectively.



Fig.1

A thin circular plate with guided edge and supported on full elastic foundation.

The homogeneous equation for Kirchhoff's plate on one parameter elastic foundation is given by the following equation [11]

$$D\nabla^4 w(r, \theta, t) + K_w w(r, \theta, t) + \rho h \partial^2 w(r, \theta, t) / \partial t^2 = 0 \quad (2)$$

Displacement in Eq. (2) can be presented as a combination of spatial and time dependent components as follows; Let

$$w(r, \theta, t) = W(r, \theta) e^{i\omega t} \quad (3)$$

Now substitute the Eq. (3) in Eq. (2)

$$D\nabla^4 W(r, \theta) + (K_w - \rho h \omega^2) W(r, \theta) = 0 \quad (4)$$

The solution to the above equation takes the following form

$$W_{mn}(r, \theta) = A_{mn} \left[J_n \left(\frac{\lambda_{mn} r}{a} \right) + C_{mn} I_n \left(\frac{\lambda_{mn} r}{a} \right) \right] \cos n\theta \quad \text{where } n = 0, 1, 2, 3, \dots, \quad m = 0, 1, 2, 3, \dots \quad (5)$$

where J_n is Bessel function of the first kind of first order and I_n is modified Bessel function of the first kind of first order. The boundary conditions can be formulated at $r = a$, as follows:

$$\frac{\partial W}{\partial r}(a, \theta) = 0 \quad (6)$$

$$V_r(a, \theta) = 0 \quad (7)$$

From Eqs. (6) and (7) yield the following:

$$\frac{\partial W}{\partial r}(a, \theta) = 0 \quad (8)$$

$$-D \left[\frac{\partial}{\partial r} \nabla^2 W + (1-\nu) \frac{1}{r} \frac{\partial}{\partial \theta} \left(\frac{1}{r} \frac{\partial^2 W}{\partial r \partial \theta} - \frac{1}{r^2} \frac{\partial W}{\partial \theta} \right) \right] = 0 \quad (9)$$

From Eqs. (5), (8) and (9), we derived the following:

$$C_{mn} = \frac{J_{m1}}{I_{p1}} \quad (10)$$

$$C_{mn} = \frac{J_{m3} - \frac{2J_{p2}}{\lambda_{mn}} - \left[3 + \frac{4+4(2-\nu)n^2}{\lambda_{mn}^2} \right] J_{m1} - \left[\frac{8(3-\nu)n^2}{\lambda_{mn}^3} - \frac{4}{\lambda_{mn}} \right] J_n(\lambda_{mn})}{I_{p3} + \frac{2I_{p2}}{\lambda_{mn}} + \left[3 - \frac{4-4(2-\nu)n^2}{\lambda_{mn}^2} \right] I_{p1} + \left[\frac{8(3-\nu)n^2}{\lambda_{mn}^3} + \frac{4}{\lambda_{mn}} \right] I_n(\lambda_{mn})} \quad (11)$$

$$J_{m1} = J_{n+1}(\lambda_{mn}) - J_{n-1}(\lambda_{mn}); J_{p2} = J_{n+2}(\lambda_{mn}) + J_{n-2}(\lambda_{mn}); J_{m3} = J_{n+3}(\lambda_{mn}) - J_{n-3}(\lambda_{mn}); \\ I_{p1} = I_{n+1}(\lambda_{mn}) + I_{n-1}(\lambda_{mn}); I_{p2} = I_{n+2}(\lambda_{mn}) + I_{n-2}(\lambda_{mn}); I_{p3} = I_{n+3}(\lambda_{mn}) + I_{n-3}(\lambda_{mn})$$

The frequency equation can be calculated From Eqs. (10) and (11), which allows determining eigenvalues λ_{mn} . The mode shape parameters C_{mn} can be determined corresponding to these eigenvalues by using either Eq. (10) or Eq. (11). The amplitude of each vibration mode in Eq. (5) is set by the normalization constant A_{mn} determined from the following condition [14].

$$\int_0^{2\pi} \int_0^a W_{mn}(r, \theta) W_{pq}(r, \theta) r dr d\theta = M_{mn} \delta_{mp} \delta_{nq} \quad (12)$$

where, M_{mn} is a mass of the plate, $\delta_{mp} = \delta_{nq} = 1$ if $m = p, n = q$ and $\delta_{mp} \delta_{nq} = 0$ if $m \neq p$ or $n \neq q$.

Dimensionless normalization constant A_{mn} can be determined from Eqs. (5) and (12) and it is given by following:

$$A_{mn} = \left[\frac{1}{\pi a^2} \cdot \int_0^{2\pi} \int_0^a \left(J_n \left(\frac{\lambda_{mn} r}{a} \right) + C_{mn} I_n \left(\frac{\lambda_{mn} r}{a} \right) \right) \cdot \cos n\theta \right]^2 r dr d\theta \quad (13)$$

In Eq (4), ω_{mn} is the natural frequency of vibrations:

$$\left(\frac{\lambda_{mn}^2}{a^2} \right) \sqrt{\frac{D}{\rho h}} \quad (14)$$

It is clear from the Eq. (14) the natural frequency of vibrations is dependent on the plate radius and eigenvalues from Eq. (14)

$$\lambda_{mn}^4 = \frac{\rho h a^4 \omega_{mn}^2}{D} \quad (15)$$

$$\lambda_{mn}^4 = \frac{\rho h a^4 \omega_{mn}^2}{D} - \frac{K_w a^4}{D} = \frac{\rho h a^4 \omega_{mn}^2}{D} - \xi^2 \quad (16)$$

where

$$\xi^2 = \frac{K_w a^4}{D} \quad (17)$$

$$\lambda_{mn}^{*4} = \lambda_{mn}^4 + \xi^2 \quad (18)$$

$$\lambda_{mn}^* = [\lambda_{mn}^4 + \xi^2]^{\frac{1}{4}} \quad (19)$$

where λ_{mn} is eigenvalue without foundation and λ_{mn}^* is eigenvalue with Winkler foundation

3 SOLUTION

Writing appropriate program and using Matlab computer software with symbolic capabilities, the above set of equations are solved for obtaining values of non-dimensional frequency parameter (λ_{mn}^*), for a given range of values Winkler foundation parameter. The following are the input parameters to the program; (i) Foundation ratio (ξ) (ii) Poisson ratio (ν) (iii) Upper bound for eigenvalues (N) (iv) Suggested for eigenvalues (d) (v) Number of mode shape parameters (n). The program finds eigenvalues λ_{mn}^* by using Matlab root finding function.

4 RESULTS AND DISCUSSIONS

The Matlab programming code is also implanted for various plate materials by adjusting the Poisson ratio. The Poisson ratio used in this case is 0.3. Results are presented for a wide range of foundation parameter as they are not presently available in the literature. The eigenvalues for the plate with guided edge and fully resting on the elastic foundation are computed. The effects of the foundation stiffness ratios on eigenvalues are plotted in Fig. 2. It has been observed from Fig. 2, that eigenvalues increases with an increment in the foundation stiffness ratio, and the plate become unstable in the region when the foundation stiffness ratio exceeds a certain value. Twelve vibration modes are presented in Fig. 2. The smoothened stepped variation is observed in Fig. 2. The stepped region increases with increase in foundation stiffness ratio and vibration modes. The location of the stepped region with respect to ξ changed gradually from the range of 0.059745[†][0.988372][‡]– 1.053192 [14.67192] to 2 [9.91694] – 1.9966 [15.3779]. Here[†]represents foundation stiffness ratio and[‡]represents eigenvalues through out the text. The eigenvalues for different plate materials, for various values of foundation parameters are computed and the results are given in Table

1. It is observed that for any value of foundation parameter (ξ), eigenvalues are independent on Poisson ratio, as presented in Fig. 3.

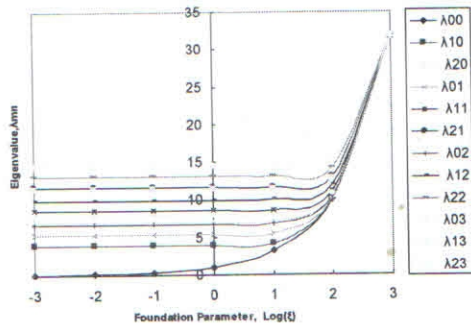


Fig.2

Effect of Foundation constraint, ξ on eigenvalues, λ_{mn} .

Table 1

Eigenvalues for different Poisson's ratio and foundation parameter

ν	$\xi = 1$	$\xi = 50$	$\xi = 100$	$\xi = 1000$	$\xi = 1e+04$	$\xi = 1e+05$
0	3.83614	7.2188	10.053	31.62448	100.0001	316.22777
0.1	3.83614	7.2188	10.053	31.62448	100.0001	316.22777
0.2	3.83614	7.2188	10.053	31.62448	100.0001	316.22777
0.3	3.83614	7.2188	10.053	31.62448	100.0001	316.22777
0.4	3.83614	7.2188	10.053	31.62448	100.0001	316.22777
0.5	3.83614	7.2188	10.053	31.62448	100.0001	316.22777

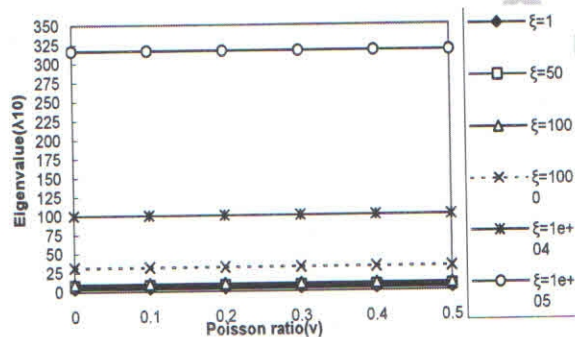


Fig.3

Effect of Poisson ratio, ν on eigenvalues, λ_{mn} .

5 CONCLUSION

The paper introduced a Matlab code for eigenvalues, of a circular plate with guided edge supports and resting on Winkler foundation. Two-dimensional plots of eigenvalues were drawn for different values of foundation stiffness ratios. It has been observed that the eigenvalues changes desperately only in a limited range of constraints specific to each vibration mode and are stable elsewhere. By knowing the position of the region where eigenvalues change rigorously is rudiment for structural design in the field of civil, marine, mechanical and aeronautical engineering applications and vibration control. It is also observed that the influence of foundation stiffness ratio on eigenvalues is more predominant.

REFERENCES

- [1] Timoshenko S., Krieger S.W., 1959, *Theory of Plates and Shells*, McGraw-Hill Book Company Inc, Newyork, Chapter 8:265.
- [2] Leissa A.W., 1969, *Vibration of Plates (NASA SP-160)*, Office of Technology Utilization, Washington, DC.
- [3] Szilard R., 2004, *Theories and Applications of Plate Analysis*, Classical Numerical and Engineering Methods, John Wiley & Sons Inc, Chapter 3.
- [4] Chakraverty S., 2009, *Vibration of Plates*, CRC Press, Taylor & Francis Group , Chapter 4.
- [5] Wang C.Y., Wang C.M., 2003, Fundamental frequencies of circular plates with internal elastic ring support, *Journal of Sound and Vibration* **263**: 1071-1078.
- [6] Leissa A. W., 1993, *Vibration of Plates*, Acoustical Society of America, Sewickley, PA.
- [7] Salari M., Bert C. M., Striz A.G., 1987, Free Vibration of a Solid Circular Plate free at its edge and attached to a Winkler foundation, *Journal of Sound and Vibration* **118**: 188-191.
- [8] Ascione L., Grimaldi A., 1984, Unilateral contact between a plate and an elastic foundation, *Mechanica* **19**: 23-233.
- [9] Kang K.H., Kim K.J., 1996, Modal properties of beams and plates on resilient supports with rotational and translational complex stiffness, *Journal of Sound and Vibration* **190**(2): 207-220.
- [10] Zheng X. J., Zhou Y. H., 1988, Exact solution of nonlinear circular plate on elastic-foundation, *Journal of Engineering Mechanics-ASCE* **114**: 1303-1316.
- [11] Ghosh A. K., 1997, Axisymmetric dynamic response of a circular plate on an elastic foundation, *Journal of Sound and Vibration* **205**: 112-120.
- [12] Winkler E., 1867, *Die Lehre von der Elasticitaet and Festigkeit*, Prag. Dominicus.
- [13] Soedel W., 1993, *Vibrations of shells and plates*, Mareel Dekker, Inc.
- [14] Weisman Y., 1970, On foundations that react in compression only, *Journal of Applied Mechanics* **37**: 1019-1030.
- [15] Dempsey J. P., Keer L. M., Patel N. B., Glasser M. L., 1984, Contact between plates and unilateral supports, *Journal of Applied Mechanics* **51**: 324-328.
- [16] Celep Z., 1988, Circular plate on tensionless Winkler foundation, *Journal of Engineering Mechanics* **114**(10): 1723-1739.

This article was downloaded by: [Aston University]

On: 04 September 2014, At: 12:27

Publisher: Taylor & Francis

Informa Ltd Registered in England and Wales Registered Number: 1072954 Registered office: Mortimer House, 37-41 Mortimer Street, London W1T 3JH, UK



Mechanics Based Design of Structures and Machines: An International Journal

Publication details, including instructions for authors and subscription information:

<http://www.tandfonline.com/loi/lmbd20>

Buckling of Annular Plates with Elastically Restrained External and Internal Edges

Lokavarapu Bhaskara Rao ^a & Chellapilla Kameswara Rao ^b

^a School of Mechanical & Building Sciences , VIT University , Chennai , Tamil Nadu , India

^b Department of Mechanical Engineering , TKR College of Engineering and Technology , Hyderabad , Andhra Pradesh , India

Published online: 20 Feb 2013.

To cite this article: Lokavarapu Bhaskara Rao & Chellapilla Kameswara Rao (2013) Buckling of Annular Plates with Elastically Restrained External and Internal Edges, Mechanics Based Design of Structures and Machines: An International Journal, 41:2, 222-235, DOI: [10.1080/15397734.2012.717495](https://doi.org/10.1080/15397734.2012.717495)

To link to this article: <http://dx.doi.org/10.1080/15397734.2012.717495>

PLEASE SCROLL DOWN FOR ARTICLE

Taylor & Francis makes every effort to ensure the accuracy of all the information (the "Content") contained in the publications on our platform. However, Taylor & Francis, our agents, and our licensors make no representations or warranties whatsoever as to the accuracy, completeness, or suitability for any purpose of the Content. Any opinions and views expressed in this publication are the opinions and views of the authors, and are not the views of or endorsed by Taylor & Francis. The accuracy of the Content should not be relied upon and should be independently verified with primary sources of information. Taylor and Francis shall not be liable for any losses, actions, claims, proceedings, demands, costs, expenses, damages, and other liabilities whatsoever or howsoever caused arising directly or indirectly in connection with, in relation to or arising out of the use of the Content.

This article may be used for research, teaching, and private study purposes. Any substantial or systematic reproduction, redistribution, reselling, loan, sub-licensing, systematic supply, or distribution in any form to anyone is expressly forbidden. Terms & Conditions of access and use can be found at <http://www.tandfonline.com/page/terms-and-conditions>

BUCKLING OF ANNULAR PLATES WITH ELASTICALLY RESTRAINED EXTERNAL AND INTERNAL EDGES[#]

Lokavarapu Bhaskara Rao¹ and Chellapilla Kameswara Rao²

¹School of Mechanical & Building Sciences, VIT University,
Chennai, Tamil Nadu, India

²Department of Mechanical Engineering, TKR College of Engineering
and Technology, Hyderabad, Andhra Pradesh, India

This article presents the exact elastic buckling of annular plates with elastically restrained edges against rotation and translation at inner and outer periphery. The classical plate theory is used to derive the governing differential equation for annular plate with elastically restrained edge support system. The buckling mode may not be axisymmetric as previously assumed. In certain cases, an asymmetric mode would yield a lower (critical) buckling load. This is due to switching of mode. This work presents the critical buckling load parameters for axisymmetric and asymmetric buckling modes. Extensive data is tabulated so that pertinent conclusions can be arrived at on the influence of rotational and translational restraints, Poisson's ratio and other boundary conditions on the buckling of uniform isotropic annular plates. The numerical results obtained are in good agreement with the previously published data. In this article, the characteristic equations are exact; therefore, the results can be calculated to any accuracy.

Keywords: Annular plate; Buckling; Elastically restrained edge; Mode switching; Rotational restraint; Translational restraint.

INTRODUCTION

Annular plates are key common structural components used in mechanical design, turbines, tanks, micro pumps, disc brakes, nuclear reactors, air crafts, submarines, etc. The prediction of buckling of structural members restrained laterally is important in the design of various engineering components. Several researchers under various loading and boundary conditions have considered the axisymmetric buckling of elastic annular plates. The earlier works based on the classical thin plate theory was done by Kawamoto (1936), Iwato (1939), Yamaki (1959), Mansfield (1960), Timoshenko and Gere (1961), Pflueger (1964), and Majumdar (1971). Laura et al. (2000) investigated the elastic buckling problem of the aforesaid type of annular plates, who modeled the plate using the classical thin plate theory. They have considered only axisymmetric modes.

Received March 6, 2012; Accepted July 27, 2012

[#]Communicated by I. Elishakoff.

Correspondence: Lokavarapu Bhaskara Rao, School of Mechanical & Building Sciences, VIT University, Chennai Campus, Vandalur-Kelambakkam Road, 600127, Tamil Nadu, India; E-mail: bhaskarbabu_20@yahoo.com

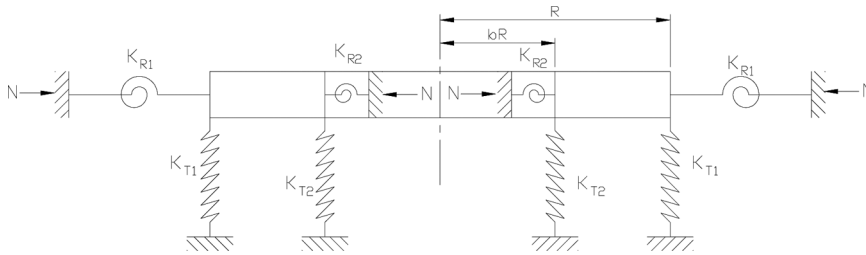


Figure 1 Buckling of an annular plate with elastically restrained edges against rotation and translation.

However, in practical industrial engineering situations, we rarely come across ideal boundary conditions such as clamped, simply supported, and free. It is an accepted fact that the condition on a periphery often tends to be in between the classical boundary conditions (clamped, simply supported, and free) and may correspond more closely to some form of elastic restraints, i.e., rotational and translational restraints (Kim and Dickinson, 1990; Wang and Wang, 2001). Very few researchers have considered the effects of rotational and translational restraints. Further, these authors, Kim and Dickinson (1990) and Xu et al. (2005), have considered only axisymmetric buckling, which may not lead to the correct buckling load. There seems to be only one article (Lokavarapu and Chellapilla, 2011) in the literature studying the vibration of annular plate with elastically restrained guided edge against translation at the inner and outer edges. In certain cases, asymmetric mode would yield a lower buckling load. It complements the mentioned article (Lokavarapu and Chellapilla, 2011) by studying the buckling of annular plate with elastically restrained edges against rotation and translation. The purpose of the present work is to complete the results of the buckling of annular plates when the edges are elastically restrained against rotation and translation by including the *asymmetric* buckling modes, thus correctly determining the buckling loads.

DEFINITION OF THE PROBLEM

Consider a thin circular annular plate of outer radius R , and inner radius bR , uniform thickness h , Young's modulus E , and Poisson's ratio ν . It is subjected to a uniform in-plane load, N along its boundary i.e., along the inner edge at $r = b$, and along the outer edge at $r = 1$, as shown in Fig. 1. This circular annular plate is assumed to be made of linearly elastic, homogeneous, and isotropic material and the effects of shear deformation and rotary inertia are neglected. The outer and inner edges of the annular plate are elastically restrained against rotation and translation as shown in Fig. 1. The problem here is to determine the elastic critical buckling loads of an annular plate with outer and inner edges that are elastically restrained against rotation and translation.

FORMULATION OF THE PROBLEM

Annular plate is elastically restrained edge against rotation and translation at outer edge of radius R and at inner edge of radius bR . The annular plate under

consideration is subjected to a uniformly distributed in-plane load N , along the inner edge $r = b$ and along the outer edge $r = 1$, as shown in Fig. 1. Let the subscript I denote the inner region $0 \leq \bar{r} \leq b$ and the subscript II denote the outer region $b \leq \bar{r} \leq 1$. Here, all lengths are normalized by R . Based on the Classical Thin Plate theory (Kirchhoff's theory), the governing fourth order differential equation for elastic buckling of an annular plate may be expressed in polar coordinates (r, θ) as

$$D\nabla^4 w + N\nabla^2 w = 0 \quad (1)$$

where w is the lateral displacement, D is the flexural rigidity, N is the uniform compressive load at inner and outer edge. After normalizing lengths by the radius of the plate R , Eq. (1) can be written as

$$D\nabla^4 \bar{w} + k^2 \nabla^2 \bar{w} = 0 \quad \text{and} \quad (2)$$

$$\nabla^2 (\nabla^2 + k^2) \bar{w} = 0 \quad (3)$$

where the Laplacian operator,

$$\nabla^2 = \frac{\partial^2}{\partial \bar{r}^2} + \frac{1}{\bar{r}} \frac{\partial}{\partial \bar{r}} + \frac{1}{\bar{r}^2} \frac{\partial^2}{\partial \theta^2} \quad (4)$$

where \bar{r} is the radial distance normalized by R . $\bar{D} = Eh^3/12(1 - \nu^2)$ is the flexural rigidity, $\bar{w} = w/R$, is normalized transverse displacement of the plate. $k^2 = R^2 N/\bar{D}$ is non-dimensional load parameter. Suppose, there are n nodal diameters. In polar coordinates (r, θ) set

$$\bar{w}(\bar{r}, \theta) = \bar{u}(\bar{r}) \cos(n\theta) \quad (5)$$

where n is the number of nodal diameters. The general solution for the governing buckling equation may be expressed as

$$\bar{u}_I(r) = C_1 J_n(k\bar{r}) + C_2 Y_n(k\bar{r}) + C_3 \bar{r}^n + C_4 \left\{ \frac{\log \bar{r}}{\bar{r}^{-n}} \right\} \quad (6)$$

Substituting Eq. (6) into Eq. (5) gives the following:

$$\bar{w}_I(\bar{r}, \theta) = \left[C_1 J_n(k\bar{r}) + C_2 Y_n(k\bar{r}) + C_3 \bar{r}^n + C_4 \left\{ \frac{\log \bar{r}}{\bar{r}^{-n}} \right\} \right] \cos(n\theta) \quad (7)$$

where top form of the Eq. (7) is used for $n = 0$ (symmetric) and the bottom form is used for $n \neq 0$ (asymmetric), C_1, C_2, C_3 , & C_4 are constants, $J_n(\cdot)$ & $Y_n(\cdot)$ are the Bessel functions of the first and second kinds of order n , respectively. Let the subscript I denote outer domain $b \leq \bar{r} \leq 1$ and the subscript II denote the inner domain $0 \leq \bar{r} \leq b$.

Case (i): Outer edge of annular plate is elastically restrained against rotation and translation

The boundary conditions at outer region of the annular plate in terms of rotational stiffness (K_{R1}) and translational stiffness (K_{T1}) is given by the following expressions:

$$M_r(\bar{r}, \theta) = K_{R1} \frac{\partial \bar{w}_I(\bar{r}, \theta)}{\partial \bar{r}} \quad \text{and} \quad (8)$$

$$V_r(\bar{r}, \theta) = -K_{T1} \bar{w}_I(\bar{r}, \theta) \quad (9)$$

The radial moment and the radial Kirchhoff shear at outer edge are defined as follows:

$$M_r(\bar{r}, \theta) = -\frac{D}{R^3} \left[\frac{\partial^2 \bar{w}_I(\bar{r}, \theta)}{\partial \bar{r}^2} + \nu \left(\frac{1}{\bar{r}} \frac{\partial \bar{w}_I(\bar{r}, \theta)}{\partial \bar{r}} + \frac{1}{\bar{r}^2} \frac{\partial^2 \bar{w}_I(\bar{r}, \theta)}{\partial \theta^2} \right) \right] \quad \text{and} \quad (10)$$

$$V_r(\bar{r}, \theta) = -\frac{D}{R^3} \left[\frac{\partial}{\partial \bar{r}} \nabla^2 \bar{w}_I(\bar{r}, \theta) + (1 - \nu) \frac{1}{\bar{r}} \frac{\partial}{\partial \theta} \left(\frac{1}{\bar{r}} \frac{\partial^2 \bar{w}_I(\bar{r}, \theta)}{\partial \bar{r} \partial \theta} - \frac{1}{\bar{r}^2} \frac{\partial \bar{w}_I(\bar{r}, \theta)}{\partial \theta} \right) \right] \quad (11)$$

Equations (8) and (10) yields the following:

$$\left[\frac{\partial^2 \bar{w}_I(\bar{r}, \theta)}{\partial \bar{r}^2} + \nu \left(\frac{1}{\bar{r}} \frac{\partial \bar{w}_I(\bar{r}, \theta)}{\partial \bar{r}} + \frac{1}{\bar{r}^2} \frac{\partial^2 \bar{w}_I(\bar{r}, \theta)}{\partial \theta^2} \right) \right] = -\frac{K_{R1} R^2}{D} \frac{\partial^2 \bar{w}_I(\bar{r}, \theta)}{\partial \bar{r}^2} \quad \text{and} \quad (12)$$

$$\left[\frac{\partial^2 \bar{w}_I(\bar{r}, \theta)}{\partial \bar{r}^2} + \nu \left(\frac{1}{\bar{r}} \frac{\partial \bar{w}_I(\bar{r}, \theta)}{\partial \bar{r}} + \frac{1}{\bar{r}^2} \frac{\partial^2 \bar{w}_I(\bar{r}, \theta)}{\partial \theta^2} \right) \right] = -R_{11} \frac{\partial \bar{w}_I(\bar{r}, \theta)}{\partial \bar{r}} \quad (13)$$

where $R_{11} = \frac{K_{R1} R^2}{D}$.

Equations (9) and (11) yields the following:

$$\begin{aligned} & \left[\frac{\partial}{\partial \bar{r}} \nabla^2 \bar{w}_I(\bar{r}, \theta) + (1 - \nu) \frac{1}{\bar{r}} \frac{\partial}{\partial \theta} \left(\frac{1}{\bar{r}} \frac{\partial^2 \bar{w}_I(\bar{r}, \theta)}{\partial \bar{r} \partial \theta} - \frac{1}{\bar{r}^2} \frac{\partial \bar{w}_I(\bar{r}, \theta)}{\partial \theta} \right) \right] \\ &= \frac{K_{T1} R^3}{D} \bar{w}_I(\bar{r}, \theta) \quad \text{and} \end{aligned} \quad (14)$$

$$\begin{aligned} & \left[\frac{\partial}{\partial \bar{r}} \nabla^2 \bar{w}_I(\bar{r}, \theta) + (1 - \nu) \frac{1}{\bar{r}} \frac{\partial}{\partial \theta} \left(\frac{1}{\bar{r}} \frac{\partial^2 \bar{w}_I(\bar{r}, \theta)}{\partial \bar{r} \partial \theta} - \frac{1}{\bar{r}^2} \frac{\partial \bar{w}_I(\bar{r}, \theta)}{\partial \theta} \right) \right] \\ &= T_{11} \bar{w}_I(\bar{r}, \theta) \end{aligned} \quad (15)$$

where $T_{11} = \frac{K_{T1} R^3}{D}$.

Boundary conditions at the outer edge: Eqs. (7), (13), and (15) yield the following at $\bar{r} = 1$:

$$\begin{aligned} & \left[\frac{k^2}{4} P_2 + \frac{k}{2} (\nu + R_{11}) P_1 - \left(\frac{k^2}{2} + \nu n^2 \right) J_n(k) \right] C_1 \\ & + \left[\frac{k^2}{4} Q_2 + \frac{k}{2} (\nu + R_{11}) Q_1 - \left(\frac{k^2}{2} + \nu n^2 \right) Y_n(k) \right] C_2 \\ & + [n((n-1)(1-\nu) + R_{11})] C_3 + \left\{ \frac{(\nu + R_{11}) - 1}{n((n+1)(1-\nu) - R_{11})} \right\} C_4 = 0 \end{aligned} \quad (16)$$

$$\begin{aligned}
& \left[\frac{k^3}{8} P_3 + \frac{k^2}{4} P_2 - \frac{k}{2} \left(\frac{3}{4} k^2 + n^2 (2 - \nu) + 1 \right) P_1 + \left(n^2 (3 - \nu) - \frac{k^2}{2} - T_{11} \right) J_n(k) \right] C_1 \\
& + \left[\frac{k^3}{8} Q_3 + \frac{k^2}{4} Q_2 - \frac{k}{2} \left(\frac{3}{4} k^2 + n^2 (2 - \nu) + 1 \right) Q_1 + \left(n^2 (3 - \nu) - \frac{k^2}{2} - T_{11} \right) Y_n(k) \right] C_2 \\
& + [n^2(n-1)\nu - n^3 - T_{11}] C_3 - \left\{ \begin{array}{c} n^2(2-\nu) \\ -n^2(n+1)\nu + n^3 - T_{11} \end{array} \right\} C_4 = 0 \quad (17)
\end{aligned}$$

where

$$\begin{aligned}
P_1 &= J_{n-1}(k) - J_{n+1}(k); & P_2 &= J_{n-2}(k) + J_{n+2}(k); & P_3 &= J_{n-3}(k) - J_{n+3}(k); \\
Q_1 &= Y_{n-1}(k) - Y_{n+1}(k); & Q_2 &= Y_{n-2}(k) + Y_{n+2}(k); & Q_3 &= Y_{n-3}(k) - Y_{n+3}(k);
\end{aligned}$$

Case (ii): Inner edge of annular plate is elastically restrained against rotation and translation

The boundary conditions at inner region of the annular plate in terms of rotational stiffness (K_{R2}) and translational stiffness (K_{T2}) is given by the following expressions:

$$M_r(\bar{r}, \theta) = -K_{R2} \frac{\partial \bar{w}_I(\bar{r}, \theta)}{\partial \bar{r}} \quad \text{and} \quad (18)$$

$$V_r(\bar{r}, \theta) = K_{T2} \bar{w}_I(\bar{r}, \theta) \quad (19)$$

The radial moment and the radial Kirchhoff shear at outer edge are defined as follows:

$$M_r(\bar{r}, \theta) = -\frac{D}{R^3} \left[\frac{\partial^2 \bar{w}_I(\bar{r}, \theta)}{\partial \bar{r}^2} + \nu \left(\frac{1}{\bar{r}} \frac{\partial \bar{w}_I(\bar{r}, \theta)}{\partial \bar{r}} + \frac{1}{\bar{r}^2} \frac{\partial^2 \bar{w}_I(\bar{r}, \theta)}{\partial \theta^2} \right) \right] \quad \text{and} \quad (20)$$

$$V_r(\bar{r}, \theta) = -\frac{D}{R^3} \left[\frac{\partial}{\partial \bar{r}} \nabla^2 \bar{w}_I(\bar{r}, \theta) + (1 - \nu) \frac{1}{\bar{r}} \frac{\partial}{\partial \theta} \left(\frac{1}{\bar{r}} \frac{\partial^2 \bar{w}_I(\bar{r}, \theta)}{\partial \bar{r} \partial \theta} - \frac{1}{\bar{r}^2} \frac{\partial \bar{w}_I(\bar{r}, \theta)}{\partial \theta} \right) \right] \quad (21)$$

Equations (18) and (20) yields the following:

$$\left[\frac{\partial^2 \bar{w}_I(\bar{r}, \theta)}{\partial \bar{r}^2} + \nu \left(\frac{1}{\bar{r}} \frac{\partial \bar{w}_I(\bar{r}, \theta)}{\partial \bar{r}} + \frac{1}{\bar{r}^2} \frac{\partial^2 \bar{w}_I(\bar{r}, \theta)}{\partial \theta^2} \right) \right] = \frac{K_{R2} R^2}{D} \frac{\partial^2 \bar{w}_I(\bar{r}, \theta)}{\partial \bar{r}^2} \quad \text{and} \quad (22)$$

$$\left[\frac{\partial^2 \bar{w}_I(\bar{r}, \theta)}{\partial \bar{r}^2} + \nu \left(\frac{1}{\bar{r}} \frac{\partial \bar{w}_I(\bar{r}, \theta)}{\partial \bar{r}} + \frac{1}{\bar{r}^2} \frac{\partial^2 \bar{w}_I(\bar{r}, \theta)}{\partial \theta^2} \right) \right] = R_{22} \frac{\partial \bar{w}_I(\bar{r}, \theta)}{\partial \bar{r}} \quad (23)$$

where $R_{22} = \frac{K_{R2} R^2}{D}$.

Equations (19) and (21) yields the following:

$$\begin{aligned}
& \left[\frac{\partial}{\partial \bar{r}} \nabla^2 \bar{w}_I(\bar{r}, \theta) + (1 - \nu) \frac{1}{\bar{r}} \frac{\partial}{\partial \theta} \left(\frac{1}{\bar{r}} \frac{\partial^2 \bar{w}_I(\bar{r}, \theta)}{\partial \bar{r} \partial \theta} - \frac{1}{\bar{r}^2} \frac{\partial \bar{w}_I(\bar{r}, \theta)}{\partial \theta} \right) \right] \\
& = -\frac{K_{T2} R^3}{D} \bar{w}_I(\bar{r}, \theta) \quad \text{and} \quad (24)
\end{aligned}$$

$$\left[\frac{\partial}{\partial \bar{r}} \nabla^2 \bar{w}_I(\bar{r}, \theta) + (1 - \nu) \frac{1}{\bar{r}} \frac{\partial}{\partial \theta} \left(\frac{1}{\bar{r}} \frac{\partial^2 \bar{w}_I(\bar{r}, \theta)}{\partial \bar{r} \partial \theta} - \frac{1}{\bar{r}^2} \frac{\partial \bar{w}_I(\bar{r}, \theta)}{\partial \theta} \right) \right] = -T_{22} \bar{w}_I(\bar{r}, \theta) \quad (25)$$

where $T_{22} = \frac{K_{T2} R^3}{D}$.

Boundary conditions at the inner edge: Eqs. (7), (23), and (25) yields the following at $\bar{r} = b$:

$$\begin{aligned} & \left[\frac{k^2}{4} P'_2 + \frac{k}{2} \left(\frac{\nu}{b} - R_{22} \right) P'_1 - \left(\frac{k^2}{2} + \frac{\nu n^2}{b^2} \right) J_n(kb) \right] C_1 \\ & + \left[\frac{k^2}{4} Q'_2 + \frac{k}{2} \left(\frac{\nu}{b} - R_{22} \right) Q'_1 - \left(\frac{k^2}{2} + \frac{\nu n^2}{b^2} \right) Y_n(kb) \right] C_2 \\ & + [n((n-1)(1-\nu) - bR_{22}) b^{n-2}] C_3 \\ & + \left\{ \frac{1}{b^2} [\nu(1 - n^2 \log b) - 1 - bR_{22}] \right. \\ & \left. + n[(n+1)(1-\nu) + R_{22} b^{-2n-3}] b^{-n-2} \right\} C_4 = 0 \end{aligned} \quad (26)$$

$$\begin{aligned} & \left[\frac{k^3}{8} P'_3 + \frac{k^2}{4b} P'_2 - \frac{k}{2} \left(\frac{3}{4} k^2 + \frac{n^2(2-\nu)+1}{b^2} \right) P'_1 \right. \\ & + \left(\frac{n^2(3-\nu)}{b^3} - \frac{k^2}{2b} + T_{22} \right) J_n(kb) \left. \right] C_1 \\ & + \left[\frac{k^3}{8} Q'_3 + \frac{k^2}{4b} Q'_2 - \frac{k}{2} \left(\frac{3}{4} k^2 + \frac{n^2(2-\nu)+1}{b^2} \right) Q'_1 \right. \\ & + \left(\frac{n^2(3-\nu)}{b^3} - \frac{k^2}{2b} + T_{22} \right) Y_n(kb) \left. \right] C_2 + b^{n-3} [n^2(n-1)(\nu-1) + T_{22} b^3] C_3 \\ & + \left\{ \frac{n^2}{b^3} [(\nu-2) + (3-\nu) \log b] + T_{22} \log b \right. \\ & \left. + \frac{n^2(1-\nu)(1+n) + T_{22} b^3}{b^3} \right\} C_4 = 0 \end{aligned} \quad (27)$$

where $R_{22} = \frac{K_{R2} R^2}{D}$, $T_{22} = \frac{K_{T2} R^3}{D}$. The top forms of Eqs. (16), (17), (26), and (27) are used for $n = 0$ (axisymmetric buckling) and the bottom forms are used for $n = 1$ (asymmetric buckling).

SOLUTION

For the given values of $n, \nu, R_{11}, T_{11}, R_{22}, T_{22}$ the above set of equations, gives an exact characteristic equation for non-trivial solutions of the coefficients C_1, C_2, C_3 & C_4 . For non-trivial solution, the determinant of $[C]_{4 \times 4}$ vanish. Using Mathematica, computer software with symbolic capabilities, solves this problem.

RESULTS AND DISCUSSIONS

The buckling load parameters are computed for various internal radii parameter b , rotational restraints R_{11} & R_{22} , and translational restraints T_{11} &

Table 1 Buckling ($n = 0$ for axisymmetric mode and $n = 1$ for asymmetric mode) load parameters for different values of rotational spring stiffness parameter, R_{11} when $R_{22} = T_{11} = T_{22} = 10$ & $\nu = 0.3$

b	$R_{11} = 0.001$		$R_{11} = 0.5$		$R_{11} = 10$		$R_{11} = 100$		$R_{11} = 10^{16}$	
	$[n = 0]$	$[n = 1]$	$[n = 0]$	$[n = 1]$	$[n = 0]$	$[n = 1]$	$[n = 0]$	$[n = 1]$	$[n = 0]$	$[n = 1]$
0	2.04986	3.62455	2.31751	3.59525	3.48925	3.44977	3.79385	3.39892	3.83184	3.39151
0.1	2.51953	3.61866	2.78811	3.59001	3.8877	3.44753	4.12692	3.39763	4.1552	3.39031
0.2	2.99333	3.58958	3.27022	3.56392	4.34119	3.4357	4.54703	3.39022	4.57077	3.38357
0.3	3.51119	3.62308	3.80159	3.59318	4.87509	3.44719	5.06483	3.39696	5.08641	3.3897
0.4	4.13835	3.84455	4.44833	3.78725	5.56585	3.52598	5.75441	3.44494	5.77562	3.43351
0.5	4.98519	4.36757	5.3215	4.23568	6.53843	3.69098	6.74155	3.54591	6.76439	3.52633
0.6	6.26967	5.38856	6.63843	5.08783	8.02657	3.9823	8.26475	3.7346	8.29143	3.70257
0.7	8.49521	7.31271	8.90093	6.65936	10.5599	4.54645	10.866	4.13491	10.9003	4.08295
0.8	13.1593	10.9636	13.6063	9.61489	15.7092	5.85539	16.1575	5.14108	16.2076	5.04988
0.9	27.7673	17.7729	28.2712	15.8321	31.306	9.88109	32.1917	8.44441	32.2919	8.24751

T_{22} . Poisson’s ratio used in these calculations is 0.3. The critical buckling load parameters, k ($n = 0$ for axisymmetric mode and $n = 1$ for asymmetric mode) for various rotational restraint at outer edge ($R_{11} = 0.001, 0.5, 10, 100$ & 10^{16}), by keeping rotational restraint, R_{22} and translational restraints (T_{11} & T_{22}), constant ($R_{22} = T_{11} = T_{22} = 10$), are presented in Table 1. Figures 2 and 3 show the variations of buckling load parameters, k ($n = 0$ for axisymmetric and $n = 1$ for asymmetric buckling load parameters), with respect to the inner radii of annular plate b .

It is observed from Fig. 2, which is for a given value of $R_{11} = 0.001$ and $R_{22} = T_{11} = T_{22} = 10$, the curve is composed of two segments. This is due to the switching of buckling modes. For a smaller internal radius b , the plate buckles in

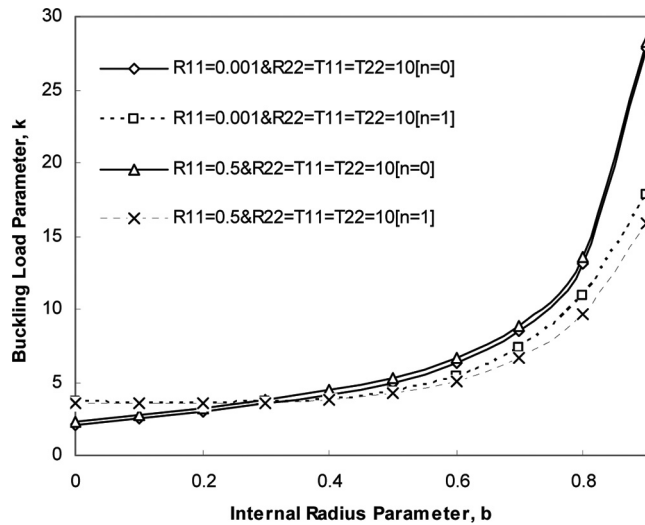


Figure 2 Buckling Load Parameter k , versus internal radius parameter b , for $R_{11} = 0.001$ & 0.5 and $R_{22} = T_{11} = T_{22} = 10$ ($n = 0$ for axisymmetric mode and $n = 1$ for asymmetric mode).

an axisymmetric mode (i.e., $n = 0$). In this segment (as shown by continuous lines in Fig. 2), the buckling load decreases as b decreases in value. For larger internal radius b , the plate buckles in an asymmetric mode (i.e., $n = 1$). In this segment (as shown by dotted lines in Fig. 2), the buckling load increases as b increases in value as shown in Fig. 2. The cross-over radius (switching of mode) is $b = 0.32891$ i.e., the buckling is governed by the axisymmetric mode $n = 0$ when $b \leq 0.32891$. When b is increased beyond 0.32891, the $n = 1$ asymmetric mode gives the correct lower buckling load. Figure 2, shows the variation of buckling load parameter k , with respect to the internal radius parameter b , for a given value of $R_{11} = 0.5$ and $R_{22} = T_{11} = T_{22} = 10$. Similarly, it is observed from the Fig. 2, the curve is composed of two segments. This is due to the switching of buckling modes. The cross-over radius (switching of mode) is $b = 0.2598$ and the corresponding buckling load is $k = 3.5777$. The buckling is governed by the axisymmetric mode $n = 0$ when $b \leq 0.2598$. When b is increased beyond 0.2598, the $n = 1$ asymmetric mode gives the correct lower buckling load. The cross-over radius parameter decreases from 0.32891 to 0.2598 as R_{11} increased from 0.001 to 0.5.

Figure 3, represent the variation of buckling load parameter k , with respect to the internal radius parameter b , for a given values of $R_{11} = 10$ & 100 and $R_{22} = T_{11} = T_{22} = 10$. It is noticed that the buckling is completely governed by asymmetric mode $n = 1$ (as shown by dotted lines in Fig. 3) and the buckling load increases as b increases in value as shown in Fig. 3.

The buckling load parameters k , ($n = 0$ for axisymmetric mode and $n = 1$ for asymmetric mode) for various rotational restraint at inner edge ($R_{22} = 5, 10, 100$ & 10^{16}), by keeping rotational restraint R_{11} , and translational restraints T_{11} & T_{22} , constant ($R_{11} = T_{11} = T_{22} = 10$), are presented in Table 2. Figures 4 and 5 show the variation of buckling load parameter k , with respect to the internal radii parameter b , for various values of rotational restraint at inner edge ($R_{22} = 5, 10, 100$ & 10^{16})

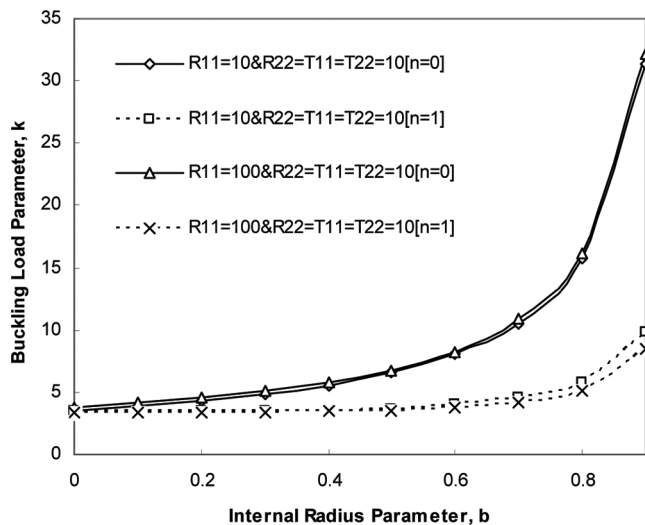


Figure 3 Buckling load parameter k , versus internal radius parameter b , for $R_{11} = 10$ & 100 and $R_{22} = T_{11} = T_{22} = 10$ ($n = 0$ for axisymmetric mode and $n = 1$ for asymmetric mode).

Table 2 Buckling ($n = 0$ for *axisymmetric* mode and $n = 1$ for *asymmetric* mode) load parameters for different values of rotational stiffness parameter, R_{22} when $R_{11} = T_{11} = T_{22} = 10$ & $\nu = 0.3$

b	$R_{22} = 5$		$R_{22} = 10$		$R_{22} = 100$		$R_{22} = 10^{16}$	
	$[n = 0]$	$[n = 1]$	$[n = 0]$	$[n = 1]$	$[n = 0]$	$[n = 1]$	$[n = 0]$	$[n = 1]$
0	3.49222	3.44977	3.49222	3.44977	3.49222	3.44977	3.49222	3.44977
0.1	3.90492	3.44753	3.8877	3.44753	3.85306	3.44753	3.84652	3.44753
0.2	4.39615	3.4357	4.34119	3.4357	4.26147	3.4357	4.2497	3.4357
0.3	4.96969	3.4472	4.87509	3.44719	4.75846	3.44709	4.74284	3.44709
0.4	5.69734	3.52668	5.56585	3.52598	5.41979	3.52538	5.40122	3.52538
0.5	6.7049	3.69497	6.53843	3.69098	6.3665	3.68738	6.34538	3.68698
0.6	8.23157	3.99995	8.02657	3.9823	7.82619	3.96595	7.80225	3.96415
0.7	10.8202	4.61191	10.5599	4.54645	10.3167	4.48418	10.2881	4.47711
0.8	16.0813	6.06545	15.7092	5.85539	15.379	5.63833	15.3406	5.61234
0.9	32.0635	10.4926	31.306	9.88109	30.7084	9.12756	30.6393	9.02702

and $R_{11} = T_{11} = T_{22} = 10$. It is noticed from Figs. 4 and 5, the buckling is completely governed by asymmetric mode $n = 1$ (as shown by dotted lines in Figs. 4 and 5) irrespective of R_{22} . The buckling load increases as b increases in value as shown in Figs. 4 and 5.

The buckling load parameters for axisymmetric and asymmetric modes and for various translational restraint at outer edge T_{11} , and keeping constant rotational restraints R_{11} & R_{22} , and translational restraint at inner edge T_{22} , ($R_{11} = R_{22} = T_{22} = 10$), are presented in Table 3 and graphically in Figs. 6 and 7. It is observed from Figs. 6 and 7, the buckling is completely governed by asymmetric mode $n = 1$ (as shown by dotted lines in Figs. 6 and 7).

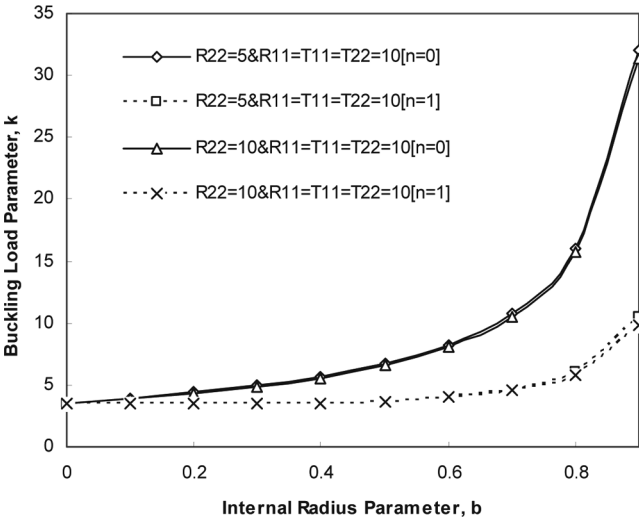


Figure 4 Buckling load parameter k , versus internal radius parameter b , for $R_{22} = 5$ & 10 and $R_{11} = T_{11} = T_{22} = 10$ ($n = 0$ for *axisymmetric* mode and $n = 1$ for *asymmetric* mode).

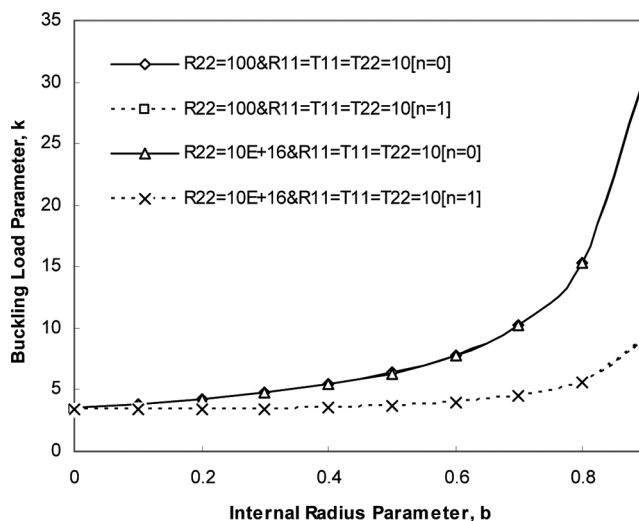


Figure 5 Buckling load parameter k , versus internal radius parameter b , for $R_{22} = 100$ & 10^{16} and $R_{11} = T_{11} = T_{22} = 10$ ($n = 0$ for axisymmetric mode and $n = 1$ for asymmetric mode).

It is observed from the Fig. 7, which for a given value of $T_{11} = 100$ and $R_{11} = R_{22} = T_{22} = 10$, the curve is composed of two segments. This is due to the switching of buckling modes. For a smaller internal radius b , the plate buckles in an axisymmetric mode (i.e., $n = 0$). For larger internal radius b , the plate buckles in an asymmetric mode (i.e., $n = 1$). The cross-over radius (switching of mode) is $b = 0.2598$. The buckling is governed by the axisymmetric mode $n = 0$ when $b \leq 0.2598$. When b is increased beyond 0.2598, the $n = 1$ asymmetric mode gives the correct lower buckling load. Similarly, Fig. 7, shows the variation of buckling load parameter k , with respect to the internal radius parameter b , for a given value of $T_{11} = 10^{16}$ and $R_{11} = R_{22} = T_{22} = 10$. It is observed from the Fig. 7, the curve

Table 3 Buckling ($n = 0$ for axisymmetric mode and $n = 1$ for asymmetric mode) load parameters for different values of rotational stiffness parameter, T_{11} when $R_{11} = R_{22} = T_{22} = 10$ & $\nu = 0.3$

b	$T_{11} = 5$		$T_{11} = 10$		$T_{11} = 100$		$T_{11} = 10^{16}$	
	$[n = 0]$	$[n = 1]$	$[n = 0]$	$[n = 1]$	$[n = 0]$	$[n = 1]$	$[n = 0]$	$[n = 1]$
0	3.49321	2.87535	3.49222	3.44977	3.49133	4.60625	3.49123	4.71989
0.1	3.95424	2.87429	3.8877	3.44753	3.82302	4.59288	3.81549	4.70422
0.2	4.43535	2.86931	4.34119	3.4357	4.24301	4.53024	4.23112	4.63398
0.3	4.98857	2.88079	4.87509	3.44719	4.74727	4.56924	4.73103	4.68091
0.4	5.70569	2.94169	5.56585	3.52598	5.39511	4.82865	5.37225	4.97532
0.5	6.72291	3.07497	6.53843	3.69098	6.29576	5.34558	6.26151	5.57066
0.6	8.28941	3.32444	8.02657	3.9823	7.65985	6.20393	7.6055	6.59859
0.7	10.976	3.82623	10.5599	4.54645	9.96414	7.66448	9.87266	8.44754
0.8	16.5391	5.00498	15.7092	5.85539	14.6039	10.5826	14.433	12.3933
0.9	-	8.60323	31.306	9.88109	28.3987	18.9687	27.9788	24.9593

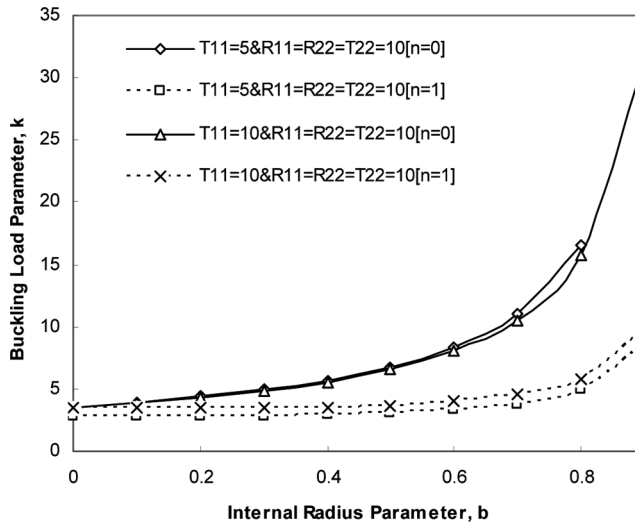


Figure 6 Buckling load parameter k , versus internal radius parameter b , for $T_{11} = 5$ & 10 and $R_{11} = R_{22} = T_{22} = 10$ ($n = 0$ for axisymmetric mode and $n = 1$ for asymmetric mode).

is composed of two segments. This is due to the switching of buckling mode. The cross-over radius (switching of mode) is $b = 0.28855$ and the corresponding buckling load is $k = 4.6901$. The buckling is governed by the axisymmetric mode $n = 0$ when $b \leq 0.28855$. When b is increased beyond 0.28855 , the $n = 1$ asymmetric mode gives the correct lower buckling load. The cross-over radius parameter increases from 0.2598 to 0.28855 as T_{11} increased from 100 to 10^{16} .

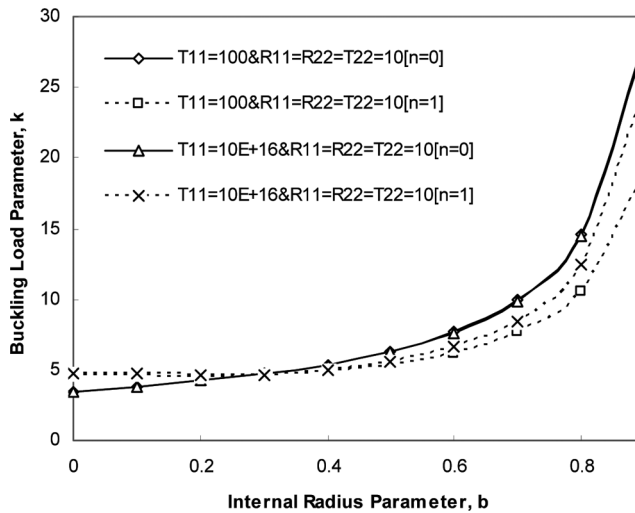


Figure 7 Buckling load parameter k , versus internal radius parameter b , for $T_{11} = 100$ & 10^{16} and $R_{11} = R_{22} = T_{22} = 10$ ($n = 0$ for axisymmetric mode and $n = 1$ for asymmetric mode).

Table 4 Comparison of critical buckling load parameter k , with Yamaki (1958) for an annular plate with both edges simply supported and Poisson's ratio = 0.3

b	0	0.1	0.3	0.5	0.7	0.9
Yamaki (1958)	—	—	4.75	6.40	10.52	31.43
Present	4.40089	4.20507	4.74929	6.40088	10.5231	31.4292

Table 5 Comparison of critical buckling load parameter k , with Yamaki (1958) for an annular plate with outer edge clamped and inner edge simply supported and Poisson's ratio = 0.3

b	0	0.1	0.3	0.5	0.7	0.9
Yamaki (1958)	—	—	7.06	9.42	15.31	45.20
Present	6.64775	6.30692	7.05846	9.416	15.3047	45.199

The cross-over radius decreases at lower values of R_{11} . The critical buckling load is completely governed by asymmetric mode $n = 1$ at higher values of R_{11} . The critical buckling load is corresponding to $n = 1$ mode irrespective of R_{22} . The critical buckling load is corresponding to $n = 1$ mode at lower values of T_{11} . The cross-over radius increases at higher values of T_{11} . The results of this kind were scarce in the literature. However, the results are compared with the following cases: (i) Table 4 presents the comparison of critical buckling load parameters k , for the annular plate with both edges simply supported (by setting the rotational translational restraints with $R_{11} = 0$ & $T_{11} \rightarrow \infty$ at outer edge and $R_{22} = 0$ & $T_{22} \rightarrow \infty$ at inner edge), against those obtained by Yamaki (1958); (ii) Table 5 presents the comparison of critical buckling load parameters k , for an annular plate with outer edge clamped and inner edge simply supported (by setting the rotational and translational restraints with $R_{11} \rightarrow \infty$ & $T_{11} \rightarrow \infty$ at outer edge and $R_{22} = 0$ & $T_{22} \rightarrow \infty$ at inner edge), against those obtained by Yamaki (1958); (iii) Table 6 presents the comparison of critical buckling load parameters k , for an annular plate with both edges clamped (by setting $R_{11} \rightarrow \infty$ & $T_{11} \rightarrow \infty$ and $R_{22} = \infty$ & $T_{22} \rightarrow \infty$ in the present problem), against those obtained by Yamaki (1958); (iv) also, the results of cross-over radius and the corresponding buckling load parameters for an annular plate with elastically restrained guided edges against translation (by setting $R_{11} \rightarrow \infty$ & $R_{22} \rightarrow \infty$ at both the edges in the present problem), are compared with the results obtained by Lokavarapu and Chellapilla (2011). The optimal ring support is affected by the rotational stiffness parameters, translational stiffness parameters. However, it is observed that the influence of rotational spring stiffness

Table 6 Comparison of critical buckling load parameter k , with Yamaki (1958) for an annular plate with both edges clamped and Poisson's ratio = 0.3

b	0	0.1	0.3	0.5	0.7	0.9
Yamaki (1958)	—	—	9.06	12.59	20.96	62.84
Present	6.64775	7.11484	9.02078	12.5861	20.9524	62.834

parameters on buckling load is much more predominant than that of translational spring stiffness parameters.

CONCLUSIONS

The buckling of thin annular plates with an elastically restrained edge against rotation and translation has been solved. Critical buckling loads are given for various rotational and translational spring stiffness parameters [R_{11} , R_{22} , T_{11} , & T_{22}] at the edges that simulate the rotational restraints, where R_{11} , R_{22} , T_{11} , & $T_{22} \rightarrow \infty$, represents a clamped edge and R_{11} & $R_{22} \rightarrow 0$ & T_{11} & $T_{22} \rightarrow \infty$, represents a simply supported edge. Also, the buckling loads are given for *axisymmetric* and *asymmetric* modes. It has been observed that the buckling mode switches from asymmetric to axisymmetric at a particular internal radius parameter. This cross-over radius depends on the rotational and translational restraints. The cross-over radius parameter decreases from 0.32891 to 0.2598 as R_{11} increased from 0.001 to 0.5. The cross-over radius parameter increases from 0.2598 to 0.28855 as T_{11} increased from 100 to ∞ . The fundamental buckling may be asymmetric, axisymmetric, or a mixture of both. In this article, the characteristic equations are exact; therefore, the results can be calculated to any accuracy. These exact solutions can be used to check numerical or approximate results. The tabulated buckling results are useful to designers in vibration control, structural monitoring and design.

NOMENCLATURE

h	Thickness of a Plate
R	Radius of a Plate
b	Non-dimensional inner radius of Annular Plate
ν	Poisson's ratio
E	Young's Modulus of a material
D	Flexural Rigidity of a Material
K_{R1}	Rotational Spring Stiffness at outer Edge
K_{T1}	Translational Spring Stiffness at outer Edge
K_{R2}	Rotational Spring Stiffness at inner Edge
K_{T2}	Translational Spring Stiffness at inner edge
R_{11}	Non-dimensional Flexibility Parameter at outer Edge
T_{11}	Non-dimensional Translational Flexibility Parameter at outer Edge
R_{22}	Non-dimensional Rotational Flexibility Parameter at inner Edge
T_{22}	Non-dimensional Translational Flexibility Parameter at inner edge
N	Uniform in-plane compressive load
k	Non-dimensional Buckling Load Parameter

REFERENCES

- Iwato, S. (1939). Stability of a circular plate with a centre hole. *Journal of the Japan Society of Mechanical Engineers* 42:663–664.
- Kawamoto, M. (1936). The stability of a thin circular plate with a concentric hole. *Journal of Japan Society Mechanical Engineering* 39:449–450.

- Kim, C. S., Dickinson, S. M. (1990). The flexural vibration of the isotropic and polar orthotropic annular and circular plates with elastically restrained peripheries. *Journal of Sound and Vibration* 143:171–179.
- Laura, P. A. A., Gutierrez, R. H., Sanzi, H. C., Elvira, G. (2000). Buckling of circular, solid and annular plates with an intermediate circular support. *Ocean Engineering* 27:749–755.
- Mansfield, E. H. (1960). On the buckling of an annular plate. *Journal of Applied Mathematics* 13:16–23.
- Majumdar, S. (1971). Buckling of a thin annular plate under uniform compression. *AIAA Journal* 9:1701–1707.
- Pflueger, A. (1964). Stabilitätsprobleme der Elastostatik. *Structural Stability Engineering Practice*. Berlin: Springer, pp. 448–453.
- Rao, L. B., Rao, C. K. (2011). Fundamental buckling of annular plates with elastically restrained guided edges against translation. *Mechanics Based Design of Structures and Machines* 39:409–419.
- Timoshenko, S. P., Gere, J. M. (1961). *Theory of Elastic Stability*. New York: McGraw-Hill.
- Wang, C. Y., Wang, C. M. (2001). Buckling of circular plates with an internal ring support and elastically restrained edges. *Thin Walled Structures* 39:821–825.
- Xu, R. Q., Wang, Y., Chen, W. Q. (2005). Axisymmetric buckling of transversely isotropic circular and annular plates. *Journal of Archive of Applied Mechanics* 74:692–703.
- Yamaki, N. (1958). Buckling of a thin annular plate under uniform compression. *Journal of Applied Mechanics* 25:267–273.

Dynamic stability and natural frequency of composite corrugated bellows expansion joint

N. Sujana Rao^{1, a}, Dr. M. Radhakrishna^{2, b} and Dr. AMK. Prasad^{3, c}

¹Assoc Professor, Sai Spurthi Institute of Technology, Sathupally,, India

²Scientist-F, Head, Design & Engineering, CSIR, IICT-Tarnaka, Hyderabad, India

³Professor, Department of Mechanical Engineering, Osmania University-Hyderabad, India

^asujan504@gmail.com, ^bradhakrishna@iict.ac.in, ^camkpr@yahoo.co.in

Key words: expansion joint, composite corrugated bellows, dynamic stability, frequency.

Abstract. The paper deals with dynamic stability and natural frequency of composite corrugated bellows expansion joint. In this simplified formulae are developed by a thin walled pipe model. The dynamic model determined by integration method. According to the EJMA formulae the torsional stability calculation is modified using two different equivalent radii. The torsional natural frequencies are calculated using the formula based on equivalent thin walled pipe model. The modified formulae are verified by those from a finite element model and good agreement is shown between the simplified formulae and the finite element model.

Introduction

Broman et al. [6] have calculated axial, transverse and torsional natural frequencies of bellows using finite element analysis (FEA). They suggested the further research work should be the torsional characteristics of bellows. The most comprehensive and widely accepted standards on corrugated bellow design are the standards of the Expansion joint manufacturing association (EJMA) [1]. Comparison of the results between the EJMA standards and finite element analysis or experimental work can be found in the literature. The dynamic behavior of the bellow has been studied, mainly concentrated on axial and transverse vibrations. M. Radhakrishna et al. [7], Jakubaukas and Weaver [4] have studied axial vibrations of bellows. EJMA [1] and Li et al. [5] have studied both the axial and transverse vibrations of bellows by considering the effect of rotary inertia in the beam model.

This paper develops simplified formulae for calculating torsional natural frequency of bellows. To calculate the torsional natural frequency of the bellows using a thin walled pipe model, its torsional stiffness and equivalent radius need to be determined. The EJMA standards have provide a simple formula of torsional stiffness calculating of bellows, in which a bellow is extended in its convolution root diameter to form an equivalent thin-walled pipe model. However, errors arise using this formula. In this paper the torsional stiffness of bellows is calculated using Chine's [2] integration method. The error source in the EJMA formulas is analyzed and two modified formulae are developed in this paper for torsional stiffness and natural frequency are verified by comparison with result from the FEA model.

Torsional natural frequency

The U-shaped bellow is composed of several circular ring shells, inverse circular ring shells and ring plates. The outer and inner radii of the bellows are represented by R_o and R_i respectively. The rotating radii of the circular ring shell and inverse circular ring shell are represented by R_1 and R_2 respectively, and are also outer and inner radii of the ring plate. The convolution crown and root radii are represented by R_c and R_r respectively. The convolution height is represented by h . for most of the bellows can be regarded as a thin walled straight pipe for simplicity in analysis. Li et al. [5] have analyzed axial vibrations of bellows using a straight pipe of model. Broman et al. [6] have calculated axial, lateral and torsional natural frequencies of bellow using the pipe model with unchanged torsional and axial stiffness in FEA.

1 Equivalent thin walled pipe model

This paper also uses an equivalent thin-walled pipe model to analyze torsional natural frequencies of bellows. Assuming that the thin-walled pipe has continuously and uniformly distributed mass, the differential for torsional vibration is given by Weaver et al [3].

$$\frac{\partial^2 \theta}{\partial x^2} - \frac{G_p}{\rho_p} \frac{\partial^2 \theta}{\partial t^2} = 0 \quad (1)$$

Where x is the axial coordinate, t is the time, θ is the torsional angle, G_p is the shear modulus of elasticity and ρ_p is the pipe density. The solution of the above differential equation can be given as

$$\theta = \left(C \sin \frac{\omega_i}{\alpha} x + D \cos \frac{\omega_i}{\alpha} x \right) (A \cos \omega_i t + B \sin \omega_i t) \quad (2)$$

Where $\alpha = \sqrt{\frac{G_p}{\rho_p}}$, the propagating speed of the torsional wave is, ω_i is the torsional frequency and A , B , C and D are constants defined by the boundary conditions.

Suppose that the torsional stiffness of the thin walled pipe is represented by K_p , the pipe mass by m_p and the polar moment of inertia by I_p .

$$\text{Then } K_p = \frac{G_p I_p}{\rho_p}, m_p = \rho_p 2 \pi R_p L s_p, I_p = 2 \pi R_p^3 s_p \quad (3) \quad (4) \quad (5)$$

Where L is the pipe length, R_p is the pipe radius and s_p is the pipe wall thickness. The torsional natural frequency of the pipe under the three different boundary conditions can be calculated using the following formula

One end is fixed and other end is freed (fixed - free). The boundary conditions are given as

$$(\theta)_{x=0} = 0, \left(\frac{\partial \theta}{\partial x} \right)_{x=L} = 0,$$

$$\text{Torsional natural frequency is } f_i = \frac{\omega_i}{2\pi} = \frac{i-0.5}{2R_p} \sqrt{\frac{K_p}{m_p}}, \text{ Where } (i=1,2,3...) \quad (6)$$

Its torsional stiffness K_b , mass m_b and equivalent radius R_b can be determined corresponding to K_p , m_p and R_p of a thin walled pipe.

2 Torsional stiffness of bellows.

A bellow is a revolutionary shell and its linear torsional deformation is axisymmetrical. The stress due to torsional deformation is also axisymmetrical. The circumferential and meridian angles are represented by θ and ϕ respectively. The parallel circle radius represented by r and the meridian and the circumferential radii of curvature are represented by r_1 and r_2 respectively, an infinitesimal section a-b-c-d is taken from the inner force analysis as shown in fig 1 sides a-b and c-d are in the meridian direction and sides a-d and b-c are in the circumferential direction. The member forces are represented by N_{11} , N_{22} , N_{12} and N_{21} where N_{12} is equal to N_{21} . The flexural torques are represented by M_{11} , M_{22} , M_{12} and M_{21} where M_{12} is equal to M_{21} .

Chien [2] has developed the equilibrium equations for revolutionary shell under torsional loading using the minimum potential energy principle. the equilibrium equations for torsion was a given as

$$-\frac{d}{d\phi} (N_{12} r^2) + \frac{1}{r_2} \frac{d}{d\phi} (M_{12} r^2) = 0 \quad (7)$$

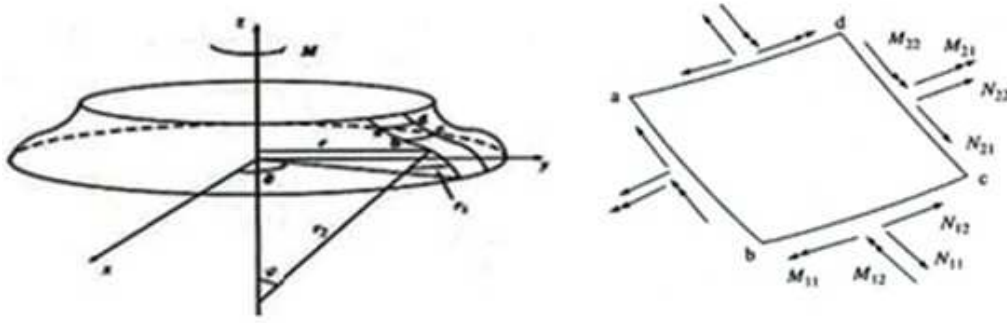


Fig 1 Element

It can be seen that only N_{12} and M_{12} have effects on the torsional deformation. According to the membrane theory, if the revolutionary shell is thin enough, the effect of M_{12} can be neglected compared with that of N_{12} the equation (12) can be simplified

$$\frac{d}{d\varphi}(N_{12}r^2) = 0 \quad (8)$$

Based on the simplification, Chien's [2] presented integration formulae for the torsional stiffness of the revolutionary shell as

$$K = \frac{T}{\theta} = \frac{\pi B(1-\nu)}{\int_{\varphi_0}^{\varphi} \frac{r_1^3}{r^3} d\varphi}, \text{ Where } K \text{ is torsional stiffness of a revolutionary shell} \quad (9)$$

T is the torsional moment, θ is the torsional angle, $B = \frac{Es}{1-\nu^2}$ is the extensional stiffness, E and ν are Young's modulus and Poisson's ratio respectively and s is the shell thickness.

One convolution of a U-shaped bellow can be seen as a composed of one circular ring shell, on inverse circular ring shell and two ring plates. If the torsional stiffness of the circular ring shell section is K_1 and that of the ring plate and the inverse circular ring shell section are K_2 and K_3 respectively. The torsional stiffness of one convolution can be given as

$$K_s = \frac{1}{1/K_1 + 2/K_2 + 1/K_3} \quad (10)$$

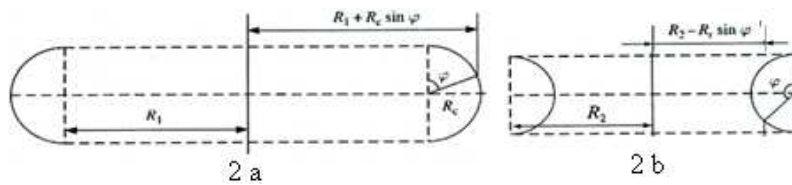


Fig.2a Sectional Bellow, 2b inverse circular ring

The circular ring shell section is shown fig 2a. Where $r_1 = R_c$ and $r = R_1 + R_c \sin \varphi$. according to equation (9) is given as

$$K_1 = \frac{\pi B(1-\nu)}{\int_0^\pi [R_c / (R_1 + R_c \sin \varphi)^3] d\varphi} \quad (11)$$

The ring plate section is shown in fig 2a. its a torsional stiffness K_2 is calculating using a torsional ring plate model and is given as

$$K_2 = \frac{\pi B(1-\nu)}{\int_{R_2}^{R_1} \frac{1}{r^3} dr} = \frac{2\pi B(1-\nu)}{1/R_2^2 - 1/R_1^2} \quad (12)$$

The inverse circular ring section is shown in fig 2b. where

$r_1 = R_r$ and $r_1 = R_r - R_r \sin \varphi$. According to the equation (9), K_3 is given as

$$K_3 = \frac{\pi B(1-\nu)}{\int_0^\pi [R_r / (R_2 - R_r \sin \varphi)^3] d\varphi}, \text{ for bellow } K_b = \frac{K_s}{n} = \frac{\pi B(1-\nu) R_m^3}{nm_b [(\pi-2)(R_c + R_r) + 2h]} \quad (13)$$

Using above equations the torsional stiffness of one convolution can be calculated. The torsional stiffness of the hole bellow as given as where n is the number of convolutions.

3 Bellows mass

Assuming that the bellows mass is continuously distributed. It can be calculated by

$$m_b = n\rho_b(A_1 + 2A_2 + A_3)s_b \quad (14)$$

Where A_1, A_2 and A_3 are the surface area of the circular ring shell section, the ring plate section and the inverse circular ring shell section respectively. ρ_b is the bellow density and s_b is the bellow wall thickness. The three surface areas are given as follows

$$A_1 = \int_0^\pi 2\pi(R_1 + R_c \sin \phi) R_c d\phi = 2\pi^2 R_1 R_c + 4\pi R_c^2, A_2 = \pi(R_1^2 - R_2^2) \quad (15), (16)$$

$$A_3 = \int_0^\pi 2\pi(R_2 - R_r \sin \phi) R_r d\phi = 2\pi^2 R_2 R_r - 4\pi r^2 \quad (17)$$

4 Equivalent radius of bellows

Assuming the bellows is extended to a circular cylindrical shell with unchanged mass and wall thickness. The equivalent radius can be calculated as

$$R_f = \frac{A_1 + 2A_2 + A_3}{2\pi[(\pi-2)(R_c + R_r) + 2h]} \quad (18)$$

Usually, R_f is not equal to the inner radius of bellows R_i . That is to say the EJMA standards are used R_i as equivalent radius to calculate the torsional stiffness of bellows. Therefore selecting R_i as the equivalent radius may not be appropriate. In fact substituting R_f for R_i in the equation (18) can be better result when verified by FEA. Broman et al. [6] have used the mean radius $R_m = \frac{R_i + R_o}{2}$ as the equivalent radius in their FEA models. This is based on the assumption that the bellow mass can be considered as concentrating on the mean radius. This paper also uses R_m as another selection of the equivalent radius.

$$\text{If } R_f \text{ is selected as the equivalent radius, } R_f = \frac{\pi B(1-\nu)R_f^3}{n[(\pi-2)(R_c + R_r) + 2h]} \quad (19)$$

The torsional natural frequency of bellow is there given as

$$f_i = \frac{\omega_i}{2\pi} = \frac{i-0.5}{2R_f} \sqrt{\frac{K_b}{m_b}}, \quad \text{Where } (i = 1, 2, 3 \dots) \text{ (fixed-free)} \quad (20)$$

Substituting the values K_b , m_b and R_f in the equation 20 yields

$$f_i = \frac{\omega_i}{2\pi} = \frac{i-0.5}{2} \sqrt{\frac{\pi B(1-\nu)R_f}{n m_b [(\pi-2)(R_c + R_r) + 2h]}}, \quad \text{Where } (i = 1, 2, 3 \dots) \text{ (fixed-free)} \quad (21)$$

Result discussion:

According to Chien's [2] integration method, torsional stiffness of bellow can be calculated by sectional integration, but this is somewhat inconvenient. This paper has simplified by two simple formulae for the equivalent radius calculation in the order to modify the EJMA formula for torsional stiffness calculations. The torsional stiffness and natural frequency of a specimen bellows have been calculated using the modified EJMA formulae, Chien's [2] integration method and equivalent thin walled pipe model. The results are compared with those from the FEA model.

Table 1 Torsional natural frequencies of composite specimen [Hz]

Condition	Modes	Methods used				FEA
		Integration		Simplified		
		R _f	R _m	R _f	R _m	
Fixed- free	1	1489	1493	1498	1496	1505
	2	4262	4280	4295	4282	4294
	3	6926	6967	6962	6982	6996
	4	9734	9754	9779	9774	9787

It can be seen from the table that no matter whether R_m or R_f is used as the equivalent radius of torsional natural frequency calculated are in good agreement with those from FEA. The simplified method is enough to satisfy engineering requirements.

Conclusion

Torsional stiffness and natural frequency of bellows are studied in this paper. The torsional vibration frequencies of bellows are calculated using an equivalent straight thin-walled pipe model. The key point using this model is to determine the torsional stiffness the equivalent radius of a bellows. Good agreement has been shown among the results from the different methods. The modified EJMA formulae for the torsional stiffness calculation and the simplified formula for the torsional natural frequency calculation of bellows can be used in engineering, as they are simple and precise.

References

- [1] Standards of the Expansion Joint Manufacturers Association, 9th edition, 2008 (EJMA, New York)
- [2] Chien, W. Z. Torsional stiffness of shells of revolution. *Appl Math. Mechanics*, 1990, 11, 403-412.
- [3] Weaver Jr, W., Timoshenko, S. P. and Young, D. H. *Vibration Problems in Engineering*, 5th edition, 1990 (John Wiley, New York).
- [4] Jakubauskas, V. F. and Weaver, D. S. Natural vibrations of fluid filled bellows, *Trans. ASME J. Pressure Vessels Technol.*, 1996, 118, 484-490.
- [5] Li, Ting-Xin, Guo, B. I. and Li, Tian-Xiang. Natural frequency of U-shaped bellows. *Int. J. Pressure Vessels and Piping*, 1990, 42, 61-74.
- [6] Broman, G. I., Jonsson, A. P. and Hermann, M. P. Determining dynamic characteristics of bellows by manipulated beam finite elements of commercial software. *Int J. Pressure Vessel and Piping*, 2000, 77, 445-453.
- [7] M. Radha krishna, C. Kameswara Rao. Axial vibrations of U-Shaped bellows with elastically restrained end conditions. *Thin-Walled structures*. 2004, 42, 415-426

Mechanics, Simulation and Control III

10.4028/www.scientific.net/AMM.367

Dynamic Stability and Natural Frequency of Composite Corrugated Bellows Expansion Joint

10.4028/www.scientific.net/AMM.367.68

Lokavarapu Bhaskara Rao

School of Mechanical and Building Sciences,
VIT University,
Chennai Campus,
Vandalur-Kelambakkam Road,
Chennai-600048, India
e-mail: bhaskarbabu_20@yahoo.com

Chellapilla Kameswara Rao

Department of Mechanical Engineering,
TKR College of Engineering and Technology,
Medbowli,
Meerpet, Saroornagar,
Hyderabad-500079, India
e-mail: chellapilla95@gmail.com

Frequencies of Circular Plates Weakened Along an Internal Concentric Circle and Elastically Restrained Edge Against Translation

The present study deals with the derivation of an exact solution for the problem of obtaining the natural frequencies of the vibration of circular plates weakened along an internal concentric circle due to the presence of a radial crack and elastically restrained along the outer edge of the plate against translation. The frequencies of the circular plates are computed for varying values of the elastic translational restraint, the radius of the radial crack, and the extent of the weakening duly simulated by considering the radial crack as a radial elastic rotational restraint on the plate. The results for the first six modes of the plate vibrations are computed. The effects of the elastic edge restraint, the radius of the weakened circle, and the extent of the weakening represented by an elastic rotational restraint on the vibration behavior of thin circular plates are studied in detail. The internal weakening due to a crack resulted in decreasing the fundamental frequency of the plate. The exact method of solution and the results presented in this paper are expected to be of specific use in analyzing the effect of a radial crack on the fundamental natural frequency of the circular plate in the presence of a translational restraint existing along the outer edge of the plate. These exact solutions can be used to check the numerical or approximate results. [DOI: 10.1115/1.4006938]

Keywords: circular plate, frequency, translational restraint, rotational restraint, weakened

1 Introduction

Circular plates are widely used as structural elements in many aeronautical, civil, mechanical, and marine applications. The vibration of circular plates is basic in structural design [1–3]. The literature on the vibration of circular plates with basic edge conditions and internal strengthening has been reviewed [4–7]. The study of free vibration and the natural frequencies of the vibration of cracked plates is essential for the detection of structural damage and also in solving the design analysis problems of mechanical systems. The natural frequencies of cracked elastic structures differ considerably from their healthy counterparts and a comprehensive literature survey of research activities regarding the vibration problems of various structures with cracks is found in the work by Dimarogonas [8]. In the case of vibration problems of cracked rectangular plates, it has been very well known for a long time that the variations in natural frequencies and mode shapes are mainly due to the crack length variations.

The initial contribution to the study of vibration problems of cracked rectangular plates was made by Lynn and Kumbasar [9], who solved the Fredholm integral equation of the first kind to numerically calculate the drop in the natural frequency of the vibration of plates due to cracking. Petyt [10] experimentally investigated the variation of the frequency of the fundamental mode due to crack length, the results of which have been verified against analytical results from the finite element formulation. A number of investigations were further carried out on the vibrations

of cracked plates by researchers such as Stahl and Keer [11], Hirano and Okazaki, [12], Solecki [13], and Yuan and Dickinson [14]. The vibrations of a cracked rectangular plate were investigated by Stahl and Keer [11] and Solecki [13] examined the problem of the bending vibrations of a simply supported rectangular plate with a crack parallel to one edge by means of the finite Fourier transformation of discontinuous functions.

By applying a domain decomposition method, Liew et al. [15] obtained the out-of-plane vibration frequencies of cracked plates, confirming the results found by Stahl and Keer [11] and Hirano and Okazaki [12], and presenting results for a wider range of crack length ratios. Furthermore, they examined a plate with a centrally-located internal crack and reported frequency crossings. Recently, for a square plate with an edge crack, Ma and Huang [16] reported variations in natural frequencies and associated mode shapes due to changes in crack length, based on both experiments and analysis using the finite element method. Ma and Huang [16] observed that the nonlinearity due to the crack closing effect has to be considered, especially for the in-plane bending case. Finite element modeling of cracked plates was studied by Qian et al. [17], deriving the element stiffness matrix of the plate by the integration of stress intensity factors. A numerical method based on the Rayleigh method for predicting the natural frequencies of a rectangular plate with a centrally located crack, including transverse shear deformation and rotary inertia, was presented by Lee and Lim [18]. Furthermore, Krawczuk [19] examined the effects of the crack location and its length on the changes of the natural frequencies of the simply supported and cantilevered rectangular plate. Liew et al. [20] investigated the vibration behavior of cracked rectangular plates, analyzing the free vibrations of rectangular plates with a crack emanating either from an edge or

Contributed by the Applied Mechanics Division of ASME for publication in the JOURNAL OF APPLIED MECHANICS. Manuscript received February 11, 2011; final manuscript received May 7, 2012; accepted manuscript posted June 6, 2012; published online October 29, 2012. Assoc. Editor: Alexander F. Vakakis.

centrally located. Khadem and Rezaee [21] presented an analytical approach to the crack detection of rectangular plates under uniform external loads using vibration analysis. Krawczuk et al. [22] studied the finite element model of a plate with an elasto-plastic through crack utilizing an element based on elasto-plastic fracture mechanics and the finite element method.

Studying the free vibration analysis of cracked annular plates, Lee [23] proposed a simple numerical method based on the Rayleigh principle for predicting the fundamental frequencies of an annular plate with an internal concentric crack and applied the same for an annular plate with two simply supported edges and two clamped edges. Ramesh et al. [24] experimentally studied the effects of the number and length of periodic radial cracks on the natural frequencies of an annular plate. Anifantis et al. [25] investigated the free vibrations of cracked annular plates by modeling a surface peripheral crack of an annular plate as a local rotational flexibility for vibration analysis. Yuan et al. [26] utilized the Ritz method of solution for the determination of the natural frequencies of the free vibration of circular and annular plates with radial or circumferential cracks or slits through the full thickness by using the minimum number of sector plate elements, which are joined together by means of artificial springs. They obtained the flexibility matrix of the sector type element with a radial through crack by using the formulas of the trapezoidal type element in the case of setting close geometric dimensions, and proved the applicability of the derived element in the dynamic analysis of annular plates with cracks. The results obtained are compared with the experimental results available in the literature.

Very few studies have been performed on the free vibrations of a circular plate weakened along a concentric circle due to the presence of a radial crack. The weakening in the plate can arise because of internal notching or partial cracks or may be caused due to fatigue cracks along a concentric circle. There are two papers [27,28] in the literature which studied the vibration of plates with internal weakening, where a clamped or simply supported [27] and movable or free edge [28] thin circular plate was studied. A hinge with an elastic rotational restraint modeled the weakened position. However, as we know, in practical industrial engineering situations, we rarely come across such ideal boundary conditions. Although the circular symmetry of the problem allows for its significant simplification, additional difficulties very often arise due to the complexity and uncertainty of boundary conditions. This uncertainty occurs because, in many practical applications, the edge of the plate is not clamped, free, or simply supported. When the plate's boundary conditions depart from classical cases, elastic translational and rotational restraints should be considered [29,30]. To the best of the authors' knowledge, there is no other research paper addressing the general boundary conditions with linear translational restraint at the plate edge. The purpose of the present paper is, therefore, to study the effect of weakening of a thin circular plate along a concentric circle due to a radial crack and the plate being elastically restrained along the outer edge against translation using the exact method of solution approach. The natural frequencies of a circular plate for varying values of translational restraint along the plate edge, the radius of the weakened circle, Poisson's ratio and the rotational restraint with the hinge of the cracked region are obtained for a wide range of nondimensional parameters and are presented in both tabular and graphical form for use in the design of such cracked and weakened circular plates which are applicable in the engineering industry.

2 Definition of the Problem

Consider a circular plate of radius R , uniform thickness h , Poisson's ratio ν , and Young's modulus E . The circular plate is also assumed to be made of a linearly elastic, homogeneous, and isotropic material. The problem at hand is to determine the frequencies of a circular plate with an elastically restrained outer edge against translation and weakened along an internal concentric circle, as shown in Fig. 1.

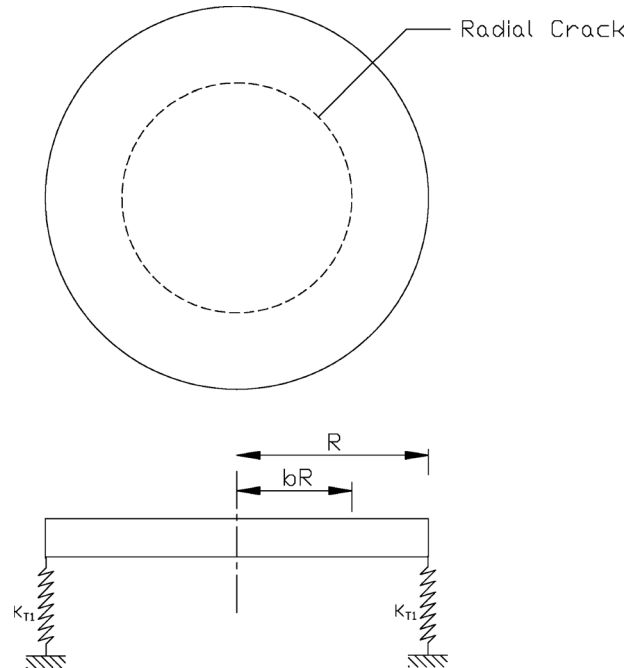


Fig. 1 Circular plate with elastically restrained outer edge against translation and weakened along an internal concentric circle

3 Analytical Formulation of the System

The plate is elastically restrained against translation at the outer edge of the plate at a radius of R from the center. The radius of the weakened circle because of the crack is considered as bR , where b is only a fraction of 1. Here, all lengths are normalized with respect to R , i.e., the radius of the outer region is 1 and the radius of the inner cracked region is b . Let the subscript I denote the outer region $b \leq r \leq 1$ and the subscript II denote the inner region $0 \leq r \leq b$. The general form of the lateral displacement of the vibration of a classical thin plate in polar coordinates can be expressed as $w = u(r) \cos(n\theta) e^{i\Omega t}$, where (r, θ) are polar coordinates, w is the transverse displacement, n is the number of modal diameters, t is time, and Ω is the frequency. The function $u(r)$ is a linear combination of the Bessel $J_n(kr)$, $Y_n(kr)$, $I_n(kr)$, $K_n(kr)$, and $k = R(\rho\Omega^2/D)^{1/4}$, where R is the plate radius, ρ is the density, D is the flexural rigidity, and k is the square root of the nondimensional frequency [2]. The general solutions for the two regions are

$$u_I(r) = C_1 J_n(kr) + C_2 Y_n(kr) + C_3 I_n(kr) + C_4 K_n(kr) \quad (1)$$

$$u_{II}(r) = C_5 J_n(kr) + C_6 I_n(kr) \quad (2)$$

where r designates the distance measured from the center of the plate whose maximum value is R . Considering an elastically restrained outer edge against translation, the boundary conditions at the outer regions of the circular plate are

$$M_r(r, \theta) = 0 \quad (3)$$

$$V_r(r, \theta) = -K_{T1} w_I(r, \theta) \quad (4)$$

where the bending moment and the Kelvin-Kirchhoff's shearing force are defined as

$$M_r(r, \theta) = -\frac{D}{R} \left[\frac{\partial^2 w_I(r, \theta)}{\partial r^2} + \nu \left(\frac{1}{r} \frac{\partial w_I(r, \theta)}{\partial r} + \frac{1}{r^2} \frac{\partial^2 w_I(r, \theta)}{\partial \theta^2} \right) \right] \quad (5)$$

$$V_r(r, \theta) = -\frac{D}{R^3} \left[\frac{\partial}{\partial r} \nabla^2 w_I(r, \theta) + (1 - \nu) \frac{1}{r} \frac{\partial}{\partial \theta} \left(\frac{1}{r} \frac{\partial^2 w_I(r, \theta)}{\partial r \partial \theta} - \frac{1}{r^2} \frac{\partial w_I(r, \theta)}{\partial \theta} \right) \right] \quad (6)$$

Equations (3)–(6) yield the following expressions

$$\left[\frac{\partial^2 w_I(r, \theta)}{\partial r^2} + \nu \left(\frac{1}{r} \frac{\partial w_I(r, \theta)}{\partial r} + \frac{1}{r^2} \frac{\partial^2 w_I(r, \theta)}{\partial \theta^2} \right) \right] = 0 \quad (7)$$

$$\left[\frac{\partial}{\partial r} \nabla^2 w_I(r, \theta) + (1 - \nu) \frac{1}{r} \frac{\partial}{\partial \theta} \left(\frac{1}{r} \frac{\partial^2 w_I(r, \theta)}{\partial r \partial \theta} - \frac{1}{r^2} \frac{\partial w_I(r, \theta)}{\partial \theta} \right) \right] = T_{11} w_I(r, \theta) \quad (8)$$

Equations (7) and (8) can be written as

$$u_I''(r) + \nu [u_I'(r) - n^2 u_I(r)] = 0 \quad (9)$$

$$u_I'''(r) + u_I''(r) - [1 + n^2(2 - \nu)] u_I'(r) + n^2(3 - \nu) u_I(r) = -T_{11} u_I(r) \quad (10)$$

where $T_{11} = K_{T1} R^3 / D$ are the normalized spring constant K_{T1} of the translational spring stiffness.

Except for the slope, the plate is continuous in terms of displacement, moment, and shear at $r = b$. The continuity conditions [8] at the interface of the two regions (i.e., at $r = b$) can be obtained as

$$u_I(b) = u_{II}(b) \quad (11)$$

$$b u_I''(b) + \nu u_I'(b) = b u_{II}''(b) + \nu u_{II}'(b) \quad (12)$$

$$b^2 u_I'''(b) - [1 + n^2(2 - \nu) + \nu] u_I'(b) = b^2 u_{II}'''(b) - [1 + n^2(2 - \nu) + \nu] u_{II}'(b) \quad (13)$$

$$b^2 u_{II}''(b) + \nu [b u_{II}'(b) - n^2 u_{II}(b)] = b^2 R_{22} [u_I'(b) - u_{II}'(b)] \quad (14)$$

where $R_{22} = K_{R2} R / D$ is the normalized spring constant and K_{R2} is the rotational spring stiffness, which is utilized for modeling the rotational restraint created by the circular crack at $r = b$. The non-trivial solutions to Eqs. (9)–(14) are sought. Equations (1), (2), and (9)–(14) yield the following equations

$$\left[\frac{k^2}{4} P_2 + \frac{k}{2} (\nu) P_1 - \left(\frac{k^2}{2} + \nu n^2 \right) J_n(k) \right] C_1 + \left[\frac{k^2}{4} Q_2 + \frac{k}{2} (\nu) Q_1 - \left(\frac{k^2}{2} + \nu n^2 \right) Y_n(k) \right] C_2 + \left[\frac{k^2}{4} R_2 + \frac{k}{2} (\nu) R_1 + \left(\frac{k^2}{2} - \nu n^2 \right) I_n(k) \right] C_3 - \left[\frac{k^2}{4} S_2 - \frac{k}{2} (\nu) S_1 + \left(\frac{k^2}{2} - \nu n^2 \right) K_n(k) \right] C_4 = 0 \quad (15)$$

$$\left[\frac{k^3}{8} P_3 + \frac{k^2}{4} P_2 - \frac{k}{2} \left(\frac{3}{4} k^2 + n^2(2 - \nu) + 1 \right) P_1 + \left(n^2(3 - \nu) - \frac{k^2}{2} - T_{11} \right) J_n(k) \right] C_1 + \left[\frac{k^3}{8} Q_3 + \frac{k^2}{4} Q_2 - \frac{k}{2} \left(\frac{3}{4} k^2 + n^2(2 - \nu) + 1 \right) Q_1 + \left(n^2(3 - \nu) - \frac{k^2}{2} - T_{11} \right) Y_n(k) \right] C_2 + \left[\frac{k^3}{8} R_3 + \frac{k^2}{4} R_2 + \frac{k}{2} \left(\frac{3}{4} k^2 - n^2(2 - \nu) + 1 \right) R_1 + \left(n^2(3 - \nu) + \frac{k^2}{2} - T_{11} \right) I_n(k) \right] C_3 + \left[-\frac{k^3}{8} S_3 + \frac{k^2}{4} S_2 + \frac{k}{2} \left(-\frac{3}{4} k^2 + n^2(2 - \nu) + 1 \right) S_1 + \left(n^2(3 - \nu) + \frac{k^2}{2} - T_{11} \right) K_n(k) \right] C_4 = 0 \quad (16)$$

$$J_n(kb) C_1 + Y_n(kb) C_2 + I_n(kb) C_3 + K_n(kb) C_4 - J_n(kb) C_5 - I_n(kb) C_6 = 0 \quad (17)$$

$$\left[\frac{b k^2}{4} P_2' + \frac{\nu k}{2} P_1' - \frac{b k^2}{2} J_n(kb) \right] C_1 + \left[\frac{b k^2}{4} Q_2' + \frac{\nu k}{2} Q_1' - \frac{b k^2}{2} Y_n(kb) \right] C_2 + \left[\frac{b k^2}{4} R_2' + \frac{\nu k}{2} R_1' + \frac{b k^2}{2} I_n(kb) \right] C_3 + \left[\frac{b k^2}{4} S_2' - \frac{\nu k}{2} S_1' + \frac{b k^2}{2} K_n(kb) \right] C_4 - \left[\frac{b k^2}{4} P_2' + \frac{\nu k}{2} P_1' - \frac{b k^2}{2} J_n(kb) \right] C_5 - \left[\frac{b k^2}{4} R_2' + \frac{\nu k}{2} R_1' + \frac{b k^2}{2} I_n(kb) \right] C_6 = 0 \quad (18)$$

$$\left[\frac{b^2 k^3}{8} P_3' - \frac{k}{2} \left(\frac{3 b^2 k^2}{4} + (1 + n^2(2 - \nu) + \nu) \right) P_1' \right] C_1 + \left[\frac{b^2 k^3}{8} Q_3' - \frac{k}{2} \left(\frac{3 b^2 k^2}{4} + (1 + n^2(2 - \nu) + \nu) \right) Q_1' \right] C_2 + \left[\frac{b^2 k^3}{8} R_3' + \frac{k}{2} \left(\frac{3 b^2 k^2}{4} - (1 + n^2(2 - \nu) + \nu) \right) R_1' \right] C_3 + \left[-\frac{b^2 k^3}{8} S_3' + \frac{k}{2} \left(-\frac{3 b^2 k^2}{4} + (1 + n^2(2 - \nu) + \nu) \right) S_1' \right] C_4 + \left[\frac{b^2 k^3}{8} P_3' + \frac{k}{2} \left(\frac{3 b^2 k^2}{4} + (1 + n^2(2 - \nu) + \nu) \right) P_1' \right] C_5 + \left[-\frac{b^2 k^3}{8} R_3' + \frac{k}{2} \left(-\frac{3 b^2 k^2}{4} + (1 + n^2(2 - \nu) + \nu) \right) R_1' \right] C_6 = 0 \quad (19)$$

$$\begin{aligned} & \left[\frac{b^2 k R_{22}}{2} P'_1 \right] C_1 + \left[\frac{b^2 k R_{22}}{2} Q'_1 \right] C_2 + \left[\frac{b^2 k R_{22}}{2} R'_1 \right] C_3 - \left[\frac{b^2 k R_{22}}{2} S'_1 \right] C_4 \\ & - \left[\frac{b^2 k^2}{4} P'_2 + \frac{k b}{2} (\nu + b R_{22}) P'_1 - \left(\frac{b^2 k^2}{2} + n^2 \right) J_n(k b) \right] C_5 \\ & - \left[\frac{b^2 k^2}{4} R'_2 + \frac{k b}{2} (\nu + b R_{22}) R'_1 + \left(\frac{b^2 k^2}{2} - n^2 \right) I_n(k b) \right] C_6 = 0 \end{aligned} \quad (20)$$

where

$$\begin{aligned} P_1 &= J_{n-1}(k) - J_{n+1}(k); & P_2 &= J_{n-2}(k) + J_{n+2}(k); \\ P_3 &= J_{n-3}(k) - J_{n+3}(k) \\ Q_1 &= Y_{n-1}(k) - Y_{n+1}(k); & Q_2 &= Y_{n-2}(k) + Y_{n+2}(k); \\ Q_3 &= Y_{n-3}(k) - Y_{n+3}(k) \\ R_1 &= I_{n-1}(k) + I_{n+1}(k); & R_2 &= I_{n-2}(k) + I_{n+2}(k); \\ R_3 &= I_{n-3}(k) + I_{n+3}(k) \\ S_1 &= K_{n-1}(k) + K_{n+1}(k); & S_2 &= K_{n-2}(k) + K_{n+2}(k); \\ K_3 &= K_{n-3}(k) + K_{n+3}(k) \\ P'_1 &= J_{n-1}(k b) - J_{n+1}(k b); & P'_2 &= J_{n-2}(k b) + J_{n+2}(k b); \\ P'_3 &= J_{n-3}(k b) - J_{n+3}(k b) \\ Q'_1 &= Y_{n-1}(k b) - Y_{n+1}(k b); & Q'_2 &= Y_{n-2}(k b) + Y_{n+2}(k b); \\ Q'_3 &= Y_{n-3}(k b) - Y_{n+3}(k b) \\ R'_1 &= I_{n-1}(k b) + I_{n+1}(k b); & R'_2 &= I_{n-2}(k b) + I_{n+2}(k b); \\ R'_3 &= I_{n-3}(k b) + I_{n+3}(k b) \\ S'_1 &= K_{n-1}(k b) + K_{n+1}(k b); & S'_2 &= K_{n-2}(k b) + K_{n+2}(k b); \\ S'_3 &= K_{n-3}(k b) + K_{n+3}(k b) \end{aligned}$$

4 Solution

For the given values of n , ν , T_{11} , R_{22} , and b , the preceding set of equations gives an exact characteristic equation for nontrivial solutions of the coefficients C_1 , C_2 , C_3 , C_4 , C_5 , and C_6 . For a nontrivial solution, the determinant of $[C]_{6 \times 6}$ must be factored out. The value of k is calculated from the characteristic equation by a simple root search. Using Mathematica, computer software with symbolic capabilities, solves this problem.

5 Results and Discussion

The code developed in Mathematica is used to determine the fundamental frequency for any range of translational and rotational restraints. Since Poisson's ratio occurs as a parameter in most of the equations, the effect of this ratio on the roots of the equations is also considered. The findings are presented in both

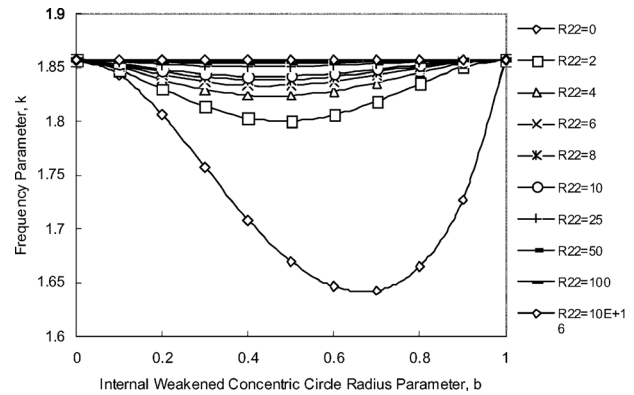


Fig. 2 The fundamental frequency parameter k versus the internal concentric weakened radius parameter b for various values of R_{22} and $T_{11} = 10$ [$\nu = 0.3$ and $n = 0$]

tabular and graphical form. The Poisson's ratio used in these calculations is 0.3.

The frequency values for various values of R_{22} , keeping T_{11} constant [$T_{11} = 10$], are tabulated. The first frequencies [k] of $n \leq 5$ modes with $R_{22} = 0, 2, 4, 6, 8, 10, 25, 50$, and 10^{16} and $T_{11} = 10$ are computed. For $b = 1$ and $R_{22} = 0$, the frequencies of the plate are the same as that of the plate without the weakening. For a given value of b and ν , the first frequency of the $n = 0$ mode converges to that of the plate without the weakening as R_{22} increases from 0. When $\nu = 0.3$, the first six frequencies of the plate without the weakening are 1.85759 [$n = 0$], 2.31479 [$n = 2$], 3.52684 [$n = 3$], 4.52488 [$n = 1$], 4.67279 [$n = 4$], and 5.7874 [$n = 5$]. It is observed that the fundamental frequency of the plate weakened along an internal concentric circle and resting on an elastically restrained edge against translation occurs at the $n = 0$ mode. The fundamental frequency of the plate varying with the radius of the weakened circle and the elastic rotational restraint of the hinge are shown in Fig. 2. The internal weakening decreases the fundamental frequency 1.85759, which is the fundamental frequency of the plate without the weakening, by less than 12% [11.57%]. The frequency decreases with R_{22} , and is lowest when $R_{22} = 0$ or when there is a frictionless circular hinge. For a given value of R_{22} , the frequency k decreases from 1.85759 to 1.64266 and again increases to 1.85759 as the radius b of the weakened circle varies from 0 to 1. The first frequencies k for higher modes ($n = 1$, $n = 3$, and $n = 5$) are presented in Tables 1–3.

The frequency values for various T_{11} by keeping R_{22} constant [$R_{22} = 10$] are computed. The first frequencies [k] of the $n \leq 5$ modes with $T_{11} = 0, 2, 4, 6, 8, 10, 25, 50$, and 10^{16} and $R_{22} = 10$ are computed. For $b = 1$ and $R_{22} = 0$, the frequency of the plate is the same as that of the plate without weakening. When $\nu = 0.3$, the first six frequencies of the plate without the

Table 1 The first frequency parameter k [$n = 1$ mode], for different R_{22} and the internal concentric weakened radius parameter b , $T_{11} = 10$, and $\nu = 0.3$

b	$R_{22} = 0$	$R_{22} = 2$	$R_{22} = 4$	$R_{22} = 6$	$R_{22} = 8$	$R_{22} = 10$	$R_{22} = 25$	$R_{22} = 50$	$R_{22} = 100$	$R_{22} = 10^{16}$
0	2.44	2.44	2.44	2.44	2.44	2.44	2.44	2.44	2.44	2.44
0.1	2.42983	2.43393	2.43572	2.43663	2.43723	2.43772	2.9279	3.24723	3.4657	3.71354
0.2	4.45878	1.66922	1.97279	2.1697	2.31693	2.43442	2.92111	3.23535	3.44813	3.68699
0.3	4.40239	1.66792	1.97089	2.1671	2.31373	2.43063	2.91212	3.21898	3.4238	3.65049
0.4	4.36099	1.66673	1.96899	2.16451	2.31044	2.42654	2.90225	3.20134	3.39838	3.6145
0.5	4.3567	1.66583	1.9675	2.16241	2.30764	2.42315	2.89427	3.18809	3.38085	3.59266
0.6	4.39391	1.66543	1.9668	2.16142	2.30635	2.42155	2.89129	3.1848	3.37856	3.59435
0.7	4.45577	1.66583	1.9674	2.16222	2.30735	2.42286	2.89549	3.19429	3.39471	3.62187
0.8	4.50687	1.66703	1.9694	2.16502	2.31105	2.42745	2.90696	3.21523	3.42552	3.66733
0.9	4.52437	1.66912	1.97269	2.1695	2.31664	2.43423	2.92212	3.24005	3.45902	3.71053
1	4.52488	1.67172	1.97609	2.1737	2.32172	2.43992	2.9322	3.25412	3.47558	3.72801

Table 2 The first frequency parameter k [$n = 3$ mode], for different R_{22} and the internal concentric weakened radius parameter b , $T_{11} = 10$, and $\nu = 0.3$

b	$R_{22} = 0$	$R_{22} = 2$	$R_{22} = 4$	$R_{22} = 6$	$R_{22} = 8$	$R_{22} = 10$	$R_{22} = 25$	$R_{22} = 50$	$R_{22} = 100$	$R_{22} = 10^{16}$
0	3.84103	3.84103	3.84103	3.84103	3.84103	3.84103	3.84103	3.84103	3.84103	3.84103
0.1	3.52693	3.59781	3.66418	3.72657	3.78546	3.84106	4.1844	4.58121	5.06797	6.32144
0.2	3.52743	3.5983	3.66468	3.72707	3.78586	3.84156	4.1849	4.58171	5.06867	6.32373
0.3	3.52893	3.5998	3.66608	3.72846	3.78726	3.84295	4.1862	4.5831	5.07025	6.32509
0.4	3.53152	3.60229	3.66857	3.73086	3.78955	3.84514	4.18799	4.58428	5.07003	6.3036
0.5	3.53451	3.60498	3.67096	3.73295	3.79144	3.84683	4.18807	4.58157	5.06112	6.23237
0.6	3.5355	3.60548	3.67095	3.73244	3.79043	3.84533	4.18297	4.57058	5.03796	6.13414
0.7	3.53241	3.60159	3.66627	3.72705	3.78435	3.83864	4.1717	4.55233	5.00775	6.07717
0.8	3.52533	3.594	3.65819	3.71857	3.77547	3.82927	4.15994	4.53828	4.99291	6.11732
0.9	3.51984	3.58892	3.6536	3.71439	3.77178	3.82608	4.16045	4.54598	5.01628	6.24422
1	3.52684	3.59781	3.66418	3.72657	3.78536	3.84106	4.18431	4.58111	5.06787	6.32115

Table 3 The first frequency parameter k [$n = 5$ mode], for different R_{22} and the internal concentric weakened radius parameter b , $T_{11} = 10$, and $\nu = 0.3$

b	$R_{22} = 0$	$R_{22} = 2$	$R_{22} = 4$	$R_{22} = 6$	$R_{22} = 8$	$R_{22} = 10$	$R_{22} = 25$	$R_{22} = 50$	$R_{22} = 100$	$R_{22} = 10^{16}$
0	5.88972	5.88972	5.88972	5.88972	5.88972	5.88972	5.88972	5.88972	5.88972	5.88979
0.1	5.7874	5.80846	5.82923	5.8497	5.86987	5.88974	6.03071	6.23828	6.57691	8.7294
0.2	5.7874	5.80846	5.82923	5.8497	5.86986	5.88973	6.03071	6.23828	6.57691	8.72949
0.3	5.78749	5.80856	5.82933	5.84979	5.86996	5.88983	6.03081	6.23837	6.5771	8.73067
0.4	5.78819	5.80925	5.83002	5.85049	5.87066	5.89053	6.0316	6.23916	6.57799	8.73282
0.5	5.79047	5.81154	5.83221	5.85268	5.87285	5.89281	6.03369	6.24125	6.57987	8.7097
0.6	5.79366	5.81462	5.83529	5.85565	5.87572	5.89549	6.03577	6.24212	6.57814	8.60155
0.7	5.79175	5.81232	5.83268	5.85275	5.87252	5.89199	6.02986	6.23223	6.55996	8.44264
0.8	5.77578	5.79595	5.81572	5.83529	5.85456	5.87353	6.00781	6.20449	6.52206	8.39009
0.9	5.75623	5.7762	5.79597	5.81534	5.83451	5.85348	5.98727	6.18406	6.50382	8.56007
1	5.7874	5.80846	5.82923	5.8497	5.86987	5.88973	6.03071	6.23828	6.57691	8.7294

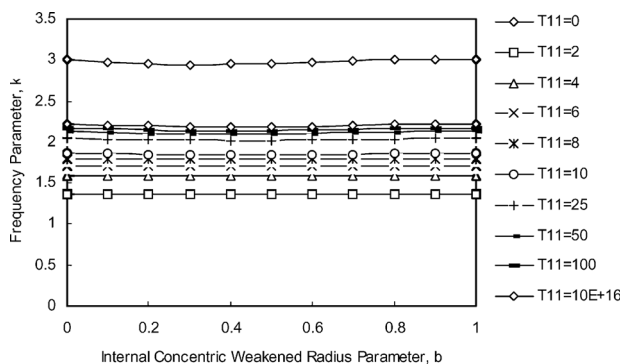


Fig. 3 The fundamental frequency parameter k versus the internal concentric weakened radius parameter b for various values of T_{11} and $R_{22} = 10$ [$\nu = 0.3$ and $n = 0$]

weakening are 2.31479 [$n = 2$], 3.00049 [$n = 0$], 3.52684 [$n = 3$], 4.52488 [$n = 1$], 4.67279 [$n = 4$], and 5.7874 [$n = 5$]. The fundamental frequency of the plate varying with the radius of the weakened circle and the elastic rotational restraint of the hinge are shown in Fig. 3, corresponding to the $n = 0$ mode. It is observed that the fundamental frequency corresponds to $T_{11} = 2$. The first frequencies k of the $n \leq 5$ modes with different T_{11} are shown in Tables 4–5. The frequency values k for higher modes ($n = 1$ and $n = 2$) are presented in Tables 4–5.

The frequency values for various R_{22} and T_{11} are determined. For $b = 1$ and $R_{22} = 0$, the frequency of the plate is same as that of the plate without the weakening. The first frequencies [k] of the $n \leq 5$ modes with $R_{22} = T_{11} = 0, 2, 4, 6, 8, 10, 25, 50$, and 10^{16} are shown in Figs. 4–6. When $\nu = 0.3$, the first six frequencies of the plate without the weakening are 2.24932 [$n = 2$], 3.00049 [$n = 0$], 3.37051 [$n = 3$], 4.43268 [$n = 4$], 4.49574 [$n = 1$], and 5.47116 [$n = 5$]. The fundamental frequency of the plate varying with the radius of the weakened circle and the elastic rotational restraint of the hinge are shown in Figs. 4–6,

Table 4 The first frequency parameter k [$n = 1$ mode], for different T_{11} and the internal concentric weakened radius parameter b , $R_{22} = 10$, and $\nu = 0.3$

b	$T_{11} = 0$	$T_{11} = 2$	$T_{11} = 4$	$T_{11} = 6$	$T_{11} = 8$	$T_{11} = 10$	$T_{11} = 25$	$T_{11} = 50$	$T_{11} = 100$	$T_{11} = 10^{16}$
0	0.115234	1.67178	1.97615	2.17378	2.32169	2.44	2.93215	3.25411	3.47565	3.72798
0.1	4.5029	1.67062	1.97469	2.172	2.31963	2.43772	2.9279	3.24723	3.4657	3.71354
0.2	4.45878	1.66922	1.97279	2.1697	2.31693	2.43442	2.92111	3.23535	3.44813	3.68699
0.3	4.40239	1.66792	1.97089	2.1671	2.31373	2.43063	2.91212	3.21898	3.4238	3.65049
0.4	4.36099	1.66673	1.96899	2.16451	2.31044	2.42654	2.90225	3.20134	3.39838	3.6145
0.5	4.3567	1.66583	1.9675	2.16241	2.30764	2.42315	2.89427	3.18809	3.38085	3.59266
0.6	4.39391	1.66543	1.9668	2.16142	2.30635	2.42155	2.89129	3.1848	3.37856	3.59435
0.7	4.45577	1.66583	1.9674	2.16222	2.30735	2.42286	2.89549	3.19429	3.39471	3.62187
0.8	4.50687	1.66703	1.9694	2.16502	2.31105	2.42745	2.90696	3.21523	3.42552	3.66733
0.9	4.52437	1.66912	1.97269	2.1695	2.31664	2.43423	2.92212	3.24005	3.45902	3.71053
1	4.52488	1.67172	1.97609	2.1737	2.32172	2.43992	2.9322	3.25412	3.47558	3.72801

Table 5 The first frequency parameter k [$n = 2$ mode], for different T_{11} and the internal concentric weakened radius parameter b , $R_{22} = 10$, and $\nu = 0.3$

b	$T_{11} = 0$	$T_{11} = 2$	$T_{11} = 4$	$T_{11} = 6$	$T_{11} = 8$	$T_{11} = 10$	$T_{11} = 25$	$T_{11} = 50$	$T_{11} = 100$	$T_{11} = 10^{16}$
0	2.31478	2.50429	2.65599	2.78312	2.8929	2.98959	3.4871	3.93604	4.36699	5.06089
0.1	2.31679	2.50601	2.6575	2.78453	2.89421	2.9909	3.48831	3.93745	4.3689	5.06459
0.2	2.31978	2.5085	2.65969	2.78653	2.8961	2.9927	3.4899	3.93894	4.37048	5.06587
0.3	2.32248	2.51069	2.66149	2.78813	2.8975	2.99399	3.49019	3.93793	4.36667	5.04858
0.4	2.32447	2.51199	2.66228	2.78852	2.89749	2.99359	3.48749	3.93103	4.35098	4.9988
0.5	2.32487	2.51159	2.66128	2.78682	2.89529	2.99089	3.4806	3.91675	4.32295	4.92929
0.6	2.32347	2.50929	2.65829	2.78313	2.8909	2.9858	3.47062	3.8988	4.29285	4.87674
0.7	2.32028	2.5056	2.6539	2.77834	2.88561	2.98001	3.46165	3.88625	4.27771	4.87383
0.8	2.31639	2.50181	2.65031	2.77475	2.88223	2.97673	3.45996	3.88876	4.29069	4.93135
0.9	2.3137	2.50052	2.65021	2.77565	2.88403	2.97953	3.46975	3.91002	4.33079	5.01845
1	2.31479	2.50431	2.6559	2.78304	2.89291	2.98961	3.48711	3.93606	4.367	5.0609

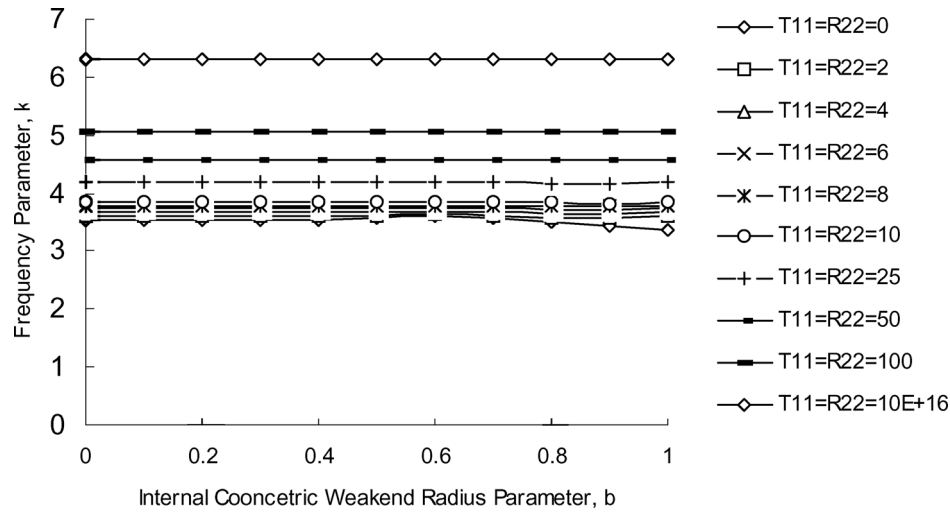


Fig. 4 The fundamental frequency parameter k versus the internal concentric weakened radius parameter b for various values of T_{11} and R_{22} [$\nu = 0.3$ and $n = 3$]

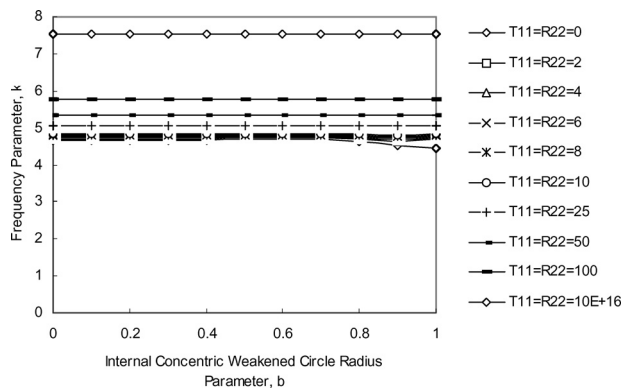


Fig. 5 The fundamental frequency parameter k versus the internal concentric weakened radius parameter b for various values of T_{11} and R_{22} [$\nu = 0.3$ and $n = 4$]

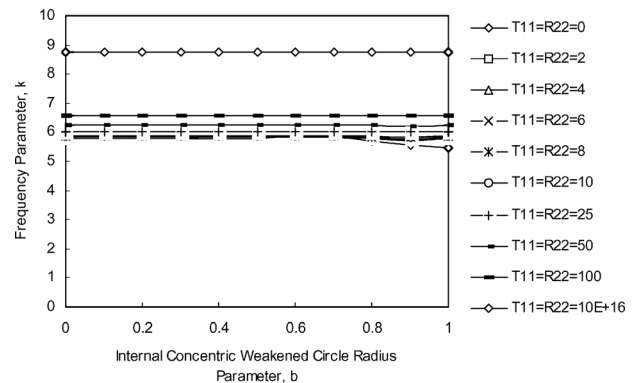


Fig. 6 The fundamental frequency parameter k versus the internal concentric weakened radius parameter b for various values of T_{11} and R_{22} [$\nu = 0.3$ and $n = 5$]

corresponding to the $n = 3$, $n = 4$, and $n = 5$ modes. The fundamental frequency corresponds to $R_{22} = T_{11} = 0$, as shown in Figs. 4–6. Results of this kind were scarce in the literature. However, the results are compared with the simply supported plate [27] and the free plate [28] by setting the translational restraint with $T_{11} \rightarrow \infty$ and $T_{11} \rightarrow 0$, respectively. The internal weakening decreases the fundamental frequency by less than 1% when b is near 0 or 1 for the simply supported plate [27] and less than 1% for the free plate [28].

6 Conclusions

The frequencies of a circular plate varying with the values of an elastic translational restraint T_{11} , the radius of the weakened circle, and the elastic rotational restraint of the hinge are determined. The internal weakening decreases the fundamental frequency by less than 12% [11.57%] for a circular plate with an elastically restrained outer edge against translation. Additionally, the frequencies are given for various values of an elastic translational restraint T_{11} at the edges that simulate the translational

restraints, where $T_{11} \rightarrow \infty$ represents a simply supported edge and $T_{11} \rightarrow 0$ represents a free edge. In this paper, the characteristic equations are exact; therefore, the results can be calculated to any accuracy. These exact solutions can be used to check the numerical or approximate results. A comparison of studies demonstrates the accuracy and stability of the present work. The tabulated results are useful to designers in the design of the plate with an internal weakened circle, such as doors and hatches (used in airplanes or spaceships), in vibration control, and structural design.

Nomenclature

- b = nondimensional radius of concentric ring support
- D = flexural rigidity of a material
- E = Young's modulus of a material
- h = thickness of a plate
- k = nondimensional frequency parameter
- K_{T1} = translational spring stiffness at the outer edge
- K_{R2} = rotational spring stiffness at the crack
- R = radius of a plate
- R_{22} = nondimensional rotational spring parameter at the crack
- T_{11} = nondimensional translational spring parameter at the outer edge
- $w(r, \theta)$ = transverse deflection of the plate
- ν = Poisson's ratio

References

- [1] Timoshenko, S., and Woinowsky-Krieger, S., 1959, *Theory of Plates and Shells*, McGraw-Hill, New York.
- [2] Leissa, A. W., 1969, *Vibration of Plates*, NASA SP-160, Office of Technology Utilization, Washington, D.C.
- [3] Szilard, R., 1974, *Theory and Analysis of Plates*, Prentice-Hall, New Jersey.
- [4] Azimi, S., 1988, "Free Vibrations of Circular Plates With Elastic or Rigid Interior Support," *J. Sound Vib.*, **120**, pp. 37–52.
- [5] Weisensel, G. N., 1989, "Natural Frequency Information for Circular and Annular Plates," *J. Sound Vib.*, **133**(1), pp. 129–137.
- [6] Ding, Z., 1994, "Free Vibration of Arbitrarily Shaped Plates With Concentric Ring Elastic and/or Rigid Supports," *Comput. Struct.*, **50**(5), pp. 685–692.
- [7] Wang, C. Y., and Wang, C. M., 2003, "Fundamental Frequencies of Circular Plates With Internal Elastic Ring Support," *J. Sound Vib.*, **263**(5), pp. 1071–1078.
- [8] Dimarogonas, A. D., 1996, "Vibration of Cracked Structures: A State of the Art Review," *Eng. Fract. Mech.*, **55**(5), pp. 831–857.
- [9] Lynn, P. P., and Kumbasar, N., 1967, "Free Vibrations of Thin Rectangular Plates Having Narrow Cracks With Simply Supported Edges," *Dev. Mech.*, **4**, pp. 911–928.
- [10] Petyt, M., 1968, "The Vibration Characteristics of a Tensioned Plate Containing a Fatigue Crack," *J. Sound Vib.*, **8**(3), pp. 377–389.
- [11] Stahl, B., and Keer, L. M., 1972, "Vibration and Stability of Cracked Rectangular Plates," *Int. J. Solids Struct.*, **8**(1), pp. 69–91.
- [12] Hirano, Y., and Okazaki, K., 1980, "Vibration of Cracked Rectangular-Plates," *Bull. JSME*, **23**, pp. 732–740.
- [13] Solecki, R., 1983, "Bending Vibration of a Simply Supported Rectangular Plate With a Crack Parallel to One Edge," *Eng. Fract. Mech.*, **18**(6), pp. 1111–1118.
- [14] Yuan, J., and Dickinson, S. M., 1992, "The Flexural Vibration of Rectangular Plate Systems Approached by Using Artificial Springs in the Rayleigh-Ritz Method," *J. Sound Vib.*, **159**(1), pp. 39–55.
- [15] Liew, K. M., Hung, K. C., and Lim, M. K., 1994, "A Solution Method for Analysis of Cracked Plates Under Vibration," *Eng. Fract. Mech.*, **48**(3), pp. 393–404.
- [16] Ma, C. C., and Huang, C. H., 2001, "Experimental and Numerical Analysis of Vibrating Cracked Plates at Resonant Frequencies," *Exp. Mech.*, **41**(1), pp. 8–18.
- [17] Qian, G. L., Gu, S. N., and Jiang, J. S., 1991, "A Finite Element Model of Cracked Plates and Applications to Vibration Problems," *Comput. Struct.*, **39**, pp. 483–487.
- [18] Lee, H. P., and Lim, S. P., "Vibration of Cracked Rectangular Plates Including Transverse Shear Deformation and Rotary Inertia," *Comput. Struct.*, **49**, pp. 715–718.
- [19] Krawczuk, M., 1993, "Natural Vibrations of Rectangular Plates With a Through Crack," *Arch. Appl. Mech.*, **63**, pp. 491–504.
- [20] Liew, K. M., Hung, K. C., and Lim, M. K., 1994, "A Solution Method for Analysis of Cracked Plates Under Vibration," *Eng. Fract. Mech.*, **48**, pp. 393–404.
- [21] Khadem, S. E., and Rezaee, M., 2000, "An Analytical Approach for Obtaining the Location and Depth of an All-Over Part-Through Crack on Externally In-Plane Loaded Rectangular Plate Using Vibration Analysis," *J. Sound Vib.*, **230**, pp. 291–308.
- [22] Krawczuk, M., Zak, A., and Ostachowicz, W., 2001, "Finite Element Model of Plate With Elasto-Plastic Through Crack," *Comput. Struct.*, **79**, pp. 519–532.
- [23] Lee, P., 1992, "Fundamental Frequencies of Annular Plates With Internal Cracks," *Comput. Struct.*, **43**, pp. 1085–1089.
- [24] Ramesh, K., Chauhan, D. P. S., and Mallik, A. K., 1997, "Free Vibration of an Annular Plate With Periodic Radial Cracks," *J. Sound Vib.*, **206**, pp. 266–274.
- [25] Anifantis, N. K., Actis, R. L., and Dimarogonas, A. D., 1994, "Vibration of Cracked Annular Plates," *Eng. Fract. Mech.*, **49**, pp. 371–379.
- [26] Yuan, J., Young, P. G., and Dickinson, S. M., 1994, "Natural Frequencies of Circular and Annular Plates With Radial or Circumferential Cracks," *Comput. Struct.*, **53**, pp. 327–334.
- [27] Wang, C. Y., 2002, "Fundamental Frequency of a Circular Plate Weakened Along a Concentric Circle," *Z. Angew. Math. Mech.*, **82**(1), pp. 70–72.
- [28] Yu, L. H., 2009, "Frequencies of Circular Plate Weakened Along an Internal Concentric Circle," *Int. J. Struct. Stab. Dyn.*, **9**(1), pp. 179–185.
- [29] Kim, C. S., and Dickinson, S. M., 1990, "The Flexural Vibration of the Isotropic and Polar Orthotropic Annular and Circular Plates With Elastically Restrained Peripheries," *J. Sound Vib.*, **143**(1), pp. 171–179.
- [30] Wang, C. Y., and Wang, C. M., 2001, "Buckling of Circular Plates With an Internal Ring Support and Elastically Restrained Edges," *Thin-Walled Struct.*, **39**(5), pp. 821–825.

Lokavarapu Bhaskara Rao, Chellapilla Kameswara Rao

Fundamental buckling of circular plates with elastically restrained edges and resting on concentric rigid ring support

© Higher Education Press and Springer-Verlag Berlin Heidelberg 2013

Abstract This work presents the existence of buckling mode switching with respect to the radius of concentric rigid ring support. The buckling mode may not be axisymmetric as previously assumed. In general, the plate may buckle in an axisymmetric mode but when the radius of the ring support becomes small, the plate may buckle in an asymmetric mode. The optimum radius of the concentric rigid ring support for maximum buckling load is also determined. Introducing internal rigid ring support, when placed at an optimal position increases the elastic buckling load capacity by 149.39 percent. The numerical results obtained are in good agreement with the previously published data.

Keywords buckling, circular plate, elastically restrained edge, rigid ring support, mode switching

1 Introduction

Buckling of plates is an important topic in many mechanical, civil, marine and aircraft structures. Their buckling load capacities need to be determined in situations where in-plane compressive forces act on the plates. In fact, the first theoretical examination of buckling of plates was attributed to Bryan [1]. He presented the buckling analysis for rectangular plates under uniform uniaxial compression using the energy criterion of stability. It should be noted that he was not only

the first to analyze the stability of plates, but also the first to apply the energy criterion of stability to the buckling problem of plate. The first event that highlighted the importance of plate buckling was related to a series of tests carried out in the labs of University of London on box beams for Britannia Bridge in 1845 [2]. Many researchers [3–6] have studied the elastic axisymmetric buckling problems of circular and annular plates.

Exact analytical solutions are available for circular plates without internal concentric ring support [7,8]. In particular, circular plates with concentric ring supports find applications in aeronautical (instrument mounting bases for space vehicles), rocket launching pads, aircrafts and naval vessels (instrument mounting bases). Based on the Kirchhoff's theory, the elastic buckling of thin circular plates has been extensively studied by many authors after the pioneering work published by Bryan [1]. Since then, there have been extensive studies on the subject covering various aspects such as different materials, boundary and loading conditions. Also the buckling of circular plates was studied by different authors [9,10]. However, these sources only considered axisymmetric case, which may not lead to the correct buckling load. Introducing an internal ring support may increase the elastic buckling capacity of in-plane loaded circular plates significantly. Laura et al. [6] investigated the elastic buckling problem of the aforesaid type of circular plates, who modeled the plate using the classical thin plate theory. In their study only axisymmetric modes are considered. The assumption of axisymmetric buckling, however, does not necessarily lead to the desired lowest critical load. Therefore, the asymmetric buckling problems of circular and annular plates have also been studied [11–13].

Although the circular symmetry of the problem allows for its significant simplification, many difficulties very often arise due to complexity and uncertainty of boundary conditions. This uncertainty could be due to practical applications where the edge of the plate does not fall into the classical boundary conditions. It is an accepted fact that the condition on a periphery often tends to be in between

Received November 30, 2012; accepted March 16, 2013

Lokavarapu Bhaskara Rao (✉)
School of Mechanical and Building Sciences, VIT University, Vandalur-
Kelambakkam Road, Chennai 600127, Tamil Nadu, India
E-mail: bhaskarbabu_20@yahoo.com

Chellapilla Kameswara Rao (✉)
Department of Mechanical Engineering, Guru Nanak Institutions
Technical Campus, Ibrahimpatnam, Hyderabad 501506, A.P, India
E-mail: chellapilla95@gmail.com

the classical boundary conditions (free, clamped and simply supported) and may correspond more closely to some form of elastic restraints, i.e., translational and rotational restraints [14–17]. In a recent study, Wang and Wang [4] showed that when the ring support has a small radius, the buckling mode takes the asymmetric form. But they have studied only the circular plate with ring support and elastically restrained edge against rotation. Bhaskara Rao and Kameswara Rao [17] studied the buckling of circular plates with an internal elastic ring support and elastically restrained edges against translation and rotation. Wang and Wang [14] showed that the axisymmetric mode assumed by the previous authors might not yield the correct buckling load. In certain cases, an asymmetric mode would yield a lower buckling load. But they have studied only the circular plate with ring support and elastically restrained edge against rotation. The purpose of the present work is to complete the results of the buckling of circular plates with an internal rigid ring support and elastically restrained edges against translation and rotation by including the asymmetric modes, thus correctly determining the buckling loads.

2 Definition of the problem

Consider a thin circular plate of radius R , uniform thickness h , Young's modulus E and Poisson's ratio ν and subjected to a uniform in-plane load, N along its boundary, as shown in Fig. 1. The circular plate is also assumed to be made of linearly elastic, homogeneous and isotropic material. The edge of the circular plate is elastically restrained edge against rotation and translation and supported by an internal rigid ring support, as shown in Fig. 1. The problem here is to determine the elastic critical buckling load of a circular plate with concentric rigid ring support and elastically restrained edge against rotation and translation.

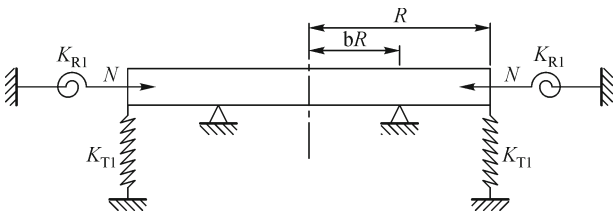


Fig. 1 Buckling of a circular plate with concentric rigid ring support and elastically restrained edge against rotation and translation

3 Formulation of the problem

The plate is elastically restrained against rotation and translation at the edge of radius, R and supported on an

internal rigid ring of smaller radius bR as shown in Fig. 1. Let subscript I denote the inner region $0 \leq \bar{r} \leq b$ and the subscript II denote the outer region $b \leq \bar{r} \leq 1$. Where r is the normalized radial distance with R . Here, all lengths are normalized by R . Using classical (Kirchhoff's) plate theory, the following fourth order differential equation for buckling in polar coordinates (r, θ) .

$$D\nabla^4 w + N\nabla^2 w = 0, \quad (1)$$

where w is the lateral displacement, N is the uniform compressive load at the edge. After normalizing the lengths by the radius of the plate R , Eq. (1) can be written as

$$D\nabla^4 \bar{w} + k^2 \nabla^2 \bar{w} = 0, \quad (2)$$

where $\nabla^2 = \frac{\partial^2}{\partial \bar{r}^2} + \frac{1}{\bar{r}} \frac{\partial}{\partial \bar{r}} + \frac{1}{\bar{r}^2} \frac{\partial^2}{\partial \theta^2}$ is the Laplace operator in the polar coordinates r and θ .

After normalization, the inner and outer radius parameters are b and 1 respectively. $\bar{D} = Eh^3/12(1-\nu^2)$ is the flexural rigidity, $\bar{w} = w/R$, is normalized transverse displacement of the plate. $k^2 = R^2 N/\bar{D}$ is non-dimensional load parameter. Suppose there are n nodal diameters. In polar coordinates (r, θ) set

$$\bar{w}(\bar{r}, \theta) = \bar{u}(\bar{r}) \cos(n\theta). \quad (3)$$

Considering the boundness at the origin, the general solution [16] for the two regions is

$$\begin{aligned} \bar{u}_I(r) = & C_1 J_n(k\bar{r}) + C_2 Y_n(k\bar{r}) + C_3 \bar{r}^n \\ & + C_4 \left\{ \frac{\log \bar{r}}{\bar{r}^{-n}} \right\}, \end{aligned} \quad (4)$$

$$\bar{u}_{II}(r) = C_5 J_n(k\bar{r}) + C_6 \bar{r}^n, \quad (5)$$

where top form of the Eq. (4) is used for $n = 0$ (Axisymmetric) and the bottom form is used for $n \neq 0$ (Asymmetric), C_1, C_2, C_3, C_4, C_5 & C_6 are constants, $J_n(\cdot)$ & $Y_n(\cdot)$ are the Bessel functions of the first and second kind of order, n , respectively. Substituting Eq. (4) into Eq. (3), gives the following

$$\begin{aligned} \bar{w}_I(\bar{r}, \theta) = & \left[C_1 J_n(k\bar{r}) + C_2 Y_n(k\bar{r}) + C_3 \bar{r}^n \right. \\ & \left. + C_4 \left\{ \frac{\log \bar{r}}{\bar{r}^{-n}} \right\} \right] \cos(n\theta), \end{aligned} \quad (6)$$

$$\bar{w}_{II}(\bar{r}, \theta) = [C_5 J_n(k\bar{r}) + C_6 \bar{r}^n] \cos(n\theta). \quad (7)$$

The boundary conditions at outer region of the circular plate in terms of rotational stiffness (K_{RI}) and translational stiffness (K_{TI}) are given by the following expressions

$$M_r(\bar{r}, \theta) = K_{RI} \frac{\partial \bar{w}_I(\bar{r}, \theta)}{\partial \bar{r}}, \quad (8)$$

$$V_r(\bar{r}, \theta) = -K_{T1} \bar{w}_I(\bar{r}, \theta). \quad (9)$$

From Eqs. (8) and (9) it can be easily seen that as K_{R1} and K_{T1} become equal to infinity, the slope and deflection become zero and hence corresponds to the case of a clamped end conditions. The translational spring stiffness K_{T1} becomes very important in simulating practical cases such as a guided end by making K_{R1} to be equal to infinity and K_{T1} equal to zero.

The radial moment and the radial Kirchhoff shear at outer edge are defined as follows

$$M_r(\bar{r}, \theta) = -\frac{D}{R^3} \left[\frac{\partial^2 \bar{w}_I(\bar{r}, \theta)}{\partial \bar{r}^2} + \nu \left(\frac{1}{\bar{r}} \frac{\partial \bar{w}_I(\bar{r}, \theta)}{\partial \bar{r}} + \frac{1}{\bar{r}^2} \frac{\partial^2 \bar{w}_I(\bar{r}, \theta)}{\partial \theta^2} \right) \right], \quad (10)$$

$$V_r(\bar{r}, \theta) = -\frac{D}{R^3} \left[\frac{\partial}{\partial \bar{r}} \nabla^2 \bar{w}_I(\bar{r}, \theta) + (1-\nu) \frac{1}{\bar{r}} \frac{\partial}{\partial \theta} \left(\frac{1}{\bar{r}} \frac{\partial \bar{w}_I(\bar{r}, \theta)}{\partial \bar{r}} - \frac{1}{\bar{r}^2} \frac{\partial \bar{w}_I(\bar{r}, \theta)}{\partial \theta} \right) \right]. \quad (11)$$

Equations (8) and (10) yield the following

$$\left[\frac{\partial^2 \bar{w}_I(\bar{r}, \theta)}{\partial \bar{r}^2} + \nu \left(\frac{1}{\bar{r}} \frac{\partial \bar{w}_I(\bar{r}, \theta)}{\partial \bar{r}} + \frac{1}{\bar{r}^2} \frac{\partial^2 \bar{w}_I(\bar{r}, \theta)}{\partial \theta^2} \right) \right] = -R_{11} \frac{\partial \bar{w}_I(\bar{r}, \theta)}{\partial \bar{r}}. \quad (12)$$

From Eqs. (9) and (11) we get the following

$$\left[\frac{\partial}{\partial \bar{r}} \nabla^2 \bar{w}_I(\bar{r}, \theta) + (1-\nu) \frac{1}{\bar{r}} \frac{\partial}{\partial \theta} \left(\frac{1}{\bar{r}} \frac{\partial \bar{w}_I(\bar{r}, \theta)}{\partial \bar{r}} - \frac{1}{\bar{r}^2} \frac{\partial \bar{w}_I(\bar{r}, \theta)}{\partial \theta} \right) \right] = T_{11} \bar{w}_I(\bar{r}, \theta), \quad (13)$$

where $R_{11} = \frac{K_{R1} R^2}{D}$ and $T_{11} = \frac{K_{T1} R^3}{D}$.

Apart from the elastically restrained edge against rotation and translation, there is an internal rigid ring support constraint and the continuity requirements of slope and curvature at the support, i.e., at $\bar{r} = b$

$$\bar{w}_I(b, \theta) = 0, \quad (14)$$

$$\bar{w}_{II}(b, \theta) = 0, \quad (15)$$

$$\bar{w}_I'(b, \theta) = \bar{w}_{II}'(b, \theta), \quad (16)$$

$$\bar{w}_I''(b, \theta) = \bar{w}_{II}''(b, \theta). \quad (17)$$

The non-trivial solutions to Eq. (12), (13), (14)–(17) are sought. The lowest value of k is the square root of the normalized buckling load. From Eqs. (4), (5), (12), (13)

and (14)–(17) yields the following equations.

$$\begin{aligned} & \left[\frac{k^2}{4} P_2 + \frac{k}{2} (\nu + R_{11}) P_1 - \left(\frac{k^2}{2} + \nu n^2 \right) J_n(k) \right] C_1 \\ & + \left[\frac{k^2}{4} Q_2 + \frac{k}{2} (\nu + R_{11}) Q_1 - \left(\frac{k^2}{2} + \nu n^2 \right) Y_n(k) \right] C_2 \\ & + [n((n-1)(1-\nu) + R_{11})] C_3 \\ & + \left\{ \frac{(\nu + R_{11}) - 1}{n((n+1)(1-\nu) - R_{11})} \right\} C_4 = 0, \end{aligned} \quad (18)$$

$$\begin{aligned} & \left[\frac{k^3}{8} P_3 + \frac{k^2}{4} P_2 - \frac{k}{2} \left(\frac{3}{4} k^2 + n^2(2-\nu) + 1 \right) P_1 \right. \\ & + \left. \left(n^2(3-\nu) - \frac{k^2}{2} - T_{11} \right) J_n(k) \right] C_1 \\ & + \left[\frac{k^3}{8} Q_3 + \frac{k^2}{4} Q_2 - \frac{k}{2} \left(\frac{3}{4} k^2 + n^2(2-\nu) + 1 \right) Q_1 \right. \\ & + \left. \left(n^2(3-\nu) - \frac{k^2}{2} - T_{11} \right) Y_n(k) \right] C_2 \\ & + [n^2(n-1)\nu - n^3 - T_{11}] C_3 \\ & - \left\{ \frac{n^2(2-\nu)}{-n^2(n+1)\nu + n^3 - T_{11}} \right\} C_4 = 0, \end{aligned} \quad (19)$$

where

$$P_1 = J_{n-1}(k) - J_{n+1}(k); P_2 = J_{n-2}(k) + J_{n+2}(k);$$

$$P_3 = J_{n-3}(k) - J_{n+3}(k); Q_1 = Y_{n-1}(k) - Y_{n+1}(k);$$

$$Q_2 = Y_{n-2}(k) + Y_{n+2}(k); Q_3 = Y_{n-3}(k) - Y_{n+3}(k);$$

$$J_n(kb)C_1 + Y_n(kb)C_2 + b^n C_3 + \left\{ \frac{\log b}{b^{-n}} \right\} C_4 = 0, \quad (20)$$

$$J_n(kb)C_5 + b^n C_6 = 0, \quad (21)$$

$$\begin{aligned} & \frac{k}{2} P_1' C_1 + \frac{k}{2} Q_1' C_2 + n b^{n-1} C_3 \\ & + \left\{ \frac{1}{b} \right\} C_4 - \frac{k}{2} P_1' C_5 - n b^{n-1} C_6 = 0, \end{aligned} \quad (22)$$

$$\begin{aligned} & \frac{k^2}{4} (P_2' - 2J_n(kb)) C_1 + \frac{k^2}{4} (Q_2' - 2Y_n(kb)) C_2 \\ & + n(n-1) b^{n-2} C_3 - \left\{ \frac{1}{b^2} \right\} C_4 \\ & - \frac{k^2}{4} (P_2' - 2J_n(kb)) C_5 - n(n-1) b^{n-2} C_6 = 0, \end{aligned} \quad (23)$$

where

$$P'_1 = J_{n-1}(kb) - J_{n+1}(kb); P'_2 = J_{n-2}(kb) + J_{n+2}(kb);$$

$$Q'_1 = Y_{n-1}(kb) - Y_{n+1}(kb); Q'_2 = Y_{n-2}(kb) + Y_{n+2}(kb);$$

The coefficient of C_4 has two values corresponding to region I in Eqs. (18)–(23). Therefore, the top form of Eqs. (18)–(23) corresponding to region, I is used for $n = 0$ (axisymmetric buckling) and the bottom form is used for $n \neq 0$ (asymmetric buckling). Therefore, the top form of Eqs. (18)–(23) are used for $n = 0$ (axisymmetric buckling) and the bottom form is used for $n \neq 0$ (asymmetric buckling).

4 Solution

For the given values of n, ν, R_{11}, T_{11} , and b the above set of equations, gives an exact characteristic equation for non-trivial solutions of the coefficients C_1, C_2, C_3, C_4, C_5 , and C_6 . Non-trivial solution, the determinant of $[C]_{6 \times 6}$ vanishes. The value of k , calculated from the characteristic equation by a simple root search method. Using Maple, computer software with symbolic capabilities, solves this problem. Here, all equations have been written in the format of the programming, which are compatible with the maple computer software.

5 Results and discussion

Poisson's ratio used in the calculations is 0.3. Buckling load parameters for axisymmetric and asymmetric modes and for various values of rotational and translational spring stiffness parameters are determined. Figures 2–5 show the variations of buckling load parameter k , with respect to the internal rigid ring support radius b , for various values of rotational and translational spring stiffness parameters. It is observed from Figs. 2–5, that for a given value of rotational and translational spring stiffness parameters, the curve is composed of two segments. This is due to the switching of buckling modes. For a smaller internal rigid ring support radius b , the plate buckles in an asymmetric mode (i.e., $n \neq 0$). In this segment (as shown by dotted lines in Figs. 2–5) the buckling load decreases as b decreases in value. For a larger internal rigid ring support radius b , the plate buckles in an axisymmetric mode (i.e., $n = 0$). In this segment (as shown by continuous lines in Figs. 2–5) the buckling load increases as b decreases up to a peak point corresponds to maximum buckling load and thereafter decreases as b decreases in value as shown in Figs. 2–5. The cross over radius i.e., mode switching for

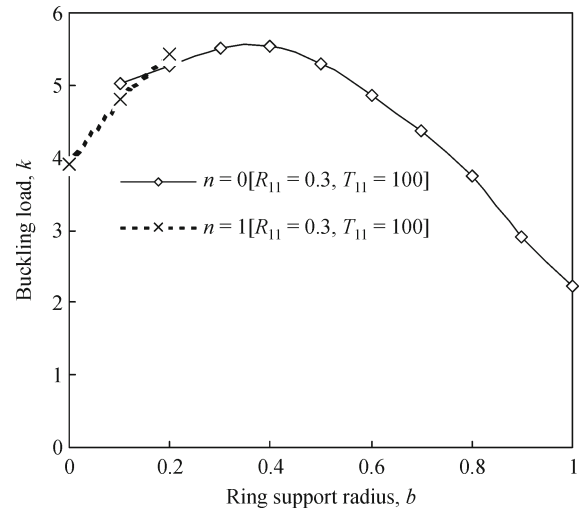


Fig. 2 Buckling load parameter k , versus internal rigid ring support radius b , for $R_{11} = 0.3$ and $T_{11} = 100$

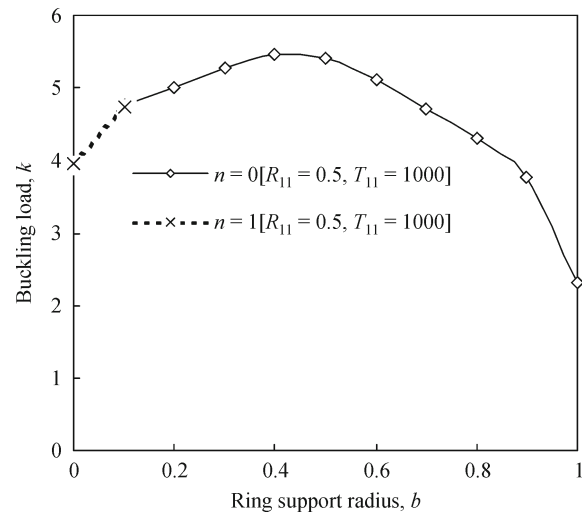


Fig. 3 Buckling load parameter k , versus internal rigid ring support radius b , for $R_{11} = 0.5$ and $T_{11} = 1000$

various values of rotational and translational spring stiffness parameters are presented in Table 1. Here, 10^{16} has been considered as infinity (∞). As $R_{11} & T_{11} \rightarrow \infty$, the edge of the plate becomes clamped and as $b \rightarrow 1$, buckling solution for axisymmetric case is 3.83163, which is in good agreement with that of Wang and Wang [14].

The optimum location of the ring support and the corresponding buckling load parameters for various rotational spring stiffness parameters ($R_{11} = 0.350$ & ∞)

Table 1 The Cross over radius (switching of buckling mode) of the rigid ring support for various values of rotational, R_{11} and translational stiffness, T_{11} parameters when $\nu = 0.3$

	$R_{11} = 0.3, T_{11} = 100$	$R_{11} = 0.5, T_{11} = 1000$	$R_{11} = 50, T_{11} = 1000$	$R_{11} = T_{11} = \infty$
b	0.1589	0.1102	0.1557	0.1523

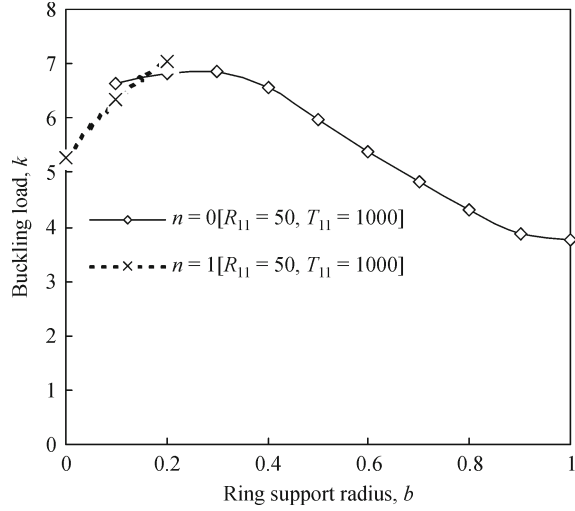


Fig. 4 Buckling load parameter k , versus internal rigid ring support radius b , for $R_{11} = 50$ and $T_{11} = 1000$

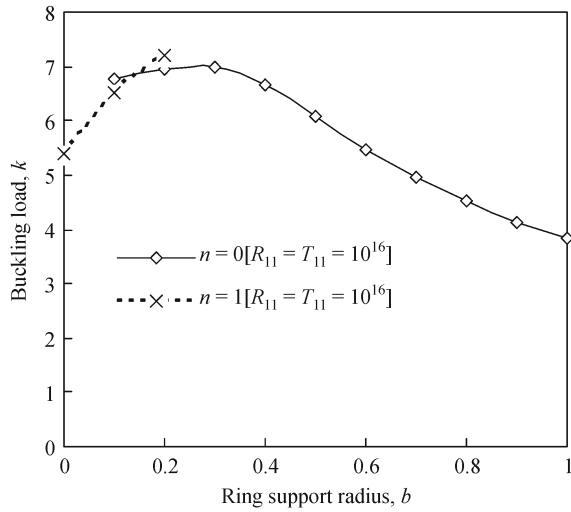


Fig. 5 Buckling load parameter k , versus internal rigid ring support radius b , for $R_{11} = T_{11} = 10^{16}$

and translational spring stiffness parameters ($T_{11} = 1001000$ & ∞) are presented in the Table 2. The

optimum location is the location of the ring support at which the buckling load parameter k becomes maximum. It is observed that the optimal rigid ring support radius parameter decrease with increase in rotational spring stiffness parameter and also the optimal buckling load capacity increases with rotational spring stiffness parameter. Introducing internal rigid ring support, when placed at an optimal position increases the elastic buckling capacity significantly, and the percentage of increase in buckling loads is presented in Table 2. The percentage increase in buckling load is calculated by comparing the buckling load parameter value obtained when the circular plate is having the ring support with that of circular plate without having the ring support. It is observed that the percentage increase in buckling load parameter decreases with increase in R_{11} . This is due to the amount of increase in buckling load without ring support with R_{11} is more than that of increase in buckling load with rigid ring support with R_{11} .

The results of this kind were scarce in the literature. However, the results are compared with the following cases. Table 3, presents the buckling load parameters k , for a circular plate with an internal rigid ring support and elastically restrained edge against rotation, against those obtained by Wang et al. [4], Laura et al. [6] and Wang et al. [18]. Reference [4] is considered because the plate can be considered as thin for $\tau = h/R = 0.001$. It shows that the present results are in good agreement. The buckling load parameters k , for clamped and simply supported edges are compared with those obtained by Wang et al. [4] and Wang et al. [18] as shown in Tables 3 and 4 respectively. The buckling load parameters for rotational stiffness parameter $R_{11} = \infty$ are shown in Table 5. Also the optimum location of the rigid ring support and the corresponding buckling load parameters for rotational spring stiffness parameter 0.3, 50 and ∞ are calculated by substituting $T_{11} = \infty$ and it is in good agreement with earlier results obtained by Wang [13].

6 Conclusions

The fundamental buckling of thin circular plates with an internal rigid ring support and elastically restrained edge against rotation and translation is presented in this paper. It

Table 2 Optimum location of the rigid ring support; the corresponding buckling load parameters and percentage increase in buckling load parameters

R_{11}	0.3	50	∞
T_{11}	100	1000	∞
b_{opt}	0.3211	0.27022	0.2600
k_{opt}	5.53449	6.87832	7.01485
age increase in buckling load/%	149.39	83.11	83.07

Table 3 Comparison of buckling load parameter k , with Laura et al. [6] and Wang et al. [18] for simply supported edge for rotational stiffness parameter $R_{11} = 0$ & $\nu = 0.3$

Rigid ring support radius, b	Wang et al. [4]	Laura et al. [6]	Wang et al. [18]	Present
0.1	—	4.5244	4.5235	4.52341
0.2	4.7703	4.7718	4.7702	4.77018
0.3	5.0711	5.0725	5.0710	5.07091
0.4	5.3297	5.3301	5.3296	5.32964
0.5	5.3667	5.3666	5.3666	5.36659
0.6	5.1264	5.1284	5.1261	5.12606
0.7	4.7730	4.7789	4.7727	4.77266
0.8	4.4219	4.4249	4.4215	4.42141
0.9	4.1069	4.1122	4.1063	4.10629

Table 4 Comparison of buckling load parameter k , with Wang et al. [4] and Wang et al. [18] for clamped edge for rotational stiffness parameter

Rigid ring support radius, b	Wang et al. [4]	Wang et al. [18]	Present
0.1	—	6.5009*	6.50095*
0.2	6.9559	6.9558	6.95582
0.3	6.9948	6.9947	6.99475
0.4	6.6627	6.6625	6.66248
0.5	6.0749	6.0745	6.07454
0.6	5.4760	5.4755	5.4755
0.7	4.9532	4.9526	4.95263
0.8	4.5134	4.5127	4.51266
0.9	4.1448	4.1436	4.14357
0.99	3.8667	3.8604	3.86061

* Asymmetric buckling load parameters

Table 5 Comparison of buckling load parameter k , with Laura et al. [6] for rotational stiffness parameter

Rigid ring support radius, b	Laura et al. [6]	Present
0.1	6.7720	6.50105
0.2	6.9649	6.95592
0.3	6.9964	6.99485
0.4	6.6693	6.66257
0.5	6.0852	6.07454
0.6	5.4845	5.47550
0.7	4.9588	4.95263
0.8	4.5277	4.51266
0.9	4.1509	4.14357

is observed that the buckling mode switches from asymmetric mode to *axisymmetric* mode at a particular rigid ring support radius. The cross over radius (switching of mode) is determined for different values of rotational and translational constraints. The optimal location of the

internal rigid ring support for maximum buckling load is also found. The optimal location of internal rigid ring support is affected by the rotational and translational stiffness parameters. Also, it is observed that for $T_{11} = 0$, the symmetric buckling mode is independent of the

internal elastic rigid ring support and gives a constant buckling load. The percentage of increase in buckling load capacity by introducing concentric rigid ring support, when it is placed at an optimal position is also determined. These exact solutions can be used to check numerical or approximate results.

Nomenclature

$w(r, \theta)$	Transverse deflection of the plate
h	Thickness of a plate
R	Radius of a plate
b	Non-dimensional radius of ring support
ν	Poisson's ratio
E	Young's modulus of a material
D	Flexural rigidity of a material
K_{R1}	Rotational spring stiffness
K_{T1}	Translational spring stiffness
T_{11}	Non-dimensional translational Flexibility parameter
R_{11}	Non-dimensional rotational Flexibility parameter
N	Uniform in-plane compressive load
k	Non-dimensional Buckling Load Parameter

References

1. Bryan G H. On the stability of a plane plate under thrust in its own plane with application to the buckling of the side of a ship. Proceedings of the London Mathematical Society, 1891, 22(1): 54–67
2. Walker A C. A Brief Review of Plate Buckling Research In Behaviour of Thin-Walled Structures, ed. by Rhodes J, Spence J, Elsevier: London, 1984, 375–397
3. Raju K K, Rao G V. Stability of moderately thick annular plates subjected to a uniform radial compressive load at the outer edge. Computers & Structures, 1989, 33(2): 477–482
4. Wang C M, Xiang Y, Kitipornchai S, Liew K M. Axisymmetric buckling of circular mindlin plates with ring supports. Journal of Structural Engineering, 1993, 119(3): 782–793
5. Liew K M, Xiang Y, Kitipornchai S, Wang C M. Buckling and vibration of annular Mindlin plates with internal concentric ring supports subject to in-plane radial pressure. Journal of Sound and Vibration, 1994, 177(5): 689–707
6. Laura P A A, Gutierrez R H, Sanzi H C, Elvira G. Buckling of circular, solid and annular plates with an intermediate circular support. Ocean Engineering, 2000, 27(7): 749–755
7. Timoshenko S P, Gere J M. Theory of Elastic Stability. New York: McGraw Hill, 1961
8. Szilard R. Theory and Analysis of Plates. NJ: Prentice-Hall, Englewood Cliffs, 1974
9. Wolkowisky J H. Buckling of the circular plate embedded in elastic springs, an application to geophysics. Communications on Pure and Applied Mathematics, 1969, 22(5): 367–667
10. Brusher D O, Almroth B O. Buckling of Bars, Plates and Shells, New York: McGraw-Hill, 1975
11. Gerard C P. Asymmetric vibration and stability of circular plates. Computers & Structures, 1978, 9(1): 89–95
12. Thevendran V, Wang C M. Buckling of annular plates elastically restrained against rotation along edges. Thin-walled Structures, 1996, 25(3): 231–246
13. Wang C Y. Buckling of a circular plate with internal elastic ring support. Mechanics Based Design of Structures and Machines, 2003, 31(1): 93–102
14. Wang C Y, Wang C M. Buckling of circular plates with an internal ring support and elastically restrained edges. Thin-walled Structures, 2001, 39(9): 821–825
15. Kim C S, Dickinson S M. The flexural vibration of the isotropic and polar orthotropic annular and circular plates with elastically restrained peripheries. Journal of Sound and Vibration, 1990, 143 (1): 171–179
16. Yamaki N. Buckling of a Thin annular plate under uniform compression. Journal of Applied Mechanics, 1958, 25: 267–273
17. Bhaskara Rao L, Kameswara Rao C. Buckling analysis of circular plates with elastically restrained edges and resting on internal elastic ring support. Mechanics Based Design of Structures and Machines, 2010, 38(4): 440–452
18. Wang C M, Aung T M, Tun Myint Aung. Buckling of circular mindlin plates with an internal ring support and elastically restrained edge. Journal of Engineering Mechanics, 2005, 131(4): 359–366

Buckling of circular plate with foundation and elastic edge

Lokavarapu Bhaskara Rao · Chellapilla Kameswara Rao

Received: 6 December 2013 / Accepted: 27 May 2014
© Springer Science+Business Media Dordrecht 2014

Abstract This paper deals with stability of circular plate with foundation and elastic edge against translation and rotation. Exact solution is utilized for development of governing equation for the problem under consideration. This paper reveals the subsistence of mode switching and it varies with foundation parameter. Fundamental buckling may not relate to axisymmetric as earlier implicated. The buckling load parameter rises monotonically with the foundation parameter. Percent of increase in load-carrying ability with foundation is calculated. A wide range of data is generated based on the dominance of rotational, translational, and foundation parameters on the stability of the system.

Keywords Buckling · Circular plate · Elastically restrained edge · Foundation · Mode switching

1 Introduction

Circular plates are important components in many structural engineering applications (Szilard 1974). Circular plates on continuous elastic foundation find many applications in the static and dynamic design of vibration exciters and vibration absorbers and also in the design of sloshing and earthquake resistant large storage vessels for nuclear power plants etc. One can find several such applications in many civil, aeronautical and mechanical supporting structures and foundations.

Based on exact and approximate methods of solution, many authors have studied the problem of static stability and Bryan (1891) carried out buckling of circular plates and the earliest innovative work in this area. A wide range of studies on the theme covers different aspects of design of structures and mechanical equipment involving various complex boundaries and loading conditions.

Different elastic foundation models like Winkler (Chonan 1980; Gupta et al. 1990; Liew et al. 1996), Pasternak (Wang and Stephens 1977; Bhattacharya 1977) and generalized foundation (Karasin 2004) has been studied and analyzed by many researchers in the available literature. Ensuring elastic stability of various structural members is imperative in structural design wherever they are supported on different types of elastic foundations. Holanda (2000) studied the affect of foundation on stability. Hetenyi (1946) has also studied buckling of beams on foundation. It was found that for stiffer foundations, the buckling load

L. B. Rao (✉)
School of Mechanical & Building Sciences, VIT
University, Chennai Campus, Vandalur-Kelambakkam
Road, Chennai 600127, India
e-mail: bhaskarbabu_20@yahoo.com

C. K. Rao
Department of Mechanical Engineering, Guru Nanak
Institutions Technical Campus, Ibrahimpatnam,
Hyderabad 501506, AP, India
e-mail: chellapilla95@gmail.com

corresponds to a mode with increased number of nodes. Various researchers studied the stability of plates taking into consideration independent contact constraints. Seide (1958) deliberated substantially long plate and established which rigid restriction, buckling load increased by 33 % comparative to unconstrained case. Analytical solution for the buckling loads for a rectangular plate is possible if two opposite sides are simply supported (Warren 1980), otherwise numerical solutions are necessary (Laura et al. 1977; Raju and Rao 1988; Yu 1957; Galletly 1959; Kline and Hancock 1965; Wolkowisky 1969; Gupta and Lal 1978, 1979, 1993, 2006; Singh and Jain 2004) studied stability of circular plates. Yu and Wang (2010) studied the buckling mosaic of plate with foundation. In a recent study, Wang (2005) found buckling load not only by the axisymmetric modes considered by earlier authors, but also by the asymmetric modes as well. There seems to be only one article (Wang 2005) in the literature studying buckling of circular plate on foundation, where boundary is a clamped, simply supported, or free edge thin circular plate.

Generally, lot of difficulties encountered due to complication of boundary condition. This complication may be because of various realistic situations when boundary may not relate to the standard boundary situations. Therefore, there is a need to consider non-classical boundary situations such as elastically restrained edge, such as translational, rotational constraints (Wang and Wang 2001; Rao and Rao 2010; Kim and Dickinson 1990; Yamaki 1958; Wang et al. 2005).

Plates are frequently exposed to in-plane stresses. This could be due to in-plane loads. This may leads to buckling of structures, which is detrimental. This occurrence is significant in different applications. Therefore, the buckling analysis of plates plays a vital role. The present work is carried out to compute elastic critical buckling loads of plate with elastic edges (against rotation, translation) and rests on foundation. In addition, the buckling loads are premeditated correctly by considering asymmetric mode.

2 Mathematical formulation

Circular plate under consideration is supported on foundation, its boundary is elastic edge (against

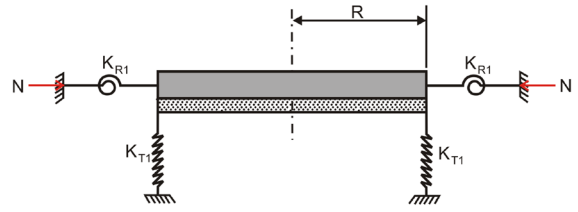


Fig. 1 Circular plate with foundation and elastic edge against rotation and translation

rotation and translation) and also it is subjected to in-plane load, N shown in Fig. 1. Here, R , ν , h and E represents radius, Poisson's ratio, thickness and modulus of elasticity of plate respectively.

According to Yu (1957), the fourth order differential equation proposed by the Classical Plate Theory (Kirchhoff's theory), for plate on foundation is given below

$$D\nabla^4 w + N\nabla^2 w + K_w w = 0 \quad (1)$$

Here, D , w , N and K_w represents flexural rigidity, lateral displacement, compressive load and foundation modulus respectively. After normalizing all lengths by R , Eq. (1) becomes

$$\nabla^4 \bar{w} + k^2 \nabla^2 \bar{w} + \xi^4 \bar{w} = 0 \quad (2)$$

$$\nabla^2 (\nabla^2 + k^2) \bar{w} + \xi^4 \bar{w} = 0 \quad (3)$$

where, $k^2 = NR^2/D$ is a non-dimensional buckling load parameter and $\xi^4 = K_w R^4/D$ is a non-dimensional foundation stiffness parameter, ∇^2 is the Laplacian parameter. In polar coordinates (r, θ) set

$$\bar{w}(\bar{r}, \theta) = \bar{u}(\bar{r}) \cos(n\theta) \quad (4)$$

Here, $\bar{w}(\bar{r}, \theta)$ represents transverse deflection of plate and n represents the nodal diameters, the general solution that is bounded at the origin is as follows. Let J_n represents Bessel function of order n . General solution to the Eq. (3) is more complicated. Therefore, the following three cases are considered.

Case (i) If $k > \sqrt{2}\xi$, the solution to Eq. (3) is given by

$$u(\bar{r}) = A_1 J_n(\alpha \bar{r}) + A_2 J_n(\beta \bar{r}) \quad (5)$$

Substituting Eq. (5) in Eq. (4), we obtain

$$\bar{w}(\bar{r}, \theta) = (A_1 J_n(\alpha \bar{r}) + A_2 J_n(\beta \bar{r})) \cos(n\theta) \quad (6)$$

$$\text{where } \alpha = \left(\frac{k^2 + \sqrt{k^4 - 4\xi_1^4}}{2} \right)^{1/2}, \quad (7)$$

$$\beta = \left(\frac{k^2 - \sqrt{k^4 - 4\xi_1^4}}{2} \right)^{1/2}$$

Case (ii) If $k = \sqrt{2}\xi$, the solution to Eq. (3) is given by

$$u(\bar{r}) = A_1 J_n(\xi \bar{r}) + A_2 \bar{r} J_{n+1}(\xi \bar{r}) \quad (8)$$

Substituting Eq. (8) in Eq. (4), we obtain

$$\bar{w}(\bar{r}, \theta) = (A_1 J_n(\xi \bar{r}) + A_2 \bar{r} J_{n+1}(\xi \bar{r})) \cos(n\theta) \quad (9)$$

Case (iii) If $k < \sqrt{2}\xi$, the solution to Eq. (3) is given by

$$u(\bar{r}) = A_1 \operatorname{Re}[J_n(i\delta \bar{r})] + A_2 \operatorname{Im}[J_n(i\delta \bar{r})] \quad (10)$$

Substituting Eq. (10) in Eq. (4), we obtain

$$\bar{w}(\bar{r}, \theta) = (A_1 \operatorname{Re}[J_n(i\delta \bar{r})] + A_2 \operatorname{Im}[J_n(i\delta \bar{r})]) \cos(n\theta) \quad (11)$$

$$\text{where } i = \sqrt{-1} \text{ and } \delta = \left(\frac{-k^2 + \sqrt{4\xi^4 - k^4}}{2} \right)^{1/2} \quad (12)$$

Considering an elastically restrained edge (Fig. 1), boundary conditions can be expresses as

$$M_r(\bar{r}, \theta) = K_{R1} \frac{\partial \bar{w}(\bar{r}, \theta)}{\partial \bar{r}} \quad (13)$$

$$V_r(\bar{r}, \theta) = -K_{T1} \bar{w}(\bar{r}, \theta) \quad (14)$$

Here bending moment and shear force can be defined as follows

$$M_r(\bar{r}, \theta) = -\frac{D}{R^3} \left[\frac{\partial^2 \bar{w}(\bar{r}, \theta)}{\partial \bar{r}^2} + \nu \left(\frac{1}{\bar{r}} \frac{\partial \bar{w}(\bar{r}, \theta)}{\partial \bar{r}} + \frac{1}{\bar{r}^2} \frac{\partial^2 \bar{w}(\bar{r}, \theta)}{\partial \theta^2} \right) \right] \quad (15)$$

$$V_r(\bar{r}, \theta) = -\frac{D}{R^3} \left[\frac{\partial}{\partial \bar{r}} \nabla^2 \bar{w}(\bar{r}, \theta) + (1 - \nu) \frac{1}{\bar{r}} \frac{\partial}{\partial \theta} \left(\frac{1}{\bar{r}} \frac{\partial^2 \bar{w}(\bar{r}, \theta)}{\partial \bar{r} \partial \theta} - \frac{1}{\bar{r}^2} \frac{\partial \bar{w}(\bar{r}, \theta)}{\partial \theta} \right) \right] \quad (16)$$

From Eqs. (13) and (15) yields the following expression

$$\left[\frac{\partial^2 \bar{w}(\bar{r}, \theta)}{\partial \bar{r}^2} + \nu \left(\frac{1}{\bar{r}} \frac{\partial \bar{w}(\bar{r}, \theta)}{\partial \bar{r}} + \frac{1}{\bar{r}^2} \frac{\partial^2 \bar{w}(\bar{r}, \theta)}{\partial \theta^2} \right) \right] = -\frac{K_{R1} R^2}{D} \frac{\partial \bar{w}(\bar{r}, \theta)}{\partial \bar{r}} \quad (17)$$

$$\left[\frac{\partial^2 \bar{w}(\bar{r}, \theta)}{\partial \bar{r}^2} + \nu \left(\frac{1}{\bar{r}} \frac{\partial \bar{w}(\bar{r}, \theta)}{\partial \bar{r}} + \frac{1}{\bar{r}^2} \frac{\partial^2 \bar{w}(\bar{r}, \theta)}{\partial \theta^2} \right) \right] = -R_{11} \frac{\partial \bar{w}(\bar{r}, \theta)}{\partial \bar{r}} \quad (18)$$

Substituting Eq. (14) in Eq. (16), we obtain

$$\left[\frac{\partial}{\partial \bar{r}} \nabla^2 \bar{w}(\bar{r}, \theta) + (1 - \nu) \frac{1}{\bar{r}} \frac{\partial}{\partial \theta} \left(\frac{1}{\bar{r}} \frac{\partial^2 \bar{w}(\bar{r}, \theta)}{\partial \bar{r} \partial \theta} - \frac{1}{\bar{r}^2} \frac{\partial \bar{w}(\bar{r}, \theta)}{\partial \theta} \right) \right] = \frac{K_{T1} R^3}{D} \bar{w}(\bar{r}, \theta) \quad (19)$$

$$\left[\frac{\partial}{\partial \bar{r}} \nabla^2 \bar{w}(\bar{r}, \theta) + (1 - \nu) \frac{1}{\bar{r}} \frac{\partial}{\partial \theta} \left(\frac{1}{\bar{r}} \frac{\partial^2 \bar{w}(\bar{r}, \theta)}{\partial \bar{r} \partial \theta} - \frac{1}{\bar{r}^2} \frac{\partial \bar{w}(\bar{r}, \theta)}{\partial \theta} \right) \right] = T_{11} \bar{w}(\bar{r}, \theta) \quad (20)$$

where $R_{11} = \frac{K_{R1} R^2}{D}$ and $T_{11} = \frac{K_{T1} R^3}{D}$ are non-dimensional rotational and translational flexibility parameter respectively.

Case (i) If $k > \sqrt{2}\xi$

2.1 Rotationally restrained boundary at outer edge

Substituting Eq. (6) in Eq. (18), we obtain the following at $r = 1$

$$\left[\frac{\alpha^2}{4} P_{88} + \frac{\alpha}{2} (\nu + R_{11}) P_{77} - \left(\frac{\alpha^2}{2} + \nu n^2 \right) J_n(\alpha) \right] A_1 + \left[\frac{\beta^2}{4} P'_{88} + \frac{\beta}{2} (\nu + R_{11}) P'_{77} - \left(\frac{\beta^2}{2} + \nu n^2 \right) J_n(\beta) \right] A_2 = 0 \quad (21)$$

where

$$P_{77} = J_{n-1}(\alpha) - J_{n+1}(\alpha); \quad P'_{77} = J_{n-1}(\beta) - J_{n+1}(\beta);$$

$$P_{88} = J_{n-2}(\alpha) + J_{n+2}(\alpha); \quad P'_{88} = J_{n-2}(\beta) + J_{n+2}(\beta)$$

2.2 Translational restrained boundary at outer edge

Substituting Eq. (6) in Eq. (20), we obtain the following at $r = 1$

$$\begin{aligned} & \left[\frac{\alpha^3}{8} (P_{99} - 3P_{77}) + \frac{\alpha^2}{4} P_{88} + \frac{\alpha}{2} (n^2(v-2) - 1) P_{77} \right. \\ & \quad \left. + \left(n^2(3-v) - \frac{\alpha^2}{2} - T_{11} \right) J_n(\alpha) \right] A_1 \\ & \quad + \left[\frac{\beta^3}{8} (P'_{99} - 3P'_{77}) + \frac{\beta^2}{4} P'_{88} + \frac{\beta}{2} (n^2(v-2) - 1) P'_{77} \right. \\ & \quad \left. + \left(n^2(3-v) - \frac{\beta^2}{2} - T_{11} \right) J_n(\beta) \right] A_2 = 0 \end{aligned} \quad (22)$$

where

$$\begin{aligned} P_{77} &= J_{n-1}(\alpha) - J_{n+1}(\alpha); P'_{77} = J_{n-1}(\beta) - J_{n+1}(\beta); \\ P_{88} &= J_{n-2}(\alpha) + J_{n+2}(\alpha); P'_{88} = J_{n-2}(\beta) + J_{n+2}(\beta); \\ P_{99} &= J_{n-3}(\alpha) - J_{n+3}(\alpha); P'_{99} = J_{n-3}(\beta) - J_{n+3}(\beta); \end{aligned}$$

Case (ii) If $k = \sqrt{2}\xi$

2.3 Rotationally restrained boundary at outer edge

Substituting Eq. (9) in Eq. (18), we obtain the following at $r = 1$

$$\begin{aligned} & \left[\frac{\xi^2}{4} P_{13} + \frac{\xi}{2} (v + R_{11}) P_{12} - \left(\frac{\xi^2}{2} + v n^2 \right) J_n(\xi) \right] A_1 \\ & \quad + \left[\frac{\xi^2}{4} (P_{12} - P_{14}) + \frac{\xi}{2} (v + R_{11} + 2) P'_{12} \right. \\ & \quad \left. + (v(1 - n^2) + R_{11}) J_{n+1}(\xi) \right] A_2 = 0 \end{aligned} \quad (23)$$

2.4 Translational restrained boundary at outer edge

Substituting Eq. (9) in Eq. (20), we obtain the following at $r = 1$

$$\begin{aligned} & \left[\frac{\xi^3}{8} (P_{15} - 3P_{12}) + \frac{\xi^2}{4} P_{13} + \frac{\xi}{2} (n^2(v-2) - 1) P_{12} \right. \\ & \quad \left. + \left(n^2(3-v) - \frac{\xi^2}{2} - T_{11} \right) J_n(\xi) \right] A_1 \\ & \quad + \left[\frac{\xi^3}{8} (P_{16} - 3P'_{12}) + \xi^2 (P_{12} - P_{14}) \right. \\ & \quad \left. + \frac{\xi}{2} (n^2(v-2) + 1) P'_{12} + (n^2 - 1 - T_{11}) J_{n+1}(\xi) \right] A_2 \\ & = 0 \end{aligned} \quad (24)$$

where

$$\begin{aligned} P_{12} &= J_{n-1}(\xi) - J_{n+1}(\xi); P'_{12} = J_n(\xi) - J_{n+1}(\xi); \\ P_{13} &= J_{n-2}(\xi) + J_{n+2}(\xi); P_{14} = J_{n+2}(\xi) - J_{n+3}(\xi); \\ P_{15} &= J_{n-3}(\xi) - J_{n+3}(\xi); P_{16} = J_{n-2}(\xi) - J_{n+4}(\xi); \end{aligned}$$

Case (iii) If $k < \sqrt{2}\xi$

2.5 Rotationally restrained boundary at outer edge

Substituting Eq. (11) in Eq. (18), we obtain the following at $r = 1$

$$\begin{aligned} & \left[\operatorname{Re} \left[(P_{31}) \frac{i^2 \delta^2}{4} \right] + (v + R_{11}) \operatorname{Re} \left[(P_{21}) \frac{i\delta}{2} \right] \right. \\ & \quad \left. + \left(\frac{\delta^2}{2} - v n^2 \right) \operatorname{Re} [J_n(i\delta)] \right] A_1 \\ & \quad + \left[\operatorname{Im} \left[(P_{31}) \frac{i^2 \delta^2}{4} \right] + (v + R_{11}) \operatorname{Im} \left[(P_{21}) \frac{i\delta}{2} \right] \right. \\ & \quad \left. + \left(\frac{\delta^2}{2} - v n^2 \right) \operatorname{Im} [J_n(i\delta)] \right] A_2 = 0 \end{aligned} \quad (25)$$

2.6 Translational restrained boundary at outer edge

Substituting Eq. (11) in Eq. (20), we obtain the following at $r = 1$

$$\begin{aligned} & \left[\operatorname{Re} \left[(P_{41}) \frac{i^3 \delta^3}{8} \right] + \operatorname{Re} \left[(P_{31}) \frac{i^2 \delta^2}{4} \right] \right. \\ & \quad \left. + \frac{i\delta}{2} \left(\frac{3\delta^2}{4} + n^2(v-2) - 1 \right) \operatorname{Re} [P_{21}] \right. \\ & \quad \left. + \left(\frac{\delta^2}{2} + n^2(3-v) - T_{11} \right) \operatorname{Re} [J_n(i\delta)] \right] A_1 \\ & \quad + \left[\operatorname{Im} \left[(P_{41}) \frac{i^3 \delta^3}{8} \right] + \operatorname{Im} \left[(P_{31}) \frac{i^2 \delta^2}{4} \right] \right. \\ & \quad \left. + \frac{i\delta}{2} \left(\frac{3\delta^2}{4} + n^2(v-2) - 1 \right) \operatorname{Im} [P_{21}] \right. \\ & \quad \left. + \left(\frac{\delta^2}{2} + n^2(3-v) - T_{11} \right) \operatorname{Im} [J_n(i\delta)] \right] A_2 = 0 \end{aligned} \quad (26)$$

The above equations listed in above three cases are used for axisymmetric ($n = 0$) and asymmetric ($n \neq 0$) buckling modes. Here, A_1 and A_2 are constants. Here, 0.3 is used as Poisson's ratio in all calculations.

Table 1 Buckling ($n = 0$ and $n = 1$ mode) loads for various translational, rotational, and foundation restraints (R_{11} , T_{11} and ξ) and $\nu = 0.33$

ξ	$R_{11} = T_{11} = 1$		$R_{11} = T_{11} = 10$		$R_{11} = T_{11} = 100$	
	$n = 0$	$n = 1$	$n = 0$	$n = 1$	$n = 0$	$n = 1$
0	2.52051	2.74951	3.48887	2.74951	3.79365	2.74951
2.5	4.38057	5.10167	4.23479	4.65156	4.39922	5.27624
5	7.78999	7.6852	7.73659	7.34844	7.75413	7.39619
7.5	11.1116	12.4921	10.9502	12.3471	11.6795	10.8835
10	14.4752	14.4927	15.3885	15.1862	15.333	14.4861
12.5	18.8247	17.9778	17.9051	18.5461	18.5706	18.2913
15	22.1629	22.0849	22.0444	22.0627	21.4294	21.9807
17.5	24.9567	25.5571	24.9517	25.5522	26.4594	25.5071
20	29.8829	29.007	29.8341	28.9668	28.8349	28.4275

Table 2 Comparison of mode switches with Wang (2005) Clamped boundary and $\nu = 0.3$

	$n = 0$		$n = 1$		$n = 0$		$n = 1$		$n = 0$		$n = 1$	
	ξ	k	ξ	k	ξ	k	ξ	k	ξ	k	ξ	k
Wang (2005)	0	3.8317	3.644	6.022	5.185	7.994	6.912	10.265	8.446	12.355	9.059	13.213
Present	0	3.8317	3.644	6.022	5.185	7.994	6.912	10.265	8.446	12.355	9.059	13.213

3 Solution

Equations mentioned above are solved to obtain an exact characteristic buckling equation by eliminating the coefficients A_1 and A_2 . For non-trivial elucidation, the determinant $[A]_{2 \times 2}$ become extinct. This exact characteristic buckling equation is solved by using a bisection algorithm. The buckling load parameter can be determined for a given set of n , ν , R_{11} , T_{11} and ξ values.

4 Numerical results

Buckling loads are calculated by considering a wide range of rotational, translational and foundation parameters and presented in Table 1. Figure 2 represents variant of buckling load, with foundation by considering a set of values elastic restraints, i.e., $R_{11} = T_{11} = 1$. It is noticed from Fig. 2, that curve is tranquil of bi segments because of mode switch. Figure 2, shows buckling load, k rises monotonically with the foundation stiffness parameter, ξ . It is observed that the symmetric (i.e., $n = 0$) solution weaves with the asymmetric solution (i.e., $n = 1$).

When the foundation stiffness is zero, the plate buckles axisymmetrically with $k = 2.52051$. When ξ increased beyond 4.67891 ($k = 7.35415$), $n = 1$ mode (asymmetric) gives correct fundamental buckling. This persists until $\xi = 5.17926$ ($k = 8.022311$) where the $n = 0$ mode again determines the lower buckling load. The next three switches of mode are at $\xi = 10.05204$ ($k = 14.5642$), $\xi = 15.2891$ ($k = 22.4873$) and $\xi = 18.5192$ ($k = 26.962$).

Figure 3 shows buckling parameter k , increases monotonically with the foundation stiffness parameter, ξ . It is observed that the asymmetric (i.e., $n = 1$) solution weaves with the symmetric solution (i.e., $n = 0$). When foundation stiffness is zero, the plate buckles asymmetrically with $k = 2.74951$. When ξ increased beyond 1.60085 ($k = 3.9656$), the symmetric mode $n = 0$ gives the correct lower buckling load. This persists until $\xi = 3.7944$ ($k = 6.05096$) where the $n = 1$ mode again determines the lower buckling load. The next four switches of mode are at $\xi = 5.5486$ ($k = 8.4391$), $\xi = 9.6868$ ($k = 14.8302$), $\xi = 10.596$ ($k = 15.9952$) and $\xi = 18.5240$ ($k = 26.9427$).

Figure 4, shows buckling parameter, k increases with the foundation stiffness parameter, ξ . It is

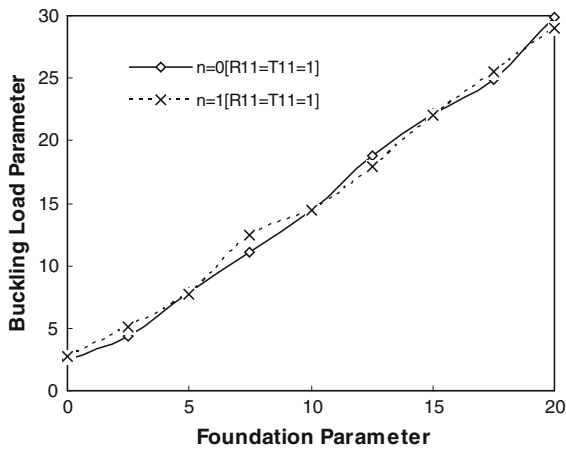


Fig. 2 Buckling parameter k , and foundation stiffness parameter ζ , for rotational and translational parameters of $R_{11} = T_{11} = 1$

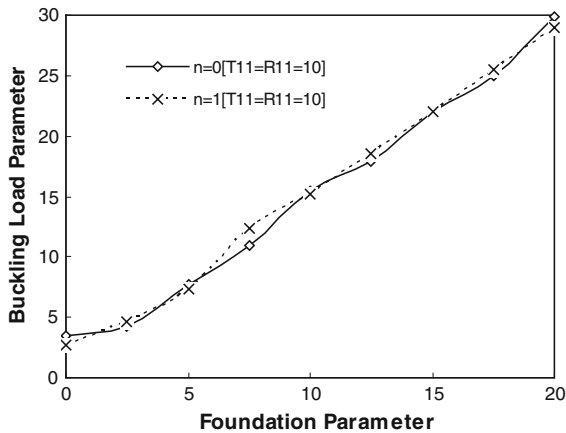


Fig. 3 Buckling parameter k , and foundation stiffness parameter ζ , for rotational and translational parameters of $R_{11} = T_{11} = 10$

observed that the asymmetric (i.e., $n = 1$) solution weaves with the symmetric solution (i.e., $n = 0$). When foundation stiffness is zero, the plate buckles asymmetrically with $k = 2.74951$. When ζ increased beyond 1.35405 ($k = 4.118$), the symmetric mode $n = 0$ gives the correct lower buckling load. When ζ increases beyond 4.27350 the $n = 1$ mode again gives the lower buckling load. The next two switches of mode are at $\zeta = 13.3435$ ($k = 19.5308$) and $\zeta = 15.9176$ ($k = 23.2749$).

Results of this sort are rare in literature. Figure 5 shows the comparison of results with the clamped boundary condition. Table 2 shows the comparison of

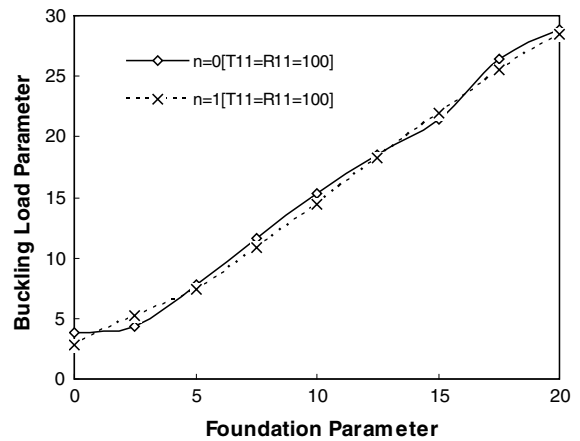


Fig. 4 Buckling parameter k , and foundation stiffness parameter ζ , for rotational and translational parameters of $R_{11} = T_{11} = 100$

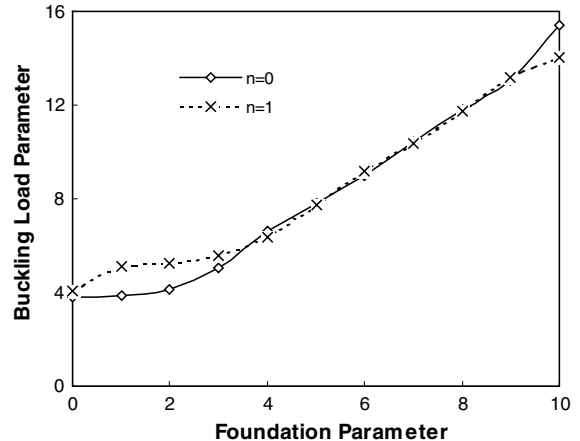


Fig. 5 Buckling parameter k , and foundation stiffness parameter ζ , for clamped boundary condition

mode switches against those obtained by Wang (2005) for clamped boundary by setting $R_{11} \rightarrow \infty$ and $T_{11} \rightarrow \infty$ in the present study. Similarly, Tables 3 and 4 shows the comparison of results for simply supported boundary (by setting $R_{11} \rightarrow 0$ and $T_{11} \rightarrow \infty$ in the present study) and free boundary condition (by setting $R_{11} \rightarrow 0$ and $T_{11} \rightarrow 0$ in the present study) respectively. The buckling load starts from zero, corresponding to the $n = 1$ mode. Kline and Hancock (1965) obtained only the symmetric $n = 0$ curve, thus overestimated the fundamental buckling where $n = 1$ mode gives correct buckling load. The buckling load of elastically restrained

Table 3 Comparison of mode switches with Wang (2005) simply supported boundary and $\nu = 0.3$

	$n = 0$		$n = 1$		$n = 0$		$n = 1$		$n = 0$	
	ξ	k	ξ	k	ξ	k	ξ	k	ξ	k
Wang (2005)	0	2.04881	3.047	4.359	4.604	6.605	6.228	8.843	7.795	11.072
Present	0	2.04881	3.047	4.359	4.604	6.605	6.228	8.843	7.795	11.072

Table 4 Comparison of mode switches with Wang (2005) free boundary and $\nu = 0.3$

	$n = 1$		$n = 2$		$n = 0$	
	ξ	k	ξ	k	ξ	k
Wang (2005)	0	0	2.059	2.046	2.550	2.502
Present	0	0	2.059	2.046	2.550	2.502

circular plate on elastic foundation is now correctly estimated.

5 Concluding remarks

The buckling of elastically restrained thin circular plate on elastic foundation is premeditated. The buckling load parameters are presented for different values of translational T_{11} and rotational restraints R_{11} . In addition, it simulates clamped boundary when $R_{11} \rightarrow \infty$ and $T_{11} \rightarrow \infty$. In addition, buckling parameters are presented for a range of elastic foundation restraints ξ . Buckling load is increased due to foundation restraint irrespective of additional plate parameters. At a particular foundation parameter, buckling mode switch from $n = 1$ to $n = 0$. Switching of mode is calculated for different translational, rotational and foundation restraints. In addition, here the equations are exact, and the solutions can be found to any precision and can be used as benchmark solution. This data would be useful during basic design of embedded circular plates, and circular anchor embedded plates.

References

- Bryan, G.H.: On the stability of a plane plate under thrust in its own plane with application to the buckling of the side of a ship. *Proc. Lond. Math. Soc.* **22**(1), 54–67 (1891)
- Bhattacharya, B.: Free vibration of plates on Vlasov's foundation. *J. Sound Vib.* **54**(3), 464–467 (1977)
- Chonan, S.: Random vibration of an initially stressed thick plate on an elastic foundation. *J. Sound Vib.* **71**(1), 117–127 (1980)
- Gupta, U.S., Lal, R., Jain, S.K.: Effect of elastic foundation on axisymmetric vibration of polar orthotropic circular plates of variable thickness. *J. Sound Vib.* **139**(3), 503–513 (1990)
- Galletly, G.D.: Circular plates on a generalized elastic foundation. *J. Appl. Mech.* **26**, 297 (1959)
- Gupta, U.S., Lal, R.: Buckling and vibrations of circular plates of variable thickness. *J. Sound Vib.* **58**(4), 501–507 (1978)
- Gupta, U.S., Lal, R.: Vibrations and buckling of parabolically tapered circular plates. *Indian J. Pure Appl. Math.* **10**(3), 347–356 (1979)
- Gupta, U.S., Lal, R., Jain, S.K.: Vibration and buckling of parabolically tapered polar orthotropic circular plates on an elastic foundation. *Indian J. Pure Appl. Math.* **24**(10), 607–631 (1993)
- Gupta, U.S., Ansari, A.H., Sharma, S.: Buckling and vibration of polar orthotropic circular plate resting on Winkler foundation. *J. Sound Vib.* **297**(3), 457–476 (2006)
- Holanda, A.S.: Analysis of the equilibrium and stability of plates with contact constraints. Ph.D. Thesis, Civil engineering Dept. PUC-Rio (in Portuguese) (2000)
- Hetenyi, M.: Beams on elastic foundations. University of Michigan Press, Ann Arbor (1946)
- Kline, L.V., Hancock, J.O.: Buckling of circular plate on elastic foundation. *J. Eng. Ind.* **87**(3), 323–324 (1965)
- Kim, C.S., Dickinson, S.M.: The flexural vibration of the isotropic and polar orthotropic annular and circular plates with elastically restrained peripheries. *J. Sound Vib.* **143**(1), 171–179 (1990)
- Karasin A.: An improved finite grid solution for plates on generalized foundations, Doctoral Thesis, Submitted to the Graduate School of Natural and Applied Sciences of The Middle East Technical University, Department of Civil Engineering, January 2004
- Laura, P.A.A., Filipich, C., Santos, R.D.: Vibration and buckling of parabolically tapered polar orthotropic circular plates on an elastic foundation. *J. Sound Vib.* **52**(2), 243–251 (1977)

- Liew, K.M., Han, J.B., Xiao, M., Do, H.: Differential quadrature method for Mindlin plates on Winkler foundation. *Int. J. Mech. Sci.* **38**(4), 405–421 (1996)
- Rao, L.B., Rao, C.K.: Buckling analysis of circular plates with elastically restrained edges and resting on internal elastic ring support. *Mech. Based Des. Struct. Mech.* **38**(4), 440–452 (2010)
- Raju, K.K., Rao, G.V.: Thermal post-buckling of square plate resting on an elastic foundation by finite element method. *Comput. Struct.* **28**, 195–199 (1988)
- Singh, R.P., Jain, S.K.: Free asymmetric transverse vibration of parabolically varying thickness polar orthotropic annular plate with flexible edge conditions. *Tamkang J. Sci. Eng.* **7**(1), 41–52 (2004)
- Seide, P.: Compressive buckling of a long simply supported plate on an elastic foundation. *J. Aeronaut. Sci.* **25**(6), 382–384 (1958)
- Szilar, R.: *Theory and analysis of plates*. Prentice-Hall, Englewood Cliffs (1974)
- Wang, T.M., Stephens, J.E.: Natural frequencies of Timoshenko beams on Pasternak foundation. *J. Sound Vib.* **51**(2), 149–155 (1977)
- Warren, R.C.: Buckling of a rectangular plate on an elastic foundation. Compressed in Two Directions. Ph.D. Thesis, Michigan State University (1980)
- Wolkowisky, J.H.: Buckling of the circular plate embedded in elastic springs, an application to geophysics. *Commun. Pure Appl. Math.* **22**(5), 367–667 (1969)
- Wang, C.Y.: On the buckling of a circular plate on an elastic foundation. *J. Appl. Mech.* **72**(5), 795–796 (2005)
- Wang, C.Y., Wang, C.M.: Buckling of circular plates with an internal ring support and elastically restrained edges. *Thin Walled Struct.* **39**(9), 821–825 (2001)
- Wang, C.M., Wang, C.Y., Reddy, J.N.: *Exact solutions for buckling of structural members*. CRC, Boca Raton (2005)
- Yu, Y.Y.: Axisymmetrical bending of circular plates under simultaneous action of lateral load, force in the middle plane, and elastic foundation. *J. Appl. Mech.* **24**(1), 141–143 (1957)
- Yu, L.H., Wang, C.Y.: Buckling mosaic of a circular plate on a partial elastic foundation. *Struct. Eng. Mech.* **34**(1), 135–138 (2010)
- Yamaki, N.: Buckling of a thin annular plate under uniform compression. *J. Appl. Mech.* **25**(2), 267–273 (1958)

Lokavarapu Bhaskara RAO, Chellapilla Kameswara RAO

Frequencies of circular plate with concentric ring and elastic edge support

© Higher Education Press and Springer-Verlag Berlin Heidelberg 2014

Abstract Exact solutions for the flexural vibrations of circular plates having elastic edge conditions along with rigid concentric ring support have been presented in this paper. Values of frequency parameter for the considered circular plate are computed for different sets of values of elastic rotational and translation restraints and the radius of internal rigid ring support. The results for the first three modes of plate vibrations are computed and are presented in tabular form. The effects of rotational and linear restraints and the radius of the rigid ring support on the vibration behavior of circular plates are studied over a wide range of non-dimensional parametric values. The values of the exact frequency parameter presented in this paper for varying values of restraint parameters and the radius of the rigid ring support can better serve in design and as benchmark solutions to validate the numerical methods obtained by using other methods of solution.

Keywords circular plate, frequency, elastic edge, rigid ring, mode switching

1 Introduction

Circular plates are extensively used in various aeronautical, civil, mechanical and marine applications. The latest literature on the problem of flexural vibrations of circular plates, with different edge conditions, has been extensively

reviewed [1–5]. Axi-symmetric vibrations of the circular plates have been studied by Bodine [6]. Laura et al. presented more accurate results for the case of axi-symmetric mode of vibration [7]. However, the fundamental frequency may not be only axi-symmetric. This fact was implied by a graph of Bodine et al. who plotted mode shapes of some higher mode frequencies [8]. Literature on vibration of circular plates with different edge conditions and internal strengthening has been reviewed by a number of researchers [9–13] utilizing methods such as Green's functions and others. Wang [17] presented values of fundamental frequency parameter of a circular plate with free edge, supported on an internal rigid ring support, and showed that the fundamental frequency is corresponding to the asymmetric mode for lower values of the radius of internal rigid ring support [14].

However, as we know, in practical industrial engineering situations, we rarely come across ideal boundary conditions. It is a widely accepted fact that the condition on a periphery often tends to be partially between the classical boundary conditions such as simply supported, clamped and free and may correspond more closely to some form of elastic restraints, i.e., rotational and translational restraints [14–16]. To the best of authors' knowledge, there is no other research paper other than the present one, addressing the vibrations of circular plates with elastically restrained boundary involving rotational and translation restraints at the edge of the circular plate along with an internal rigid ring support.

The main purpose of this paper is therefore to study the effects of the radius of the internal rigid ring support, the circular plate being elastically restrained along the outer edge against rotation and translation making use of the exact method of solution. The natural frequencies of circular plate for varying values of rotational and translational restraints along the plate edge, rigid ring support radius for a wide range of non-dimensional parameters and are expressed in graphical and tabular form for use in design of such circular plates which has application in engineering industry.

Received February 14, 2014; accepted March 23, 2014

Lokavarapu Bhaskara RAO (✉)
SMBS, VIT University, Chennai Campus, Vandalur-Kelambakkam
Road, Chennai-600127, Tamil Nadu, India
E-mail: bhaskarbabu_20@yahoo.com

Chellapilla Kameswara RAO (✉)
Department of Mechanical Engineering, Guru Nanak Institutions
Technical Campus, Ibrahimpatnam, Hyderabad - 501506, A.P, India
E-mail: chellapilla95@gmail.com

2 Mathematical formulation

The circular plate under consideration is of radius R , Poisson's ratio ν , density ρ , thickness h , and elastic constant E . In Fig. 1 is shown a circular plate, which has outer boundary elastically restrained against translation and rotation (at radius R) and supported on a rigid internal ring support (at radius bR), b being a fraction and less than 1.

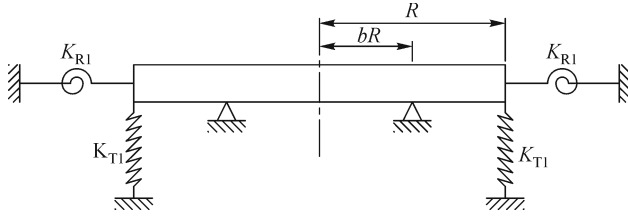


Fig. 1 Concentric rigid ring supported circular plate with elastically restrained boundary

All lengths are normalized with respect to plate radius R . That is how the outer boundary radius is 1 and ring radius is b . Subscript I denotes outer region $b \leq r \leq 1$, subscript II denotes inner region $0 \leq r \leq b$. According to the circular plate theory given by Leissa, the following fourth - order differential equation describes the flexural vibrations of the plate [2]:

$$D\nabla^4 w + \rho h \frac{\partial^2 w}{\partial t^2} = 0 \quad (1)$$

where D is the flexural rigidity of the plate. General form of lateral displacement of vibration of plate can be represented as $w = u(r)\cos(n\theta)e^{i\omega t}$ where (r, θ) are polar coordinates, w is the transverse displacement, n is the number of nodal diameters, ω is the frequency and t the time. The function $u(r)$ is a linear combination of Bessel functions $J_n(kr), Y_n(kr), I_n(kr), K_n(kr)$ and $k = R(\rho\omega^2/D)^{1/4}$ is the square root of the non-dimensional frequency of the plate [3]. General solutions for regions I and II are as follows:

$$u_I(r) = C_1 J_n(kr) + C_2 Y_n(kr) + C_3 I_n(kr) + C_4 K_n(kr) \quad (2)$$

$$u_{II}(r) = C_5 J_n(kr) + C_6 I_n(kr) \quad (3)$$

Considering the elastically restrained edge at the outer region, boundary conditions can be formulated as

$$M_r(r, \theta) = K_{R1} \frac{\partial w_I(r, \theta)}{\partial r} \quad (4)$$

$$V_r(r, \theta) = -K_{T1} w_I(r, \theta) \quad (5)$$

Here bending moment and shear force can be represented as

$$M_r(r, \theta) = -\frac{D}{R} \left[\frac{\partial^2 w_I(r, \theta)}{\partial r^2} + \nu \left(\frac{1}{r} \frac{\partial w_I(r, \theta)}{\partial r} + \frac{1}{r^2} \frac{\partial^2 w_I(r, \theta)}{\partial \theta^2} \right) \right] \quad (6)$$

$$V_r(r, \theta) = -\frac{D}{R^3} \left[\frac{\partial}{\partial r} \nabla^2 w_I(r, \theta) + (1-\nu) \frac{1}{r} \frac{\partial}{\partial \theta} \left(\frac{1}{r} \frac{\partial^2 w_I(r, \theta)}{\partial r \partial \theta} - \frac{1}{r^2} \frac{\partial w_I(r, \theta)}{\partial \theta} \right) \right] \quad (7)$$

From Eqs. (4), (6) and (5), (7) yields the following expressions

$$\left[\frac{\partial^2 w_I(r, \theta)}{\partial r^2} + \nu \left(\frac{1}{r} \frac{\partial w_I(r, \theta)}{\partial r} + \frac{1}{r^2} \frac{\partial^2 w_I(r, \theta)}{\partial \theta^2} \right) \right] = -R_{11} \frac{\partial w_I(r, \theta)}{\partial r} \quad (8)$$

$$\left[\frac{\partial}{\partial r} \nabla^2 w_I(r, \theta) + (1-\nu) \frac{1}{r} \frac{\partial}{\partial \theta} \left(\frac{1}{r} \frac{\partial^2 w_I(r, \theta)}{\partial r \partial \theta} - \frac{1}{r^2} \frac{\partial w_I(r, \theta)}{\partial \theta} \right) \right] = T_{11} w_I(r, \theta) \quad (9)$$

At $r = 1$, the Eqs. (8) and (9) can be expressed as

$$u_I''(1) + \nu[u_I'(1) - n^2 u_I(1)] = -R_{11} u_I'(1) \quad (10)$$

$$u_I'''(1) + u_I''(1) - [1 + n^2(2-\nu)]u_I'(1) + n^2(3-\nu)u_I(1) = -T_{11} u_I(1) \quad (11)$$

where $R_{11} = \frac{K_{R1}R}{D}$ and $T_{11} = \frac{K_{T1}R^3}{D}$ are the normalized spring constants K_{R1} & K_{T1} of the rotational and translational elastic springs respectively.

Apart from the elastically restrained conditions at the outer boundary, continuity requirements at the rigid ring support (at $r = b$) are as follows

$$u_I(b) = 0 \quad (12)$$

$$u_{II}(b) = 0 \quad (13)$$

$$u_I'(b) = u_{II}'(b) \quad (14)$$

$$u_I''(b) = u_{II}''(b) \quad (15)$$

The non-trivial solutions to Eqs. (10) – (15) are required to be obtained.

From Eqs. (1), (2), (10)–(15), we obtain the following consequent equations:

$$\left[\frac{k^2}{4}P_2 + \frac{k}{2}(\nu + R_{11})P_1 - \left(\frac{k^2}{2} + \nu n^2 \right) J_n(k) \right] C_1 + \left[\frac{k^2}{4}Q_2 + \frac{k}{2}(\nu + R_{11})Q_1 - \left(\frac{k^2}{2} + \nu n^2 \right) Y_n(k) \right] C_2 + \left[\frac{k^2}{4}R_2 + \frac{k}{2}(\nu + R_{11})R_1 + \left(\frac{k^2}{2} - \nu n^2 \right) I_n(k) \right] C_3 - \left[\frac{k^2}{4}S_2 - \frac{k}{2}(\nu + R_{11})S_1 + \left(\frac{k^2}{2} - \nu n^2 \right) K_n(k) \right] C_4 = 0 \quad (16)$$

$$\begin{aligned} & \left[\frac{k^3}{8}P_3 + \frac{k^2}{4}P_2 - \frac{k}{2} \left(\frac{3}{4}k^2 + n^2(2-\nu) + 1 \right) P_1 + \left(n^2(3-\nu) - \frac{k^2}{2} - T_{11} \right) J_n(k) \right] C_1 \\ & + \left[\frac{k^3}{8}Q_3 + \frac{k^2}{4}Q_2 - \frac{k}{2} \left(\frac{3}{4}k^2 + n^2(2-\nu) + 1 \right) Q_1 + \left(n^2(3-\nu) - \frac{k^2}{2} - T_{11} \right) Y_n(k) \right] C_2 \\ & + \left[\frac{k^3}{8}R_3 + \frac{k^2}{4}R_2 + \frac{k}{2} \left(\frac{3}{4}k^2 - n^2(2-\nu) + 1 \right) R_1 + \left(n^2(3-\nu) + \frac{k^2}{2} - T_{11} \right) I_n(k) \right] C_3 \\ & + \left[-\frac{k^3}{8}S_3 + \frac{k^2}{4}S_2 + \frac{k}{2} \left(-\frac{3}{4}k^2 + n^2(2-\nu) + 1 \right) S_1 + \left(n^2(3-\nu) + \frac{k^2}{2} - T_{11} \right) K_n(k) \right] C_4 = 0 \end{aligned} \quad (17)$$

$$J_n(kb)C_1 + Y_n(kb)C_2 + I_n(kb)C_3 + K_n(kb)C_4 = 0 \quad (18) \quad \left[\frac{k}{2}P'_1 \right] C_1 + \left[\frac{k}{2}Q'_1 \right] C_2 + \left[\frac{k}{2}R'_1 \right] C_3 - \left[\frac{k}{2}S'_1 \right] C_4 - \left[\frac{k}{2}P'_1 \right] C_5 - \left[\frac{k}{2}R'_1 \right] C_6 = 0 \quad (20)$$

$$J_n(kb)C_5 + I_n(kb)C_6 = 0 \quad (19)$$

$$\begin{aligned} & \left[\frac{k^2}{4}P'_2 - \frac{k^2}{2}J_n(kb) \right] C_1 + \left[\frac{k^2}{4}Q'_2 - \frac{k^2}{2}Y_n(kb) \right] C_2 + \left[\frac{k^2}{4}R'_2 + \frac{k^2}{2}I_n(kb) \right] C_3 + \\ & \left[\frac{k^2}{4}S'_2 + \frac{k^2}{2}K_n(kb) \right] C_4 - \left[\frac{k^2}{4}P'_2 - \frac{k^2}{2}J_n(kb) \right] C_5 - \left[\frac{k^2}{4}R'_2 + \frac{k^2}{2}I_n(kb) \right] C_6 = 0 \end{aligned} \quad (21)$$

where

$$\begin{aligned} P_1 &= J_{n-1}(k) - J_{n+1}(k); P_2 = J_{n-2}(k) + J_{n+2}(k); P_3 = J_{n-3}(k) - J_{n+3}(k); \\ Q_1 &= Y_{n-1}(k) - Y_{n+1}(k); Q_2 = Y_{n-2}(k) + Y_{n+2}(k); Q_3 = Y_{n-3}(k) - Y_{n+3}(k); \\ R_1 &= I_{n-1}(k) + I_{n+1}(k); R_2 = I_{n-2}(k) + I_{n+2}(k); R_3 = I_{n-3}(k) + I_{n+3}(k); \\ S_1 &= K_{n-1}(k) + K_{n+1}(k); S_2 = K_{n-2}(k) + K_{n+2}(k); K_3 = K_{n-3}(k) + K_{n+3}(k); \\ P'_1 &= J_{n-1}(kb) - J_{n+1}(kb); P'_2 = J_{n-2}(kb) + J_{n+2}(kb); Q'_1 = Y_{n-1}(kb) - Y_{n+1}(kb); Q'_2 = Y_{n-2}(kb) + Y_{n+2}(kb); \\ R'_1 &= I_{n-1}(kb) + I_{n+1}(kb); R'_2 = I_{n-2}(kb) + I_{n+2}(kb); S'_1 = K_{n-1}(kb) + K_{n+1}(kb); S'_2 = K_{n-2}(kb) + K_{n+2}(kb); \end{aligned}$$

using bisection method of iteration technique. In generating the results in this paper, we considered the value of Poisson's ratio as 0.3.

3 Solution

Given the set of values of n , ν , T_{11} , R_{11} , R_{22} & b , equations mentioned above are utilized in obtaining an exact characteristic frequency equation by suitably eliminating the coefficients C_1 , C_2 , C_3 , C_4 , C_5 & C_6 . The values of non-dimensional frequency parameter k can be obtained by solving the nonlinear characteristic equation

4 Results and discussions

Values of frequency parameter are computed for different values of elastic restraint parameters (rotational and translational) and the radius of the concentric rigid ring

support. Values of fundamental frequency parameter for axi-symmetric and asymmetric modes of vibration for a given set of values of rotational restraint parameters ($R_{11} = 2.5, 5, 20, 50, 100, 500, 100 \text{ \& } 10^{16}$) are computed by keeping T_{11} as constant i.e., $T_{11} = 10$. Results for the first three modes of plate vibrations are obtained and presented in Figs. 2–9.

It can be observed from Fig. 2, which for a given set of values of $R_{11} = 2.5$ & $T_{11} = 10$, the given curve is composed of two segments due to the occurrence of vibration mode switching. For lower values of the radius of concentric rigid ring support, the fundamental frequency is corresponding to asymmetric $n = 1$ mode. In this region (as represented by dotted lines in Fig. 2) fundamental frequency decreases as b decreases in value. For higher values of concentric rigid ring support radius, the fundamental frequency is corresponding to axisymmetric mode ($n = 0$). In this segment (as represented by continuous lines in Fig. 2) the fundamental frequency increases as b decreases up to a peak point and correspond to the maximum frequency and decreases thereafter as b decreases as shown in Fig. 2.

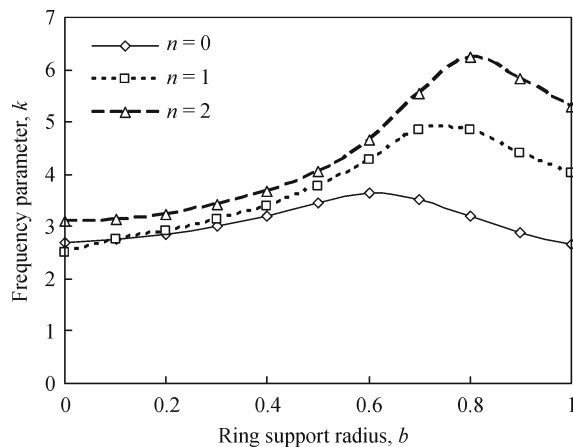


Fig. 2 Fundamental frequency of circular plate and concentric rigid support radius for $R_{11} = 2.5$ & $T_{11} = 10$

It can be observed from Fig. 2, that the cross over radius for mode switching from asymmetric to axisymmetric mode in this case becomes $b = 0.09985$. Fundamental frequency is governed by asymmetric mode when $b \leq 0.09985$ (as shown by the dotted lines in Fig. 2). When b is increased beyond 0.09985, axisymmetric mode gives the correct fundamental frequency as shown by continuous lines in Fig. 2. Optimal solutions (concentric ring support, b_{opt} and the subsequent fundamental frequency, k_{opt}) are $b = 0.6$ and $k = 3.63298$ respectively, which is equal to nodal radius of the axisymmetric mode and frequency.

Similarly, it is observed from Figs. 3–9, that for a given set of values of rotational restraint parameters ($R_{11} = 5, 20, 50, 100, 500, 100 \text{ \& } 10^{16}$) and $T_{11} = 10$,

the curve shown is composed of two segments due to the occurrence of vibration mode switching. For lower values of concentric rigid ring support radius, the fundamental frequency corresponds to the asymmetric mode. In this segment (as represented by dotted lines in Figs. 3–9), we can find that the fundamental frequency decreases as the value of b decreases. For higher values of the radius of concentric rigid ring support, the fundamental frequency corresponds to axisymmetric mode. In this region (as represented by continuous lines in Figs. 3–9), the fundamental frequency increases as b decreases up to a peak point corresponding to the maximum frequency and, decreases thereafter as b decreases as shown in Figs. 3–9. Using Figs. 3–9, the cross over radius, b_{cor} and corresponding frequency parameters, k_{cor} are computed and presented in Table 1. Further, the optimal solutions (concentric ring support, b_{opt} and the subsequent fundamental frequency, k_{opt}) are also obtained and presented in Table 2.

Mode switching (crossover) radius decreases from 0.09985 to 0.08597 as R_{11} varies from 2.5 to 10^{16} and $T_{11} = 10$. The optimal location is 0.6, which remains constant for $R_{11} = 2.5$ to 0.6 and $T_{11} = 10$. However, the fundamental frequency can be seen to be increasing from 3.63298 to 3.9227 at the respective optimal locations.

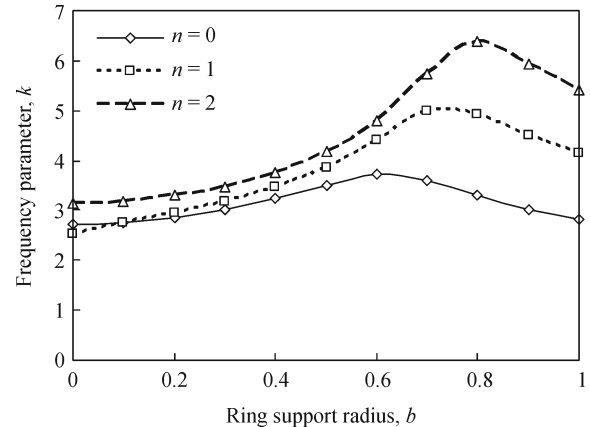


Fig. 3 Frequency of circular plate and concentric rigid support radius for $R_{11} = 5$ & $T_{11} = 10$

The fundamental frequency for $n = 0$ and $n = 1$ modes for different sets of values of translation restraint parameter ($T_{11} = 2.5, 5, 20, 50, 100, 500, 100 \text{ \& } 10^{16}$) are computed keeping R_{11} constant ($R_{11} = 10$). Results for the first three modes of vibrations are obtained and presented in Figs. 10–17. It is observed from Fig. 10, for a given set of values of $T_{11} = 2.5$ and $R_{11} = 10$, the curve presented is composed of two segments due to the occurrence of vibration mode switching. For lower values of the radius of concentric rigid ring support, the fundamental frequency is corresponding to asymmetric mode. In this region (as

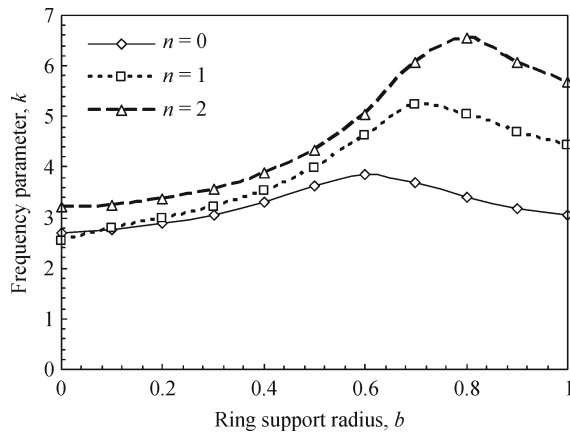


Fig. 4 Fundamental frequency of circular plate and concentric rigid support radius for $R_{11} = 20$ & $T_{11} = 10$

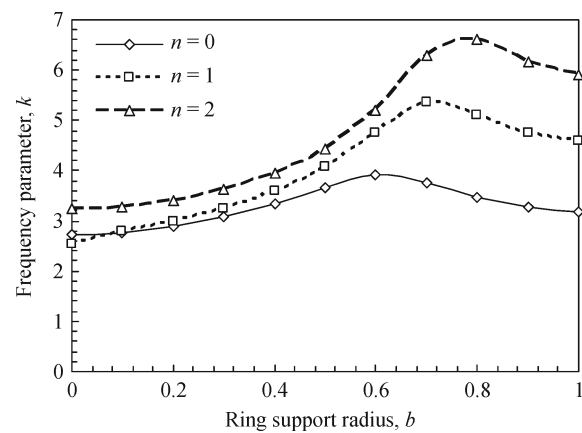


Fig. 7 Fundamental frequency of circular plate and concentric rigid support radius for $R_{11} = 500$ & $T_{11} = 10$

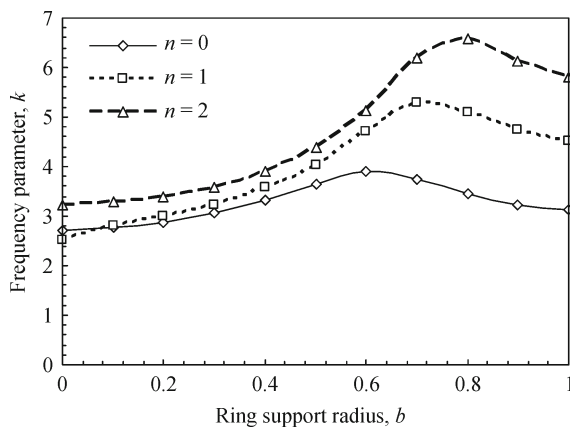


Fig. 5 Fundamental frequency of circular plate and concentric rigid support radius for $R_{11} = 50$ & $T_{11} = 10$

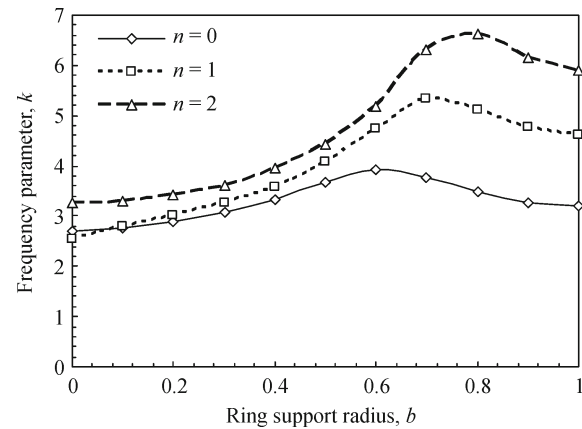


Fig. 8 Fundamental frequency of circular plate and concentric rigid support radius for $R_{11} = 1000$ & $T_{11} = 10$

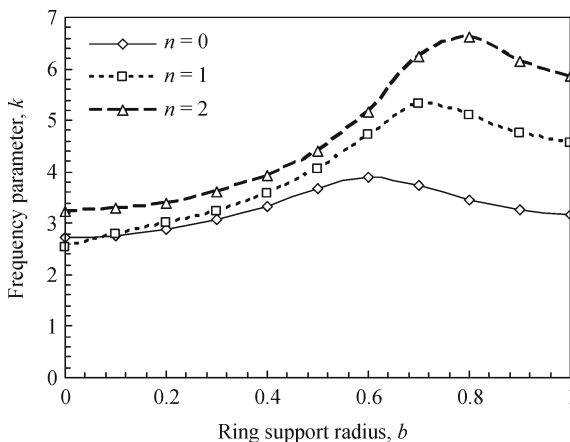


Fig. 6 Fundamental frequency of circular plate and concentric rigid support radius for $R_{11} = 100$ & $T_{11} = 10$

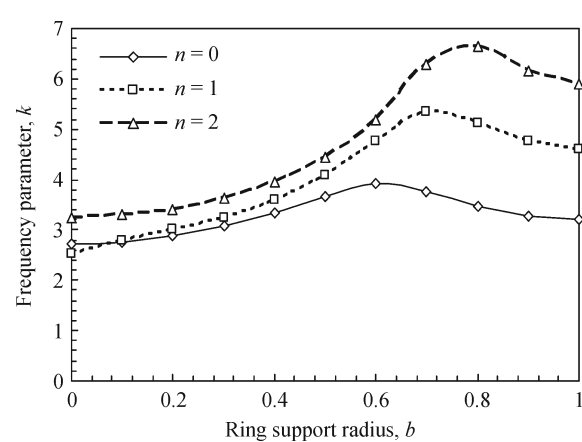


Fig. 9 Fundamental frequency of circular plate and concentric rigid support radius for $R_{11} = 10^{10}$ & $T_{11} = 10$

represented by dotted lines in Fig. 10) fundamental frequency decreases as b decreases in value. For higher

values of concentric rigid ring support radius, the fundamental frequency is corresponding to an axisym-

Table 1 The cross over radius, b_{cor} and the corresponding frequency parameters, k_{cor} for various values of R_{11} and $T_{11} = 10$

R_{11}	2.5	5	20	50	100	500	1000	10^{16}
b_{cor}	0.09985	0.09530	0.08911	0.08701	0.08679	0.08614	0.08601	0.08597
k_{cor}	2.75033	2.75477	2.76	2.76050	2.76163	2.76246	2.76273	2.76272

Table 2 Optimal locations (concentric ring support, b_{opt} and subsequent frequency parameter, k_{opt} for various values of R_{11} and $T_{11} = 10$

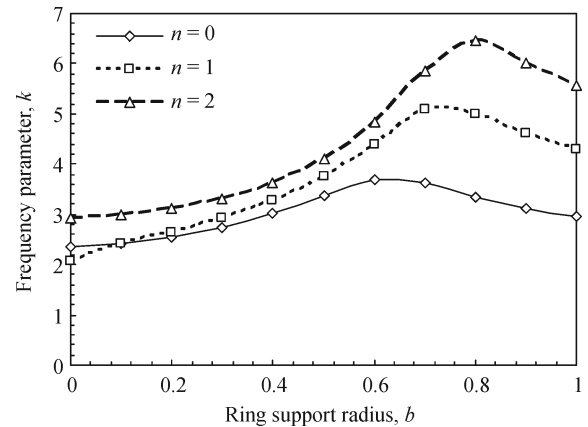
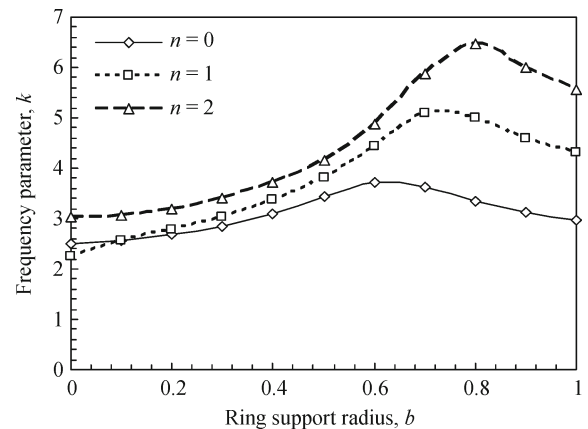
R_{11}	2.5	5	20	50	100	500	1000	10^{16}
b_{opt}	0.6	0.6	0.6	0.6	0.6	0.6	0.6	0.6
k_{opt}	3.63298	3.72601	3.85606	3.89405	3.90808	3.91972	3.92121	3.9227

metric mode. In this region (as represented by continuous lines in Fig. 10), the fundamental frequency increases as b decreases up to a peak point corresponding to maximum frequency and decreases thereafter as b decreases as shown in Fig. 10.

It is observed from Fig. 10, which the cross over radius for mode switching from asymmetric to axisymmetric mode in this case is $b = 0.098370$. Fundamental frequency is governed by $n = 1$ mode when $b \leq 0.098370$ (as represented by the dotted lines in Fig. 10). When b is increased beyond 0.098370, $n = 0$ mode gives correct fundamental frequency as shown by continuous lines in Fig. 10. Optimal solutions (concentric ring support, b_{opt} and the subsequent fundamental frequency, k_{opt}) are $b = 0.6$ and $k = 3.67998$ respectively, which is equal to the nodal radius of the axisymmetric mode and frequency.

Similarly, it is observed from the Figs. 11–17, for a given set of translational restraints ($T_{11} = 5, 20, 50, 100, 500, 1000$ & 10^{16}), and $R_{11} = 10$, the given curve is composed of two segments due to the occurrence of vibration mode switching. For lower values of concentric rigid ring support radius, fundamental frequency is corresponding to asymmetric mode. In this region (as represented by dotted lines in Figs. 11–17) fundamental frequency decreases as b decreases in value. For higher values of concentric rigid ring support radius, fundamental frequency is corresponding to an axisymmetric mode. In this region (as represented by continuous lines in Figs. 11–17) fundamental frequency increases as b decreases up to a peak point corresponds to maximum frequency and decreases thereafter as b decreases as shown in Figs. 11–17. It is observed from Figs. 11–17, the cross over radius, b_{cor} and corresponding frequency parameters, k_{cor} are computed and presented in Table 3. In addition, optimal solutions (concentric ring support, b_{opt} and the subsequent fundamental frequency, k_{opt}) are obtained and presented in Table 4.

The mode switching (cross over) radius varies (decreases) from 0.09837 to 0.016 as T_{11} varies 2.5 to 10^{16} and $R_{11} = 10$. The optimal location varies (decreases) from 0.6 to 0.4 as T_{11} varies from 2.5 to 10^{16} and $R_{11} = 10$. However, the fundamental frequency increases from 3.67998 to 4.48074 at the respective optimal locations.

**Fig. 10** Fundamental frequency of circular plate and concentric rigid support radius for $T_{11} = 2.5$ & $R_{11} = 10$ **Fig. 11** Fundamental frequency of circular plate and concentric rigid support radius for $T_{11} = 5$ & $R_{11} = 10$

Optimal location of rigid ring support is of great importance in design of supported structures. Optimal solution for the above two cases are presented in Tables 2 and 4. Results are compared as follows: (a) Frequencies ($n = 0$ mode) agree with Laura et. al. [7] (b) Table 5 presents exact fundamental frequency with free boundary

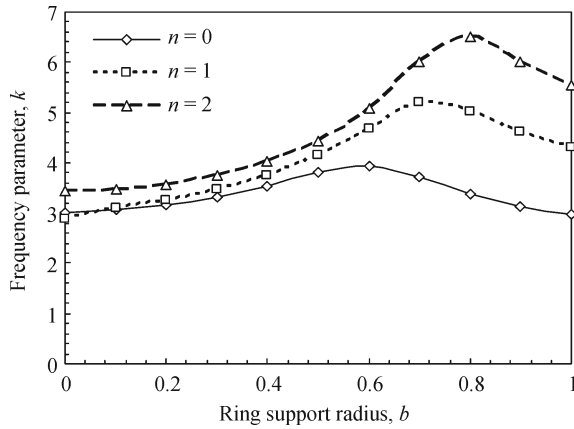


Fig. 12 Fundamental frequency of circular plate and concentric rigid support radius for $T_{11} = 20$ & $R_{11} = 10$

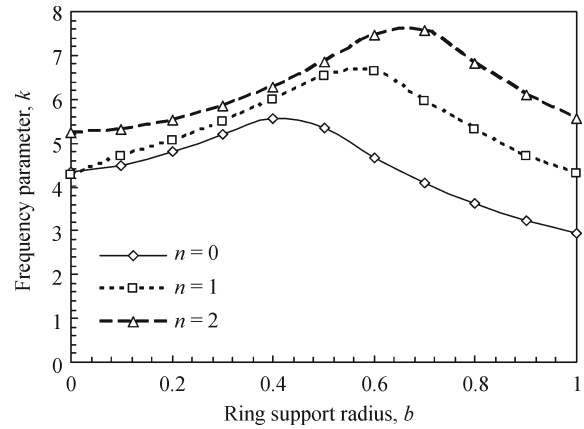


Fig. 15 Fundamental frequency of circular plate and concentric rigid support radius for $T_{11} = 500$ & $R_{11} = 10$

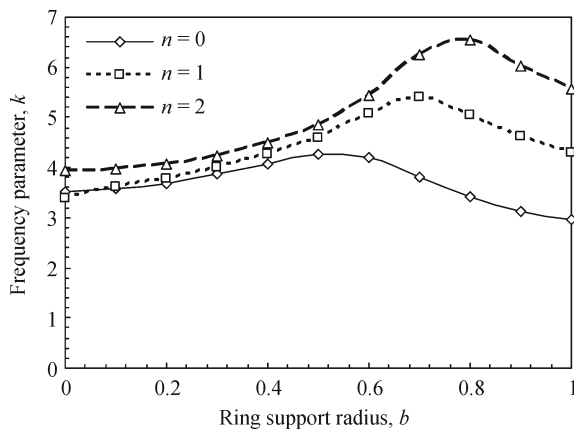


Fig. 13 Fundamental frequency of circular plate and concentric rigid support radius for $T_{11} = 50$ & $R_{11} = 10$

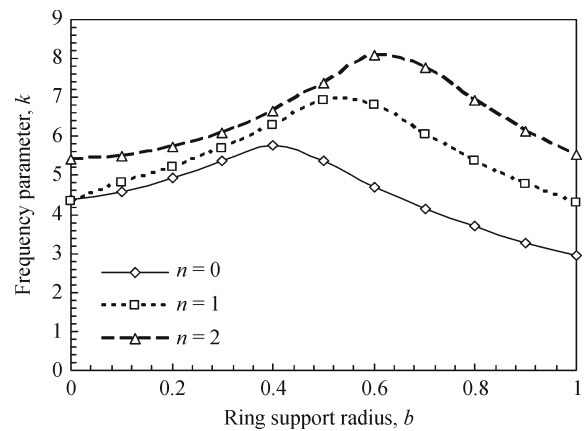


Fig. 16 Fundamental frequency of circular plate and concentric rigid support radius for $T_{11} = 1000$ & $R_{11} = 10$

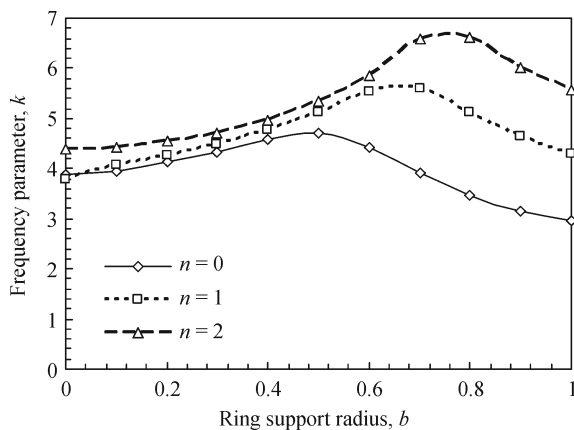


Fig. 14 Fundamental frequency of circular plate and concentric rigid support radius for $T_{11} = 100$ & $R_{11} = 10$

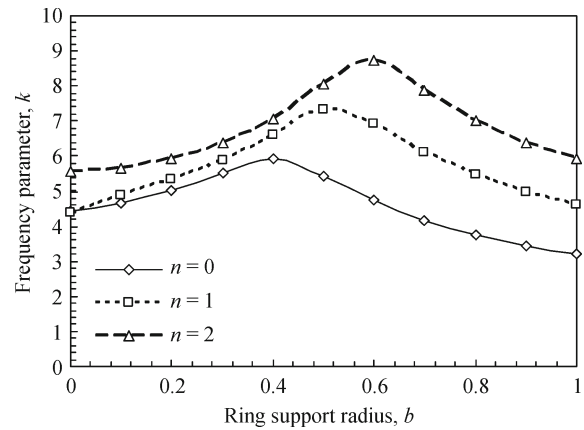


Fig. 17 Fundamental frequency of circular plate and concentric rigid support radius for $T_{11} = 10^{16}$ & $R_{11} = 10$

(by substituting $R_{11} \rightarrow 0$ in the current problem), with results obtained by Wang [17] (c) the fundamental frequency for clamped boundary (by substituting $R_{11} \rightarrow$

∞ & $T_{22} \rightarrow \infty$ in current problem) compared well with that of Wang et al. [17] (d) the fundamental frequency parameter k , for sliding edge against translation (by setting

Table 3 The cross over radius, b_{cor} and the corresponding frequency parameters, k_{cor} for various values of T_{11} and $R_{11} = 10$

T_{11}	2.5	5	20	50	100	500	1000	10^{16}
b_{cor}	0.09837	0.09640	0.08282	0.06378	0.04602	0.02184	0.01924	0.016
k_{cor}	2.41573	2.54833	3.05268	3.54305	3.90990	4.36130	4.42406	4.48074

Table 4 Optimal locations (ring support, b_{opt} and subsequent frequency, k_{opt}) for $R_{11} = 10$ and different values of T_{11}

T_{11}	2.5	5	20	50	100	500	1000	10^{16}
b_{opt}	0.6	0.6	0.6	0.5	0.5	0.4	0.4	0.4
k_{opt}	3.67998	3.72379	3.93665	4.26143	4.7033	5.75927	5.93386	4.48074

$R_{11} \rightarrow \infty$ & T_{11}) with a frequency parameter $k = 3.8711$, the fundamental frequency parameter k , for sliding edge (by setting $R_{11} \rightarrow \infty$) with a frequency parameter of $k = 3.8711$ and, the fundamental frequency parameter k , for rotationally restrained and simply supported edge (by setting R_{11} & $T_{11} \rightarrow \infty$) with a frequency parameter of $k = 3.8711$ agree well with those corresponding results presented by Wang [13].

Table 5 Comparison of Fundamental frequency for $\nu = 0.3$, with Wang et al. [14] for free Edge

Ring support radius, b	Wang et al. [14])	Present
0	0	0
0.02	1.501	1.50077
0.05	1.634	1.63422
0.1	1.789	1.78911
0.15	1.922	1.92226
0.2	2.051	2.05103

5 Conclusions

From the results presented in this paper, it can be easily seen that the fundamental mode of frequency switches from *asymmetric* to *axisymmetric* mode at specific rigid support radii. Change of mode (crossover) has been computed and shown graphically for varying values of elastic edge restraints against rotation and translation. The optimal solutions such as radius of optimum internal ring support and the corresponding fundamental frequency are computed for a wide variety of cases and are presented in a form convenient for use in design. The optimal rigid support radius is significantly influenced by variations in the edge elastic restraint parameters. Further, it is observed that the translation restraint parameter has relatively higher influence on frequency parameters than the rotational restraint parameter. As the results obtained in this paper are from exact method of solution in closed form, the presented results very well serve in designing such structures and as benchmark, solutions for assessing the

accuracy of the frequency results obtained using other approximate techniques.

References

1. Timoshenko S, Woinowsky-Krieger S. Theory of Plates and Shells. McGraw-Hill, New York, 1959
2. Leissa A W. Vibration of Plates. NASA SP-160, 1969
3. Mcleod A J, Bishop R E D. The Forced Vibration of Circular Flat Plates. Mechanical Engineering Science Monograph, 1965, 1: 1–33
4. Szilard R. Theory and Analysis of Plates. Prentice-Hall, New Jersey, 1974
5. Jawad M H. Design of plate and shell structures. ASME Three Park Avenue, New York, NY 10016, 2004
6. Bodine R Y. The fundamental frequency of a thin, flat circular plate supported along a circle of arbitrary radius. Journal of Applied Mechanics, 1959, 26: 666–668
7. Laura P A A, Gutierrez R H, Vera S A, Vega D A. Transverse vibrations of a circular plate with a free edge and a concentric circular support. Journal of Sound and Vibration, 1999, 223(5): 842–845
8. Bodine R Y. Vibration of Circular Plate supported by a concentric ring of arbitrary radius. Journal of the Acoustical Society of America, 1967, 41(6): 1551
9. Kukla S, Szewczyk M. The Green's functions for vibration problems of circular plates with elastic ring supports. Scientific Research of the Institute of Mathematics and Computer Science, 2004, 1(3): 67–72
10. Magrab E B. Vibrations of Elastic Structural Members. Sijthoff & Noordhoff. The Netherlands, 1979
11. Weisensel G N. Natural Frequency Information for Circular and Annular Plates. Journal of Sound and Vibration, 1989, 133(1): 129–134
12. Azimi S. Free Vibration of circular plates with elastic or rigid interior support. Journal of Sound and Vibration, 1988, 120(1): 37–52
13. Wang C Y, Wang C M. Fundamental Frequencies of Circular Plates with internal elastic ring support. Journal of Sound and Vibration, 2003, 263(5): 1071–1078
14. Wang C Y, Wang C M. Buckling of Circular Plates with an internal ring support and elastically restrained edges. Thin-walled Structures, 2004, 40(12): 1205–1215

- tures, 2001, 39(9): 821–825
15. Kim C S, Dickinson S M. The Flexural Vibration of the Isotropic and Polar Orthotropic Annular and Circular Plates with elastically restrained peripheries. *Journal of Sound and Vibration*, 1990, 143 (1): 171–179
16. Rao L B, Rao C K. Buckling of Annular Plates with Elastically Restrained External and Internal Edges. *Mechanics Based Design of Structures and Machines: An International Journal*, 2013, 41(2): 222–235
17. Wang C Y. On the fundamental frequency of a circular plate supported on a ring. *Journal of Sound and Vibration*, 2001, 243(5): 945–946



Frequency analysis of annular plates with inner and outer edges elastically restrained and resting on Winkler foundation



Lokavarapu Bhaskara Rao ^{a,*}, Chellapilla Kameswara Rao ^{b,1}

^a School of Mechanical and Building Sciences, VIT University, Chennai Campus, Vandalur-Kelambakkam Road, Chennai 600127, India

^b Department of Mechanical Engineering, Guru Nanak Institutions Technical Campus, Khanapur, Manchal (M), Ibrahimpatnam, Hyderabad 501508, A.P., India

ARTICLE INFO

Article history:

Received 29 October 2012

Received in revised form

11 February 2014

Accepted 18 February 2014

Available online 28 February 2014

Keywords:

Annular plate

Frequency

Elastic edge conditions

Winkler foundation

ABSTRACT

The present paper deals with exact analysis of free lateral vibrations of annular plates with inner and outer edges elastically restrained and resting on Winkler type elastic foundation. Exact solution is obtained from the formulation based on the classical plate theory assumptions. The frequencies of the annular plate are computed for various values of elastic rotational and translational restraints, foundation restraint and radius of an annular plate and the results for the first three modes of the plate vibrations are presented in both graphical and tabular form suitable for use in design. The effect of varying values of rotational and translational restraints, foundation restraint and radius of the annular plate on the vibration behavior of annular plates is studied in detail. The exact frequencies of vibration presented in non-dimensional form can serve as benchmark values for researchers to validate their numerical methods when applied for such annular plate problems.

© 2014 Elsevier Ltd. All rights reserved.

1. Introduction

Leissa [1] and Kim and Dickinson [2] have studied lateral vibration of thin annular plate subject to certain complicating effects. Kim and Dickinson [3] have also studied the flexural vibration of isotropic annular and circular plates with elastically restrained peripheries, using the Rayleigh–Ritz method. Wang et al. [4,5] used the differential quadrature method and Civalek [25] utilized the harmonic differential quadrature method in studying free vibration problems of annular plates with different boundary conditions. Liu and Chen [6] studied the problem of axisymmetric vibration of annular and circular plates, isotropic or polar orthotropic using an axisymmetric finite element. Vera et al. [8,9] have studied free vibration of annular plates with four combinations of boundary conditions Case (i) clamped at both edges, Case(ii) clamped at outer edge and simply supported at inner edge, and Case (iii) simply supported at outer edge and clamped at inner edge. Case (iv) simply supported at both edges and also the free-free edge conditions. Romanelli et al. [7], Vega et al. [10] and Laura et al. [11] studied the problem of free vibrations of annular plates with various boundary conditions and having an intermediate concentric circular support. Wang [12] has studied the vibration of an annular membrane attached to a free rigid core. Wang et al. [13] studied the effect of core on the fundamental

frequencies of annular plates with four different types of ideal boundary conditions.

Many authors [14,15,29] have studied the problem of free vibration of uniform and stepped circular plates resting on elastic foundation. The problem of free vibration of circular plate with stepped thickness is studied by Avlos et al. [16] both experimentally and analytically and by Kukla and Szweczyk [27] using Green's function method. Singh and Jain [17,18], studied the problem of free vibration of polar orthotropic annular and annular sector plates with thickness taper and with elastic edge conditions. Gupta and Bhargadwaj [19] studied the problem of free vibration of polar orthotropic circular plates resting on elastic foundation with quadratic variation in plate thickness. Hsu [20,21] studied the free vibrations of annular plates with different boundary conditions using the modified differential quadrature method. Ambali et al. [22] study the effect of fluid inertia on frequencies of vibration of annular plates.

In practical situations in industry, the plate periphery often tends to be part way between the classical boundary conditions such as free, clamped or simply supported and may correspond more closely to some form of appropriate combination of elastic restraints, i.e., translational and rotational restraints. Kim and Dickinson [2], Wang and Wang [23], Vera et al. [24], Kukla and Szweczyk [26,28], and Rao and Rao [30–32] studied the effect of such elastic restraints on plate frequencies of vibration and stability criterion. However, the problem of generally restrained annular plate resting on Winkler's foundation is not fully studied in the available literature and the present paper addresses the same giving an exact solution to the problem.

* Corresponding author. Tel.: +91 9949976175; fax: +91 44 3993 2555.

E-mail addresses: bhaskarbabu_20@yahoo.com (L.B. Rao),

chellapilla95@gmail.com (C.K. Rao).

¹ Tel.: +91 9849198548.

Nomenclature

$w(r, \theta)$	transverse deflection of the plate
r	plate radius at any point on the plate
θ	angle of radius
ω	circular frequency
h	thickness of the plate
R	radius of the plate
b	non-dimensional radius of ring support
ν	Poisson's ratio
E	Young's modulus of a material

D	flexural rigidity of a material
k_w	Winkler foundation stiffness
K_{T1}, K_{T2}	translation spring stiffnesses
K_{R1}, K_{R2}	rotational spring stiffnesses
T_{11}, T_{22}	non-dimensional translational flexibility parameter
R_{11}, R_{22}	non-dimensional rotational flexibility parameter
n	number of nodal diameters
t	time
\bar{k}_1	non-dimensional Frequency parameter without foundation,
\bar{k}_2	non-dimensional Frequency parameter with foundation

The present paper therefore deals with the free vibrations of annular plate considering both inner and outer peripheries of the plate elastically restrained against rotation and translation and resting on Winkler type elastic foundation and results are presented for the first three modes of vibration for a wide range of non-dimensional parameters in both graphical and tabular form suitable for use in design.

2. Problem definition

Consider a thin annular plate of radius R , uniform thickness h , Young's modulus E , density ρ , flexural rigidity D and Poisson's ratio ν , as shown in Fig. 1. The plate is also assumed to be made of linearly elastic, homogeneous and isotropic material. Moreover, the effects of shear deformation and rotary inertia are neglected. The edge of the annular plate is elastically restrained against rotation and translation at inner and outer periphery. The annular plate is supported by an elastic foundation as shown in Fig. 1. The present study is to determine the frequency of annular plate when both the peripheries are elastically restrained against rotation and translation and it is resting on elastic foundation.

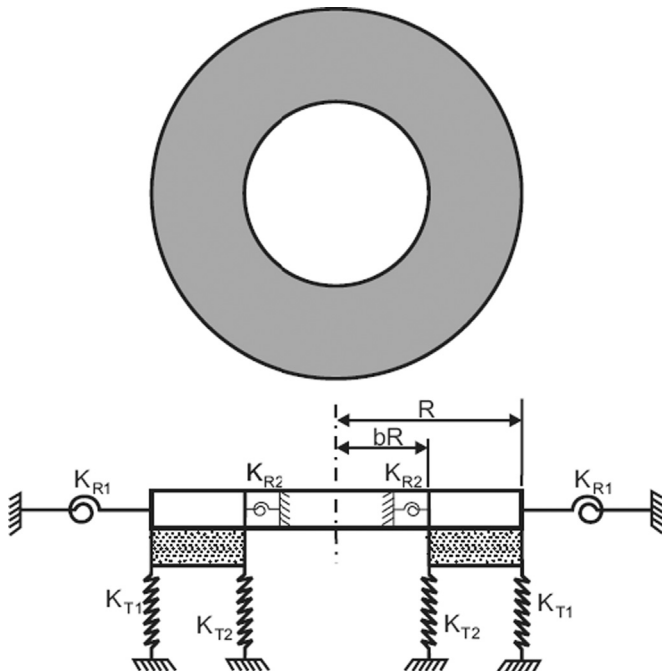


Fig. 1. Annular plate with rotational and translational constraints at inner and outer edge and resting on elastic foundation.

3. Mathematical formulation of the problem

Consider an annular plate of outer radius, R and inner radius bR as shown in Fig. 1. The annular plate is supported by an elastic foundation. Let subscript I denote the annular portion $0 \leq \bar{r} \leq b$ and the subscript II denote the outer region $b \leq \bar{r} \leq 1$. Here, all lengths are normalized by plate radius R . As per the Kirchhoff's classical plate theory, the following fourth order differential equation describes the free flexural vibrations of an annular plate

$$D\nabla^4 w + \rho h \frac{\partial^2 w}{\partial t^2} = 0 \quad (1)$$

where

$$\nabla^2 = \frac{\partial^2}{\partial \bar{r}^2} + \frac{1}{\bar{r}} \frac{\partial}{\partial \bar{r}} + \frac{1}{\bar{r}^2} \frac{\partial^2}{\partial \theta^2} \quad (2)$$

is the Laplace operator expressed in the polar coordinates r and θ . The first studies of Eq. (1) were those of Poisson and Kirchhoff and the classical methods of finding the solution of this equation is based on the separation of variables. After considering the foundation parameter Eq. (1) becomes

$$D\nabla^4 w + \xi w + \rho h \frac{\partial^2 w}{\partial t^2} = 0 \quad (3)$$

where \bar{r} is the radial distance normalized by R , $D = Eh^3/12(1-\nu^2)$ the flexural rigidity, $\bar{w} = w/R$ the normalized transverse displacement of the plate, $\xi = R^4 k_w/D$ the non-dimensional foundation parameter and k_w the Winkler foundation stiffness.

Using the separation of variables approach, the general solution to the classical plate vibration Eq. (3) in polar coordinates can be assumed as

$$\bar{w} = u(\bar{r}) \cos(n\theta) e^{i\omega t} \quad (4)$$

where n is the number of nodal diameters, ω the frequency and t the time. The function u is a linear combination of the Bessel functions $J_n(\bar{k}_1 \bar{r})$, $Y_n(\bar{k}_1 \bar{r})$, $I_n(\bar{k}_1 \bar{r})$ and $K_n(\bar{k}_1 \bar{r})$ and $\bar{k}_1 = R(\rho\omega^2/D)^{1/4}$, is the square root of the non-dimensional frequency. The annular plate of normalized radius at outer edge is 1 and the normalized radius at inner edge is b . There are therefore two plate regions. The general solutions for the outer region are giving by the following equation.

$$\bar{w}_I(\bar{r}, \theta) = [C_1 J_n(\bar{k}_1 \bar{r}) + C_2 Y_n(\bar{k}_1 \bar{r}) + C_3 I_n(\bar{k}_1 \bar{r}) + C_4 K_n(\bar{k}_1 \bar{r})] \cos(n\theta) \quad (5)$$

3.1. Application of boundary conditions at the outer edge

The boundary conditions at outer edges of the annular plate in terms of rotational stiffness (K_{R1}) and translational stiffness (K_{T1}) is given by the following expressions

$$M_r(\bar{r}, \theta) = K_{R1} \frac{\partial \bar{w}_I(\bar{r}, \theta)}{\partial \bar{r}} \quad (6)$$

$$V_r(\bar{r}, \theta) = -K_{T1} \bar{w}_l(\bar{r}, \theta) \quad (7)$$

The radial moment and the radial Kirchhoff shear at outer edge are defined as follows

$$M_r(\bar{r}, \theta) = -\frac{D}{R^3} \left[\frac{\partial^2 \bar{w}_l(\bar{r}, \theta)}{\partial \bar{r}^2} + \nu \left(\frac{1}{\bar{r}} \frac{\partial \bar{w}_l(\bar{r}, \theta)}{\partial \bar{r}} + \frac{1}{\bar{r}^2} \frac{\partial^2 \bar{w}_l(\bar{r}, \theta)}{\partial \theta^2} \right) \right] \quad (8)$$

$$V_r(\bar{r}, \theta) = -\frac{D}{R^3} \left[\frac{\partial}{\partial \bar{r}} \nabla^2 \bar{w}_l(\bar{r}, \theta) + (1-\nu) \frac{1}{\bar{r}} \frac{\partial}{\partial \theta} \left(\frac{1}{\bar{r}} \frac{\partial^2 \bar{w}_l(\bar{r}, \theta)}{\partial \bar{r} \partial \theta} - \frac{1}{\bar{r}^2} \frac{\partial \bar{w}_l(\bar{r}, \theta)}{\partial \theta} \right) \right] \quad (9)$$

Substituting Eq. (6) in Eq. (8) yields the following:

$$\left[\frac{\partial^2 \bar{w}_l(\bar{r}, \theta)}{\partial \bar{r}^2} + \nu \left(\frac{1}{\bar{r}} \frac{\partial \bar{w}_l(\bar{r}, \theta)}{\partial \bar{r}} + \frac{1}{\bar{r}^2} \frac{\partial^2 \bar{w}_l(\bar{r}, \theta)}{\partial \theta^2} \right) \right] = -\frac{K_{R1} R^2}{D} \frac{\partial^2 \bar{w}_l(\bar{r}, \theta)}{\partial \bar{r}^2} \quad (10)$$

$$\left[\frac{\partial^2 \bar{w}_l(\bar{r}, \theta)}{\partial \bar{r}^2} + \nu \left(\frac{1}{\bar{r}} \frac{\partial \bar{w}_l(\bar{r}, \theta)}{\partial \bar{r}} + \frac{1}{\bar{r}^2} \frac{\partial^2 \bar{w}_l(\bar{r}, \theta)}{\partial \theta^2} \right) \right] = -R_{11} \frac{\partial^2 \bar{w}_l(\bar{r}, \theta)}{\partial \bar{r}^2} \quad (11)$$

where

$$R_{11} = \frac{K_{R1} R^2}{D}$$

Substituting Eq. (7) in Eq. (9) yields the following:

$$\left[\frac{\partial}{\partial \bar{r}} \nabla^2 \bar{w}_l(\bar{r}, \theta) + (1-\nu) \frac{1}{\bar{r}} \frac{\partial}{\partial \theta} \left(\frac{1}{\bar{r}} \frac{\partial^2 \bar{w}_l(\bar{r}, \theta)}{\partial \bar{r} \partial \theta} - \frac{1}{\bar{r}^2} \frac{\partial \bar{w}_l(\bar{r}, \theta)}{\partial \theta} \right) \right] = \frac{K_{T1} R^3}{D} \bar{w}_l(\bar{r}, \theta) \quad (12)$$

$$\left[\frac{\partial}{\partial \bar{r}} \nabla^2 \bar{w}_l(\bar{r}, \theta) + (1-\nu) \frac{1}{\bar{r}} \frac{\partial}{\partial \theta} \left(\frac{1}{\bar{r}} \frac{\partial^2 \bar{w}_l(\bar{r}, \theta)}{\partial \bar{r} \partial \theta} - \frac{1}{\bar{r}^2} \frac{\partial \bar{w}_l(\bar{r}, \theta)}{\partial \theta} \right) \right] = T_{11} \bar{w}_l(\bar{r}, \theta) \quad (13)$$

where

$$T_{11} = \frac{K_{T1} R^3}{D}$$

3.2. Application of boundary conditions at the inner edge

Similarly, the boundary conditions at the inner edge of the annular plate in terms of rotational stiffness (K_{R2}) and translational stiffness (K_{T2}) are given by the following expressions.

$$M_r(\bar{r}, \theta) = -K_{R2} \frac{\partial \bar{w}_l(\bar{r}, \theta)}{\partial \bar{r}} \quad (14)$$

$$V_r(\bar{r}, \theta) = K_{T2} \bar{w}_l(\bar{r}, \theta) \quad (15)$$

The radial moment and the radial Kirchhoff shear at inner edge are defined as follows

$$M_r(\bar{r}, \theta) = -\frac{D}{R^3} \left[\frac{\partial^2 \bar{w}_l(\bar{r}, \theta)}{\partial \bar{r}^2} + \nu \left(\frac{1}{\bar{r}} \frac{\partial \bar{w}_l(\bar{r}, \theta)}{\partial \bar{r}} + \frac{1}{\bar{r}^2} \frac{\partial^2 \bar{w}_l(\bar{r}, \theta)}{\partial \theta^2} \right) \right] \quad (16)$$

$$V_r(\bar{r}, \theta) = -\frac{D}{R^3} \left[\frac{\partial}{\partial \bar{r}} \nabla^2 \bar{w}_l(\bar{r}, \theta) + (1-\nu) \frac{1}{\bar{r}} \frac{\partial}{\partial \theta} \left(\frac{1}{\bar{r}} \frac{\partial^2 \bar{w}_l(\bar{r}, \theta)}{\partial \bar{r} \partial \theta} - \frac{1}{\bar{r}^2} \frac{\partial \bar{w}_l(\bar{r}, \theta)}{\partial \theta} \right) \right] \quad (17)$$

Substituting Eq. (14) in Eq. (16) yields the following:

$$\left[\frac{\partial^2 \bar{w}_l(\bar{r}, \theta)}{\partial \bar{r}^2} + \nu \left(\frac{1}{\bar{r}} \frac{\partial \bar{w}_l(\bar{r}, \theta)}{\partial \bar{r}} + \frac{1}{\bar{r}^2} \frac{\partial^2 \bar{w}_l(\bar{r}, \theta)}{\partial \theta^2} \right) \right] = \frac{K_{R2} R^2}{D} \frac{\partial^2 \bar{w}_l(\bar{r}, \theta)}{\partial \bar{r}^2} \quad (18)$$

$$\left[\frac{\partial^2 \bar{w}_l(\bar{r}, \theta)}{\partial \bar{r}^2} + \nu \left(\frac{1}{\bar{r}} \frac{\partial \bar{w}_l(\bar{r}, \theta)}{\partial \bar{r}} + \frac{1}{\bar{r}^2} \frac{\partial^2 \bar{w}_l(\bar{r}, \theta)}{\partial \theta^2} \right) \right] = R_{22} \frac{\partial^2 \bar{w}_l(\bar{r}, \theta)}{\partial \bar{r}^2} \quad (19)$$

where

$$R_{22} = \frac{K_{R2} R^2}{D}$$

Substituting Eq. (15) in Eq. (17) yields the following:

$$\left[\frac{\partial}{\partial \bar{r}} \nabla^2 \bar{w}_l(\bar{r}, \theta) + (1-\nu) \frac{1}{\bar{r}} \frac{\partial}{\partial \theta} \left(\frac{1}{\bar{r}} \frac{\partial^2 \bar{w}_l(\bar{r}, \theta)}{\partial \bar{r} \partial \theta} - \frac{1}{\bar{r}^2} \frac{\partial \bar{w}_l(\bar{r}, \theta)}{\partial \theta} \right) \right] = -\frac{K_{T2} R^3}{D} \bar{w}_l(\bar{r}, \theta) \quad (20)$$

$$\left[\frac{\partial}{\partial \bar{r}} \nabla^2 \bar{w}_l(\bar{r}, \theta) + (1-\nu) \frac{1}{\bar{r}} \frac{\partial}{\partial \theta} \left(\frac{1}{\bar{r}} \frac{\partial^2 \bar{w}_l(\bar{r}, \theta)}{\partial \bar{r} \partial \theta} - \frac{1}{\bar{r}^2} \frac{\partial \bar{w}_l(\bar{r}, \theta)}{\partial \theta} \right) \right] = -T_{22} \bar{w}_l(\bar{r}, \theta) \quad (21)$$

where

$$T_{22} = \frac{K_{T2} R^3}{D}$$

The inner and outer edges of the annular plate considered in this paper are thus elastically restrained against rotation and translation and the problem is formulated for obtaining an exact solution.

Substituting Eq. (5) in Eq. (11) yields the following equation, at outer edge situated at location $\bar{r} = 1$:

$$\begin{aligned} & \left[\frac{\bar{k}_1^2}{4} T_2 + \frac{\bar{k}_1}{2} (\nu + R_{11}) T_1 - \left(\frac{\bar{k}_1^2}{2} + \nu n^2 \right) J_n(\bar{k}_1) \right] C_1 \\ & + \left[\frac{\bar{k}_1^2}{4} U_2 + \frac{\bar{k}_1}{2} (\nu + R_{11}) U_1 - \left(\frac{\bar{k}_1^2}{2} + \nu n^2 \right) Y_n(\bar{k}_1) \right] C_2 \\ & + \left[\frac{\bar{k}_1^2}{4} V_2 + \frac{\bar{k}_1}{2} (\nu + R_{11}) V_1 + \left(\frac{\bar{k}_1^2}{2} - \nu n^2 \right) I_n(\bar{k}_1) \right] C_3 \\ & + \left[\frac{\bar{k}_1^2}{4} W_2 - \frac{\bar{k}_1}{2} (\nu + R_{11}) W_1 + \left(\frac{\bar{k}_1^2}{2} - \nu n^2 \right) K_n(\bar{k}_1) \right] C_4 = 0 \end{aligned} \quad (22)$$

where

$$\begin{aligned} T_1 &= J_{n-1}(\bar{k}_1) - J_{n+1}(\bar{k}_1); \quad U_1 = Y_{n-1}(\bar{k}_1) - Y_{n+1}(\bar{k}_1); \\ V_1 &= I_{n-1}(\bar{k}_1) + I_{n+1}(\bar{k}_1); \quad W_1 = K_{n-1}(\bar{k}_1) + K_{n+1}(\bar{k}_1); \\ T_2 &= J_{n-2}(\bar{k}_1) + J_{n+2}(\bar{k}_1); \quad U_2 = Y_{n-2}(\bar{k}_1) + Y_{n+2}(\bar{k}_1); \\ V_2 &= I_{n-2}(\bar{k}_1) + I_{n+2}(\bar{k}_1); \quad W_2 = K_{n-2}(\bar{k}_1) + K_{n+2}(\bar{k}_1); \end{aligned}$$

Similarly, substituting Eq. (5) in Eq. (14) yields the following equation, at the outer edge located at $\bar{r} = 1$:

$$\begin{aligned} & \left[\frac{\bar{k}_1^3}{8} T_3 + \frac{\bar{k}_1^2}{4} T_2 - \frac{\bar{k}_1}{2} \left(\frac{3}{4} \bar{k}_1^2 + n^2(2-\nu) + 1 \right) T_1 \right. \\ & \left. + \left(n^2(3-\nu) - \frac{\bar{k}_1^2}{2} - T_{11} \right) J_n(\bar{k}_1) \right] C_1 \\ & + \left[\frac{\bar{k}_1^3}{8} U_3 + \frac{\bar{k}_1^2}{4} U_2 - \frac{\bar{k}_1}{2} \left(\frac{3}{4} \bar{k}_1^2 + n^2(2-\nu) + 1 \right) U_1 \right. \\ & \left. + \left(n^2(3-\nu) - \frac{\bar{k}_1^2}{2} - T_{11} \right) Y_n(\bar{k}_1) \right] C_2 \\ & + \left[\frac{\bar{k}_1^3}{8} V_3 + \frac{\bar{k}_1^2}{4} V_2 + \frac{\bar{k}_1}{2} \left(\frac{3}{4} \bar{k}_1^2 + n^2(-2+\nu) - 1 \right) V_1 \right. \\ & \left. + \left(n^2(3-\nu) + \frac{\bar{k}_1^2}{2} - T_{11} \right) I_n(\bar{k}_1) \right] C_3 \\ & + \left[-\frac{\bar{k}_1^3}{8} W_3 + \frac{\bar{k}_1^2}{4} W_2 + \frac{\bar{k}_1}{2} \left(-\frac{3}{4} \bar{k}_1^2 + n^2(2-\nu) + 1 \right) W_1 \right. \\ & \left. + \left(n^2(3-\nu) + \frac{\bar{k}_1^2}{2} - T_{11} \right) K_n(\bar{k}_1) \right] C_4 = 0 \end{aligned} \quad (23)$$

where

$$\begin{aligned} T_1 &= J_{n-1}(\bar{k}_1) - J_{n+1}(\bar{k}_1); T_2 = J_{n-2}(\bar{k}_1) + J_{n+2}(\bar{k}_1); T_3 = J_{n-3}(\bar{k}_1) - J_{n+3}(\bar{k}_1); \\ U_1 &= Y_{n-1}(\bar{k}_1) - Y_{n+1}(\bar{k}_1); U_2 = Y_{n-2}(\bar{k}_1) + Y_{n+2}(\bar{k}_1); U_3 = Y_{n-3}(\bar{k}_1) - Y_{n+3}(\bar{k}_1); \\ V_1 &= I_{n-1}(\bar{k}_1) + I_{n+1}(\bar{k}_1); V_2 = I_{n-2}(\bar{k}_1) + I_{n+2}(\bar{k}_1); V_3 = I_{n-3}(\bar{k}_1) + I_{n+3}(\bar{k}_1); \\ W_1 &= K_{n-1}(\bar{k}_1) + K_{n+1}(\bar{k}_1); W_2 = K_{n-2}(\bar{k}_1) + K_{n+2}(\bar{k}_1); W_3 = K_{n-3}(\bar{k}_1) + K_{n+3}(\bar{k}_1); \\ T_3 &= J_{n-3}(\bar{k}_1) - J_{n+3}(\bar{k}_1); U_3 = Y_{n-3}(\bar{k}_1) - Y_{n+3}(\bar{k}_1); \\ V_3 &= I_{n-3}(\bar{k}_1) + I_{n+3}(\bar{k}_1); W_3 = K_{n-3}(\bar{k}_1) + K_{n+3}(\bar{k}_1); \end{aligned}$$

Substituting Eq. (5) in Eq. (19) yields the following equation, at inner edge located at $\bar{r} = b$:

$$\left[\frac{\bar{k}_1^2}{4} T_2' + \frac{\bar{k}_1}{2} \left(\frac{\nu}{b} - R_{22} \right) T_1' - \left(\frac{\bar{k}_1^2}{2} + \frac{\nu n^2}{b^2} \right) J_n(\bar{k}_1 b) \right] C_1$$

$$\begin{aligned} &+ \left(\frac{n^2(3-\nu)}{b^3} - \frac{\bar{k}_1^2}{2b} + T_{22} \right) Y_n(\bar{k}_1 b) \left] C_2 \right. \\ &+ \left[\frac{\bar{k}_1^3}{8} V_3' + \frac{\bar{k}_1^2}{4b} V_2' + \frac{\bar{k}_1}{2} \left(\frac{3}{4} \bar{k}_1^2 + n^2(-2+\nu) - 1 \right) V_1' \right. \\ &+ \left. \left(\frac{n^2(3-\nu)}{b^3} + \frac{\bar{k}_1^2}{2b} + T_{22} \right) I_n(\bar{k}_1 b) \right] C_1 \\ &+ \left[-\frac{\bar{k}_1^3}{8} W_3' + \frac{\bar{k}_1^2}{4b} W_2' + \frac{\kappa}{2} \left(-\frac{3}{4} \bar{k}_1^2 + n^2(2-\nu) + 1 \right) W_1' \right. \\ &+ \left. \left(\frac{n^2(3-\nu)}{b^3} + \frac{\bar{k}_1^2}{2b} + T_{22} \right) K_n(\bar{k}_1 b) \right] C_4 = 0 \end{aligned} \quad (25)$$

where

$$\begin{aligned} T_1' &= J_{n-1}(\bar{k}_1 b) - J_{n+1}(\bar{k}_1 b); T_2' = J_{n-2}(\bar{k}_1 b) + J_{n+2}(\bar{k}_1 b); T_3' = J_{n-3}(\bar{k}_1 b) - J_{n+3}(\bar{k}_1 b); \\ U_1' &= Y_{n-1}(\bar{k}_1 b) - Y_{n+1}(\bar{k}_1 b); U_2' = Y_{n-2}(\bar{k}_1 b) + Y_{n+2}(\bar{k}_1 b); U_3' = Y_{n-3}(\bar{k}_1 b) - Y_{n+3}(\bar{k}_1 b); \\ V_1' &= I_{n-1}(\bar{k}_1 b) + I_{n+1}(\bar{k}_1 b); V_2' = I_{n-2}(\bar{k}_1 b) + I_{n+2}(\bar{k}_1 b); V_3' = I_{n-3}(\bar{k}_1 b) + I_{n+3}(\bar{k}_1 b); \\ W_1' &= K_{n-1}(\bar{k}_1 b) + K_{n+1}(\bar{k}_1 b); W_2' = K_{n-2}(\bar{k}_1 b) + K_{n+2}(\bar{k}_1 b); W_3' = K_{n-3}(\bar{k}_1 b) + K_{n+3}(\bar{k}_1 b); \end{aligned}$$

$$\begin{aligned} &+ \left[\frac{\bar{k}_1^2}{4} U_2' + \frac{\bar{k}_1}{2} \left(\frac{\nu}{b} - R_{22} \right) U_1' - \left(\frac{\bar{k}_1^2}{2} + \frac{\nu n^2}{b^2} \right) Y_n(\bar{k}_1 b) \right] C_2 \\ &+ \left[\frac{\bar{k}_1^2}{4} V_2' + \frac{\bar{k}_1}{2} \left(\frac{\nu}{b} - R_{22} \right) V_1' + \left(\frac{\bar{k}_1^2}{2} - \frac{\nu n^2}{b^2} \right) I_n(\bar{k}_1 b) \right] C_3 \\ &+ \left[\frac{\kappa^2}{4} W_2' - \frac{\bar{k}_1}{2} \left(\frac{\nu}{b} - R_{22} \right) W_1' + \left(\frac{\bar{k}_1^2}{2} - \frac{\nu n^2}{b^2} \right) K_n(\bar{k}_1 b) \right] C_4 = 0 \end{aligned} \quad (24)$$

where

$$\begin{aligned} T_1' &= J_{n-1}(\bar{k}_1 b) - J_{n+1}(\bar{k}_1 b); U_1' = Y_{n-1}(\bar{k}_1 b) - Y_{n+1}(\bar{k}_1 b); \\ V_1' &= I_{n-1}(\bar{k}_1 b) + I_{n+1}(\bar{k}_1 b); W_1' = K_{n-1}(\bar{k}_1 b) + K_{n+1}(\bar{k}_1 b); \\ T_2' &= J_{n-2}(\bar{k}_1 b) + J_{n+2}(\bar{k}_1 b); U_2' = Y_{n-2}(\bar{k}_1 b) + Y_{n+2}(\bar{k}_1 b); \\ V_2' &= I_{n-2}(\bar{k}_1 b) + I_{n+2}(\bar{k}_1 b); W_2' = K_{n-2}(\bar{k}_1 b) + K_{n+2}(\bar{k}_1 b); \end{aligned}$$

Substituting Eq. (5) in Eq. (21) yields the following equation at the inner edge located at $\bar{r} = b$:

$$\begin{aligned} &\left[\frac{\bar{k}_1^3}{8} T_3' + \frac{\bar{k}_1^2}{4b} T_2' - \frac{\bar{k}_1}{2} \left(\frac{3}{4} \bar{k}_1^2 + n^2(2-\nu) + 1 \right) T_1' \right. \\ &+ \left. \left(\frac{n^2(3-\nu)}{b^3} - \frac{\bar{k}_1^2}{2b} + T_{22} \right) J_n(\bar{k}_1 b) \right] C_1 \\ &+ \left[\frac{\bar{k}_1^3}{8} U_3' + \frac{\bar{k}_1^2}{4b} U_2' - \frac{\bar{k}_1}{2} \left(\frac{3}{4} \bar{k}_1^2 + n^2(2-\nu) + 1 \right) U_1' \right. \end{aligned}$$

Let us define

$$\bar{k}_2 = (\bar{k}_1^4 + \xi^2)^{1/4} \quad (26)$$

where \bar{k}_1 is the non-dimensional frequency parameter without foundation and \bar{k}_2 is the non-dimensional frequency parameter with the inclusion of the effect of Winkler foundation. The boundary conditions used for this case have yielded the Eqs. (11), (13), (19) and (21) and the final set of equations to be solved for this case are therefore Eqs. (22)–(25) in combination with Eq. (26).

4. Method of solution

To obtain the values of natural frequencies for any given set of values of parameters such as n , ν , R_{11} , T_{11} , R_{22} , T_{22} and ξ , firstly the above-derived set of Eqs. (22)–(25) along with Eq. (26) are solved for getting non-trivial solutions by setting the resulting determinant of matrix of coefficients $[C]_{4 \times 4}$ to be equal to zero. All the above set of equations are coded accordingly in a computer program written in the well known Mathematica software with symbolic capabilities and the problem is solved repeatedly for various sets of values of the rotational restraint, translation restraint and other parameters such as n , ν , R_{11} , T_{11} , R_{22} , T_{22} and ξ . Root searching method is utilized in getting the real roots of the determinant for the given set of parameter values to obtain the corresponding values of natural

Table 1

Frequency parameter ($n=0$ mode) for different rotational stiffness parameters R_{11} , when $T_{11} = R_{22} = T_{22} = 100$ and $\xi = 10$ and $\nu = 0.3$.

R_{11}	$b=0.1$	$b=0.2$	$b=0.3$	$b=0.4$	$b=0.5$	$b=0.6$	$b=0.7$	$b=0.8$	$b=0.9$
0	3.63258	3.84745	4.05488	4.27604	4.52517	4.82115	5.19732	5.73715	6.76639
5	3.80489	4.00748	4.19703	4.39537	4.61716	4.88213	5.22794	5.74634	6.76727
10	3.85428	4.05362	4.23774	4.42886	4.64223	4.89851	5.23655	5.7494	6.76768
15	3.87769	4.07551	4.25699	4.44457	4.65389	4.90609	5.24061	5.75093	6.76793
20	3.89135	4.08828	4.26819	4.45368	4.66062	4.91047	5.24296	5.75185	6.76808
50	3.92017	4.11525	4.29179	4.47278	4.67466	4.91958	5.24792	5.75385	6.76847
100	3.93126	4.12562	4.30084	4.48007	4.68	4.92304	5.24982	5.75464	6.76865
500	3.94076	4.13451	4.30859	4.48629	4.68454	4.92599	5.25144	5.75533	6.76881
1000	3.94199	4.13566	4.30959	4.4871	4.68513	4.92637	5.25165	5.75542	6.76883
2000	3.94261	4.13624	4.31009	4.4875	4.68543	4.92656	5.25176	5.75547	6.76884
10000	3.94311	4.1367	4.3105	4.48783	4.68566	4.92671	5.25184	5.7555	6.76885
1.00E+17	3.94323	4.13682	4.3106	4.48791	4.68572	4.92675	5.25187	5.75551	6.76885

frequency parameters \bar{k}_1 and \bar{k}_2 . Various combinations of the restraint parameters are considered for analysis so that the range is sufficiently covered to yield useful results. One of the aims of this paper is to provide results useful for designing such circular plates with high accuracy. The results for the extreme cases of values of restraint parameters R_{11} , T_{11} , R_{22} , and T_{22} between zeros to infinity are obtained and the same are compared with the results for ideal boundary conditions such as simply supported, clamped and free and found to be in excellent agreement with ones available in the published literature. With this convergence checked thoroughly, we believe that the results presented in this paper are more exact and can therefore be utilized in designing such circular plates with combination of rotational and translation elastic restraints.

5. Presentation of results

For the purpose of present study, the Poisson's ratio is considered as $\nu=0.3$. The numerical results obtained are presented in both tabular and graphical form convenient for use in design. The variation of the non-dimensional frequency parameter with rotational constraint is presented in Table 1 for $n=0$ mode. It is calculated for different values of non-dimensional rotational spring stiffness parameters R_{11} , and non-dimensional radii. i.e., from $b=0.1$ to 0.9 by keeping T_{11} , R_{22} , T_{22} , and ξ constant. Figs. 2–4 show the effect of rotational spring stiffness parameter on frequency parameter for $n=0$, 1 and 2 modes. It is observed from the Figs. 2–4, that the frequency increases with increase in rotational spring stiffness parameter. However, it is observed that the influence of rotational spring stiffness parameter on the natural frequencies is comparatively less than that due to translational spring stiffness. For a given radius parameter $b=0.1$, the frequency parameter is increased by 8.55% for $n=0$, 5.15% for $n=1$ and 1% for $n=2$ modes when R_{11} increased from 0 to ∞ . Similarly for a given R_{11} (0 and ∞), the frequency parameter is increased by 86.27% and 71.66% for $n=0$, 65.53% and 57.46% for $n=1$ and 46.13% and 44.95% for $n=2$ mode respectively when b increased from 0.1 to 0.9. It is found that the $n=0$ axisymmetric mode gives the fundamental frequency. When $b=0$, the plate has full foundation support and the frequency is $\bar{k}_2=10.0056$. This is in excellent agreement with the results ($\bar{k}_2=10.00568$) presented by Bhaskara Rao and Kameswara Rao in Ref. [31]. Table 2, shows the comparison of results (for $R_{11}=20$, $T_{11}=R_{22}=T_{22}=100$ and $\xi=0$), with the values presented by Bhaskara Rao and Kameswara Rao in Ref. [32].

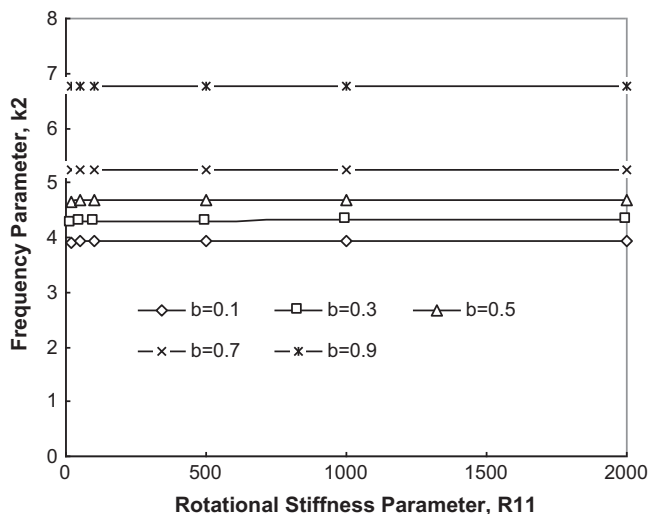


Fig. 2. Effect of non-dimensional rotational spring stiffness R_{11} , on frequency parameter for $T_{11}=R_{22}=T_{22}=100$, $\xi=10$ and $n=0$.

The variation of the non-dimensional frequency with translational spring stiffness parameter is presented in Table 3 for $n=0$ mode. It is calculated for different values of non-dimensional translational spring stiffness parameter T_{11} , and non-dimensional radii. i.e., from $b=0.1$ to 0.9 by keeping R_{11} , R_{22} , T_{22} , and ξ constant. The effect of translational spring stiffness parameter on frequency is plotted in Figs. 5–7 for $n=0$, 1 and 2. It is noticed from Figs. 5–7, that the frequency increases with increase in translational spring stiffness parameter. For a given radius parameter $b=0.1$, the frequency parameter is increased by 27.35% for $n=0$, 51.09% for $n=1$ and 64.24% for $n=2$ mode when T_{11} increased from 0 to ∞ . Similarly for

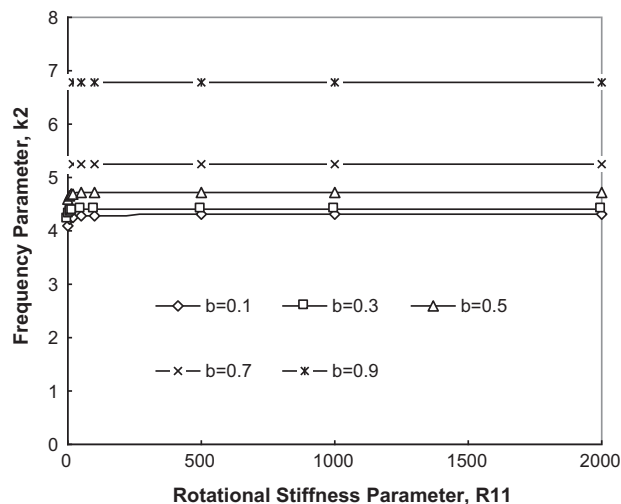


Fig. 3. Effect of non-dimensional rotational spring stiffness R_{11} , on Frequency Parameter for $T_{11}=R_{22}=T_{22}=100$, $\xi=10$ & $n=1$.

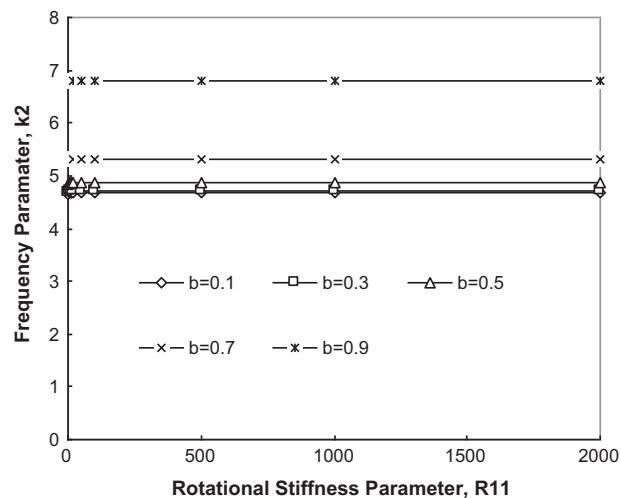


Fig. 4. Effect of non-dimensional rotational spring stiffness R_{11} , on frequency parameter for $T_{11}=R_{22}=T_{22}=100$, $\xi=10$ and $n=2$.

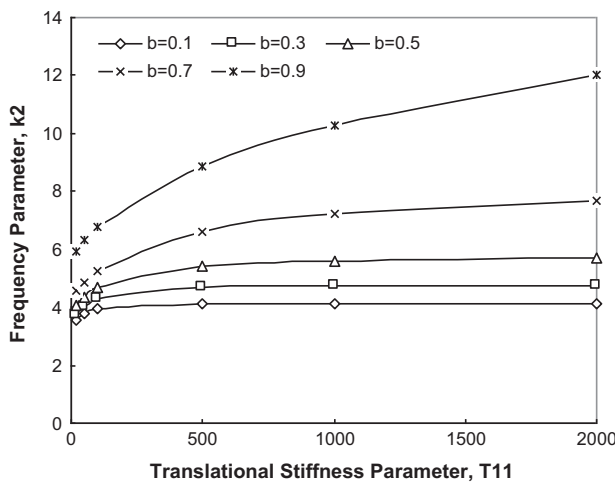
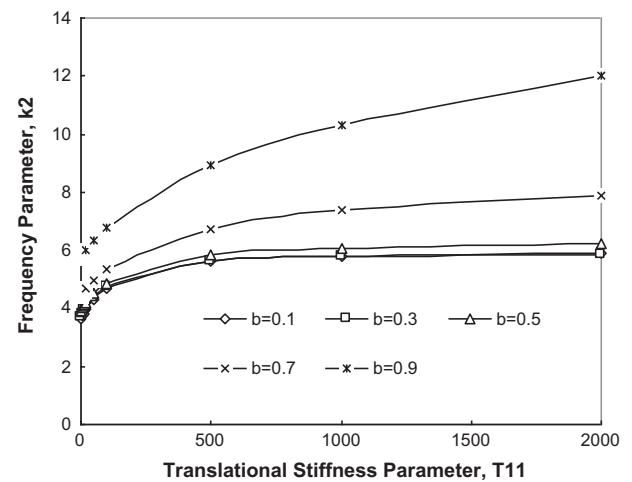
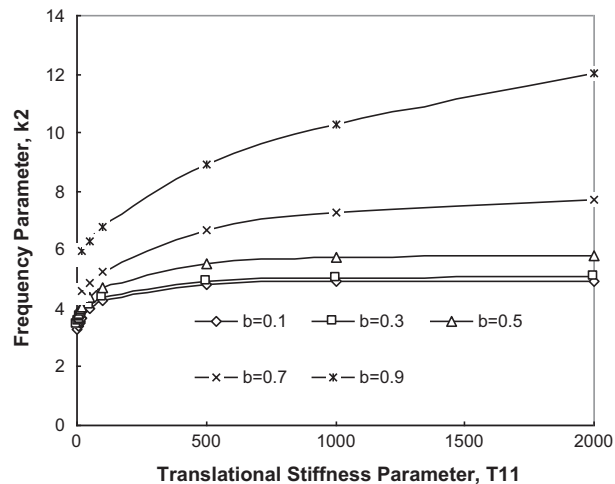
Table 2

Comparison of frequency parameter for $R_{11}=20$, $T_{11}=R_{22}=T_{22}=100$ and $\xi=0$.

b	Bhaskara Rao and Kameswara Rao [31]
0.1	3.3721
0.3	3.90231
0.5	4.39123
0.7	5.06017

Table 3Frequency parameter ($n=0$ mode) for different translational stiffness parameter T_{11} , when $R_{11}=R_{22}=T_{22}=100$ and $\xi=10$ and $\nu=0.3$.

T_{11}	$b=0.1$	$b=0.2$	$b=0.3$	$b=0.4$	$b=0.5$	$b=0.6$	$b=0.7$	$b=0.8$	$b=0.9$
0	3.25945	3.33815	3.44098	3.5829	3.77362	4.02115	4.34404	4.80796	5.68426
5	3.34418	3.42658	3.52876	3.66636	3.85014	4.0903	4.40805	4.8713	5.75497
10	3.41781	3.50478	3.60749	3.74231	3.9209	4.15529	4.46899	4.93212	5.82315
15	3.4822	3.57443	3.67859	3.81186	3.98666	4.21658	4.52717	4.99065	5.88899
20	3.53878	3.63682	3.74316	3.87586	4.04802	4.27454	4.58283	5.04706	5.95267
50	3.7658	3.90366	4.03252	4.17484	4.34673	4.5682	4.87433	5.34908	6.29712
100	3.93126	4.12562	4.30084	4.48007	4.68	4.92304	5.24982	5.75464	6.76865
500	4.10705	4.39444	4.68777	5.02522	5.44109	5.96746	6.62394	7.46605	8.8894
1000	4.12919	4.42907	4.74195	5.11503	5.60356	6.28449	7.23442	8.47348	10.3016
2000	4.14008	4.44594	4.76834	5.1594	5.68758	6.46844	7.68424	9.48856	12.0056
10000	4.14868	4.45917	4.78897	5.19419	5.75453	6.62279	8.12828	11.0338	16.6507
1.00E+16	4.15081	4.46244	4.79405	5.20275	5.77108	6.66164	8.24751	11.5861	21.4874

**Fig. 5.** Effect of non-dimensional translational spring stiffness parameter T_{11} , on frequency parameter for $R_{11}=R_{22}=T_{22}=100$, $\xi=10$ and $n=0$.**Fig. 7.** Effect of non-dimensional translational spring stiffness parameter T_{11} , on frequency parameter for $R_{11}=R_{22}=T_{22}=100$, $\xi=10$ and $n=2$.**Fig. 6.** Effect of non-dimensional translational spring stiffness parameter T_{11} , on frequency parameter for $R_{11}=R_{22}=T_{22}=100$, $\xi=10$ and $n=1$.

a given T_{11} (0 and ∞), the frequency parameter is increased by 74.39% and 417.66% for $n=0$, 72.35% and 331.26% for $n=1$ and 56.87% and 260.08% for $n=2$ mode respectively when b increased from 0.1 to 0.9. It is observed from Figs. 2–4 and 5–7, that in the former case, the higher values of frequencies are recorded at lower values of R_{11} , but in the latter case, lower values of frequency parameters are observed at lower values of T_{11} . Therefore, it is observed from the above, that the influence of T_{11} is relatively more

than that of R_{11} on frequency parameter. It was found that the $n=0$ axisymmetric mode gives the fundamental frequency. When $b=0$, the plate has full foundation support and the frequency is $\bar{k}_2=10$. This is in excellent agreement with the results ($\bar{k}_2=10$) presented by Bhaskara Rao and Kameswara Rao in Ref. [31].

The variation of the non-dimensional frequency with foundation constraint is presented in Table 4 for $n=0$ mode. It is calculated for different values of non-dimensional foundation stiffness parameter ξ , and non-dimensional radii, i.e., from $b=0.1$ to 0.9 by keeping R_{11} , T_{11} , R_{22} and T_{22} constant for $n=0, 1$ and 2 modes. It is observed from Figs. 8–10, the frequency increases with increase in foundation stiffness parameter. For a given radius parameter, the frequency increases with increase in foundation stiffness parameter. For a given radius parameter $b=0.1$, the frequency parameter is increased by 192.32% for $n=0$, 155.74% for $n=1$ and 128.48% for $n=2$ modes when ξ increased from 0 to 100. Similarly for a given ξ (0 and 100), the frequency parameter increased by 94.79% and 4.3% for $n=0$, 70% and 4% for $n=1$ and 51.86% and 3.75% for $n=2$ mode respectively when b increased from 0.1 to 0.9. As observed from Figs. 2–4, 5–7 and 8–10, the influence of foundation constraint is more on the frequency when compared to rotational and translational constraints. It was found that the $n=0$ axisymmetric mode gives the fundamental frequency. When $b=0$, the plate has full foundation support and the frequency is $\bar{k}_2=2.94751$. This is in excellent agreement with the results ($\bar{k}_2=2.94751$) presented by Bhaskara Rao and Kameswara Rao in Ref. [31].

The variation of the non-dimensional frequency with rotational, translational and foundation constraints is presented in

Table 4Frequency ($n = 0$ mode) for different foundation stiffness parameters ξ , when $T_{11} = R_{11} = R_{22} = T_{22} = 100$ and $\nu = 0.3$.

ξ	$b=0.1$	$b=0.2$	$b=0.3$	$b=0.4$	$b=0.5$	$b=0.6$	$b=0.7$	$b=0.8$	$b=0.9$
0	3.43271	3.71125	3.94476	4.17163	4.41432	4.69863	5.06778	5.61871	6.68655
2.5	3.47071	3.74145	3.96997	4.19298	4.43238	4.71362	5.07974	5.6275	6.69177
5	3.57777	3.8279	4.04285	4.25517	4.48526	4.75776	5.11513	5.65362	6.70735
7.5	3.73736	3.96017	4.15622	4.35314	4.56944	4.8287	5.17254	5.69637	6.7331
10	3.93126	4.12562	4.30084	4.48007	4.68	4.92304	5.24982	5.75464	6.76865
12.5	4.1447	4.31276	4.46765	4.62888	4.81154	5.03689	5.34442	5.82705	6.81354
15	4.36748	4.51269	4.64904	4.79321	4.95893	5.16632	5.45362	5.91205	6.86724
17.5	4.59319	4.71912	4.8392	4.96788	5.11771	5.30771	5.57476	6.00798	6.92912
20	4.818	4.92787	5.03395	5.14891	5.28426	5.45795	5.70537	6.11326	6.99852
50	7.16727	7.20155	7.2364	7.27612	7.3255	7.39305	7.49735	7.68977	8.1899
100	10.0345	10.0471	10.06	10.0749	10.0936	10.1197	10.161	10.2404	10.4661
500	22.3638	22.3649	22.3661	22.3674	22.3692	22.3716	22.3754	22.3829	22.4052
1000	31.6239	31.6243	31.6247	31.6252	31.6258	31.6266	31.628	31.6307	31.6386
2000	44.7217	44.7219	44.722	44.7222	44.7224	44.7227	44.7232	44.7241	44.7269
10000	100	100	100	100	100	100	100	100	100
1.00E+17	1.00E+08	1.00E+08	1.00E+08	1.00E+08	1.00E+08	1.00E+08	1.00E+08	1.00E+08	1.00E+08

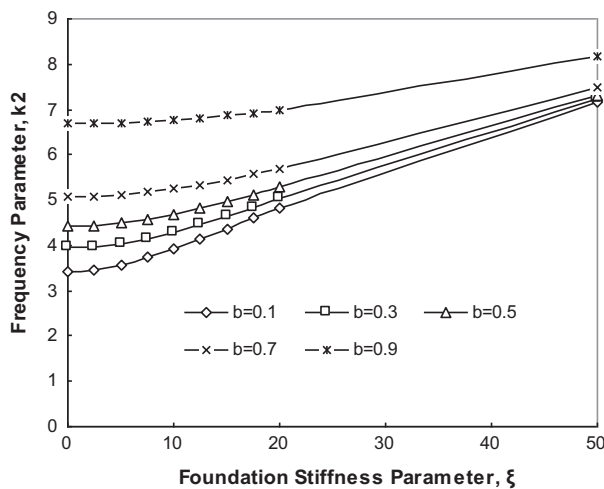
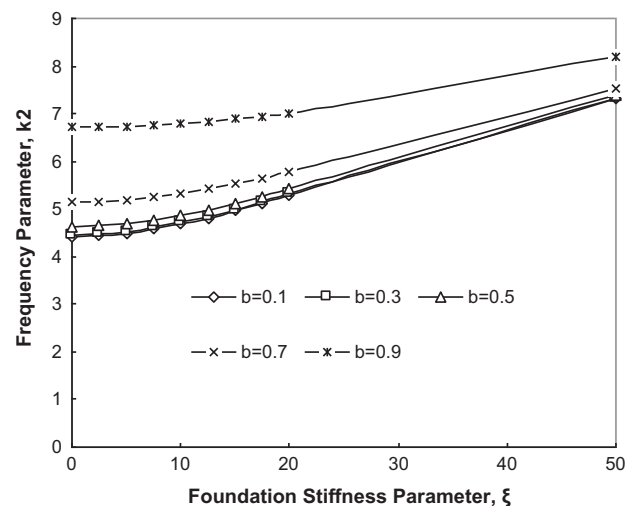
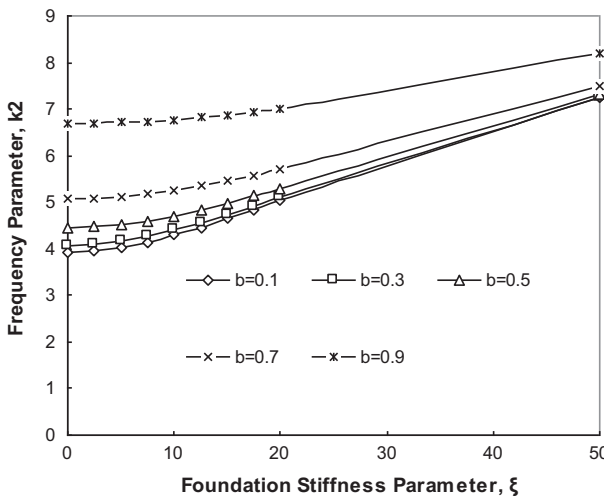
**Fig. 8.** Effect of non-dimensional foundation stiffness ξ , on frequency parameter for $R_{11} = T_{11} = R_{22} = T_{22} = 100$ and $n = 0$.**Fig. 10.** Effect of non-dimensional foundation stiffness ξ , on frequency parameter for $R_{11} = T_{11} = R_{22} = T_{22} = 100$ and $n = 2$.**Fig. 9.** Effect of non-dimensional foundation stiffness ξ , on frequency parameter for $R_{11} = T_{11} = R_{22} = T_{22} = 100$ and $n = 1$.

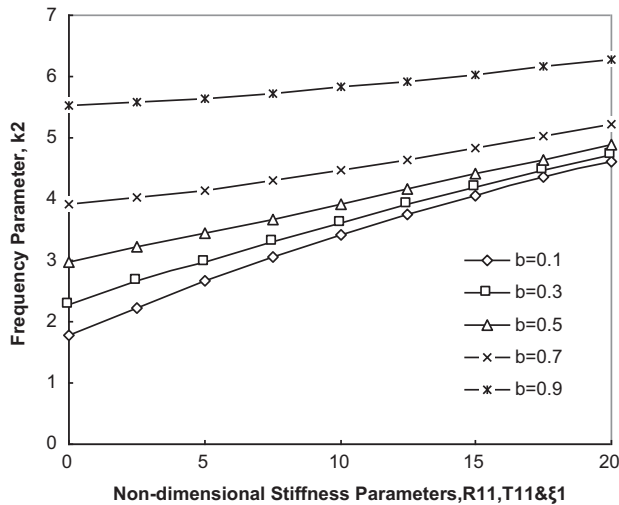
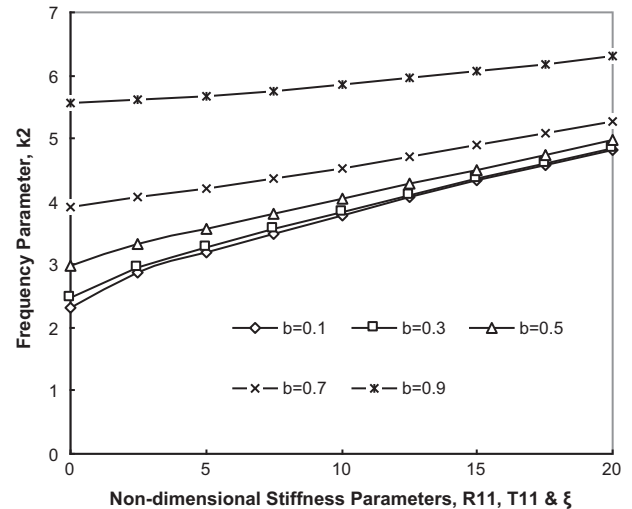
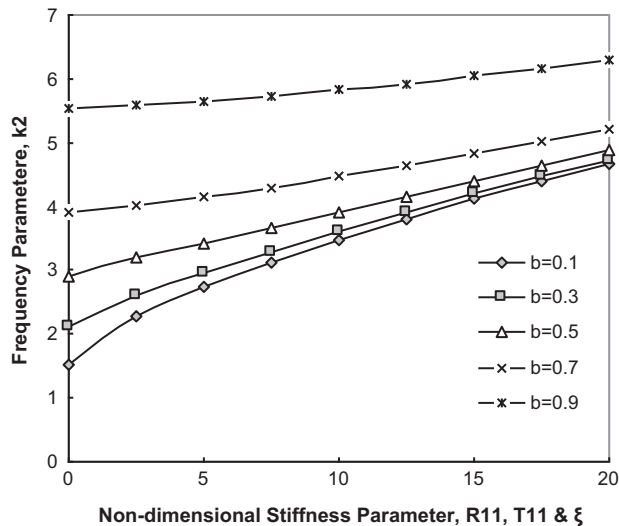
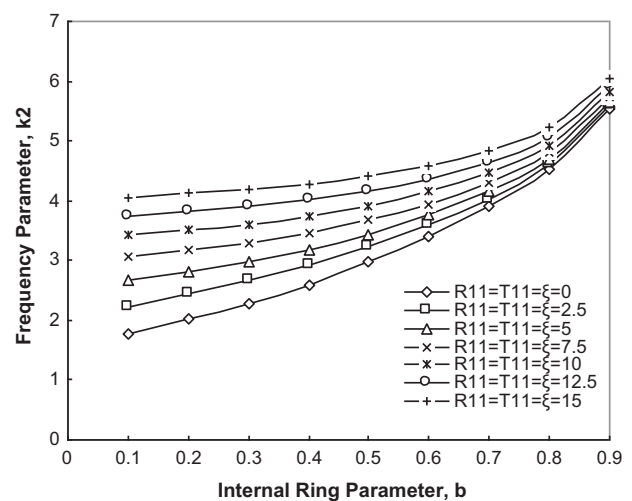
Table 5 for $n = 0$ mode. It is calculated for different values of non-dimensional rotational, translational, foundation constraints, and non-dimensional radii. i.e., from $b = 0.1$ to 0.9 by keeping R_{22} and T_{22} constant for $n = 0, 1$ and 2 modes. In Figs. 11–13, the effect of the three elastic constraints on frequency has been

plotted and it is observed that the frequency increases with increase in the three elastic constraints. It is also shown frequency versus internal radius parameter in Fig. 14. For a given radius parameter $b = 0.1$, the frequency parameter is increased by 161.19% for $n = 0$, 206.14% for $n = 1$ and 107.8% for $n = 2$ modes when R_{11} , T_{11} and ξ increased from 0 to 20. Similarly for a given R_{11} , T_{11} and ξ (0 and 20), the frequency parameter is increased by 212.93% and 35.87% for $n = 0$, 263% and 34.51% for $n = 1$ and 139.24% and 30.53% for $n = 2$ mode respectively when b increased from 0.1 to 0.9. It was found that the $n = 0$ axisymmetric mode gives the fundamental. When $b = 0$, the plate has full foundation support and the frequency is $k_2 = 0.211466$. This is in excellent agreement with the results ($k_2 = 0.211466$) presented by Bhaskara Rao and Kameswara Rao in Ref. [31]. Figs. 2–4, 5–7, 8–10, and 11–13 depict the variation of frequency as a function of the non-dimensional spring parameters i.e., both rotational and translational at inner and outer periphery of the annular plate and elastic foundation parameter.

The variation of the non-dimensional frequency parameter with rotational constraint R_{22} , is presented in Table 6 for $n = 0$ mode. It is calculated for different values of non-dimensional rotational spring stiffness parameters R_{22} , and non-dimensional radii. i.e., from $b = 0.1$ to 0.9 by keeping R_{11} , T_{11} , T_{22} , & ξ constant for $n = 0, 1$ and 2 modes. Figs. 15–17 show the effect of rotational spring stiffness parameter on frequency parameter for $n = 0, 1$ and 2 modes. It is

Table 5Frequency ($n=0$ mode) for different rotational R_{11} , translational T_{11} , and foundation ξ , stiffness parameters when $R_{22} = T_{22} = 100$ and $\nu = 0.3$.

R_{11}, T_{11} & ξ	$b=0.1$	$b=0.2$	$b=0.3$	$b=0.4$	$b=0.5$	$b=0.6$	$b=0.7$	$b=0.8$	$b=0.9$
0	1.76955	2.02461	2.28783	2.59986	2.97468	3.41419	3.91811	4.53447	5.53745
2.5	2.23244	2.43938	2.65666	2.91404	3.22274	3.58906	4.02777	4.60166	5.58666
5	2.65932	2.80828	2.9742	3.18014	3.43748	3.7547	4.15021	4.69005	5.65138
7.5	3.05508	3.16621	3.29371	3.45733	3.66964	3.94209	4.2962	4.79985	5.73031
10	3.41743	3.50455	3.6055	3.73744	3.9133	4.14667	4.46175	4.92784	5.82182
12.5	3.75083	3.82204	3.90451	4.01317	4.16054	4.36122	4.64106	5.07014	5.92418
15	4.06014	4.1203	4.18954	4.28091	4.40616	4.58005	4.82904	5.22313	6.03568
17.5	4.34941	4.40154	4.46101	4.53932	4.6473	4.79934	5.02179	5.38367	6.15471
20	4.62181	4.6679	4.71995	4.78817	4.88251	5.01671	5.21651	5.54926	6.27984

**Fig. 11.** Effect of non-dimensional rotational R_{11} , translational T_{11} , and foundation ξ , stiffness parameters on frequency parameter for $R_{22} = T_{22} = 100$ and $n=0$.**Fig. 13.** Effect of non-dimensional rotational R_{11} , Translational T_{11} , and foundation ξ , stiffness parameters on frequency parameter for $R_{22} = T_{22} = 100$ and $n=2$.**Fig. 12.** Effect of non-dimensional rotational R_{11} , translational T_{11} , and foundation ξ , stiffness parameters on frequency parameter for $R_{22} = T_{22} = 100$ and $n=1$.**Fig. 14.** Effect of non-dimensional rotational stiffness R_{11} , translational stiffness T_{11} , and foundation stiffness ξ , parameters on frequency parameter for $R_{22} = T_{22} = 100$ and $n=0$.

observed from Figs. 15–17 that the frequency increases with increase in rotational spring stiffness parameter. However, it is observed that the influence of rotational spring stiffness parameter is very less. For a given radius parameter $b=0.1$, the frequency parameter is increased by 0.09% for $n=0$, 2.47% for $n=1$ and 0.36% for $n=2$ modes when R_{22} increased from 0 to ∞ . Similarly for a given R_{22} (0 and ∞), the frequency parameter is increased by 72.27% and 72.17% for $n=0$, 61.13% and 57.27% for $n=1$ and 45.4% and 44.89% for $n=2$ mode respectively when b increased from 0.1 to 0.9. It was

found that the $n=0$ axisymmetric mode gives the fundamental frequency.

The variation of the non-dimensional frequency with translational spring stiffness parameter T_{22} is presented in Table 7 for $n=0$ mode. It is calculated for different values of non-dimensional translational spring stiffness parameter T_{22} , and non-dimensional radii. i.e., from $b=0.1$ to 0.9 by keeping R_{11} , R_{22} , T_{11} , and ξ constant. The effect of translational spring stiffness parameter on frequency is plotted in Figs. 18–20 for $n=0$, 1 and 2 modes. It is

Table 6
Frequency ($n = 0$ mode) for different rotational stiffness parameters R_{22} , when $R_{11} = T_{11} = T_{22} = 100$, $\xi = 10$ and $\nu = 0.3$.

R_{22}	$b=0.1$	$b=0.2$	$b=0.3$	$b=0.4$	$b=0.5$	$b=0.6$	$b=0.7$	$b=0.8$	$b=0.9$
0	3.92815	4.11186	4.2803	4.45695	4.65683	4.90211	5.23425	5.74694	6.76718
5	3.92939	4.1185	4.29092	4.46938	4.66965	4.91388	5.24286	5.75082	6.76773
10	3.92996	4.12099	4.29454	4.47338	4.67359	4.9174	5.24551	5.75219	6.768
15	3.93029	4.12229	4.29637	4.47535	4.67551	4.9191	5.24679	5.75289	6.76816
20	3.93051	4.12309	4.29747	4.47653	4.67664	4.9201	5.24755	5.75332	6.76827
50	3.93103	4.12489	4.29988	4.47907	4.67906	4.92222	5.24918	5.75426	6.76853
100	3.93126	4.12562	4.30084	4.48007	4.68	4.92304	5.24982	5.75464	6.76865
500	3.93147	4.12627	4.30168	4.48094	4.68081	4.92375	5.25037	5.75497	6.76875
1000	3.9315	4.12636	4.30179	4.48105	4.68092	4.92384	5.25044	5.75502	6.76877
2000	3.93152	4.1264	4.30185	4.48111	4.68097	4.92389	5.25047	5.75504	6.76878
10000	3.93153	4.12643	4.30189	4.48115	4.68101	4.92393	5.2505	5.75506	6.76878
1.00E+16	3.93153	4.12644	4.3019	4.48116	4.68102	4.92394	5.25051	5.75506	6.76878

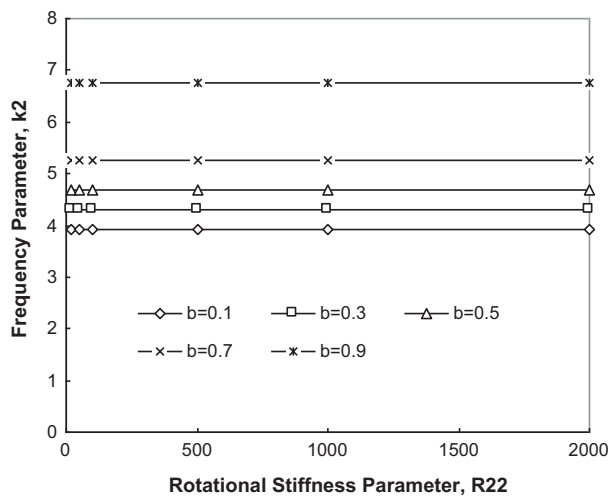


Fig. 15. Effect of non-dimensional rotational spring stiffness R_{22} , on frequency parameter for $R_{11} = T_{11} = T_{22} = 100$, $\xi = 10$ and $n = 0$.

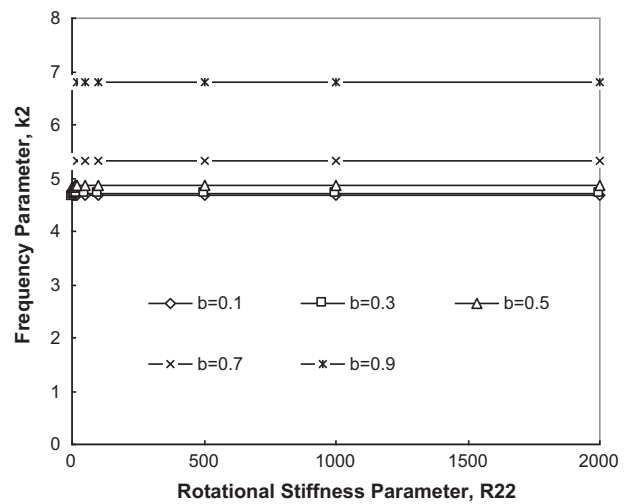


Fig. 17. Effect of non-dimensional rotational spring stiffness R_{22} , on frequency parameter for $R_{11} = T_{11} = T_{22} = 100$, $\xi = 10$ and $n = 2$.

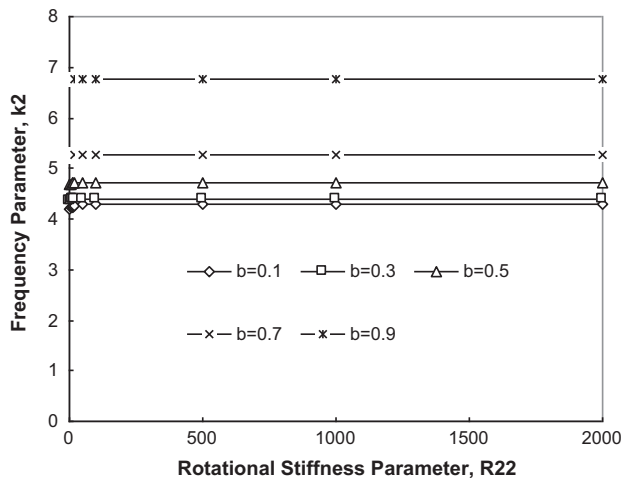


Fig. 16. Effect of non-dimensional rotational spring stiffness R_{22} , on frequency parameter for $R_{11} = T_{11} = T_{22} = 100$, $\xi = 10$ and $n = 1$.

noticed from Figs. 18–20, that the frequency increases with increase in translational spring stiffness parameter. It was found that the $n = 0$ axisymmetric mode gives the fundamental frequency. For a given radius parameter $b = 0.1$, the frequency parameter is increased by 20.84% for $n = 0$, 3.99% for $n = 1$ and 0.6% for $n = 2$ modes when T_{22} increased from 0 to ∞ . Similarly for a given T_{22} (0 and ∞), the frequency parameter is increased by 58.93% and 376.52% for $n = 0$, 36.1% and 374.02% for $n = 1$ and

25.1% and 348.91% for $n = 2$ mode respectively when b increased from 0.1 to 0.9.

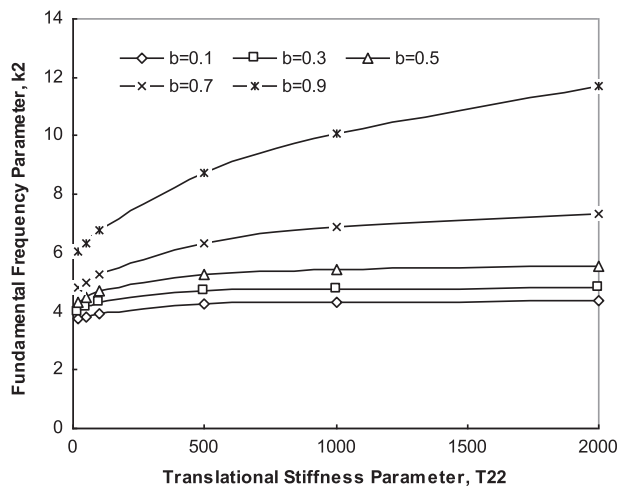
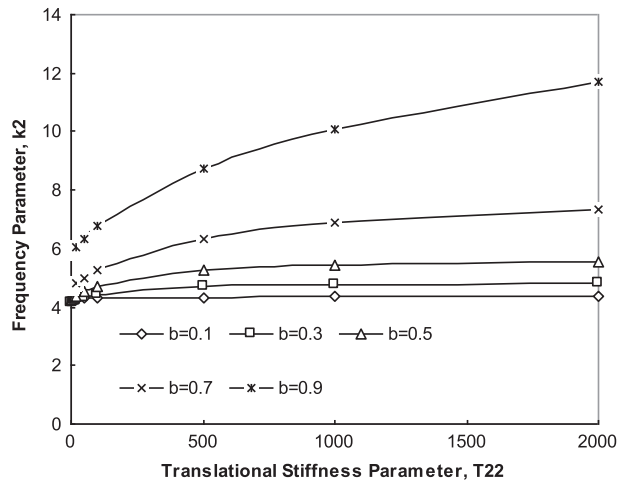
It is observed from the above discussion that the influence of foundation stiffness parameter is more on frequency than that of rotational and translational stiffness parameters at inner and outer edges R_{11} , R_{22} , T_{11} and T_{22} . In addition, it observed that the influence of translational stiffness parameters is more on frequency than that of rotational stiffness parameters R_{11} and R_{22} . It also noticed that the influence of elastic constraints at outer edge R_{11} and T_{11} , on frequency is more predominant than that of elastic constraints at inner edge R_{22} and T_{22} .

An investigation on the effect of Poisson's ratio, on the frequency is also studied. Each of the equations is reevaluated for values of Poisson's ratio between 0 and 0.5, and no significant variation is observed. However, natural frequencies of two cases are determined to confirm the validation of certain results. Table 8, shows a comparison of results, in the case where both boundaries of the plate are rigidly clamped with the values obtained by Leissa [1], Avalos et al. [16]) and Amabili et al. [22]. However, in the reference (Avalos et al. [16]), the results were obtained by the approximate method.

Table 9, deals with the case where the inner boundary of the plate is simply supported and the outer boundary are rigidly clamped. Present results are compared with the results obtained by Leissa [1] and Avalos et al. [16] where in Poisson's ratio is considered as $\nu = 1/3$. Also, the results are in good agreement with the results obtained by Amabili et al. [22] for the following two cases. (i) Annular plate with outer clamped edge and inner free

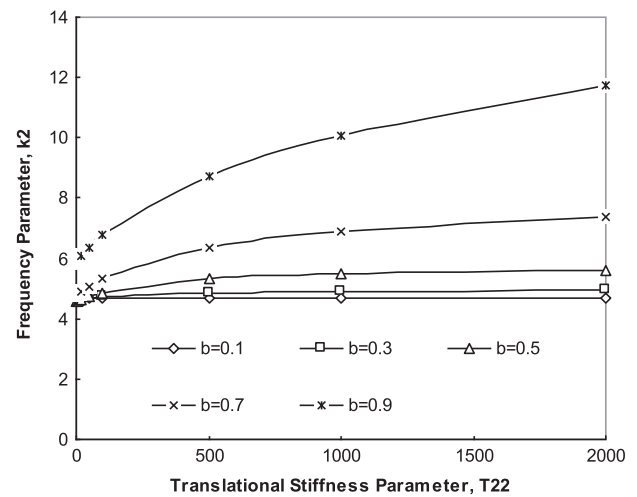
Table 7Frequency ($n = 0$ mode) for different translational stiffness parameters T_{22} when $R_{11} = R_{22} = T_{11} = 100$ and $\xi = 10$ and $\nu = 0.3$.

T_{22}	$b=0.1$	$b=0.2$	$b=0.3$	$b=0.4$	$b=0.5$	$b=0.6$	$b=0.7$	$b=0.8$	$b=0.9$
0	3.66318	3.73218	3.84143	3.98742	4.16619	4.37874	4.64501	5.03547	5.82194
5	3.68156	3.76209	3.87708	4.02468	4.20296	4.41524	4.68353	5.08024	5.88141
10	3.69925	3.79047	3.9108	4.06002	4.23809	4.45039	4.72087	5.12377	5.93911
15	3.7163	3.81743	3.94272	4.09359	4.27168	4.4843	4.75711	5.16611	5.99515
20	3.73274	3.84307	3.97298	4.1255	4.30384	4.51703	4.79232	5.20736	6.04965
50	3.81994	3.97338	4.12543	4.28801	4.47143	4.69216	4.98464	5.43465	6.34889
100	3.93126	4.12562	4.30084	4.48007	4.68	4.92304	5.24982	5.75464	6.76865
500	4.24848	4.46954	4.68681	4.94135	5.27003	5.71987	6.34349	7.22232	8.73899
1000	4.33208	4.54037	4.76481	5.04475	5.43192	6.00926	6.88341	8.13689	10.0868
2000	4.37837	4.57721	4.80527	5.09989	5.52379	6.19455	7.31088	9.08465	11.7285
10000	4.41683	4.6069	4.83787	5.14493	5.60137	6.36261	7.77088	10.6049	16.2457
1.00E+16	4.42655	4.61431	4.846	5.15625	5.62117	6.40691	7.90275	11.19	21.0936

**Fig. 18.** Effect of non-dimensional translational spring stiffness parameter T_{22} , on natural frequency for $R_{11} = R_{22} = T_{11} = 100$, $\xi = 10$ and $n = 0$.**Fig. 19.** Effect of non-dimensional translational spring stiffness parameter T_{22} , on natural frequency for $R_{11} = R_{22} = T_{11} = 100$, $\xi = 10$ and $n = 1$.

edge as shown in Table 10. (ii) Annular plate with both edges free is shown in Table 11.

It is observed that, the influence of translational stiffness parameter on frequency is more predominant than that of rotational stiffness parameter. In addition, it is observed that the influence of foundation parameter on frequency is more predominant than that of translational or rotational parameters. It is also noticed that the influence of elastic constraints at outer edge R_{11} and T_{11} , on frequency is more predominant than that of elastic

**Fig. 20.** Effect of non-dimensional translational spring stiffness parameter T_{22} , on natural frequency for $R_{11} = R_{22} = T_{11} = 100$, $\xi = 10$ and $n = 2$.**Table 8**

Comparison of frequency parameters when both the boundaries of the plate are rigidly clamped.

b	Present	Leissa [1]	Avalos et al. [16]	Amabili et al. [22]
0.1	27.280	27.3	27.67	27.280
0.3	45.346	45.2	45.37	45.346
0.5	89.250	89.2	89.31	89.250
0.7	248.399	248	248.9	248.40

Table 9

Comparison of frequency parameters when both the inner boundary of the plate is simply supported and outer boundary of the plate is rigidly clamped.

b	Present	Leissa [1]	Avalos et al. [16]
0.1	22.595	22.58	22.83
0.3	33.663	33.66	33.66
0.5	63.977	64	63.94

Table 10

Comparison of frequency parameters when outer boundary is clamped and inner boundary is free.

b	0	0.1	0.3	0.5	0.7
Present work	3.19622	3.18736	3.37991	4.20886	6.56827
Amabili et al. [22]	3.19622	3.18736	3.37991	4.20886	6.56828

Table 11
Comparison of frequency parameters when both edges free ends.

b	0	0.1	0.3	0.5	0.7
Present Work	3.00052	2.96219	2.89024	3.0518	3.62809
Amabili, M et al. [22]	3.00052	2.96219	2.89024	3.05180	3.62809

constraints at inner edge R_{22} and T_{22} . An investigation on the effect of Poisson's ratio, on the frequency is studied. Each of the equations is reevaluated for values of Poisson's ratio between 0 and 0.5, and no significant variation is observed. The wide range of values could be potentially used in vibration control and structural design.

6. Conclusions

In this paper, an exact solution to the problem of free vibration of annular plates with inner and outer edges and resting on elastic foundation is presented. The frequencies for the first three modes of plate vibration are given for various values of rotational and translational spring stiffness parameters [R_{11} , R_{22} , T_{11} , T_{22} and ξ] at the edges that simulate the rotational and translational restraints where $R_{11} \rightarrow \infty$ and $T_{11} \rightarrow \infty$ and $R_{22} \rightarrow \infty$ and $T_{22} \rightarrow \infty$ represents a clamped edge. Two-dimensional plots are drawn for a wide range of rotational, translational restraints and foundation restraint. Presented here is the influence of parameters on the first three frequencies of vibration. Also, the percentage increase in the fundamental as well as higher mode frequency parameters with rotational, translational and foundation restraints are calculated and presented in graphical form for use in design as well for understanding the trends. However, it is observed that the influence of foundation stiffness parameter on fundamental as well as higher mode frequency parameters is much more predominant than that of rotational and translational spring stiffness parameters. In this paper, the characteristic solutions are derived in an exact manner and hence, the results can be obtained to any desired accuracy. The results presented in this paper can also serve as benchmark solutions, which can be used to check the accuracy of approximate methods of solutions for their convergence. The tabulated frequency results are useful for designers working in the area of vibration control and structural design applications.

References

- [1] Leissa AW. Vibration of plates, SP-160. Washington, DC: US Government Printing Office; 1969.
- [2] Kim CS, Dickinson SM. On the lateral vibration of thin annular and circular composite plates subject to certain complicating effects. *J Sound Vib* 1989;130:363–77.
- [3] Kim CS, Dickinson SM. The flexural vibration of the isotropic and polar orthotropic annular and circular plates with elastically restrained peripheries. *J Sound Vib* 1990;143:171–9.
- [4] Wang X, Striz AG, Bert CW. Free vibration analysis of annular plates by the DQ method. *J Sound Vib* 1993;164:173–5.
- [5] Larrando H, Topalian V, Avalor DR, Laura PAA. Comments on free vibration analysis of annular plates by the DQ method. *J Sound Vib* 1994;177:137–9.
- [6] Liu CF, Chen GT. A simple finite element analysis of axisymmetric vibration of annular and circular plates. *Int J Mech Sci* 1995;8:861–71.
- [7] Romanelli E, Rossi RE, Laura PAA, Gutierrez RH. Transverse vibrations of a circular annular plate with an intermediate circular support and a free inner edge. *J Sound Vib* 1997;212(3):564–71.
- [8] Vera SA, Sanchez MD, Laura PAA, Vega DA. Transverse vibrations of circular, annular plates with several combinations of boundary conditions. *J Sound Vib* 1998;213(4):757–62.
- [9] Vera SA, Laura PAA, Vega DA. Transverse vibrations of a free-free circular annular plate. *J Sound Vib* 1999;224(2):379–83.
- [10] Vega DA, Vera SA, Laura PAA, Gutierrez RH, Pronato ME. Transverse vibrations of an annular circular plate with free edges and an intermediate concentric circular support. *J Sound Vib* 1999;223(3):493–6.
- [11] Laura PAA, Gutierrez RH, Rossi RE. Transverse vibration of a circular, annular plate with free edges and two, intermediate concentric circular supports. *J Sound Vib* 1999;226(5):1043–7.
- [12] Wang CY. Vibration of an annular membrane attached to a free, rigid core. *J Sound Vib* 2003;260:776–82.
- [13] Wang CY, Wang CM. Examination of the fundamental frequencies of annular plates with small core. *J Sound Vib* 2005;280:1116–24.
- [14] Celep Z, Turhan D. Axisymmetric vibrations of circular plates on tensionless elastic foundation. *J Appl Mech—Trans ASME* 1990;57:677–81.
- [15] Utku M, Citipitiglu E, Inceleme I. Circular plates on elastic foundation modelled with annular plates. *Comput Struct* 2000;78:365–74.
- [16] Avalos D, Laura PAA, Bianchi AM. Analytical and experimental investigation on vibrating circular plate with stepped thickness over a concentric circular region. *J Acoust Soc Am* 1987;82(1):13–6.
- [17] Singh RP, Jain SK. Free asymmetric transverse vibration of parabolically varying thickness polar orthotropic annular plate with flexible edge conditions. *Tamkang J Sci Eng* 2004;7(1):41–52.
- [18] Singh RP, Jain SK. Free asymmetric transverse vibration of polar orthotropic annular sector plate with thickness varying parabolically in radial direction. *Sadhana* 2004;29(5):415–28.
- [19] Gupta AP, Bhargadwaj N. Free vibration of polar orthotropic circular plates of quadratically varying thickness resting on elastic foundation. *Appl Math Model* 2005;29:137–57.
- [20] Hsu MH. Vibration analysis of annular plates using the modified generalized differential quadrature method. *J Appl Sci* 2006;6(7):1591–5.
- [21] Hsu MH. Vibration analysis of annular plates. *Tamkang J Sci Eng* 2007;10(3):193–9.
- [22] Amabili M, Frosali G, Kwak MK. Free vibrations of annular plates coupled with fluids. *J Sound Vib* 1996;191(5):825–46.
- [23] Wang CY, Wang CM. Buckling of circular plates with an internal ring support and elastically restrained edges. *Thin Wall Struct* 2001;39:821–5.
- [24] Vera SA, Febbo M, Rossit CA, Dolinko AE. Transverse vibrations of circular annular plates with edges elastically restrained against rotation, used in acoustic underwater transducers. *Ocean Eng* 2002;29:1201–8.
- [25] Civaletk Ö, Ülker M. Harmonic differential quadrature (HDQ) for axisymmetric bending analysis of thin isotropic circular plates. *Struct Eng Mech* 2004;17(1):1–14.
- [26] Kukla S, Szewczyk M. Application of Green's function method in frequency analysis of axisymmetric vibration of annular plates with elastic ring supports. *Sci Res Inst Math Comput Sci* 2005;1(4):79–86.
- [27] Kukla S, Szewczyk M. Free vibration of annular and circular plates of stepped thickness-application of Green's function method. *Sci Res Inst Math Comput Sci* 2006;1(5):46–54.
- [28] Kukla S, Szewczyk M. Frequency analysis of annular plates with elastic concentric supports by using a Green's function method. *J Sound Vib* 2007;300(1–2):387–93.
- [29] Kukla S, Szewczyk M. Free vibration of annular plates of stepped thickness resting on Winkler elastic foundation. *Sci Res Inst Math Comput Sci* 2007;1(6):109–16.
- [30] Lokavarapu Bhaskara Rao, Chellapilla Kameswara Rao. Fundamental buckling of annular plates with elastically restrained guided edges against translation. *Mech Based Des Struct* 2011;39(4):409–19.
- [31] Bhaskara Rao L, Kameswara Rao C. Frequency analysis of annular plate with internal and external elastically restrained edge. In: Proceedings of international conference on advances in machine design and industry automation. Pune, India; 2007. p. 171–175.
- [32] Bhaskara Rao L, Kameswara Rao C. Natural frequency of circular plate elastically restrained against rotation and resting on Winkler foundation. In: Proceedings of eight international conference on vibration problems. Howrah, India; 2007. p. 182–186.

See discussions, stats, and author profiles for this publication at: <https://www.researchgate.net/publication/320087533>

Exact Closed-Form Solution of Vibrations of a Generally Restrained Circular Plate with Crack and Weakened Along an Internal Concentric Circle

Article in *International Journal of Acoustics and Vibrations* · October 2017

DOI: 10.20855/ijav.2017.22.3479

CITATIONS

4

READS

182

3 authors, including:



Lokavarapu Bhaskara Rao
VIT University Chennai

105 PUBLICATIONS 349 CITATIONS

[SEE PROFILE](#)



Kameswara Rao Chellapilla
NNRG

108 PUBLICATIONS 593 CITATIONS

[SEE PROFILE](#)

Some of the authors of this publication are also working on these related projects:



Vibrations and Stability of Plates [View project](#)



Poetry [View project](#)

Exact Closed-Form Solution of Vibrations of a Generally Restrained Circular Plate with Crack and Weakened Along an Internal Concentric Circle

Lokavarapu Bhaskara Rao

School of Mechanical and Building Sciences, VIT University, Chennai Campus, Vandalur-Kelambakkam Road, Chennai-600127, Tamil Nadu, India.

Chellapilla Kameswara Rao

Department of Mechanical Engineering, Nalla Narasimha Reddy Engineering College, Ghatkesar (M), Ranga Reddy (Dt.) Hyderabad-501506, Telangana State, India.

(Received 4 December 2014; accepted 18 January 2017)

A thin circular plate with generally restrained periphery and weakened along an internal concentric circle due to a crack, is considered in this paper for studying its vibration characteristics. The frequency for first six modes of plate vibration is computed for varying values of radius of crack, elastic rotational and translational restraints, and the extent of weakening duly simulated by considering the crack as a rotational restraint on the plate. From the results obtained, it is observed that for a plate with translation and rotational restraints, the internal weakening decreases the fundamental frequency by around 31 per cent.

NOMENCLATURE

K_{T1}	Translational spring stiffness at outer periphery;
K_{R1}	Rotational spring stiffness at outer periphery;
K_{R2}	Rotational spring stiffness at the cracked region;
T_{11}	Non-dimensional translational Flexibility parameter at the outer edge;
R_{11}	Non-dimensional rotational flexibility parameter at the outer edge;
R_{22}	Non-dimensional rotational flexibility parameter at the cracked region;
k	Non-dimensional frequency parameter;

1. INTRODUCTION

Many structural elements are composed of circular plates in aeronautical, civil, mechanical, and marine applications. The problem of determination of vibration characteristics of circular plates is basic to engineering design.¹⁻⁴ Several researchers reviewed the literature on vibrations of circular plates with basic edge conditions and internal strengthening.⁵⁻⁹ Detection of structural damage through analytical and experimental investigations of vibration characteristics of cracked plates has become essential for solving design analysis problems of various types of mechanical systems. The natural frequencies and mode shapes of cracked elastic circular plates considerably differ from their healthy counterparts. In this respect, Dimarogonas has conducted a comprehensive literature search regarding the effects of cracks on the vibrations of various types and shapes of structures.¹⁰ Papadopoulos has briefly described the history of the strain energy release rate (SERR) theory as well as different methods of crack identification.¹¹ Broda et al. have discussed various models of classical and non-classical

crack- induced elastic, thermo-elastic, and dissipative nonlinearities.¹²

Lynn and Kumbasar investigated the problem of vibrations of cracked rectangular plates by presenting the solution for the Fredholm integral equation of the first kind and calculating numerically the drop in the natural frequency of vibration of plates due to the presence of cracks.¹³ Petyt investigated experimentally the variation of fundamental frequency of vibration as the crack length changes and, the results were verified against analytical ones using finite element method.¹⁴ Stahl and Keer, Hirano and Okazaki, Solecki and Yuan, and Dickinson studied further on vibrations of cracked plates using different methods of analysis.¹⁵⁻¹⁸ Huang and Ma studied the problem of vibrations of circular plate with a radial crack using an optical measurement system known as the AF-ESPI method.¹⁹

Liew et al.²⁰ studied the problem of out-of-plane vibrations of cracked plates utilizing the domain decomposition method, confirming the results presented by Stahl and Keer, Hirano and Okazaki, and presented results for a wide range of crack length ratios.^{15,16} Further, they examined the vibrations of a plate having a centrally located internal crack and reported results of frequency crossings. Ma and Huang recently studied the problem of vibrations of a square plate with an edge crack utilizing both experimental and finite element analysis.²¹ They found that the variations in crack length to be having considerable influence on the natural frequencies and mode shapes of the plate. Si et al. recently studied the free vibrations of circular plates with radial side cracks considering the presence of water on one side utilizing Rayleigh-Ritz method.²²

By the integration of stress intensity factors, the stiffness matrix was derived for the cracked plate by Qian et al. for carrying out the finite element analysis.²³ Utilizing Rayleigh's

method and including effects of shear deformation and rotary inertia, Lee and Lim presented results for the natural frequencies and mode shapes of thick rectangular plate with a centrally located crack.²⁴ Krawczuk studied the influence of the crack location and crack length on the natural frequencies of both simply supported and cantilever rectangular plates.²⁵ The dynamic behaviour of cracked rectangular plates was investigated by Liew et al. analysing the free vibrations of rectangular plates either with a crack emanating from an edge or that which is centrally located.²⁶ Khadem and Rezaee carried out vibration analysis for crack detection in a rectangular plate subjected to uniform external loads.²⁷ Krawczuk et al. studied the fracture mechanics of a plate with an elasto-plastic through crack by using the finite element method.²⁸

Based on Rayleigh's principle, Lee proposed a simple numerical method for computing the first natural frequencies of an annular plate with an internal concentric crack and applied the same for an annular plate with two opposite edges simply supported and the other two edges clamped.²⁹ The effect of the number and length of periodic radial cracks on the natural frequencies of an annular plate was investigated experimentally by Ramesh et al.³⁰ By modelling a surface peripheral crack as a local rotational flexibility, Anifantis et al. investigated the problem identifying free vibration characteristics of cracked annular plates.³¹ Utilizing the Ritz method, Yuan et al. studied the influence of radial or circumferential cracks or slits through the full thickness on the natural frequencies of free vibration of circular and annular plates.³² By using the optimum number of sector plate elements and joining them together with artificial spring elements, they obtained the flexibility matrix of sector-type element with radial crack and proved the applicability of the derived element in the dynamic analysis of annular plates with cracks eventually comparing the results with the experimental ones available in the literature.

Very few studies^{33–35} exist in the literature on the vibrations of circular plate weakened along a concentric circle due to crack where Wang³³ and Yu³⁴ considered the basic boundary conditions and Bhaskara Rao and Kameswara Rao³⁵ considered an elastically restrained edge against translation. Due to internal notching, partial crack, or fatigue crack along a concentric circle, the plate may become weak in its bending strength. A hinge with an elastic rotational restraint can be considered to model the weakened position. In realistic engineering circumstances, a perfect boundary condition is hardly present. Therefore, when the boundary departs from such realistic situation, an elastically restrained edge must be considered.^{36–39} Main intention of this work is therefore to study the effect of weakening of thin plate along concentric circle due to crack and the plate being elastically restrained along the outer edge against translation and rotation using exact method of solution approach. The natural frequencies of circular plate for varying values of translation restraint and rotational restraint along the plate periphery, along with the variations in the radius of weakened circle, Poisson's ratio and rotational restraint with hinge of cracked region are obtained for a wide range of non-dimensional parameters. The results are expressed in graphical and tabular formats for ease of use in understand-

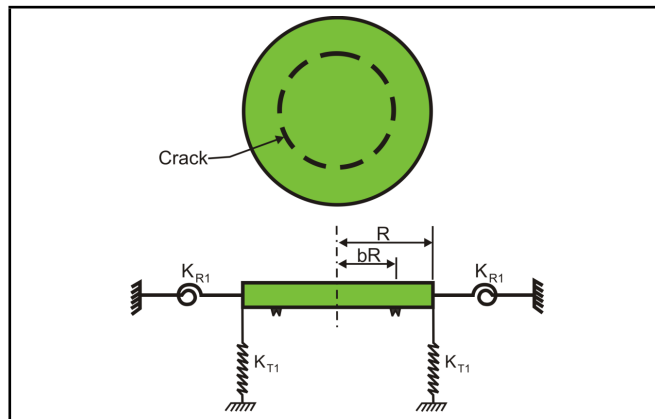


Figure 1. Generally restrained circular plate with crack.

ing the design of such cracked and weakened circular plates in engineering industry.

2. MATHEMATICAL FORMULATION

The circular plate under consideration is of radius R , Poisson's ratio ν , density ρ , thickness h , and elastic constant E . Figure 1 shows a circular plate that has an outer periphery, a generally restrained edge (at radius R), and an edge weakened along an internal concentric circle (at radius bR). Here, b is a fraction and is less than 1.

Here, all lengths are normalized with respect to R i.e., the radius of outer region is 1 and radius of inner cracked region is b . Here, r designates the distance measured from the centre of plate whose maximum value is R . Here subscript I represents outer region $b \leq r \leq 1$ and subscript II represents inner region $0 \leq r \leq b$. General form of lateral displacement of vibration of classical thin plate can be expressed as²

$$w = u(r) \cos(n\theta) e^{i\omega t}; \quad (1)$$

where n is the number of modal diameters, ω is the frequency, w is the transverse displacement, and t is time.

The function $u(r)$ is a linear combination of Bessel functions $J_n(kr)$, $Y_n(kr)$, $I_n(kr)$, $K_n(kr)$ and $k = R(\rho\omega^2/D)^{1/4}$; here D is flexural rigidity and k is the square root of the non-dimensional frequency.³ General solutions for regions I & II are

$$u_I(r) = C_1 J_n(kr) + C_2 Y_n(kr) + C_3 I_n(kr) + C_4 K_n(kr); \quad (2)$$

$$u_{II}(r) = C_5 J_n(kr) + C_6 I_n(kr). \quad (3)$$

Considering the generally restrained edge at the outer periphery, the boundary conditions can be formulated as

$$M_r(r, \theta) = K_{R1} \frac{\partial w_I(r, \theta)}{\partial r}; \quad (4)$$

$$V_r(r, \theta) = -K_{T1} w_I(r, \theta); \quad (5)$$

where K_{R1} and K_{T1} are, respectively, the rotational and linear spring stiffness of the elastically restrained circular plate

boundary. Here, bending moment ($M_r(r, \theta)$) & Kelvin-Kirchhoff's ($V_r(r, \theta)$) shear force can be represented as

$$M_r(r, \theta) = -\frac{D}{R} \left[\frac{\partial^2 w_I(r, \theta)}{\partial r^2} + \nu \left(\frac{1}{r} \frac{\partial w_I(r, \theta)}{\partial r} + \frac{1}{r^2} \frac{\partial^2 w_I(r, \theta)}{\partial \theta^2} \right) \right]; \quad (6)$$

$$V_r(r, \theta) = -\frac{D}{R^3} \left[\frac{\partial}{\partial r} \nabla^2 w_I(r, \theta) + (1 - \nu) \frac{1}{r} \frac{\partial}{\partial \theta} \left(\frac{1}{r} \frac{\partial^2 w_I(r, \theta)}{\partial r \partial \theta} - \frac{1}{r^2} \frac{\partial w_I(r, \theta)}{\partial \theta} \right) \right]; \quad (7)$$

From Eqs. (4), (6) and (5), Eq. (7) yields the following expressions

$$\left[\frac{\partial^2 w_I(r, \theta)}{\partial r^2} + \nu \left(\frac{1}{r} \frac{\partial w_I(r, \theta)}{\partial r} + \frac{1}{r^2} \frac{\partial^2 w_I(r, \theta)}{\partial \theta^2} \right) \right] = -R_{11} \frac{\partial w_I(r, \theta)}{\partial r}; \quad (8)$$

$$\left[\frac{\partial}{\partial r} \nabla^2 w_I(r, \theta) + (1 - \nu) \frac{1}{r} \frac{\partial}{\partial \theta} \left(\frac{1}{r} \frac{\partial^2 w_I(r, \theta)}{\partial r \partial \theta} - \frac{1}{r^2} \frac{\partial w_I(r, \theta)}{\partial \theta} \right) \right] = T_{11} w_I(r, \theta); \quad (9)$$

Equations (8) and (9) can be presented as

$$\ddot{u}_I(r) + \nu [\dot{u}_I(r) - n^2 u_I(r)] = -R_{11} \dot{u}_I(r); \quad (10)$$

$$\ddot{u}_I + \ddot{u}_I(r) - [1 + n^2(2 - \nu)] \dot{u}_I(r) + n^2(3 - \nu) u_I(r) = -T_{11} u_I(r); \quad (11)$$

where $R_{11} = \frac{K_{R1}R}{D}$ & $T_{11} = \frac{K_{T1}R}{D}$ are, respectively, the non-dimensional rotational and translational spring parameters involving the springs constants K_{R1} & K_{T1} , which are the elastic spring stiffnesses simulating the elastic restraints at the circular plate outer periphery.

Apart from the generally restrained edge at the outer periphery, the continuity requirements³³ at $r = b$ are as follows

$$u_I(b) = u_{II}(b); \quad (12)$$

$$b\ddot{u}_I(b) + \nu \dot{u}_I(b) = b\ddot{u}_{II}(b) + \nu \dot{u}_{II}(b); \quad (13)$$

$$b^2 \ddot{u}_I(b) - [1 + n^2(2 - \nu) + \nu] \dot{u}_I(b) = b^2 \ddot{u}_{II}(b) - [1 + n^2(2 - \nu) + \nu] \dot{u}_{II}(b); \quad (14)$$

$$b^2 \ddot{u}_{II}(b) + \nu [b\dot{u}_{II}(b) - n^2 u_{II}(b)] = b^2 R_{22} [\dot{u}_I(b) - u_{II}(b)]; \quad (15)$$

where $R_{22} = \frac{K_{R2}R}{D}$ is the normalized spring constant with K_{R2} being the rotational spring stiffness, which is utilized for modelling the rotational restraint, created by the presence of

circular crack at $r = b$. The non-trivial solutions to Eqs. (10)–(15) are sought. From Eqs. (2), (3), and (10)–(15) we derive the following equations.

$$\begin{aligned} & \left[\frac{k^2}{4} P_2 + \frac{k}{2} (\nu + R_{11}) P_1 - \left(\frac{k^2}{2} + \nu n^2 \right) J_n(k) \right] C_1 + \\ & \left[\frac{k^2}{4} Q_2 + \frac{k}{2} (\nu + R_{11}) Q_1 - \left(\frac{k^2}{2} + \nu n^2 \right) Y_n(k) \right] C_2 + \\ & \left[\frac{k^2}{4} R_2 + \frac{k}{2} (\nu + R_{11}) R_1 + \left(\frac{k^2}{2} - \nu n^2 \right) I_n(k) \right] C_3 - \\ & \left[\frac{k^2}{4} S_2 - \frac{k}{2} (\nu + R_{11}) S_1 + \left(\frac{k^2}{2} - \nu n^2 \right) K_n(k) \right] C_4 = 0; \end{aligned} \quad (16)$$

$$\begin{aligned} & \left[\frac{k^3}{8} P_3 + \frac{k^2}{4} P_2 - \frac{k}{2} \left(\frac{3}{4} k^2 + n^2(2 - \nu) + 1 \right) P_1 \right. \\ & \quad \left. + \left(n^2(3 - \nu) - \frac{k^2}{2} - T_{11} \right) J_n(k) \right] C_1 + \\ & \left[\frac{k^3}{8} Q_3 + \frac{k^2}{4} Q_2 - \frac{k}{2} \left(\frac{3}{4} k^2 + n^2(2 - \nu) + 1 \right) Q_1 \right. \\ & \quad \left. + \left(n^2(3 - \nu) - \frac{k^2}{2} - T_{11} \right) Y_n(k) \right] C_2 + \\ & \left[\frac{k^3}{8} R_3 + \frac{k^2}{4} R_2 + \frac{k}{2} \left(\frac{3}{4} k^2 - n^2(2 - \nu) + 1 \right) R_1 \right. \\ & \quad \left. + \left(n^2(3 - \nu) + \frac{k^2}{2} - T_{11} \right) I_n(k) \right] C_3 + \\ & \left[-\frac{k^3}{8} S_3 + \frac{k^2}{4} S_2 + \frac{k}{2} \left(-\frac{3}{4} k^2 + n^2(2 - \nu) + 1 \right) S_1 \right. \\ & \quad \left. + \left(n^2(3 - \nu) + \frac{k^2}{2} - T_{11} \right) K_n(k) \right] C_4 = 0; \end{aligned} \quad (17)$$

$$J_n(kb)C_1 + Y_n(kb)C_2 + I_n(kb)C_3 + K_n(kb)C_4 - J_n(kb)C_5 - I_n(kb)C_6 = 0; \quad (18)$$

$$\begin{aligned} & \left[\frac{bk^2}{4} \dot{P}_2 + \frac{\nu k}{2} \dot{P}_1 - \frac{bk^2}{2} J_n(kb) \right] C_1 + \\ & \left[\frac{bk^2}{4} \dot{Q}_2 + \frac{\nu k}{2} \dot{Q}_1 - \frac{bk^2}{2} Y_n(kb) \right] C_2 + \\ & \left[\frac{bk^2}{4} \dot{R}_2 + \frac{\nu k}{2} \dot{R}_1 + \frac{bk^2}{2} I_n(kb) \right] C_3 + \\ & \left[\frac{bk^2}{4} \dot{S}_2 - \frac{\nu k}{2} \dot{S}_1 + \frac{bk^2}{2} K_n(kb) \right] C_4 - \\ & \left[\frac{bk^2}{4} \dot{P}_2 + \frac{\nu k}{2} \dot{P}_1 - \frac{bk^2}{2} J_n(kb) \right] C_5 - \\ & \left[\frac{bk^2}{4} \dot{R}_2 + \frac{\nu k}{2} \dot{R}_1 + \frac{bk^2}{2} I_n(kb) \right] C_6 = 0; \end{aligned} \quad (19)$$

(See Eqs. (20) and (21) on the top of the next page.)

3. SOLUTION

Given the set of values of n , ν , T_{11} , R_{11} , R_{22} , and b , equations listed above are utilized in obtaining exact characteristics

$$\begin{aligned} & \left[\frac{b^2 k^3}{8} \dot{P}_3 - \frac{k}{2} \left(\frac{3b^2 k^2}{4} + (1 + n^2(2 - \nu) + \nu) \right) \dot{P}_1 \right] C_1 + \left[\frac{b^2 k^3}{8} \dot{Q}_3 - \frac{k}{2} \left(\frac{3b^2 k^2}{4} + (1 + n^2(2 - \nu) + \nu) \right) \dot{Q}_1 \right] C_2 + \\ & \left[\frac{b^2 k^3}{8} \dot{R}_3 + \frac{k}{2} \left(\frac{3b^2 k^2}{4} - (1 + n^2(2 - \nu) + \nu) \right) \dot{R}_1 \right] C_3 + \left[-\frac{b^2 k^3}{8} \dot{S}_3 + \frac{k}{2} \left(-\frac{3b^2 k^2}{4} + (1 + n^2(2 - \nu) + \nu) \right) \dot{S}_1 \right] C_4 + \\ & \left[\frac{b^2 k^3}{8} \dot{P}_3 + \frac{k}{2} \left(\frac{3b^2 k^2}{4} + (1 + n^2(2 - \nu) + \nu) \right) \dot{P}_1 \right] C_5 + \left[-\frac{b^2 k^3}{8} \dot{R}_3 + \frac{k}{2} \left(-\frac{3b^2 k^2}{4} + (1 + n^2(2 - \nu) + \nu) \right) \dot{R}_1 \right] C_6 = 0; \end{aligned} \quad (20)$$

$$\begin{aligned} & \left[\frac{b^2 k R_{22}}{2} \dot{P}_1 \right] C_1 + \left[\frac{b^2 k R_{22}}{2} \dot{Q}_1 \right] C_2 + \left[\frac{b^2 k R_{22}}{2} \dot{R}_1 \right] C_3 - \left[\frac{b^2 k R_{22}}{2} \dot{S}_1 \right] C_4 - \\ & \left[\frac{b^2 k^2}{4} \dot{P}_2 + \frac{kb}{2} (\nu + b R_{22}) \dot{P}_1 - \left(\frac{b^2 k^2}{2} + n^2 \right) J_n(kb) \right] C_5 - \left[\frac{b^2 k^2}{4} \dot{R}_2 + \frac{kb}{2} (\nu + b R_{22}) \dot{R}_1 + \left(\frac{b^2 k^2}{2} - n^2 \right) I_n(kb) \right] C_6 = 0; \end{aligned} \quad (21)$$

where $P_1 = J_{n-1}(k) - J_{n+1}(k)$; $P_2 = J_{n-2}(k) + J_{n+2}(k)$; $P_3 = J_{n-3}(k) - J_{n+3}(k)$;
 $Q_1 = Y_{n-1}(k) - Y_{n+1}(k)$; $Q_2 = Y_{n-2}(k) + Y_{n+2}(k)$; $Q_3 = Y_{n-3}(k) - Y_{n+3}(k)$;
 $R_1 = I_{n-1}(k) + I_{n+1}(k)$; $R_2 = I_{n-2}(k) + I_{n+2}(k)$; $R_3 = I_{n-3}(k) + I_{n+3}(k)$;
 $S_1 = K_{n-1}(k) + K_{n+1}(k)$; $S_2 = K_{n-2}(k) + K_{n+2}(k)$; $S_3 = K_{n-3}(k) + K_{n+3}(k)$;
 $\dot{P}_1 = J_{n-1}(kb) - J_{n+1}(kb)$; $\dot{P}_2 = J_{n-2}(kb) + J_{n+2}(kb)$; $\dot{P}_3 = J_{n-3}(kb) - J_{n+3}(kb)$;
 $\dot{Q}_1 = Y_{n-1}(kb) - Y_{n+1}(kb)$; $\dot{Q}_2 = Y_{n-2}(kb) + Y_{n+2}(kb)$; $\dot{Q}_3 = Y_{n-3}(kb) - Y_{n+3}(kb)$;
 $\dot{R}_1 = I_{n-1}(kb) + I_{n+1}(kb)$; $\dot{R}_2 = I_{n-2}(kb) + I_{n+2}(kb)$; $\dot{R}_3 = I_{n-3}(kb) + I_{n+3}(kb)$;
 $\dot{S}_1 = K_{n-1}(kb) + K_{n+1}(kb)$; $\dot{S}_2 = K_{n-2}(kb) + K_{n+2}(kb)$; $\dot{S}_3 = K_{n-3}(kb) + K_{n+3}(kb)$;

equations by suitably eliminating coefficients of C_1, C_2, C_3, C_4, C_5 , and C_6 . The values of non-dimensional frequency parameters k are obtained by solving the exact characteristic equation by utilizing a root search method based on bisection method and coding the same appropriately in MATHEMATICA.

4. RESULTS AND DISCUSSIONS

Poisson's ratio employed here is 0.3. The values (R_{11} and T_{11}) are chosen to cover both classical and nonclassical boundary conditions. Also, the values of rotational spring R_{22} are chosen to simulate the intensity of the crack appropriately. A smaller value of R_{22} represents that the crack is very small and higher value of R_{22} represents a concentric rigid ring support. Frequency values for various values of R_{22} keeping R_{11} and T_{11} constant [$R_{11} = T_{11} = 0.0001$] are computed. The first frequencies [k] of $n \leq 5$ modes with $R_{22} = 0, 2, 4, 6, 8, 10, 25, 50$, and 10^{16} and $R_{11} = T_{11} = 0.0001$ are computed. For $b = 1$ and $R_{22} = 0$, the frequency of plate is same as that of plate without having weakening crack. For a given value of b & ν , the first frequency of $n = 0$, the modal frequency converges to that of plate without weakening as R_{22} is increased from a value of 0. When $\nu = 0.3$, first six frequencies of plate without weakening are obtained as 2.31479 [$n = 2$], 3.00049 [$n = 0$], 3.52684 [$n = 3$], 4.52488 [$n = 1$], 4.67279 [$n = 4$], and 5.7874 [$n = 5$]. Notice that the fundamental frequency of plate weakened along an internal concentric circle and generally restrained edge against translation and rotation occurs at $n = 2$ mode. The variation of fundamental frequency of plate for varying values of radius of weakened circle and rotational restraint parameter of hinge are given in Fig. 2, for $n = 0$ mode. As $R_{22} \rightarrow \infty$ (as the spring becomes rigid),

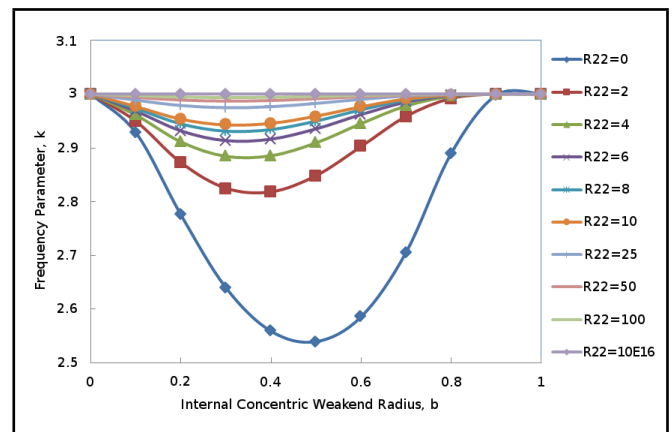


Figure 2. Fundamental frequency and concentric weakened radius parameter for different R_{22} and $R_{11} = T_{11} = 0.0001$, $\nu = 0.3$, and $n = 0$.

the frequency parameter stays at 3.00049. For the remaining values of R_{22} , the frequency parameter decreases except when $b = 0$ or 1.

The frequency values for various values of R_{22} keeping R_{11} and T_{11} constant [$R_{11} = T_{11} = 2$] are computed. First frequencies of $n \leq 5$ modes with $R_{22} = 0, 2, 4, 6, 8, 10, 25, 50$, and 10^{16} and $R_{11} = T_{11} = 2$ are computed. For $b = 1$ and $R_{22} = 0$, the frequency of plate is same as that of plate without having weakening crack. For a given value of b & ν , the first frequency of $n = 0$ modal frequency converges to that of plate without weakening as R_{22} is increased from a value of 0. When $\nu = 0.3$, first six frequencies of plate without weakening are obtained as 1.39366 [$n = 0$], 1.82795 [$n = 1$], 2.73255 [$n = 2$], 3.78917 [$n = 3$], 4.86708 [$n = 4$], and 5.94356 [$n = 5$]. Notice that the fundamental frequency of plate weakened along an internal concentric circle and resting on generally restrained edge against translation and rotation occurs at

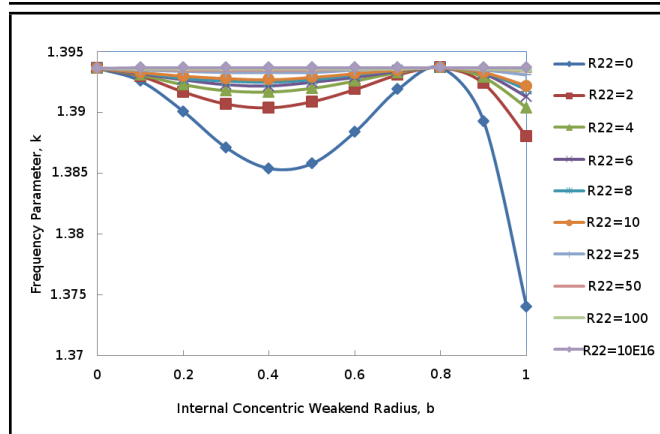


Figure 3. Fundamental frequency and concentric weakened radius parameter for different R_{22} and $R_{11} = T_{11} = 2$, $\nu = 0.3$, and $n = 0$.

$n = 0$ mode. As $R_{22} \rightarrow \infty$ (as the spring becomes rigid), the frequency parameter stays at 1.39366. For the remaining values of R_{22} , the variation of frequency parameter is shown in Fig. 3. There is an optimum location within the plate.

Internal weakening decreases fundamental frequency 1.39366, which is the fundamental frequency of plate without the weakening by less than 1% (0.5948%). For a given value of R_{22} , the frequency k decreases from 1.39366 to 1.38537, increases to 1.39366, and finally decreases to 1.374 as the radius of the weakened circle varies from 0 to 1. The local maximum frequency 1.39366 occurs at $b = 0.8$. Thus $b = 0.8$ is the optimum radius if the plate needs to be notched, such as a closed hatch. The internal weakening has minute effect [decreases fundamental frequency by less than 1% (0.5948%)] on the fundamental frequency when $0 \leq b \leq 0.4$. Where as it has little effect on fundamental frequency [decreases the fundamental frequency by less than 2% (1.41%)] when $b > 0.8$.

The frequency values for various values of R_{22} keeping R_{11} and T_{11} constant [$R_{11} = T_{11} = 5$] are computed. The first frequencies of $n \leq 5$ modes with $R_{22} = 0, 2, 4, 6, 8, 10, 25, 50$, and 10^{16} and $R_{11} = T_{11} = 10$ are computed. For $b = 1$ and $R_{22} = 0$, the frequency of plate is same as that of plate without having weakening crack. For a given value of b & ν , the first frequency of $n = 0$ modal frequency converges to that of plate without weakening as R_{22} is increased from a value of 0. When $\nu = 0.3$, first six frequencies of plate without weakening are obtained as 1.73363 [$n = 0$], 2.16554 [$n = 1$], 2.97556 [$n = 2$], 3.97353 [$n = 3$], 5.01943 [$n = 4$], and 6.07607 [$n = 5$]. Notice that the fundamental frequency of plate weakened along an internal concentric circle and resting on generally restrained edge against translation and rotation occurs at $n = 0$ mode. As $R_{22} \rightarrow \infty$ (as the spring becomes rigid), the frequency parameter stays at 1.73363. For the remaining values of R_{22} , the variation of frequency parameter is shown in Fig. 4. There is an optimum location within the plate.

Internal weakening decreases the fundamental frequency 1.73363, which is fundamental frequency of the plate without the weakening by less than 1% (0.8%). For a given value of R_{22} , the frequency k decreases from 1.73363 to 1.71975, increases to 1.73363, and finally decreases to 1.65872 as radius b of weakened circle varies from 0 to 1. Here, local maximum

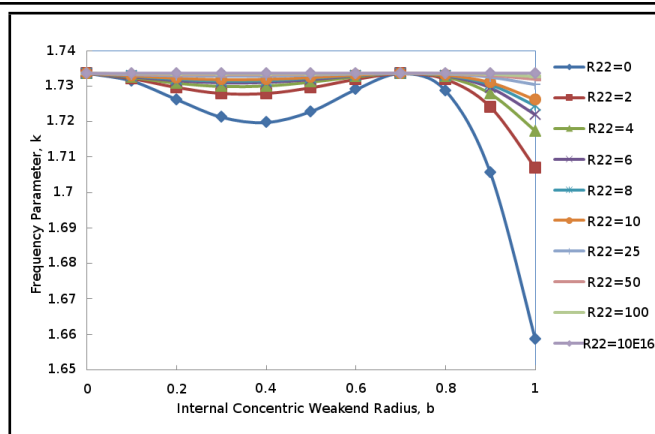


Figure 4. Fundamental frequency and concentric weakened radius parameter for different R_{22} and $R_{11} = T_{11} = 5$, $\nu = 0.3$, and $n = 0$.

frequency 1.73363 occurs at $b = 0.7$. Thus $b = 0.7$ is optimum radius if the plate needs to be notched, such as a closed hatch. Here, internal weakening has minute effect [decreases fundamental frequency by less than 1% (0.8%)] on fundamental frequency when $0 \leq b \leq 0.4$. Where as it has more effect on fundamental frequency [decreases the fundamental frequency by less than 5% (4.32%)] when $b > 0.7$.

The frequency values for various values of R_{22} keeping R_{11} and T_{11} constant [$R_{11} = T_{11} = 10$] are tabulated. First frequencies of $n \leq 5$ modes with $R_{22} = 0, 2, 4, 6, 8, 10, 25, 50$, and 10^{16} and $R_{11} = T_{11} = 10$ are presented in Tables 1 to 6. For $b = 1$ and $R_{22} = 0$, the frequency of plate is same as that of plate without having weakening crack. For a given value of b & ν , first frequency of $n = 0$ modal frequency converges to that of plate without weakening as R_{22} is increased from a value of 0. When $\nu = 0.3$, first six frequencies of plate without weakening are obtained as 2.03159 [$n = 0$], 2.46241 [$n = 1$], 3.19071 [$n = 2$], 4.13574 [$n = 3$], 5.15511 [$n = 4$] and 6.19719 [$n = 5$]. Notice that the fundamental frequency of plate weakened along an internal concentric circle and resting on generally restrained edge against translation and rotation occurs at $n = 0$ mode. As $R_{22} \rightarrow \infty$ (as the spring becomes rigid), the frequency parameter stays at 2.03159. For the remaining values of R_{22} , the variation of frequency parameter is shown in Fig. 5. There is an optimum location within the plate.

Internal weakening decreases fundamental frequency 2.03159, which is fundamental frequency of plate without weakening by less than 9% (8.5647%). For a given value of R_{22} , the frequency k decreases from 2.03159 to 2.00913, increases to 2.03063 and finally decreases to 1.85759 as radius b of weakened circle varies from 0 to 1. Here, local maximum frequency 2.03063 occurs at $b = 0.7$. Thus $b = 0.7$ is the optimum radius if plate needs to be notched, such as a closed hatch. The internal weakening has little effect [decreases fundamental frequency by less than 1% (1.11%)] on fundamental frequency when $0 \leq b \leq 0.4$. Where as it has more effect on fundamental frequency [decreases the fundamental frequency by less than 9% (8.5647%)] when $b > 0.7$.

The frequency values for various values of R_{22} keeping R_{11} & T_{11} constant [$R_{11} = T_{11} = 50$] are computed. First frequencies of $n \leq 5$ modes with $R_{22} = 0, 2, 4, 6, 8, 10, 25, 50$, and 10^{16} and $R_{11} = T_{11} = 10$ are computed. For $b = 1$

Table 1. First frequency parameter, ($n = 0$) for different R_{22} and internal concentric weakened radius parameter, b , $R_{11} = T_{11} = 10$, and $\nu = 0.3$.

b	$R_{22} \rightarrow 0$	2	4	6	8	10	25	50	100	10^6
0	2.03159	2.03159	2.03159	2.03159	2.03159	2.03159	2.03159	2.03159	2.03159	2.03159
0.1	2.02739	2.02869	2.02929	2.02979	2.02999	2.03029	2.03089	2.03119	2.03139	2.03159
0.2	2.0178	2.024	2.02639	2.0276	2.02839	2.02889	2.03039	2.03089	2.0312	2.03159
0.3	2.00962	2.0214	2.025	2.0267	2.0277	2.0284	2.03019	2.0308	2.03119	2.03159
0.4	2.00913	2.02221	2.0257	2.0273	2.0282	2.0288	2.03039	2.0309	2.03129	2.03159
0.5	2.01691	2.0259	2.028	2.029	2.0296	2.0299	2.03089	2.03119	2.03139	2.03159
0.6	2.02778	2.03019	2.03069	2.03099	2.03109	2.03119	2.03139	2.03149	2.03149	2.03159
0.7	2.03063	2.03127	2.03138	2.03139	2.03149	2.03149	2.03149	2.03159	2.03159	2.03159
0.8	2.00906	2.02368	2.02678	2.02809	2.02889	2.02939	2.03059	2.03109	2.03129	2.03159
0.9	1.94995	2.00144	2.01312	2.01831	2.02121	2.02301	2.0279	2.0297	2.0306	2.03159
1	1.85759	1.96079	1.98721	1.99928	2.00616	2.01065	2.02252	2.02691	2.0292	2.03159

Table 2. First frequency parameter, ($n = 1$) for different R_{22} and internal concentric weakened radius parameter b , $R_{11} = T_{11} = 10$, and $\nu = 0.3$.

b	$R_{22} \rightarrow 0$	2	4	6	8	10	25	50	100	10^6
0	2.46239	2.46239	2.46239	2.46239	2.46239	2.46239	2.46239	2.46239	2.46239	2.46241
0.1	2.44903	2.45442	2.45672	2.45802	2.45882	2.45932	2.46101	2.46161	2.46201	2.46241
0.2	2.4067	2.43805	2.44684	2.45093	2.45333	2.45492	2.45912	2.46071	2.46151	2.46241
0.3	2.33785	2.41649	2.43436	2.44215	2.44654	2.44943	2.45682	2.45952	2.46092	2.46241
0.4	2.26443	2.39335	2.42069	2.43247	2.43906	2.44335	2.45433	2.45822	2.46032	2.46241
0.5	2.21468	2.37421	2.40883	2.4239	2.43238	2.43776	2.45193	2.45702	2.45972	2.46241
0.6	2.20233	2.36444	2.40195	2.41871	2.42819	2.43428	2.45034	2.45623	2.45932	2.46241
0.7	2.22629	2.36744	2.40286	2.41902	2.4283	2.43428	2.45024	2.45613	2.45922	2.46241
0.8	2.27925	2.384	2.41253	2.4258	2.43348	2.43857	2.45204	2.45703	2.45972	2.46241
0.9	2.35036	2.41172	2.42968	2.43816	2.44325	2.44654	2.45543	2.45882	2.46052	2.46241
1	2.42166	2.44274	2.44943	2.45272	2.45472	2.45602	2.45952	2.46091	2.46161	2.46241

Table 3. First frequency parameter, ($n = 2$) for different R_{22} and internal concentric weakened radius parameter b , $R_{11} = T_{11} = 10$, and $\nu = 0.3$.

b	$R_{22} \rightarrow 0$	2	4	6	8	10	25	50	100	10^6
0	3.1908	3.1908	3.1908	3.1908	3.1908	3.1908	3.1908	3.1908	3.1908	3.1908
0.1	3.1948	3.1939	3.19331	3.19291	3.19261	3.19241	3.19161	3.19121	3.19101	3.19071
0.2	3.20557	3.20009	3.19759	3.1962	3.1952	3.1945	3.19251	3.19171	3.19121	3.19071
0.3	3.21492	3.20346	3.19938	3.19729	3.19599	3.1952	3.1927	3.19181	3.19131	3.19071
0.4	3.19851	3.19426	3.19298	3.19239	3.19209	3.1919	3.1912	3.19101	3.19091	3.19071
0.5	3.12095	3.16202	3.17262	3.17752	3.18041	3.18221	3.18701	3.18881	3.18981	3.19071
0.6	2.98278	3.10605	3.1376	3.15208	3.16036	3.16565	3.17993	3.18522	3.18792	3.19071
0.7	2.83663	3.04051	3.0953	3.12085	3.13562	3.1452	3.17105	3.18063	3.18562	3.19071
0.8	2.73415	2.98644	3.05879	3.09331	3.11347	3.12674	3.16277	3.17634	3.18343	3.19071
0.9	2.7072	2.96328	3.04172	3.07984	3.10249	3.11736	3.15838	3.17404	3.18223	3.19071
1	2.77645	2.98702	3.05558	3.08961	3.10997	3.12345	3.16087	3.17524	3.18283	3.19071

Table 4. First frequency parameter, ($n = 3$) for different R_{22} and internal concentric weakened radius parameter b , $R_{11} = T_{11} = 10$, and $\nu = 0.3$.

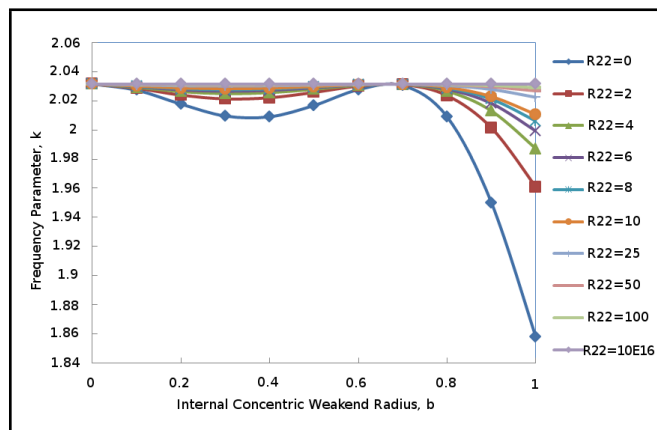
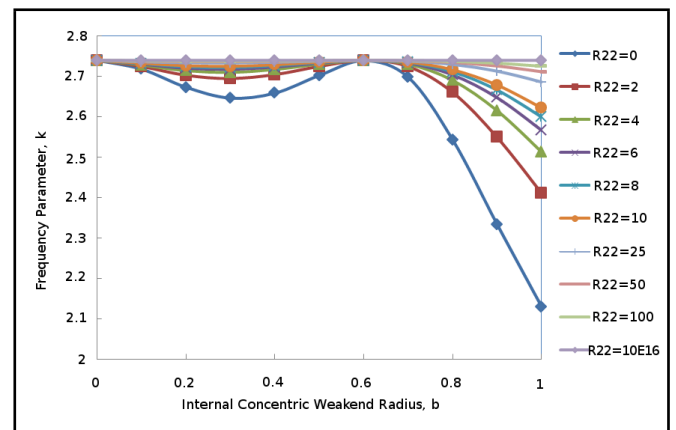
b	$R_{22} \rightarrow 0$	2	4	6	8	10	25	50	100	10^6
0	4.13572	4.13572	4.13571	4.13572	4.13571	4.13572	4.13571	4.13572	4.13571	4.13572
0.1	4.13584	4.13584	4.13574	4.13574	4.13574	4.13574	4.13574	4.13574	4.13574	4.13574
0.2	4.13774	4.13724	4.13684	4.13664	4.13654	4.13644	4.13604	4.13594	4.13584	4.13574
0.3	4.14541	4.14182	4.14013	4.13923	4.13863	4.13813	4.13684	4.13634	4.13604	4.13574
0.4	4.15824	4.14818	4.1444	4.14231	4.14111	4.14022	4.13773	4.13674	4.13624	4.13574
0.5	4.15298	4.14426	4.14139	4.1399	4.13911	4.13851	4.13693	4.13634	4.13604	4.13574
0.6	4.07023	4.10553	4.11613	4.12123	4.12424	4.12614	4.13154	4.13354	4.13464	4.13574
0.7	3.88275	4.01772	4.05886	4.07873	4.09041	4.0982	4.11926	4.12715	4.13135	4.13574
0.8	3.65521	3.90077	3.98002	4.01925	4.04271	4.05828	4.1014	4.11787	4.12666	4.13574
0.9	3.46495	3.79616	3.90776	3.96405	3.99799	4.02075	4.08433	4.10899	4.12207	4.13574
1	3.38479	3.75423	3.8792	3.94249	3.98072	4.00627	4.07784	4.10559	4.12037	4.13574

Table 5. First frequency parameter, ($n = 4$) for different R_{22} and internal concentric weakened radius parameter b , $R_{11} = T_{11} = 10$, and $\nu = 0.3$.

b	$R_{22} \rightarrow 0$	2	4	6	8	10	25	50	100	10^6
0	5.1551	5.1551	5.1551	5.1551	5.1551	5.1551	5.1551	5.1551	5.1551	5.1551
0.1	5.15511	5.15511	5.15511	5.15511	5.15511	5.15511	5.15511	5.15511	5.15511	5.15511
0.2	5.15531	5.15531	5.15521	5.15521	5.15521	5.15521	5.15512	5.15511	5.15511	5.15511
0.3	5.1573	5.1567	5.15631	5.15611	5.15591	5.15581	5.15541	5.15531	5.15521	5.15511
0.4	5.16545	5.16158	5.15979	5.1588	5.1582	5.1577	5.15631	5.15581	5.15541	5.15511
0.5	5.17786	5.16793	5.16406	5.16197	5.16068	5.15978	5.1572	5.15621	5.15571	5.15511
0.6	5.15333	5.15422	5.15445	5.15467	5.15477	5.15478	5.155	5.15501	5.15511	5.15511
0.7	5.00234	5.07817	5.10375	5.11664	5.12434	5.12943	5.14372	5.14922	5.15212	5.15511
0.8	4.7276	4.92987	5.00226	5.0394	5.06206	5.07734	5.12017	5.13694	5.14583	5.15511
0.9	4.4342	4.76097	4.88337	4.94766	4.98739	5.01435	5.09122	5.12167	5.13794	5.15511
1	4.22661	4.65672	4.81367	4.89544	4.94555	4.9794	5.07574	5.11368	5.13385	5.15511

Table 6. First frequency parameter, ($n = 5$) for different R_{22} and internal concentric weakened radius parameter b , $R_{11} = T_{11} = 10$, and $\nu = 0.3$.

b	$R_{22} \rightarrow 0$	2	4	6	8	10	25	50	100	10^6
0	6.19718	6.19718	6.19718	6.19718	6.19718	6.19718	6.19718	6.19718	6.19718	6.19718
0.1	6.19719	6.19719	6.19719	6.19719	6.19719	6.19719	6.19719	6.19719	6.19719	6.19719
0.2	6.19719	6.19719	6.19719	6.19719	6.19719	6.19719	6.19719	6.19719	6.19719	6.19719
0.3	6.19768	6.19748	6.19748	6.19739	6.19739	6.19739	6.19729	6.19729	6.19719	6.19719
0.4	6.20095	6.19976	6.19917	6.19877	6.19848	6.19838	6.19778	6.19749	6.19739	6.19719
0.5	6.21167	6.20622	6.20374	6.20235	6.20146	6.20076	6.19888	6.19808	6.19769	6.19719
0.6	6.21357	6.20646	6.2037	6.20212	6.20124	6.20055	6.19877	6.19798	6.19759	6.19719
0.7	6.11202	6.15145	6.16596	6.17347	6.17807	6.18117	6.18998	6.19349	6.19529	6.19719
0.8	5.8271	5.99107	6.05448	6.08814	6.10891	6.12309	6.16354	6.17961	6.1882	6.19719
0.9	5.4652	5.77154	5.89685	5.96505	6.00808	6.03754	6.1237	6.15845	6.17732	6.19719
1	5.17181	5.61856	5.79369	5.88735	5.94577	5.98571	6.10064	6.14657	6.17123	6.19719


Figure 5. Fundamental frequency and concentric weakened radius parameter for different R_{22} and $R_{11} = T_{11} = 10$, $\nu = 0.3$, and $n = 0$.

Figure 6. Fundamental frequency and concentric weakened radius parameter for different R_{22} and $R_{11} = T_{11} = 50$, $\nu = 0.3$, and $n = 0$.

and $R_{22} = 0$, the frequency of plate is same as that of plate without having weakening crack. For a given value of b & ν , first frequency of $n = 0$ modal frequency converges to that of plate without weakening as R_{22} is increased from a value of 0. When $\nu = 0.3$, first six frequencies of plate without weakening are obtained as 2.73971 [$n = 0$], 3.36961 [$n = 1$], 3.93897 [$n = 2$], 4.67971 [$n = 3$], 5.56452 [$n = 4$], and 6.52888 [$n = 5$]. Notice that the fundamental frequency of plate weakened along an internal concentric circle and resting on generally restrained edge against translation and rotation occurs at $n = 0$ mode. As $R_{22} \rightarrow \infty$ (as the spring becomes rigid), the frequency parameter stays at 2.73971. For the remaining values of R_{22} , the variation of frequency parameter is shown in Fig. 6. There is an optimum location within the plate.

Internal weakening decreases fundamental frequency 2.73971, which is fundamental frequency of the plate without weakening by less than 4% (3.4%). For a given value of R_{22} , the frequency k decreases from 2.73971 to 2.64629,

increases to 2.73971 and finally decreases to 2.12973 as radius b of weakened circle varies from 0 to 1. Here, local maximum frequency 2.73971 occurs at $b = 0.6$. Thus, $b = 0.6$ is optimum radius if plate needs to be notched, such as a closed hatch. Here, the internal weakening has considerable effect [decreases the fundamental frequency by less than 4% (3.4%)] on fundamental frequency when $0 \leq b \leq 0.3$. Where as it has more effect on fundamental frequency [decreases the fundamental frequency by less than 23% (22.264%)] when $b > 0.6$.

The frequency values for various values of R_{22} keeping R_{11} & T_{11} constant [$R_{11} = T_{11} = 100$] are computed. First frequencies of $n \leq 5$ modes with $R_{22} = 0, 2, 4, 6, 8, 10, 25, 50$, and 10^{16} and $R_{11} = T_{11} = 100$ are computed. For $b = 1$ and $R_{22} = 0$, the frequency of plate is as that of plate without having weakening crack. For a given value of b & ν , the first frequency of $n = 0$ modal frequency converges to that of plate without weakening as R_{22} is increased from a value of 0.

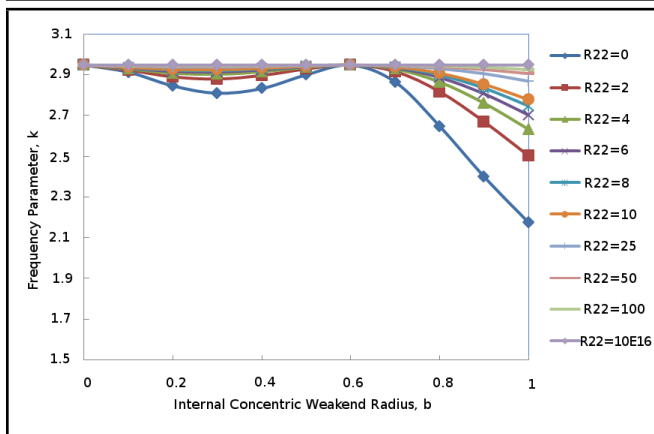


Figure 7. Fundamental frequency and concentric weakened radius parameter for different R_{22} and $R_{11} = T_{11} = 100$, $\nu = 0.3$, and $n = 0$.

When $\nu = 0.3$, first six frequencies of plate without weakening are obtained as 2.94749 [$n = 0$], 3.80332 [$n = 1$], 4.41124 [$n = 2$], 5.0759 [$n = 3$], 5.86747 [$n = 4$], and 6.75891 [$n = 5$]. Notice that the fundamental frequency of plate weakened along an internal concentric circle and resting on generally restrained edge against translation and rotation occurs at $n = 0$ mode. As $R_{22} \rightarrow \infty$ (as the spring becomes rigid), the frequency parameter stays at 2.94749. For the remaining values of R_{22} , the variation of frequency parameter is shown in Fig. 7. There is an optimum location within the plate.

Here, the internal weakening decreases fundamental frequency 2.94749 that is fundamental frequency of plate without weakening by less than 5% (4.69%). For a given value of R_{22} , the frequency k decreases from 2.94749 to 2.80925, increases to 2.94749 and finally decreases to 2.17453 as radius b of weakened circle varies from 0 to 1. Here, local maximum frequency 2.94749 occurs at $b = 0.6$. Thus, $b = 0.6$ is optimum radius if the plate needs to be notched, such as a closed hatch. Here, internal weakening has considerable effect [decreases fundamental frequency by less than 5% (4.69%)] on fundamental frequency when $0 \leq b \leq 0.3$. Where as it has more effect on fundamental frequency [decreases the fundamental frequency by less than 27% (26.22%)] when $b > 0.6$.

The frequency values for various values of R_{22} keeping R_{11} & T_{11} constant [$R_{11} = T_{11} = 1000$] are computed. First frequencies of $n \leq 5$ modes with $R_{22} = 0, 2, 4, 6, 8, 10, 25, 50$, and 10^{16} and $R_{11} = T_{11} = 1000$ are computed. For $b = 1$ and $R_{22} = 0$, the frequency of plate is same as that of plate without having weakening crack. For a given value of b & ν , first frequency of $n = 0$ modal frequency converges to that of plate without weakening as R_{22} is increased from a value of 0. When $\nu = 0.3$, first six frequencies of plate without weakening are 3.17078 [$n = 0$], 4.52162 [$n = 1$], 5.68836 [$n = 2$], 6.7132 [$n = 3$], 7.61683 [$n = 4$], and 8.43981 [$n = 5$]. Notice that the fundamental frequency of plate weakened along an internal concentric circle and resting on generally restrained edge against translation and rotation occurs at $n = 0$ mode. As $R_{22} \rightarrow \infty$ (as the spring becomes rigid), the frequency parameter stays at 3.17078. For the remaining values of R_{22} , the variation of frequency parameter is shown in Fig. 8. There is an optimum location within the plate.

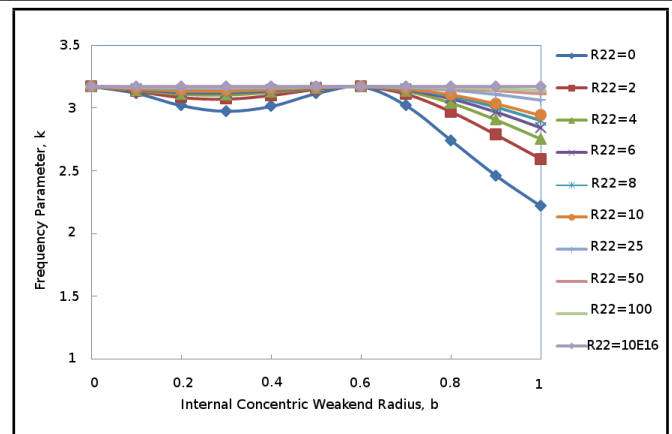


Figure 8. Fundamental frequency and concentric weakened radius parameter for different R_{22} and $R_{11} = T_{11} = 1000$, $\nu = 0.3$, and $n = 0$.

Internal weakening decreases fundamental frequency 3.17078, which is the fundamental frequency of plate without the weakening by less than 7% (6.22%). For a given value of R_{22} , the frequency k decreases from 3.17078 to 2.97341, increases to 3.17078 and finally decreases to 2.21675 as radius b of weakened circle varies from 0 to 1. Here, local maximum frequency 3.17078 occurs at $b = 0.6$. Thus $b = 0.6$ is optimum radius if a plate needs to be notched, such as a closed hatch. The internal weakening has significant effect [decreases the fundamental frequency by less than 7% (6.22%)] on fundamental frequency when $0 \leq b \leq 0.3$. Where as it has enormous effect on fundamental frequency [decreases the fundamental frequency by less than 31% (30.0856%)] when $b > 0.6$.

The frequency values for various values of R_{22} keeping R_{11} & T_{11} constant [$R_{11} = T_{11} = 100000$] are computed. First frequencies of $n \leq 5$ modes with $R_{22} = 0, 2, 4, 6, 8, 10, 25, 50$, and 10^{16} and $R_{11} = T_{11} = 100000$ are computed. For $b = 1$ and $R_{22} = 0$, the frequency of plate is same as that of plate without having weakening crack. For a given value of b & ν , first frequency of $n = 0$ modal frequency converges to that of plate without weakening as R_{22} is increased from value of 0. When $\nu = 0.3$, first six frequencies of plate without weakening are 3.19596 [$n = 0$], 4.61 [$n = 1$], 5.90356 [$n = 2$], 7.13955 [$n = 3$], 8.33993 [$n = 4$], and 9.51523 [$n = 5$]. Notice that the fundamental frequency of plate weakened along an internal concentric circle and resting on generally restrained edge against translation and rotation occurs at $n = 0$ mode. As $R_{22} \rightarrow \infty$ (as the spring becomes rigid), the frequency parameter stays at 3.19596. For the remaining values of R_{22} , the variation of frequency parameter is shown in Fig. 9. There is an optimum location within the plate.

Here, internal weakening decreases fundamental frequency 3.19596, which is the fundamental frequency of plate without weakening by less than 7% (6.39%). For a given value of R_{22} , the frequency k decreases from 3.19596 to 2.9916, increases to 3.19596 and finally decreases to 2.22145 as radius b of weakened circle varies from 0 to 1. Here, local maximum frequency 3.19596 occurs at $b = 0.6$. Thus $b = 0.6$ is optimum radius if the plate needs to be notched, such as a closed hatch. Here, internal weakening has significant effect [decreases fundamental frequency by less than 7% (6.39%)] on fundamental frequency

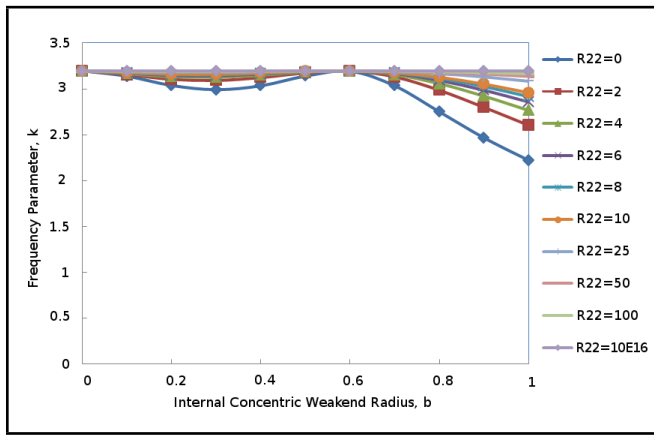


Figure 9. Fundamental frequency and concentric weakened radius parameter for different R_{22} and $R_{11} = T_{11} = 100000$, $\nu = 0.3$, and $n = 0$.

when $0 \leq b \leq 0.3$. Whereas it has enormous effect on fundamental frequency [decreases the fundamental frequency by less than 31% (30.49%)] when $b > 0.6$.

A reduction in fundamental frequency increases from 1% (at lower values of R_{22} , i.e. $R_{22} = 2$) to 8% (at higher values of R_{22} , i.e. $R_{22} = 10^5$) through 4% (for $R_{22} = 50$), 5% (for $R_{22} = 100$), 7% (for $R_{22} = 1000$) at lower values of internal concentric weakened radius parameter, b . A reduction in fundamental frequency increases as rotational restraint parameter R_{22} increases.

A reduction in fundamental frequency increases from 2% (at lower values of R_{22} , i.e. $R_{22} = 2$) to 31% (at higher values of R_{22} , i.e. $R_{22} = 10^5$) through 23% (for $R_{22} = 50$), 27% (for $R_{22} = 100$), 31% (for $R_{22} = 1000$) at higher values of internal concentric weakened radius parameter, b . A reduction in fundamental frequency increases with increase in rotational spring stiffness parameter R_{22} . The rotational spring stiffness parameter R_{22} has immense influence on percentage decrease in fundamental frequency parameter, at higher values of internal concentric weakened radius parameter b that greatly decreases the fundamental frequency.

In all the cases discussed above, when $b = 1$, the structure is corresponding to circular plate with elastic edge. Fundamental frequencies for $R_{22} = 0$ case, which impersonates a frictionless hinge/trough circular crack, are shown in the Table 7.

The frequency values for various values of R_{11} keeping R_{22} & T_{11} constant ($R_{22} = T_{11} = 10$) are tabulated. First frequencies [k] of $n \leq 5$ modes with $R_{11} = 0, 2, 4, 6, 8, 10, 25, 50$, and 10^{16} and $R_{22} = T_{11} = 10$ are shown in Tables 8 to 13. For $b = 1$ and $R_{11} = 0$, the frequency of plate is same as that of plate without having weakening crack. For a given value of b & ν , first frequency of $n = 0$ modal frequency converges to that of plate without weakening as R_{11} is increased from a value of 0. When $\nu = 0.3$, first six frequencies of plate without weakening are obtained as 1.85759 [$n = 0$], 2.43992 [$n = 1$], 2.98961 [$n = 2$], 3.84106 [$n = 3$], 4.84171 [$n = 4$], and 5.88973 [$n = 5$]. Notice that the fundamental frequency of plate weakened along an internal concentric circle and resting on elastically restrained edge occurs at $n = 0$ mode.

The frequency values for various values of T_{11} keeping R_{11} & R_{22} constant ($R_{11} = R_{22} = 10$) are tabulated. First frequencies [k] of $n \leq 5$ modes with $T_{11} = 0, 2, 4, 6, 8, 10, 25$,

50, and 10^{16} and $R_{11} = R_{22} = 10$ are shown in Tables 14 to 19. For $b = 1$ and $T_{11} = 0$, the frequency of plate is same as that of plate without having weakening crack. For a given value of b & ν , the first frequency of $n = 0$ modal frequency converges to that of plate without weakening as T_{11} is increased from a value of 0. When $\nu = 0.3$, first six frequencies of plate without weakening are obtained as 1.56837 [$n = 1$], 2.69693 [$n = 2$], 3.5696 [$n = 0$], 3.78149 [$n = 3$], 4.8612 [$n = 4$] and 5.89884 [$n = 5$]. Notice that the fundamental frequency of plate weakened along an internal concentric circle and resting on elastically restrained edge occurs at $n = 1$ mode.

According to the author's acquaintance, the results for circular plate with generally restrained edge conditions presented here, are quite new and are not available in literature. Hence, results could be compared only with those available in the literature as follows. (i) For the basic boundary such as simply supported and clamped plate³³ by setting the translational and rotational restraints with $T_{11} \rightarrow \infty$ & $R_{11} \rightarrow 0$ and $T_{11} \rightarrow \infty$ & $R_{11} \rightarrow \infty$, respectively. Here, internal weakening decreases fundamental frequency by less than 1% when b is 0 or 1 for simply supported plate and less than 1% for clamped plate. (ii) For the basic boundary such as movable edge and free³⁴ by setting the translational and rotational restraints with $T_{11} \rightarrow 0$ & $R_{11} \rightarrow \infty$ and $T_{11} \rightarrow 0$ & $R_{11} \rightarrow 0$, respectively. Here, internal weakening decreases fundamental frequency by less than 1% when $0 \leq b \leq 0.26$ for the plate with movable edge and less than 1% for the free plate. (iii) For non-classical boundary such as translational restrained edge³⁵ by setting rotational restraint $R_{11} \rightarrow 0$. Here, an internal weakening decreases fundamental frequency by less than 12% for a circular plate with translational restrained edge.

5. CONCLUSIONS

The exact vibration solutions of plates that are weakened along internal circle and that have generally restrained edges are presented. It is observed that the fundamental frequency of plate weakened along internal circle due to a crack and resting on generally restrained edges against translation and rotation occurs at $n = 0$ mode corresponding to $R_{22} = 0, 2, 4, 6, 8, 10, 25, 50$, and 10^{16} , $R_{11} = T_{11} = 2, 5, 50, 10, 50, 100, 1000$, and 10^5 , and $R_{11} = 0, 2, 4, 6, 8, 10, 25, 50$, and 10^{16} , $R_{22} = T_{11} = 10$ and at $n = 1$ mode corresponding to $T_{11} = 0, 2, 4, 6, 8, 10, 25, 50$, and 10^{16} & $R_{11} = R_{22} = 10$. Here, an internal weakening greatly decreases the fundamental frequency by less than 31% (30.49%). In addition, the frequencies are given for variable elastic restraints (T_{11} & R_{11}) at boundary which simulate the translational and rotational restraints where $T_{11} \rightarrow \infty$ & $R_{11} \rightarrow \infty$ represents a clamped support and $T_{11} \rightarrow \infty$ & $R_{11} \rightarrow 0$ represents a simply supported boundary. These exact solutions serve as benchmark solutions for verifying approximate results by other methods. Here, results presented are useful in the design of hatches and doors used in various industrial applications such as aerospace and automobile.

In summary, in this paper, the effect on fundamental frequency due to the influence of the presence of a crack is in-

Table 7. Fundamental frequency parameters, k for a circular hinge ($R_{22} = 0$, and for different values of R_{11} and $\nu = 0.3$).

b	$R_{22} \rightarrow 0$	0.1	0.2	0.3	0.4	0.5	0.6	0.7	0.8	0.9	1.0
$R_{11} = T_{11} = 10^{-3}$	2.31479	2.31968	2.33405	2.3561	2.38104	2.40017	2.40176	2.37951	2.33862	2.29143	2.17876
$R_{11} = T_{11} = 0.5$	2.03159	2.02739	2.0178	2.00962	2.00913	2.01691	2.02778	2.03063	2.00906	1.94995	1.85759
$R_{11} = T_{11} = 2$	1.39361	1.39256	1.39006	1.38707	1.38537	1.38577	1.38837	1.39186	1.39365	1.38926	1.374
$R_{11} = T_{11} = 5$	1.73362	1.73143	1.72623	1.72124	1.71975	1.72285	1.72903	1.73351	1.7287	1.70556	1.65872
$R_{11} = T_{11} = 10$	2.03159	2.02739	2.0178	2.00962	2.00913	2.01691	2.02778	2.03063	2.00906	1.94995	1.94995
$R_{11} = T_{11} = 50$	2.73979	2.71805	2.67328	2.64629	2.65856	2.70238	2.73905	2.69805	2.5432	2.33372	2.12973
$R_{11} = T_{11} = 100$	2.94748	2.91268	2.84521	2.80925	2.83227	2.89985	2.94745	2.86418	2.6474	2.3993	2.17453
$R_{11} = T_{11} = 1000$	3.17077	3.11603	3.01805	2.97341	3.01324	3.11488	3.16778	3.01734	2.73996	2.45934	2.45934
$R_{11} = T_{11} = 10^5$	3.19596	3.13862	3.03715	2.9916	3.03373	3.13965	3.19206	3.03315	2.74966	2.46594	2.22145
$R_{11} = T_{11} = 10^{16}$	3.19616	3.13892	3.03735	2.9918	3.03393	3.13995	3.19235	3.03325	2.74976	2.46603	2.22145

Table 8. First frequency parameter, ($n = 0$) for different R_{11} and internal concentric weakened radius parameter b , $R_{22} = T_{11} = 10$, and $\nu = 0.3$.

b	$R_{11} \rightarrow 0$	2	4	6	8	10	25	50	100	10^6
0	1.85759	1.96996	2.00196	2.01702	2.0258	2.03159	2.04705	2.05282	2.05592	2.05902
0.1	1.8532	1.96776	2.00027	2.01553	2.02441	2.03029	2.04595	2.05184	2.05483	2.05802
0.2	1.84802	1.96527	1.99837	2.01393	2.02301	2.02889	2.04485	2.05074	2.05383	2.05702
0.3	1.84413	1.96387	1.99748	2.01324	2.02241	2.0284	2.04445	2.05044	2.05353	2.05682
0.4	1.84224	1.96387	1.99768	2.01354	2.02281	2.0288	2.04486	2.05094	2.05403	2.05722
0.5	1.84254	1.96517	1.99898	2.01484	2.02391	2.0299	2.04596	2.05194	2.05503	2.05822
0.6	1.84483	1.96727	2.00067	2.01633	2.02531	2.03119	2.04695	2.05274	2.05583	2.05892
0.7	1.84852	1.96926	2.00187	2.01703	2.0258	2.03149	2.04675	2.05233	2.05532	2.05832
0.8	1.85261	1.96995	2.00117	2.01563	2.0239	2.02939	2.04385	2.04924	2.05203	2.05482
0.9	1.8561	1.96766	1.99688	2.01034	2.01802	2.02301	2.03637	2.04136	2.04395	2.04654
1	1.85759	1.96079	1.98721	1.99928	2.00616	2.01065	2.02252	2.02691	2.0292	2.03159

vestigated. Also, the variation of fundamental frequency with respect to the location of the crack is investigated for different values of R_{11} and T_{11} . In addition, the influence of the intensity of the crack on fundamental frequency is investigated in detail. From the various results obtained and presented, it is found that the fundamental frequency decreases as the crack moves away from the centre of the plate and it reduces with the reduction in the intensity of the crack.

REFERENCES

- Timoshenko, S. and Woinowsky-Krieger, S. *Theory of Plates and Shells*, McGraw-Hill, New York, (1959).
- Leissa, A. W. *Vibration of Plates*, (NASA SP-160). Office of Technology Utilization, Washington, DC, (1969).
- Szilar, R. *Theory and Analysis of Plates*, Prentice-Hall, New Jersey, (1974).
- Maan, H. Jawad. *Design of plate and shell structures*, ASME Three Park Avenue, New York, NY 10016, (2004).
- Magrab, E. B. *Vibrations of Elastic Structural Members*, Sijthoff & Noordhoff, The Netherlands, (1979).
- Azimi, S. Free Vibrations of Circular Plates with elastic or rigid interior support, *Journal of Sound and Vibration*, **120** (1), 37–52, (1988). [https://dx.doi.org/10.1016/0022-460X\(88\)90333-1](https://dx.doi.org/10.1016/0022-460X(88)90333-1)
- Weisensel, G. N. Natural Frequency Information for Circular and Annular Plates, *Journal of Sound and Vibration*, **133** (1), 129–137, (1989). [https://dx.doi.org/10.1016/0022-460X\(89\)90987-5](https://dx.doi.org/10.1016/0022-460X(89)90987-5)
- Ding, Z. Free Vibration of arbitrarily shaped plates with concentric ring elastic and/or rigid supports, *Computers & Structures*, **50** (5), 685–692, (1994). [https://dx.doi.org/10.1016/0045-7949\(94\)90427-8](https://dx.doi.org/10.1016/0045-7949(94)90427-8)
- Wang, C. Y. and Wang, C. M. Fundamental Frequencies of Circular Plates with internal elastic ring support, *Journal of Sound and Vibration*, **263** (5), 1071–1078, (2003). [https://dx.doi.org/10.1016/S0022-460X\(03\)00275-X](https://dx.doi.org/10.1016/S0022-460X(03)00275-X)
- Dimarogonas, A. D. Vibration of Cracked Structures: A State of the Art Review, *Engineering Fracture Mechanics*, **55** (5), 831–857, (1996). [https://dx.doi.org/10.1016/0013-7944\(94\)00175-8](https://dx.doi.org/10.1016/0013-7944(94)00175-8)
- Papadopoulos Chris, A. The strain energy release approach for modeling cracks in rotors: A state of the art review, *Mechanical Systems and Signal Processing*, **22** (4), 763–789, (2008). <https://dx.doi.org/10.1016/j.ymssp.2007.11.009>
- Broda, D., Staszewski, W. J., Martowicz, A., Uhl, T., and Silberschmidt, V. V. Modeling of nonlinear crack-wave interactions for damage detection based on ultrasound: A review, *Journal of Sound and Vibration*, **333** (4), 1097–1118, (2014). <https://dx.doi.org/10.1016/j.jsv.2013.09.033>
- Lynn, P. P. and Kumbasar, N. Free Vibrations of Thin Rectangular Plates Having Narrow Cracks with Simply Supported Edges, *Dev Mech*, **4**, 911–928, (1967).
- Petyt, M. The Vibration Characteristics of a Tensioned Plate Containing a Fatigue Crack, *Journal of Sound and Vibration*, **8** (3), 377–389 (1968). [https://dx.doi.org/10.1016/0022-460X\(68\)90244-7](https://dx.doi.org/10.1016/0022-460X(68)90244-7)
- Stahl, B. and Keer, L. M. Vibration and Stability of Cracked Rectangular Plates, *International Journal of Solids and Structures*, **8** (1), 69–91, (1972). [https://dx.doi.org/10.1016/0020-7683\(72\)90052-2](https://dx.doi.org/10.1016/0020-7683(72)90052-2)
- Hirano, Y. and Okazaki, K. Vibration of Cracked Rectangular-Plates, *Bulletin of the JSME*, **23** (179), 732–740, (1980). <https://dx.doi.org/10.1299/jsme1958.23.732>

Table 9. First frequency parameter, ($n = 1$) for different R_{11} and internal concentric weakened radius parameter b , $R_{22} = T_{11} = 10$, and $\nu = 0.3$.

b	$R_{11} \rightarrow 0$	2	4	6	8	10	25	50	100	10^6
0	2.44	2.45249	2.45729	2.45978	2.46129	2.46239	2.4654	2.46658	2.46719	2.46788
0.1	2.43772	2.44982	2.45442	2.45682	2.45832	2.45932	2.46222	2.46342	2.46402	2.46462
0.2	2.43442	2.44592	2.45023	2.45252	2.45392	2.45492	2.45762	2.45872	2.45932	2.45992
0.3	2.43063	2.44113	2.44513	2.44723	2.44853	2.44943	2.45193	2.45284	2.45343	2.45394
0.4	2.42654	2.43604	2.43955	2.44145	2.44255	2.44335	2.44555	2.44635	2.44685	2.44735
0.5	2.42315	2.43146	2.43456	2.43616	2.43706	2.43776	2.43967	2.44037	2.44077	2.44117
0.6	2.42155	2.42887	2.43157	2.43287	2.43378	2.43428	2.43588	2.43658	2.43688	2.43719
0.7	2.42286	2.42947	2.43187	2.43308	2.43378	2.43428	2.43568	2.43629	2.43659	2.43689
0.8	2.42745	2.43386	2.43616	2.43737	2.43807	2.43857	2.43987	2.44037	2.44067	2.44097
0.9	2.43423	2.44144	2.44394	2.44524	2.44604	2.44654	2.44795	2.44845	2.44875	2.44905
1	2.43992	2.44962	2.45282	2.45442	2.45532	2.45602	2.45772	2.45842	2.45882	2.45922

Table 10. First frequency parameter, ($n = 2$) for different R_{11} and internal concentric weakened radius parameter b , $R_{22} = T_{11} = 10$, and $\nu = 0.3$.

b	$R_{11} \rightarrow 0$	2	4	6	8	10	25	50	100	10^6
0	2.98959	3.09309	3.1382	3.16344	3.17951	3.1908	3.22393	3.23752	3.24499	3.25278
0.1	2.9909	3.0945	3.13971	3.16506	3.18123	3.19241	3.22565	3.23932	3.24671	3.25459
0.2	2.9927	3.09649	3.1418	3.16705	3.18332	3.1945	3.22784	3.24151	3.2489	3.25688
0.3	2.99399	3.09748	3.1426	3.16785	3.18392	3.1952	3.22833	3.24191	3.24929	3.25718
0.4	2.99359	3.09578	3.1402	3.16505	3.18082	3.1919	3.22433	3.23761	3.2449	3.25258
0.5	2.99089	3.08999	3.13271	3.15656	3.17173	3.18221	3.21316	3.22583	3.23272	3.24001
0.6	2.9858	3.07971	3.11974	3.1419	3.15597	3.16565	3.1942	3.20588	3.21217	3.21886
0.7	2.98001	3.06715	3.10368	3.12374	3.13642	3.1452	3.17076	3.18114	3.18673	3.19262
0.8	2.97673	3.05697	3.08991	3.10778	3.11896	3.12674	3.14911	3.15819	3.16308	3.16827
0.9	2.97953	3.05468	3.08452	3.10059	3.11057	3.11736	3.13712	3.14501	3.1493	3.1537
1	2.98961	3.06436	3.0929	3.10788	3.11716	3.12345	3.14151	3.1486	3.15239	3.15638

Table 11. First frequency parameter, ($n = 3$) for different R_{11} and internal concentric weakened radius parameter b , $R_{22} = T_{11} = 10$, and $\nu = 0.3$.

b	$R_{11} \rightarrow 0$	2	4	6	8	10	25	50	100	10^6
0	3.84103	3.97959	4.04817	4.08909	4.11635	4.13572	4.19552	4.22127	4.23555	4.25104
0.1	3.84106	3.97961	4.04819	4.08922	4.11637	4.13574	4.19564	4.2214	4.23567	4.25105
0.2	3.84156	3.98011	4.04879	4.08982	4.11697	4.13644	4.19634	4.22209	4.23637	4.25184
0.3	3.84295	3.98171	4.05048	4.09151	4.11876	4.13813	4.19813	4.22399	4.23826	4.25374
0.4	3.84514	3.98389	4.05257	4.0936	4.12085	4.14022	4.20012	4.22587	4.24015	4.25562
0.5	3.84683	3.98429	4.05216	4.09259	4.11945	4.13851	4.19741	4.22267	4.23675	4.25182
0.6	3.84533	3.97839	4.04368	4.08241	4.10797	4.12614	4.18204	4.2059	4.21918	4.23346
0.7	3.83864	3.96303	4.02312	4.05846	4.08172	4.0982	4.14851	4.16988	4.18166	4.19434
0.8	3.82927	3.94078	3.99349	4.02414	4.0442	4.05828	4.10111	4.11918	4.12917	4.13975
0.9	3.82608	3.92312	3.96744	3.9928	4.00917	4.02075	4.05529	4.06967	4.07756	4.08604
1	3.84106	3.92661	3.96355	3.98411	3.99719	4.00627	4.03303	4.04401	4.05	4.05629

Table 12. First frequency parameter, ($n = 4$) for different R_{11} and internal concentric weakened radius parameter b , $R_{22} = T_{11} = 10$, and $\nu = 0.3$.

b	$R_{11} \rightarrow 0$	2	4	6	8	10	25	50	100	10^6
0	4.84169	4.97687	5.05146	5.09868	5.13132	5.1551	5.23208	5.26682	5.2866	5.30826
0.1	4.84171	4.9769	5.05148	5.0987	5.13125	5.15511	5.2321	5.26684	5.28661	5.30828
0.2	4.84181	4.97699	5.05158	5.0988	5.13135	5.15521	5.23219	5.26694	5.28671	5.30838
0.3	4.84221	4.97749	5.05207	5.0994	5.13195	5.15581	5.23289	5.26764	5.28741	5.30908
0.4	4.8437	4.97918	5.05386	5.10119	5.13384	5.1577	5.23488	5.26973	5.2895	5.31126
0.5	4.84639	4.98167	5.05625	5.10347	5.13602	5.15978	5.23666	5.27131	5.29098	5.31265
0.6	4.84787	4.98086	5.05384	5.09997	5.13162	5.15478	5.22937	5.26292	5.28199	5.30286
0.7	4.84258	4.96808	5.03617	5.07891	5.10816	5.12943	5.19763	5.22809	5.24536	5.26413
0.8	4.82842	4.93914	4.99805	5.0345	5.05936	5.07734	5.13435	5.15952	5.1738	5.18928
0.9	4.81795	4.90771	4.95384	4.9819	5.00077	5.01435	5.05669	5.07526	5.08565	5.09683
1	4.84171	4.90831	4.94006	4.95863	4.97081	4.9794	5.00566	5.01675	5.02293	5.02952

Table 13. First frequency parameter, ($n = 5$) for different R_{11} and internal concentric weakened radius parameter b , $R_{22} = T_{11} = 10$, and $\nu = 0.3$.

b	$R_{11} \rightarrow 0$	2	4	6	8	10	25	50	100	10^6
0	5.88972	6.01304	6.08684	6.13595	6.171	6.19718	6.28555	6.32739	6.35177	6.37902
0.1	5.88974	6.01305	6.08685	6.13598	6.17103	6.19719	6.28557	6.32741	6.35178	6.37894
0.2	5.88973	6.01305	6.08685	6.13598	6.17103	6.19719	6.28557	6.32741	6.35178	6.37904
0.3	5.88983	6.01315	6.08704	6.13617	6.17113	6.19739	6.28576	6.32761	6.35197	6.37924
0.4	5.89053	6.01395	6.08784	6.13707	6.17212	6.19838	6.28685	6.3287	6.35316	6.38033
0.5	5.89281	6.01623	6.09022	6.13945	6.1745	6.20076	6.28934	6.33118	6.35564	6.3829
0.6	5.89549	6.01811	6.0913	6.14003	6.17468	6.20055	6.28782	6.32906	6.35303	6.37979
0.7	5.89199	6.00912	6.07852	6.12445	6.15691	6.18117	6.26246	6.30061	6.32278	6.34735
0.8	5.87353	5.97629	6.0361	6.07515	6.10262	6.12309	6.1908	6.22216	6.24034	6.26041
0.9	5.85348	5.93148	5.97542	6.00358	6.02316	6.03754	6.08458	6.10595	6.11824	6.13182
1	5.88973	5.93358	5.95615	5.96983	5.97902	5.98571	6.00638	6.01547	6.02056	6.02606

Table 14. First frequency parameter, ($n = 0$) for different T_{11} and internal concentric weakened radius parameter b , $R_{11} = R_{22} = 10$, and $\nu = 0.3$.

b	$T_{11} \rightarrow 0$	2	4	6	8	10	25	50	100	10^6
0	3.67597	1.40294	1.65497	1.81687	1.9368	2.03159	2.41131	2.64156	2.79104	2.95826
0.1	3.64793	1.40274	1.65458	1.81618	1.9358	2.03029	2.40753	2.63439	2.78059	2.94293
0.2	3.62648	1.40254	1.65418	1.81548	1.9347	2.02889	2.40364	2.62751	2.77063	2.92897
0.3	3.62838	1.40244	1.65398	1.81518	1.9343	2.0284	2.40225	2.62533	2.76804	2.92579
0.4	3.64843	1.40254	1.65408	1.81538	1.9346	2.0288	2.40374	2.62842	2.77283	2.93356
0.5	3.67026	1.40264	1.65448	1.81598	1.9355	2.0299	2.40713	2.63479	2.78219	2.9471
0.6	3.67445	1.40284	1.65488	1.81668	1.9365	2.03119	2.41052	2.64057	2.79005	2.95746
0.7	3.65221	1.40294	1.65498	1.81687	1.9367	2.03149	2.41091	2.64036	2.78875	2.95387
0.8	3.61401	1.40264	1.65438	1.81577	1.9351	2.02939	2.40453	2.6286	2.77152	2.92887
0.9	3.58008	1.40174	1.65218	1.81228	1.93021	2.02301	2.38799	2.60111	2.73496	2.88173
1	3.5696	1.39985	1.6479	1.80531	1.92054	2.01065	2.3588	2.55688	2.68026	2.81682

Table 15. First frequency parameter, ($n = 1$) for different T_{11} and internal concentric weakened radius parameter b , $R_{11} = R_{22} = 10$, and $\nu = 0.3$.

b	$T_{11} \rightarrow 0$	2	4	6	8	10	25	50	100	10^6
0	1.66531	1.9257	2.10646	2.24722	2.36323	2.46239	2.94164	3.34731	3.72084	4.30624
0.1	1.66095	1.92223	2.10329	2.24415	2.36026	2.45932	2.93797	3.34204	3.71257	4.28781
0.2	1.65486	1.91734	2.0988	2.23976	2.35587	2.45492	2.93218	3.33315	3.69779	4.25278
0.3	1.64738	1.91145	2.09332	2.23447	2.35048	2.44943	2.92469	3.32157	3.67844	4.20901
0.4	1.6382	1.90437	2.08703	2.22838	2.3445	2.44335	2.91701	3.3103	3.6612	4.17802
0.5	1.62743	1.89669	2.08035	2.2223	2.33871	2.43776	2.91153	3.30434	3.65524	4.17933
0.6	1.61535	1.88891	2.07446	2.21752	2.33473	2.43428	2.91084	3.30754	3.66592	4.2176
0.7	1.60259	1.88222	2.07047	2.21522	2.33363	2.43428	2.91633	3.32031	3.69034	4.27481
0.8	1.58992	1.87754	2.06938	2.21642	2.33653	2.43857	2.927	3.33765	3.71545	4.30623
0.9	1.57824	1.87584	2.07207	2.2215	2.3433	2.44654	2.93826	3.34751	3.71704	4.26818
1	1.56837	1.87793	2.07845	2.22998	2.35258	2.45602	2.94125	3.33206	3.67021	4.15757

Table 16. First frequency parameter, ($n = 2$) for different T_{11} and internal concentric weakened radius parameter b , $R_{11} = R_{22} = 10$, and $\nu = 0.3$.

b	$T_{11} \rightarrow 0$	2	4	6	8	10	25	50	100	10^6
0	2.83713	2.92015	2.99601	3.06574	3.13043	3.1908	3.54753	3.93833	4.39911	5.55402
0.1	2.83915	2.92207	2.99782	3.06747	3.13214	3.19241	3.54904	3.93984	4.40082	5.55823
0.2	2.84184	2.92467	3.00021	3.06986	3.13433	3.1945	3.55083	3.94143	4.4023	5.558
0.3	2.84323	2.92586	3.00121	3.07066	3.13512	3.1952	3.55072	3.94022	4.39889	5.53072
0.4	2.84083	2.92326	2.99851	3.06776	3.13192	3.1919	3.54602	3.93282	4.3856	5.4648
0.5	2.83185	2.91418	2.98932	3.05848	3.12254	3.18221	3.53454	3.91765	4.36235	5.39402
0.6	2.81409	2.89692	2.97236	3.04171	3.10588	3.16565	3.51769	3.89891	4.33973	5.37288
0.7	2.78795	2.87227	2.94901	3.01947	3.08463	3.1452	3.50103	3.88606	4.33318	5.4288
0.8	2.75621	2.84413	2.92387	2.99682	3.06418	3.12674	3.49286	3.88886	4.35193	5.52572
0.9	2.72378	2.81818	2.90311	2.98045	3.0516	3.11736	3.49983	3.9098	4.38672	5.54383
1	2.69693	2.80112	2.89373	2.97725	3.05349	3.12345	3.52218	3.93583	4.3971	5.40798

Table 17. First frequency parameter, ($n = 3$) for different T_{11} and internal concentric weakened radius parameter b , $R_{11} = R_{22} = 10$, and $\nu = 0.3$.

b	$T_{11} \rightarrow 0$	2	4	6	8	10	25	50	100	10^6
0	3.95635	3.99457	4.03153	4.06736	4.10208	4.13572	4.35999	4.65502	5.07354	6.75599
0.1	3.95638	3.99461	4.03164	4.06747	4.1021	4.13574	4.36011	4.65503	5.07356	6.75632
0.2	3.95707	3.9953	4.03233	4.06807	4.1028	4.13644	4.36071	4.65573	5.07435	6.7591
0.3	3.95887	3.9971	4.03413	4.06986	4.10459	4.13813	4.3624	4.65732	5.07594	6.75865
0.4	3.96126	3.99948	4.03632	4.07205	4.10668	4.14022	4.36399	4.6583	5.07562	6.72428
0.5	3.96055	3.99848	4.03521	4.07074	4.10518	4.13851	4.36098	4.6531	5.06582	6.63323
0.6	3.94947	3.9872	4.02363	4.05896	4.0931	4.12614	4.34661	4.63523	5.04067	6.541
0.7	3.92153	3.95926	3.99569	4.03092	4.06506	4.0982	4.31817	4.60551	5.00837	6.53889
0.8	3.87662	3.91545	3.95298	3.98921	4.02434	4.05828	4.28395	4.57838	4.99242	6.65873
0.9	3.82431	3.86644	3.90706	3.94629	3.98412	4.02075	4.26259	4.57598	5.01536	6.75635
1	3.78149	3.8304	3.87711	3.92183	3.96485	4.00627	4.27486	4.61219	5.06654	6.61541

Table 18. First frequency parameter, ($n = 4$) for different T_{11} and internal concentric weakened radius parameter b , $R_{11} = R_{22} = 10$, and $\nu = 0.3$.

b	$T_{11} \rightarrow 0$	2	4	6	8	10	25	50	100	10^6
0	5.05056	5.07222	5.09341	5.11427	5.13483	5.1551	5.29775	5.50518	5.83866	7.93035
0.1	5.05059	5.07216	5.09342	5.11428	5.13485	5.15511	5.29777	5.5052	5.83869	7.93038
0.2	5.05069	5.07226	5.09352	5.11438	5.13495	5.15521	5.29777	5.5053	5.83878	7.93097
0.3	5.05129	5.07285	5.09411	5.11498	5.13554	5.15581	5.29846	5.5059	5.83948	7.93393
0.4	5.05328	5.07484	5.09601	5.11687	5.13744	5.1577	5.30035	5.50778	5.84126	7.92598
0.5	5.05557	5.07713	5.09829	5.11915	5.13962	5.15978	5.30194	5.50866	5.84064	7.8587
0.6	5.05156	5.07292	5.09389	5.11445	5.13482	5.15478	5.29553	5.49986	5.82684	7.72757
0.7	5.02751	5.04857	5.06933	5.0897	5.10976	5.12943	5.26819	5.46933	5.79003	7.64986
0.8	4.97431	4.99558	5.01654	5.03711	5.05737	5.07734	5.2174	5.42034	5.74435	7.74586
0.9	4.90284	4.9259	4.94856	4.97082	4.99279	5.01435	5.16549	5.38401	5.73237	7.92328
1	4.84612	4.87388	4.90113	4.92779	4.95384	4.9794	5.1568	5.40656	5.79155	7.79604

Table 19. First frequency parameter, ($n = 5$) for different T_{11} and internal concentric weakened radius parameter b , $R_{11} = R_{22} = 10$, and $\nu = 0.3$.

b	$T_{11} \rightarrow 0$	2	4	6	8	10	25	50	100	10^6
0	6.12986	6.14357	6.15713	6.17061	6.18399	6.19718	6.29282	6.43937	6.69385	9.08574
0.1	6.1299	6.14358	6.15715	6.17063	6.18401	6.19719	6.29284	6.4394	6.69387	9.08575
0.2	6.1299	6.14357	6.15715	6.17063	6.18401	6.19719	6.29284	6.4394	6.69387	9.08585
0.3	6.13	6.14377	6.15735	6.17083	6.18411	6.19739	6.29293	6.43959	6.69407	9.08732
0.4	6.13099	6.14467	6.15824	6.17172	6.1851	6.19838	6.29393	6.44059	6.69516	9.08865
0.5	6.13347	6.14725	6.16083	6.1742	6.18758	6.20076	6.29631	6.44286	6.69713	9.05246
0.6	6.13375	6.14733	6.16081	6.17419	6.18747	6.20055	6.29539	6.44075	6.69251	8.9186
0.7	6.11558	6.12896	6.14224	6.15532	6.1683	6.18117	6.27422	6.41659	6.66236	8.77277
0.8	6.05799	6.07127	6.08435	6.09743	6.11031	6.12309	6.21534	6.35641	6.60001	8.81281
0.9	5.96765	5.98192	5.996	6.00998	6.02386	6.03754	6.13658	6.28804	6.54981	9.05407
1	5.89884	5.91661	5.93419	5.95156	5.96873	5.98571	6.10702	6.28922	6.59581	8.95778

- 17 Solecki, R. Bending Vibration of a Simply Supported Rectangular Plate with a Crack Parallel to One Edge, *Engineering Fracture Mechanics*, **18** (6), 1111–1118, (1983). [https://dx.doi.org/10.1016/0013-7944\(83\)90004-8](https://dx.doi.org/10.1016/0013-7944(83)90004-8)
- 18 Yuan, J. and Dickinson, S. M. The Flexural Vibration of Rectangular Plate Systems Approached by Using Artificial Springs in the Rayleigh-Ritz Method, *Journal of Sound and Vibration*, **159** (1), 39–55, (1992). [https://dx.doi.org/10.1016/0022-460X\(92\)90450-C](https://dx.doi.org/10.1016/0022-460X(92)90450-C)
- 19 Huang Chi-Hung, Ma Chien-Ching. Vibration of cracked circular plates at resonance frequencies, *Journal of Sound and Vibration*, **236** (4), 637–656, (2001). <https://dx.doi.org/10.1006/jsvi.2000.2974>
- 20 Liew, K. M., Hung, K. C. and Lim, M. K. A Solution Method for Analysis of Cracked Plates under Vibration, *Engineering and Fracture Mechanics*, **48** (3), 393–404, (1994). [https://dx.doi.org/10.1016/0013-7944\(94\)90130-9](https://dx.doi.org/10.1016/0013-7944(94)90130-9)
- 21 Ma, C. C. and Huang, C. H. Experimental and Numerical Analysis of Vibrating Cracked Plates at Resonant Frequencies, *Experimental Mechanics*, **41** (1), 8–18, (2001). <https://dx.doi.org/10.1007/BF02323099>
- 22 Si, X. H., Lu, W. X., and Chu, F. L. Modal analysis of circular plates with radial side cracks and in contact with water on one side based on the Rayleigh-Ritz method, *Journal of Sound and Vibration*, **331** (1), 231–251, (2012). <https://dx.doi.org/10.1016/j.jsv.2011.08.026>
- 23 Qian, G. L., Gu, S. N., and Jiang, J. S. A finite element model of cracked plates and applications to vibration problems, *Computers & Structures*, **39** (5), 483–487, (1991). [https://dx.doi.org/10.1016/0045-7949\(91\)90056-R](https://dx.doi.org/10.1016/0045-7949(91)90056-R)
- 24 Lee, H. P. and Lim, S. P. Vibration of cracked rectangular plates including transverse shear deformation and rotary inertia, *Computers & Structures*, **49** (4), 715–718, (1993). [https://dx.doi.org/10.1016/0045-7949\(93\)90074-N](https://dx.doi.org/10.1016/0045-7949(93)90074-N)
- 25 Krawczuk, M. Natural vibrations of rectangular plates with a through crack, *Archives of Applied Mechanics*, **63** (7), 491–504, (1993). <https://dx.doi.org/10.1007/BF00788047>
- 26 Liew, K. M., Hung, K. C., and Lim, M. K. A solution method for analysis of cracked plates under vibration, *Engineering and Fracture Mechanics*, **48** (3), 393–404, (1994). [https://dx.doi.org/10.1016/0013-7944\(94\)90130-9](https://dx.doi.org/10.1016/0013-7944(94)90130-9)
- 27 Khadem, S. E. and Rezaee, M. An analytical approach for obtaining the location and depth of an all-over part-through crack on externally in-plane loaded rectangular plate using vibration analysis, *Journal of Sound and Vibration*, **230** (2), 291–308, (2000). <https://dx.doi.org/10.1006/jsvi.1999.2619>
- 28 Krawczuk, M., Zak, A., and Ostachowicz, W. Finite element model of plate with elasto-plastic through crack, *Computers & Structures*, **79** (5), 519–532, (2001). [https://dx.doi.org/10.1016/S0045-7949\(00\)00156-5](https://dx.doi.org/10.1016/S0045-7949(00)00156-5)
- 29 Lee, P. Fundamental frequencies of annular plates with internal cracks, *Computers & Structures*, **43** (6), 1085–1089, (1992). [https://dx.doi.org/10.1016/0045-7949\(92\)90009-O](https://dx.doi.org/10.1016/0045-7949(92)90009-O)
- 30 Ramesh, K., Chauhan, D. P. S., and Mallik, A. K. Free vibration of an annular plate with periodic radial cracks, *Journal of Sound and Vibration*, **206** (2), 266–274, (1997). <https://dx.doi.org/10.1006/jsvi.1997.1028>
- 31 Anifantis, N. K., Actis, R. L., and Dimarogonas, A. D. Vibration of cracked annular plates, *Engineering Fracture Mechanics*, **49** (3), 371–379, (1994). [https://dx.doi.org/10.1016/0013-7944\(94\)90265-8](https://dx.doi.org/10.1016/0013-7944(94)90265-8)
- 32 Yuan, J., Young, P. G. and Dickinson, S. M. Natural frequencies of circular and annular plates with radial or circumferential cracks, *Computers & Structures*, **53** (2), 327–334, (1994). [https://dx.doi.org/10.1016/0045-7949\(94\)90205-4](https://dx.doi.org/10.1016/0045-7949(94)90205-4)
- 33 Wang, C. Y. Fundamental frequency of a circular plate weakened along a concentric circle, *Journal of Applied Mathematics and Mechanics*, **82** (1), 70–72, (2002). [https://dx.doi.org/10.1002/1521-4001\(200201\)82:1<70::AID-ZAMM70>3.0.CO;2-A](https://dx.doi.org/10.1002/1521-4001(200201)82:1<70::AID-ZAMM70>3.0.CO;2-A)
- 34 Yu, L. H. Frequencies of circular plate weakened along an internal concentric circle, *International Journal of Structural Stability and Dynamics*, **9** (1), 179–185, (2009). <https://dx.doi.org/10.1142/S021945540900293X>
- 35 Bhaskara Rao, L. and Kameswara Rao, C. Frequencies of circular plates weakened along an internal concentric circle and elastically restrained edge against translation, *Journal of Applied Mechanics-T ASME*, 1-7, (2013). <https://dx.doi.org/10.1115/1.4006938>
- 36 Kim, C. S. and Dickinson, S. M. The flexural vibration of the isotropic and polar orthotropic annular and circular plates with elastically restrained peripheries, *Journal of Sound and Vibration*, **143** (1), 171–179(1990). [https://dx.doi.org/10.1016/0022-460X\(90\)90576-L](https://dx.doi.org/10.1016/0022-460X(90)90576-L)
- 37 Wang, C. Y. and Wang, C. M. Buckling of circular plates with an internal ring support and elastically restrained edges, *Thin Walled Structures*, **39** (5), 821–825, (2001). [https://dx.doi.org/10.1016/S0263-8231\(01\)00031-3](https://dx.doi.org/10.1016/S0263-8231(01)00031-3)
- 38 Rao, L. B. and Rao, C. K. Buckling of annular plates with elastically restrained external and internal edges, *Mechanics Based Design of Structures and Machines*, **41** (2), 222–235, (2013). <https://dx.doi.org/10.1080/15397734.2012.717495>
- 39 Bhaskara Rao, L. and Kameswara Rao, C. Vibrations of elastically restrained circular plates resting on Winkler foundation, *Arabian Journal for Science and Engineering*, **38** (11), 3171–3180, (2013). <https://dx.doi.org/10.1007/s13369-012-0457-1>

See discussions, stats, and author profiles for this publication at: <https://www.researchgate.net/publication/316462738>

Torsional post-buckling of thin-walled open section clamped beam supported on Winkler–Pasternak foundation

Article in Thin-Walled Structures · July 2017

DOI: 10.1016/j.tws.2017.03.017

CITATIONS

8

READS

233

2 authors:



Kameswara Rao Chellapilla

NNRG

105 PUBLICATIONS 459 CITATIONS

[SEE PROFILE](#)



Lokavarapu Bhaskara Rao

VIT University Chennai

80 PUBLICATIONS 198 CITATIONS

[SEE PROFILE](#)

Some of the authors of this publication are also working on these related projects:



Computational Mechanics [View project](#)



Nanotechnology [View project](#)



Full length article

Torsional post-buckling of thin-walled open section clamped beam supported on Winkler-Pasternak foundation



Chellapilla Kameswara Rao^a, Lokavarapu Bhaskara Rao^{b,*}

^a Nalla Narsimha Reddy Engineering College, Chowdariguda (V), Ghatkesar (M), Ranga Reddy (Dt) - 500088, Telangana, India

^b School of Mechanical & Building Sciences, VIT University, Chennai Campus, Vandalur-Kelambakkam Road, Chennai 600127, India

ARTICLE INFO

Keywords:

Beam
Open section
Post-buckling
Warping
Winkler-Pasternak foundation

ABSTRACT

The study presents the post-buckling behaviour of thin-walled beam of open section supported by Winkler-Pasternak foundation and it is subjected to an axial compressive load. Here, the assumptions are the strains to be small and elastic, in-plan cross-sectional deformations and the shear deformations to be negligible. The post-buckling paths are determined for clamped beam of I - cross-section which is constant. The point of bifurcation for clamped beam is calculated. It is found to be symmetric and stable for various values of Winkler-Pasternak foundation parameters and Warping parameter.

1. Introduction

The study of the post-buckling response of thin-walled prismatic beam of open section has many applications in civil, naval, rail, aircraft and automotive structures. Furthermore, several of the base-frame structures of rotating equipment consist of thin-walled beams of open section which are either partially or continuously supported by other structural members or concrete foundations. Under some critical loading conditions these beams undergo either coupled flexural-torsional or pure torsional buckling which poses critical design problems in industry. Practical problems involving beams supported on a grid-type support structure or different types of machine foundations come under the category of beams on Winkler-Pasternak foundation and this improved model is being adopted for getting more accurate dynamic characteristics of the supported beam in bending, torsion and coupled bending-torsion type of problems.

The problem of linear torsional buckling has been widely investigated and the results for such cases are presented [1,2]. Although, the classical linear buckling theories for elastic beams necessarily predict buckling at loads that remain constant as the buckling amplitude increases. YOUNG [3] was the first person who investigated the nonlinear behaviour of circular members in uniform torsion. The related problem of torsional stiffness of narrow rectangular sections under axial tension was examined by BUCKLEY [4]. The behaviour of thin-walled I and Z sections was investigated by CULLIMORE [5]. GHOBARAH and TSO [6,7] presented more accurate theory of non-linear non-uniform torsion of thin-walled beams of open section by using the principle of minimum potential energy and taking into

account large torsional deformations under general loading and boundary conditions.

Bazant and Nimeiri [8], Epstein and Murray [9], Szymczak [10], Roberts and Azizian [11] and Wekezer [12,13] studied the nonlinear torsional behaviour of thin-walled beams in a great detail. The post buckling behaviour of thin-walled open cross-section compression members using the general nonlinear theory of elastic stability was studied by Grimaldi et al. [14]. However, in all these studies the effect of continuous elastic foundation was not considered. Kameswara Rao et al. [15,16] studied the effect of Winkler-type elastic foundation on the linear torsional stability of thin-walled beams of open section, but its effect on post-buckling behaviour was not studied. KAMESWARA RAO ET AL., [17] investigated the post-buckling behaviour of thin-walled beams of open section subjected to an axial compressive load and resting on a Winkler-type continuous elastic foundation.

Winkler model of elastic foundation, also known as one-parameter model, is the simplest and the widely used model which is based on the assumption that the respective displacement is proportional to the pressure at the contact surface all along the beam length and that the soil foundation is composed of closely spaced, independent and linear elastic springs. As this Winkler model suffers from the deficiency of assuming that no interaction takes place between these soil springs, it does not accurately predict the dynamic response of practical foundations such as pavements or machine foundations [18]. In order to overcome this deficiency, a two-parameter foundation model such as Winkler-Pasternak foundation model is developed by PASTERNAK [19] who introduced an additional shear layer in the Winkler model and thus including the effect of shear interactions between the springs.

* Corresponding author.

E-mail addresses: chellapilla95@gmail.com (C.K. Rao), bhaskarababu_20@yahoo.com (L.B. Rao).

Nomenclature

A	Area of cross-section and length of the beam
L	Length of the beam
G	Shear modulus
E	Young's modulus
\varnothing	Angle of twist
$x(z)$	Normal function of angle of twist
z	Distance along the length of beam
C_w	Warping constant
C_s	Torsion constant
K	Warping parameter
K_w	Winkler foundation modulus
K_p	Pasternak foundation modulus

P	Axial compressive load
P_{cr}	Linear buckling load
P_{cr}^*	Non-linear buckling load
σ	P/A , axial compressive stress
K^2	$GC_s L^2/EC_w$ Warping parameter
Δ^2	$\sigma I_p L^2/EC_w$; load parameter
Δ_{cr}	Linear buckling load parameter
Δ_{cr}^*	Non-linear buckling load parameter
F	$I_R - (I_{PC}/A)^2$, cross-sectional property
I_R	Polar moment of inertia of beam, also $I_{PC} = 1/2 I_p$
δ	F/C_w
λ^2	$K_w L^4/EC_w$ Winkler foundation parameter
ξ^2	$K_p L^2/EC_w$ Pasternak foundation parameter

SIMÃO [20] presented post-buckling bi-furcational analysis of thin-walled prismatic members in the context of the generalized beam theory. He presented a series of analytical models, based on the generalized beam theory (GBT), investigating the buckling and post-buckling behaviour of thin-walled prismatic cold-formed steel structural members under compression and/or bending. The effect of warping constraints on the buckling of thin-walled structures was studied by Pignataro et al. [21]. They have considered various warping constraints at the bar ends and the relevant buckling modes and loads are numerically evaluated. Camotim et al. [22] presented a state-of-the-art report on the use of Generalized Beam Theory (GBT) to assess the buckling behaviour of plane and space thin-walled steel frames. The torsion of restrained thin-walled bars of open constant bi-symmetric cross-section was investigated by Kujawa [23] using Castiglione's first theorem. The exact solutions were simplified by expanding them in a power series. The effect of warping on the post-buckling behaviour of thin-walled structures was investigated by Rizzi and Varano [24]. They have used a direct one-dimensional model to describe the mechanical behaviour of thin-walled beams to analyse the initial post buckling of some sample framed structures. Kujawa and Szymczak [25] studied the elastic stability of axially compressed bar related to the cross-section distortion using the principle of stationary total potential energy. The aim of present paper is to study in detail, the effect of continuous Winkler-Pasternak elastic foundation on the torsional post-buckling behaviour of clamped uniform thin-walled beam of open cross-section.

2. Mathematical formulation of the problem

The purpose of this work is to study theatrically the elastically torsional post buckling behaviour of statically indeterminate (or hyperstatic) beam of I-section supported on Winkler-Pasternak foundation as shown in Fig. 1(a). The beam under consideration is doubly symmetric thin-walled beam of constant cross-section undergoing pure torsion and subjected to an axial compressive load. The constant cross-section of I-section is shown in Fig. 1(b).

Assumptions in the present study are, neglect the effects of (i) shear deformations (ii) large and inelastic strains, and (iii) in-plane cross-sectional deformations.

Considering \varnothing as the angle of twist undergone by the thin-walled open section beam, the torque developed in the beam T under non-linear torsional deformation is given by

$$T = GC_s \varnothing' - EC_w \varnothing''' + 2EF(\varnothing')^3 \quad (1)$$

where C_w is the warping constant $= I_f h^2/2$, C_s = shear constant $= (1/3)(2b_f t_f^3 + h t_w^3)$, the prime denotes differentiation with respect to z , E the Young's modulus, G the shear modulus, I_R the fourth moment of inertia about the shear centre, I_{PC} the half of the polar moment of inertia about the shear center and F is a constant depending on cross-sectional properties of the beam defined as $F = I_R - (I_{PC}/A)^2$.

Further, the reaction offered by the foundation (FR) is given by

$$FR = K_w \varnothing - K_p \varnothing'' \quad (2)$$

where K_w is the Winkler foundation modulus and K_p is the modulus of Pasternak foundation.

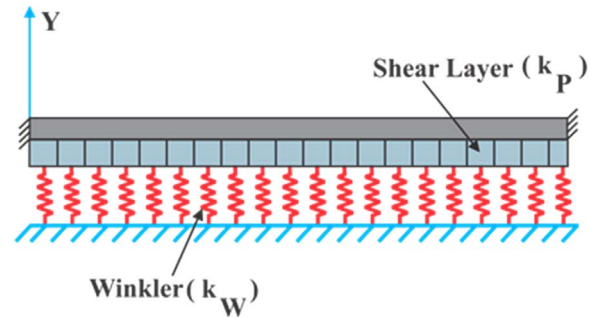
Considering a thin - walled doubly symmetric I-beam as shown in Fig. 1(a) and (b) having web and flange thickness t_f and t_w respectively, height between the centre lines of the flanges, h , flange width b_f , and flange and web thickness being assumed as small compared with height h , i.e., $t_f \ll h$ and $t_w \ll h$, the geometric properties in Eq. (1) can be evaluated as follows [6]

$$I_R = \frac{h^5 t_w}{320} + \frac{b_f h^4 t_f}{32} + \frac{b_f^5 t_f}{160} + \frac{b_f^3 h^2 t_f}{48} \quad (3)$$

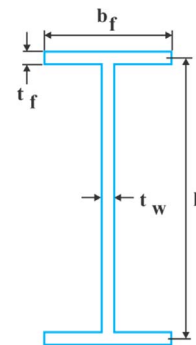
where

$$I_{PC} = \frac{1}{24}(h^3 t_w + 2b_f^3 t_f + 6b_f h^2 t_f) \quad (4)$$

The total potential energy, consisting of the strain energy of deformation of the beam, the work done by the external axial



(a) Clamped beam resting on Pasternak foundation



(b) American steel thin-walled I-beam

Fig. 1. (a) Clamped beam resting on Pasternak foundation. (b) American steel thin-walled I-beam.

compressive load and the reaction offered by the continuous elastic foundation, is given by [10,14,19].

$$V = \frac{1}{2} \int_0^L [EC_w(\varphi')^2 + (GC_s - \sigma I_p + K_p)(\varphi')^2 + EF(\varphi')^4 + K_w(\varphi)^2] dz = 0 \quad (5)$$

The fundamental differential equation resulting from the Euler condition of stationary potential energy given by Eq. (5) can be expressed as

$$EC_w \varphi^{iv} - 6EF(\varphi')^2 \varphi'' - (GC_s - \sigma I_p + K_p) \varphi'' + K_w \varphi = 0 \quad (6)$$

where $\sigma = P/A$ is the axial compressive stress acting on the beam due to load P .

The general solution of Eq. (6) with the clamped boundary condition can be obtained by numerical methods using computer techniques. Here, the Galerkin's technique is used to obtain the approximate solution.

Eq. (6) can be re-written in non-dimensional form as

$$\varphi^{iv} - 6\delta(\varphi')^2 \varphi'' - (K^2 - \Delta^2 + \xi^2) \varphi'' + 4\lambda^2 \varphi = 0 \quad (8)$$

Here, the parameter $\delta = \frac{F}{C_w}$. To solve Eq. (6) by Galerkin's method, the angle of twist, $\varphi(Z)$ is assumed to be of the form

$$\varphi(Z) = \beta x(Z) \quad (9)$$

where β is the torsional amplitude. The approximate function $\varphi(Z)$ is assumed to satisfy the boundary conditions. On substituting Eq. (9) in (8), the error function, ϵ can be estimated as follows

$$\epsilon = \beta [x^{iv} - 6\beta^2 \delta (x')^2 x'' - (K^2 - \Delta^2 + \xi^2) x'' + 4\lambda^2 x] \quad (10)$$

In order to minimize the error ϵ , the Galerkin's integral is given by the following equation:

$$\int_0^1 \epsilon x(Z) dZ = 0 \quad (11)$$

Substituting Eqs. (10) into Eq. (11), the expression for the torsional post-buckling load for a thin-walled beam of open section can be obtained as

$$\Delta_{cr}^{*2} = (K^2 + \xi^2) + \left(\frac{I_1}{I_3}\right) + 6\beta^2 \delta \left(\frac{I_2}{I_3}\right) - 4\lambda^2 \left(\frac{I_4}{I_3}\right) \quad (12)$$

where

$$I_1 = \int_0^1 x^{iv} x dz; \quad I_2 = \int_0^1 (x')^2 x'' x dz; \quad I_3 = \int_0^1 x'' x dz; \quad I_4 = \int_0^1 x^2 x dz \quad (13)$$

The case considered here is a beam with clamped edge on both the ends. The boundary conditions associated with clamped edges are:

$$\varphi = 0; \quad \varphi' = 0 \text{ at } Z = 0,$$

$$\text{where the non-dimensional beam length } Z = (z/L) \quad (14)$$

$$\varphi = 0; \quad \varphi' = 0 \text{ at } Z = 1 \quad (15)$$

We assume the following function for $x(Z)$ which satisfies the clamped boundary conditions given by Eqs. (14) and (15) as

$$x(Z) = \beta(1 - \cos 2\pi Z) \quad (16)$$

Evaluating the integrals I_1, I_2, I_3 and I_4 given in Eq. (13) utilising the function given in Eq. (16) and substituting the same in Eq. (12) we obtain the expression for the critical post-buckling load as

$$\Delta_{cr}^{*2} = K^2 + \xi^2 + 4\pi^2 + \frac{3\lambda^2}{\pi^2} + 6\pi^2 \delta \beta^2 \quad (17)$$

The corresponding linear torsional buckling load for a clamped beam is given by

$$\Delta_{cr}^2 = K^2 + \xi^2 + 4\pi^2 + \frac{3\lambda^2}{\pi^2} \quad (18)$$

Therefore, the ratio of the nonlinear to linear buckling load can be expressed as

$$\frac{P^*}{P_{cr}} = \frac{\Delta_{cr}^{*2}}{\Delta_{cr}^2} = 1 + (6\pi^4 \delta \beta^2) / [\pi^2 (K^2 + \xi^2 + 4\pi^2) + 3\lambda^2] \quad (19)$$

In the absence of Pasternak elastic foundation, i.e., $\xi = 0$, Eq. (19) reduces to

$$\frac{P^*}{P_{cr}} = \frac{\Delta_{cr}^{*2}}{\Delta_{cr}^2} = 1 + 6\pi^4 \delta \beta^2 / [\pi^2 (K^2 + 4\pi^2) + 3\lambda^2] \quad (20)$$

In the absence of an Winkler elastic foundation, i.e., $\lambda^2 = 0$, Eq. (20) reduces to

$$\frac{P^*}{P_{cr}} = \frac{\Delta_{cr}^{*2}}{\Delta_{cr}^2} = 1 + 6\pi^4 \delta \beta^2 / [\pi^2 (K^2 + 4\pi^2)] \quad (21)$$

3. Results and conclusions

Consider a doubly symmetric I-beam (see Fig. 1(b)) for the analysis with the following dimensions (all dimensions are in mm):

Length of the beam (L) = 760; Web thickness (t_w) = 2.13; Flange thickness (t_f) = 3.11; Flange width (b_f) = 31.55; Depth of the beam (d) = 72.76; Distance between center lines of flanges = h = 69.65.

The non-dimensional parameters K and δ are determined from the beam properties and obtained as $K = 3.106$ and $\delta = 1.1095$. The ratio of nonlinear buckling load to linear buckling load can be determined from Eq. (20). Arithmetical values of the ratio of nonlinear buckling load to linear buckling load (P^*/P_{cr}) against values of torsional amplitude (β) for different values of Winkler stiffness parameter (λ) and Pasternak stiffness parameter (ξ) are obtained using Eq. (20).

The values of the ratio of nonlinear buckling to linear buckling loads (P^*/P_{cr}) against torsional amplitude (β) for various values of Winkler stiffness parameter ($\lambda = 0, 5, 10, 15, 20, 25$ & 30) by keeping Pasternak stiffness parameter constant ($\xi = 0$) are obtained and results are plotted in Fig. 2. Similarly, the values of the ratio of nonlinear buckling to linear buckling loads (P^*/P_{cr}) against torsional amplitude (β) for various values of Winkler stiffness parameter ($\lambda = 0, 5, 10, 15, 20, 25$ & 30) by keeping Pasternak stiffness parameter constant ($\xi = 25, 50, 75$ & 100) are obtained and the resulting plots are given in Figs. 3–6. The selected values of Winkler and Pasternak stiffness parameters (λ & ξ), provide a wide range of foundations characteristics varying from no torsional stiffness to high torsional stiffness values. It is observed from the Fig. 2, that the ratio of nonlinear buckling load to linear torsional buckling load (P^*/P_{cr}) increases with increasing values of the torsional amplitude

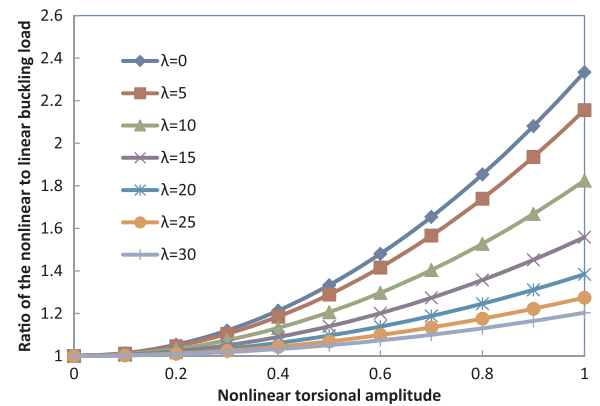


Fig. 2. The effect of elastic foundation (for various values of Winkler stiffness parameter, λ , with Pasternak stiffness parameter, $\xi=0$) on torsional post-buckling behaviour of clamped thin-walled beam of open section.

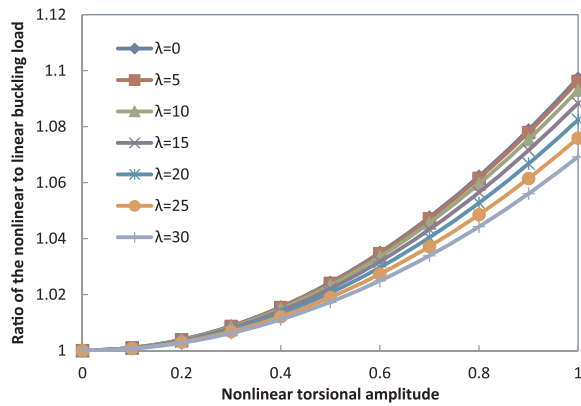


Fig. 3. The effect of elastic foundation (for various values of Winkler stiffness parameter, λ , with Pasternak stiffness parameter, $\xi=25$) on torsional post-buckling behaviour of clamped thin-walled beam.

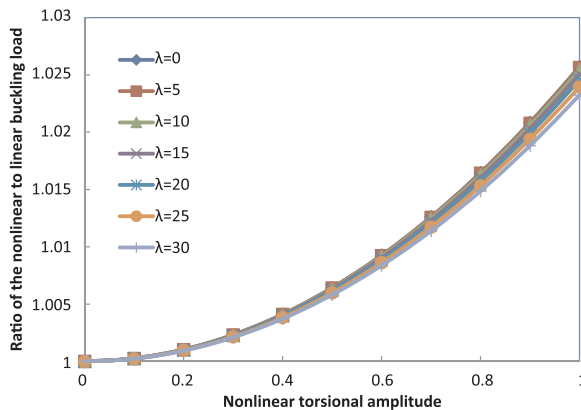


Fig. 4. The effect of elastic foundation (for various values of Winkler stiffness parameter, λ , with Pasternak stiffness parameter, $\xi=50$) on torsional post-buckling behaviour of clamped thin-walled beam.

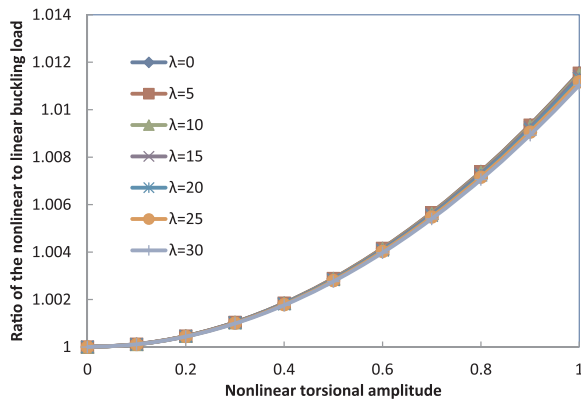


Fig. 5. The effect of elastic foundation (for various values of Winkler stiffness parameter, λ , with Pasternak stiffness parameter, $\xi=75$) on torsional post-buckling behaviour of clamped thin-walled beam.

(β) for a given values of Winkler stiffness parameter ($\lambda = 0, 5, 10, 15, 20, 25$ & 30) by keeping Pasternak stiffness parameter, $\xi = 0$. The equilibrium configurations in the torsional post-buckling region exist only for axial compressive loads in excess of the critical load of small deflection theory. It is also observed that for lower values of β , the nonlinear buckling load increases rapidly as β increases. Also, as λ increases, the nonlinear buckling load decreases as β increases as shown in Figs. 2–6. Also, as λ increases, the curves become flatter indicating that the influence of β on nonlinear buckling load becomes gradually less significant.

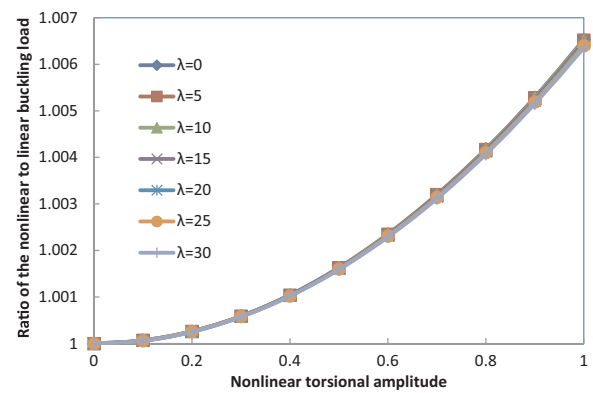


Fig. 6. The effect of elastic foundation (for various values of Winkler stiffness parameter, λ , with Pasternak stiffness parameter, $\xi=100$) on torsional post-buckling behaviour of clamped thin-walled beam.

From the results presented in Figs. 2–6, we can easily observed that the ratio of the nonlinear to linear torsional buckling load (P^*/P_{cr}) increases consistently with increasing values of torsional amplitude (β). The values of ratio of the nonlinear to linear torsional buckling load (P^*/P_{cr}) increases with increasing values of the torsional amplitude (β) for various values of Winkler stiffness parameter, λ , as Pasternak stiffness parameter, ξ increases from 0 to 100. Also, for various values of λ , the influence of β on nonlinear buckling load becomes gradually less significant as ξ increases.

The percentage variation of the ratio of nonlinear to linear buckling load (P^*/P_{cr}) as β varies from 0.1 to 1, with Winkler stiffness parameter, λ , for various values of Pasternak stiffness parameter, ($\xi = 0, 25, 50, 75$ & 100) is computed and shown in Fig. 7. The percentage increase of the ratio of nonlinear to linear buckling load (P^*/P_{cr}) is more for $\xi = 0$ and decreases with increase in λ . Also, the percentage variation is less significant as ξ increases.

The values of the ratio of nonlinear to linear buckling loads (P^*/P_{cr}) against torsional amplitude (β) for various values of Pasternak stiffness parameter in the range ($\xi = 0, 5, 10, 15, 20, 25$ & 30) are obtained by keeping Winkler stiffness parameter constant ($\lambda = 0$) are obtained and results are plotted in Fig. 8. Similarly, the values of the ratio of nonlinear to linear buckling loads (P^*/P_{cr}) against torsional amplitude (β) for various values of Pasternak stiffness parameter ($\xi = 0, 5, 10, 15, 20, 25$ & 30) by keeping Winkler stiffness parameter constant ($\lambda = 25, 50, 75$ & 100) are obtained and the resulting plots are shown in Figs. 8–12.

It can be easily observed from the Fig. 8, that the ratio of nonlinear to linear torsional buckling load (P^*/P_{cr}) increases with increasing values of the torsional amplitude (β) for a given values set of values of Pasternak stiffness parameter ($\xi = 0, 5, 10, 15, 20, 25$ & 30) by keeping

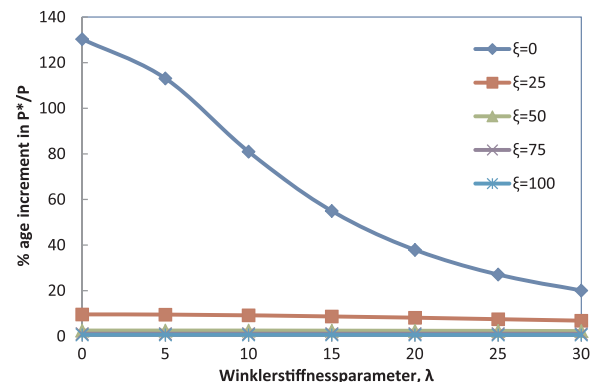


Fig. 7. The percentage variation of the ratio of nonlinear to linear buckling load (P^*/P_{cr}) as β varies from 0.1 to 1, with Winkler stiffness parameter, λ , for different values of Pasternak stiffness parameter, ($\xi=0, 25, 50, 75$ & 100).

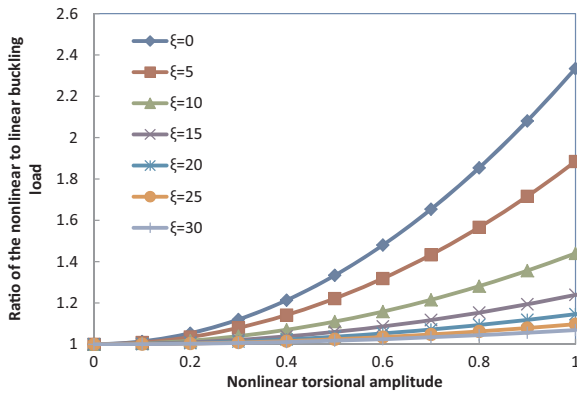


Fig. 8. The effect of elastic foundation (for various values of Pasternak stiffness parameter, ξ , with Winkler stiffness parameter, $\lambda=0$) on torsional post-buckling behaviour of clamped thin-walled beam.

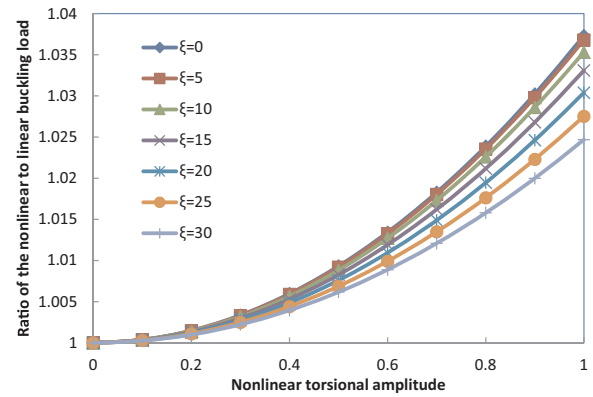


Fig. 11. The effect of elastic foundation (for various values of Pasternak stiffness parameter, ξ , with Winkler stiffness parameter, $\lambda=75$) on torsional post-buckling behaviour of clamped thin-walled beam.

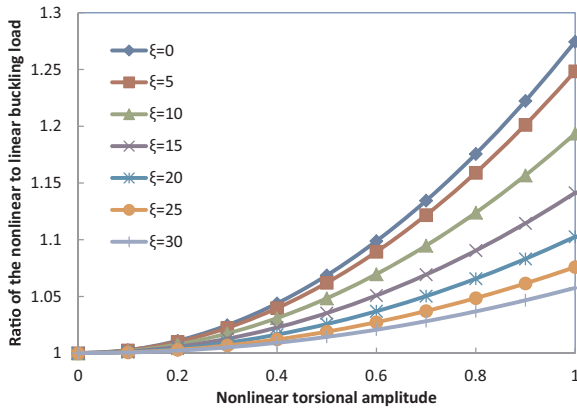


Fig. 9. The effect of elastic foundation (for various values of Pasternak stiffness parameter, ξ , with Winkler stiffness parameter, $\lambda=25$) on torsional post-buckling behaviour of clamped thin-walled beam.

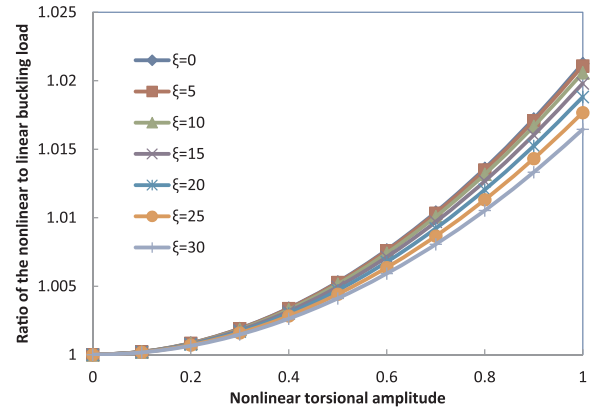


Fig. 12. The effect of elastic foundation (for various values of Pasternak stiffness parameter, ξ , with Winkler stiffness parameter, $\lambda=100$) on torsional post-buckling behaviour of clamped thin-walled beam.

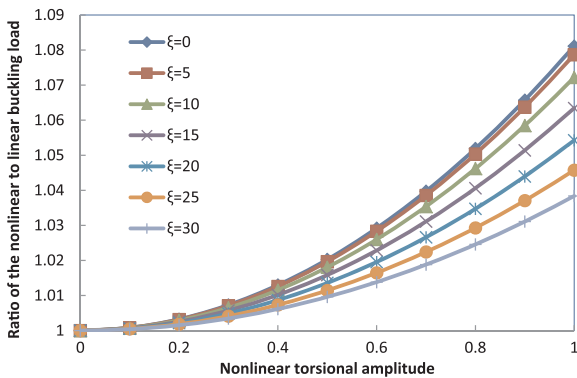


Fig. 10. The effect of elastic foundation (for various values of Pasternak stiffness parameter, ξ , with Winkler stiffness parameter, $\lambda=50$) on torsional post-buckling behaviour of clamped thin-walled beam.

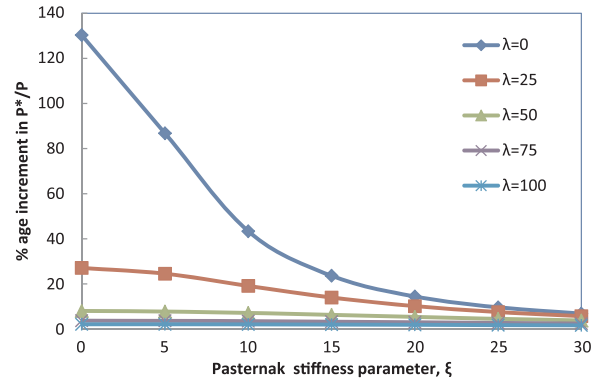


Fig. 13. The percentage variation of the ratio of nonlinear to linear buckling load (P^*/P_{cr}) as β varies from 0.1 to 1, with Pasternak stiffness parameter, ξ , for different values of Winkler stiffness parameter, $\lambda=0, 25, 50, 75$ & 100 .

Winkler stiffness parameter, $\lambda = 0$. It is also observed that for lower values of β , the nonlinear buckling load increase rapidly as β increases. Also, as ξ increases, the nonlinear buckling load decreases as β increases as shown in Figs. 8–12. Also, as ξ increases, the curves become flatter indicating that the influence of β on nonlinear buckling load becomes gradually decreases.

From the Figs. 8–12 presented, it can be also observed that the ratio of the nonlinear to linear torsional buckling load (P^*/P_{cr}) increases with increasing values of torsional amplitude (β). The values of the ratio of nonlinear to linear torsional buckling load (P^*/P_{cr}) can be seen to be increasing with increasing values of the torsional amplitude (β) for

various values of ξ , as λ increases from 0 to 100. Also, for different values of ξ , the influence of β on nonlinear buckling load becomes gradually less significant as λ increases.

The percentage variation of the ratio of nonlinear to linear buckling load (P^*/P_{cr}) as β varies from 0.1 to 1, with Pasternak stiffness parameter, ξ , for various values of Winkler stiffness parameter, ($\lambda=0, 25, 50, 75$ & 100) is computed and shown in Fig. 13. The percentage increase of the ratio of nonlinear to linear buckling load (P^*/P_{cr}) is more for $\lambda = 0$ and decreases with increase in ξ . Also, the percentage variation is less significant as λ increases.

The variation of the nonlinear buckling load with increasing values

of torsional amplitude for different values of λ is more convergence (as ξ increases from 0 to 100, shown in Figs. 2–6) than the variation of the nonlinear buckling load with increasing values of torsional amplitude for different values of ξ as λ increases from 0 to 100 (as shown in Figs. 8–12). It is observed from the Eq. (19) that as δ increases the nonlinear buckling load P^* increases for constant values of β , K , ξ & λ . It is also observed that the effect of increase in values of Warping parameter, K , Pasternak stiffness parameter ξ , and/or Winkler stiffness parameter λ is to decrease the nonlinear buckling load, P^* considerably. It is noticed that the rate of change in the nonlinear buckling load, P^* is gradually reduces due to increase in β & λ as ξ increases and for any constant values of K & δ (Refer Figs. 2–6). It is also observed that the rate of change in the nonlinear buckling load P^* is more significant due to increase in β & ξ as λ increases and for any constant values of K & δ (Refer Figs. 8–12).

References

- [1] S.P. Timoshenko, J.M. Gere, *Theory of Elastic Stability*, 2 ed, McGraw-Hill, New York, 1961, pp. 212–229.
- [2] V.Z. Vlasov, *Thin-walled Elastic Beams*, 2 ed., National Science Foundation, Washington, DC, 1961.
- [3] S.P. Timoshenko, *Strength of Materials-Part-I*, 3rd ed, D.Van Nostrand, Co. Inc, Washington, Dc, 1961.
- [4] J.C. Buckley, The Bifilar Property of Twisted Stripes 28 Phil.Mag., London, 1914, p. 778.
- [5] M.S.G. Cullimore, The Shortening Effect-A Non-linear Feature of Pure Torsion, *Engineering structures* 153 Butterworths, London, 1949.
- [6] W.K. Tso, A.A. Ghobarah, Non-linear non-uniform torsion of thin-walled beams, *Int. J. Mech. Sci.* 13 (1971) 1039–1047.
- [7] A.A. Ghobarah, W.K. Tso, A non-linear thin-walled beam theory, *Int. J. Mech. Sci.* 13 (1971) 1025–1038.
- [8] Z.P. Bazant, M.E.I. Nimeiri, Large deflections spatial buckling of thin-walled beams and frames (ASCE), *J. Eng. Mech. Div.* 99 (1973) 1259–1281.
- [9] M. Epstein, D.W. Murray, Three-dimensional large deformation analysis of thin-walled beams, *Int. J. Solids Struct.* 12 (1976) 867–876.
- [10] C. Szymczak, Buckling and initial post-buckling behaviour of thin-walled I-column, *Comput. Struct.* 11 (1980) 481–487.
- [11] T.M. Roberts, Z.G. Azizian, Instability of thin-walled bars (ASCE), *J. Eng. Mech.* 109 (1983) 781–794.
- [12] J.W. Wekezer, Instability of thin walled bars (ASCE), *J. Eng. Mech.* 111 (1985) 923–935.
- [13] J.W. Wekezer, Non-linear of torsion of thin-walled bars of variable cross-sections, *Int. J. Mech. Sci.* 27 (1985) 631–641.
- [14] C. Grimaldi, M. Pignataro, Postbuckling behavior of thin-walled open cross-section compression members, *J. Struct. Mech.: Int. J.* 7 (2) (1979) 143–159.
- [15] C. Kameswara Rao, B.V.R. Gupta, D.L.N. Rao, Torsional vibrations of thin-walled beams on continuous elastic foundations using finite element method. In: *Proceedings of the International conference on Finite Element Methods in Engineering*. Coimbatore Institute of technology, pp. 231–248, 1974.
- [16] C. Kameswara Rao, A. Appala Satyam, Torsional vibrations and stability of thin-walled beams on continuous elastic foundation, *AIAA J.* 13 (1975) 232–234.
- [17] C. Kameswara Rao, S. Mirza, Torsional post-buckling of thin-walled open section beams resting on a continuous elastic foundation, *Thin-walled Struct.* 8 (1989) 55–62.
- [18] V.Z. Vlasov, U.N. Leontiev, *Beams, Plates, and Shells on elastic foundation*, Israel program for scientific translations [translated from Russian], Jerusalem, 1966.
- [19] P.L. Pasternak, On a New Method of Analysis of an Elastic Foundation by Means of Two-Constants, USSR: Gosudarstvennoe Izdatelstvo Literaturi po Stroitelstvu I Arkhitekture [in Russian], Moscow, 1954.
- [20] P.D. Simão, Post-buckling bifurcational analysis of thin-walled prismatic members in the context of the Generalized Beam Theory, (Ph.D. thesis), Departamento de Engenharia Civil, Faculdade de Ciências e Tecnologia da Universidade de Coimbra, 2007.
- [21] M. Pignataro, N. Rizzi, V. Varano, The effects of warping constraints on the buckling of thin-walled structures, *J. Mech. Mater.* 4 (2009) 10.
- [22] D. Camotim, C. Basaglia, N. Silvestre, GBT buckling analysis of thin-walled steel frames: a state-of-the-art report, *Thin-walled Struct.* 48 (2010) 726–743.
- [23] M. Kujawa, Torsion of restrained thin-walled bars of open constant bi-symmetric cross-section, *Task. Q.* 16 (1) (2011) 5–15.
- [24] N.L. Rizzi, V. Varano, The effects of warping on the post-buckling behaviour of thin-walled structures, *Thin-walled Struct.* 49 (2011) 1091–1097.
- [25] M. Kujawa, C. Szymczak, Elastic distortional buckling of thin-walled bars of closed quadratic cross section, *Mech. Mech. Eng.* 17 (2) (2013) 119–126.

A Critical Review of Strategies Being Adopted in Artificial Intelligence-Aided Engineering Education

Chellapilla Kameswara Rao¹ and G. Janardhana Raju²

¹Ex-Professor (chellapilla95@gmail.com) & ²Dean (SOE) (gjraju@rediffmail.com),

Department of Mechanical Engineering, Nalla Narasimha Reddy Group of Institutions,
Korremula X Road, Via Narapally, Ghatkesar Mandal, Chowdariguda, Telangana 500088.

ABSTRACT

As we all know, in the last two decades, the scientific methods such as Pattern Recognition, Image Processing, Automation, Artificial Intelligence, Evolutionary Neural Networks, Self-driven Cars and Vehicles and Robotics have become household names. Last decade has also witnessed phenomenal transformations in various fields of industrial sector and in creating innovative paradigms, such as “Industry 4.0”, initially in Germany and then spread throughout the whole European Union, and of “Society 5.0” in Japan, among other transformations with global impact. How the mind works is still a real mystery and is undoubtedly a very complex part of the human body still to be understood well. The Human being is presently categorised as a “Naturally-Born and Brought-up Robot” having only 10% of its memory available for exercising its “Free-Will”. The concept of “artificial intelligence-aided engineering education” being articulated in this paper refers to applying artificial intelligence techniques and resources for improving the whole teaching-learning process in engineering education. All the areas of educational practice such as planning and organization of teaching programmes and courses including final assessment of learning results and outcomes can be smartly organised through Artificial Intelligence software tools .

The present review paper includes a brief discussion on strategies being adopted in reputed Technical Universities on Computer-assisted instruction and intelligent teaching programs, AI-supported courses, Virtual laboratories, AI for supporting educational and curricular planning, AI for developing sustaining teaching-learning activities and helping with student assessment. The main aim of this paper is to provide necessary background that will facilitate discussion on these and other important questions that need to be investigated further. Even though there are several things that AI can be do, there are many other essential things it cannot do even in the future. How AI works is still a “Black Box” and is very important for us right now to understand some key characteristics of current AI to be able to apply them effectively.

Introduction:

Over the last decade or so, there is a high pitch of discussion on “student-centred learning” and NAAC and NBA certifications are being sought by many engineering colleges and the same are being awarded to those engineering colleges which are showing serious and honest interest in digital maintenance of student admission data, various course objectives, achieved student performances and the ultimate outcomes.

Higher education in engineering is being slowly geared to maintain and perfect institutional organization and their governance using Artificial Intelligence tools and technologies such as desktops, LAN, internet and skype-enabled video conferencing in organising technical seminars and conferences. Technological advances achieved through these activities can be seen to have resulted in extensive digitization, e-learning, self-study through Google search and watching of streaming educational videos on YouTube etc.

In view of the recent advances in artificial intelligence (AI) all over the world, the non-invasive brain-computer interfaces are opening up new and innovative strategies being implemented in the “teaching and learning process”, resulting in seriously reducing the role of a teacher to just a mere ‘facilitator of learning’ in the classroom and outside as “a coach or a guide” only. Many of the educational institutions all over the world are taking incremental steps towards the replacement of teachers with virtual “teacherbots” [1,2].

Providing affordable solutions to use brain computer interface (BCI) devices capable to measure when a student is fully focused on the content and learning tasks [3,4] is already possible, and super-computers, such as IBM’s Watson, can provide an automated teacher presence for the entire duration of a course.

The possibility to communicate and command computers through thought and wider applications of AI in teaching and learning represents the real technological revolution that will dramatically change the structure of higher education across the world.

A ‘teacherbot’ or ‘cloud-lecturer’, can be adopted for personalized learning with a blended delivery of opted courses or for fully online courses. Already presenting as a disruptive alternative to traditional teaching assistants, the ‘Teacherbots’ are assisting in providing computing solutions for the administrative part of teaching, dealing mainly with content delivery, basic and administrative feedback and supervision.

As an example, we can look at the course on knowledge based artificial intelligence (KBAI), offered by Professor Ashok Goel, in the online M.S. Computer Sciences program, at Georgia Tech in the USA. The teaching assistant (TA) was highly successful in its performance and hence valued by the class students that they wanted to nominate her to the outstanding TA award. At the end of this course it was quite surprising to know that Jill Watson was only a ‘teacherbot’ and not a real person.

Google hacking [5,6,7] or ‘advanced search’ is a very intensive and intelligent activity of retrieving related documents for study or research projects on hand. Lot of patience and crazy love, towards locating and downloading all relevant material available on the internet, is required in this effort to complete the task without missing even one related one. That is the reason why this google searching becomes a real art and hence, it is not surprising that many people fail to succeed with complete satisfaction in this important activity related to ‘Literature Search’. Many a time, the searcher has to even go to the extent of browsing the 30th page of the google search result pages in the process. Also, no judgement should be applied while plucking all the fruits from the garden onto the mat on the floor.

Segregation of these downloads into most relevant, distantly related and unrelated should be done only after a close and critical look at all these items.

Educating Millenials:

Millennial Student Attributes which are listed in the following paragraphs include several attributes of students who have grown up with technology that may influence the way you teach [9-11]:

1. **“Computers are not technology”**. Development of Computers, availability of Internet, and the World Wide Web are being used by Millennials’ and a part of their lives as the landline telephones and black and colour television are to the earlier generations.
2. **“Reality is no longer real”**. Using advanced digital technologies like “morphing”, the so-called original images can easily be modified and distorted and hence may not be real. Even the emails received by you also may be coming from an address which may not be from the real owner of that address.
3. **“Doing is more important than knowing”**. Slowly an attitude of thinking that views acquiring Knowledge is no longer becoming the ultimate goal as they think that half-life of information is very short and hence not very important. Today’s generation thinks that really what matters is practical actions and the consequential results are the ones that are more important than the simple and trivial accumulation of mere facts.
4. **“Learning more closely resembles Nintendo than logic”**. Nintendo is a Japanese multinational consumer electronics and video game which involves a trial-and-error approach in solving the problems where in, the more you lose the more you learn and reach knowledge in a fastest way in mastering the game, because **“losing leads to more experience and thus ultimately leading to intelligent learning.”**
5. **“Multitasking is a way of life”**. In view of the fast changing way of life, many students who are pursuing higher studies today are forced to and adopted to getting engaged in several activities at the same time. That is how the “Millenials” get through their day, doing home work while listening to music with ear phones on and, chatting with their friends on whatsapp.
6. **“Consumer and creator are blurring”**. As we all know, most of the IT service companies functioning in India keep their employees busy in a “time-taking and patience-testing” job of “simple and trivial Copy-Pasting”, from the material obtained through internet-searching and downloading the documents, on the particular subject referred by a foreign customer, into an Excel sheet and/or into a PPT file, **without adding a “single creative word” of their own**. Such is the IT services business and complex money-making world today. This type of life and work is leading to the “operative assumption” that if something which is in digital form and is freely available on the world wide web in the “Pdfdrive” or “Archive.Org” or “YouTube”, being felt and treated as everyone’s property.

We can see the consequences of this “**consumer and creator are blurring**” talk above in developing a mental make-up in blatantly and openly violating the copyrights of both all published books and the internationally made “All Videos and Movies and Artistic and Performance event videos”. The word “**Plagiarism**” is internationally silently heckled and mass violated bringing down the death of the authors, creators and artists. All movie makers and authors are immediately selling or licensing their movies to Amazon for safe selling, to the extent possible, in this “uncontrollable global hacking”, digital and cyber crime age.

In addition to the above, we should not forget that latest trend of large scale publication of research papers in “Fake and Predatory International Research Journals”. Of course, UGC and AICTE and other international research organisations are issuing serious warnings and circulars in trying to reduce such publications getting undue advantage and promotion through such publications.

People must have noticed that the emergence of the new (word) requirement of job related “**employability**” is a direct consequence of “commercialising education” globally through the mask of “Right to Education”. Thus “Rote Learning” is given free chit “**to be the order of the day**” in getting higher education degrees and certificates without having any capability in “**writing in their words**”. This has brought in the so called “Soft Skills”, “Critical Thinking” and “Problem Solving Capability”, “Spoken English”, “Communication Skill” and “Group Discussion Skill” for consequential “commercialisation” on a large scale for certifying the students for this so-called “Employability”. All this is going on in the name of “Development” and as a part of “Global High Capitalism” and “Liberal Activism” brutally crushing down the “Conservative and classical disciplined thinking” which was prevalent in the earlier decades. In what direction this trend will end, is any one’s guess!

Right to Education (RTI) Law, enacted in India in 2010, led to the implementation of “No Detention up to Eighth Class” which is unofficially extended up to the final year of the Engineering and other Degrees also, has resulted in serious consequence of large scale “Joblessness”. Slowly, following the rudimentary principle of crude “Market Economy”, the admissions in to these educational institutions started falling down leading to summary closure of these institutions. We all know how randomly the so-called “market economy” works! Suddenly, markets collapse resulting in heavy monetary and reputational losses. In view of this the educational Institutions adopting the policy of “Pay the fees and get whatever degree you want”, “ensuring freely the A++ grade and unabated pass in the examinations” leading to “Severe decline in the degree holders having “employability criteria” not being satisfied!!

Like the cruel fall of infamous “ISO” certifications, which no one talks about now, the latest liberal certifications by NAAC and NBA to educational institutions, even with lowest quality of teaching and research faculty, is slowly becoming useless and is not in a position to attract large demand as expected in the student admissions into these institutions

Death of the Author, Publisher and the CopyRights:

In view of the above type of mindset being developed silently and promoted all over the world unabated, over the last two decades, there is an immediate need to develop and adopt improved methods and technologies in educating 'Millennials' need to be quite different from those classical ones adopted in the case of educating their earlier generation, as the 'Millennials' learn differently compared to the previous generations. A vast amount of literature exists on the internet and a serious study suggests that this new generation which was born between 1982 to 2000 are quite different in nature compared to behaviour and working of earlier generation. Their outlook about life also is quite bizarre when looked at critically from the ideals, experience and outlook of their predecessors.

While there are different observations and judgements about their worldly outlook, one thing is clear that the growing technological knowledge and resources on the internet and the gadgets and smart mobiles have got profound influence on their life in general and the learning habits and also their mental makeup.

Many researchers categorise, these '**millenials**', also named as products of "**Generation Y**" as, more philosophical and spiritual than the earlier generation. They have intimately observed the miserable failures and suffering undergone by their parents and elders particularly in terms of lack of quality of life and enjoyment. Earlier generation has worked hard throughout their life in terms of acquiring educational qualifications and in building up great careers, and sacrificing their personal hard earned money, happiness and enjoyment in bringing up their children to have a better social status and richness in their life. In the process, they had no enjoyment of travelling to great places in the world or enjoying the benefits of their earnings. They were generally satisfied in sacrificing everything for their children and hence they are also called as "baby boomers".

From a close look at these studies and reports on this 'millennial' generation, we understand that these people process their information, collected from social interactions, movies and visuals, and further their knowledge through personal experiences more than listening to their elders and their experiences and views about life and living. Hence, they follow and exhibit a self-learning process much different from the previous generations.

They have a lot of literature, videos and movies, gadgets like ipads, notebooks, Kindle for easy reading, plenty of news and entertainment channels, digitised books and news papers in view of the advances in and availability of internet and web technologies, and all merged, combined and comfortably and conveniently made available on their smart mobiles.

While Millennials have almost unlimited access to more information on areas of interest to them, the accumulation of knowledge is seen as less important than the ability to perform a task. As one can see today, a new terms 'employability' and 'soft skills' have entered into the education and learning outputs required for getting a suitable job in this 'knowledge and market economy' and booming IT services all over the world.

Literature suggests that these expected learning outcomes and preferences clash with the traditional teaching methods still being employed in engineering and technology education today. Though the curriculum is evolving to incorporate the ever increasing volume of data and skills needed to compete in today's environment, traditional teaching styles such as the largely adopted "black board" and 'power point lecturing' have yet to get moulded themselves suitably to motivate and enthuse today's student who is largely addicted whatsapp, facebook and use of mobile phone all the 24 hours of the day. Continuous viewing of information and chatting on the smart mobile phone has become quite normal in kids as well as elderly people today leading to accidents on the road and in growth of impatience in listening to others teaching or advice. Students today including their teachers feel that all necessary information is available in plenty utilising the internet, web and cloud computing technologies and hence need not be memorised or stored anywhere anymore. Data storage available on laptops and mobile phones is also increasing significantly almost every day.

Current discussions and deliberations made on this topic in different platforms all over the world [12-14], suggests that a phenomenal and significant change is needed within engineering education. Some educators feel it is critical to change the traditional teaching methods to adapt to today's student. Through the goal of analyzing perceptions Millennial engineering and technology students have towards traditional teaching methods, this study could help to either validate or invalidate the prior concerns of educators. Recommendations were given based on the results of the study in efforts to engage and attract students to engineering studies.

Artificial Intelligence and Mobile Technologies for Learning and Teaching:

Instead of negatively reacting, to the uncontrollable and huge growth of possession and use of mobile phones in large scale communication and online e-commerce, as a threat to general living carrying mobile always holding it in their left hand, boarding and getting down the buses and vehicles, crossing the road looking at the whatsapp, facebook on mobile, driving scooter and motor-bike with mobiles in hand causing deadly accidents on the road and casually sitting in classes paying no attention to the teaching going on in the class room formal education not focussing on learning, we need to explore how learning can be transformed for the mobile age. This needs to be done through an honest dialogue between the two facets of education. The first facet involves in knowledge being given authority through the command on curriculum and the other facet in which it emerges through organising necessary negotiation process of coming to mutual agreement on the quality and expected outcomes to be achieved.

The challenge of integrating the Information and communications technology (ICT), Artificial Intelligence (AI) [15-17] and Mobile Technologies [18-20] needs to be carried out with an honest and serious focus on reforming the teaching and learning process involving innovative modes of learning which can keep and enthuse the active learner's concentration in the construction of knowledge with a hands-on training in practical and productive project execution under the able guidance of a professional experienced teacher. The classical thinking about "**learning**" as a process that extends beyond individual capability to mental

and brainy distributed systems that miraculously and artificially learn, acquire and develop knowledge, brings in the issue of ontological role of technology only as a participant in the process of learning. As described in latest cognitive science literature, learning and cognition are diffused in the distributed learning systems. The unique interaction between the elements of the humans or technological system carried out successfully within a distributed context is the one which creates meaning in this act of interaction and exchange. It is a recognisable and significant fact that, through selective, productive and useful conversations and interactions only, the “learning system as a whole” advances evolving as a continuum of advanced knowledge. Understanding and realising the fact that, we human beings are all “naturally born and brought-up robots” we can acquire useful and profound knowledge only through group discussions and fruitful interactions only and not by mere “rote learning involving “memorisation”. The take away at the end of this process is the real knowledge which settles and solidifies in the memory in the form of the enlightened experience. To acquire such experience, we need to innovate and evolve excellent combinations of all the available ICT, AI and mobile technologies appropriate and suitable to the technical subjects to be taught for imparting the rightful learning in the student.

REFERENCES:

1. Bayne, S. (2015). Teacherbot: interventions in automated teaching. *Teaching in Higher Education*, 20(4). doi:10.1080/ 13562517.2015.1020783
2. Botrel, L, Holz, EM, Kübler, A. (2015). Brain painting V2: evaluation of P300-based brain-computer interface for creative expression by an end-user following the user-centered design. *Brain-Computer Interfaces*, 2(2–3),1–15.
3. Chen, X, Wang, Y, Nakanishi, M, Gao, X, Jung, TP, Gao, S. (2015). High-speed spelling with a noninvasive brain– computer interface. *Proceedings of the National Academy of Sciences*, 112(44), E6058–E6067.
4. González, VM, Robbes, R, Góngora, G, Medina, S (2015). Measuring concentration while programming with low-cost BCI devices: differences between debugging and creativity tasks. In *Foundations of augmented cognition*, (pp. 605– 615). Los Angeles, CA: Springer International Publishing.
5. Google Hacking 101, <https://www.oakton.edu/user/2/rjtaylor/cis101/GoogleHacking101.pdf>
6. Johnny Long, “The Google Hacker’s Guide: Understanding and Defending Against the Google Hacker”, *Googlehacker.pdf* (<http://johnny.ihackstuff.com/>).
7. Harnish, R. J., Bridges, K. R., Sattler, D. N., Signorella, M. L., & Munson, M. (Eds.). “The Use of Technology in Teaching and Learning”, 2018, Retrieved from the Society for the Teaching of Psychology web site:.,<http://teachpsych.org/ebooks/>
8. “Millennials: Our Newest Generation in Higher Education”, Northern Illinois University, Faculty Development and Instructional Design Center, facdev@niu.edu, www.niu.edu/facdev,

(https://www.niu.edu/facdev/pdf/guide/students/millennials_our_newest_generation_in_higher_education.pdf)

9. McBride, T., & Nief, R. (2011). "The mindset list", http://www.beloit.edu/mindset/tps://dmartindale.weebly.com/uploads/8/8/5/9/8859853/starlink-educatingthenet-gen_strategiesthatwork_packet.pdf

10. Elizabeth A. Howard, "How do Millennial Engineering and Technology Students Experience Learning Through Traditional Teaching Methods Employed in the University Setting", M.S. Thesis, Department of Computer Graphics, Perdue University, 2011.

11. Manoj Joseph D'Souza and Paul Rodrigues, "Engaging Millennial Students in an Engineering Classroom using Extreme Pedagogy", Indian Journal of Science and Technology, Vol 8(24), IPL0313, September 2015.

12. Manoj Joseph D'Souza and Paul Rodrigues, "eXtreme Teaching-Learning Paradigm: A pedagogical framework for higher education", International Journal of Applied Engineering Research, ISSN 0973-4562 Vol. 10 No.69 (2015).

13. "Educating the Engineer of 2020: A Practical Implementation", National Academy of Engineers of the National Academies, The National Academies Press, Washington, DC, 2015.

14. M. U. Bokhari, Sadaf Ahmad, Shadab Alam and Faheem Masoodi, "Modern Tools and Technologies for Interactive Learning", Proceedings of the 5th National Conference; INDIACOM-2011 Computing For Nation Development, Bharati Vidyapeeth's Institute of Computer Applications and Management, New Delhi, March 10 – 11, 2011.

15. Discussion Paper- "National Strategy for Artificial Intelligence", Niti Aayog, June 2018, https://www.niti.gov.in/writereaddata/files/document_publication/NationalStrategy-for-AI-Discussion-Paper.pdf

16. Stefan A. D. Popenici and Sharon Kerr, Exploring the impact of artificial intelligence on teaching and learning in higher education", Popenici and Kerr Research and Practice in Technology Enhanced Learning (2017) 12:22 DOI 10.1186/s41039-017-0062-8

17. Uchechukwu Ajuzieogu, "The Role of AI In Modern Computing and Education", Computer Education Seminar 2019, UNN, A seminar approach to understanding the underlying principles of AI and its relevance to Education, in the 21st Century, 2019.

18. Bin Zou and Jiaying Li, "Exploring mobile apps for English language teaching and learning". In F. Helm, L. Bradley, M. Guarda, & S. Thouèsny (Eds), Critical CALL – Proceedings of the 2015 EUROCALL Conference, Padova, Italy, Aug. 26-29, 2015 (pp. 564-568). Dublin: Research-publishing.net. <http://dx.doi.org/10.14705/rpnet.2015.000394>

19. Mohamed Ally (Ed.), Mobile Learning Transforming the Delivery of Education and Training, © 2009 Mohamed Ally, Published by AU Press, Athabasca University, 2009.

20. Mike Sharples, Josie Taylor, Giasemi Vavoula. A Theory of Learning for the Mobile Age. R. Andrews and C. Haythornthwaite. The Sage Handbook of Elearning Research, Sage publications, pp.221-247, 2006. ffhal-00190276



Determination of Natural Frequencies of Fluid Conveying Pipes using Muller's Method

Shankarachar Sutar¹ · Radhakrishna Madabhushi¹ · Kameswara Rao Chellapilla² · Ramesh Babu Poosa³

Received: 7 September 2015 / Accepted: 15 February 2018
© The Institution of Engineers (India) 2018

Abstract In the present paper the natural frequencies of fluid-conveying pipes with guided-clamped, guided-simply supported, guided-free and guided-guided boundary conditions are derived explicitly. Numerical results are presented for four cases, and the effect of fluid flow velocity on the natural frequencies is discussed. Critical velocities are determined to find the point of flutter. The pipe is modelled as an Euler–Bernoulli beam. The differential equation of motion for free vibration is established using Hamilton's principle. The transcendental frequency equation is derived using Muller's bisection method. By varying the non-dimensional velocities the frequencies are determined for the said boundary conditions. It is observed that there is a reduction in natural frequency with an increase in velocity, for all the boundary conditions. The influence of fluid velocity on the instability of the pipe is determined. The results obtained analytically were validated by experiment for guided-guided end condition only.

Keywords Fluid-conveying pipes · Muller's method · Natural frequency · Guided pipe support

Introduction

Pipes are widely used for transfer of fluids from one point to the other and are susceptible to vibrations. Flow-induced vibration analysis of pipes conveying fluid is thus important in structural dynamics. It is well known that pipeline systems may undergo divergence and flutter type of instability due to fluid-structure interaction. Over the last 60 years, extensive studies have been carried out on dynamic analysis of piping systems subjected to different boundary conditions and loadings. Ashley and Haviland [1] studied the cross wind force on fluid conveying pipes supported above ground. Naguleswaran and Williams [2] developed solutions for natural frequencies in axial mode for hinged-hinged, fixed-hinged, fixed-fixed boundary conditions. Stein and Tobriner [3] discussed vibration of pipes containing flowing fluid, in which the effects of foundation modulus, flow velocity and internal pressure on the dynamic stability, frequency response and wave propagation characteristics of an undamped system was studied.

Notable contributions in the area of piping vibrations also include the works of Chen [4]. In most of the cases, the differential equation of motion of fluid-conveyed pipe is deduced using the Galerkin's method in Lagrange system. Subsequently, the solution of the differential equation is obtained by considering many numerical methods such as transfer matrix, finite element, perturbation, Runge-Kutta and differential quadrature.

Weaver and Unny [5] studied the dynamic stability of finite length of pipe conveying fluid using Flugge-Kempner equation to find the critical flow velocities. Paidoussis [6] presented a general transverse frequency equation with gravitational force, pressurization effects, material damping and viscous damping effects. Shizhong, et al [7] had conducted research on solid liquid coupling dynamics of pipe conveying fluid, where they studied the influence of flowing

✉ Radhakrishna Madabhushi
mradhakrishna@iict.res.in

¹ Design and Engineering Division, CSIR-Indian Institute of Chemical Technology, Hyderabad 500007, India

² Department of Mechanical Engineering, Nalla Narasimha Reddy Engineering College, Hyderabad 500088, India

³ Department of Mechanical Engineering, College of Engineering, Osmania University, Hyderabad 500007, India

velocity, pressure, solid–liquid coupling damping and solid–liquid coupling stiffness on natural frequency for simply supported ends. Zhang, et al [8] studied the vibration of pipes conveying fluid and developed dynamic equilibrium matrix using Lagrange principle for discretized pipe element flowing fluid for simply supported end condition which is subjected to initial axial tension and frequencies were compared with experimental results.

Oz and Boyaci [9] developed a mathematical model for transverse vibrations of tensioned pipes conveying fluid with time dependent velocity. The principal parametric resonance cases were studied for the boundary conditions and results are presented for the first two modes.

Chaos, et al [10] found new closed-form solutions for the natural frequency of a clamped-guided beam are derived for their investigation. By postulating the mode shape of the clamped-guided beam, whose material density and stiffness are taken as polynomial functions, a closed-form solution was calculated for the natural frequency. Wiggert, et al [11] have reviewed fluid structure interaction in piping and highlighted the effects of fluid forces on piping and its support structure. The work dealt on how transfer of momentum and forces between piping and the contained liquid during unsteady flow and excitation mechanisms are caused by rapid changes in flow and pressure or may be initiated by mechanical action of the piping. Sinha, et al [12] developed a finite element model for cantilever pipe conveying fluid. The instability in the pipe was inferred due to change in the natural frequencies for its dynamic behavior and compared the results of a FE model with experimental data.

Zhang, et al [13] developed a FE model to predict the vibration of cylindrical shells conveying fluid and validated the results with experiment. Seo, et al [14] also have studied the frequency analysis for cylindrical shells using the finite element approach and understood the effective thickness of fluid according to circumferential modes in the study. The influence of fluid velocity on the frequency response function is illustrated. Rao [15] had determined natural frequencies for all the classical and elastically restrained boundary conditions.

Chellapilla and Simha [16] studied two parameter foundation effects of fluid conveying pipes resting on soil media and found the frequencies. Aldraihem [17] studied the dynamic stability of a collar-stiffened pipe conveying fluid using the Euler-Bernoulli theoretical approach. FE model was developed to predict the dynamic stability of the stiffened pipe under the influence of flowing fluid. It is found that the collar stiffened pipe exhibit unique stability characteristics when compared to uniform pipe. Huang, et al [18] considered Galerkin's method and obtained natural frequencies for fluid conveying pipeline with different boundary conditions. The four variables mass, stiffness, length and flow velocity were studied in detail to estimate the effect of flow velocity on the natural frequency. Jweeg,

et al [19] estimated through experiments the critical buckling velocities for pinned–pinned–clamped–pinned and clamped–clamped end conditions and also measured the fundamental natural frequencies for the end conditions.

Drozyner [20] developed a method for determining the acceptable limits of piping vibration and corresponding natural frequencies. Acceptance criteria for the vibrations were based on the allowable limits of deformation and stress of the pipeline. Huang, et al [21] developed a mathematical model using Ferraris method of natural frequency analysis on pipeline conveying fluid with both ends supported. The natural frequencies and critical flow velocities were also found for clamped–simply supported, clamped–clamped and simply supported cases and found that the clamped–clamped is more stable than other two cases. Lee and Jeong [22] developed a mathematical model for vibration of three-dimensional piping system conveying a pulsating fluid. The dynamic equations of motion are further used to develop natural frequencies of fluid conveying pipe. The accuracy and efficiency of efficient numerical method were validated by comparison with conventional numerical integration method. Lee and Jeong [23] discussed the effect of rotary compressor on piping system with fluid pulsation signal in the pipe which was measured by a pressure transducer. The results were compared by developing a FE model of the same piping system and were found in agreement with the experimental results.

The present paper deals with a set of combinations of guided supports such as clamped-guided, guided–simply supported, guided–free and guided–guided, which are quite commonly used in piping as pipe supports. A mathematical model is developed for estimation of natural frequencies for these end conditions.

Euler-Bernoulli beam theory and Hamilton's energy expressions are used to derive the equation of motion for transverse vibration of the fluid conveying pipe with guided end conditions. The exact solution of the differential equation is expressed as a polynomial function. The boundary conditions are substituted in fourth order derivatives of the polynomial function and by using the Gaussian elimination rule the transcendental frequency equation is obtained. The natural frequencies for the first mode of vibration are computed by using the Muller's Bisection numerical method. Critical velocity is computed, when the flow is turbulent and frequency approaches zero. A FORTRAN computer program is developed for estimation of the frequencies in non-dimensional form.

Formulation of Problem

Consider a straight pipe having end conditions as clamped-guided, guided–simply supported, guided–free and guided–guided as shown in Figs. 1, 2, 3 and 4, respectively. It is

assumed that the fluid motion is planar, harmonic, incompressible, pipe horizontal and cross-sectional area of the flow pipe is constant.

From first principles and applying the Euler–Bernoulli beam theory and Hamilton’s energy equations for the elastically restrained pipe conveying fluid, the differential equation of motion and boundary conditions are obtained as [15]

$$EI \frac{\partial^4 w}{\partial x^4} + (m_p + m_f) \frac{\partial^2 w}{\partial t^2} + m_f U^2 \frac{\partial^2 w}{\partial x^2} + 2m_f U \frac{\partial^2 w}{\partial x \partial t} = 0 \quad (1)$$

where EI is the bending stiffness of a pipe; $m_p + m_f$, the mass of pipe and mass of fluid; U , the velocity of fluid along the x -direction; and t , the time; $EI \frac{\partial^4 w}{\partial x^4}$ is the stiffness term; $(m_p + m_f) \frac{\partial^2 w}{\partial t^2}$ is the inertia force term; $m_f U^2 \frac{\partial^2 w}{\partial x^2}$ is the curvature term; and $m_f U \frac{\partial^2 w}{\partial x \partial t}$ is the Coriolis force term.

The equation of motion, Eq. (1), can be written in the following non-dimensional form

$$\frac{\partial^4 w}{\partial \xi^4} + (V^2) \frac{\partial^2 w}{\partial \xi^2} + 2\gamma U \frac{\partial^2 w}{\partial \xi \partial \tau} - \lambda^4 w = 0 \quad (2)$$

where, γ is the damping term, ξ , the natural boundary condition; ω , the circular frequency; λ , the non-dimensional frequency; U , the flow velocity; V , the non-dimensional velocity; Ω is the natural frequency; $V^2 = \left(\frac{m_f U^2 L^2}{EI}\right)$; and $\lambda^4 = \left(\frac{(m_p + m_f) \omega^2 L^4}{EI}\right)$.

$$\frac{\partial^4 w}{\partial \xi^4} + (V^2) \frac{\partial^2 w}{\partial \xi^2} - \lambda^4 w = 0 \quad (3)$$

$$2\varepsilon^2 = (V^2); \quad \varepsilon = \frac{V}{\sqrt{2}} \quad (4)$$

When the natural frequency of the pipe approaches zero, the critical flow velocity has been computed for all the end conditions. When the flow velocity is equal to the critical velocity, the pipe bows out and buckles, as the forces required to make the fluid deform to the pipe curvature are greater than the stiffness of the pipe. The term γ in Eq. (2) represents the damping of the system and its effect on the frequency is negligible and so is ignored here, as the present work aims to obtain upper bounds for the frequencies of vibration of the fluid-conveying pipe.

The boundary conditions for the piping system are given here

$$\left[\left(-EI \frac{\partial^2 w}{\partial x^2} \right) \right]_{x=0} = 0 \quad (5)$$

$$\left[\left(EI \frac{\partial^3 w}{\partial x^3} - T^* \frac{\partial w}{\partial x} \right) \right]_{x=0} = 0 \quad (6)$$

$$\left[\left(EI \frac{\partial^2 w}{\partial x^2} \right) \right]_{x=L} = 0 \quad (7)$$

$$\left[\left(-EI \frac{\partial^3 w}{\partial x^3} + T^* \frac{\partial w}{\partial x} \right) \right]_{x=L} = 0 \quad (8)$$

where $T^* = \alpha - \beta$; and L is the length of the pipe between supports or span.

Let us consider the solution for Eq. (3), as

$$W(x) = ce^{s\xi} \quad (9)$$

where c is an arbitrary constant

$$\frac{\partial^4 w(x)}{\partial \xi^4} = cs^4 e^{s\xi}; \quad \frac{\partial^2 w}{\partial \xi^2} = cs^2 e^{s\xi} \quad (10)$$

Using Eq. (9) into Eq. (3) along with Eq. (4), one gets,

$$s^4 + 2\varepsilon^2 s^2 - \lambda^4 = 0,$$

or

$$(s^2)^2 + 2\varepsilon^2 s^2 - (\lambda^2)^2 = 0 \quad (11)$$

The roots of Eq. (11) is given by

$$s^2 = \frac{-2\varepsilon^2 \pm \sqrt{(2\varepsilon^2)^2 + 4\lambda^4}}{2}; \quad s^2 = \sqrt{-\varepsilon^2 \pm \sqrt{\varepsilon^4 + \lambda^4}}$$

$$s_1 = \alpha; \quad s_2 = i\beta; \quad s_3 = -\alpha; \quad s_4 = -i\beta$$

Considering first two roots $s_1 = \alpha$ and $s_2 = i\beta$
Then $\alpha = \sqrt{-\varepsilon^2 + \sqrt{\varepsilon^4 + \lambda^4}}$; $\beta = \sqrt{\varepsilon^2 + \sqrt{\varepsilon^4 + \lambda^4}}$.

Derivation of Natural Frequency

Let the solution of the general Eq. (2) be

$$W(x) = A \sinh \alpha x + B \cosh \alpha x + C \sin \beta x + D \cos \beta x \quad (12)$$

Then,

$$\frac{\partial W(x)}{\partial x} = A\alpha \cosh \alpha x + B\alpha \sinh \alpha x + C\beta \cos \beta x - D\beta \sin \beta x \quad (13)$$

Fig. 1 Clamped-guided support

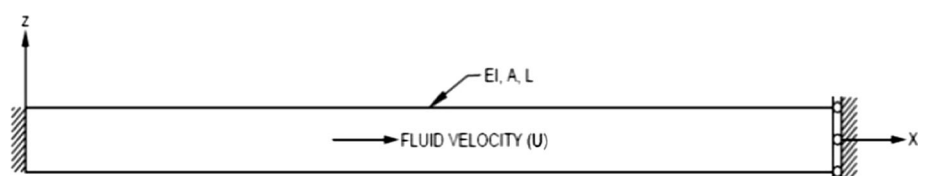
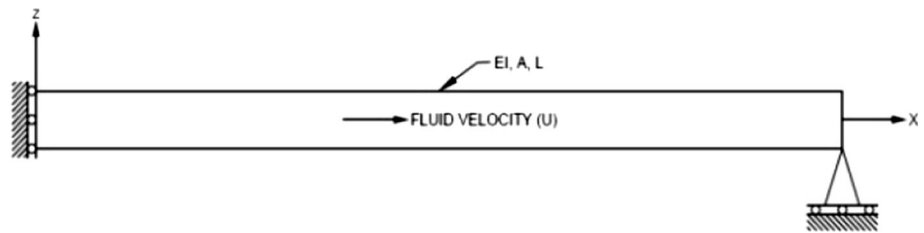
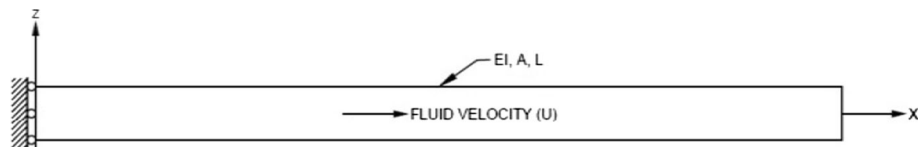
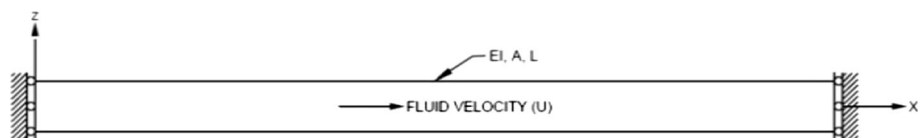


Fig. 2 Guided-simply supported**Fig. 3** Guided-free support**Fig. 4** Guided-guided support

$$\frac{\partial^2 W(x)}{\partial x^2} = A\alpha^2 \sinh \alpha x + B\alpha^2 \cosh \alpha x - C\beta^2 \sin \beta x - D\beta^2 \cos \beta x \quad (14)$$

$$\frac{\partial^3 W(x)}{\partial x^3} = A\alpha^3 \cosh \alpha x + B\alpha^3 \sinh \alpha x - C\beta^3 \cos \beta x + D\beta^3 \sin \beta x \quad (15)$$

Boundary conditions for the ends are given here

Clamped end: $w = 0, \frac{\partial w}{\partial x} = 0$

Guided end: $\frac{\partial w}{\partial x} = 0, \frac{\partial^3 w}{\partial x^3} - T^* \frac{\partial w}{\partial x} = 0$

Free end: $\frac{\partial^2 w}{\partial x^2} = 0, \frac{\partial^3 w}{\partial x^3} - T^* \frac{\partial w}{\partial x} = 0$

Simply supported: $w = 0, \frac{\partial^2 w}{\partial x^2} = 0$

Differentiating Eq. (12) and on substitution of the boundary conditions in Eqs. (13), (14) and (15), the frequency equations are obtained as

Clamped-guided:

$$\alpha\beta^2(\alpha^2 + \beta^2) \cosh(\alpha l) \sin(\beta l) + \alpha^2\beta(\alpha^2 + \beta^2) \sinh(\alpha l) \cos(\beta l) = 0 \quad (16)$$

Guided-simply supported:

$$\alpha\beta[(\alpha^4 + \beta^4) + 2\alpha^2\beta^2] \cosh(\alpha l) \cos(\beta l) = 0 \quad (17)$$

Guided-free:

$$[\alpha(\alpha^2 + \beta^2)(\alpha^4\beta^2)] \cosh(\alpha l) \sin(\beta l) + [\beta(\alpha^2 + \beta^2)(\alpha^2\beta^4)] \sinh(\alpha l) \cos(\beta l) \quad (18)$$

Guided-guided:

$$[(\alpha^2 + \beta^2)^2(\alpha^2\beta^2)] \sinh(\alpha l) \sin(\beta l) = 0 \quad (19)$$

Müllers Method

It uses parabolic interpolation to approximate the given function and then the zero is approximated by the zero of the interpolating quadratic. The quadratic equation has two roots and at any given step. The root can be chosen which is nearer to the current best estimate further, a quadratic equation with real coefficients can give complex roots. Hence this method can give complex roots, even when starting values are real.

Three points x_i, x_{i-1} and x_{i-2} are identified and the function be approximated by a parabola using quadratic interpolation.

$$g(x) = f(x_i) + (x - x_i)f[x_i, x_{i-1}] + (x - x_i) + (x - x_{i-1})f[x_i, x_{i-1}, x_{i-2}] = a_2(x - x_i)^2 + a_1(x - x_i) + a_0 \quad (20)$$

where

$$a_0 = f(x), a_1 = f[x_i, x_{i-1}] + (x_i - x_{i-1})f[x_i, x_{i-1}, x_{i-2}], a_2 = f[x_i, x_{i-1}, x_{i-2}] \quad (21)$$

The zeros of $g(x)$ is given by

$$x_i + \frac{2a_0}{-a_0 \pm \sqrt{a_1^2 - 4a_0a_2}} \quad (22)$$

where one of the two roots is chosen, if, $x_i = a$, the zero of $f(x)$ then, $x_{i+1} = a$, that is the iteration will converge if the initial value is exact.

If $x_i = a$ then $a_0 = f(x_i) = 0$ and must choose that sign before the radical which agrees with $-a_1$, so, that the denominator does not vanish, it may be noted that the

coefficients a_0 , a_1 and a_2 are in general complex and that sign before the radical always be chosen which results the larger magnitude for the denominator (that is, selection of that root of the quadratic is closer to x_i). This method is used to develop FORTRAN program code for piping support system and to find out natural frequencies of fluid conveying pipe for variable velocities with different guided end conditions.

Results and Discussions

Case I: Clamped-Guided Support

Figure 5 shows the fluid-conveying pipe with clamped-guided ends and for increasing order of non-dimensional flow velocities. It is observed that the natural frequency decreases with an increase in non-dimensional velocity. It also shows the point where the pipe flutters and gets into instability zone, that is where the fluid velocity is larger than the critical velocity. The percentage reduction in frequency is around 95% as non-dimensional flow velocity increases from $V = 0.1$ to $V = 5.251$.

Case II: Guided-Simply Supported

Figure 6 depicts the fluid conveying pipe with guided-simply supported ends. In the case of clamped-guided ends the instability region lies in the range of 5.251–5.641 and for guided-simply supported the instability region occurs at a much lower flow velocity of $V = 1.548$ to $V = 1.94$. The percentage reduction in frequency is 84% for flow velocity variation of $V = 0.1$ to $V = 1.548$.

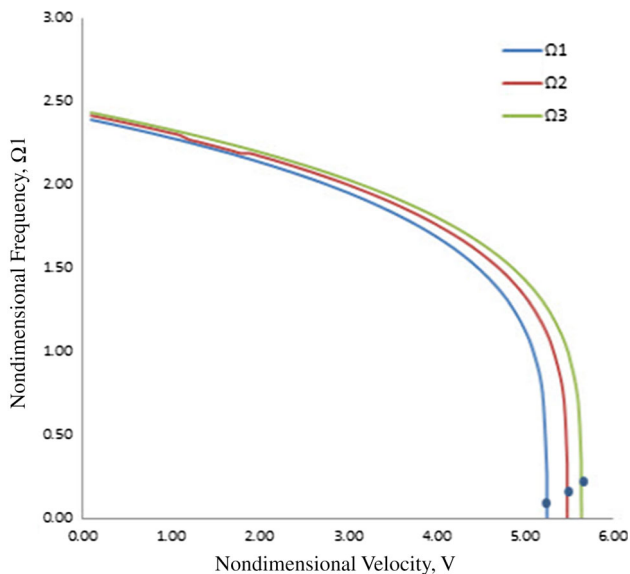


Fig. 5 Non-dimensional natural frequency against velocity and points of flutter clamped-guided end

Case III: Guided-Free Support

Figure 7 presents the guided-free ends, which is around 43.3% when flow velocity increases from 0.1 to 4.72.

Case IV: Guided-Guided Support

Figure 8 presents the guided supports at both the ends. The percentage reduction in frequency is around 62.3% as flow velocity increases from 0.1 to 5.147. For this type of end condition only, the analytical results were validated with experimental work performed and shown in Table 1 [24].

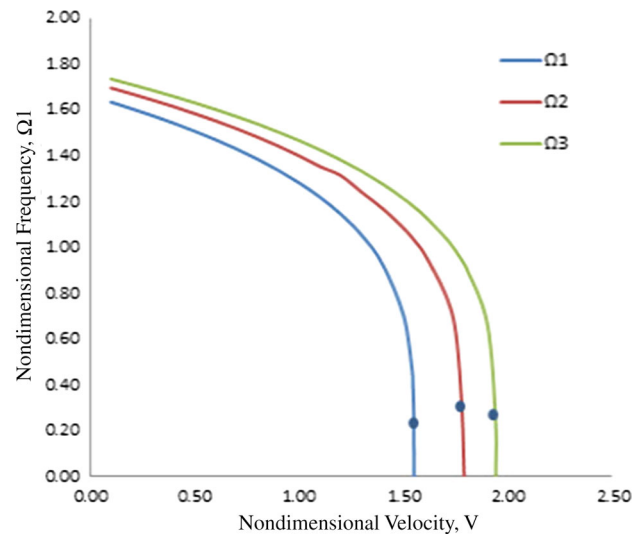


Fig. 6 Non-dimensional velocity against natural frequency and point of flutter-guided-simply supported ends

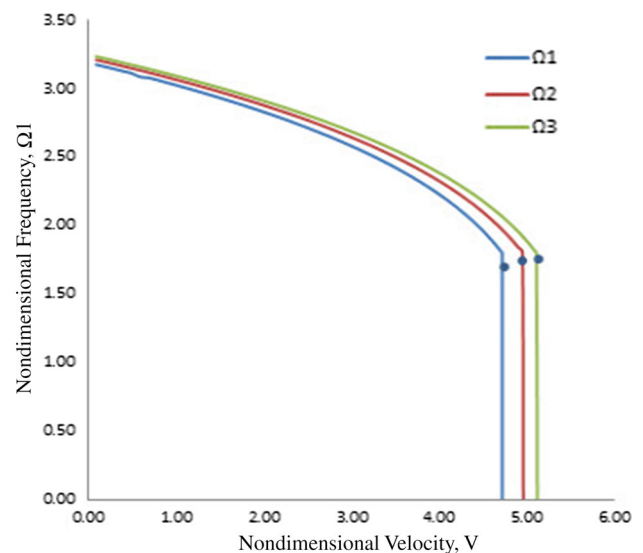


Fig. 7 Non-dimensional velocity natural frequency and points of flutter-guided-free ends

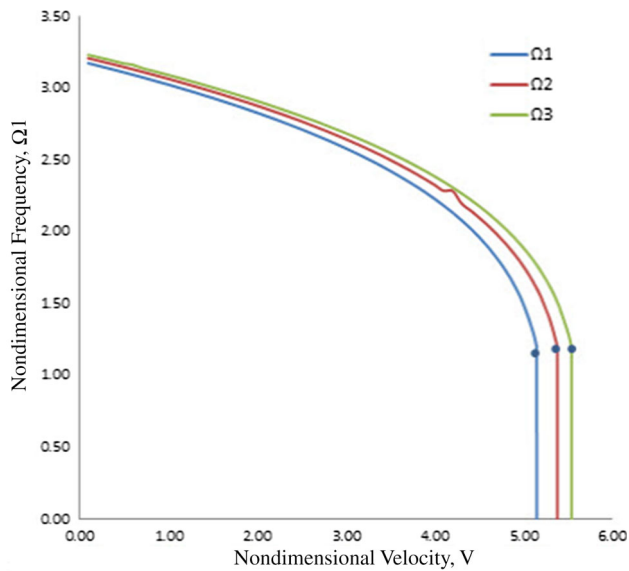


Fig. 8 Non-dimensional velocity against natural frequency and point of flutter-guided-guided ends

Table 1 Validation of experiments carried out with different velocities

Mode	V, m/s	Natural frequency of pipe with guided ends, Hz		
		Theory	Experiment	Percentage error analytical against experiment
1	20.1	3.48	5.0	30.4
2	21.2	8.0	10.0	20.0
3	23.3	8.0	10.0	20.0

Conclusion

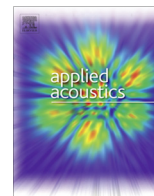
From the study, conclusion can be drawn as follows:

- Exact solution is developed for fluid-conveying pipes considering clamped-guided, guided-simply supported, guided-free and guided-guided end conditions.
- The frequencies of first three modes of vibration are computed by varying the fluid flow velocity.
- Critical velocities are obtained.
- A FORTRAN program is developed for computation of natural frequencies by using Muller's method for non-linear equations and the iterated value of 'x' representing the non-dimensional natural frequency is found by the Inverse Parabolic Interpolation method.
- Experiment was conducted for guided-guided ends and frequencies obtained and compared.

Acknowledgements The authors are thankful and acknowledge the Management of CSIR-Indian Institute of Chemical Technology, Hyderabad, India and College of Engineering, Osmania University, Hyderabad, India for providing the infrastructural facilities.

References

1. H. Ashley, G. Haviland, Bending vibration of a pipeline containing flowing fluid. *Trans. ASME J. Appl. Mech.* **17**, 229–232 (1950)
2. S. Naguleswaran, C.J.H. Williams, Lateral vibration of a pipe conveying a fluid. *J. Mech. Eng. Sci.* **10**(3), 228–238 (1968)
3. R.A. Stein, M.W. Tobriner, Vibration of pipes containing flowing fluid. *Trans. ASME* **37**(4), 906–916 (1970)
4. S.-S. Chen, Free vibration of a coupled fluid/structural system. *J. Sound Vib.* **21**(4), 387–398 (1972)
5. D.S. Weaver, T.E. Unny, On the dynamic stability of fluid conveying pipes. *Trans. ASME* **40**(1), 48–52 (1973)
6. M.P. Paidoussis, Dynamic stability of pipes conveying fluid. *J. Sound Vib.* **33**(3), 267–294 (1974)
7. W. Shizhong, L. Yulan, H. Wenhui, Research on solid-liquid coupling dynamics of pipe conveying fluid. *J. Appl. Math. Mech.* **19**(11), 1065–1071 (1998)
8. Y.L. Zhang, D.G. Gorman, J.M. Reese, Analysis of the vibration of pipes conveying fluid. *Proc. Inst. Mech. Eng. Part C* **213**, 849–860 (1999)
9. H.R. Oz, H. Boyaci, Transverse vibrations of tensioned pipes conveying fluid with time-dependent velocity. *J. Sound Vib.* **236**(2), 259–276 (2000)
10. R. Becquet, I. Elishakoff, Class of analytical closed-form polynomial solutions for clamped-Guided Inhomogeneous beams. *Chaos Solitons Fractals* **12**(9), 1657–1678 (2001)
11. D.C. Wiggert, A.S. Tijsseling, Fluid transients and fluid structure interaction in flexible liquid filled piping. *Am. Soc. Mech. Eng. J.* **54**(5), 455–481 (2001)
12. J.K. Sinha, S. Singh, A.R. Rao, Finite element simulation of dynamic behaviour of an open-ended cantilever pipe conveying fluid. *J. Sound Vib.* **240**(1), 189–194 (2001)
13. Y.L. Zhang, J.M. Reese, D.G. Gorman, Finite element analysis of the vibratory characteristics of cylindrical shells conveying fluid. *Comput. Methods Appl. Mech. Eng.* **191**, 5207–5231 (2002)
14. Y.-S. Seo, W.-B. Jeong, W.-S. Yoo, Frequency response analysis of cylindrical shells conveying fluid using finite element method. *J. Mech. Eng. Sci.* **19**(2), 625–633 (2005)
15. S.S. Rao, *Vibration of Continuous Systems* (Wiley, New York, 2007), pp. 317–328
16. K.R. Chellapilla, H.S. Simha, Critical velocity of fluid conveying pipes resting on two parameter foundation. *J. Sound Vib.* **302**, 387–397 (2007)
17. O.J. Aldraihem, Analysis of the dynamic stability of collar stiffened pipes conveying fluid. *J. Sound Vib.* **300**, 453–465 (2007)
18. Y.-M. Huang, Y.-S. Liu, B.-H. Li, Y.-J. Li, Z.-F. Yue, Natural frequency analysis of fluid conveying pipeline with different boundary conditions. *Nucl. Eng. Des.* **240**, 461–467 (2010)
19. M.J. Jweeg, A.E. Yousif, M.R. Ismail, Experimental estimation of critical buckling velocities for conservative pipes conveying fluid. *J. Al-Khwarizmi Eng.* **7**(4), 17–26 (2011)
20. P. Drozyner, Determining the limits of piping vibration. *Sci. Probl. Mach. Oper. Maint.* **1**(165), 97–103 (2011)
21. H. Yi-min, G. Seng, W. Wei, H. Jie, A direct method of natural frequency analysis on pipeline conveying fluid with both ends supported. *J. Nucl. Eng. Des.* **253**, 12–22 (2012)
22. S.-H. Lee, W.-B. Jeong, An efficient method to predict steady-state vibration of three-dimensional piping system conveying a pulsating fluid. *J. Mech. Sci. Technol.* **6**(9), 2659–2667 (2012)
23. S.-H. Lee, S.-M. Ryu, W.-B. Jeong, Vibration analysis of compressor piping system with fluid pulsation. *J. Mech. Sci. Technol.* **26**(12), 3903–3909 (2012)
24. S.M. Sutar, M. Radhakrishna, P. Ramesh Babu, A theoretical and experimental study of flow induced pipe vibrations with guided end conditions. *J. Hydrocarb. Process. USA.* 1–14. <http://www.hydrocarbonprocessing.com/Article/35670831>. Accessed 08 July 2016



Non-linear torsional vibration of lengthy thin-walled simply supported beam of open section resting on Winkler foundation

Kameswara Rao Chellapilla^a, Bhaskara Rao Lokavarapu^{b,*}

^a Department of Mechanical Engineering, Nalla Narasimha Reddy Engineering College, Ghatkesar (M), Ranga Reddy (Dt.), Hyderabad, Telangana State, India

^b School of Mechanical and Building Sciences, VIT University, Chennai Campus, Vandalur-Kelambakkam Road, Chennai, Tamil Nadu, India

ARTICLE INFO

Article history:

Received 6 November 2018

Received in revised form 30 March 2019

Accepted 10 May 2019

Keywords:

Beam

Open section

Vibration

Warping effect

Winkler foundation

ABSTRACT

The aim of this paper is to study the non-linear torsional vibrations of lengthy thin-walled simply supported beam of open section resting on Winkler foundation. The governing differential equation of motion is derived. An effort has been made to obtain and solve the governing differential equation of large amplitude torsional vibrations of doubly symmetric thin-walled beams of open section with simply supported boundary. Approximate solutions are obtained for simply supported beams using the well-known Galerkin's method. Plots specifying the effect of large amplitudes on nonlinear frequency of torsional vibrations for various non-dimensional beam constants are furnished. From the present study, we observe, that for lower values of Winkler stiffness parameter $\lambda \leq 0.1$, the non-linear frequency increases drastically as β increases. Also, it is noticed that as the value of Winkler stiffness parameter λ increases, the influence of β decreases. For higher values of $\lambda \geq 30$, the effect of β in the present range 0–0.1 on non-linear frequency seems to be negligible.

© 2019 Elsevier Ltd. All rights reserved.

1. Introduction

Study of torsional vibrations finds extensive application in aerospace (Fuselage floor beam, rail system for chamber, aircraft undercarriages, and jet engine components), civil (industrial, building and architectural applications), mechanical (trucks, transmissions, trains, rails, mining screens, fluidized bed boilers, and anchor chains), and marine (container ships and fast patrol boats, ladders, steel flooring and grating, stairs, the jacket-type pier) engineering etc. Singh et al. [1] presented an exhaustive critical review of studies of large amplitude free vibrations of beams. Many problems of vibration of thin-walled beams emerging in the state-of-the-art high-speed structures in automotive, aerospace, power, marine and launching vehicles cannot be effectively described by the classical linear theories [2–6] solely, since the torsional deformations of these beams are usually of such a magnitude that the assumption of small rotations of cross sections will not anymore be valid. During the course of an experiment, Tso [7] observed a certain behaviour which could not be foreseen from the linearized equations. He described the phenomenon in terms of the vibrational modes of the beam. He observed that when a higher mode resonant frequency of the beam is a multiple or near multiple of

the lowest mode, and when the beam is excited at this resonant frequency, there is a tendency for energy to transmit from the highest mode to the lowest mode, resulting very often in a high order sub-harmonic oscillation. He presented an analysis of such behaviour through non-linear couplings.

The behaviour of a thin-walled beam subjected to static twisting moments applied at the end cross sections, has been studied by Cullimore [8]. Cullimore considered the case of uniform torsion of a beam of narrow rectangular section and I section, subjected to static end moments. Gregory [9,10] extended the study of uniform torsion to cover a beam of mono-symmetrical angle sections. They showed that if large torsional deformation was considered, the torsional and longitudinal deformations are coupled together. Such coupling is known as the shortening effect. The effect of shear strain due to warping and bending of the beam was included by Tso [11]. He considered torsional deformations in addition to bending and shearing deformations. This approach can be considered as a “Timoshenko beam theory” analogy for thin-walled elements.

Among the available contributions in this direction [8,12–14], the one presented by Ghobarah and Tso [12] and Tso and Ghobarah [13] is an enhanced nonlinear thin-walled beam theory derived by assuming that the flexural deformations are of higher order of diminutiveness than torsional deformations. The current study ventures to determine and solve the governing differential equation of large amplitude torsional vibrations of simply supported

* Corresponding author.

E-mail address: bhaskarababu_20@yahoo.com (B.R. Lokavarapu).

Nomenclature

A, L	Area of cross-section and length of the beam	$x(z)$	Normal function of angle of twist
C_w	Warping torsion constant	z	Distance along the length of beam
C_s	Saint Venant's torsion constant	λ^2	$K_w L / 4EC_w$ Foundation parameter
G	Modulus of rigidity	δ	F/C_w
E	Modulus of elasticity	K^2	$GC_s L^2 / EC_w$ Warping parameter
F	Cross-sectional property constant = $I_R - (I_{pc}/A)^2$	P	Axial compressive load
I_{pc}	Half the polar moment of inertia of beam = $1/2 I_p$	σ	P/A , axial compressive stress
I_R	Fourth moment of inertia of beam about shear center	\varnothing	Angle of twist
K_w	Winkler foundation modulus		
K	Warping parameter		

doubly symmetric thin-walled open section beams, based on the nonlinear theory presented by Ghobarah and Tso [12] and Tso and Ghobarah [13]. Plots denoting the influence of large amplitudes on the nonlinear period of torsional vibrations for various non-dimensional beam constants are displayed. Kameswara Rao [14] studied nonlinear torsional vibrations of thin-walled beams of open-section. He has derived and solved the governing differential equation of large amplitude torsional vibrations of simply supported doubly symmetric thin-walled beams of open section using Galerkin's method [28]. A finite element method for studying non-linear free torsional vibrations of thin-walled beams with bisymmetric open cross-section is studied by Rozmarynowski and Szymczak [15].

They have derived the fundamental differential equation of the problem is based on the classical assumption of a thin-walled beam with a non-deformable cross-section. Sarma and Varadan studied Ritz finite element approach to nonlinear vibrations of beams. They have used Ritz finite element approach to study the large amplitude free flexural vibrations of beams with immovable ends [16]. Lewandowski explores the Application of the Ritz method to the analysis of non-linear free vibrations of beams. He presented an analytical solution for geometrically non-linear free vibrations of beams with elastically supported ends in the horizontal direction [17].

An analysis of the nonlinear torsion of thin-walled bars of variable, open cross-section is studied by Wekezer [18]. The finite element method is used to formulate stiffness matrices for a thin-walled bar element. Attard [19] studied the nonlinear theory of non-uniform torsion of thin-walled open beams. They have presented expressions for the finite nonlinear strains in Lagrangian coordinates and the Kirchhoff stresses for thin-walled open beams. Researchers have applied different models such as inclusion or exclusion of axial displacement, and linear or nonlinear kinematic (strain-displacement) relations. Starting with the work of Woinosky-Krieger [20] who used elliptic integrals, researchers have also utilised several methods such as perturbation, Ritz-Galerkin and the finite element method [21]. Pillai and Nageswara Rao [22] have studied the problem of large amplitude free vibration of simply supported uniform beams with immovable ends is examined. The equation of motion for this problem is found to be of Duffing type.

Foudil et al., [23] analysed the behaviour of thin-walled beams with open section in presence of large torsion. They have derived equilibrium equations for the case of elastic behaviour without any assumption on torsion angle amplitude. They have implemented an incremental-iterative Newton-Raphson method for solving nonlinear equations. Gupta et al., [23,24] studied large amplitude free vibration analysis of uniform, slender and isotropic beams through a relatively simple finite element formulation, applicable to homogenous cubic nonlinear temporal equation

(homogenous Duffing equation). Samir [25] presented approximate analytical solutions for the nonlinear free vibrations of composite beams in buckling. The governing differential equations for large amplitude vibrations of a composite beam are derived using Galerkin's discretization approach.

The current study aims to obtain and solve the governing differential equation of large amplitude torsional vibrations of doubly symmetric thin-walled open section beams resting on Winkler foundation as shown in Fig. 1. Approximate solutions are obtained for simply supported beams utilizing Galerkin's technique. Plots representing the effect of large amplitudes on the non-linear period of torsional vibrations for diverse non-dimensional beam constants are provided.

The main aim of the present study is to estimate the effect of Winkler foundation parameter λ on the torsional non-linear frequency of doubly-symmetric thin-walled beams resting on Winkler's foundation. From this study detailed here under, we observe, that for lower values of Winkler stiffness parameter $\lambda \geq 0$, the non-linear frequency increases drastically as the torsional amplitude β increases. Also, it is noticed that as the value of Winkler stiffness parameter λ increases, the influence of β decreases and for higher values of $\lambda \geq 30$, the effect of β in the present range 0 to 0.1 on non-linear frequency becomes negligible.

2. Formulation and analysis

The static nonlinear torsion equation for a doubly symmetric thin-walled beam of open section of length L , subjected to a twisting moment M_t is given by Eq. (1) [13].

$$M_t L^3 = GC_s L^2 \theta' - EC_w \theta''' + 2EF(\theta')^3 \quad (1)$$

where G is the shearing modulus, C_s is the Saint Venant's torsion constant, E is Young's modulus, C_w is the warping torsion constant, and θ is the angle of twist. Also, F is a constant dependent on cross-sectional properties and is defined by $F = I_R - (I_{pc}/A)^2$, in which I_{pc} is half the polar moment of inertia about the shear centre, I_R is the fourth moment of inertia about the shear center, A is the area, and the primes designate differentiation with respect to the non-dimensional length $Z = z/L$, where z being the distance along the length of the beam.

For free vibrations, $M_t' = \rho I_p L \ddot{\theta}$, where dots donate differentiation with respect to time t , ρ is the mass density, I_p is the polar moment of inertia, and from the Eq. (1) yields the following

$$GC_s L^2 \theta'' + 6EF(\theta')^2 \theta'' - EC_w \theta^{iv} = \rho I_p L^4 \ddot{\theta} \quad (2)$$

For the present purpose, approximate solutions are obtained using the well-known Galerkin's method for simply supported beams.

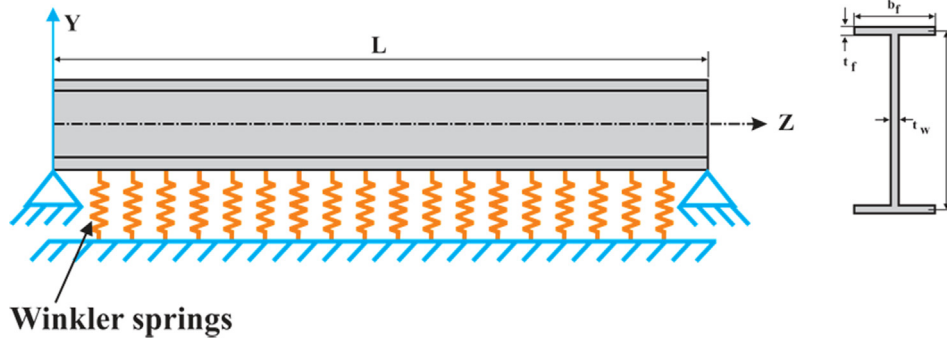


Fig. 1. Doubly symmetric Thin-walled I-beam resting on Winkler foundation.

The boundary conditions for a simply supported beam are given below

$$\varnothing = 0; \varnothing'' = 0 \quad \text{at } Z = 0 \quad (3)$$

$$\varnothing = 0; \varnothing'' = 0 \quad \text{at } Z = L \quad (4)$$

where primes designate partial differentiation with respect to the non-dimensional length $Z = z/L$

Eq. (2) can be written in a non-dimensional form as:

$$\varnothing^{iv} - 6\delta^* (\varnothing')^2 \varnothing'' - (K^2) \varnothing'' + 4\gamma_w^2 \varnothing + \bar{\mu}^* \ddot{\varnothing} = 0 \quad (5)$$

where

$$\gamma_w^2 = \frac{K_{WL}}{EC_w}; \quad \bar{\mu}^* = \rho I_p L^4 / EC_w; \quad \delta^* = \frac{F}{C_w} \quad (6)$$

And dots designate differentiation with respect to time t

In order to solve Eq. (5) by Galerkin's method [26], the angle of twist $\varnothing(Z, t)$ can be assumed as

$$\varnothing(Z, t) = \beta^* x(z) \tau^*(t) \quad (7)$$

where τ^* is a function of time. Since x will be an approximate function assumed to satisfy the boundary conditions, by substituting Eq. (7) in Eq. (5) an error function ϵ will be obtained as:

$$\epsilon^* = \beta^* \left\{ \bar{\mu}^* \ddot{\tau} x + \tau^* \left[x^{iv} - 6\delta^* \beta^{*2} (x')^2 x'' - (K^2) x'' + 4\gamma_w^2 x \right] \right\} \quad (8)$$

For minimizing the error function ϵ , the error integral according to Galerkin's Method [26] is given by

$$\int_0^1 \epsilon x(z) dz = 0 \quad (9)$$

In order to satisfy the boundary conditions, Eqs. (3) and (4) we assume

$$x(Z) = \sin \pi Z \quad (10)$$

From Eqs. (8), (9) and (10), we obtain the equation governing the time function τ^* as,

$$\bar{\mu}^* \ddot{\tau} + \left[\pi^2 (K^2 + \pi^2) + 4\gamma_w^2 \right] \tau^* + (3/2) \pi^4 \delta^* \beta^{*2} \tau^{*3} = 0 \quad (11)$$

If the initial conditions are

$$\tau^*(0) = 1 \text{ and } \dot{\tau}^*(0) = 0 \quad (12)$$

The solution of Eq. (11), which is known as Duffing's equation [27] will be given in the form of an elliptical cosine C_n^*

$$\tau^* = C_n^* (\omega_1^* t, p_1) \quad (13)$$

where

$$\omega_1^{*2} = \frac{\left[\pi^2 (K^2 + \pi^2) + 4\gamma_w^2 \right]}{\bar{\mu}^*} \left\{ 1 + \frac{1.5\pi^4 \delta^* \beta^{*2}}{\left[\pi^2 (K^2 + \pi^2) + 4\gamma_w^2 \right]} \right\} \quad (14)$$

For and $\beta \rightarrow 0$ then Eq. (13) can be written as

$$\omega_1^{*2} = \frac{\left[\pi^2 (K^2 + \pi^2) + 4\gamma_w^2 \right]}{\bar{\mu}^*} \quad (15)$$

Therefore the ratio of non-linear to linear frequency ratio can be expressed as

$$\frac{\omega_1^*}{\omega_1} = \left\{ 1 + \frac{1.5\pi^4 \delta^* \beta^{*2}}{\left[\pi^2 (K^2 + \pi^2) + 4\gamma_w^2 \right]} \right\}^{1/2} \quad (16)$$

Eq. (13) can be reduced to Eq. (17) in the absence of elastic foundation, i.e., $\gamma_w = 0$

$$\frac{\omega_1^*}{\omega_1} = \left\{ 1 + \frac{1.5\pi^4 \delta^* \beta^{*2}}{\left[\pi^2 (K^2 + \pi^2) \right]} \right\}^{1/2} \quad (17)$$

3. Numerical results and discussions

The various beam parameters involved in the analysis are obtained for three selected steel I-beams [6], knowing the width of the flange b , depth of the web h , thickness of the flange t_f , thickness of the web t_w and the beam length L . To cover a good range of values of the non-linear sectional property the non-linear sectional property $\delta^* = \frac{F}{C_w}$, Warping Parameter K and the Winkler foundation modulus λ , a total of three consisting of one Indian and two American standard steel I beams, are considered in obtaining the results for presentation in this paper to enable their use in designing such sections for application in aircraft structures. Numerical solutions of Eq. (14) showing the effect of amplitude on period of nonlinear torsional vibration are presented in Figs. 2–35, for the three steel I-beams considered, among which two are American standard wide-flanged (36WF230 and 24WF130) beams [29], for distinctive values of non-dimensional warping constant K . Poisson's ratio assumed here as 0.3.

Case (i):

Dimensions of a standard steel I-beam considered are as follows: $h = 69.65$ mm, $b_f = 31.55$ mm, $t_f = 3.11$ mm, $t_w = 2.13$ mm. The effect of torsional amplitudes on frequency of non-linear torsional vibration of simply supported I-beam for several values of the Winkler stiffness parameter, λ , Warping parameter, K and dimensionless parameter δ is determined and shown in Figs. 2–6.

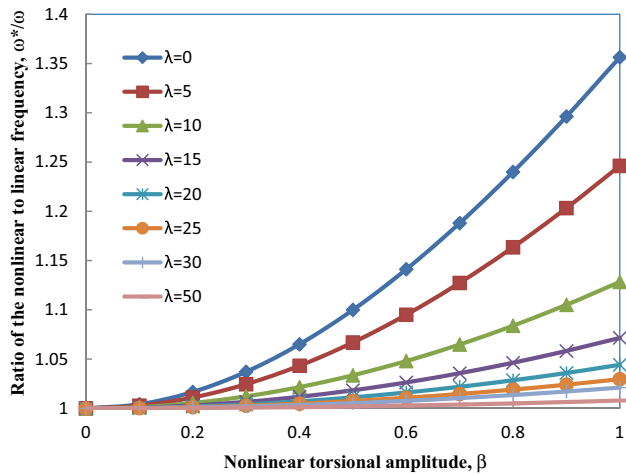


Fig. 2. The influence of elastic foundation (for different values of the Winkler stiffness parameter, λ , and $\delta = 1.1095$ and $K = 3.106$) on non-linear torsional vibration of simply supported thin-walled beam of open section.

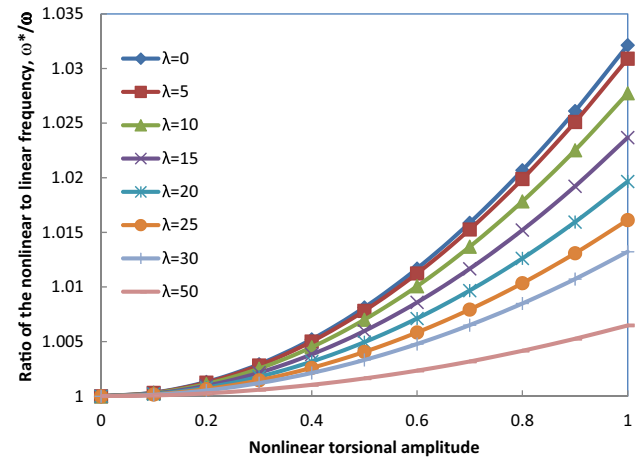


Fig. 5. The influence of elastic foundation (for different values of the Winkler stiffness parameter, λ , and $\delta = 1.1095$ and $K = 15.528$) on non-linear torsional vibration of simply supported thin-walled beam of open section.

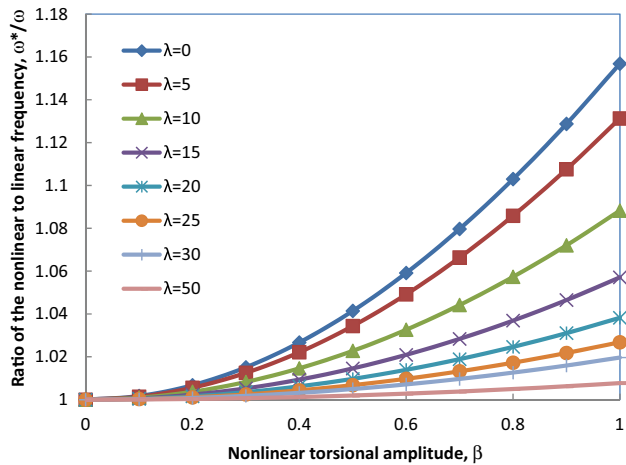


Fig. 3. The influence of elastic foundation (for different values of the Winkler stiffness parameter, λ , and $\delta = 1.1095$ and $K = 6.211$) on non-linear torsional vibration of simply supported thin-walled beam of open section.

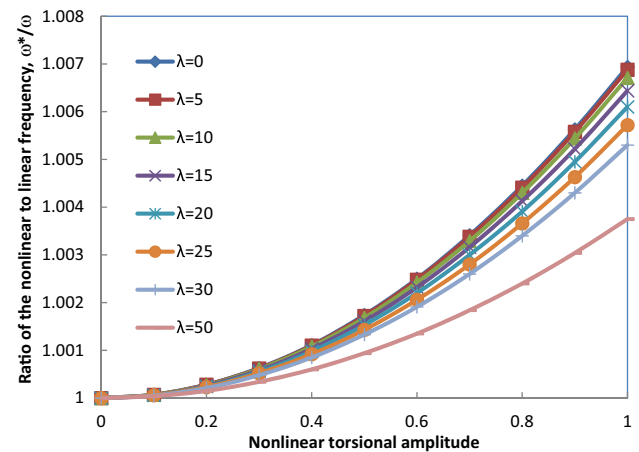


Fig. 6. The influence of elastic foundation (for different values of the Winkler stiffness parameter, λ , and $\delta = 1.1095$ and $K = 34.161$) on non-linear torsional vibration of simply supported thin-walled beam of open section.

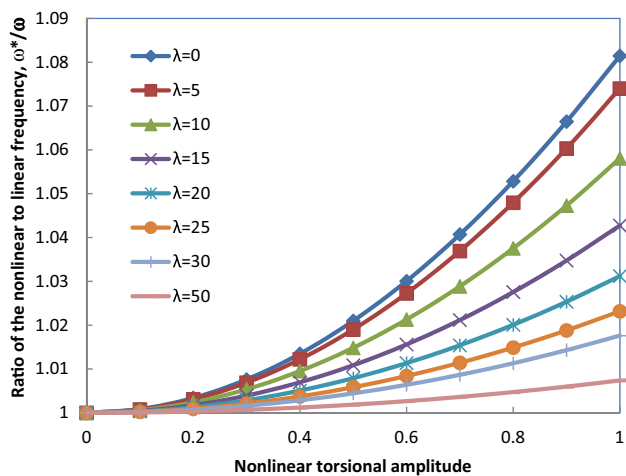


Fig. 4. The influence of elastic foundation (for different values of the Winkler stiffness parameter, λ , and $\delta = 1.1095$ and $K = 9.317$) on non-linear torsional vibration of simply supported thin-walled beam of open section.

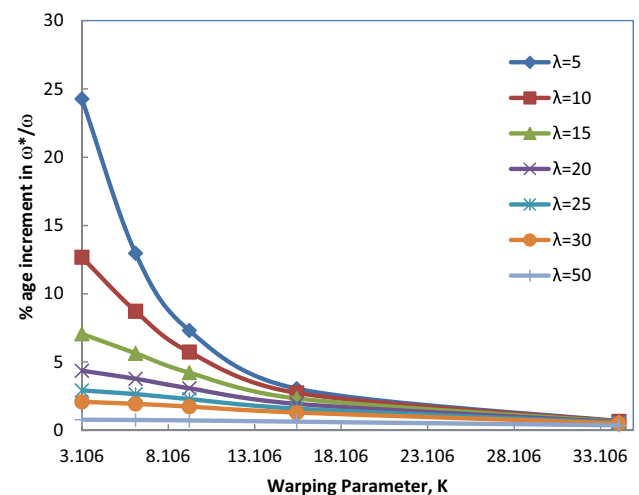


Fig. 7. The percentage variation of the ratio of nonlinear to linear frequency ratio (ω^*/ω) as β varies from 0.1 to 1, with Warping parameter, K , for various values of Winkler stiffness parameter, $\lambda = 0, 5, 10, 15, 20, 25, 30$ and 50 .

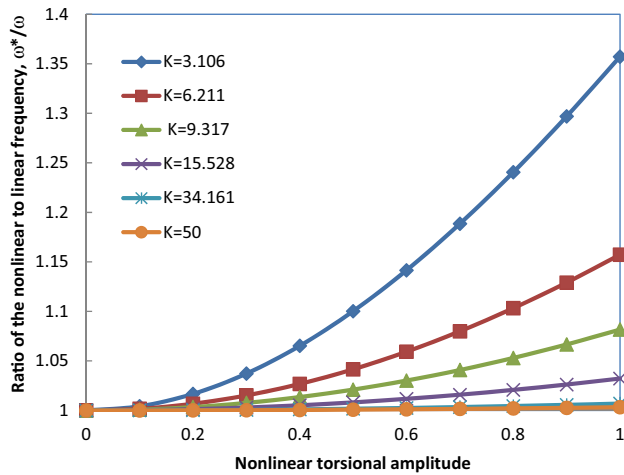


Fig. 8. The influence of Warping parameter (for different values of the Warping parameter K , and $\delta = 1.1095$ and $\lambda = 0$) on non-linear torsional vibration of simply supported thin-walled beam of open section.

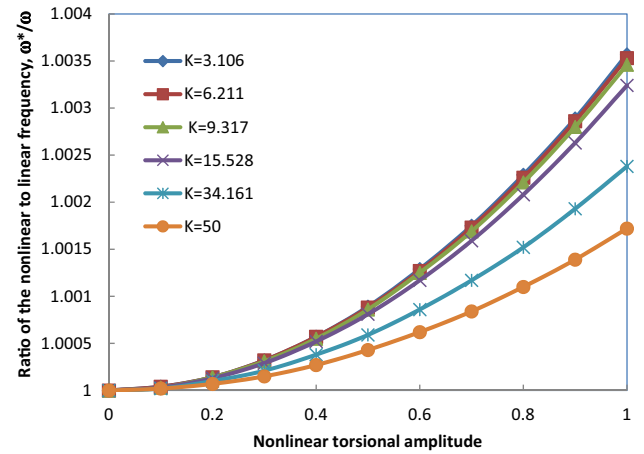


Fig. 11. The influence of Warping parameter (for different values of the Warping parameter K , and $\delta = 1.1095$ and $\lambda = 75$) on non-linear torsional vibration of simply supported thin-walled beam of open section.

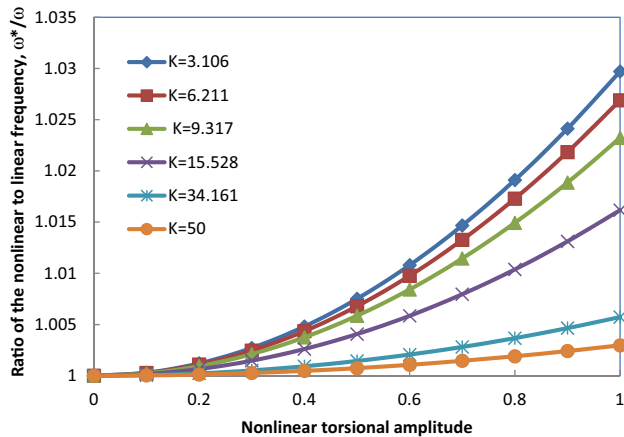


Fig. 9. The influence of Warping parameter (for different values of the Warping parameter K , and $\delta = 1.1095$ and $\lambda = 25$) on non-linear torsional vibration of simply supported thin-walled beam of open section.

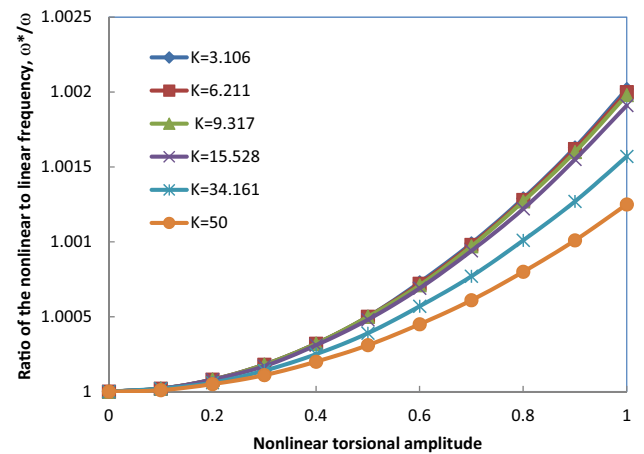


Fig. 12. The influence of Warping parameter (for different values of the Warping parameter K , and $\delta = 1.1095$ and $\lambda = 100$) on non-linear torsional vibration of simply supported thin-walled beam of open section.

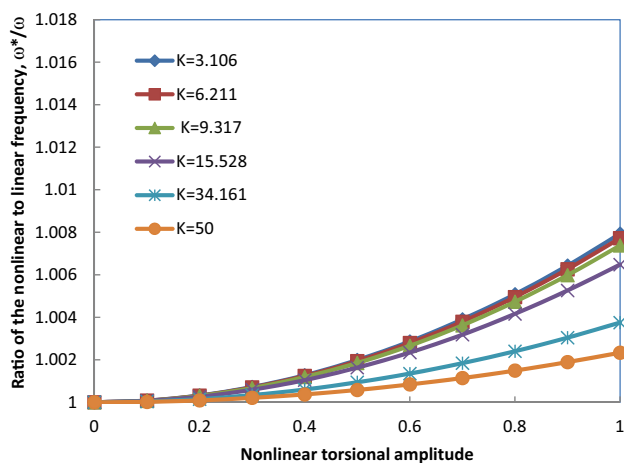


Fig. 10. The influence of Warping parameter (for different values of the Warping parameter K , and $\delta = 1.1095$ and $\lambda = 50$) on non-linear torsional vibration of simply supported thin-walled beam of open section.

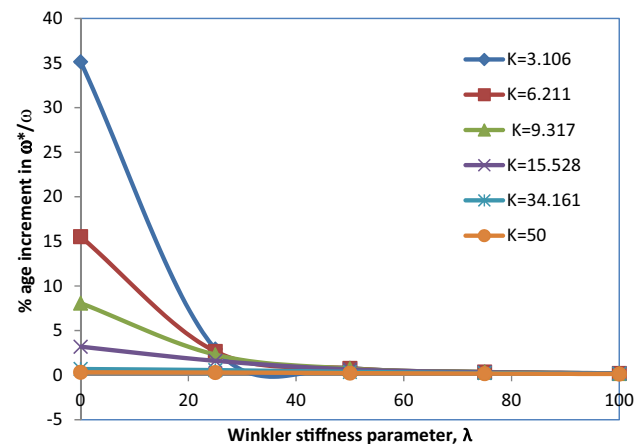


Fig. 13. The percentage variation of the ratio of nonlinear to linear frequency ratio (ω^*/ω) as β varies from 0.1 to 1, with Winkler stiffness parameter, λ for various values of Warping parameter, $K = 6.211, 9.317, 15.528$ and 34.161 .

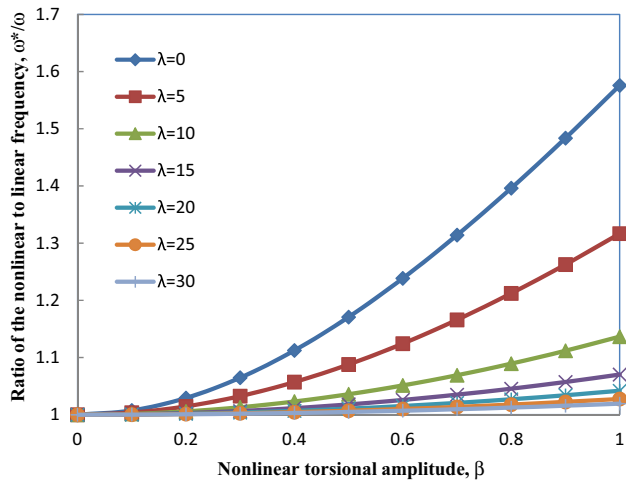


Fig. 14. The influence of elastic foundation (for different values of the Winkler stiffness parameter λ , and $\delta = 0.992$ and $K = 0.177$) on non-linear torsional vibration of simply supported thin-walled beam of open section.

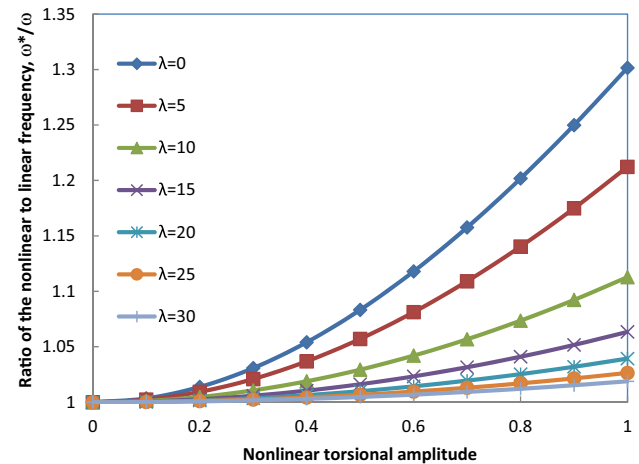


Fig. 17. The influence of elastic foundation (for different values of the Winkler stiffness parameter λ , and $\delta = 0.992$ and $K = 3.361$) on non-linear torsional vibration of simply supported thin-walled beam of open section.

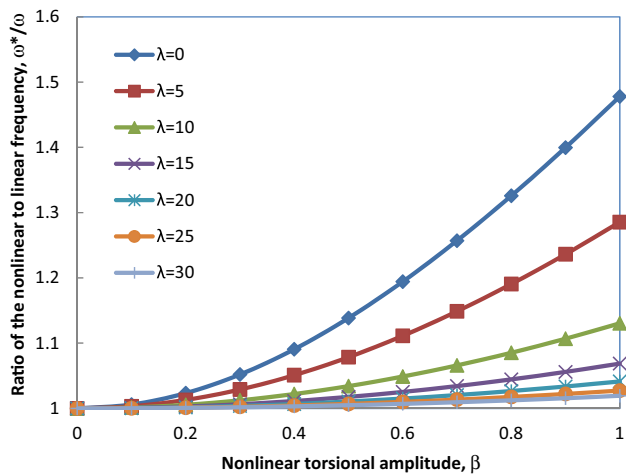


Fig. 15. The influence of elastic foundation (for different values of the Winkler stiffness parameter λ , and $\delta = 0.992$ and $K = 1.592$) on non-linear torsional vibration of simply supported thin-walled beam of open section.

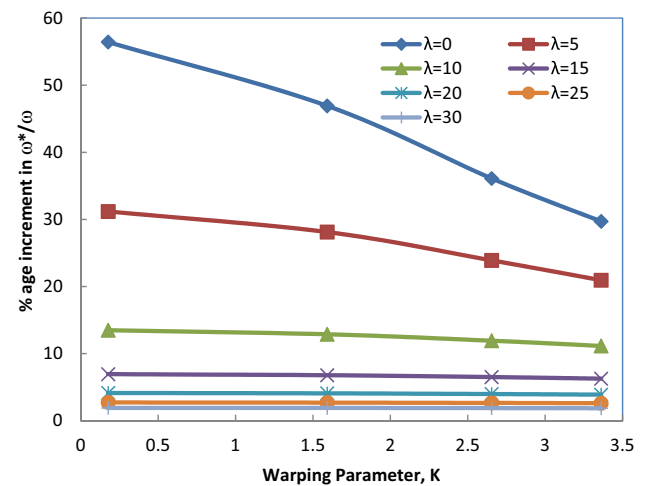


Fig. 18. The percentage variation of the ratio of nonlinear to linear frequency ratio (ω^*/ω) as β varies from 0.1 to 1, with Warping parameter K for various values of Winkler stiffness parameter $\lambda = 0, 5, 10, 15, 20, 25$ and 30.

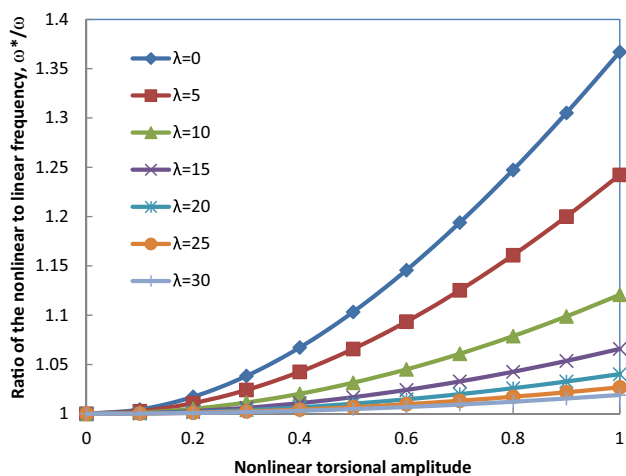


Fig. 16. The influence of elastic foundation (for different values of the Winkler stiffness parameter λ , and $\delta = 0.992$ and $K = 2.654$) on non-linear torsional vibration of simply supported thin-walled beam of open section.

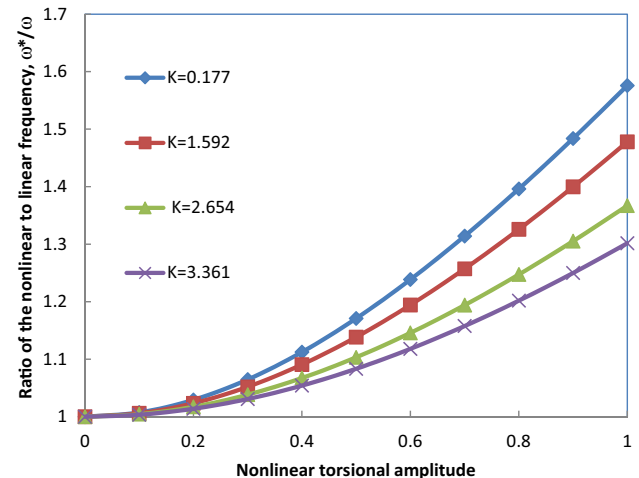


Fig. 19. The influence of Warping parameter (for different values of the Warping parameter K , and $\delta = 0.992$ and $\lambda = 0$) on non-linear torsional vibration of simply supported thin-walled beam of open section.

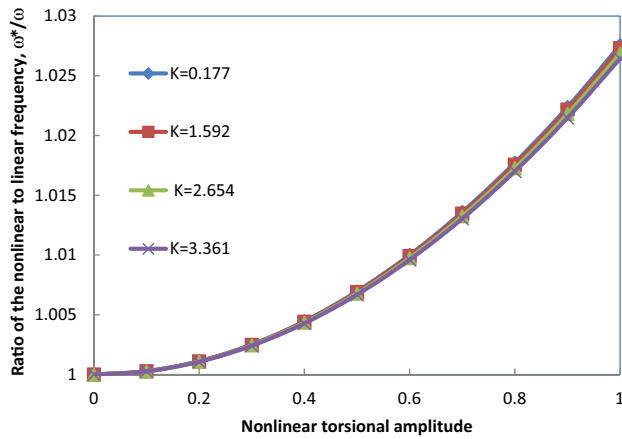


Fig. 20. The influence of Warping parameter (for different values of the Warping parameter K , and $\delta = 0.992$ and $\lambda = 25$ on non-linear torsional vibration of simply supported thin-walled beam of open section.

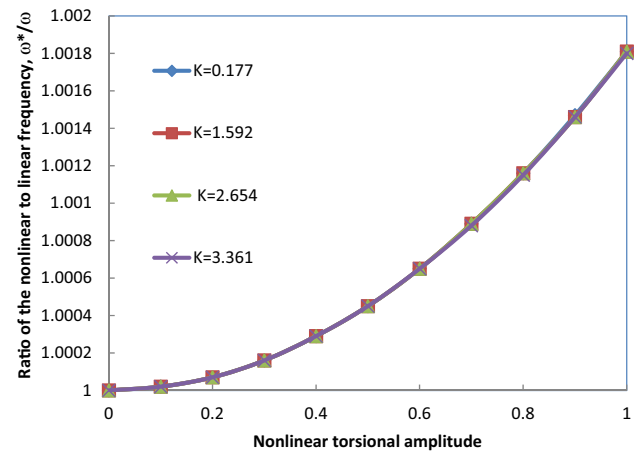


Fig. 23. The influence of Warping parameter (for different values of the Warping parameter K , and $\delta = 0.992$ and $\lambda = 100$) on non-linear torsional vibration of simply supported thin-walled beam of open section.

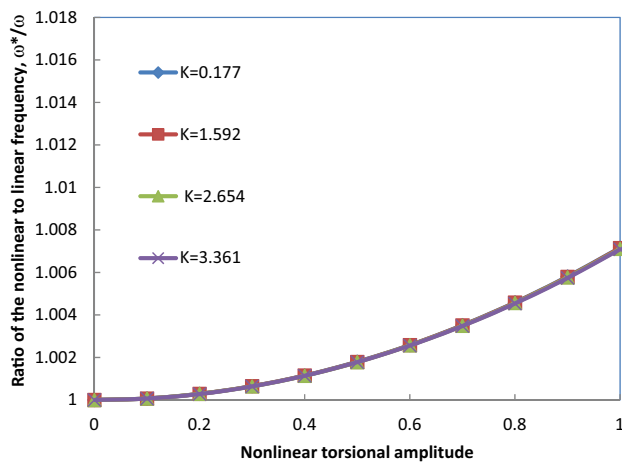


Fig. 21. The influence of Warping parameter (for different values of the Warping parameter K , and $\delta = 0.992$ and $\lambda = 50$) on non-linear torsional vibration of simply supported thin-walled beam of open section.

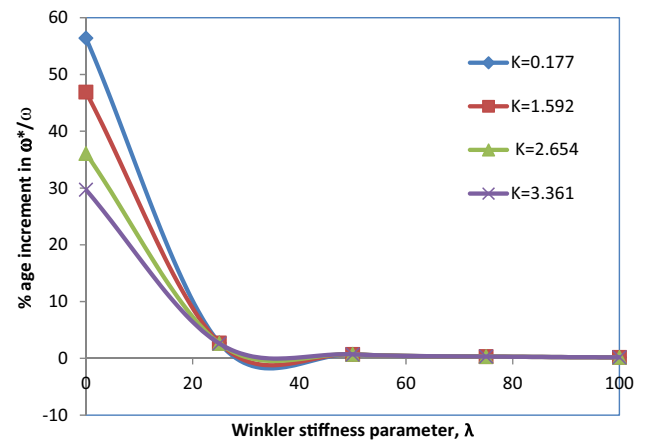


Fig. 24. The percentage variation of the ratio of nonlinear to linear frequency ratio (ω^*/ω) as β varies from 0.1 to 1, with Winkler stiffness parameter, λ for various values of Warping parameter $K = 0.177, 1.592, 2.654$ and 3.361 .

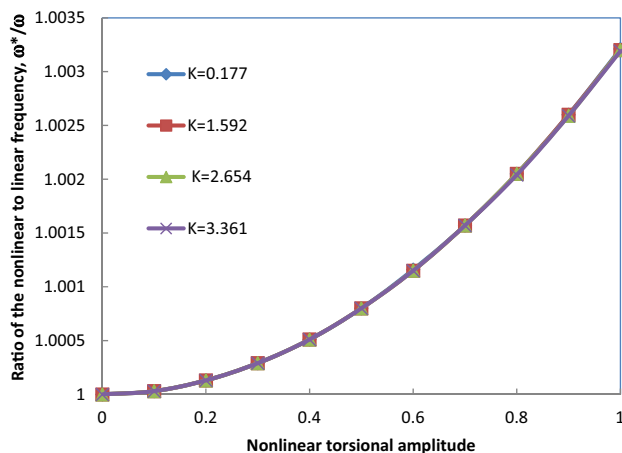


Fig. 22. The influence of Warping parameter (for different values of the Warping parameter K , and $\delta = 0.992$ and $\lambda = 75$) on non-linear torsional vibration of simply supported thin-walled beam of open section.

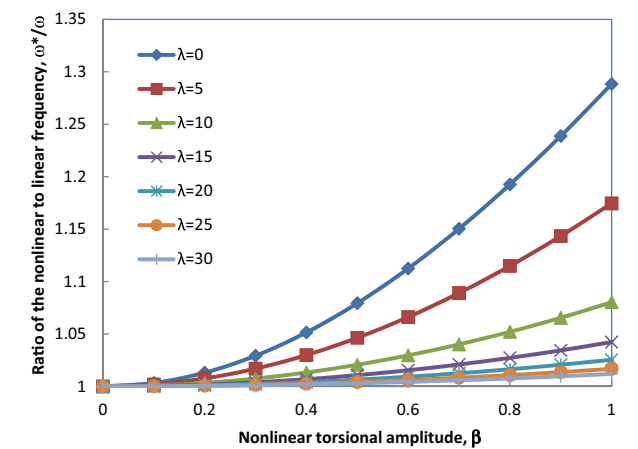


Fig. 25. The influence of elastic foundation (for different values of the Winkler stiffness parameter, λ , and $\delta = 0.6104$ and $K = 0.217$) on non-linear torsional vibration of simply supported thin-walled beam of open section.

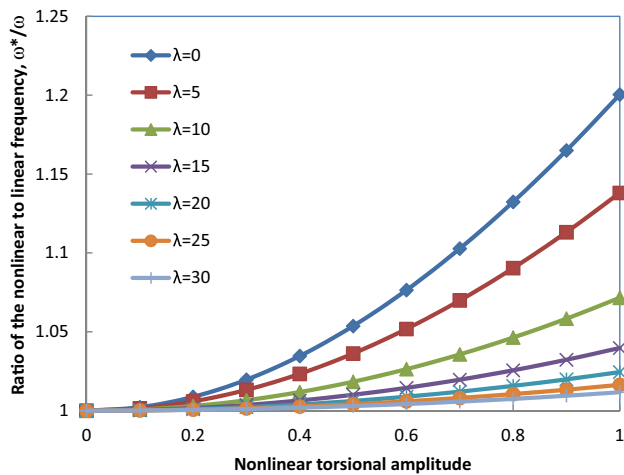


Fig. 26. The influence of elastic foundation (for different values of the Winkler stiffness parameter, λ , and $\delta = 0.6104$ and $K = 1.957$) on non-linear torsional vibration of simply supported thin-walled beam of open section.

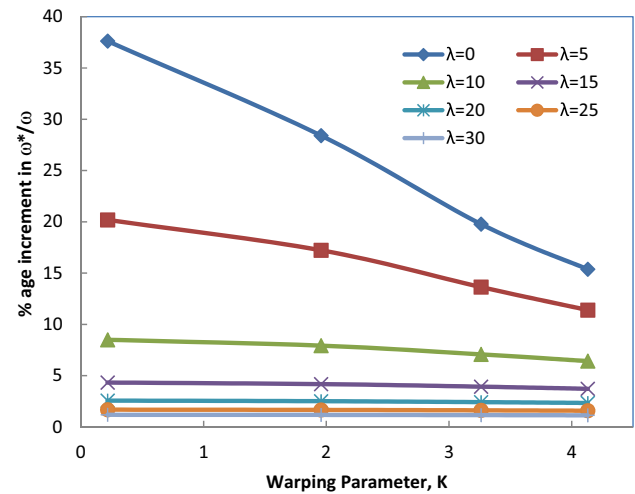


Fig. 29. The percentage variation of the ratio of nonlinear to linear frequency ratio (ω^*/ω) as β varies from 0.1 to 1, with Warping parameter K , for various values of Winkler stiffness parameter, $\lambda = 0, 5, 10, 15, 20, 25$ and 30 .

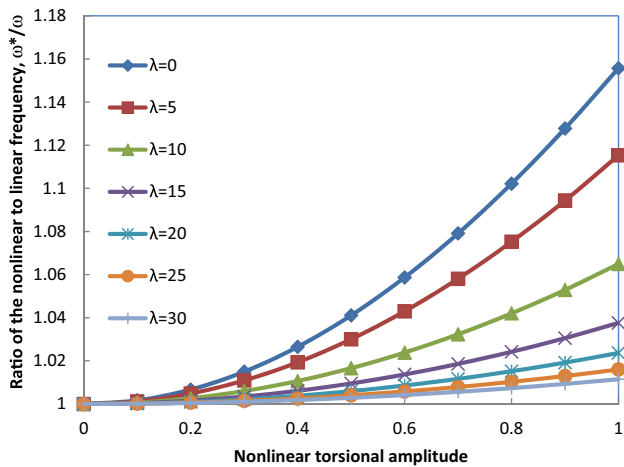


Fig. 27. The influence of elastic foundation (for different values of the Winkler stiffness parameter, λ , and $\delta = 0.6104$ and $K = 3.261$) on non-linear torsional vibration of simply supported thin-walled beam of open section.

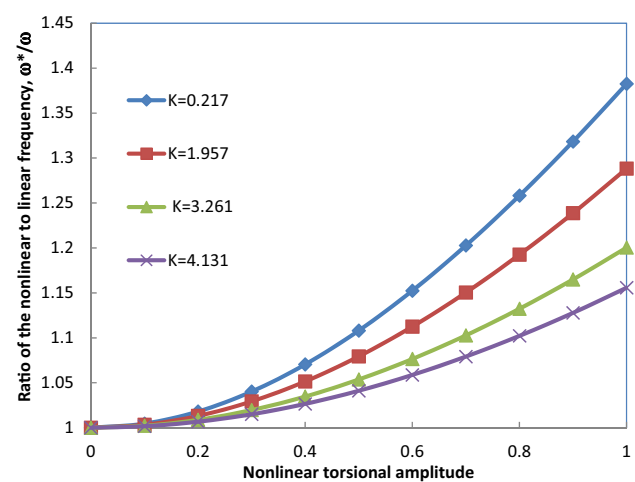


Fig. 30. The influence of Warping parameter (for different values of the Warping parameter, K , and $\delta = 0.6104$ and $\lambda = 0$) on non-linear torsional vibration of simply supported thin-walled beam of open section.

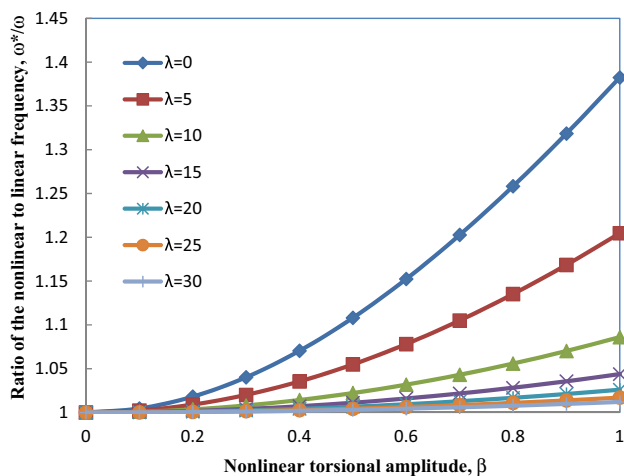


Fig. 28. The influence of elastic foundation (for different values of the Winkler stiffness parameter, λ , and $\delta = 0.6104$ and $K = 4.131$) on non-linear torsional vibration of simply supported thin-walled beam of open section.

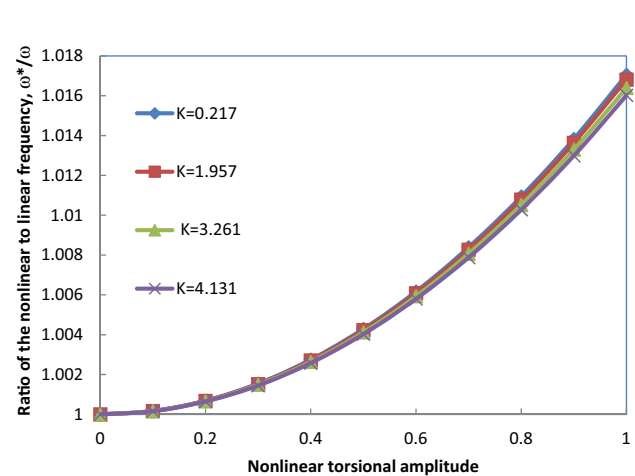


Fig. 31. The influence of Warping parameter (for different values of the Warping parameter, K , and $\delta = 0.6104$ and $\lambda = 25$) on non-linear torsional vibration of simply supported thin-walled beam of open section.

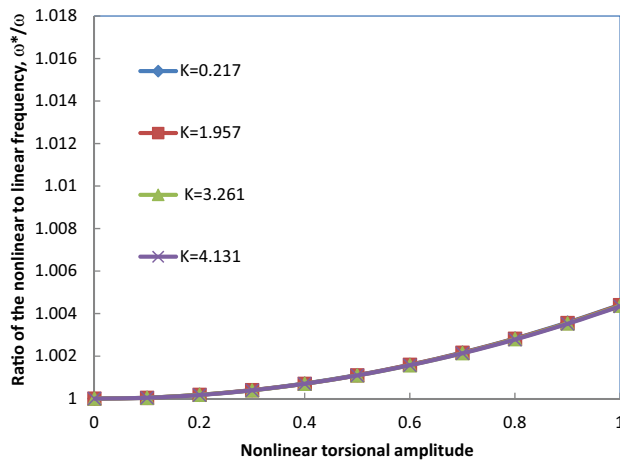


Fig. 32. The influence of Warping parameter (for different values of the Warping parameter, K , and $\delta = 0.6104$ and $\lambda = 50$) on non-linear torsional vibration of simply supported thin-walled beam of open section.

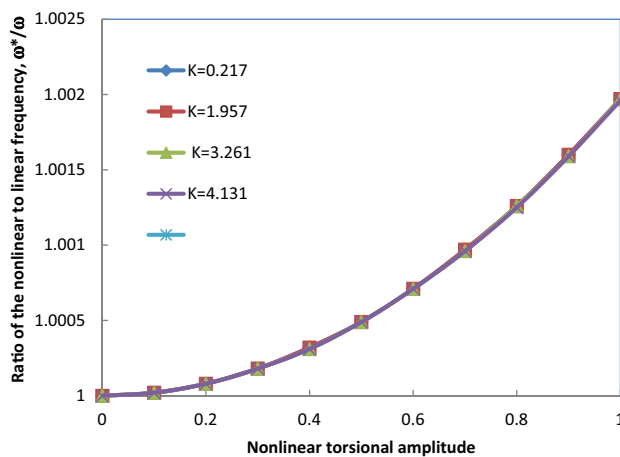


Fig. 33. The influence of Warping parameter (for different values of the Warping parameter, K , and $\delta = 0.6104$ and $\lambda = 75$) on non-linear torsional vibration of simply supported thin-walled beam of open section.

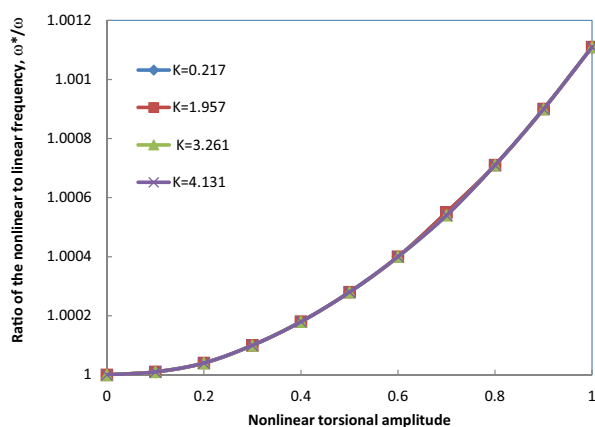


Fig. 34. The influence of Warping parameter (for different values of the Warping parameter, K , and $\delta = 0.6104$ and $\lambda = 100$) on non-linear torsional vibration of simply supported thin-walled beam of open section.

Ratio of the nonlinear to linear frequency, ω^*/ω for various values of λ and $\delta = 1.1095$ and $K = 3.106$ is computed and presented in Table 1. The effect of torsional amplitudes on frequency of

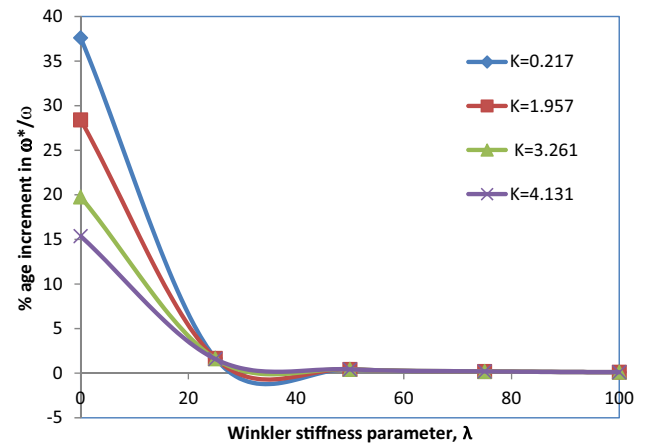


Fig. 35. The percentage variation of the ratio of nonlinear to linear frequency ratio (ω^*/ω) as β varies from 0.1 to 1, with Winkler stiffness parameter λ for various values of Warping parameter $K = 0.217, 1.957, 3.261$ and 4.131 .

non-linear torsional vibration for various values of the Winkler stiffness parameter, λ , and Warping parameter, $K = 3.106$ and dimensionless parameter $\delta = 1.1095$ is shown in Fig. 2. Similarly, the influence of torsional amplitudes on frequency of non-linear torsional vibration for various values of the Winkler stiffness parameter, λ , and Warping parameter, $K = 6.211, 9.317, 15.5288$ and 34.161 and dimensionless parameter $\delta = 1.1095$ is shown in Figs. 3–6. It is observed from the Figs. 2–6 that the non-linear behaviour is of the hard spring type. For lower values of $\lambda \leq 0.1$, the non-linear frequency increases drastically as β increases. Also, it is noticed that as the value of Winkler stiffness parameter λ increases, the influence of β decreases. For higher values of $\lambda \geq 30$, the effect of β in the present range 0 to 0.1 on non-linear frequency seems to be negligible. For a given value of λ , the non-linear frequency decreases as Warping parameter, K increases from 3.106 to 34.161. It is clear from the Figs. 2–6, there is a convergence for different values of λ as K increase from 3.106 to 34.161. The percentage deviation of the ratio of non-linear to linear frequency (ω^*/ω) as β changes from 0.1 to 1, with Warping parameter, K , for various values of Winkler stiffness parameter, $\lambda = 0.5, 10, 15, 20, 25, 30$ and 50 is shown in Fig. 7. It is noticed that the percentage variation convergence with Warping parameter K . Also, there is no considerable effect of β at higher values of Winkler stiffness parameter λ .

The effect of torsional amplitudes on frequency of non-linear torsional vibration of simply supported I-beam for different values of the Warping parameter, K , Winkler stiffness parameter, λ , and dimensionless parameter δ is determined and shown in Figs. 8–12. Ratio of the nonlinear to linear frequency, ω^*/ω for different values of K and $\delta = 1.1095$ and $\lambda = 0$ is computed and presented in Table 2. The effect of torsional amplitudes on frequency of non-linear torsional vibration for different values of the Warping parameter, K and Winkler stiffness parameter, $\lambda = 0$, and dimensionless parameter $\delta = 1.1095$ is shown in Fig. 8. Similarly, the influence of torsional amplitudes on frequency of non-linear torsional vibration for different values of the Warping parameter, K and Winkler stiffness parameter, λ and dimensionless parameter $\delta = 1.1095$ is shown in Figs. 9–12. It is observed from the Figs. 8–12, that the non-linear behaviour is of the hard spring type. For lower values of $K \leq 0.1$, the non-linear frequency increases drastically as β increases. Also, it is noticed that as the value of Warping parameter K increases, the influence of β decreases. For higher values of $K \geq 34.161$ the effect of β in the present range 0–0.1 on non-linear frequency seems to be negligible. For a given value of K , the

Table 1Ratio of the nonlinear to linear frequency, ω^*/ω for various values of λ and $\delta = 1.1095$ and $K = 3.106$.

β	$\lambda = 0$	$\lambda = 5$	$\lambda = 10$	$\lambda = 15$	$\lambda = 20$	$\lambda = 25$	$\lambda = 30$	$\lambda = 50$
0	1	1	1	1	1	1	1	1
0.1	1.00419	1.00276	1.00136	1.00074	1.00045	1.0003	1.00021	1.00008
0.2	1.01665	1.011	1.00545	1.00296	1.0018	1.0012	1.00085	1.00032
0.3	1.0371	1.02458	1.01222	1.00665	1.00406	1.0027	1.00192	1.00072
0.4	1.06506	1.0433	1.02162	1.01178	1.0072	1.0048	1.00341	1.00127
0.5	1.09996	1.06688	1.03358	1.01835	1.01123	1.00749	1.00532	1.00199
0.6	1.14117	1.09502	1.04801	1.02633	1.01613	1.01077	1.00766	1.00286
0.7	1.18804	1.12736	1.06482	1.03567	1.02189	1.01463	1.01041	1.0039
0.8	1.23991	1.16357	1.08389	1.04634	1.0285	1.01906	1.01357	1.00508
0.9	1.2962	1.20328	1.1051	1.05831	1.03593	1.02407	1.01714	1.00643
1	1.35634	1.24617	1.12834	1.07153	1.04419	1.02963	1.02112	1.00793

Table 2Ratio of the nonlinear to linear frequency, ω^*/ω for various values of K and $\delta = 1.1095$ and $\lambda = 0$.

β	$K = 3.106$	$K = 6.211$	$K = 9.317$	$K = 15.528$	$K = 34.161$	$K = 50$
0	1	1	1	1	1	1
0.1	1.0042	1.00169	1.00085	1.00033	1.00007	1.00003
0.2	1.0167	1.00676	1.00339	1.00131	1.00028	1.00013
0.3	1.0372	1.01515	1.00762	1.00294	1.00063	1.00029
0.4	1.06523	1.02678	1.01351	1.00523	1.00112	1.00052
0.5	1.10022	1.04154	1.02103	1.00815	1.00174	1.00082
0.6	1.14153	1.05931	1.03015	1.01172	1.00251	1.00118
0.7	1.18851	1.07993	1.04082	1.01592	1.00342	1.0016
0.8	1.2405	1.10324	1.053	1.02074	1.00446	1.00209
0.9	1.29691	1.12907	1.06664	1.02618	1.00564	1.00265
1	1.35718	1.15727	1.08168	1.03223	1.00696	1.00327

non-linear frequency decreases as Winkler stiffness, λ increases from 0 to 100. It is clear from the Figs. 8–12, there is a convergence for different values of K as λ increase from 0 to 100. The percentage variation of the ratio of nonlinear to linear frequency ratio (ω^*/ω) as β varies from 0.1 to 1, with Winkler stiffness parameter, $\lambda = 0, 25, 50, 75$ and 100 for Warping parameter, $K = 3.106$ is shown in Fig. 13. It is noticed that the percentage variation convergence with Winkler stiffness parameter, λ . Similarly, the percentage variation of the ratio of nonlinear to linear frequency ratio (ω^*/ω) as β varies from 0.1 to 1, with Winkler stiffness parameter λ for various values of Warping parameter $K = 6.211, 9.317, 15.528, 34.161$ and 50 is shown in Fig. 13. It is noticed that the percentage variation convergence with Winkler stiffness parameter λ . Also, there is no considerable effect of β at higher values of Warping parameter K .

Case (ii):

Dimensions of a 36 WF 230 standard steel I-beam considered are shown in Table 3. The plots (Figs. 14–17) are drawn between the ratio of ω^*/ω and the torsional amplitude β for various values of Winkler stiffness parameter, λ , Warping parameter K and, dimensionless parameter δ . Ratio of the nonlinear to linear frequency, ω^*/ω for various values of λ and $\delta = 0.992$ and $K = 0.177$ is computed and presented in Table 4. The influence of torsional amplitudes on frequency of non-linear torsional vibration for various values of the Winkler stiffness parameter, λ , and Warping parameter, $K = 0.177$ and dimensionless parameter $\delta = 0.992$ is shown in Fig. 14. Similarly, the influence of torsional amplitudes on frequency of non-linear torsional vibration for various values of the Winkler stiffness parameter, λ , and Warping parameter,

$K = 1.592, 2.654$ and 3.361 and dimensionless parameter $\delta = 0.992$ is shown in Figs. 15–17. It is observed from the Figs. 15–17 that the non-linear behaviour is of the hard spring type. For lower values of $\lambda \leq 0.1$, the non-linear frequency increases drastically as β increases. Also, it is noticed that as the value of Winkler stiffness parameter λ increases, the influence of β decreases. For higher values of $\lambda \geq 30$, the influence of β in the present range 0–0.1 on non-linear frequency seems to be negligible. For a given value of λ , the non-linear frequency decreases as Warping parameter, K increases from 0.177 to 3.361. It is clear from the Figs. 15–17, there is a convergence for different values of λ as K increase from 0.177 to 3.361. The percentage variation of the ratio of non-linear to linear frequency ratio (ω^*/ω) as β varies from 0.1 to 1, with Warping parameter K , for various values of Winkler stiffness parameter, $\lambda = 0, 5, 10, 15, 20, 25$ and 30 is shown in Fig. 18. It is noticed that the percentage variation convergence with Warping parameter K . Also, there is no considerable effect of β at higher values of Winkler stiffness parameter, λ .

The effect of torsional amplitudes on frequency of non-linear torsional vibration of simply supported I-beam for different values of the Warping parameter K , Winkler stiffness parameter λ , and dimensionless parameter δ is determined and shown in Figs. 19–23. Ratio of the nonlinear to linear frequency, ω^*/ω for various values of K and $\delta = 0.992$ and $\lambda = 0$ is computed and presented in Table 5. The effect of torsional amplitudes on frequency of non-linear torsional vibration for different values of the Warping parameter, K and Winkler stiffness parameter, $\lambda = 0$, and dimensionless parameter $\delta = 0.992$ is shown in Fig. 19. Similarly, the influence of torsional amplitudes on frequency of non-linear

Table 3

Dimensions a 36 WF 230 standard steel I-beam.

Designation	Depth	Width	Thickness Web	Thickness Flange	Sectional Area	Weight
W 36 × 230	in 35.9	in 16.47	in 0.76	in 1.26	In**2 67.6	lb/ft 230

Table 4Ratio of the nonlinear to linear frequency, ω^*/ω for different values of λ and $\delta = 0.991$ and $K = 0.177$.

β	$\lambda = 0$	$\lambda = 5$	$\lambda = 10$	$\lambda = 15$	$\lambda = 20$	$\lambda = 25$	$\lambda = 30$
0	1	1	1	1	1	1	1
0.1	1.00739	1.00366	1.00146	1.00073	1.00043	1.00028	1.0002
0.2	1.02924	1.01457	1.00582	1.00291	1.00171	1.00112	1.00078
0.3	1.06466	1.03249	1.01304	1.00653	1.00384	1.00251	1.00177
0.4	1.11235	1.05707	1.02306	1.01157	1.00682	1.00446	1.00314
0.5	1.17082	1.08785	1.03581	1.01802	1.01063	1.00696	1.0049
0.6	1.23854	1.12433	1.05118	1.02585	1.01527	1.01001	1.00704
0.7	1.31408	1.16598	1.06906	1.03503	1.02073	1.0136	1.00957
0.8	1.39618	1.21225	1.08932	1.04552	1.027	1.01773	1.01249
0.9	1.48373	1.26265	1.11184	1.05728	1.03405	1.02238	1.01578
1	1.57585	1.31669	1.13648	1.07027	1.04188	1.02756	1.01944

Table 5Ratio of the nonlinear to linear frequency, ω^*/ω for various values of K and $\delta = 0.992$ and $\lambda = 0$.

β	$K = 0.177$	$K = 1.592$	$K = 2.654$	$K = 3.361$
0	1	1	1	1
0.1	1.00739	1.0059	1.00433	1.00346
0.2	1.02924	1.02341	1.01722	1.01379
0.3	1.06466	1.05194	1.03835	1.03076
0.4	1.11235	1.09063	1.06723	1.05407
0.5	1.17082	1.13844	1.10325	1.0833
0.6	1.23854	1.19428	1.14573	1.11799
0.7	1.31408	1.25708	1.19399	1.15764
0.8	1.39618	1.32584	1.24736	1.20177
0.9	1.48373	1.3997	1.30521	1.2499
1	1.57585	1.47789	1.36697	1.30159

torsional vibration for different values of the Warping parameter, K and Winkler stiffness parameter, λ and dimensionless parameter $\delta = 0.992$ is shown in Figs. 19–23. It is observed from the Figs. 19–23, that the non-linear behaviour is of the hard spring type. For lower values of $K \leq 0.177$, the non-linear frequency increases drastically as β increases. Also, it is noticed that as the value of Warping parameter K increases, the influence of β decreases. For higher values of $K \geq 3.361$ the influence of β in the present range 0 to 0.1 on non-linear frequency seems to be decreases and the influence of β becomes negligible as the value of K increases further. For a given value of K , the non-linear frequency decreases as Winkler stiffness, λ increases from 0 to 100. It is clear from the Figs. 20–23, there is a convergence for different values of K as λ increase from 25 to 100. The influence of torsional amplitude β on non-linear frequency is same irrespective of Warping parameter K . Also, the non-linear frequency reduces slightly with increase in Winkler parameter λ . The percentage variation of the ratio of nonlinear to linear frequency ratio (ω^*/ω) as β varies from 0.1 to 1, with Winkler stiffness parameter, λ for various values of Warping parameter, $K = 0.177, 1.592, 2.654$ and 3.361 is shown in Fig. 24. It is noticed that the percentage variation convergence with Winkler stiffness parameter λ . Also, there is no considerable effect of β at higher values of Warping parameter K .

Case (iii):

Dimensions of a 24 WF 130 standard steel I-beam considered are shown in Table 6. The plots (Figs. 25–28) are drawn between the ratio of ω^*/ω and the torsional amplitude β for various values of Winkler stiffness parameter, λ , Warping parameter K and

dimensionless parameter δ . Ratio of the nonlinear to linear frequency, ω^*/ω for various values of λ and $\delta = 0.6104$ and $K = 0.217$ is computed and presented in Table 7. The influence of torsional amplitudes on frequency of non-linear torsional vibration for different values of the Winkler stiffness parameter, λ , and Warping parameter, $K = 0.217$ and dimensionless parameter $\delta = 0.6104$ is shown in Fig. 25. Similarly, the influence of torsional amplitudes on frequency of non-linear torsional vibration for various values of the Winkler stiffness parameter, λ , and Warping parameter, $K = 1.957, 3.261$ and 4.131 and dimensionless parameter $\delta = 0.6104$ is shown in Figs. 26–28. It is observed from the Figs. 25–28 that the non-linear behaviour is of the hard spring type. For lower values of $\lambda \leq 0.1$, the non-linear frequency increases drastically as β increases. Also, it is noticed that as the value of Winkler stiffness parameter λ increases, the influence of β decreases. For higher values of $\lambda \geq 30$, the influence of β in the present range 0 to 0.1 on non-linear frequency seems to be negligible. For a given value of λ , the non-linear frequency decreases as Warping parameter, K increases from 0.217 to 4.131. It is clear from the Figs. 25–28, there is a convergence for different values of λ as K increase from 0.217 to 4.131. The percentage variation of the ratio of non-linear to linear frequency ratio (ω^*/ω) as β varies from 0.1 to 1, with Warping parameter, K , for various values of Winkler stiffness parameter, $\lambda = 0, 5, 10, 15, 20, 25$ and 30 is shown in Fig. 29. It is noticed that the percentage variation convergence with Warping parameter K . Also, there is no considerable effect of β at higher values of Winkler stiffness parameter λ .

The effect of torsional amplitudes on frequency of non-linear torsional vibration of simply supported I-beam for different values of the Warping parameter K , Winkler stiffness parameter, λ , and dimensionless parameter δ is determined and shown in Figs. 30–34. Ratio of the nonlinear to linear frequency, ω^*/ω for various values of K and $\delta = 0.6104$ and $\lambda = 0$ is computed and presented in Table 8. The effect of torsional amplitudes on frequency of non-linear torsional vibration for different values of the Warping parameter, K and Winkler stiffness parameter, $\lambda = 0$, and dimensionless parameter $\delta = 0.6104$ is shown in Fig. 30. It is observed from the Fig. 30, that the non-linear behaviour is of the hard spring type. For lower values of $K \leq 0.21$, the non-linear frequency increases drastically as β increases. Similarly, the influence of torsional amplitudes on frequency of non-linear torsional vibration for different values of the Warping parameter, K and Winkler

Table 6

Dimensions a 24 WF130 standard steel I-beam.

Designation	Depth	Width	Thickness Web	Thickness Flange	Sectional Area	Weight	Moment of Inertia - Ix	Moment of Inertia - Iy	Section of Modulus - Wx	Section of Modulus - Wy
W 24 × 131	in	in	in	in	in**2	lb/ft	in**4	in**4	in**3	in**3
	24.48	12.855	0.605	0.960	38.5	131	4020	340	329	53.0

Table 7Ratio of the nonlinear to linear frequency, ω^*/ω for various values of λ , $\delta = 0.6104$ and $K = 0.217$.

β	$\lambda = 0$	$\lambda = 5$	$\lambda = 10$	$\lambda = 15$	$\lambda = 20$	$\lambda = 25$	$\lambda = 30$
0	1	1	1	1	1	1	1
0.1	1.00455	1.00225	1.0009	1.00045	1.00026	1.00017	1.00012
0.2	1.01806	1.00898	1.00358	1.00179	1.00105	1.00069	1.00048
0.3	1.0402	1.0201	1.00804	1.00402	1.00236	1.00155	1.00109
0.4	1.07042	1.03546	1.01425	1.00714	1.0042	1.00275	1.00193
0.5	1.10807	1.05488	1.02218	1.01113	1.00655	1.00429	1.00302
0.6	1.15241	1.07814	1.03178	1.01598	1.00943	1.00617	1.00434
0.7	1.20271	1.10501	1.04302	1.02169	1.01281	1.00839	1.0059
0.8	1.25825	1.13521	1.05584	1.02824	1.0167	1.01094	1.0077
0.9	1.31838	1.1685	1.07018	1.03562	1.02108	1.01383	1.00974
1	1.38248	1.20462	1.08599	1.04379	1.02597	1.01705	1.01201

Table 8Ratio of the nonlinear to linear frequency, ω^*/ω for various values of K and $\delta = 0.6104$ and $\lambda = 0$.

β	$K = 0.217$	$K = 1.957$	$K = 3.261$	$K = 4.131$
0	1	1	1	1
0.1	1.00455	1.00329	1.0022	1.00168
0.2	1.01806	1.01311	1.00878	1.00669
0.3	1.0402	1.02926	1.01965	1.01499
0.4	1.07042	1.05146	1.03467	1.0265
0.5	1.10807	1.07933	1.05367	1.04111
0.6	1.15241	1.11244	1.07644	1.0587
0.7	1.20271	1.15034	1.10275	1.07911
0.8	1.25825	1.19259	1.13234	1.10219
0.9	1.31838	1.23872	1.16496	1.12778
1	1.38248	1.28832	1.20038	1.15571

stiffness parameter, λ and dimensionless parameter $\delta = 0.6104$ is shown in Figs. 31–34. It is noticed that as the value of Warping parameter K increases, the influence of β decreases. For a given value of K , the non-linear frequency decreases as Winkler stiffness, λ increases from 0 to 100. It is clear from the Figs. 31–34, there is a convergence for different values of K as λ increase from 25 to 100. The influence of torsional amplitude β on non-linear frequency is same irrespective of warping parameter K . Also, the non-linear frequency reduces slightly with increase in Winkler parameter λ . The percentage variation of the ratio of nonlinear to linear frequency ratio (ω^*/ω) as β varies from 0.1 to 1, with Winkler stiffness parameter, λ for various values of Warping parameter, $K = 0.217, 1.957, 3.261$ and 4.131 is shown in Fig. 35. It is noticed that the percentage variation convergence with Winkler stiffness parameter, λ . Also, there is no considerable effect of β at higher values of Warping parameter K .

Table 9

Comparison of Case (i) standard I-beam, Case (ii) 24WF130 and Case (iii) 36WF230.

	Non-linear sectional property, δ	Warping parameter, K	Non-linear to linear frequency ratio, ω^*/ω	
			Winkler stiffness parameter, $\lambda = 5$ & non-linear torsional amplitude, $\beta = 0.1$	Winkler stiffness parameter, $\lambda = 30$ & non-linear torsional amplitude $\beta = 0.9$
Case(i)	1.1095	3.106	1.00276	1.01714
		6.211	1.0014	1.01595
		9.317	1.00077	1.0143
		15.528	1.00031	1.01073
Case(ii)	0.6104	34.101	1.00007	1.0043
		0.217	1.00225	1.00974
		1.957	1.0019	1.00964
		3.261	1.00147	1.00947
Case(iii)	0.992	4.131	1.00122	1.00931
		0.177	1.00366	1.01578
		1.592	1.00326	1.01567
		2.654	1.00271	1.01549
		3.361	1.00235	1.01532

4. Conclusions

The effect of torsional amplitudes on frequency of non-linear torsional vibration for different values of the Winkler stiffness parameter, λ , Warping parameter, K and dimensionless parameter δ has been investigated. It can be easily observed from the comparison Table 9, that the non-linear behaviour is of the hard spring type and that for lower values of Winkler stiffness parameter $\lambda \leq 0.1$, the non-linear to linear frequency ratio increases drastically as the torsional amplitude β increases. Also, it can be noticed that as the value of Winkler stiffness parameter λ increases, the influence of torsional amplitude β decreases on the nonlinear to linear frequency ratio. For higher values of λ , that is $\lambda \geq 30$, the effect of torsional amplitude β in the present range 0 to 0.1 on non-linear to linear frequency ratio seems to be negligible. For lower values of $K \leq 0.1$, the non-linear to linear frequency ratio increases drastically as torsional amplitude β increases. Also, it is noticed that as the value of Warping parameter K increases, the influence of torsional amplitude β on nonlinear to linear frequency ratio decreases. For higher values of $K \geq 34.161$ the effect of torsional amplitude β in the present range 0 to 0.1 on non-linear frequency ratio can be seen to become almost negligible. For a given value of λ , the non-linear frequency decreases as Warping parameter K increases from 3.106 to 34.161. For a given value of K , the non-linear frequency to linear frequency ratio decreases as Winkler stiffness, λ increases from 0 to 100. For constant values of parameters λ , K and β , the effect of decrease in the value of δ is to decrease the nonlinear to linear frequency ratio considerably.

Appendix A. Supplementary data

Supplementary data to this article can be found online at <https://doi.org/10.1016/j.apacoust.2019.05.012>.

References

- [1] Singh G, Sharma AK, Rao GV. Large-amplitude free vibrations of beams—a discussion of various formulations and assumptions. *J Sound Vib* 1990;142(1):77–85.
- [2] Vlasov VZ. *Thin-Walled Elastic Beams*; QTS61-11400. Washington, D. C.: National Science Foundations; 1961.
- [3] Nayfeh AH, Mook DT. *Nonlinear oscillations*. New York: John Wiley and Sons; 1979.
- [4] Gere JM. Torsional vibrations of beams of thin-walled open section. *J Appl Mech Trans ASME* 1954;21(4):381–7.
- [5] Aggarwal HR, Cranch ET. A theory of torsional and coupled bending torsional waves in thin-walled open section beams. *J Appl Mech Trans ASME* 1967;34(2):337–43.
- [6] Kameswara Rao C, Apparao KV, Sarma PK. Effect of longitudinal inertia and of shear deformation on the torsional frequency and normal modes of thin-walled open section beams. *J Aeronaut Soc India* 1974.
- [7] Tso WK. *Dynamics of thin-walled beams of open section*. Dynamics laboratory report, Pasadena, California, June 1964.
- [8] Cullimore MSG. The Shortening effect: a nonlinear feature of pure torsion. *Res Eng Struct Suppl London* 1949;153–63.
- [9] Gregorv M. A nonlinear bending effect when certain unsymmetrical sections are subjected to pure torque. *Aust J Appl Sci* 1960;11:33–48.
- [10] Gregory M. The bending and shortening effect of pure torque. *Aust J Appl Sci* 1960;11:209–16.
- [11] Tso WK. Coupled vibrations of thin-walled elastic bars. *J Eng Mech Div* 1965;91:33–52.
- [12] Ghobarah AA, Tso WK. A nonlinear thin-walled beam theory. *Int J Mech Sci* 1971;13(12):1025–38.
- [13] Tso WK, Ghobarah AA. Nonlinear non-uniform torsion of thin-walled beams. *Int J Mech Sci* 1971;13(12):1039–47.
- [14] Kameswara Rao C. Nonlinear torsional vibrations of thin-walled beams of open section. *J Appl Mech Trans ASME* 1975;42:240–2.
- [15] Rozmarynowski B, Szymczak C. Non-linear free torsional vibrations of thin-walled beams with bisymmetric cross-section. *J Sound Vib* 1984;97(1):145–52.
- [16] Sarma BS, Varadan TK. Ritz finite element approach to nonlinear vibrations of beams. *Int J Numer Meth Eng* 1984;20(2):353–67.
- [17] Lewandowski R. Application of the Ritz method to the analysis of non-linear free vibrations of beams. *J Sound Vib* 1987;114(1):91–101.
- [18] Wekezer JW. Nonlinear torsion of thin-walled bars of variable, open cross-sections. *Int J Mech Sci* 1985;27(10):631–41.
- [19] Attard MM. Nonlinear theory of non-uniform torsion of thin-walled open beams. *Thin-walled Struct* 1986;4(2):101–34.
- [20] Woinowsky-Krieger S. The effect of an axial force on the vibration of hinged bars. *Trans ASME* 1950;72:35–6.
- [21] Singh G, Rao GV, Iyengar NGR. Re-investigation of large-amplitude free vibrations of beams using finite elements. *J Sound Vib* 1990;143:351–5.
- [22] Pillai SRR, Nageswara Rao B. On nonlinear free vibrations of simply supported uniform beams. *J Sound Vib* 1992;159(3):527–31.
- [23] Mohri Foudil, Damil Noureddine, Ferry Michel Potier. Large torsion finite element model for thin-walled beams. *Comput Struct* 2008;86(7–8):671–83.
- [24] Gupta RK, Jagadish Babu G, Ranga Janardhan G, Venkateswara Rao G. Relatively simple finite element formulation for the large amplitude free vibrations of uniform beams. *Finite Elem Anal Des* 2009;45(10):624–31.
- [25] Emam Samir A. Approximate analytical solutions for the nonlinear free vibrations of composite beams in buckling. *Compos Struct* 2013;100:186–94.
- [26] Meirowitch. *Analytical Methods in Vibrations*. The Macmillan Company, New York 1967; P. 235.
- [27] Volterra E, Zachmanaglou EC. *Dynamics of vibrations*. Ohio: Charles E. Merrill Books Inc.; 1965. p. 496.
- [28] Axelsson O, Barker BR. *Finite element solution of boundary value problems*. Philadelphia: SIAM; 2001.
- [29] ASTM A992/A992M-06a, *Standard Specification for Structural Steel Shapes*, ASTM International, West Conshohocken, PA, 2006.

Spectral Dynamic Analysis of Torsional Vibrations of Thin-Walled Open Section Beams Restrained Against Warping at One End and Transversely Restrained at the Other End

Chellapilla Kameswara Rao¹, Lokavarapu Bhaskara Rao²

¹ Department of Mechanical Engineering, Nalla Narsimha Reddy Engineering College, Korremula 'X' Road, Chowdariguda (V), Ranga Reddy (Dist) – Hyderabad - 500088

² School of Mechanical and Building Sciences, VIT University, Chennai Campus, Vandalur-Kelambakkam Road, Chennai-600127, India

Abstract: The present paper deals with spectral dynamic analysis of free torsional vibration of doubly symmetric thin-walled beams of open section. Spectral frequency equation is derived in this paper for the case of rotationally restrained doubly-symmetric thin-walled beam with one end rotationally restrained and transversely restrained at the other end. The resulting transcendental frequency equation with appropriate boundary conditions is derived and is solved for varying values of warping parameter and the rotational and transverse restraint parameter. The influence of rotational restraint parameter, transverse restraint parameter and warping parameter on the free torsional vibration frequencies is investigated in detail. A MATLAB computer program is developed to solve the spectral frequency equation derived in this paper. Numerical results for natural frequencies for various values of rotational and transverse restraint parameters for various values of warping parameter are obtained and presented in both tabular as well as graphical form showing the influence of these parameters on the first fundamental torsional frequency parameter.

Keywords: Thin-walled beam; open section; torsion; spectral dynamic analysis; restrained cantilever

1. Introduction

It is very well known that in practical situations, the boundary conditions of structural members will be quite complex and can be simulated by using translational springs and rotational springs with appropriate combinations of the same. There exist a good number of research efforts in this direction and many researchers have addressed this problem of vibrations of generally restrained beams with various combinations of boundary conditions^[1-25]. The combined effect of rotary inertia, shear deformation and root flexibility has been investigated experimentally by Beglinger *et al.*^[12]. A considerable amount of theoretical work has been done in the field of vibration dealing with the computation of natural frequencies and mode shapes of cantilever beams with flexible roots^[6, 9, 17, 19, 20, 22]. Kameswara Rao^[23] presented a closed form equation for computing fundamental frequency of cantilever blade taking into account the resilience of the clamped end. Experimental verification of the results for this case was also carried out by Abbas and Irretier^[24]. Kameswara Rao and Mirza^[25] derived the transcendental frequency equation and mode shape expressions for the case of generally restrained Euler-Bernoulli beams and presented extensive numerical results for various values of linear and rotational restraint parameters.

While there are a number of publications on flexural vibrations of elastically restrained cantilever beams, the literature on torsional vibrations of doubly symmetric thin-walled beams of open section is rather rare. Free torsional vibrations and stability of doubly-symmetric long thin-walled beams of open section were investigated by Kameswara Rao and Appala Satyam^[26] and Christiano and Salmela^[27]. Numerical values of exact torsional natural frequencies of

Copyright © 2018 Chellapilla Kameswara Rao *et al.*

doi: 10.18063/ijmp.v1i1.746

This is an open-access article distributed under the terms of the Creative Commons Attribution Unported License

(<http://creativecommons.org/licenses/by-nc/4.0/>), which permits unrestricted use, distribution, and reproduction in any medium, provided the original work is properly cited.

beams with circular cross-section, where nonuniform warping does not arise, were presented by Gorman^[28] and Belvins^[29] for different classical boundary conditions. Torsional vibration frequencies for beams of open thin-walled sections, subjected to several combinations of classical boundary conditions, taking into account warping effects were first derived by Gere^[30]. Including elastic torsional and warping restraints, Carr^[31] and Christino and Salmela^[27] presented numerical results using approximate methods for the calculation of natural frequencies. For the case of torsional frequencies of circular shafts and piping with elastically restrained edges, Kameswara Rao^[32] derived exact frequency equation and presented corresponding numerical results for a wide range of non-dimensional parameters.

Rafezy and Howson^[33] developed an exact dynamic stiffness matrix approach for the three-dimensional, bi-material beam of doubly asymmetric cross-section. The beam comprises a thin-walled outer layer that encloses and works compositely with its shear sensitive core material. The theory has been applied successfully to the frequency analysis of various single and continuous beam structures with and without an infilled core. Bozdogan and Ozturk^[34] proposed a method for a free vibration analysis of a thin-walled beam of doubly asymmetric cross section filled with shear sensitive material. First, a dynamic transfer matrix method was obtained for planar shear flexure and torsional motion. Secondly, uncoupled angular frequencies were obtained by using dynamic element transfer matrices and boundary conditions. Finally, coupled frequencies were obtained by the well-known two-dimensional approaches.

It can be seen from the very recent review presented by Sapountzakis^[35] that the problem of free torsional vibration analysis of doubly-symmetric thin-walled I-beams or Z-beams subjected to partial warping restraint is not being addressed till now in the available literature. Burlon *et al*^[36] proposes an exact approach to coupled bending and torsional free vibration analysis of beams with monosymmetric cross section, featuring an arbitrary number of in-span elastic supports and attached masses. The proposed method relies on the elementary coupled bending-torsion theory and makes use of the theory of generalized functions to handle the discontinuities of the response variables. Burlon *et al*^[37] investigated the stochastic response of a coupled bending–torsion beam, carrying an arbitrary number of supports/masses. Using the theory of generalized functions in conjunction with the Euler–St. Venant coupled bending–torsion beam theory, exact analytical solutions under stationary inputs are obtained based on frequency response functions derived by two different closed-form expressions.

In view of the same, an attempt has been made in this paper to present a spectral dynamic analysis of free torsional vibration of doubly-symmetric thin-walled beams of open section with one end partially restrained against warping at the left end and the other end transversely restrained including the effects of warping parameter. Spectral frequency equation is derived for this case and the resulting transcendental frequency equation is solved for varying values of warping parameter and the partial restraint parameters. The influence of rotational and transverse restraint parameter along with warping parameter on the free torsional vibration frequencies is investigated in detail by utilising a Matlab computer program developed especially to solve the spectral frequency equation derived in this paper. Numerical results for natural frequencies for various values of partial rotational and transverse restraint parameters are obtained and presented in both tabular as well as graphical form for use in design, showing their parametric influence clearly.

2. Formulation and analysis

Consider a long doubly-symmetric thin-walled beam of open cross section of length L and the beam as undergoing free torsional vibrations. The corresponding differential equation of motion can be written as:

$$EC_W \frac{\partial^4 \varphi}{\partial z^4} - GC_S \frac{\partial^2 \varphi}{\partial z^2} + \rho I_P \frac{\partial^2 \varphi}{\partial t^2} = 0 \quad (1)$$

where,

E = young's modulus, C_W =warping constant, G =shear modulus, C_S = torsion constant, ρ =mass density of the material of the beam, I_P =polar moment of inertia, φ = angle of twist, z = distance along the length of the beam.

For free torsional vibrations, the angle of twist, can be expressed in the form.

$$\varphi(z,t) = x(z)e^{i\omega t}, \quad (2a)$$

$$x(z) = Ce^{mz} \quad (2b)$$

In which $x(z)$ is the modal shape function corresponding to each beam torsional natural frequency ω .

The expression for $x(z)$ which satisfies Eqn. (1) can be written as:

$$x(z) = Ae^{+\alpha z} + Be^{-\alpha z} + Ce^{+i\beta z} + De^{-i\beta z} \quad (3)$$

in which,

$$\beta L, \alpha L = \sqrt{\frac{\mp K^2 + \sqrt{K^4 + 4\lambda^2}}{2}}, \quad (4)$$

where,

$$K^2 = \left(\frac{GC_S L^2}{EC_W} \right); \quad \text{Non- dimensional warping parameter}$$

$$\lambda^2 = \left(\frac{\rho I_P \omega^2 L^4}{EC_W} \right); \quad \text{Non- dimensional frequency parameter}$$

From Eqn. (4), we have the following relation between αL and βL

$$(\alpha L)^2 = (\beta L)^2 + K^2 \quad (5)$$

Knowing α and β , the frequency parameter λ can be evaluated using the following equation:

$$\lambda^2 = (\alpha L)(\beta L) \quad (6)$$

The four arbitrary constants A, B, C and D in Eqn. (3) can be determined from the boundary conditions of the beam. For any single-span beam, there will be two boundary conditions at each end and these four conditions then determine the corresponding frequency and mode shape expressions.

3. Derivation of spectral frequency equation

Consider a thin-walled doubly symmetric I-beam with one end rotationally restrained and the other end transversely restrained as shown in figure 1, undergoing free torsional vibrations. In order to derive the spectral frequency equation for this case, let us first introduce the related nomenclature.

The variation of angle of twist ϕ with respect to z is denoted by $\theta(z)$. The flange bending moment and the total twisting moment are given by $M(z)$ and $T(z)$. Considering clockwise rotations and moments to be positive, we have

$$\theta(z) = \frac{d\phi}{dz}; \quad hM(z) = -EC_W \frac{d^2\theta}{dz^2} \quad (7)$$

$$T(z) = -EC_W \frac{d^3\theta}{dz^3} + GC_S \frac{d\theta}{dz} \quad (8)$$

where $EC_W = \frac{I_f h^2}{2}$. I_f being the flange moment of inertia and h is the distance between the center lines of the flanges of a thin-walled I-beam.

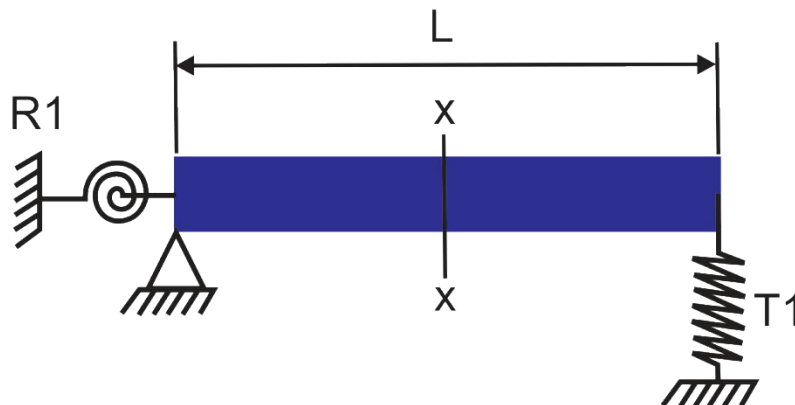


Fig.1, (a). A thin-walled open section beam rotationally restrained at one end and transversely restrained at the other end

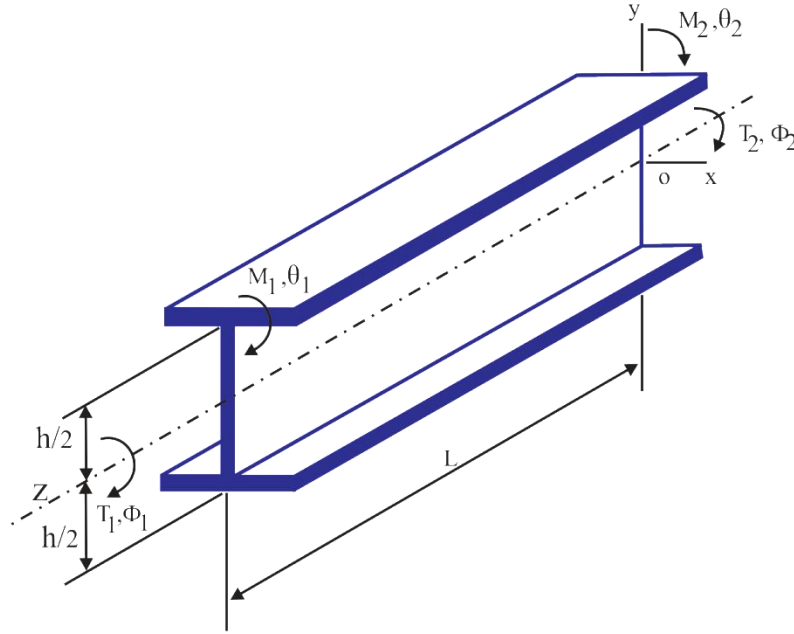


Fig. 1, (b). Cross-section of the beam at x-x.

Taking S as the stiffness of the rotational spring and $R = (SL/EC_w)$ as the non-dimensional rotational spring stiffness parameter and $Z=(z/L)$ as the non-dimensional length of the beam, the boundary conditions can be easily identified as follows:

$$\text{At } Z=0, \quad \varphi = 0, \quad \frac{d^2\varphi}{dz^2} = R \frac{d\varphi}{dz} \quad (9)$$

$$\text{And at } Z=L, \quad \frac{d^3\varphi}{dz^3} - K^2 \frac{d\varphi}{dz} = T\varphi, \quad \frac{d^2\varphi}{dz^2} = 0 \quad (10)$$

The spectral frequency equation obtained is as given below:

$$RS_1 + F_1S_2 + TF_2Q_{1m2} + RTF_3S_3 = 0 \quad (11)$$

where

$$F_1 = \frac{(\alpha^2 + \beta^2)}{(\alpha^2\beta^2)}; \quad F_2 = \frac{(\alpha^4 + 2\alpha^2\beta^2 + \beta^4)}{(\alpha^3\beta^3)}; \quad F_3 = \frac{(\alpha^2 + \beta^2)}{(\alpha^3\beta^3)} \quad (12)$$

$$Q_1 = \frac{1 + e^{2L(\alpha + i\beta)}}{A\alpha L(\alpha + i\beta)}; \quad Q_2 = \frac{1 + e^{2L(\alpha - i\beta)}}{A\alpha L(\alpha - i\beta)} \quad (13)$$

$$Q_{1m2} = (Q_1 - Q_2) \quad (14)$$

$$S_1 = (F_1Q_{1p2} + F_2Q_{1m2} + 2); \quad S_2 = (\alpha^3Q_{3p4} - \beta^3Q_{3m4}); \quad S_3 = (\alpha Q_{3m4} - \beta Q_{3p4}) \quad (15)$$

Four degenerate cases spectral frequency equations can be easily obtained from Equation (11) as follows:

Case (i). For $R = 0$ and $T = \infty$, we get the case of simply-supported beam for which we obtain

$$Q_{1m2} = 0 \quad (16)$$

Case (ii). For $R = \infty$ and $T = 0$, we get the case of cantilever beam with restrained warping for which we obtain

$$S_1 = 0 \quad (17)$$

Case (iii). For $R = 0$ and $T = 0$, we get the case of cantilever beam with unrestrained warping for which we obtain

$$S_2 = 0 \quad (18)$$

Case (iv). For $R = \infty$ and $T = \infty$, we get the clamped-simply supported beam case for which we obtain

$$S_3 = 0 \quad (19)$$

4. Results and discussions

Numerical results for the first three natural torsional frequencies of vibration of thin-walled beams of open section are obtained by solving the transcendental spectral frequency Eq. (11) using trial-and-error method. The Muller's iteration technique based on bisection method is coded in Matlab and the same is utilised in generating the numerical data and the same is presented in several tables and graphs for use in design.

It should be mentioned here that even though several studies are made by researchers in the area of torsional

frequencies of thin-walled beams of open section, numerical values are not made available for use in design. As is known, graphical results can help us only in understanding the trend of variation of natural frequencies due to the increase in warping parameter K and the partial warping restraint parameters R and T , but will not provide the frequencies to the four digit accuracy which we require for using the same for design.

For the case of thin-walled beam with partially restrained warping (R), R varying from 0 to 10^{+17} at the left end and with partial linear transverse restraint (T), T varying from 0 to 10^{+17} at the other, the fundamental mode torsional frequencies for a fixed value of warping parameter $K=0.0$ are presented in Table 1. The fundamental mode torsional frequencies are determined for a wide range of R and T but only a few are presented in Table.1. **Figure 2** represents the variation of frequency parameter with warping parameter ($K = 0$ to 10) for $R = 0$ and $R = 10^{+17}$. Whereas, **Figure 3** is drawn to clearly show the variation of the fundamental first mode frequencies with varying values of K and R . It is observed that for a given value of R , the frequency parameter increases with increase in warping parameter value K .

From figures 2 and 3, we can easily see that the increase in warping parameter K is to increase the fundamental mode torsional frequencies significantly. For values of K greater than 10, we can easily notice that the frequencies of cantilever with unrestrained as well as completely restrained thin-walled beams almost tend to converge to a constant value as K approaches higher values such as 80. For a constant value of warping parameter K , the increase in values of partial warping parameter R from 0 to infinity (10^{+18}) results in consistent increase in the values of fundamental mode frequencies as the cantilever end becomes stiffer and stiffer.

From the definition of non-dimensional warping parameter K (4b), we can understand that the torsional frequency increases for increasing values of torsion constant C_S or decreasing values of warping constant C_W . Effect of K also can be seen to be more predominant compared to the effect of partial warping restraint K . This can be seen from **Figure 3** whereas K is increasing from 0 to 80, the two curves related to cantilever beam fully restrained and the one with unrestrained warping are almost converging to the same value and hence we can conclude that the boundary condition has insignificant effect on the natural torsional frequencies of thin-walled doubly symmetric beams for very high values of warping parameter K .

Fundamental mode torsional frequencies of thin-walled beams for wide range of values of warping parameter K from 1 to 80 and the partial warping restraint R from 0 to 10^{+18} are calculated. These results are also plotted in Figures 4 to 5 showing clearly the variation of fundamental natural torsional frequency with varying values of warping parameter K and the partial warping restraint R .

The percentage variation of frequency parameter with increasing values of, as K varies from 0 to 80 is presented in Figure. 6. The percentage variation of frequency parameter changes from 96.29025 to 83.37943 when the value of K varies from 0 to 80. Similarly, the percentage variation of frequency parameter with K as R varies from 0.01 to 10^{+18} is presented in Figure. 7. The percentage variation of frequency parameter changes from 77.81 to 0.62 when the value of R varies from 0.01 to 10^{+18} .

The values of second and third mode torsional natural frequencies of thin-walled beams of open section for various values of warping parameter K from 0.01 to 200 and partial warping restraint parameter R from 0.01 to 1000 in Tables 2 and 3 respectively. These numerical values are plotted in Figures 8 and 9 for the second mode and Figures 10 and 11 for the third mode, showing clearly the influence of warping parameter K and partial warping restraint R on the non-dimensional natural frequency parameter λ .

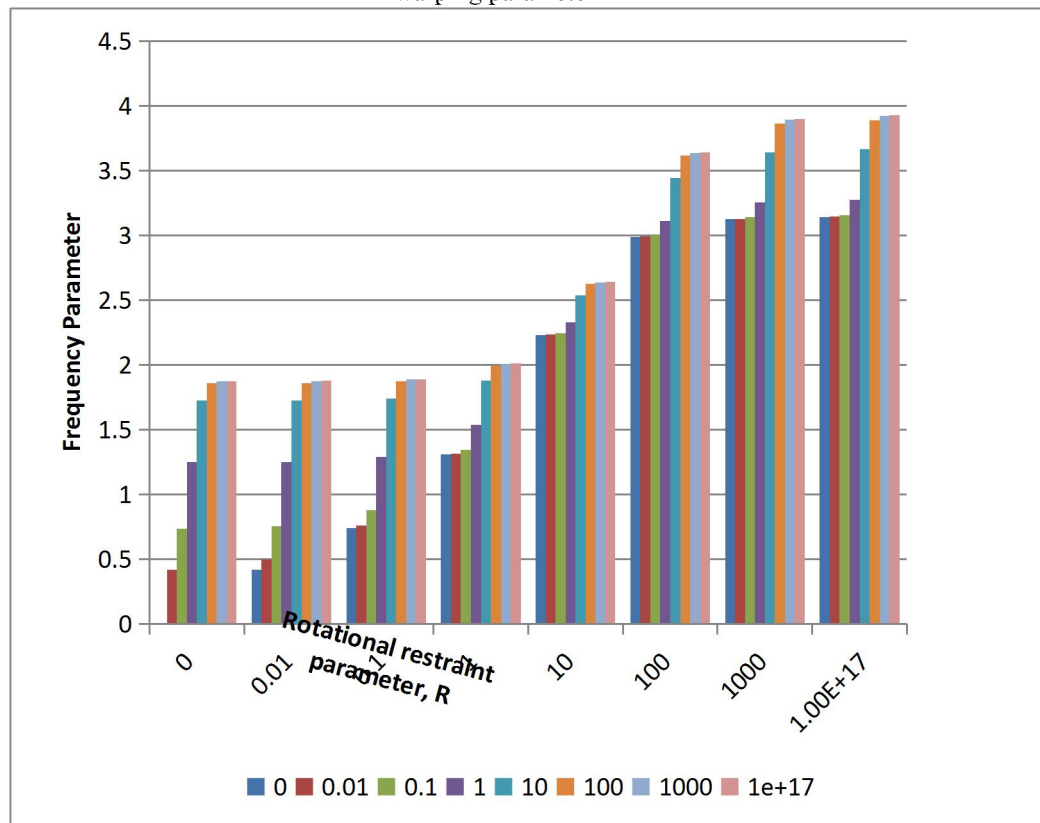
The authors sincerely hope that this detailed data presented in this paper will be quite useful in design of such systems and also to establish accuracy of frequencies obtained by using latest approximate methods such as Generalised Differential Quadrature Method (GDQM), Differential Transform Method (DTM), Adomian Decomposition Method (ADM) or any other method such as Finite Element Method.

Spectral dynamic analysis of free torsional vibration of doubly symmetric thin-walled beams of open section is carried out and detailed results of this study are presented in this paper suitable for use in design and also for checking approximate solutions obtained for their accuracy. For the case of a cantilever thin-walled beam of doubly symmetric open cross-section undergoing free

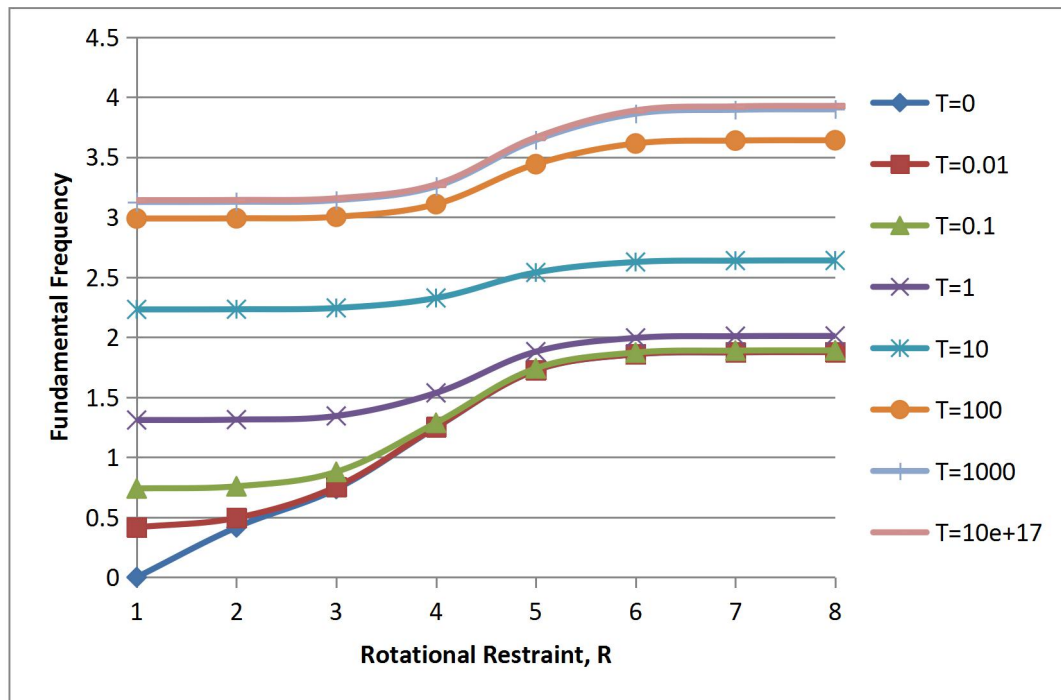
torsional vibrations and subjected to partial warping restraint, the spectral frequency equation is derived in this paper. The resulting transcendental frequency equation for the case of cantilever boundary conditions is solved for thin-walled beams of open cross section for varying values of warping parameter and the partial warping restraint parameter. The influence of partial warping restraint parameter R and the warping parameter K on the free torsional vibration frequencies is investigated in detail and significant amount of numerical frequency data is generated. Using a MATLAB computer program developed to solve the spectral frequency equation derived, numerical results for the first three modes of torsional natural frequencies for various values of rotational restraint parameter R and warping restraint parameter K are obtained and are presented in both tabular as well as graphical form showing their parametric influence clearly. In comparison with the partial warping restraint parameter R , the warping parameter K is found to have significant effect on the torsional natural frequencies not only of the fundamental mode but also of higher modes.

R	T = 0	T = 0.01	T = 0.1	T = 1	T = 10	T = 100	T = 1000	T = 10¹⁷
0	0	0.41616	0.73973	1.30981	2.23133	2.98864	3.12608	3.14159
0.01	0.41595	0.49481	0.75769	1.31339	2.23256	2.99011	3.12766	3.14318
0.1	0.73578	0.75406	0.87821	1.34368	2.24336	3.00301	3.14155	3.15718
1	1.24792	1.25200	1.28704	1.53581	2.32647	3.10846	3.25665	3.27329
10	1.72274	1.72455	1.74058	1.87929	2.53883	3.44122	3.64228	3.66464
100	1.85679	1.85833	1.87205	1.99395	2.62616	3.61335	3.86146	3.88919
1000	1.87323	1.87475	1.88824	2.00836	2.63761	3.63772	3.39401	3.92269
10 ¹⁷	1.87510	1.87662	1.89008	2.01000	2.63893	3.64054	3.89780	3.92660

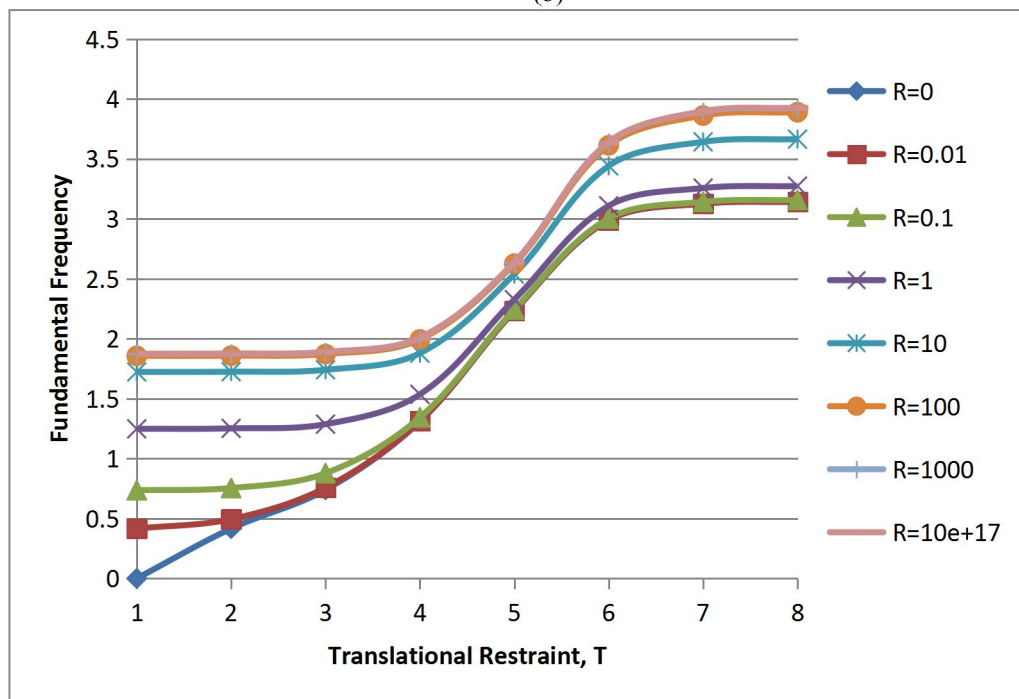
Table 1. First mode natural frequencies for various values of rotational and translational restraint parameters and for warping parameter $K = 0$



(a)



(b)



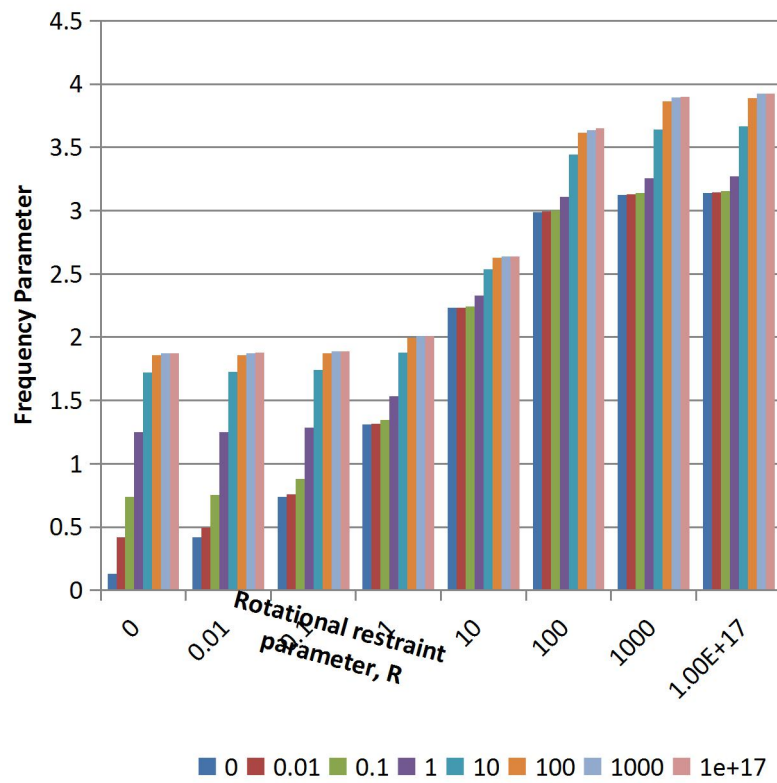
(c)

Fig. 2, (a), (b) and (c). Variation of frequency parameter with rotational and translational restraints (R & $T=0$ to 10^{17}) for a given warping parameter ($K=0$).

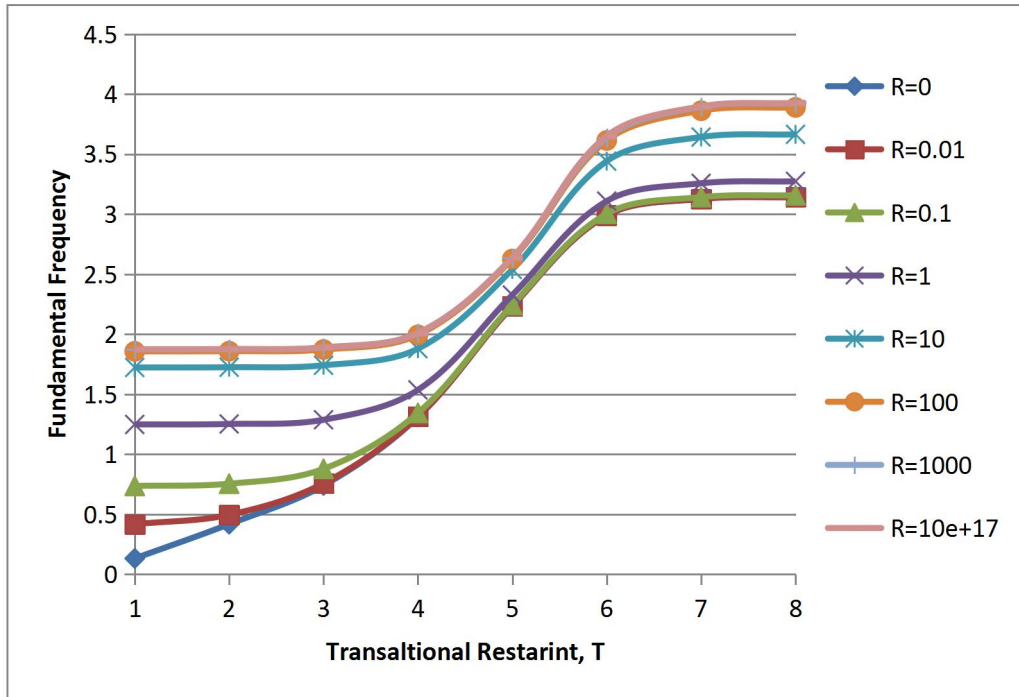
R	T = 0	T = 0.01	T = 0.1	T = 1	T = 10	T = 100	T = 1000	T = 10^{17}
0	0.1316	0.4172	0.7399	1.3098	2.2313	2.9886	3.1261	3.1416
0.01	0.417	0.4954	0.7579	1.3134	2.2326	2.9901	3.1277	3.1432
0.1	0.736	0.7542	0.8783	1.3437	2.2434	3.003	3.1416	3.1572
1	1.248	1.252	1.2871	1.5358	2.3265	3.1085	3.2567	3.2733

10	1.7228	1.7246	1.7406	1.8793	2.5388	3.4412	3.6423	3.6646
100	1.8568	1.8584	1.8721	1.994	2.6262	3.6134	3.8615	3.8892
1000	1.8733	1.8748	1.8883	2.0084	2.6376	3.6377	3.894	3.9227
10^{17}	1.8751	1.8766	1.8901	2.01	2.6389	3.6505	3.8978	3.9266

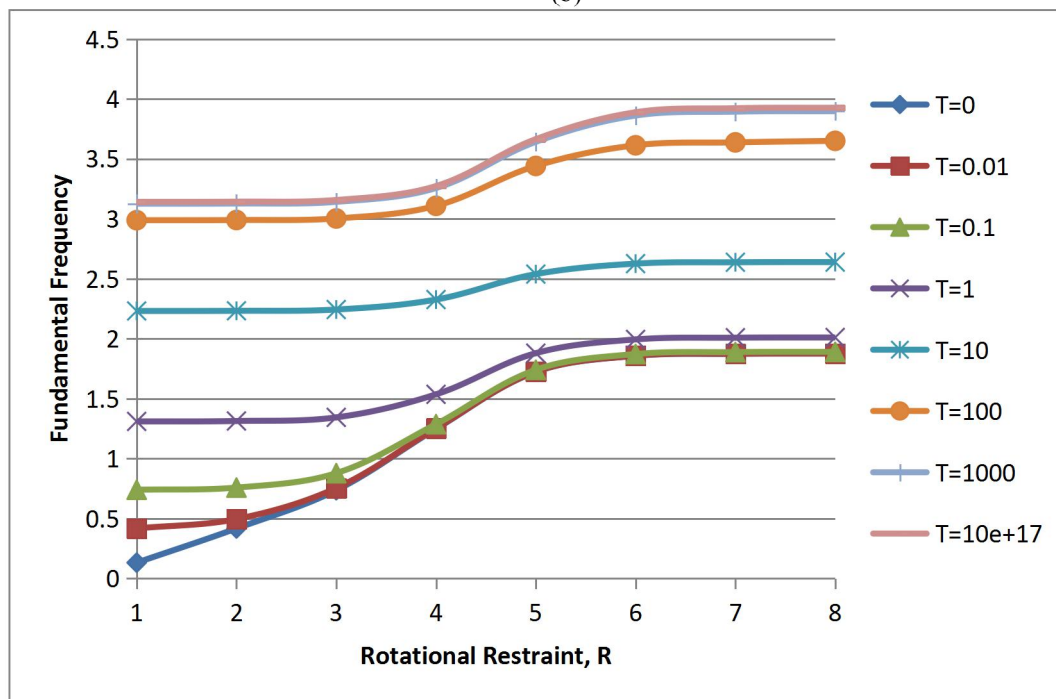
Table 2. First mode natural frequencies for various values of rotational and translational restraint parameters and for warping parameter $K = 0.01$



(a)



(b)



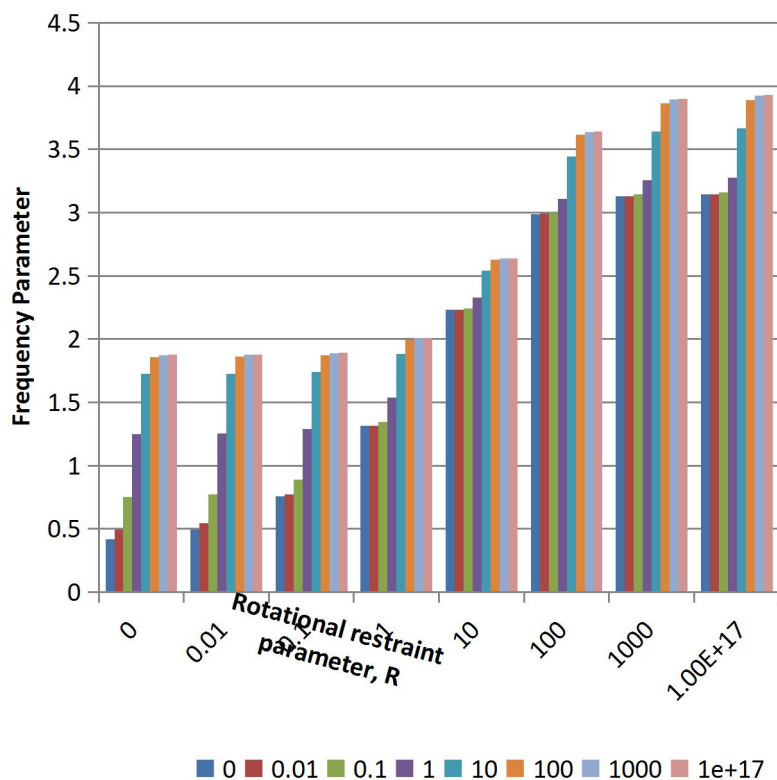
(c)

Fig. 3, (a), (b) and (c). Variation of frequency parameter with rotational and translational restraints (R & $T=0$ to 10^{17}) for a given Warping parameter ($K=0.01$).

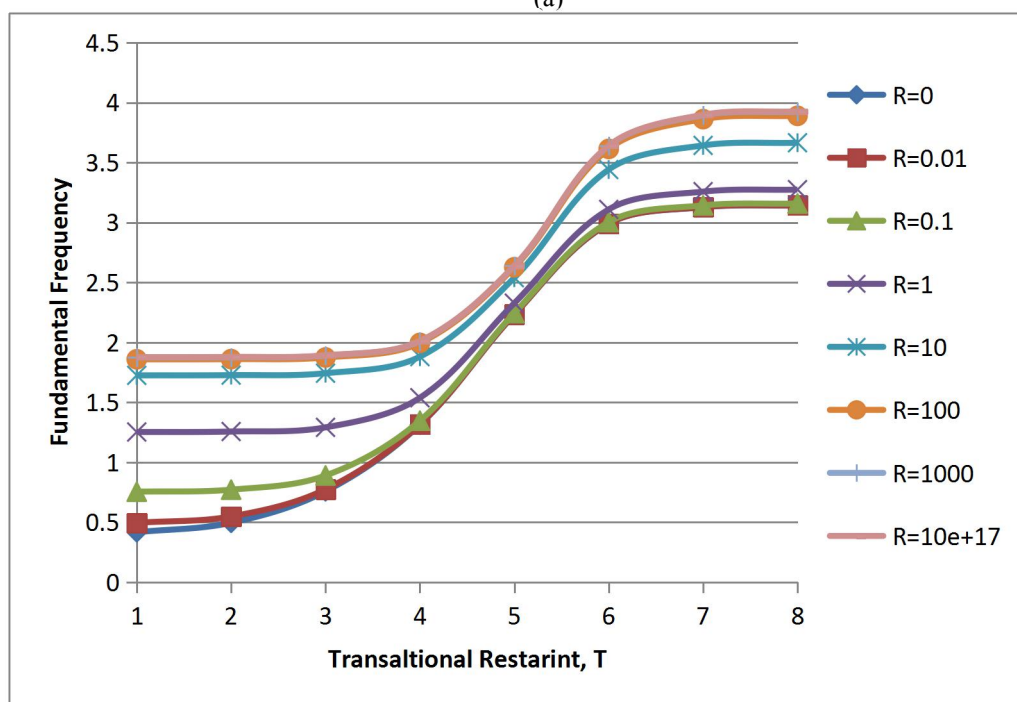
R	T = 0	T = 0.01	T = 0.1	T = 1	T = 10	T = 100	T = 1000	T = 10^{17}
0	0.4162	0.4949	0.7575	1.313	2.2317	2.9893	3.1269	3.1424
0.01	0.4948	0.5477	0.7743	1.3166	2.2331	2.9907	3.1284	3.144
0.1	0.7541	0.7711	0.8891	1.3467	2.2439	3.0036	3.1423	3.158
1	1.252	1.2561	1.2908	1.5379	2.327	3.109	3.2573	3.274
10	1.7247	1.7265	1.7425	1.8808	2.5393	3.4416	3.6428	3.6652

100	1.8586	1.8601	1.8738	1.9953	2.6266	3.6136	3.8619	3.8897
1000	1.875	1.8765	1.8899	2.0097	2.6381	3.638	3.8945	3.9232
10^{17}	1.8769	1.8784	1.8918	2.0114	2.6394	3.6408	3.8983	3.9271

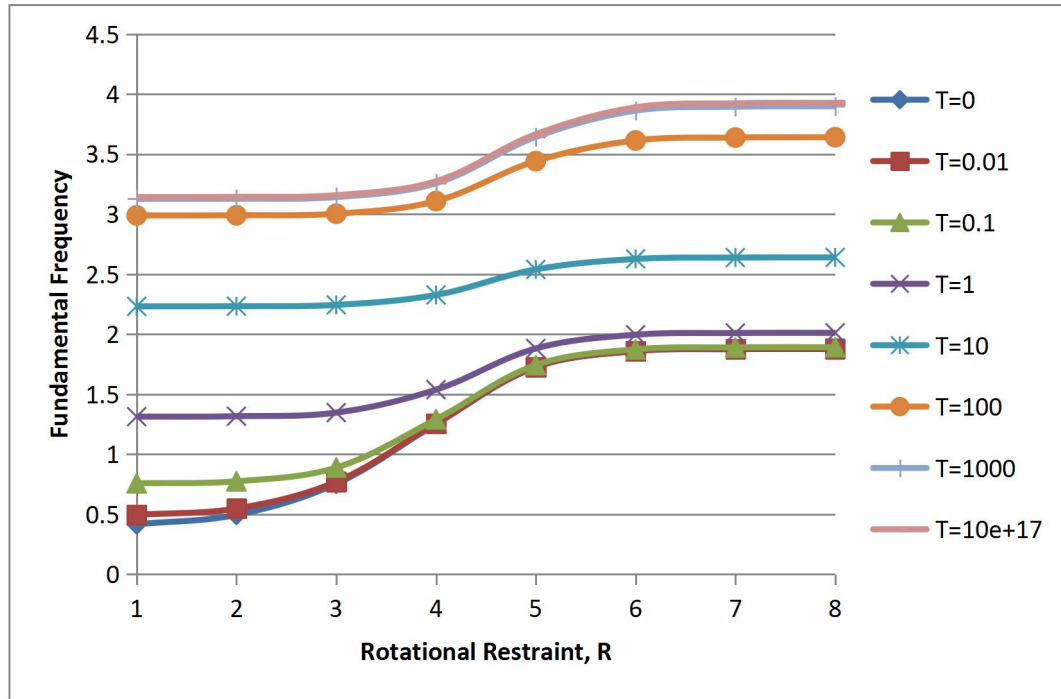
Table 3. First mode natural frequencies for various values of rotational and translational restraint parameters and for warping parameter $K = 0.1$



(a)



(b)

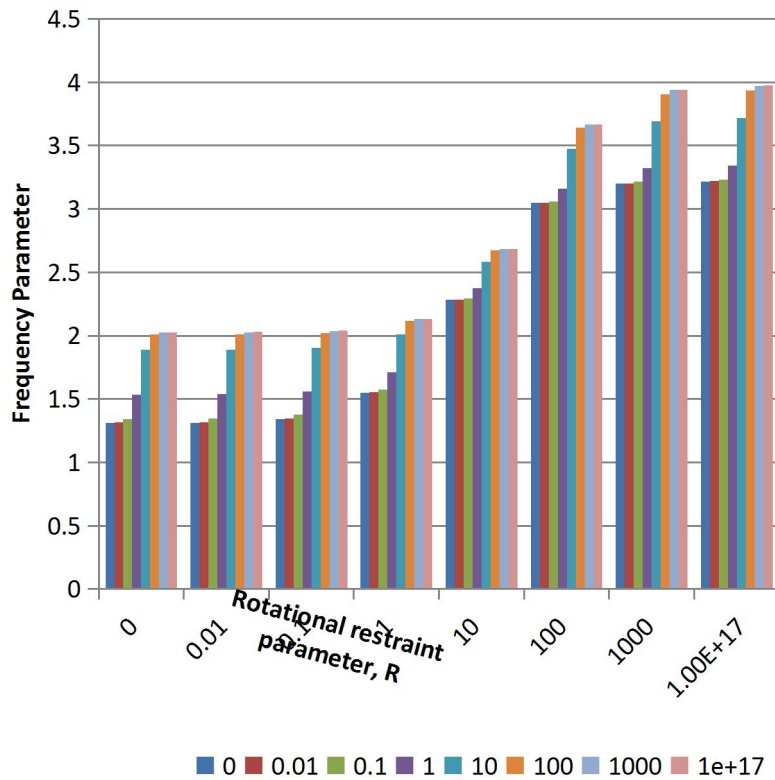


(c)

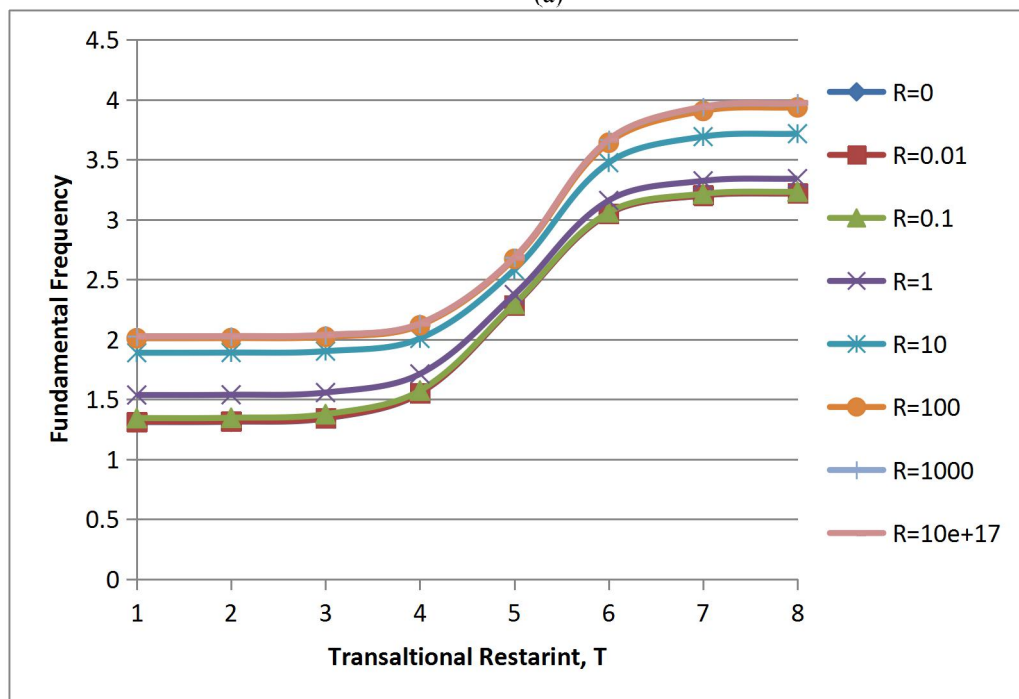
Fig. 4, (a), (b) and (c). Variation of frequency parameter with rotational and translational restraints (R & $T=0$ to 10^{17}) for a given Warping parameter ($K=0.1$).

R	T = 0	T = 0.01	T = 0.1	T = 1	T = 10	T = 100	T = 1000	T = 10^{17}
0	1.3104	1.3136	1.3414	1.5516	2.2852	3.0479	3.2008	3.2183
0.01	1.3139	1.3171	1.3447	1.5538	2.2863	3.0493	3.2023	3.2198
0.1	1.344	1.347	1.377	1.5736	2.2964	3.0612	3.2152	3.2328
1	1.5364	1.5385	1.5572	1.7125	2.3746	3.1591	3.323	3.3416
10	1.8891	1.8904	1.9022	2.0084	2.5828	3.4746	3.6919	3.7165
100	2.0102	2.0114	2.0219	2.118	2.6722	3.6413	3.9062	3.9363
1000	2.0256	2.0268	2.0371	2.1321	2.6841	3.6651	3.9383	3.9694
10^{17}	2.0274	2.0285	2.0389	2.1337	2.6854	3.6679	3.942	3.9733

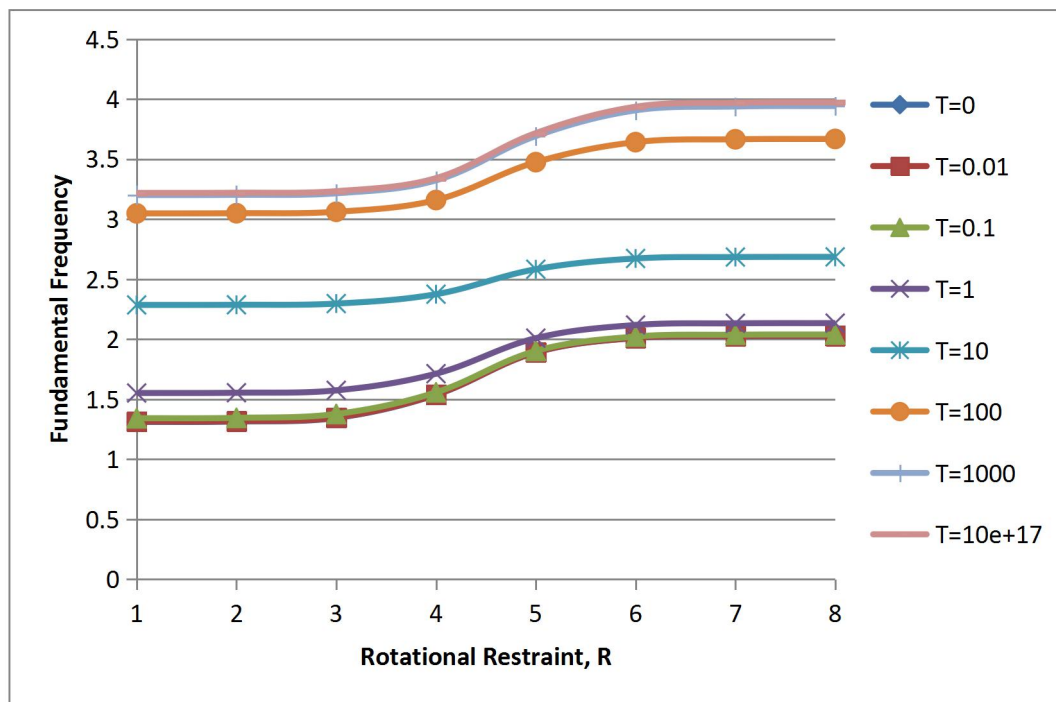
Table 4. First mode natural frequencies for various values of rotational and translational restraint parameters and for warping parameter $K = 1$



(a)



(b)

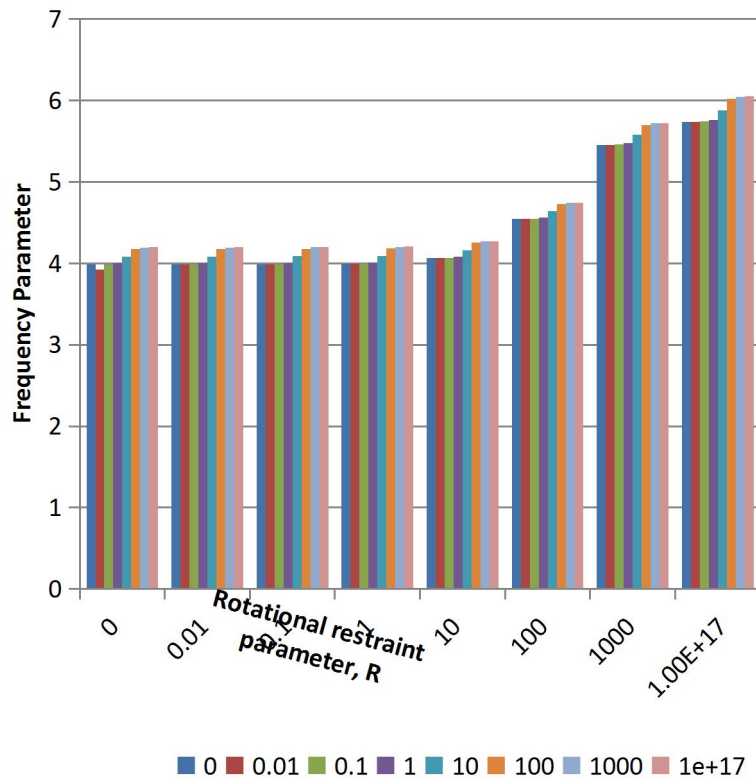


(c)

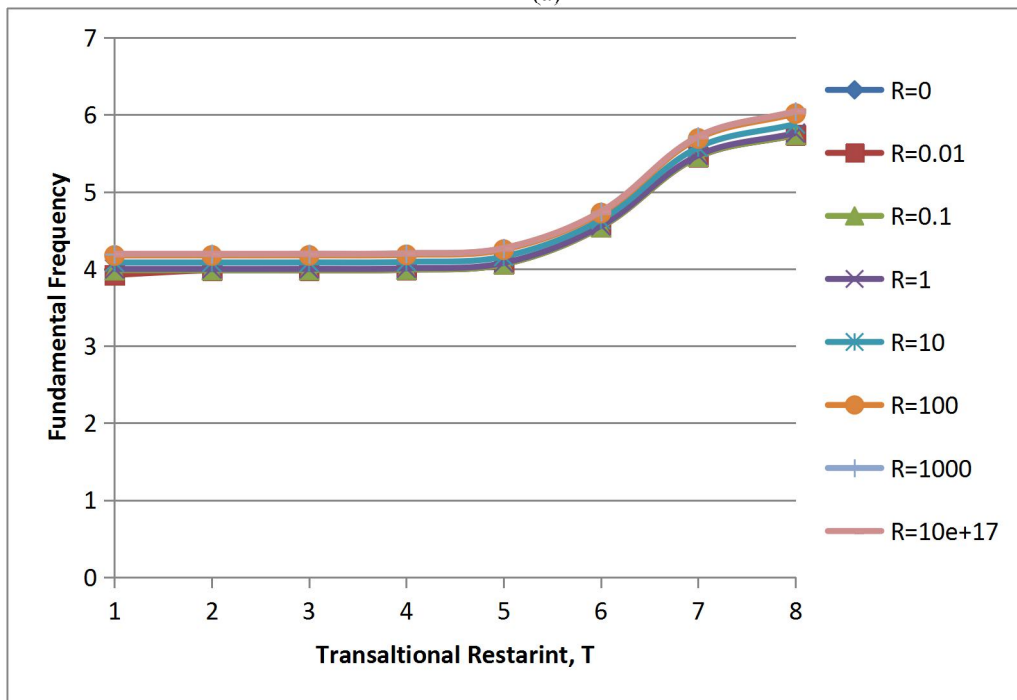
Fig. 5, (a), (b) and (c). Variation of frequency parameter with rotational and translational restraints (R & $T=0$ to 10^{17}) for a given Warping parameter ($K=1$).

R	T = 0	T = 0.01	T = 0.1	T = 1	T = 10	T = 100	T = 1000	T = 10^{17}
0	3.9827	3.9828	3.9836	3.9909	4.0613	4.5431	5.454	5.7384
0.01	3.9229	3.983	3.9837	3.9911	4.0615	4.5433	5.454	5.7387
0.1	3.9846	3.9847	3.9855	3.9928	4.0632	4.5449	5.4562	5.741
1	4.0004	4.0005	4.0013	4.0086	4.0787	4.5597	5.4751	5.7626
10	4.0842	4.0843	4.085	4.0922	4.161	4.6389	5.5778	5.8806
100	4.1752	4.1753	4.176	4.1831	4.2505	4.7258	5.6934	6.0158
1000	4.1942	4.1942	4.1949	4.202	4.2692	4.7439	5.7178	6.0447
10^{17}	4.1965	4.1966	4.1973	4.2043	4.2715	4.7462	5.7208	6.0483

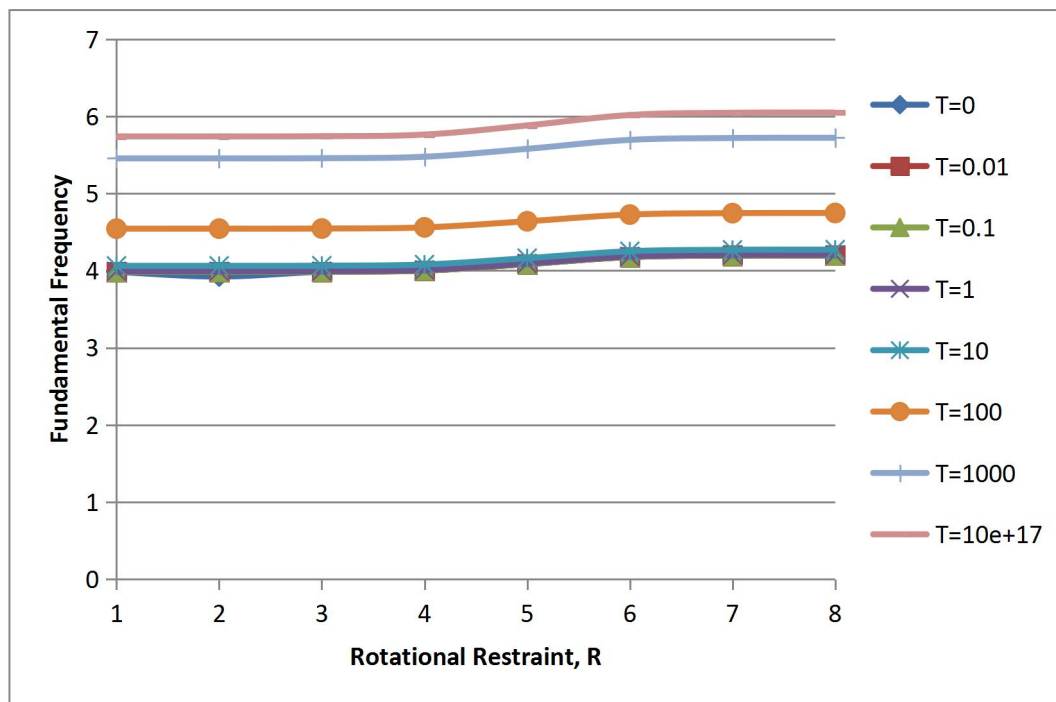
Table 5. First mode natural frequencies for various values of rotational and translational restraint parameters and for warping parameter $K = 10$



(a)



(b)

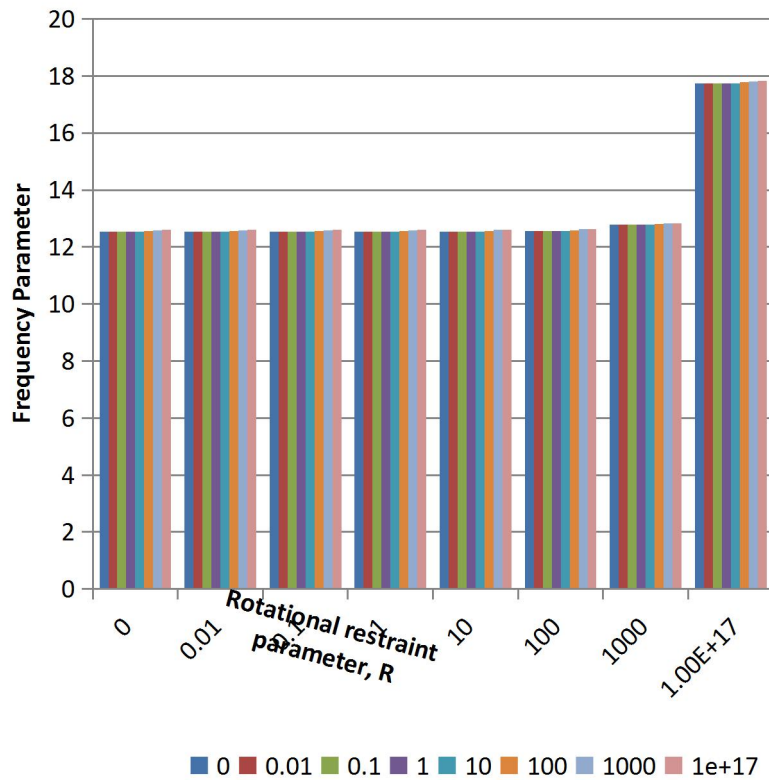


(c)

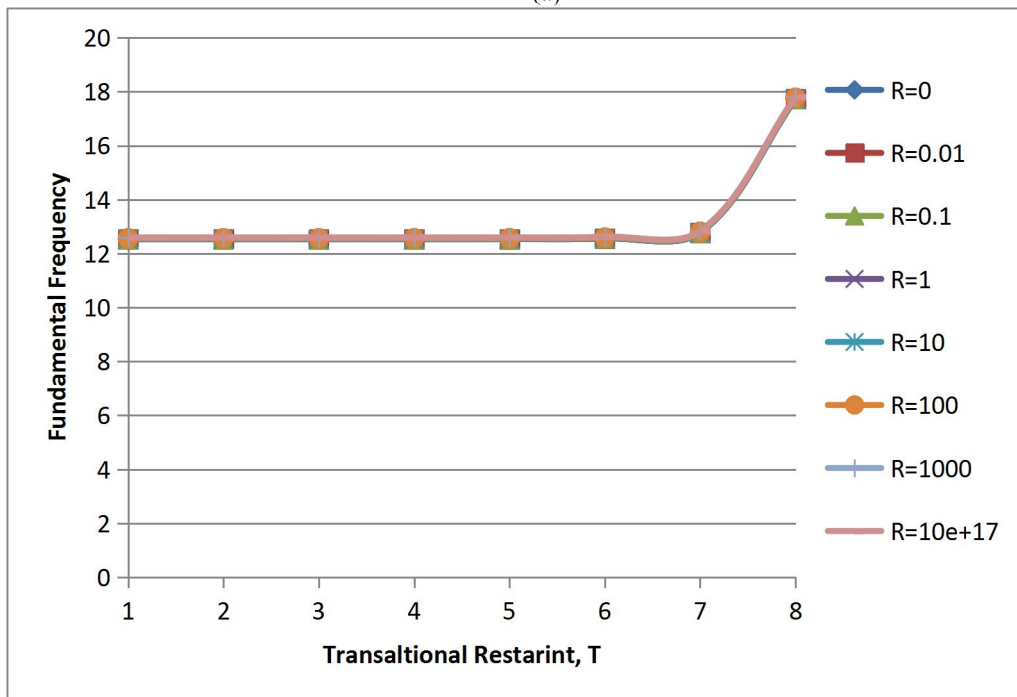
Fig. 6.(a), (b) and (c). Variation of frequency parameter with rotational and translational restraints (R & $T=0$ to 10^{17}) for a given Warping parameter ($K=10$).

R	T = 0	T = 0.01	T = 0.1	T = 1	T = 10	T = 100	T = 1000	T = 10^{17}
0	12.5339	12.5339	12.5339	12.5342	12.5364	12.5592	12.7758	17.7289
0.01	12.5339	12.5339	12.5339	12.5342	12.5364	12.5592	12.7758	17.7289
0.1	12.534	12.534	12.534	12.5342	12.5365	12.5592	12.7758	17.729
1	12.5345	12.5345	12.5345	12.5348	12.5371	12.5598	12.7764	17.7298
10	12.5396	12.5396	12.5396	12.5399	12.5421	12.5649	12.7814	17.737
100	12.5653	12.5654	12.5654	12.5656	12.5679	12.5906	12.8067	17.7734
1000	12.5913	12.5913	12.5913	12.5915	12.5938	12.6164	12.8332	17.8101
10^{17}	12.597	12.5976	12.5971	12.5973	12.5996	12.6222	12.8378	17.8182

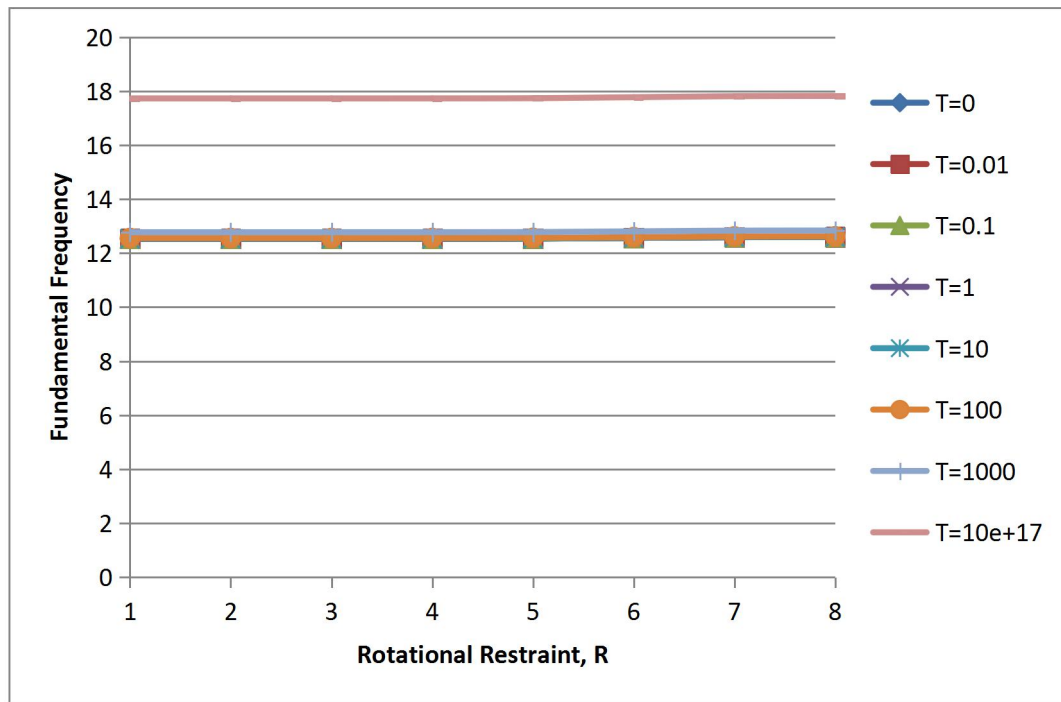
Table 6. First mode natural frequencies for various values of rotational and translational restraint parameters and for warping parameter $K = 100$



(a)



(b)

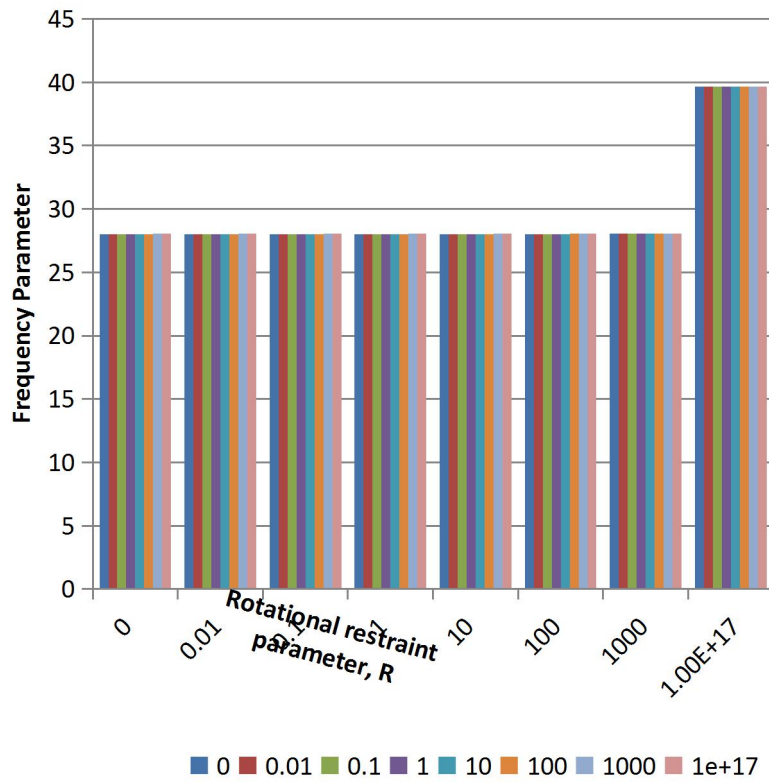


(c)

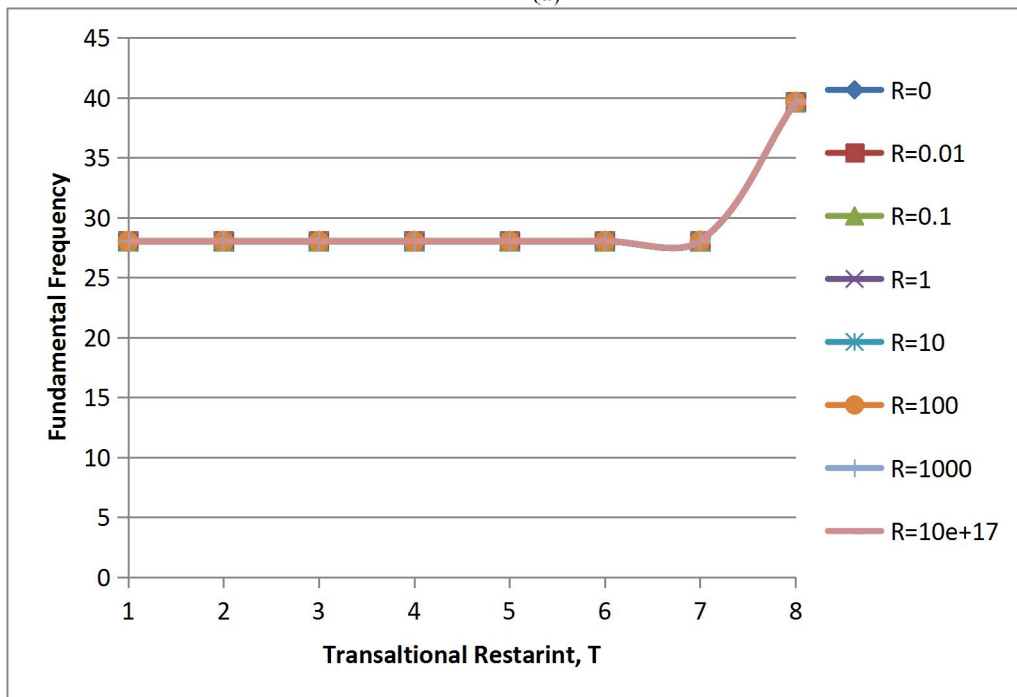
Fig. 7, (a), (b) and (c). Variation of frequency parameter with rotational and translational restraints (R & $T=0$ to 10^{17}) for a given Warping parameter ($K=100$).

R	T = 0	T = 0.01	T = 0.1	T = 1	T = 10	T = 100	T = 1000	T = 10^{17}
0	28.025	28.025	28.025	28.025	28.0253	28.0273	28.0477	39.6337
0.01	28.025	28.025	28.025	28.025	28.0253	28.0273	28.0477	39.6337
0.1	28.025	28.025	28.025	28.0251	28.0253	28.0273	28.0477	39.6337
1	28.0251	28.0251	28.0251	28.0251	28.0253	28.0274	28.0478	39.6337
10	28.0256	28.0256	28.0256	28.0256	28.0258	28.0278	28.0482	39.6344
100	28.0297	28.0297	28.0297	28.0287	28.0299	28.032	28.0524	39.6403
1000	28.0437	28.0437	28.0437	28.0437	28.044	28.046	28.0664	39.6601
10^{17}	28.0531	28.0531	28.0531	28.0531	28.0533	28.0554	28.0757	39.6734

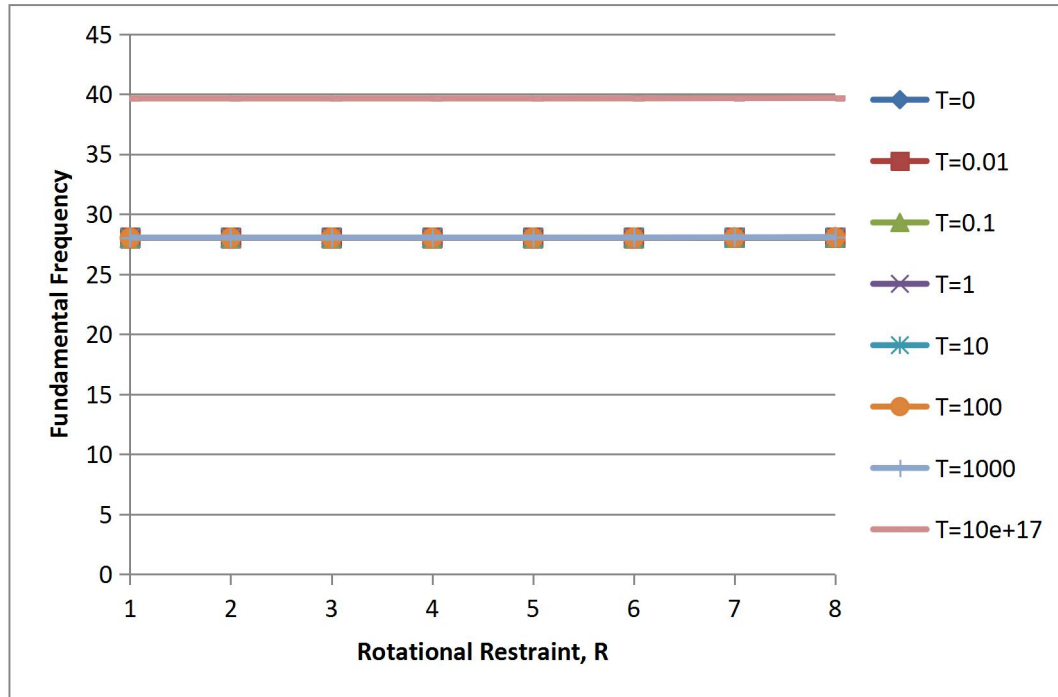
Table 7. First mode natural frequencies for various values of rotational and translational restraint parameters and for warping parameter $K = 500$



(a)



(b)



(c)

Fig. 8, (a), (b) and (c). Variation of frequency parameter with rotational and translational restraints (R & $T=0$ to 10^{17}) for a given Warping parameter ($K=500$).

6. Conclusions

Spectral dynamic analysis of free torsional vibration of doubly-symmetric thin-walled beams of open section is carried out and detailed results of this study are presented in this paper suitable for use in design and also for checking approximate solutions obtained for their accuracy. For the case of a thin-walled beam of doubly-symmetric open cross-section partially restrained against warping at one end transversely restrained at the other, undergoing free torsional vibrations, the spectral frequency equation is derived in this paper. The resulting transcendental frequency equation for the case of rotationally restrained cantilever with transverse restraint on the other end is solved for thin-walled beams of open cross section for varying values of warping parameter and the partial rotational and transverse restraint parameters. The influence of partial rotational restraint parameter R , transverse restraint parameter T and the warping parameter K on the free torsional vibration frequencies is investigated in detail and significant amount of numerical frequency data is generated. Using a MATLAB computer program developed to solve the spectral frequency equation derived in this study, numerical results for the first three modes of torsional natural frequencies for various values of, and warping K are obtained and are presented in both tabular as well as graphical form showing their parametric influence clearly. In comparison with the partial restraint parameters R and T , the warping parameter K is found to have significant effect on the torsional natural frequencies not only of the fundamental mode but also on higher modes as well.

References

1. D. YOUNG, R. P. FELGAR JR. 1949 Tables of characteristic functions representing normal modes of vibration of a beam. university of texas publication, No. 4913.
2. R. E. D. BISHOP, D. C. JOHNSON. Vibration Analysis Tables. Cambridge University Press. 1956.
3. T. C. CHANG, R. R. CRAIG. Normal modes of uniform beams. Journal of the Engineering Mechanics Division, American Society of Civil Engineers I, 95, 1027-1031. 1969.
4. E. G. PASSIG. End slope and fundamental frequency of vibrating fuel rods. Nuclear Engineering and Design 14 (2): 198-200. 1970.
5. K. R. CHUN. Free vibration of a beam with one end spring-hinged and other free. Journal of Applied Mechanics 39

- (4), 1154-1155. 1972.
6. J. C. MCBAIN, J. GENIN. Natural frequencies of a beam considering support characteristics. *Journal of Sound and Vibration* 27 (2): 197-206. 1973.
7. J. C. MCBAIN, J. GENIN. Effect of support flexibility on the fundamental frequency of vibrating beams. *Journal of the Franklin Institute* 296, 259-273. 1973.
8. R. C. HIBBELER. Free vibration of a beam supported by unsymmetrical spring-hinges. *Journal of Applied Mechanics* 42, 501-502. 1975.
9. D.A. GRANT. Vibration frequencies for a uniform beam with one end elastically supported and carrying a mass at the other end. *Journal of Applied Mechanics* 42 (2): 878-880. 1975.
10. G.L. ANDERSON. On the extensional and flexural vibrations of rotating bars. *International Journal of Non-linear Mech.*, 1975, 10, 223.
11. E. M. NASSAR, W. H. HORTON. Static deflection of beams subjected to elastic rotational restraints, *American Institute of Aeronautics and Astronautics Journal* 14, 1976, 122-123.
12. V. BEGLINGER, U. BOLLETER, W.E. LOCHER. Effects of shear deformation, rotary inertia and elasticity of the support on the resonance frequencies of short cantilever beams. *Journal of Engineering for Power, ASME*, 98(1): 79-87. 1976.
13. M.J. MAURIZI, R. E. ROSSI, J. A. REYES. Vibration frequencies for a beam with one end spring-hinged and subjected to a translational restraint at the other end. *Journal of Sound and Vibration* 48(4): 565-568. 1976.
14. R. P. GOEL. Free vibrations of a beam-mass system with elastically restrained ends. *Journal of Sound and Vibration* 47, 9-14. 1976.
15. R. D. BLEVINS. *Formulas for Natural Frequency and Mode Shape*. New York: Van Nostrand. 1979.
16. C. SUNDARARAJAN. Fundamental frequency of beams with elastic rotational restraints. *Journal of Mechanical Design* 101 (4): 711-712. 1979.
17. T. JUSTINE, A. KRISHNAN. Effect of support flexibility on fundamental frequency of beams. *Journal of Sound and Vibration* 68 (2): 310-312. 1980.
18. R. FOSSMAN, A. SORENSEN. Influence of flexible connections on response characteristics of a beam. *Journal of Mechanical Design* 102, 829-834. 1980.
19. H. IRRETIER, O. MAHRENHOLTZ. Eigen-frequencies and mode shapes of a free-standing, twisted, tapered and rotating blade with respect to an elastically support root. ASME publication, 81-DET-125, 1-9. 1981.
20. B. A. H. ABBAS. Vibrations of Timoshenko beams with elastically restrained ends. *Journal of Sound and Vibration* 97(4): 541-548. 1984.
21. B. A. H. ABBAS. Dynamic analysis of thick rotating blades with flexible roots. *The Aeronautical Journal* 89, 10-16. 1985.
22. D. AFOLABI. Natural frequencies of cantilever blades with resilient roots. *Journal of Sound and Vibration* 110(6): 429-441. 1986.
23. C. KAMESWARA RAO. Fundamental Frequencies of Cantilever Blades with Resilient Roots. *Journal of Sound and Vibration*. 126(2): 363-366. 1988.
24. B.A.H. ABBAS, H. IRRETIRE. Experimental and theoretical investigations of the effect of root flexibility on the vibration characteristics of cantilever beams. *Journal of Sound and Vibration* 130(3): 353-362. 1989.
25. C. KAMESWARA RAO. A note on vibrations of generally restrained beams. *Journal of Sound and Vibration* 130(3): 453-465. 1989.
26. C. KAMESWARA RAO , A. APPALA SATYAM. Torsional vibration and stability of thin-walled beams on continuous elastic foundation. *AIAA Journal*. 13, 232-234, 1975.
27. P. CHRISTIANO, L. SALMELA. Frequencies of beams with elastic warping restraint. *Journal of the Structural Division* 97(6): 1835-1840. 1971.
28. D. J. GORMAN. *Free vibration analysis of beams and shafts*. Wiley, New York, USA. 1975.
29. R. D. BLEVINS. *Formulas for Natural Frequency and Mode Shape*. D. Van Nostrand, New York, USA. 1979.
30. J.M. GERE. Torsional vibrations of beams of thin-walled open section. *Journal of Applied Mechanics*. 21(4): 381-387. 1954.
31. J. B. CARR. Torsional vibration of uniform thin-walled beams of open section. *Aeronautical Journal*. 73(704): 672-674. 1969.
32. C. KAMESWARA RAO. Torsional frequencies and mode shapes of generally constrained shafts and piping. *Journal of Sound and Vibration*. 125(1): 115-121. 1988.
33. B. RAFEZY, W. P. HOWSON. Exact dynamic stiffness matrix for a thin-walled beam of doubly asymmetric cross-section filled with shear sensitive material, *International Journal for Numerical Methods in Engineering*. 69: 2758-2779. 2007.
34. K. B. BOZDOGAN, D. OZTURK. Free vibration analysis of a thin-walled beam with shear sensitive material. *Mathematical Problems in Engineering* Volume 1-7. 2013.
35. E. J. SAPOUNTZAKIS. Bars under torsional loading: A generalized beam theory approach. *ISRN Civil*

Engineering, 1-39. 2013.

36. A. BURLO, G. FAILLA, F. ARENA. Coupled bending and torsional free vibrations of beams with in-span supports and attached masses. *European Journal of Mechanics / A Solids*. 66, 387-411, 2017.
37. ANDREA BURLON, GIUSEPPE FAILLA, FELICE ARENA. Exact stochastic analysis of coupled bending–torsion beams with in-span supports and masses. *Probabilistic Engineering Mechanics*. Volume 54, October 2018, 53-64.